2012

# Freeze-thaw performance of pavement foundation materials

Alex Johnson
*Iowa State University*

**Freeze-thaw performance of pavement foundation materials**

by

**Alex Edwin Johnson**

A thesis submitted to the graduate faculty

In partial fulfillment of the requirements for the degree of

MASTER OF SCIENCE

Major: Civil Engineering (Geotechnical Engineering)

Program of Study Committee:
David J. White, Major Professor
Robert Horton
Peter Taylor
Pavana Vennapusa

Iowa State University

Ames, Iowa

2012

*For*

*My wife, Sadie*

## TABLE OF CONTENTS

## LIST OF TABLES

## LIST OF FIGURES

## ABSTRACT

Freezing and thawing processes damage pavement foundation systems; increase pavement and vehicle maintenance costs; reduce traveler comfort and safety; decrease fuel economy; and decrease pavement life spans. Current pavement design methods provide limited guidance for characterizing frost-susceptible materials. A laboratory frost-heave and thaw-weakening test could be used to differentiate frost-susceptible materials from non-frost-susceptible materials to reduce the effects of frost action.

The goal of this research was to provide guidance for selecting pavement foundation materials based on their freeze-thaw durability. The objectives of this study were to use ASTM D5918 *Standard Test Methods for Frost Heave and Thaw Weakening Susceptibility of Soils* to determine the relative frost-susceptibility of various soil types; study the effects of stabilizers on reducing frost-susceptibility; and determine seasonal changes of in situ pavement support conditions.

The important outcomes of this research are that it is difficult to predict frost-heave susceptibility from USCS classifications; the coefficients of variation for ASTM D5918 test results were similar to published results; when stabilizing loess with cement, increased cement content decreased the range of initial moisture contents that result in maximum compressive strength; and compared to unstabilized loess, cement-stabilized loess was found to be non-frost-susceptible, but fly ash-stabilized loess showed only slight improvement.

This research suggests that using a test such as ASTM D5918 to compare the relative frost-susceptibility of pavement foundation materials in the design phase may reduce the effects of frost action.

# CHAPTER 1. INTRODUCTION

This chapter describes the industry and technical problems associated with this research, the goals and objectives of the research, and the significance of the research. The final section discusses how the chapters are organized in this thesis.

## INDUSTRY PROBLEM

Freezing and thawing processes severely affect pavement foundation systems in the northern regions of the United States, which result in damage to pavement systems and increased costs over the life of these systems.

The effects of freezing and thawing processes, also known as frost action, on pavement structures are difficult to predict. Many variables (e.g., material type and depth of water table) must be considered when determining how to prevent frost action from causing damage and reducing the service life of pavement systems. Typical effects of frost action are rough pavement surfaces, cracking, and potholes (Simonsen and Isacsson 1999). Frost action damages the pavement system, which increases costs by requiring additional pavement and automobile maintenance; decreasing road users' comfort; causing safety hazards (e.g., increased maintenance or reconstruction); decreasing the life span of the pavement system; and decreasing fuel economy because of increased roughness (Spizziri 2012).

Current pavement design methods (e.g., AASHTO 1993 and NCHRP) provide limited guidance for reducing the effects of frost action. In order to effectively consider frost action, the design process should include laboratory tests that measure the frost susceptibility of materials rather than use correlations that do not account for variations in soil response and in situ conditions. The laboratory test should be applied among design agencies to develop a uniform design process in areas affected by frost action.

This research will be a part of a pavement foundation manual that is being prepared through a federal highway pooled fund study – Improving the Foundation Layers for Concrete Pavements FHWA TPF-5 (183). The following departments of transportation (DOT) are contributing to the study: California DOT, Iowa DOT, Michigan DOT, Pennsylvania DOT, and Wisconsin DOT.

## TECHNICAL PROBLEM

The Pavement Design for Seasonal Frost Conditions manual states that "the detrimental effects of frost action in subsurface materials are manifested by nonuniform heave of pavements during the winter and by loss of strength of affected soils during the ensuing thaw period" (Joint Departments of the Army and Air Force Manual 1985, 2–1). Highly variable responses of pavement foundation layers to frost action result from in situ conditions (e.g., depth of the water table), unpredictable climate conditions, and differences in material properties. The first two conditions can be accounted for but not easily modified in the pavement design process. However, pavement designers can and should understand the properties of site materials so they can specify materials that would reduce frost susceptibility. In general, laboratory tests used to establish frost susceptibility are not performed during the design process. This problem is compounded because several frost-heave and thaw-weakening laboratory tests use different equipment and thermal boundary conditions, which makes it difficult to use in pavement design and correlate to long-term pavement performance.

## GOAL OF THE RESEARCH

The first goal of this research was to provide guidance for the selection of pavement foundation materials based on their freeze-thaw durability. The second goal of this research is to better understand how pavement support conditions change on a seasonal basis.

## OBJECTIVES

The objectives of this study are to:

- determine the relative frost-susceptibility of various soil types according to ASTM D5918 Standard Test Methods for Frost Heave and Thaw Weakening Susceptibility of Soils and obtain repeatable results,
- study the effects of stabilizers on reducing frost susceptibility, and
- determine seasonal changes of in situ pavement support conditions.

## SIGNIFICANCE OF THE RESEARCH

Improving the resilience of pavement structures to the effects of frost action is critical for increasing the long-term quality of pavement projects. This resilience is directly related to the

materials used in foundation layers. However, current design methods do not require that pavement foundation materials be tested for frost susceptibility.

This research demonstrates the benefits of a laboratory testing program that evaluates the frost susceptibility of materials and argues that frost susceptibility tests should be conducted early in the pavement design process so designers can identify and specify optimum pavement foundation materials. In some cases, specifying the optimum materials that may cost more initially may provide long-term economic benefits.

This improvement in the design process could reduce recurring maintenance or reconstruction costs, lead to more economical designs, improve the overall safety of the roadway system and result in the user experiencing smoother rides and saving money on automobile maintenance in the long term.

This thesis also discusses long-term in situ seasonal variation findings.

## ORGANIZATION OF THE DOCUMENT

Following this introduction chapter, the thesis is organized into five additional chapters. Chapter 2 provides a review of relevant literature and a background for this research. Chapter 3 describes the test procedures used in this research, and chapter 4 presents the results of laboratory soil index tests. Chapter 5 presents the results and analysis of the laboratory and in situ tests performed in this research. Chapter 6 includes conclusions and recommendations for future research and practice. A list of references and appendices are located at the end.

# CHAPTER 2. LITERATURE REVIEW

This chapter presents a literature review of the effects of freezing and thawing processes on the pavement foundation system. The material contained in this chapter will describe how this research is related to and builds off of past research.

The literature review covers five main topics: freeze-thaw theory, freeze-thaw laboratory testing, in situ seasonal pavement testing, chemical stabilization techniques to reduce freeze-thaw effects, and applicable methods of design to frost affected areas.

## FREEZE-THAW THEORY

Freezing temperatures in pavement structures can lead to damaging heave and an eventual loss of pavement support conditions. Heave in pavements is caused by the formation of ice lenses, also known as ice segregation. In order for ice lenses to develop, three conditions must be present: the soil must be frost susceptible (i.e., supply water to the freezing front by capillary action), there must a sufficient supply of water (i.e., high ground water table), and there must be freezing temperatures present (Taber 1929). Iowa, Michigan, Pennsylvania, and Wisconsin are in wet-freeze regions. In wet-freeze regions, there is a sufficient supply of water, due to high water tables, and there are freezing temperatures present, so the only condition that is missing is frost-susceptible materials (American Concrete Pavement Association 2008). Portions of California are located in dry-freeze, dry-nonfreeze, and wet-nonfreeze regions. All three regions are less susceptible to frost heave compared to wet-freeze regions because they typically only have one or none of the three conditions required for frost heaving to occur.

### Ice Lens Theory

Taber (1929) showed that frost heave is a result of ice lens formation in the soil, which is primarily caused by an addition of water to the freezing front. However, Benkelman and Olmstead (1931) proposed that frost heave is a result of soil saturation and seepage. According to their theory, as the frost line moves into the soil layers, free water and water held in films around soil particles freeze. Thus, according to Benkelman and Olmstead (1931), heave is as a result of the volume expansion of water, which is around 10% (Taber 1929). The volume expansion of water limits the total amount of heave to around 5 cm in situ

instead of the 15 cm that have been observed (Taber 1929). Therefore, Benkelman and Olmstead's theory does not properly explain in situ conditions. Benkelman and Olmstead's theory was tested on laboratory samples enclosed in a glass tube with a pervious cork at the bottom which acted as a water supply (1931). As the frost line moved toward the surface of the sample, during thawing, a void appeared where water would gather. As freeze-thaw cycles were repeated, more voids formed, showing that ice lenses were forming.

Casagrande (et al. 1931) observed that Benkelman and Olmstead's theory of frost heave was based on defective laboratory tests which led to misleading results. When Benkelman and Olmstead would freeze and thaw their sample, they would move the depth of frost penetration up and down. This led to the top layers of soil being frozen to the side walls of the glass tube. The upper frozen layers were prevented from settling in the tube, which caused a void to form. The process resulted in the development of a pocket of water which froze when the frost depth was eventually lowered. Cassagrande agreed with Taber's theory that frost heave is a result of a constant supply of water to the freezing front instead of freeze-thaw cycling. Penner (1966) also performed experiments and confirmed that freeze-thaw cycling is not required for significant heaving to occur.

### Movement of Water

The degree of frost heave is dependent on the pore size which determines the magnitude of capillary stress. Capillary stress is caused by the surface tension of free water and as the capillary stress increases, the height that water can be pulled above the water table increases (Taber 1929). The main factors that affect capillary action are the distance to the water table and the soil particle size (Beskow [1935] 1991). The amount of water available to a growing ice lens is directly related to the degree of heaving. Kaplar (1970) found that the supply of water is dependent on the pumping rate, suction head, distance to free water, size and number of water passages, freezing rate of active film water, and characteristics of air bubbles in the soil. In fine-grained materials the permeability can be low enough to limit the supply of water to the freezing front and significantly reduce the potential for frost heave (Beskow [1935] 1991). Beskow stated that "for coarse silty clays frost heaving decreases with increasing grain size, and for fine it decreases with decreasing grain size" ([1935] 1991, p. 87). Taber

also showed that a layer of coarse material can be used as a capillary break to stop the movement of water to the frost line.

Taber (1929) performed dilatometer tests to closely measure the volume change during freezing in a closed freezing system, where additional water is not made available during freezing. Taber found that water froze completely in clean sand or other materials with large voids. However, in finer grained materials a portion of water does not freeze but is tightly held in films around the soil particles. Beskow ([1935] 1991) theorized that adsorption films form around fine grained soil particles and as freezing occurs, water is pulled from the film to form ice crystals. Negative pressures develop as a result of water being pulled from the films, which leads to water being drawn from below to replenish the films (Beskow [1935] 1991). Penner (1966) also theorized that as water held in films turns to ice a negative pressure gradient in the soil is formed. Beskow compared the freezing process in soils to the evaporation or drying that takes place in soils. The soil drying process is similar to freezing because, they both remove water that is in the soil pore space. As water freezes in ice lenses it separates or removes itself from the soil structure, as it would during evaporation.

### Frost-Heave Process

Stratification in soil layers can provide optimal conditions for frost heave because the boundaries of layers are typically where ice crystals begin to form (Beskow [1935] 1991). Taber (1929) theorized that for the frost depth to remain at the same location as the freezing front, a heat balance must be reached between the extraction of heat moving through frozen layers and heat moving through unfrozen layers. Heat exchanged through rising water and heat lost while transitioning from water to ice must also be considered (Taber 1929). If the heat balance is maintained, then the ice lens will continue to grow, but if the frost depth moves down, a new ice lens will form. The thickness of an ice lens is dependent on the relationship between the supply of water and the movement of heat in the soil (Penner 1966). For slow frost penetration, a thicker ice lens can be expected, but for a quick freeze, many thin ice lenses can develop.

Taber (1929) reported that ice lenses form when growing ice crystals move towards soil particles and the water between them is reduced to a film around the soil particles. Taber further explained that

> if the soil particle is relatively small so that the molecules do not have far to travel through the film, and if growth is relatively slow, so that they have time to enter between the ice and the particle, then the growing crystal will exclude the particle; but if the particle is relatively large and if freezing is relatively rapid, the particle is gradually surrounded by ice. (1929, p. 439)

This process explains why ice banding forms in soil, as opposed to one thick ice lens. In order for an ice lens to form, the soil particle must be excluded by the ice crystals. Taber found that ice lenses form more easily when the soil has a high water content. Therefore, when repeated freezing and thawing cycles occur, heaving in the soil could be greater. The freezing and thawing cycles also break apart consolidated soils which reduces the tensile strength of the soil that is resisting heave.

The vertical heave can be attributed to the vertical direction being the one that conducts the majority of heat away from the soil and being the direction of least resistance. Taber found that a growing ice lens can exert a pressure of 1,300 kPa. Increasing the pressure on a soil sample leads to a lower soil water freezing temperature, as well as reducing the permeability by consolidating the soil.

### Frost-Heave Theories

Penner (1959) theorized that the energy required to bring water to the freezing front is supplied by the supercooling of water in the soil pore space. Smaller soil pores lower the required temperature for the pore water to freeze. A portion of water that is held in adsorbed films on soil particles is frozen when the freezing front moves into the soil. As water is removed from the films to freeze, it is replaced by water held in films below. Penner suggested that in the process of water freezing in soil, water goes from being supercooled in the pores to being adsorbed in films to becoming a part of the growing ice lens. For this to happen, the soil temperatures must be below freezing to supercool the water. He theorized that an increase in overburden pressure can slow or stop the growth of an ice lens by reducing the freezing point of the adsorbed water on the soil particles. The best situation for frost heave to occur is one where there is a shallow freezing front, which lowers the overburden pressure, and a high water table, which provides a constant supply of water.

Penner's theory suggested that the maximum moisture suction and heaving pressures should decrease as the pore size increases. This supports the use of particle size limitations. The permeability can also decrease with decreasing particle size, which can lead to smaller amounts of heave even though the particle size may be smaller; this is the case for clay soils. Penner found that an increase in density also has the same effect as decreasing the grain size, because the pore size is decreased. This can potentially make a coarse grained material more susceptible to frost heave (Penner 1959). In a discussion of Penner's theory (1959), Miller disagreed with the theory that supercooling of water is the main supply of energy for frost heave. He hypothesized that recharging adsorbed films is not a result of phase change or supercooling, because if film water is supercooled it would instantaneously freeze the entire film when it came into contact with ice crystals. If the adsorbed film froze, it would completely end the movement of water. Miller believed water was supercooled, but the effect took a passive role. Water must be supercooled to an extent in order for water to freeze under increasing overburden pressures. Miller hypothesized that the freezing point of water held in films is depressed by adsorption forces rather than being supercooled. The adsorption forces also bring water from below to replace water being frozen. Miller states that "water acquired by the surface film is constantly being borrowed and stored as ice" (Penner 1959, p.21).

Primary heaving occurs when water flows through unfrozen soil to the base of a growing ice lens (Miller 1972). The growing ice lens is the interface between ice and water. The end of primary heaving occurs when the frozen pore size becomes too small to allow water movement to the freezing front. The theory which Taber and Beskow worked on was based on primary heaving. However, Miller argued that there is another process taking place, which is called secondary heaving. Secondary heaving is a process where ice exists in the pores below the base of the growing ice lens. The development of a new ice lens takes place behind the freezing front. Like Taber, Miller assumes that the soil particles are covered in a film. However, Miller was interested in the films surrounding particles below a growing ice lens as they become partially frozen. A pressure potential develops as water is pulled from films by the forces created from the pore water freezing. The pressure potential pulls water from below to replenish the films. Once the films are replenished they supply water needed for the

continual growth of the ice lens. Chamberlain (1981) found that secondary heave theory depends on the following factors:

- Rate of heat extraction
- Size of soil pores
- Freezing point of the water
- Hydraulic conductivity of frozen fringe
- Temperature gradient in the frozen fringe
- Thickness of frozen fringe
- In situ moisture tension in unfrozen soil
- Hydraulic conductivity of unfrozen soil
- Compressibility of unfrozen soil
- Magnitude of the overburden pressure

Kaplar (1970) theorized that adsorbed water on soil particles resulted in the energy required to supply water to the freezing front. Fine grained soils are affected more by the adsorbed films than coarser particles. Kaplar compared the force caused by the freezing films to miniature hydraulic jacks that lift the soil up, as long as they are supplied with water. Lifting the soil particles creates suction in the water which causes a pressure gradient to develop. The principle of free energy can be used to define the work being done in the films to create a pressure gradient. The amount of free energy that is available to create suction is related to the size of the film area, which is related to the size of the particle and the thickness of the film. Larger particles are less susceptible to frost heave because they induce lower pressure gradients. The relation between the size of particles and frost heave would lead to the assumption that highly plastic clays would be very susceptible to frost heave, but they typically are not because they have such a low permeability that the water supply is inhibited.

Once the pressure in the pore ice reaches the overburden pressure, the stresses between the grains becomes zero which allows the above particles to freely move with the ice (Miller 1972). This is the beginning of a new ice lens. Miller defined this area in which ice and water exist together, below the base of the ice lens, as the frozen fringe. The frozen fringe is compared to quicksand where the seepage forces reduce the effective stress to zero. Miller theorized that if primary heaving is limited by heat extraction, secondary heaving will not

occur because ice will most likely not appear below the ice lens. But, if the supply of water is the limiting factor, then the creation of new ice lenses below the current one will take place, by the penetration of ice into the pore structure below the current ice lens.

Miller (1978) went on to describe the forces acting in the frozen fringe. As the freezing front penetrates the soil, films on the top side of the particle becomes cooler than on the bottom side. As the film on the top of the particle begin to swell and push the particle away from the ice, a surface force is applied to the particle. On the bottom side of the particle, the only surface force acting is from the pore water pressure. This difference in forces results in a net downward force acting on the particle. The downward force results in the tendency to separate the ice and soil mass by pushing the soil particle out of the ice lens. The temperature gradient also causes a gradient in the particle film pressure, which leads to water being pulled up to the freezing front. Miller supported his theory with experimental observations where an induced temperature gradient resulted in particles trapped in ice to move down or towards increasing temperatures.

The ice lenses that form during frost penetration will then thaw from the top down as the temperatures begin to warm. This leads to the resulting water being trapped in the upper levels, because the lower levels are frozen (Taber 1929). This can cause differential settlement and be more damaging than frost heave.

## FREEZE-THAW LABORATORY TESTING

Laboratory testing provides useful indications of how soils will perform when exposed to frost action. The following sections discuss how freeze-thaw laboratory testing can be used to determine the effects of frost action on soils. The first section discusses how particle size tests and mineral properties can be used to predict frost susceptibility. The second section gives background information and results, from the literature, for the frost-heave and thaw-weakening test outlined in ASTM D5918. The final section gives a brief overview of chemical stabilization techniques and how they can be used to reduce the effects of frost action.

### Particle Size Frost Susceptibility Tests

Cassagrande (1931) performed in situ frost-heave tests on square slabs placed over various soil types. He recorded the temperature beneath the slab and the total amount of

heave during freezing. He concluded that in non-uniform soils a considerable amount of frost heave could be expected when more than 3% of the particles are smaller than 0.02 mm. He also stated that in uniform soils, considerable heave could be expected if more than 10% of the particles are smaller than 0.02 mm. In soils with less than 1% smaller than 0.02 mm, he observed no frost heave. Chamberlain (1981) mentions that Cassagrande's criteria are still the most widely used even though Cassagrande most likely never meant it to be widely applied. The criteria are only based on frost-heave test results, not thaw weakening.

Chamberlain (1981) found that there were no available tests to completely evaluate the freeze-thaw performance of soils in the laboratory. Chamberlain critiqued over 100 test methods related to freeze-thaw performance. He separated the test methods used to classify frost susceptibility into five categories particle size properties, pore size properties, soil/water interaction, soil/water/ice interaction, and frost-heave properties.

The most used methods to determine frost-susceptibility characteristics are the ones related to the particle size of the soils because they do not require testing in addition to what is typically performed on a road project. Chamberlain reported that, the grain size criteria used by the U.S. Army Corps of Engineers (USACE) are the most reliable based on laboratory tests (Table 1). The laboratory tests compared grain size criteria used by various agencies with laboratory frost-heave tests on 16 soil samples.

The USACE criteria used three levels to determine the extent of testing that would be required to determine a material's frost susceptibility. A type 1 criterion describes gravels with 1.5% < 0.02 mm and sands with 3% < 0.02 mm to be non-frost-susceptible. If a soil does not meet the type 1 criterion, a complete soil classification would be required to fulfill the type 2 criteria. A type 3 criterion requires a frost-heave test for gravels with 1.5-3% smaller than 0.02 mm and sands with 3-10% smaller than 0.02 mm. Because the degree of frost susceptibility is highly variable, it was recommended that a frost-heave test be performed when accurate information is required.

**Table 1. U.S. Army Corps of Engineers Frost Susceptibility Classification System (Chamberlain 1981)**

| Frost susceptibility* | Frost group | Kind of soil | Amount finer than 0.02 mm (% by weight) | Typical soil type under USCS[x] |
|---|---|---|---|---|
| Negligible to low | NFS** | Gravels | 0-1.5 | GW, GP |
| | | Sands | 0-3 | SW,SP |
| Possible | PFS[xx] | Gravels | 1.5-3 | GW, GP |
| | | Sands | 3-10 | SW, SP |
| Low to medium | S1 | Sands | 3-6 | GW, GP, GW-GM, GP-GM |
| Very low to high | S2 | Sands | 3-6 | SW,SP, SW-SM, SP-SM |
| Very low to high | F1 | Gravels | 6-10 | GM, GW-GM, GP-GM |
| Medium to high | F2 | Gravels | 10-20 | GM, GM-GC, GW-GM, GP-GM |
| Very low to very high | F2 | Sands | 6-15 | SM, SW-SM, SP-SM |
| Medium to high | F3 | Gravels | > 20 | GM, GC |
| Low to high | F3 | Sands except very fine silty sands | > 15 | SM, SC |
| Very low to very high | F3 | Clays, PI > 12 | — | CL, CH |
| Low to very high | F4 | All silts | — | ML, MH |
| Very low to high | F4 | Very fine silty sands | > 15 | SM |
| Low to very high | F4 | Clays, PI < 12 | — | CL, CL-ML |
| Very low to very high | F4 | Varved clays and other fine-grained, banded sediments | — | CL and ML; CL, ML and SM; CL, CH, and ML; CL, CH, ML and SM |

*Based on laboratory frost-heave tests
[x]G–gravel, S–sand, M–silt, C–clay, W–well-graded, P–poorly graded, H–high plasticity, L–low plasticity
**Non-frost-susceptible
[xx]Requires laboratory frost-heave test to determine frost susceptibility

The U.S. Army Cold Regions Research Engineering Laboratory (CRREL) used a frost-heave test, to determine frost-heave classifications, which is known as the CRREL

frost-heave test. The USACE grain size criteria can be compared to the frost-heave results and classifications (Figure 1).

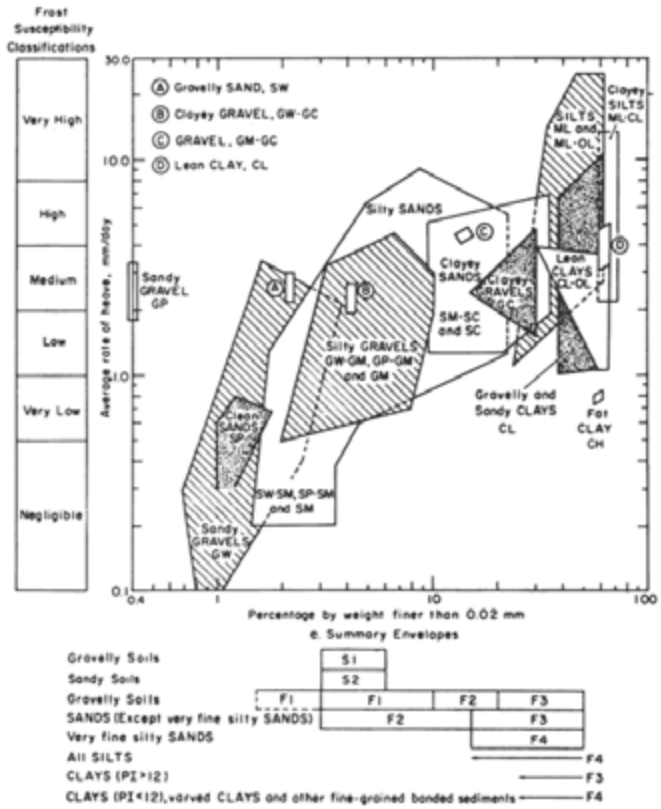


**Figure 1. U.S. Army Corps of Engineers frost susceptibility of soils (Joint Departments of the Army and Air Force 1985)**

A study performed by the Massachusetts Department of Public Works and the Federal Highway Administration (FHWA) at the Winchendon field test site, observed frost heave, thaw weakening, and frost penetration over a period of three winters (Edgers et al. 1988). Twelve soil types were used in the foundations of the test road, to compare their frost-susceptibility in situ. The 12 soil types included fine grained and coarse grained soils. They found that simple grain size criteria, such as percent smaller than 0.02 mm or 0.074 mm did not predict reliable results when compared to in situ observations. The results showed that soils with a small percentage of fines passing 0.074 mm performed well, but for soils with fines the results were unpredictable. They found that the USACE criteria predicted the frost-susceptibility quite well, but the ranges of susceptibility are so wide that they cannot accurately predict field performance and the method could reject many acceptable materials.

**Mineral Properties that Affect Test Results**

Brandl (2008) indicated that the grain size limitations proposed by Cassagrande have been widely used, but the maximum of 3% > 0.02 mm for non-uniform soils is strict and typically uneconomical. He proposed that knowing the mineral types in the soils would better describe the frost susceptibility. He describes the USACE figure that compares percent passing 0.02 mm and frost heave (Figure 1) as having a wide range of scatter that is mostly due to the differences in mineral composition.

Brandl (2008) reported results from studies he conducted in the 1970s. He conducted numerous laboratory tests and reported that the clay mineral type can affect a soil's frost susceptibility. He found that kaolin is more susceptible to frost heave than montmorillonite, because montmorillonite has a lower hydraulic conductivity. He performed tests on sandy gravel with different proportions of clay minerals. In Figure 2, which is taken from his 2008 paper, curve 1 is kaolin and curve 4 is montmorillonite.

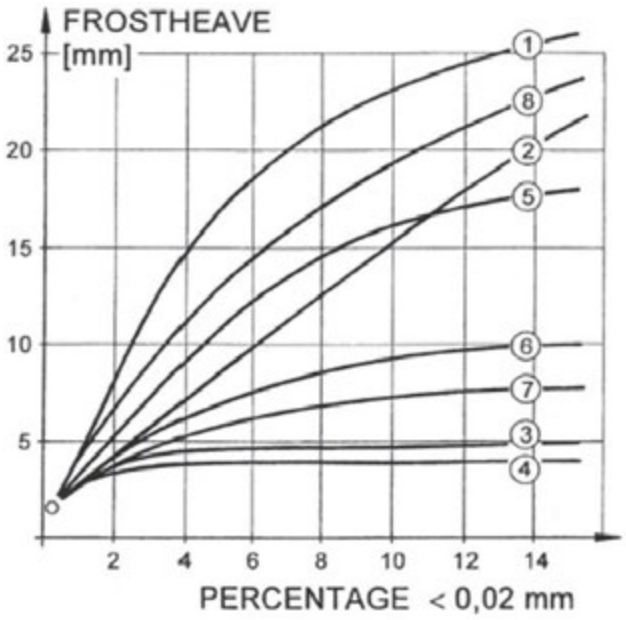


**Figure 2. Frost heave reaction to changes in added clay minerals for a sandy gravel (Brandl 2008)**

Brandl (2008) also found that montmorillonite is more susceptible to thaw weakening than kaolinite (Figure 3).

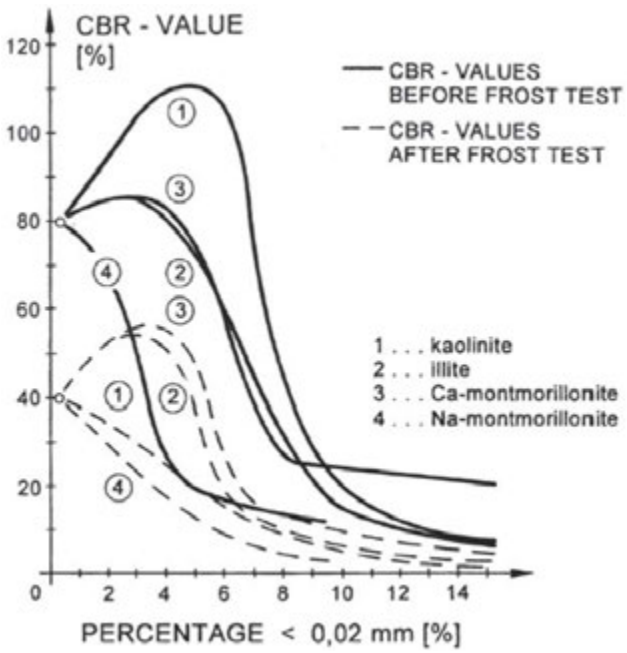


**Figure 3. CBR reaction to changes in added clay minerals for a sandy gravel (Brandl 2008)**

Brandl (2008) also reported that minerals with a neutral reaction (i.e., rock-forming minerals) to frost action are carbonates, quartz, and feldspars with the exception of several laminated silicate groups (i.e., iron hydroxides that result from weathering, kaolinite, chlorite, vermiculite, montmorillonite, and mica). He established frost-susceptibility criteria based on the percentage of mineral type that is finer than 0.02 mm. Certain mineral types should be required to have less passing 0.02 mm. Frost action in base and subbase materials is typically ignored, because they are thought to be non-frost-susceptible (Konrad and Lemieux 2005). However, if these materials have enough fines present, the frost susceptibility can change. It is typically accepted that frost susceptibility increases with increasing fines content, but it is not common to acknowledge the mineral composition of the fines.

## Frost-Heave and Thaw-Weakening Tests

Particle size analysis only represents a portion of the freeze-thaw problem. Chamberlain (1981) found that using grain size criteria was effective for rejecting frost-susceptible material. But this approach can also reject non-frost-susceptible materials, resulting in overly conservative selection criteria. Chamberlain suggested that the degree of frost susceptibility

is related to the rate of heat removal, temperature gradient in the soil, moisture conditions, overburden stress, pore size, freeze-thaw cycling, and soil texture. He concluded that a new procedure for testing freeze-thaw performance, in the laboratory, was needed to account for these properties and proposed the following process:

1. particle size analysis;
2. moisture tension hydraulic conductivity test; and
3. a new frost-heave test with a California bearing ratio (CBR) test performed in the thawed state ( Chamberlain 1981).

Chamberlain (1986) evaluated his proposed three-part procedure by comparing laboratory and field results. He reported that the original CRREL frost-heave test (1965) had several problems: poor temperature control, side friction, a long testing period, no way to test thaw weakening, and only one freeze-thaw cycle. He presented some guidelines for a new freezing test, which Tester and Gaskin (1992) referred to as the CRREL II test. Chamberlain (1986) outlined that test should be simple, repeatable, and reliable; it should correlate with in situ frost heave; it should have a shorter test period; it should cover a wide range of materials; and the equipment should be cheap to manufacture. Chamberlain designed the CRREL II frost-heave and thaw-weakening test that was the basis for the 1996 version of ASTM D5918: Standard Test Methods for Frost Heave and Thaw Weakening Susceptibility of Soils.

The CRREL II test was designed to address top and bottom temperature control, reducing radial heat flow, reducing side friction, providing access to water, allowing for freeze-thaw cycling, and thaw weakening. Chamberlain (1986) achieved these goals by using a multi-ring freezing cell, a membrane liner, circulating liquid temperature plates, a temperature controlled cabinet, a constant surcharge, and a constant head water supply. The 50-100 $W/m^2$ rate of heat removal was chosen to replicate field conditions. A temperature gradient of 0.25°C/cm was proposed as a compromise between field observations and what is possible in a laboratory setting. However, the actual temperature gradient used in ASTM D5918 is 0.4°C/cm during the first 8 hours of freezing and 0.8°C/cm during the last 16 hours, which has drawn criticism as being very high (Henry and Holtz 2003). Typical in situ temperature gradients are around 0.1°C/cm. Svec (1989) also thought the temperature gradient was much

too high and that it is unrepresentative of field conditions. He found that a more typical gradient would be between 0 and 0.15°C/cm.

The temperature gradients in the soil affect the rate and amount of frost heave (Henry and Holtz 2003). Higher temperature gradients result in higher heave rates and greater heave. Svec (1989) explained that a low frost-penetration rate would result in a lower heave rate because the frozen fringe is thicker and a higher frost-penetration rate would result in lower heave rates because the soil freezes so quickly that water cannot be drawn to the freezing front. Whereas a middle ranged frost-penetration rate would result in higher heave rates because of a thinner frozen fringe. Henry and Holtz (2003) are in favor of replicating in situ conditions rather than having a high temperature gradient test that is more of an index test (i.e., CRREL II). Temperature gradients affect the rate of heave, because the temperatures in the soil profile determine how much water is frozen in the soil which controls the hydraulic conductivity in the frozen fringe.

The need for freeze-thaw cycling in the CRREL II test is to allow for physical changes to take place in the sample, which can include changes in density, structure, and permeability (Chamberlain 1986). Freeze-thaw cycling can increase the vertical permeability of thawed soils by 2-10 times (Andersland and Ladanyi 2004). The majority of the changes in permeability take place during the first three cycles.

The surcharge weight used in the CRREL II test was selected to represent loading from a pavement structure (Chamberlain 1986). It was also decided to saturate the sample by soaking, and to allow a constant supply of water at the base of the sample during testing. Finally a CBR test would be performed at the end of the test to determine the thaw weakening. Four samples were tested for each soil. Brandl stated "Freezing-thawing tests inevitably exhibit a scatter of results, in spite of the most careful test performance. (Brandl 2008, p.10)" He recommended that at least three samples be tested for each soil. Kestler (2003) concluded that laboratory frost-heave tests are the most direct method for determining a soil's frost susceptibility, but they are typically not performed on pavement projects due to their expensive and time consuming nature.

Johnson et al. (1986) suggested that the results of the heave rate portion of the freeze-thaw test be implemented into pavement design systems as a roughness factor. It was also

suggested that the results of the CBR after thawing be implemented into pavement designs as an indicator of loss in pavement support capacity.

**ASTM D5918 in the Literature**

This section discusses four seminal works having to do with tests conducted according to ASTM D5918. To create a rating system for frost susceptibility, Chamberlain (1986) compared the results of the CRREL II freeze-thaw test with in situ observations. The in situ measurements were chosen from a six week period during the initial freeze (Chamberlain 1986). The in situ data was from the Winchendon field test site that was observed by the Massachusetts Department of Public Works. Of the 12 soils observed at the Winchendon field test site, 6 were chosen to compare the results of the new CRREL II test to in situ test data. An additional three soils were tested from and observed at the Albany County Airport in New York. The Albany test site consisted of a taxiway that was in service and another that was not. Index test results for the 9 soils tested are provided in Table 2. Frost-heave measurements were taken at regular intervals during winter months. The falling weight deflectometer (FWD) and repeated-load plate-bearing (RPB) tests were performed during peak thawing period.

**Table 2. Material index properties from Chamberlain (1986)**

| Material | Percent finer than 0.074 mm | Percent finer than 0.02 mm | Uniformity coefficient | Liquid limit (%) | Plasticity index (%) | Specific gravity | USCS soil classification | UASCE frost-susceptibility classification |
|---|---|---|---|---|---|---|---|---|
| Dense-graded stone | 9 | 6 | 46.2 | — | NP | 2.82 | GM-GP | VL-H |
| Graves sand | 48 | 16 | 20.8 | — | NP | 2.7 | SM | L-H |
| Hart Brothers sand | 31 | 8 | 9.1 | — | NP | 2.76 | SM | VL-H* |
| Hyannis sand | 31 | 3 | 3.8 | — | NP | 2.67 | SM | N |
| Ikalanian sand | 48 | 8 | 5.2 | — | NP | 2.7 | SM-SP | VL-H* |
| Sibley till | 38 | 24 | 22.5 | 19 | 4 | 2.74 | SM-SC | LV-H |
| Taxiway A base | 15 | 10 | 95.8 | — | NP | 2.72 | SW-SM | N-H |
| Taxiway B subbase | 13 | 8 | 16.3 | — | NP | 2.68 | GW-GM | VL-H |
| Taxiway B subgrade | 16 | 6 | 2.6 | — | NP | 2.69 | SM | N-H |

*Requires CRREL laboratory frost-heave test according to USACE frost susceptibility classification system

Chamberlain (1986) compared the USACE frost-susceptibility criteria to observed frost-heave and thaw-weakening measurements. He observed that the ranges of frost

susceptibilities were too wide to be useful and that there was not a good relationship between the frost-susceptibility ratings and the in situ measurements. A typical frost-heave versus time plot for a granular material and a fine-grained material is provided in Figure 4 and Figure 5, respectively. These results indicate that the granular material heaves more during the first freeze cycle than the second, but the fine-grained sample heaves more during the second freeze cycle.

Chamberlain (1986) attributed the reason for the larger heave in the second freeze cycle, in fine-grained material, to an increase in hydraulic conductivity, which was a result of changing the clay structure. He theorized that the additional freeze-thaw cycles would only change the results significantly in clay soils, because they continue to experience structural changes after the first freeze, as opposed to other soil types where most of the change occurs during the first freeze. Chamberlain (1996) also discussed that more than one freeze-thaw cycle is needed for dirty gravels that may be used as a base or subbase material. He observed they can demonstrate a low susceptibility for frost heave during the first cycle, but the second cycle displays a higher susceptibility to frost heave.

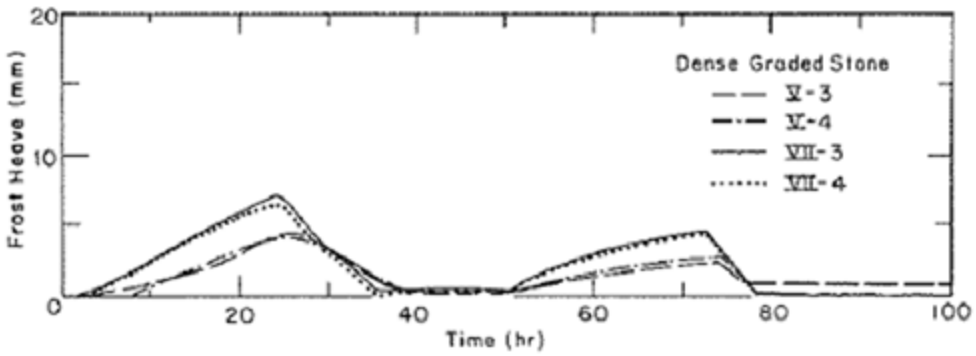


**Figure 4. Frost heave versus time for dense-graded stone (Chamberlain 1986, Fig. 41)**

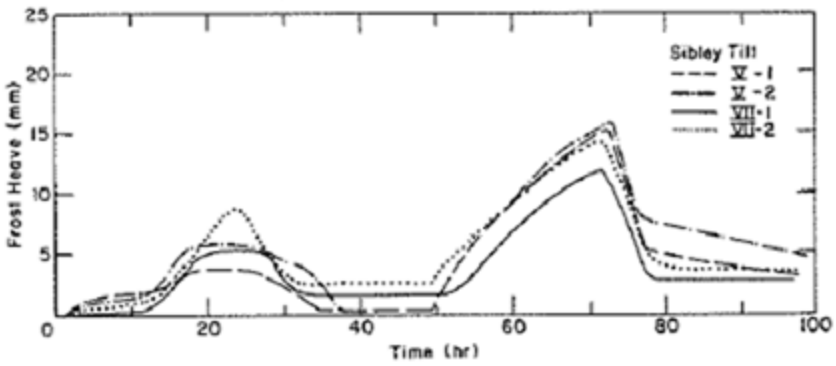


**Figure 5. Frost heave versus time for Sibley till (Chamberlain 1986. Fig. 46)**

The results of the CRREL II frost-heave and thaw-weakening test, performed by Chamberlain (1986), are summarized in Table 3. During laboratory testing, it was found that moisture tension hydraulic conductivity tests did not produce useable results because there was no apparent relationship between the laboratory results and measured in situ heave data.

When the laboratory results were compared with the field test results, a good correlation was observed for the first freezing period. The heave measurements from laboratory tests were higher by as much as ten times when compared to in situ test measurements, but the trends were similar. The test was setup to be an index test rather than a prediction of the amount of heave that would occur in situ. During the second freeze, several samples showed much higher heave rates in the laboratory than in situ. One reason for the laboratory heave rate to be higher than in situ heave measurements may be that the frost depth in situ does not reach the water table so the extent of capillary rise is not preconditioned for water movement, as it is in the laboratory test (Chamberlain 1986).

**Table 3. Summary of results from CRREL II frost-heave and thaw-weakening test (Chamberlain 1986)**

| Material | Moisture content before freezing | Rate of 1st freeze (mm/day) | Heave at 8 hr 2nd freeze (mm/day) | Thaw CBR (%) |
|---|---|---|---|---|
| Dense-graded stone | 5.0 | 3.01 | 3.01 | 6.7 |
| | 5.0 | NF | 4.34 | 10.6 |
| | 5.0 | 5.55 | 5.36 | 10.8 |
| | 5.0 | 5.33 | 5.33 | 11.8 |
| Graves sand | 19.3 | 9.25 | 6.71 | 1.6 |
| | 19.3 | 8.99 | 8.99 | 1.5 |
| | 16.3 | 9.14 | 6.46 | 1.9 |
| | 16.3 | 5.64 | 3.41 | 1.6 |
| Hart Brothers sand | 7.4 | 8.27 | 7.35 | — |
| | 7.4 | 5.72 | 5.14 | 3.8 |
| | 7.4 | 8.23 | 5.55 | 4.3 |
| | 7.4 | NF | 9.14 | 5.9 |
| Hyannis sand | 16.4 | 1.83 | 1.75 | 8.5 |
| | 16.4 | 1.52 | 1.75 | 6.8 |
| | 15.8 | 1.77 | 0.91 | — |
| | 15.8 | 1.52 | 1.16 | 9.0 |
| Ikalanian sand | 11.0 | 6.32 | 5.52 | 2.2 |
| | 11.0 | 8.38 | 7.62 | 3.2 |
| | 11.0 | NF | 5.40 | 1.3 |
| | 11.6 | 3.20 | 4.42 | 1.3 |
| Sibley till | 10.0 | 2.48 | 19.50 | 1.0 |
| | 10.0 | 2.67 | 20.73 | 0.6 |
| | 10.0 | 0.98 | 15.24 | 1.2 |
| | 10.0 | 2.01 | 16.22 | 1.4 |
| Taxiway A base | 7.2 | 3.60 | 11.83 | 13.1 |
| | 7.5 | 4.57 | 12.01 | 12.2 |
| Taxiway B subbase | 13 | 6.10 | 14.87 | 7.7 |
| | 11.4 | 6.46 | 12.01 | 8.6 |
| Taxiway B subgrade | 12.7 | 14.63 | 11.58 | 13.8 |
| | 12.8 | 10.30 | 9.14 | 18.5 |

The relationship between the thawed lab CBR values and the thawed in situ deflection measurements appeared to be nearly linear (Chamberlain 1986). Through the comparison of laboratory and field results, a frost-susceptibility classification was formed based on the average heave rate and the thawed CBR. Chamberlain (1986) reported that the particle size analysis was effective at determining which materials were frost susceptible, but did not determine the extent of frost susceptibility. He also reported that the CBR is a vital part of frost-susceptibility testing. The ASTM D5918 frost-susceptibility classifications that were derived from that study are shown in Table 4. The probable frost group, from the UASCE grain size criteria has also been added to the classifications (Chamberlain et al 1996).

**Table 4. Frost susceptibility classifications based on ASTM D5918**

| Frost susceptibility classification | 8-hr heave rate (mm/day) | Bearing ratio after thaw (%) | Probable frost group (Chamberlain et al 1996) |
|---|---|---|---|
| Negligible | <1 | >20 | NFS, PFS |
| Very low | 1 to 2 | 20 to 15 | S1, PFS |
| Low | 2 to 4 | 15 to 10 | F1,S2, PFS |
| Medium | 4 to 8 | 10 to 5 | F2 |
| High | 8 to 16 | 5 to 2 | F3 |
| Very High | >16 | <2 | F4 |

Tester and Gaskin (1992) performed a fines (i.e., passing 0.074 mm) content study on a crushed limestone material using the CRREL II test. Limestone fines were collected and added to the limestone aggregate to create samples that had non-plastic fines contents of: 2%, 6%, 8%, 10%, and 14%. They found that the first and second heave rates were very similar for the material with varying fines contents. They found that the rate of frost heave increased linearly as the fines content increased, this lead to the conclusion that even a slight increase from the allowable fines content could result in higher susceptibility to heave. The frost heave versus non-plastic fines content plot from their study is provided in Figure 6 which shows that there is an increase in frost-heave rate of about 0.5 mm/day for every 1% increase in fines content. The resulting frost-susceptibility classifications for the varying fines contents are provided in Table 5. Tester and Gaskin (1992) recommended that the maximum fines content be set at 8% to keep the frost-susceptibility classification at a low rating. They found that there was some variation in the CBR results, but overall the fines content did not affect the CBR value of the crushed limestone in a thawed state.

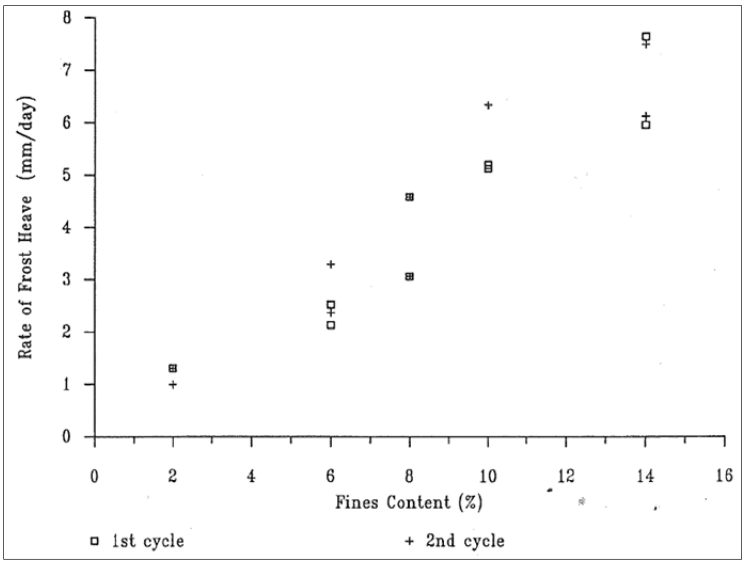


**Figure 6. Heave rates for a crushed limestone with non-plastic fines based on an 8 hour freezing period (Tester and Gaskin 1992, Fig. 6)**

**Table 5. Frost-susceptibility classification of crushed limestone with varying non-plastic fines content (Tester and Gaskin1992)**

| % Fines | Frost-heave classification | Unfrozen CBR (%) | Thawed CBR (%) |
|---|---|---|---|
| 2 | Very low | 24 | 19, 19 |
| 6 | Low | 13 | 23, 12 |
| 8 | Low | 20 | 19,14 |
| 10 | Medium | 20 | 20,14 |
| 14 | Medium | 19 | 26,16 |

Tester and Gaskin (1992) repeated the tests by adding 2%, 8%, and 14% of three plastic fines—kaolinite, illite/chlorite, and bentonite— to the limestone material. The frost heave versus plastic fines content is provided in Figure 7. The resulting frost-heave susceptibility classifications are provided in Table 6 and thaw-weakening classifications in Table 7. The kaolinite fines produced the highest frost-heave rate. This supports Brandl's (2008) conclusions. Tester and Gaskin (1992) concluded that kaolin fines should be limited to a maximum of 5%, whereas illite/chlorite and bentonite fines can be acceptable up to 14%. The test only subjects the material to freezing conditions, so it is mentioned that additional tests are required to test the effects of applying multiple loads to the materials, in order to simulate pavement conditions and determine if pumping of the fines will be a problem.

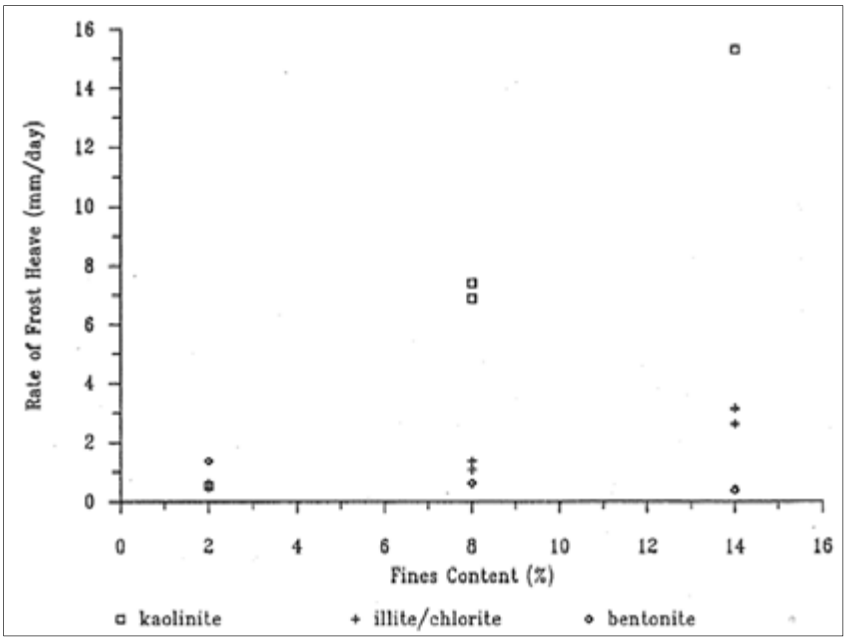


**Figure 7. Heave rates for a crushed limestone with plastic fines based on an 8 hour freezing period (Tester and Gaskin 1992, Fig. 7).**

**Table 6. Frost-heave susceptibility classification of crushed limestone with varying plastic fines content (Tester and Gaskin1992)**

| % Fines | Kaolinite | Illite/chlorite | Bentonite |
|---|---|---|---|
| 2 | Negligible | Negligible | Very low |
| 8 | Medium | Very low | Negligible |
| 14 | High-very high | Low | Negligible |

**Table 7. Thaw-weakening susceptibility classification of crushed limestone with varying plastic fines content (Tester and Gaskin 1992)**

| % Fines | Kaolinite | Illite/chlorite | Bentonite |
|---|---|---|---|
| 2 | 17, 10 | 16, 15 | 10, 10 |
| 8 | 13, 13 | 12, 11 | 12, 12 |
| 14 | 13, 12 | 7, 7 | 14, 14 |

Bigl and Berg (1996) performed the CRREL II test on pavement materials collected from MnRoad research testing facility located in Albertville, Minnesota. The purpose of the tests was to determine the materials behavior when exposed to frost action and to provide input parameters for modeling the materials using CRREL's Mechanistic Pavement Design and Evaluation Procedure. The materials tested included four samples of clay subgrade and two base materials. They also presented a dense-graded stone material that has previously been presented by Chamberlain (1986) and will not be mentioned here. The material index

properties are provided in Table 8 and the results of the CRREL II frost-heave and thaw-weakening test are provided in Table 9.

**Table 8. Material index properties from Mn/ROAD (Bigl and Berg 1996)**

| Material | ASTM classification | AASHTO classification | Specific gravity | Liquid limit (%) | Plasticity index (%) | % Passing 0.074 mm |
|---|---|---|---|---|---|---|
| **Subgrade** | | | | | | |
| 1171 (563) | SC | A-6 | 2.70 | 30.6 | 10.6 | 50 |
| 1193 (564) | CL | A-6 | 2.70 | 31.2 | 14.3 | 68 |
| 1206 (565) | CL | A-6 | 2.70 | 37.0 | 18.5 | 65 |
| 1232 (566) | CL | A-6 | 2.71 | 26.4 | 10.9 | 51 |
| **Base** | | | | | | |
| Blended Stone | GW | A-1-a with sand | 2.79 | 2.74 | — | 4 |

**Table 9. Summary of results from CRREL II frost-heave and thaw-weakening test (Bigl and Berg 1996)**

| Material | 1st Freeze | | 2nd Freeze | | Thawed CBR test | |
|---|---|---|---|---|---|---|
| | Heave rate (mm/day) | Rating | Heave rate (mm/day) | Rating | CBR (%) | Rating |
| **Subgrade** | | | | | | |
| 1171 (563) | 1 | Very low | 7.5 | Medium | 2 | Medium |
| 1193 (564) | 9.3 | High | 22.5 | Very high | <1 | Very high |
| 1206 (565) | 9.3 | High | 16 | High | <1 | Very high |
| 1232 (566) | 1 | Very low | 7.5 | Medium | 2 | Medium |
| **Base** | | | | | | |
| Blended Stone | <1 | Negligible | <1 | Negligible | Negligible | Negligible |

Janoo et al. (1997) conducted the CRREL II test on a granular subbase material used under a pavement at the Raymark Superfund site in Stratford, Connecticut. The subbase material had approximately 20% of material finer than 0.074 mm and approximately 14% of

material finer than 0.02 mm. The frost-heave test was performed on the material in saturated (Samples 1–4) and unsaturated (Samples 5–8) conditions. The frost heave versus time plots for the saturated material is provided in Figure 8, and for the unsaturated material in Figure 10. The moisture content profile for the saturated material is provided in Figure 9, and the profile for the unsaturated material is shown in Figure 11. The saturated condition was thought to represent the foundation conditions after cracking had occurred (i.e., later in the life of the pavement), while the unsaturated condition was meant to represent the pavement at the beginning of the pavement life. The results and classifications of the tests are shown in Table 10.

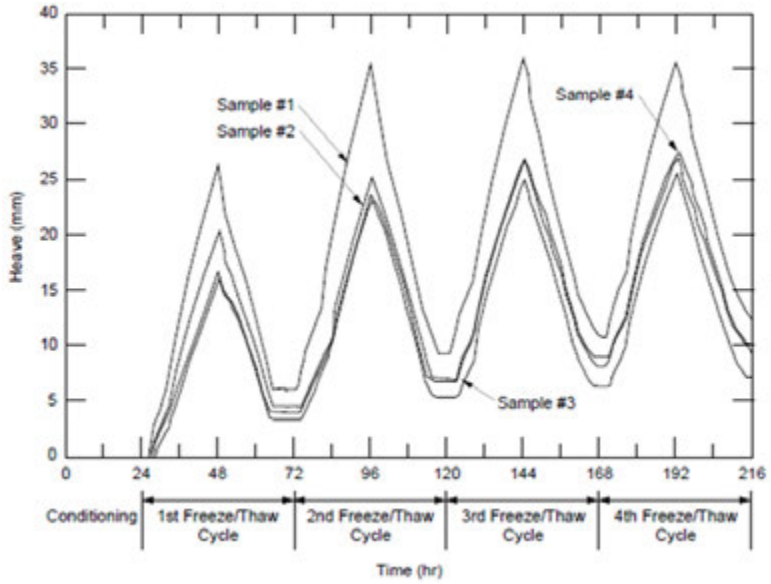


**Figure 8. Frost-susceptibility testing for saturated soil samples (Janoo et al. 1997, Fig. 3)**

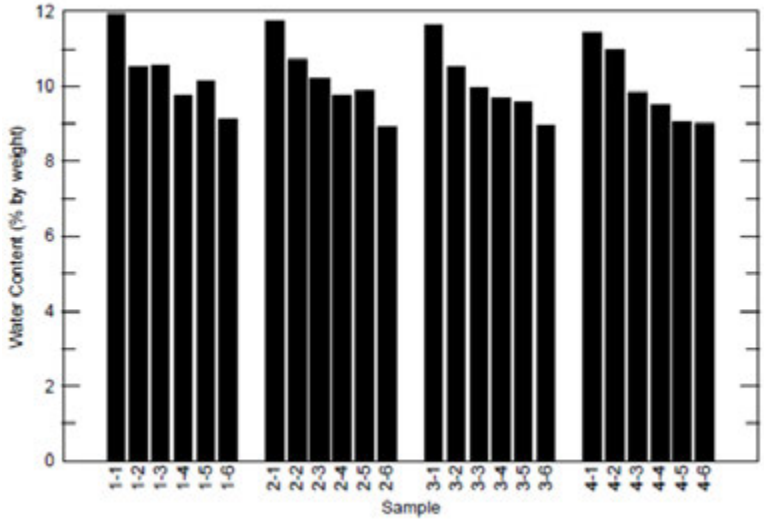


**Figure 9. Sample moisture profile for saturated samples (Janoo et al. 1997, Fig. 4)**

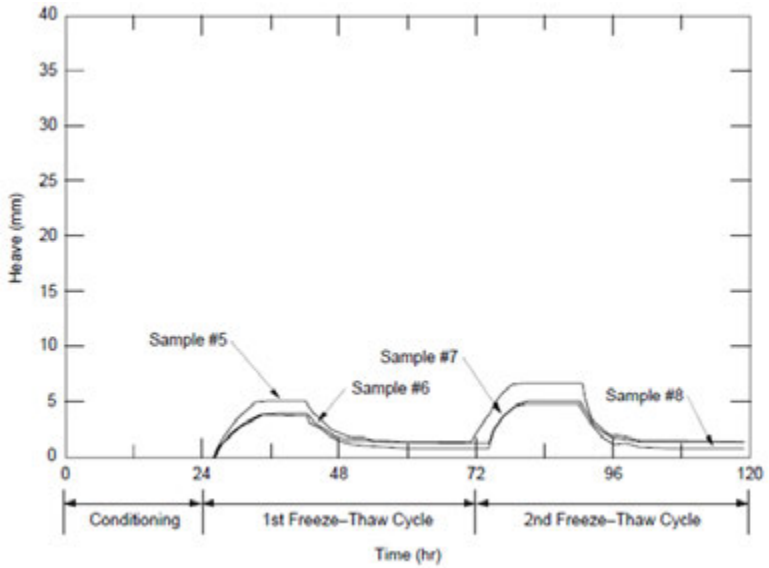


**Figure 10. Frost-susceptibility testing for unsaturated soil samples (Janoo et al. 1997, Fig. 5)**

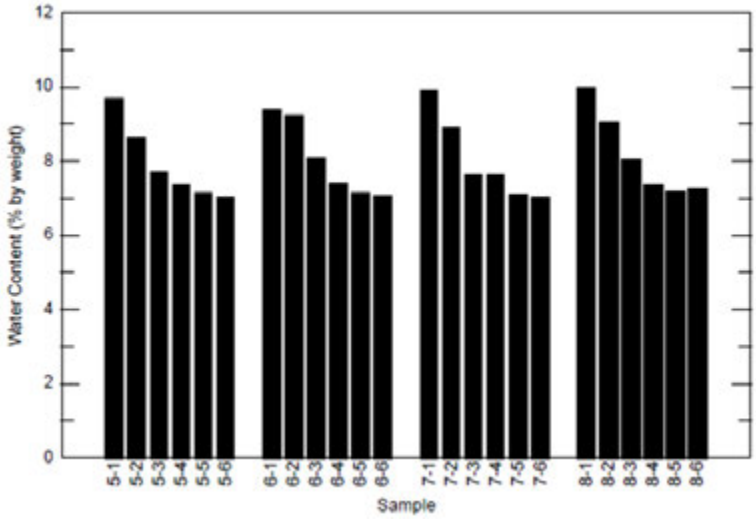


**Figure 11. Sample moisture profile for unsaturated samples (Janoo et al. 1997, Fig. 6)**

**Table 10. Summary of frost-heave and thaw-weakening test results (Janoo et al. 1997)**

| Sample | Pretest moisture (%) | Heave rate (mm/day) | Classification | Pretest CBR (%) | Post-test CBR (%) | UASCE Frost-susceptibility classification |
|---|---|---|---|---|---|---|
| 1 | 7.66 | 20.2 | Very high | 45 | 4 | F2 |
| 2 | 7.56 | 15.4 | High | 40 | 3 | F2 |
| 3 | 7.11 | 15.0 | High | 43 | 3 | F2 |
| 4 | 7.72 | 14.9 | High | 35 | 4 | F2 |
| 5 | 8.35 | 6 | Low | 44 | 10 | F2 |
| 6 | 8.25 | 4 | Medium | 45 | 9 | F2 |
| 7 | 8.36 | 4 | Medium | 34 | 8 | F2 |
| 8 | 8.77 | 4 | Medium | 39 | 9 | F2 |

## Chemical Stabilization Techniques

Chemical stabilizers that are typically considered effective in resisting frost action are lime, fly ash, cement, or some combination of these (Joint Departments of the Army and Air Force 1985). Stabilized geomaterials can provide a durable and stable foundation for pavement systems that are exposed to frost action. However, stabilized materials should be thoroughly tested to ensure they are durable and can withstand repeated freeze-thaw cycles. It should also be verified that the addition of a stabilizer does not increase the frost

susceptibility of the material. The frost susceptibility can potentially increase when soil modification (i.e., the soil properties are improved rather than significantly strengthened) is applied, which can result in a soil structure that is conducive for ice lens creation and increased capillary action. A soil, in frost affected areas, is only considered to be stabilized if it meets durability and strength requirements; otherwise it is considered to be a modified soil (Joint Departments of the Army and Air Force 1985). Modified soils require additional attention, compared to stabilized soils to verify that the properties will not deteriorate as they are exposed to multiple freeze-thaw cycles (Joint Departments of the Army and Air Force 1985).

The durability of stabilized soils is important for determining if the stabilized soil is capable of enduring harsh environments while remaining stable and effective (Shihata and Baghdadi 2001). There is very little document guidance on the durability aspects of stabilized soils in frost areas. The durability of stabilized materials is typically determined by measuring material loss as a result of freeze-thaw cycling and brushing. The unconfined compressive strength after freeze-thaw cycling or vacuum saturation can also be an indicator of stabilized soil durability.

Brushing samples, as in ASTM D560, can create a large source of error between laboratory technicians (Shihata and Baghdadi 2001), because it is so dependent on how much pressure is applied and how it is applied. The USACE omits the brushing portion of ASTM D560 in order to remove the inconsistency associated with that portion of the test (Joint Departments of the Army and Air Force 1994). ASTM D560 is not widely used to test stabilizers other than cement, because the standard does not address the problem of frost heave and strength loss that results from freeze-thaw cycling (Chamberlain et al. 1996). The Portland Cement Association (PCA) provides guidelines on maximum allowable percent mass loss after freeze-thaw cycling for cement stabilized soils as summarized in Table 11. Similarly, the USACE provides guidelines on maximum allowable percent mass loss (Table 12), and the minimum compressive strength guidelines (Table 13). ASTM D560 does not include acceptable weight loss percentages. Hausmann (1990) found from a review of the literature that the compressive strength typically increases linearly with increases in cement content.

**Table 11. PCA durability criteria for cement stabilized materials (Portland Cement Association 1992)**

| AASHTO soil group | Maximum allowable mass loss (%) |
|---|---|
| A-1, A-2-4, A-2-5, and A-3 | <14 |
| A-2-6, A-2-7, A-4, and A-5 | <10 |
| A-6 and A-7 | <7 |

**Table 12. USACE durability requirements for cement, lime, lime-cement, and lime-cement-fly ash stabilized materials (Joint Departments of the Army and Air Force 1994)**

| Type of soil stabilized | Maximum allowable weight loss after 12 wet-dry or freeze-thaw cycles percent of initial specimen weight |
|---|---|
| Granular, PI < 10 | 11 |
| Granular, PI > 10 | 8 |
| Silt | 8 |
| Clays | 6 |

**Table 13. USACE minimum unconfined compressive strength for cement, lime, lime-cement, and lime-cement-fly ash stabilized soils (Joint Departments of the Army and Air Force 1994)**

| Stabilized soil layer | Minimum unconfined compressive strength (psi)[a] | |
|---|---|---|
| | Flexible pavement | Rigid pavement |
| Base course | 750 | 500 |
| Subbase course, select material, subgrade | 250 | 250 |

[a]Unconfined compressive strength determined at 7 days for cement stabilization and 28 days for lime, lime fly ash, or lime-cement-fly ash stabilization.

Dempsey and Thompson (1973) performed a study to determine if vacuum saturation could be used as an indication of freeze-thaw durability. The unconfined compressive strength and moisture content, after vacuum saturation, was used as an indicator of durability. It had been previously determined that the unconfined compressive strength correlated well with the durability of stabilized materials. They performed unconfined compression tests and moisture content tests on samples that had been vacuum saturated or had been through 5 to 10 freeze-thaw cycles. They performed a linear regression analysis on the results of the

compressive strength after freeze-thaw cycling and vacuum saturation. The results showed strong correlations between compressive strength measurements obtained after 10 freeze-thaw cycles and compressive strength measurements after vacuum saturation (Figure 12). They also found from linear regression analysis that the moisture contents after freeze-thaw cycling are strongly related to moisture contents after vacuum saturation (Figure 13). The vacuum saturation method was found to provide a much quicker method of determining the durability of stabilized materials, compared to freeze-thaw cycling.

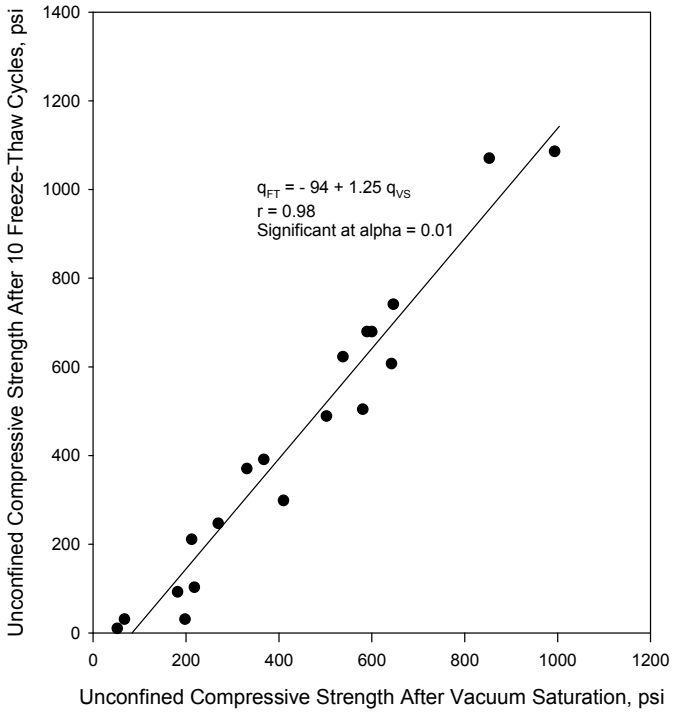


**Figure 12. Relationship between unconfined compressive strength after 10 freeze-thaw cycles and after vacuum saturation (Dempsey and Thompson 1973)**

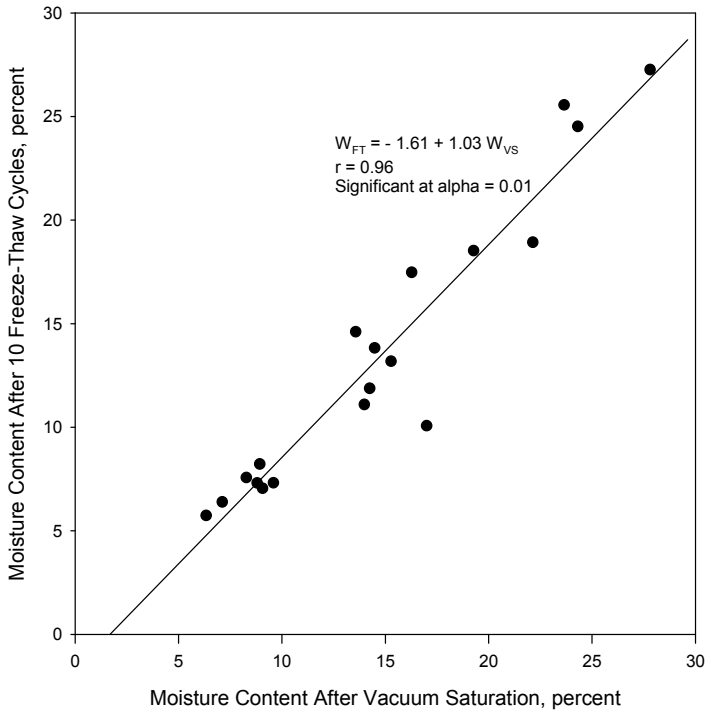


**Figure 13. Relationship between moisture content after 10 freeze-thaw cycles and after vacuum saturation (Dempsey and Thompson 1973)**

The PCA Soil-Cement Laboratory Handbook recommends that 2-in. x 2-in. samples be used, when all soil particles pass 4.76 mm (Portland Cement Association 1992). The Iowa State compaction apparatus is one method that can be used to make 2-in. x 2-in. samples (O'Flaherty et al. 1963). The PCA Soil-Cement Laboratory Handbook also mentioned that the size of the stabilized samples is not that important, because the goal of the testing is not to determine a design compressive strength but to determine how the stabilizer and soil react.

Shihata and Baghdadi (2001) performed freeze-thaw durability tests, according to ASTM D560, to determine if the unconfined compressive strength could be used as an indicator of freeze-thaw durability. They made one set of samples that were brushed during freeze-thaw cycling, as specified in ASTM D560 for durability classification, and another set of samples that were not brushed for unconfined compression testing. All samples were allowed to cure for seven days at 21°C and 100% humidity. They concluded that the unconfined compressive strength measurements after freeze-thaw cycling can be used as an indicator of durability, because there was a good correlation between the two parameters (Figure 14). They also found that the compressive strength after freeze-thaw cycling showed correlations with the

seven day compressive strength, which could allow for an even more simplified method of determining durability. They recommended that the unconfined compressive strength testing is better than the percent loss testing as brushing leads to inconsistent results with different operators.

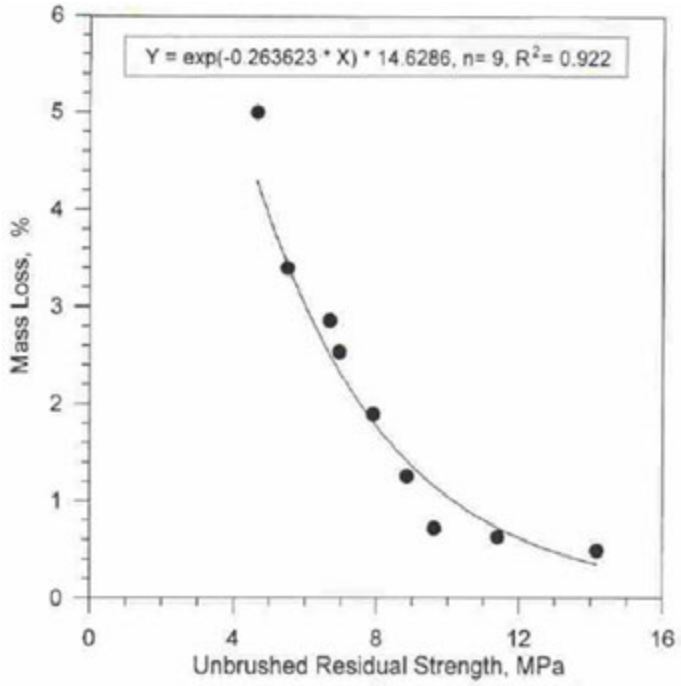


**Figure 14. Relationship between unconfined compressive strength after 12 freeze-thaw cycles and after 7-day curing (Shihata and Baghdadi 2001)**

Guthrie et al. (2007) performed frost-heave tests on a silty subgrade sample stabilized with 0, 2, 3.5, and 5 % cement. The soil had a USCS classification of ML and a USACE frost group classification of F-4. The frost-heave test setup was different from that used in ASTM D5918. They found that a cement content of 3.5% and 5% completely prevent frost heave, but a cement content of 2% resulted in more heaving than the 0%. This supports the recommendations of the Joint Departments of the Army and Air Force (1985) that tests should be performed to verify that the specified stabilizer content is not increasing the frost-heave susceptibility of the soil. They found that the material with 2% cement had considerably higher moisture contents than the other tests and resulted in more capillary action prompting higher amounts of frost heave. Guthrie et al. (2007) mentioned that there are two extremes to the amount of cement added to a soil. If the cement content is too low,

the frost heave can be higher and if the cement content is too high, significant shrinking can occur. One significant conclusion from Guthrie et al. (2007) was that the cement content to be added to a soil must be justified based on detailed laboratory test results.

## IN SITU SEASONAL PAVEMENT TESTING

The follow sections outline the effects of and in situ measurements of frost action in pavements.

### Frost Action in Pavements

When pavement structures are exposed to frost heaving and thaw weakening, the mechanical properties can be significantly affected by the seasonal changes in temperature and soil moisture conditions (Simonsen and Isacsson 1999). The stiffness of supporting layers typically increases when frozen, due to the soil particles being frozen together in the base and subbase materials and ice lens formation in the subgrade materials. This results in an increase in foundation layer bearing capacity. The damage caused by freezing in asphalt cement (AC) layers is due to differential frost heave and thermal cracks. Salour and Erlingsson (2012) found that among pavements that are subjected to frost action, spring thaw is responsible for the highest amount of deterioration in AC pavements.

Andersland and Ladanyi (2004) mentioned that snow on roadway shoulders can insulate the underlying material and cause problems during freezing. The problem can occur if the material under the center of the roadway begins to freeze, but the snow insulates the material under the shoulders enough to prevent freezing. This causes a temperature differential between the shoulder and center of the roadway, which can result in an increased supply of water and differential frost heave to occur between the two locations. Ultimately, the result is longitudinal cracking in the center of the roadway, as illustrated by Nordal and Refsdal (1989 in Andersland and Ladanyi 2004) (Figure 15).

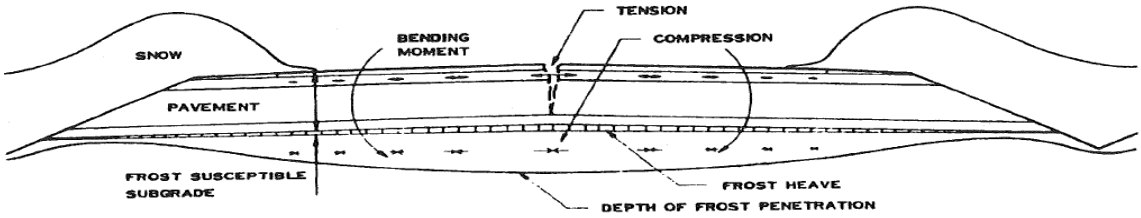


**Figure 15. Longitudinal frost cracks due to thermal shielding of road edges by snow (Andersland and Ladanyi 2004, 302)**

Once pavement begins to thaw in the spring, bearing capacity can be drastically reduced (Simonsen and Isacsson 1999). The loss in bearing capacity is due to the supporting layers becoming saturated. Simonsen and Isacsson (1999) found that drainage in pavement systems is very important in general, but it is even more important in cold regions. An increase in moisture content, due to ice thawing, in the foundation layers can cause high pore water pressures to develop which will lead to a reduction in the effective stress. This results in a reduction in shear stress and bearing capacity. Salour and Erlingsson (2012) found that water saturation and excess pore water can cause reduction in internal frictional forces between aggregate materials. Additional water can be a result of the melting ice being trapped between the pavement material and the remaining frozen layers below (Simonsen and Isacsson 1999). They found that less severe winters produce conditions for larger amounts of heave for a given depth of frost. The slow frost penetration rates can result in more ice lenses being formed. The slow frost penetration leads to the majority of the ice accumulating near the surface of the pavement foundation layers. Once the ice begins to melt, there is a rapid release of water that can create detrimental support conditions. Severe winters result in deeper frost penetration, which results in the main concentration of ice being deeper in the pavement foundation. Even though there may be more ice present, the effect of the melting ice on the pavement is less rapid and is spread out over a longer period of time. If there is good drainage in the pavement system, the effects of the additional water on the pavement will be reduced. The ability of the system to drain is related to the fines content of the materials.

Thawing typically progresses from the pavement surface down, resulting in a condition where melted water can become trapped between the pavement surface and the frozen layers below. In this condition, where thawing is rapid, the drainage path is constrained in the

vertical direction so transverse drainage paths must be available. If the edge of the pavement surface is covered in snow during thawing, the snow can insulate the ground below it and the soil will remain frozen. When this occurs, the transverse drainage direction is cutoff. If the thawing takes place much slower, the thawing front will work its way from the lower layers up and the water will be allowed to drain. The thaw depth affects the amount of settlement that will take place and the rate of thawing affects the magnitude of change in pore water pressure. The amount of settlement that takes place depends on ice lens formation, soil density, pore water pressures, and soil compressibility.

Simonsen and Isacsson (1999) found that the following factors can impact the amount of thaw-weakening damage on pavement systems: road structure, frost susceptibility, subgrade conditions, temperature, precipitation, and traffic. They found that the length of recovery from thaw weakening is dependent on the frost depth, soil type, water content, and drainage conditions. It can take weeks to months to fully recover, depending on the drainage conditions. Load restrictions can be used to reduce pavement damage during periods of thaw weakening (Andersland and Ladanyi 2004). However, load restrictions are mostly used on flexible pavements, because most rigid pavements were determined to be able to resist the loss of strength during thawing.

Simonsen and Isacsson (1999) described that when pavement foundation layers are deformed under traffic loads, most of the deflection rebounds once the load has been removed. The remaining deformation that does not rebound is called permanent deformation and occurs when there is excess water present. The spring thawing condition presents the ideal opportunity for permanent deformation to occur. When the base materials are saturated, the vehicle load is initially placed on the pore water. When the pore water is loaded it makes the base material unstable and can cause upward stress that can cause cracks in the pavement system. After this process occurs many times, it can cause holes in the pavement layer and a loss of base material; this is especially true for AC pavements. Salour and Erlingsson (2012) found that when the base course is saturated, there can be a pumping of fines in the base course which eventually leads to a weaker and less drainable material than what was initially designed.

Another type of failure can occur when the subgrade is frost susceptible and has been frozen (Simonsen and Isacsson 1999). Once, the subgrade begins to thaw and the pore water pressures increase due to the additional water, the subgrade is displaced and is unable to sustain the loads that are applied from the upper pavement layers. When the subgrade is displaced, a loss of support for the pavement layer occurs which can cause deformations in the pavement. Salour and Erlingsson (2012) found that the relative damage caused during thaw weakening, due to traffic loads, is 1.5 to 3 times higher than the average annual damage on AC pavements.

## In Situ Measurements of Frost Action in Pavements

Some in situ studies examine frost heave while others focus on thaw weakening.

### Frost Heave

In a study at MnRoad (Lukanen et al. 2006), frost pins were placed in sections of AC and Portland cement concrete (PCC). The AC sections had sand, clay, and granular base as foundation materials. The PCC sections had a granular base with either sand or clay underneath. The frost pins were placed at 15 m intervals in the five 152 m test sections. The frost pins were observed over a period of four years. The results revealed that the heave across each of the sections was not even. This differential heave affects pavement ride and performance. Differential heave can greatly increase pavement roughness and occurs when material types or properties change (e.g., a change from cut to fill or an area with increased moisture content) (Joint Departments of the Army and Air Force 1985).

Many states require a 1–1.5 m subcut into the subgrade, which consists of removing the subgrade material and recompacting it in place, a process that helps create a uniform subgrade that will reduce differential heave. The test sections at MnRoad were undercut 5 m and still showed signs of differential heave. The sections with clay subgrade in the pavement structure, showed the highest amount of frost heave. Also the AC on clay sections showed an increase in the International Roughness Index (IRI) as the subgrade heaved. The AC on sand sections showed smaller increases in IRI because the subgrade had small amounts of heave. Although the PCC section with a clay subgrade heaved significantly, the PCC sections showed no increases in IRI. Lukanen et al. (2006) reported that ride quality is minimally related to differential frost heave in the subgrade and many other factors can affect the IRI in

addition to frost heave. They concluded that current empirical design and mechanistic empirical design processes do not account for differential frost-heave movements.

**Thaw Weakening**

Increased moisture content in supporting layers during thawing weakens pavement structures (Janoo and Berg 1996). This additional water in the pavement structure reduces the bearing capacity because of the reduced strength of the supporting layers. The strength of AC pavements is largely dependent on the temperature, this results in large variations in strength during the high temperature swings that occur during freezing and thawing periods. PCC can also be negatively affected during thawing periods because of curling effects that are caused by high temperature differentials in the pavement layer. The curling can occur at the edges and corners of the pavement which will affect the load transfer efficiency. Janoo and Berg (1996) conducted a study of the effects of thaw weakening on PCC for airfields. They conducted falling weight deflectometer (FWD) tests and measured temperatures in the pavement structure. Frost depths were determined based on where the temperature was 0°C. An example of their frost depth versus time can be seen in Figure 16.

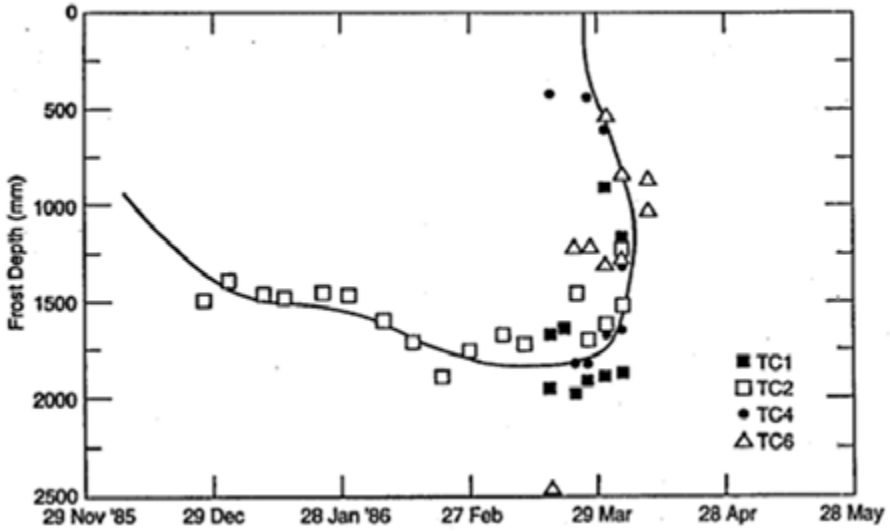


**Figure 16. Frost penetration plot (Janoo and Berg 1996)**

Janoo and Berg (1996) used the basin area FWD index to analyze the effects of thaw weakening. Equation (1) shows the calculation of the basin area FWD index from seven deflection sensors.

$$\frac{1}{2}\sum_{i=0}^{6}\left[(\delta_i+\delta_{i+1})(r_{i+1}-r_i)\right] \quad (1)$$

where $\delta_i$ = the deflection at sensor i and

$r_i$ = the distance of sensor i from the center of the loading plate

An example of the data can be seen in Figure 17, which displaces the results of the indices for several test locations. The higher the basin area measurement is, the lower the strength of the pavement structure. They measure joint transfer efficiency (JTE) which is a measure of how well load is distributed from one PCC slab to the next. They found that the JTE typically decreased as the temperature increased as the beginning of the spring thaw. However, as thawing progressed, the JTE began to increase (Figure 18). They found from a review of the literature that the JTE was not affected by the load applied during the FWD test.

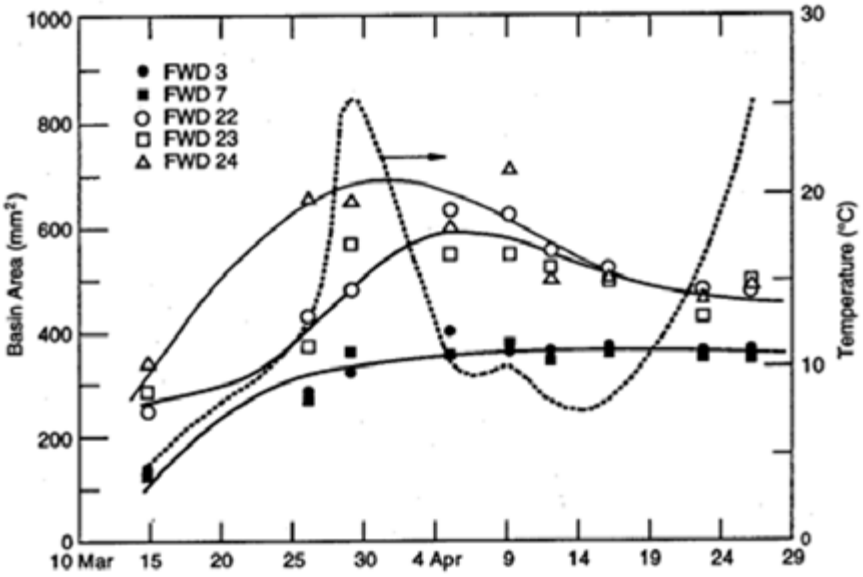


**Figure 17. Change in basin area during spring thaw (Janoo and Berg 1996)**

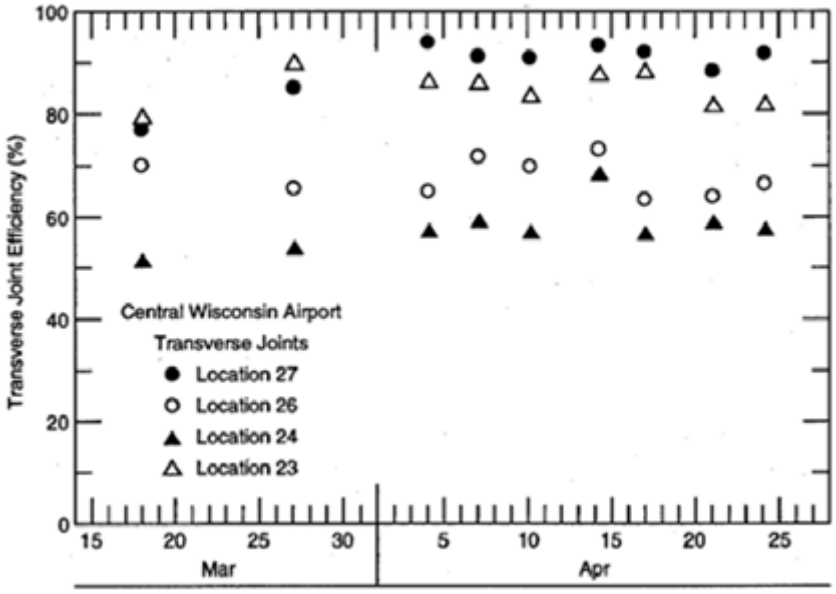


**Figure 18. Joint transfer efficiency during spring thaw (Janoo and Berg 1996)**

Drumm and Meier (2003) compiled seasonal test data from sites across North America. The research was conducted as a part of the Long Term Pavement Performance (LTPP) Seasonal Monitoring Program (SMP). They collected data from temperature sensors, moisture sensors, and FWD tests. They discussed that the temperature in PCC does not affect the performance as much as the gradient in the PCC slab. Curling of the slabs can result of the temperature gradient. Upward curling will occur when the temperature is cooler on the top compared to the bottom (i.e., at night) and downward curling can occur when the temperature on the top is warmer than the bottom (i.e., during day). When the temperature in the slab is colder, the joints open which can result in reduced load transfer efficiencies. Reductions in load transfer efficiencies can also be caused by curling. FWD testing can be performed at the edge of slabs to observe daily and seasonal changes in load transfer efficiency due to curling and opening of joints. FWD deflections, from increasing loads, from the slab edges and the center of slab can be compared. If the deflections have a near linear relationship between the drop height and response, it is an indication that the slab is in good contact with the underlying layers. Any deviations from linear can indicate curling.

Drumm and Meier (2003) mentioned that it is a typical misunderstanding that granular base material do not undergo thaw weakening. This is a result of a strong base material requiring a significant amount of fines, which as discussed can decrease the permeability and

increase the frost-heave potential. They found, from several sources, that there is no relationship between amount of rainfall and subgrade moisture content variation. Joint faulting in PCC, can be a result of pumping (i.e., loss of material), frost heave, or expansive subgrade soils.

Drumm and Meier stated that, "even under the best of circumstances, FWD backcalculation is as much an art as it is a science" (2003, p. 4-5). Spring thaw and recovery moduli are difficult to backcalculate, because of the pavement structure not being adequately modeled by the elastic layer theory that was used. It is difficult for the theory to represent a soft saturated layer trapped between a much stiffer base material and the frost subgrade that lies below. It was recommended that advanced modeling would be required to represent this situation. The backcalculated moduli during frozen periods are typically too high and inconsistent. They found that it was difficult to determine when slab curling was affecting the results and when it was not. It was recommended that deflection basins be used rather than backcalculated moduli to determine the effects of frost action on the pavement system.

Drumm and Meier (2003) found that the following indices were used at Mn/ROAD to determine spring thaw conditions: SCI, BDI, and $D_0$. The definitions of the FWD indices are shown in Table 14. The indices are expected to decrease during the frozen period (Figure 19). A stress level of 550 kPa was used in the study, because it corresponds to a stress level that is typically used in pavement design. They recommended, from FWD results on AC pavements, that the following FWD indices be used to observe the effect of frost action: BCI, SDI, SI, and PA. With the data available, they were not able to detect a significant thaw-weakening period. They hypothesized that it was a result of one or a combination of the following factors: thaw weakening occurred between their site visits, the subgrade soils were not frost susceptible, or the pavements were designed to minimize the effects of thaw weakening. The LTPP SMP sites were only visited once a month. Drumm and Meier analyzed FWD results on AC pavements from the U.S. Army Frost Effects Research Facility and other locations that were collected on a daily basis during thawing. They found that the effects of thawing could be seen from the SI and SDI indices.

**Table 14. FWD indices (Drumm and Meier 2003)**

| Parameter | Formula |
|---|---|
| AREA | $6 * [(D_0/D_0) + (2*D_{305}/D_0) + (2*D_{610}/D_0) + (D_{914}/D_0)]$ |
| Deflection at load plate ($D_0$) | $D_0$ |
| Deflection at 1524 mm ($D_{1524}$) | $D_{1524}$ |
| Base curvature index (BCI) | $D_{610} - D_{914}$ |
| Surface curvature index (SCI) | $D_0 - D_{305}$ |
| Basin damage index (BDI) | $D_{305} - D_{610}$ |
| Partial area (PA), $m^2$ | $[(D_{457}+D_{610})/2*0.153] + [(D_{610}+D_{914})/2*0.304] + [(D_{914}+D_{1524})/2*0.610]$ |
| Subgrade damage index (SDI) | $D_{610} - D_{1524}$ |
| Subsurface index (SI) | $D_{305} - D_{1524}$ |

$D_x$ is the surface deflection measured x mm from the loading plate.

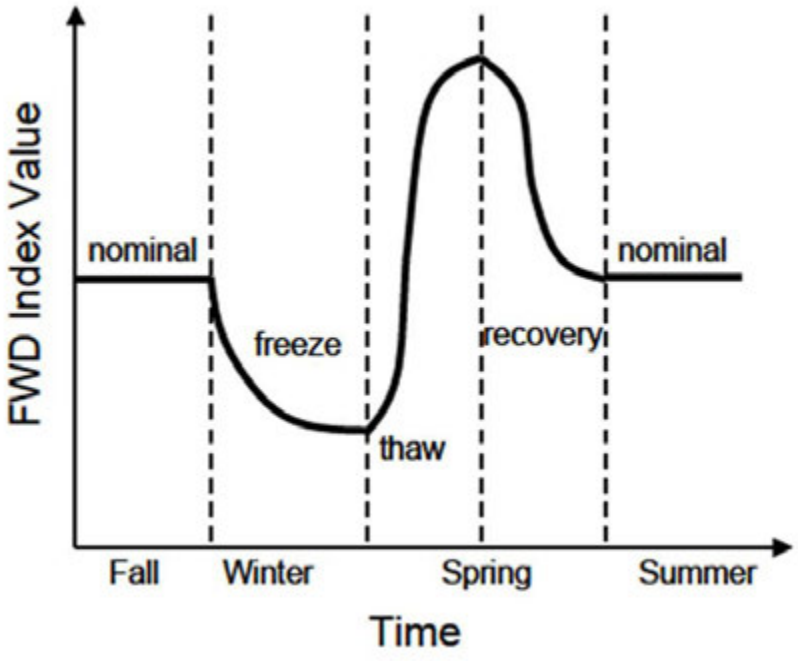


**Figure 19. Expected seasonal variation of FWD indices (Drumm and Meier 2003)**

Salour and Erlingsson (2012) recommended, based on a literature review, that the following FWD indices be used to determine the effects of frost action on pavement systems: $D_0$, SCI, BCI, BDI and a subgrade strength index (SSI) be used to determine the effects of spring thaw on pavements. The SSI is determined by dividing $D_{900}$ during thaw by the $D_{900}$ after recovery. Salour and Erlingsson (2012) studied the structural performance of a flexible

pavement in Sweden. The use of the FWD indices can be seen in (Figure 20). Just as Drumm and Meier (2003) found, the FWD indices values reduce when frozen and increase during thawing.

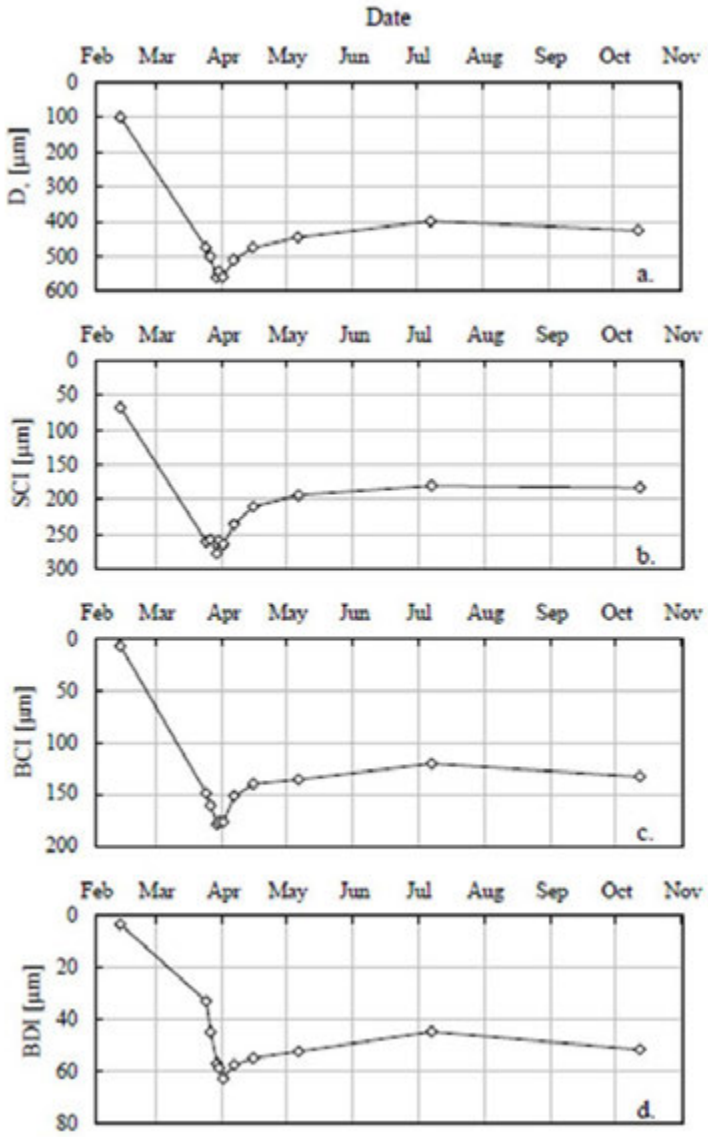


**Figure 20. Seasonal variation of $D_0$, SCI, BCI, and BDI (Salour and Erlingsson 2012, Fig. 13)**

Jong et al. (1998) performed a study to develop a method for determining when load restrictions should be implemented. The data collected measured air and subsurface temperatures, subsurface water contents, water phase changes, and pavement moduli. Thermocouples and thermistors were used to measure temperature, time domain

reflectometry probes were used to determine water contents and phase changes, and FWD tests were used to determine the pavement moduli. Flexible pavements (i.e., AC pavements) were tested over an 18 month period on three secondary highways. They found that the thermocouples, thermistors, and time domain reflectometry probes all resulted in approximately the same frost depth profiles (Figure 21). They presented the structural capacity of the pavement in the form of FWD deflection basins and backcalculated FWD moduli. An example of the FWD deflection basin can be seen in Figure 22. The basins show that the deflection is very low during winter and very high during spring, with the deflections for the summer period falling in between.

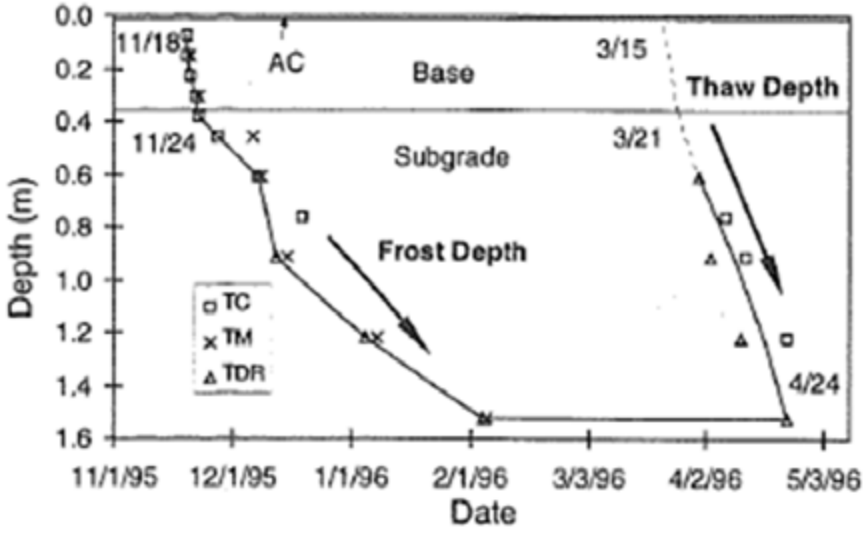


**Figure 21. Frost depth measured with thermocouples, thermistors, and time domain reflectometry probes (Jong et al. 1998)**

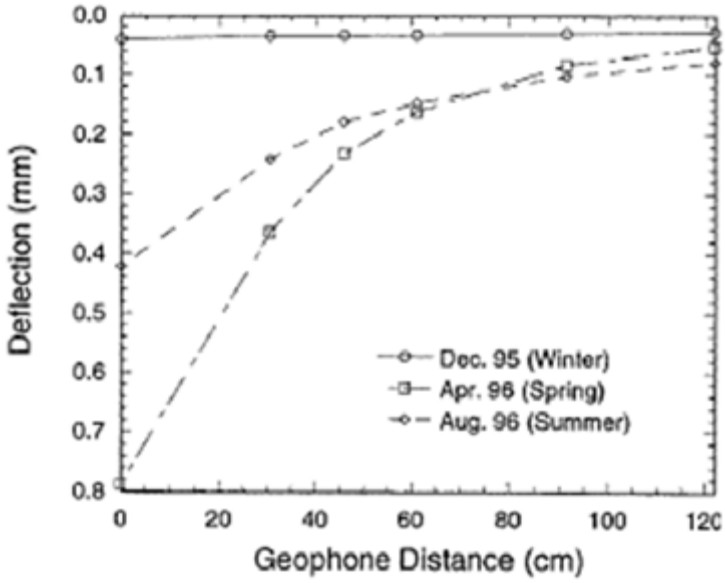


**Figure 22. Changes in seasonal FWD deflection basins (Jong et al. 1998)**

Jong et al. (1998) performed FWD tests at approximately 15 m intervals and found that overall; the modulus did not vary significantly for the intervals tested, so it was assumed that one interval could be used to represent the test section. They found that the moduli of the base and subgrade continued to weaken, after thawing began, until both layers were completely thawed (Figure 23). The thaw weakening stage lasted approximately one month and continued to recover for an additional four months. Figure 23 also shows that the subgrade has a higher modulus than the base for a brief period during thawing.

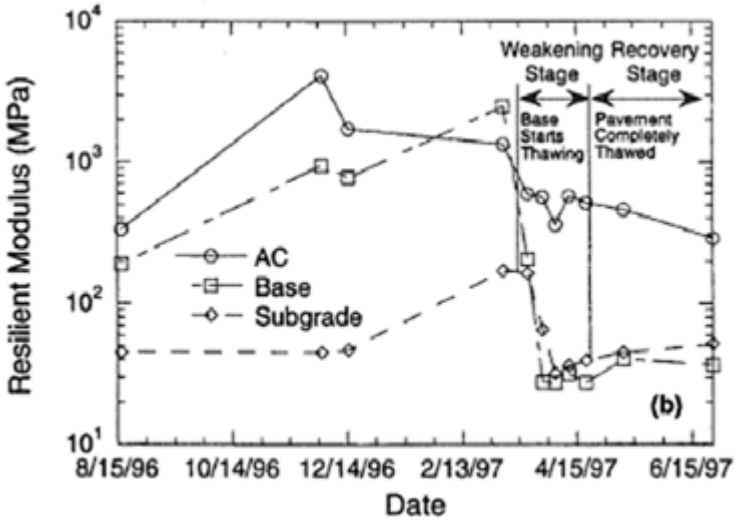


**Figure 23. Changes in seasonal resilient modulus (Jong et al. 1998)**

Newcomb and Birgisson (1999) showed a typically understanding of how a roadway is impacted by frost action (Figure 24). The deflection response from an applied load is reduced during periods of freezing and then drastically increases during the following thaw period. They found from other studies that the critical period during thawing is when water is trapped in the base layer between the pavement and the frozen subgrade.

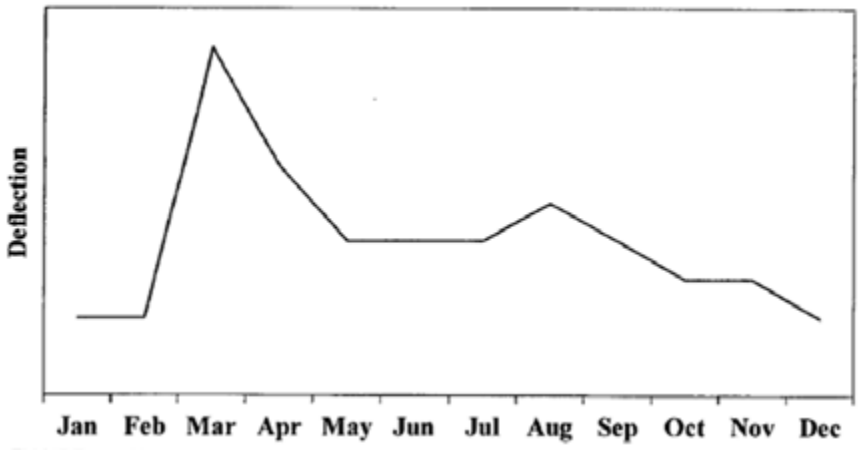


**Figure 24. Typical pavement deflection response due to seasonal changes (Newcomb and Birgisson 1999)**

The effect on the resilient modulus can be seen in (Figure 25). The result of water being trapped in the base course is that the modulus of the subgrade is actually higher than that of the base course for a short time, which supports Jong et al. (1998).

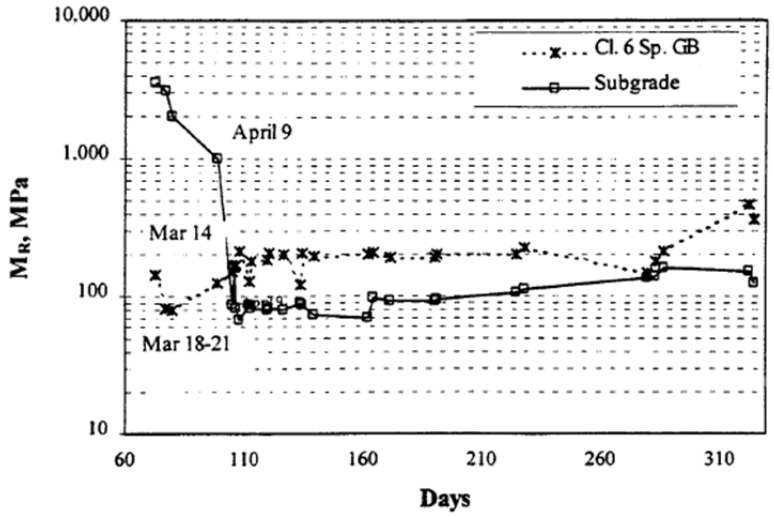


**Figure 25. Seasonal changes in the resilient moduli of the base and subgrade layers (Newcomb and Birgisson 1999)**

As a part of the ROADEX II Project in Northern Europe, the effect of thaw weakening was studied on low volume gravel roads (Saarenketo and Saara 2005). One method used to determine the changes in stiffness and thickness of pavement layers was the dynamic cone penetration (DCP) test. They used the results of the DCP test to determine the depths to layer interfaces and to determine the location of the frost line. They backcalculated a modulus, based on the shear strength, from the DCP data. Figure 26 shows the DCP moduli being used to track the thawing process. They concluded that the DCP test is very useful for monitoring the frost depth and the stiffness of the road structure, but they found that it has problems penetrating stiff base course so it is not suitable for observing well-built roads.

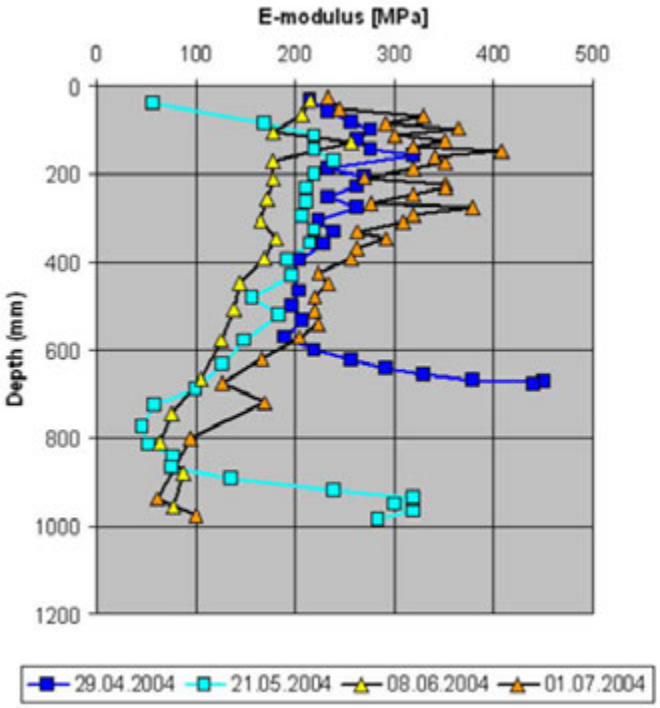


**Figure 26. Tracking thawing process by using DCP backcalculated moduli (Saarenketo and Saara 2005, Fig. 80)**

Christopher et al. (2006) mentioned that the DCP is an efficient means to characterize the subgrade conditions. The DCP provides information on the subsurface materials without sampling disturbance, allows for a continuous collection of data, indicates stratigraphy, indicates strength, and no laboratory samples are required.

## APPLICABLE DESIGN GUIDES

Pavement systems should be designed to account for the effects of frost heave so traffic flow is not interrupted and for thaw weakening so the pavement life is not decreased from the design life (Joint Departments of the Army and Air Force 1985). The following sections discuss how the 1993 AASHTO Guide and the NCHRP 1–37A Mechanistic-Empirical Design Guide (MEPDG) address frost action in pavement design and the final section discusses suggestions for pavement design drawn from the guides and other sources.

### 1993 AASHTO Guide for Design of Pavement Structures

The 1993 AASHTO Guide is based on the relationship between serviceability and performance, which results in pavement structures designed to meet the needs of an expected traffic volume but also meets the minimum serviceability at the end of the design life (AASHTO 1993).

The 1993 AASHTO Guide states that "A reliable method for recognizing a frost susceptible material for site specific conditions has not, as yet, been identified" (p. I-25). Therefore, the guide includes a method that uses the following three empirical parameters to estimate the effect of frost heave on the pavement system: frost-heave rate, maximum potential serviceability loss, and frost-heave probability. The frost-heave rate is in mm per day and is determined from the USACE plot of average rate of heave versus the percentage of material finer than 0.02 mm (Figure 1). The maximum potential serviceability loss from frost heave depends on the depth of frost penetration and the drainage quality in the pavement system (AASHTO 1993). The drainage quality of the pavement system is determined by how long it takes for water to leave the pavement system. A chart is used to determine the maximum potential serviceability loss from frost heave. The frost-heave probability is based on the designer's estimate of the area of the project that will be exposed to frost heave. The probability depends on how frost susceptible the subgrade is, the amount of moisture available to the system, the quality of drainage, the number of freeze-thaw cycles, and the frost-penetration depth (AASHTO 1993). The probability relies heavily on past experiences, because there is no process to follow.

The three empirical parameters are used in a nomograph to determine the potential serviceability loss due to frost heave (AASHTO 1993). The potential serviceability loss due

to frost heave is very approximate, because of the parameters used in its determination (Christopher et al. 2006). Curves are developed for the potential serviceability loss due to frost heave and the potential serviceability loss due to swelling to get a curve that represents the total environmental potential serviceability loss over time (AASHTO 1993). The total environmental potential serviceability loss over time is added to the potential serviceability loss due to the cumulative traffic loads to determine the maximum potential serviceability loss. The maximum potential serviceability loss is then used in the pavement design process.

There are two methods available to define the seasonal variation in pavement support conditions in the 1993 AASHTO Guide (AASHTO 1993). One method is to determine laboratory resilient modulus based on moisture contents representative of seasonal conditions. The other method is to backcalculate the resilient modulus from deflections measured in the pavement system for different seasonal conditions. Rigid pavements only require the length of the seasons to be known and the representative moduli for the seasons. However, flexible pavements require the seasonal moduli values to be combined into an effective roadbed soil resilient modulus.

Andersland and Ladanyi (2004) recommended that the 1993 AASHTO Guide should be used when experience indicates that frost heave will be mostly uniform along the length of pavement system or if additional frost action control procedures will be used.

### NCHRP 1–37A Mechanistic-Empirical Design Guide

The Mechanistic-Empirical Design Guide (MEPDG) allows for seasonal variations in resilient modulus to be accounted for by either directly inputting values for each month or by inputting moisture and freeze-thaw predictions into models that predict the resilient modulus (NCHRP 2004). The moisture and freeze-thaw predictions are determined from the Enhanced Integrated Climate Model (EICM), which consists of three main parts: the Climatic-Materials-Structural Model; the CRREL Frost Heave and Thaw Settlement Model; and the Infiltration and Drainage Model. EICM computes and predicts temperature, resilient modulus adjustment factors, pore water pressure, water content, frost and thaw depths, frost heave, and drainage performance for the entire pavement structure. The LTTP SMP test sites were used to develop the EICM. The EICM outputs the following to be used in other aspects of design in the guide: unbound material resilient modulus adjustment factors, volumetric

moisture content, temperature profile in PCC, number of freeze-thaw cycles and freezing index, and relative humidity values for determining moisture gradients in a PCC slab.

The EICM requires information concerning the following categories: general information, weather, ground water, drainage and surface properties, and pavement structure and materials. Several input parameters are required to produce quality output parameters. For each input parameter there are three levels of importance. For example a level one input parameter would be a result of direct measurements, whereas a level three input parameter would be a result of estimations or predictions. The higher quality input parameters will lead to a higher accuracy structural design.

MEPDG provides some guidance on how to identify frost-susceptible materials, but the classifications are not explicitly used in the design process. MEPDG does not directly account for the effects of frost heave; rather it provides methods to reduce the effects of frost heave. The maximum frost depth, from EICM, is meant to be used to determine layering configurations that will be required to prevent freezing of frost-susceptible soil. The guide presents the USACE soil frost-susceptibility classifications and plot comparing percent passing #200 and heave rate as references.

Andersland and Ladanyi (2004) mention that mechanistic pavement design models used in frost regions requires several predictions including: the stresses, strains, and deflections in the pavement system. The properties and thickness of the pavement layers need to adjusted to make sure that the predicted stress, strains, and deflections are in an acceptable range based on the loading that the pavement system is expected to have. The stresses, strains, and deflections of the pavement layer are predicted from the resilient modulus of the pavement foundation.

### Design Suggestions for Reducing the Effects of Frost Action

In addition to specifying the steps of the design process, the 1993 AASHTO Guide and MEPDG include additional suggestions for reducing the effects of frost action or addressing problem areas. The suggestions have indirect effects on the design process, but they may negate detrimental effects of frost action. The AASHTO Guide recommends that agencies reduce the effects of frost action by using design methods that are based on local conditions.

For example, the AASHTO Guide recommends that frost-susceptible materials should be removed and replaced with non-frost-susceptible material to a depth of one half or more of the expected frost-penetration depth. The MEPDG recommends stabilizing fines in frost-susceptible materials by mechanically removing or physically bonding them; reducing the amount of water available; or reduce the freezing point of the soil pore water. The Joint Departments of the Army and Air Force recommends that the distance between the pavement structure and the ground water table be at least 1.5 m, but preferably 3 m to reduce capillary action (1985). Table 15 shows several design suggestions taken from the 1993 AASHTO Guide, MEPDG (NCHRP 2004), and other sources.

**Table 15. Samples of design suggestions for areas exposed to frost action**

| Design Suggestion | Source |
|---|---|
| Remove frost-susceptible soil and replace with non-frost-susceptible soil | AASHTO 1993; NCHRP 2004; Tighe et al. 2007 |
| Place additional layers of non-frost-susceptible material sufficiently thick so the subgrade does not freeze | American Concrete Pavement Association 2008; NCHRP 2004 |
| Remove pockets of frost-susceptible soils to increase subgrade uniformity | American Concrete Pavement Association 2008; NCHRP 2004 |
| Use a capillary break or increase the distance between the pavement structure and water table | American Concrete Association 2008; NCHRP 2004; Tighe et al. 2007 |
| Design the pavement structure to resist poor subgrade conditions that result from frost action | NCHRP 2004; Tighe et al. 2007 |
| Stabilize the fines of frost-susceptible material | NCHRP 2004 |
| Provide sufficient drainage in the pavement structure | American Concrete Pavement Association 2008 |
| Control subgrade uniformity by monitoring compaction and moisture content during placement | American Concrete Pavement Association 2008 |

# CHAPTER 3. METHODS

This chapter explains the methods used to address the following three objectives:

- To determine the frost heave and thaw weakening susceptibility of various soil types with laboratory testing equipment and obtain repeatable results.
- To determine seasonal changes of in situ pavement support parameters.
- To study the effects of stabilizers and changing material gradations for reducing frost heave and thaw weakening susceptibility.

The methods describe material types (e.g., soil index properties), strength characteristics, and responses to repeated freezing and thawing cycles.

## RESEARCH DESIGN

The research conducted includes laboratory and in situ test methods.

Laboratory tests were performed to determine how various soil types respond to repeated freezing and thawing cycles. The laboratory tests included:

- soil classification and index tests
- compaction tests
- strength tests
- durability tests
- frost heave and thaw weakening test

The results of the frost heave and thaw weakening test can be compared to results of soil classification and index tests to gain an understanding of how the frost heave and thaw weakening parameters vary as the material characteristics change. This process will assist in determining which parameters are the most important in predicting a soils response to freezing and thawing.

In situ testing data was gathered from seven pavement sections across Iowa to quantify the seasonal changes in pavement support parameters. In situ tests are an effective method of quantifying the effect of freezing and thawing on pavement systems.

The laboratory test methods are described first, followed by the in situ tests.

## LABORATORY TEST METHODS

**Table 16. Summary of laboratory test methods**

| Test Method | Test |
|---|---|
| **Soil classification and index tests** | |
| ASTM D422-63 | Standard Test Method for Particle-Size Analysis of Soils |
| ASTM C117-04 | Standard Test Method for Materials Finer than 75-µm (No. 200) Sieve in Mineral Aggregates by Washing |
| ASTM C136-06 | Standard Test Method for Sieve Analysis of Fine and Coarse Aggregates |
| ASTM D4318-05 | Standard Test Methods for Liquid Limit, Plastic Limit, and Plasticity Index of Soils |
| ASTM D2487-06 | Standard Practice for Classification of Soils for Engineering Purposes (Unified Soil Classification System) |
| ASTM D3282-93 | Standard Practice for Classification of Soils and Soil-Aggregate Mixtures for Highway Construction Purposes |
| ASTM D854-06 | Standard Test Methods for Specific Gravity of Soil Solids by Water Pycnometer |
| ASTM C127-07 | Standard Test Method for Density, Relative Density (Specific Gravity), and Absorption of Coarse Aggregate |
| **Compaction tests** | |
| ASTM D698-07 | Standard Test Methods for Laboratory Compaction Characteristics of Soil Using Standard Effort |
| ASTM D4253-00 | Standard Test Methods for Maximum Index Density and Unit Weight of Soils Using a Vibratory Table |
| ASTM D4254-00 | Standard test Methods for Minimum Index Density and Unit Weight of Soils and Calculation of Relative Density |
| O'Flaherty et al. 1963 | 2-in. x 2-in. Iowa State Compaction Method |
| **Strength tests** | |
| ASTM D1883-07 | Standard Test Method for CBR (California Bearing Ratio) of Laboratory-Compacted Soils |
| O'Flaherty et al. 1963 | 2-in. x 2-in. Compressive Strength Tests |
| **Durability tests** | |
| ASTM D559-03 | Standard Test Methods for Wetting and Drying Compacted Soil-Cement Mixtures |
| ASTM D560-03 | Standard Test Methods for Freezing and Thawing Compacted Soil-Cement Mixtures |
| Dempsey et al. 1973 | Vacuum Saturation of Stabilized Soils |
| **Frost heave and thaw weakening test** | |
| ASTM D5918-06 | Standard Test Methods for Frost Heave and Thaw Weakening Susceptibility of Soils |

## Soil Classification and Index Properties

Soil index properties are physical properties that can be observed and can have a significant impact on a soil's response to factors such as water and changes in temperature. Soil index properties describe the soils particle size, particle density, and soil consistency. The tests used to define these properties are particle size analysis, Atterberg limits, and specific gravity.

Particle size analyses were performed according to ASTM D422-63, ASTM C117-04, and ASTM C136-06 (Figure 27). ASTM D422-63 was used for fine-grained samples where the particle size distribution smaller than 0.075 mm was needed. The hydrometer method for determining the particle size analysis smaller than 0.075 mm was also conducted on aggregate materials. ASTM C117-04 and ASTM C136-06 were followed to determine the particle size distribution and percent passing 0.075 mm for aggregate materials. The sample size for each material was approximately 2,500 g, based on the criteria in ASTM D422-63. This was done to preserve material for future testing.

**Figure 27. Sieve shaker**

Atterberg limit tests were performed according to ASTM D4318-05 to determine a soil's liquid limit (LL), plastic limit (PL), and plasticity index (PI) (Figure 28). The dry preparation method was used for these tests. The results of the particle size analysis and Atterberg limits testing were then used to determine the classification according to the unified soil

classification system (USCS) and American Association of State Highway and Transportation Officials (AASHTO). The USCS classification was determined in accordance with ASTM D2487-06 and the AASHTO classification was determined in accordance with ASTM D3282-93.

**Figure 28. Atterberg limits test**

The specific gravity of the materials passing the No. 4 sieve was determined according to ASTM D854-06 and the specific gravity of the materials retained on the No. 4 sieve was determined according to ASTM C127-07. Method B of ASTM D854-06 was used, which requires the sample to be initially oven-dry. The apparent specific gravity of the materials retained on the No. 4 sieve was determined. The average specific gravity was determined when a soil contained particles larger and smaller than the No. 4 sieve. The average specific gravity was calculated according ASTM D854-06, based on the specific gravity of the soil passing the No. 4 sieve, the apparent specific gravity of the soil retained on the No. 4 sieve, the percent of soil passing the No. 4 sieve, and the percent of soil retained on the No. 4 sieve.

### Compaction Tests

Standard Proctor compaction tests were conducted using a mechanical Proctor setup (Figure 29) to determine the relationship between moisture content and dry unit weight. The testing was carried out in accordance with ASTM D698-07. Minimum and maximum index

density properties were determined for granular materials according to ASTM D4253-00 and ASTM D4254-00 using a vibratory table.

**Figure 29. Automatic Proctor compactor**

The 2-in. x 2-in. method was used to form samples of stabilized soil that are 5.1 cm in diameter and 5.1 cm in height. The 2-in. x 2-in. samples allow for a quick determination of the combination of water content/cement content that will produce the highest compressive strength. The samples were prepared and tested in general accordance with the procedure provided by O'Flaherty et al. (1963). The method is applicable to soils where there is either no material retained or the No. 4 sieve or where the material larger than the No. 4 sieve has been removed. Samples were moisture conditioned to target moisture contents and mellowed for a period of 24 hours. Stabilizers were added to the soil at target percentages based on the dry soil weight and were hand mixed.

The soil was compacted by dropping a 2268 g (5 lb.) hammer from a 305 mm (12 in.) height (Figure 30). The diameter of the hammer was nearly the same as the diameter of the

compaction cylinder. For the first drop, a temporary support was in place under the compaction cylinder. The temporary support was then removed and the sample was compacted by applying half of the total blows to the top of the sample, then inverting the sample and applying the remaining blows. The number of blows applied depended on the soil type and desired compaction level. The number of blows required to reach the same density as a standard Proctor sample can vary for different soil types. The sample was then extruded from the compaction cylinder and measured to verify that the height was 305 mm ±1.3 mm (2 in. ±0.05 in.) The sample was wrapped in plastic wrap and aluminum foil and was cured at 38°C (100°F) for seven days. Three samples were made at each moisture content/stabilizer content combination.

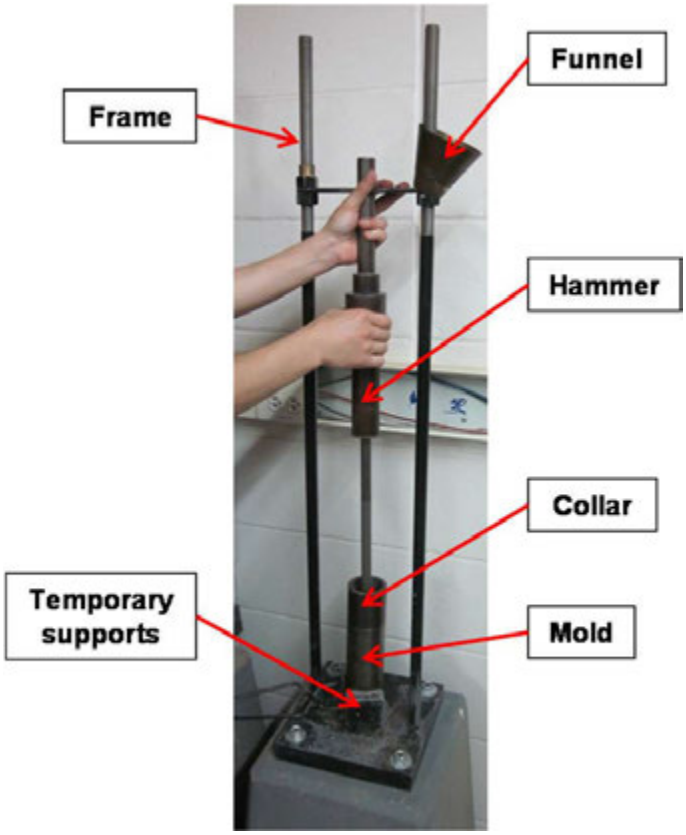


**Figure 30. Compaction of 2-in. x 2-in. samples**

## Strength Tests

The California bearing ratio (CBR) and unconfined compression tests were used to determine strength characteristics of the materials.

The California bearing ratio test is a strength test that can be used to determine the effectiveness of a material as a foundation layer for roadways (Figure 31). The test was performed in accordance with ASTM D1883-07. The particles retained on the 19 mm sieve were removed from the sample. The CBR was determined either at the optimum water content or at the natural water content. The moisture content chosen for the CBR test was based on the moisture content used to form the samples for the frost heave and thaw weakening test. The CBR samples were not soaked prior to testing.

**Figure 31. California bearing ratio (CBR) test**

Unconfined compression tests were performed on the 2-in. x 2-in (Figure 32) samples that were made using the Iowa State 2-in. x 2-in. compaction apparatus. The samples were loaded until they reached failure at a loading rate of 1.3 mm (0.05 in.) per minute.

**Figure 32. 2-in. x 2-in. unconfined compression test**

## Durability Tests

Wetting and drying, freezing and thawing, and vacuum saturation tests were performed to assess the durability of stabilized materials.

Wetting and drying durability tests were conducted according to ASTM D559-03 test method A (Figure 33) with the exceptions of the following steps: the gradation was not modified for some materials and the cement was not added before moisture conditioning the samples. Water was added to the soil the day prior to compaction to allow for the sample to mellow. The samples were compacted within 10 minutes of adding the stabilizer.

**Figure 33. Brushing the durability sample**

A cement treated base material from MI I-96 was tested directly from the batching plant, therefore the mixing and compaction procedures in ASTM D559-03 were not followed. A Marshall hammer was used to compact the specimen in a Proctor mold in three lifts with nine blows per lift. The compaction energy applied to the sample was the same as the standard Proctor test.

Freezing and thawing durability tests were conducted according to ASTM D560-03, with the same deviations during sample preparation as those for ASTM D559-03.

The 2-in. x 2-in.compacted and cured samples were vacuum saturated in accordance with the method proposed by Dempsey et al. (1973) using a vacuum chamber and water supply as shown in (Figure 34).

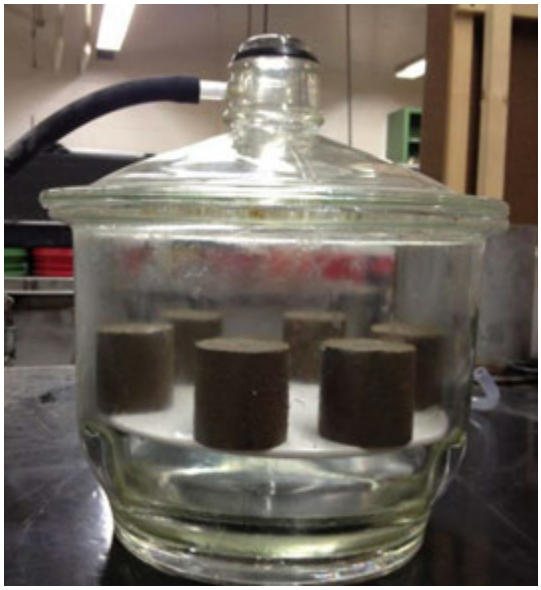

**Figure 34. 2-in. x 2-in. vacuum saturation**

The steps followed for vacuum saturating the samples and performing unconfined compression tests are as follows:

1. The samples were removed from the oven and allowed to equilibrate to room temperature for two hours.
2. The samples were placed on a perforated plate in a vacuum desiccation chamber.
3. The chamber was evacuated to 24 in. of mercury for 30 minutes.
4. The chamber was flooded with water until the samples were covered. The samples were soaked at atmospheric pressure for one hour.

5. The samples were removed from the chamber and the free water was allowed to drain.
6. The unconfined compressive strength and moisture content was determined for each sample.

## Frost Heave and Thaw Weakening Test

This section describes the procedures used to determine the frost heave and thaw weakening susceptibility for various soil samples. The following topics are discussed in the following subsections:

- Frost heave and thaw weakening test background
- Equipment development and setup
- Overview of the test method

### Frost Heave and Thaw Weakening Test Background

The frost heave and thaw weakening test was performed in general accordance with ASTM D5918-06. The test classifies soils based on the heave rate and thawed bearing ratio values determined from the test. The values are compared with a classification system to determine the susceptibility ratings. The test is primarily designed for classifying pavement foundation soils. The test can only be used to compare the relative frost heave and thaw weakening susceptibility between material types. ASTM D591806 mentions that the results cannot be used to directly determine the amount of frost heave or thaw weakening in a pavement system.

The test was carried out on four specimens for each soil type by subjecting each sample to two freeze-thaw cycles over a five day period. The samples dimensions were 146 mm (5.75 in.) in diameter and 152 mm (6 in.) in height. The samples were compacted inside six rings with a rubber membrane between the soil and the rings. A water supply was made available at a level of 13 mm (0.5 in.) above the bottom of the sample. A surcharge weight was applied to the sample to simulate the loading of a typical pavement section. During the test, laser displacement transducers took measurements of the samples' heave and thermocouple sensors recorded the temperature profile within the sample. The samples were placed in a temperature controlled chest freezer and then frozen and thawed by changing the temperature at the top and bottom of the samples. Once the test sequence was completed, a

CBR test was performed on the thawed samples and a moisture content profile was determined by carefully trimming the samples and obtaining moisture contents at various depths.

**Equipment Development and Setup**

This section outlines the development of the setup described in ASTM D5918-06 and discusses deviations or modifications from the standard. The setup used in this study was designed and fabricated at Iowa State University. Detailed drawings, model numbers, and serial numbers of all parts used in the setup are provided in Appendix B.

*Compaction Mold*. The compaction mold consists of the base plate, compaction cylinder, spacer disks, acrylic rings, collar, rubber membrane, and clamps (Figure 35 and Figure 36).

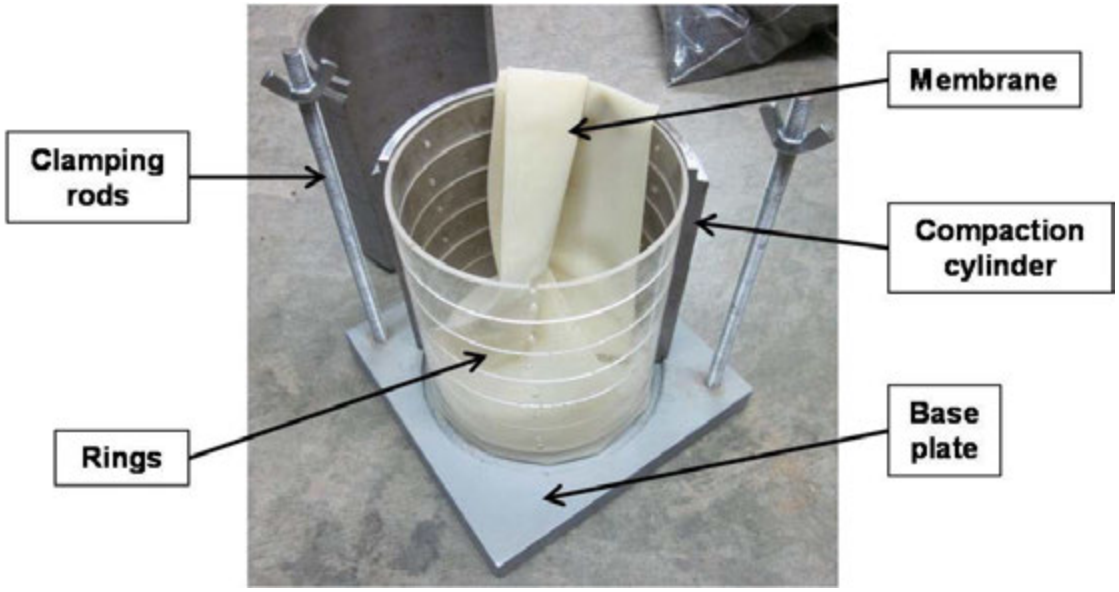


**Figure 35. Inside view of the frost-heave and thaw-weakening test compaction mold**

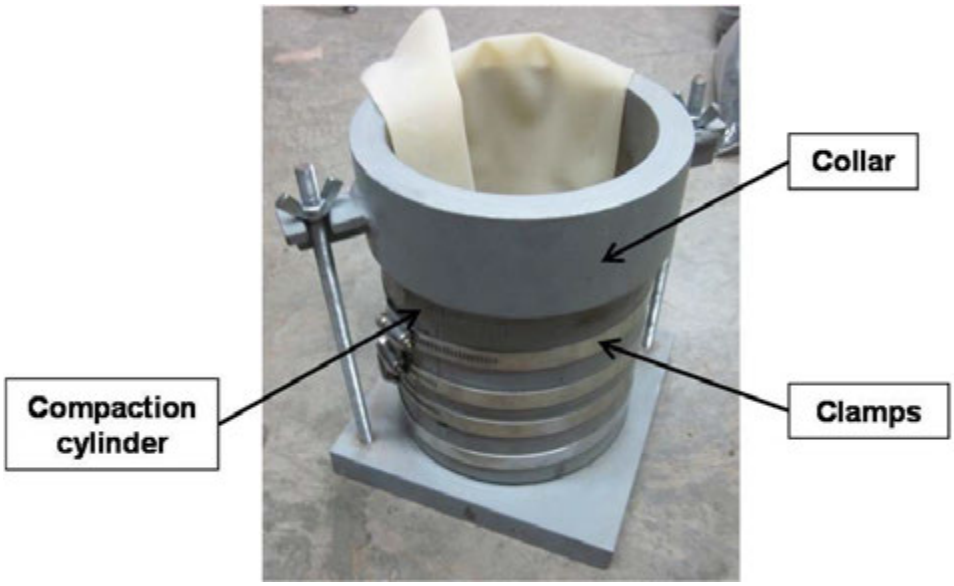


**Figure 36. Frost-heave and thaw-weakening test compaction mold**

*Compaction cylinder*. The compaction cylinder was about 13mm (0.5 in.) taller than the specified height in the standard, with a total height of 178 mm (7 in.), to accommodate a thicker spacer disk. ASTM D5918-06 specifies that the compaction cylinder should be split vertically into three side walls. However, because of the difficulty in cutting three equal pieces, the cylinder was split into two side pieces (Figure 37). There were no apparent problems observed with two pieces versus three.

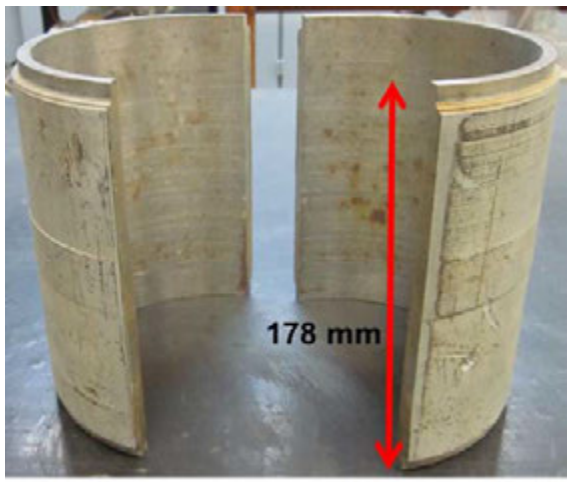


**Figure 37. Compaction cylinder for the frost-heave and thaw-weakening compaction mold**

*Collar*. In order to fit the collar over the compaction cylinder, the diameter of the recess bored into the collar was manufactured as 171 mm (6.75 in.) rather than the specified 152 mm (6.0 in.) (Figure 38).

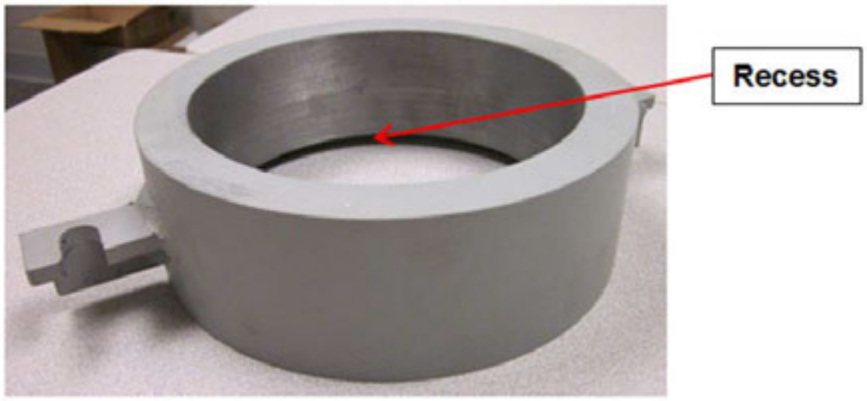


**Figure 38. Collar for the frost-heave and thaw-weakening compaction mold**

*Spacer disk*. Acrylic spacer disks were made with a diameter of 151 mm (5.95 in.) to allow for the membrane to fit between the spacer disk and the compaction cylinder (Figure 39). The bottom spacer disk was 19 mm (0.75 in.) to add durability to the spacer so it would better withstand the compaction blows.

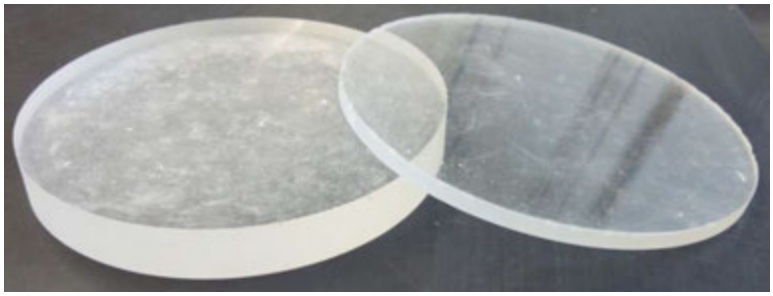

**Figure 39. Spacer disks for frost-heave and thaw-weakening sample preparation**

*Rings*. The acrylic rings were manufactured as specified with the exception of the split cut through the height (Figure 40). The acrylic rings in the prototype were split cut, but the inherent stresses in the rings resulted in the rings not holding a circular shape after being cut. The split in the rings is not an issue if the samples being tested are remolded.

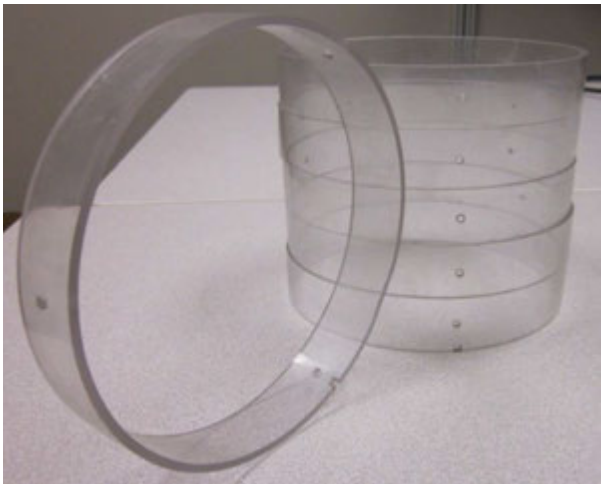

**Figure 40. Rings for frost-heave and thaw-weakening sample preparation**

*Rubber membrane*. The membranes used were 0.4 mm (0.014 in.) thick and 152 mm (6 in.) in diameter (Figure 35). A 146 mm (5.75 in.) diameter membrane could not be found in the marketplace and custom made membranes were found to be uneconomical. The 6 in. diameter membrane proved to perform sufficiently.

*Sample freezing assembly.* The variations in the sample freezing assembly included how the displacement measuring system was supported and the type of sensor used to measure the displacement. Figure 41 is adapted from Figure 2 in ASTM D5918-06 and shows the deviations made from the standard.

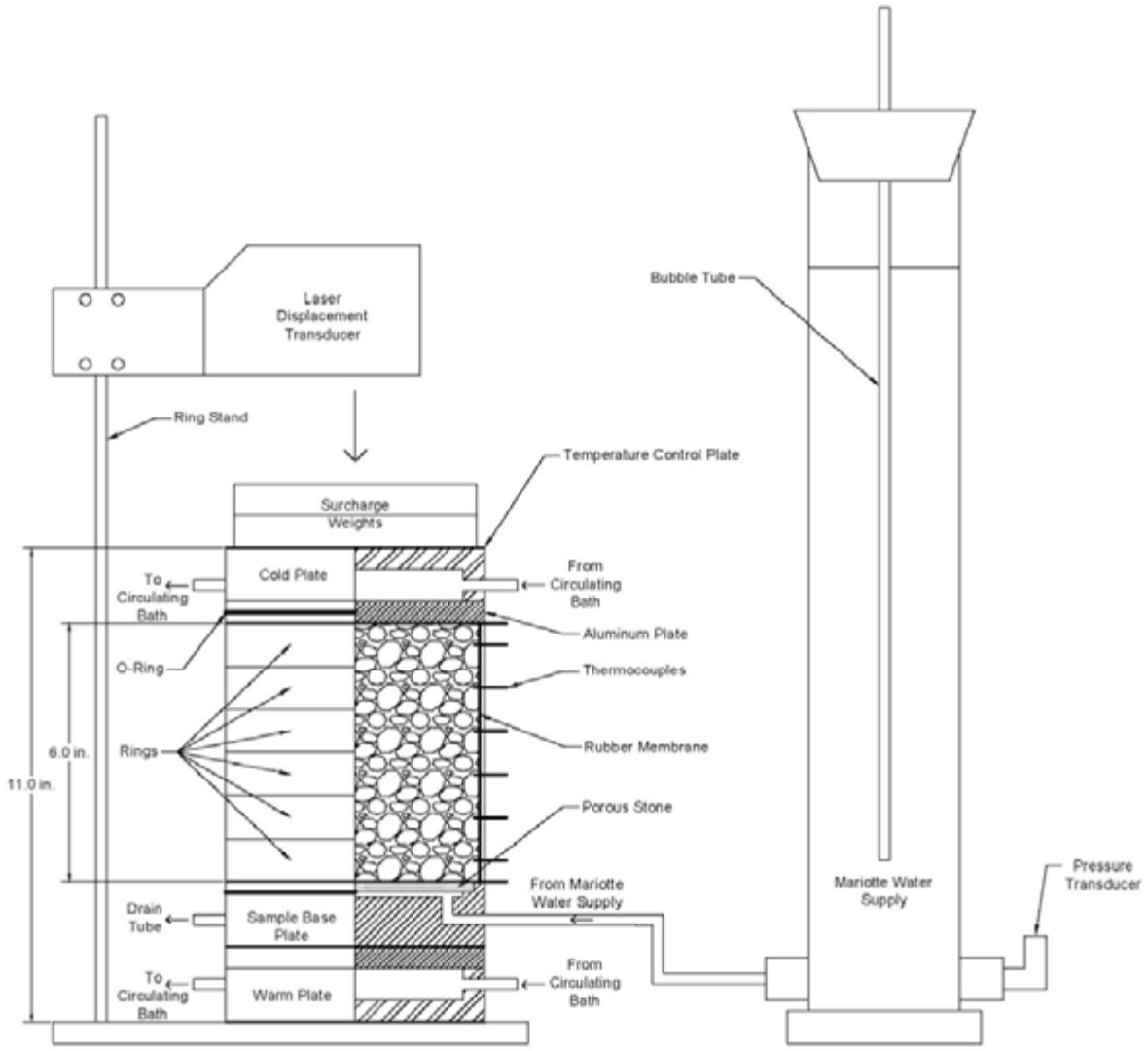


**Figure 41. Frost-heave and thaw-weakening sample assembly**

*Top and bottom temperature control end plates*. The temperature control end plates were made out of an acrylic disk, with a serpentine path cut into it, and an aluminum plate (Figure 42). The serpentine path was cut on the top of the acrylic disk so the circulating liquid is in directed contact with the aluminum disk. The aluminum plate and acrylic disk were bolted together with a rubber O-ring between them near the outside diameter to prevent leaks. The serpentine path began near the outside of the disk and continued toward the center where it then returned to the water bath.

**Figure 42. Acrylic side (left) and aluminum side (right) of temperature control end plate used to freeze and thaw samples**

**Figure 43. Sample base plate without porous stone (left) and with porous stone (right)**

*Constant head (Mariotte) water supply*. The water supply was made out of acrylic tubing with a diameter of 76 mm (3 in.) and a height of 508 mm (20 in.). The thickness of the wall was initially 3 mm (0.125 in.), but over time they began to crack. The wall thickness of the next set of water supplies was 10 mm (0.375 in.). The top of the water supply was sealed off by a rubber stopper. A hole was drilled in the rubber stopper for the glass bubble tube. A valve was placed at the base of the water supply to allow for easy shut off. A quick disconnect was installed on the flexible tube connecting the water supply and the sample base plate to ease the process of setting up the equipment. A pressure transducer was also installed at the base of the water supply to measure the water head being applied to the sample. It was initially thought that the pressure transducer would measure the level of water in the reservoir, but it actually measures the elevation of the water in the bubble tube. If the

elevation of the water in the reservoir is to be measured, the pressure transducer should be placed above the water level.

*Surcharge weight*. The surcharge weight consisted of two 2268 g (5 lb.) steel disks, rather than the specified single lead disk.

*Heave and consolidation measuring apparatus*. Laser displacement transducers were used to measure the heave and consolidation. The lasers had a measurement range of 50 mm and a resolution of 0.75 µm. The lasers were connected to a data acquisition system that recorded the temperature at one-minute intervals. The lasers were mounted on a laboratory ring stand using a custom-made bracket.

*Temperature control baths.* The water baths had an operating range of -30° to +200°C and a stability of ±0.01°C. The water baths were programmable and were filled with a 50% ethylene glycol-water solution (Figure 44). Insulating tape was wrapped around the flexible tubing, between the water baths and the temperature control end plates, to reduce the temperature change of the solution.

3

**Figure 44. Temperature control baths used to freeze and thaw samples**

The ideal temperature profiles (Figure 45) were programmed into to the temperature control baths; however the actual temperature profiles (Figure 46) measured were higher during freezing and lower during thawing periods than the target values. This discrepancy occurred because of temperature losses in the glycol solution as it was transported from the

temperature control baths to the temperature control end plates. It was also observed that this discrepancy was greater for some cohesionless and cement-treated materials. One possibility for the difference in top and bottom temperatures is a lack of good contact between the soil and the thermocouples. Despite the decrease in temperature, all samples were completely frozen. The increased temperatures and poor thermocouple contact caused difficulty in accurately determining the frost depths.

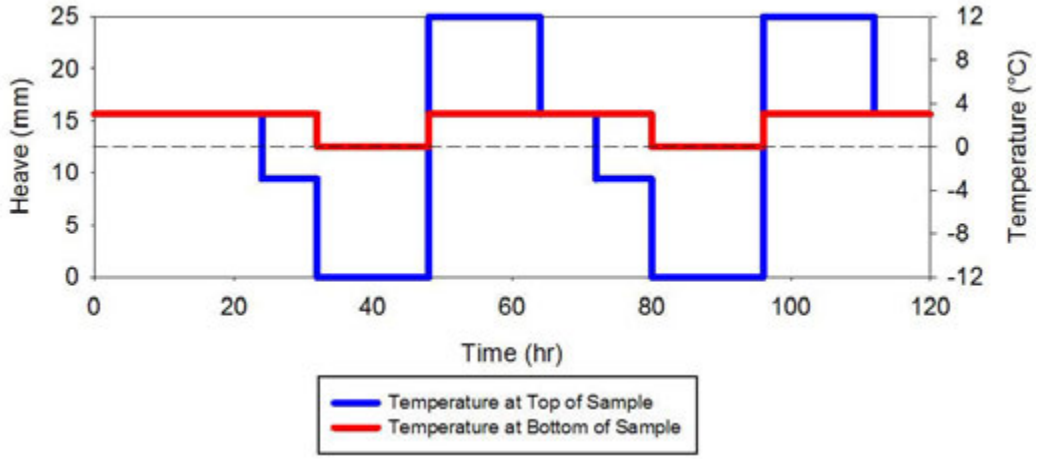


**Figure 45. Ideal top and bottom temperature profiles**

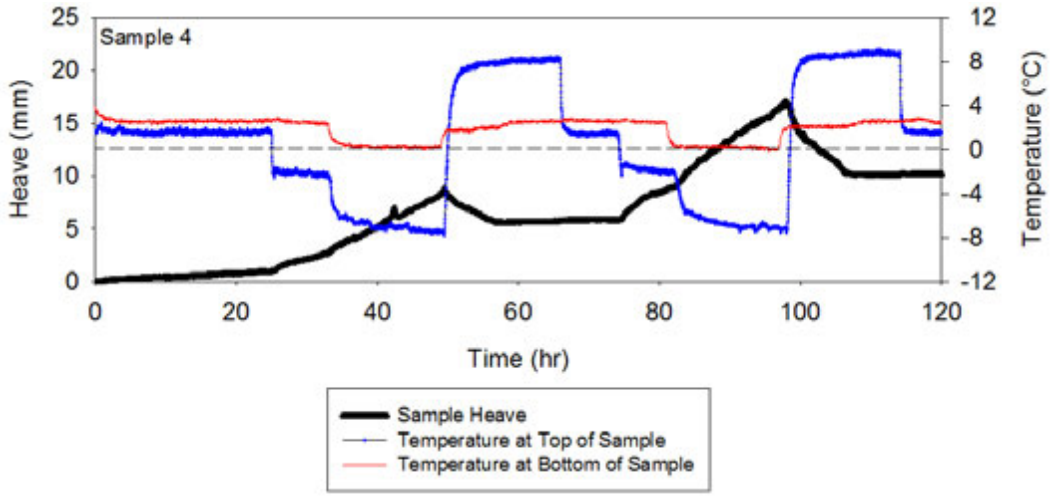


**Figure 46. Example measurements of top and bottom temperature profiles**

*Temperature control chamber.* A 0.42 $m^3$ (14.8 $ft^3$) chest freezer (Figure 47) was used as a temperature control chamber. The temperature was regulated using a temperature controller with a thermocouple placed inside the freezer. ASTM D5918-06 specifies that the air temperature in the chamber should be between 2°C ±1.5. An example air temperature profile

with the specified range is shown in Figure 48. Results indicated that the measured air temperature was mostly within the specified range; however the temperatures varied from test to test. One possibility for this variation is the location of the thermocouple in the chamber not being constant.

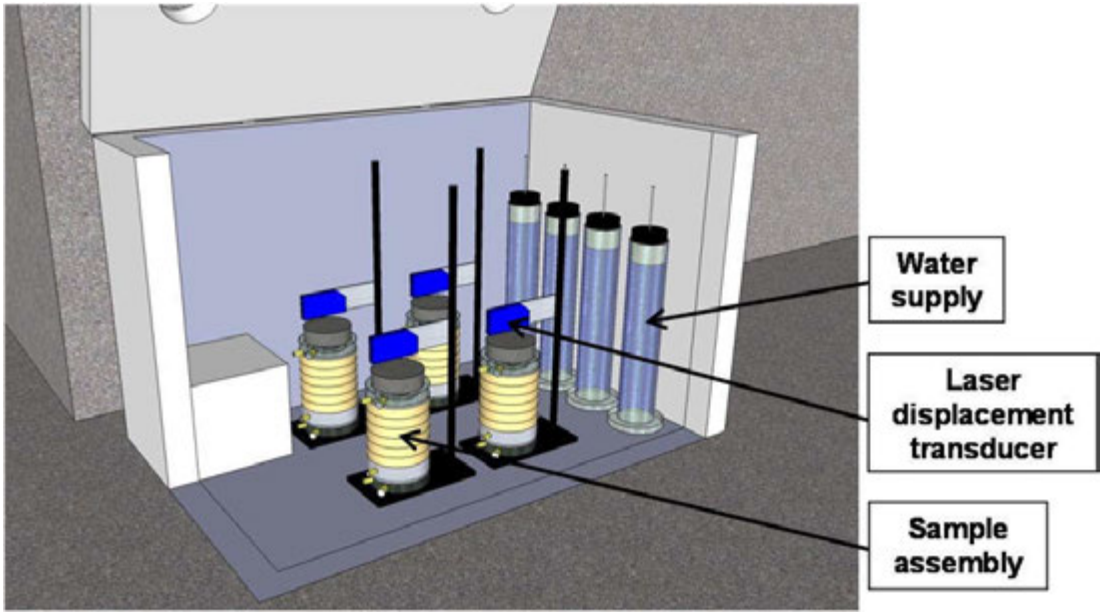


**Figure 47. Idealized view of the temperature control chamber**

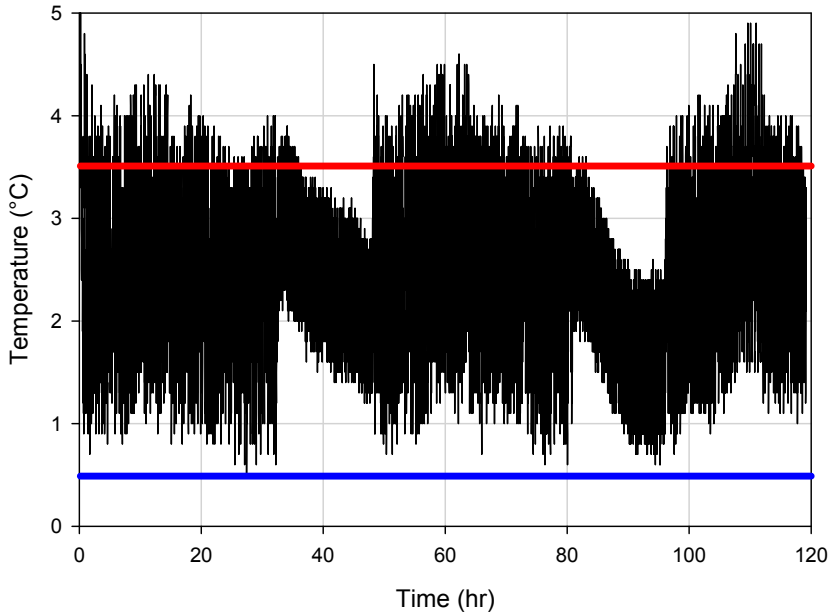


**Figure 48. Example measurements of temperature control air chamber**

*Temperature measuring system*. The temperature measuring system consisted of Type T thermocouple wire connected to a data acquisition system. The data acquisition system automatically took readings at one-minute intervals. The two thermocouple wires were twisted together and soldered. The measurement range of the thermocouples is -200°C to +400°C and has an accuracy of ±1.8°C. The standard specifies that the thermocouples have an accuracy of ±0.1°C, but the data acquisition system that was already available for this study was used to reduce costs.

The standard specifies that 33 thermocouples are needed, 32 for the samples and 1 for the air temperature. However, the data acquisition system used only had the capacity for 31 thermocouples, so one of the middle sensors was omitted from two samples. A middle sensor was omitted because temperature data from the middle of a sample is less important than data from the top and bottom thermocouples.

**Overview of Test Method**

This section discusses the additional steps and deviations from the procedure described in sections 7 through 10 of ASTM D5918-06. A detailed procedural manual is included in Appendix C. A flow chart of the general testing procedure for one sample is provided in Figure 49. According to the standard, four samples are typically tested for the same material. For stabilized materials only two samples are tested at each moisture content/stabilizer content.

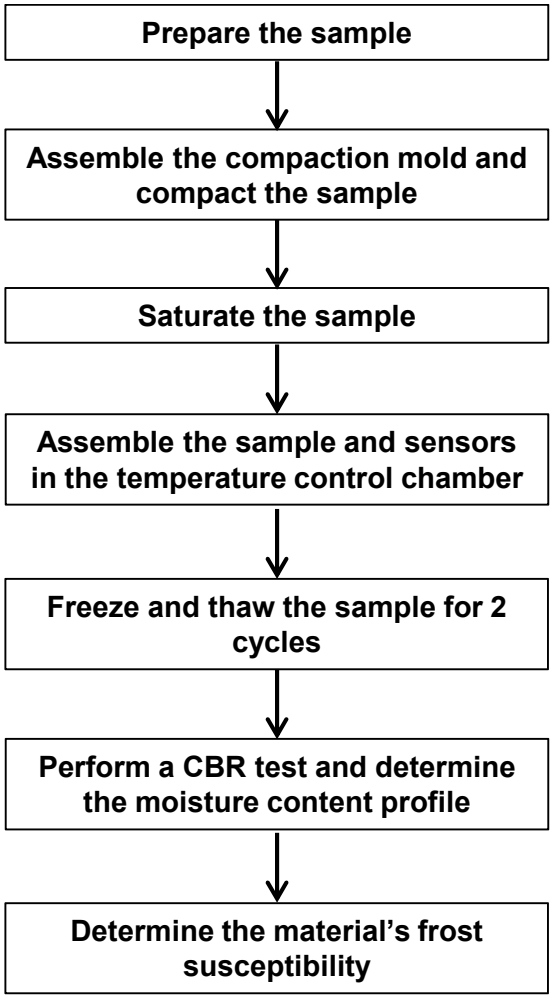


**Figure 49. General frost heave and thaw weakening test procedure**

*Remolded samples.* Remolded samples were used for all material types. For some cohesionless materials, the in situ moisture content was used. This typically resulted in the material being compacted at their bulking moisture content, which resulted in a lower density than the maximum. The in situ moisture content was used to better represent field conditions. Particles larger than 19 mm (0.75 in.) were scalped from the original gradation.

*Compaction.* All samples were compacted using standard Proctor energy. The samples were compacted in 5 equal layers with 40 blows in each layer from a standard Proctor hammer. The hammer weighed 2495 g (5.5 lb.) and was dropped from a height of 305 mm (12 in.). The samples were compacted to slightly above the top of the sixth ring and the remaining material above the ring was removed with a straightedge.

*Freezing point depression determination.* The freezing point depression was not determined due to the inaccuracy of the temperature measuring system. The decision to not measure the freezing point depression was based off of the temperature profile results during the test sequence. It was not possible to effectively determine the point of nucleation.

*Mounting the sample for testing.* A hose clamp was placed over the rubber O-ring to seal the sample and prevent water from exiting the sample between the sample base plate and the membrane (Figure 50).

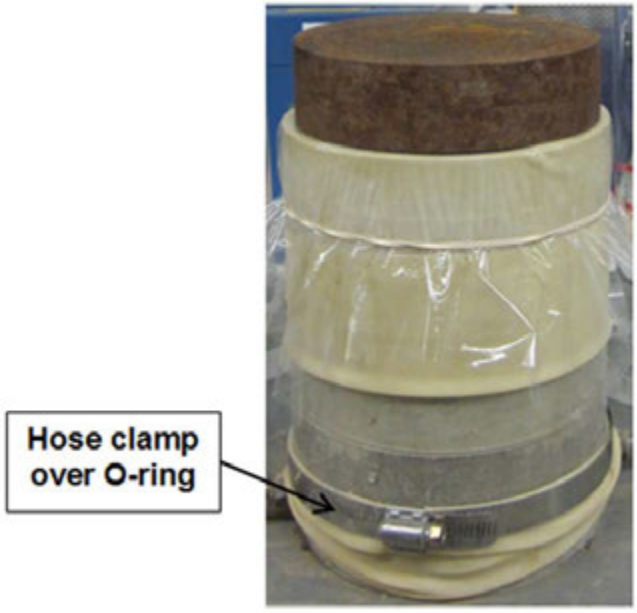


**Figure 50. Sample on a base plate**

*Completing the test assembly.* Loose insulation was not always added to the temperature control chamber. It was determined, from test data, that the loose insulation had little effect on the air temperature around the samples.

*Nucleation.* The accuracy of the temperature measurement system was not high enough to effectively determine when ice nucleation was occurring. Therefore, the possibility of instantaneous freezing was not considered.

*Purging air from base.* It was noticed after several attempts to purge air from the sample base, that there was no air exiting from the base. The reason for this is unknown. Therefore, the test sequence was no longer interrupted for the purpose of purging air from the base.

*Conducting the bearing ratio test after thawing.* The penetration of the plunger was allowed to be 10 mm (0.4 in.) as opposed to specified limit of 8 mm (0.3 in.) The penetration was increased in order to allow for the correction, due to surface irregularities, that is specified in ASTM D1883-07.

**Analysis of Frost-Heave Data**

The heave rate is determined from the slope of the heave versus time plot. ASTM D5918-06 specifies that the frost-heave rate should be determined during the first eight hours of each freeze thaw cycle. However, the samples did not always heave during the first 8 hours of each freeze cycle. The heave rate determined from the first 8 hours of each freeze cycle was very similar to the heave rate determined for the entire 24 hours of each freeze cycle. Therefore, it was decided that the 24 hour frost-heave rate would be reported to keep the analysis procedure uniform, whether the samples did or did not heave during the first 8 hours of each freeze cycle. The heave rate was determined from the time the sample began to heave until heaving had ceased and the temperature began to rise. The slope of the line was determined by performing a linear regression analysis. The red lines in Figure 51 show the portions of the heave versus time line that is used to determine the frost-heave rate.

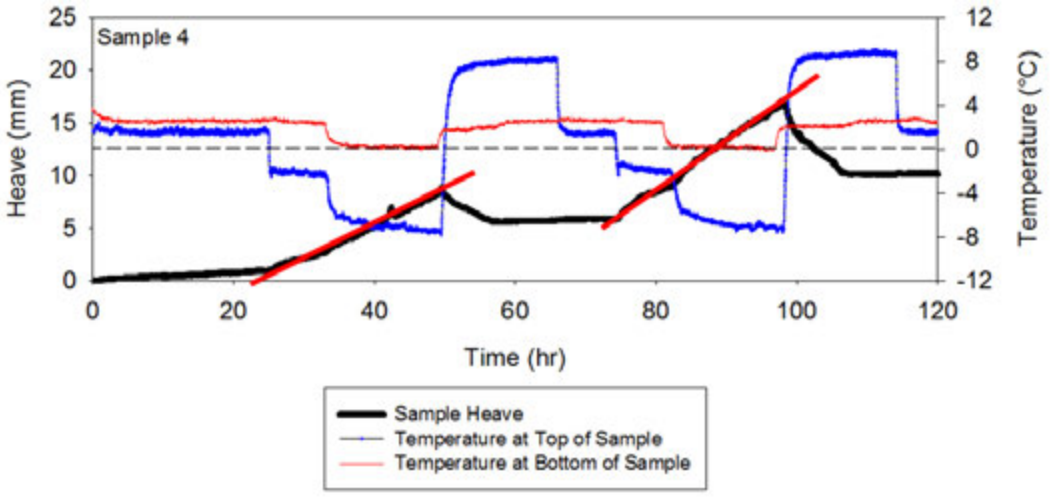


**Figure 51. Determination of frost-heave rate from plot of heave versus time**

## IN SITU TEST METHODS

The in situ test methods that were followed can be seen in Table 17.

**Table 17. Summary of in situ test methods**

| Test Method | Test |
|---|---|
| ASTM D6951-03 | Standard Test Method for Use of the Dynamic Cone Penetrometer in Shallow Pavement Applications |
| FHWA 2000 | Falling weight deflectometer (FWD) |

### Dynamic Cone Penetrometer

The dynamic cone penetrometer (DCP) test was performed in accordance with ASTM D6951-03 (Figure 52). The dynamic cone penetrometer test was used to determine CBR values of the pavement foundation layers. The layering of the underling materials can be determined from changes in slope on the cumulative blows versus depth plot. The DCP was used to test down to an approximate depth of 2 m (79 in.) using extension rods.

**Figure 52. Dynamic cone penetration (DCP) test**

### Falling Weight Deflectometer

The falling weight deflectometer (FWD) tests were performed in accordance with the LTPP Manual for Falling Weight Deflectometer Measurements Operational Field Guidelines (FHWA 2000) using a Kuab Model 150 2 m FWD (Figure 53). The FWD was used to

perform non-destructive evaluations of the pavement system throughout the year. The FWD test was performed by dropping a mass from four specified heights, to simulate pavement loading. The first drop was a seating load of approximately 26.7 kN (6000 lb.), followed by four test loads that were approximately 26.7 kN (6000 lb.), 40.0 kN (9000 lb.), 53.4 kN (12000 lb.), and 75.6 kN (17000). The actual load applied was measured using a load cell. The deflection basin was measured using seismometers. The seismometers were located at 305 mm (12 in.) in front of the loading plate, at the center of loading plate, and 305 mm (12 in.), 610 mm (24 in.), 914 mm (36 in.), 1219 mm (48 in.), and 1524 mm (60 in.) behind the loading plate.


**Figure 53. Falling weight deflectometer (FWD) test**

## U.S. Highway 30 Ames, IA Temperature Probe

A vertical and horizontal temperature probe was installed on U.S. Highway 30 near Ames, IA before the pavement surface was constructed. The purpose of the horizontal temperature probe was to determine if there are differences in the subsurface temperature under the shoulder compared to the center of the roadway when snow is piled on the shoulders. The top of the vertical temperature probe and the horizontal temperature probe is located approximately 0.15 m under the bottom of the pavement surface between the RPCC and RPCC/RAP interface (Figure 54). The vertical temperature probe is located on the centerline of the roadway and extends to an approximate depth of 1.2 m. The horizontal

temperature probe begins at the centerline of the roadway and extends approximately 4.57 m to the shoulder. Type T thermocouple wire was used in the temperature probe and was connected to a Campbell Scientific CR5000 datalogger (Figure 54). The datalogger recorded temperature measurements every hour and was powered by a 12 volt battery, which was subsequently charged by a solar panel.

**Figure 54. U.S. Highway 30 vertical and horizontal temperature probes (left) and temperature probe data acquisition set up (right)**

Figure 55 shows a cross sectional view of the vertical and horizontal temperature probes in the right East bound lane of U.S. Highway 30.

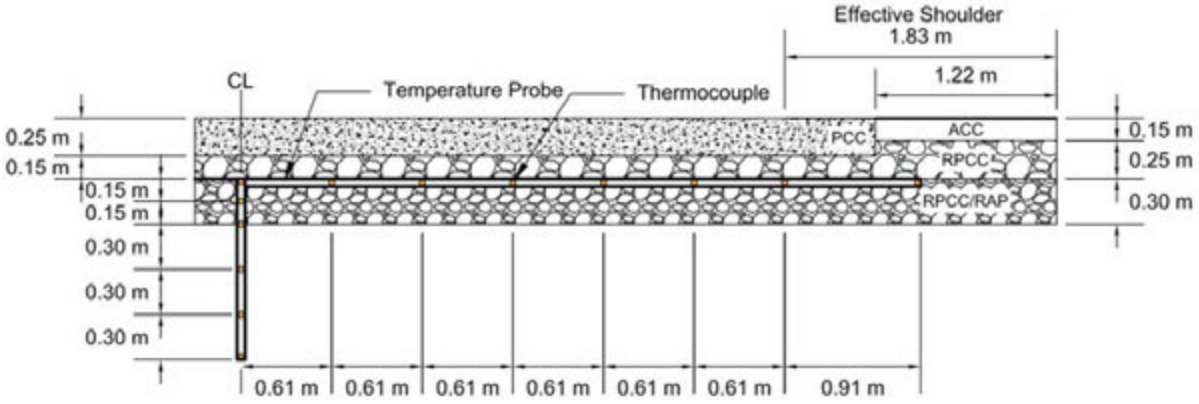


**Figure 55. Vertical and horizontal temperature probes on U.S. Highway 30**

# CHAPTER 4. MATERIALS

This chapter presents soil index properties for a wide variety of soil types that were sampled from various road construction projects and quarries for this research (Table 18). The materials are typically found in pavement foundation layers and have a wide range of classifications from well-graded gravels to lean clays with fines contents ranging between 0 and 100%.

**Table 18. Summary of source/project location and materials investigated**

| Project/Source location | Materials |
|---|---|
| Pottawattamie County, Iowa, 160th Street | Low volume unpaved granular surfacing material collected from the ditch and roadway |
| Monona County, Iowa, Interstate 29 (IA I-29) | Lean clay subgrade, silt with sand subgrade (also in Wolfe 2011) |
| Story County, Iowa, U.S. Highway 30 (IA US-30) | Clayey sand subgrade, recycled portland cement concrete (RPCC) subbase, RPCC/recycled asphalt pavement (RPCC/RAP) subbase, Limestone subbase |
| Story County, Iowa, Manatts | Concrete sand subbase, RAP subbase, RPCC/RAP subbase |
| Story County, Iowa, Martin Marietta Materials | Crushed limestone subbase |
| Clinton and Eaton Counties, Michigan, Interstate 96, (MI I-96) | Clayey sand subgrade (also in Wolfe 2011), RPCC cement treated base (CTB) |
| Indiana County, Pennsylvania, U.S. Highway 22 (PA US-22) | Sandy lean clay subgrade (also in Wolfe 2011) |
| Pottawattamie County, Iowa | Loess, cement-treated loess, fly ash-treated loess |
| Portage County, Wisconsin, U.S. Highway 10 (WI US-10) | Sandy lean clay subgrade (also in Wolfe 2011) |

The following sections present the laboratory soil index properties (i.e., soil classifications, grain size criteria, Atterberg limits, specific gravity, and compaction data) in a table for each of the project/source locations. The grain size distribution and compaction curves, where applicable, are presented. In addition to typical grain size criteria, the percent smaller than 0.074 mm and 0.02 mm have also been included. As Tester and Gaskin (1992) found, the frost susceptibility of a material can increase as the percent passing 0.074 mm increases. Cassagrande (1931) originally recommended using the percent passing 0.02 mm as an indication of frost susceptibility, but the criteria was also adopted for use in the USACE frost susceptibility classification system. The compaction data for the samples tested

according to ASTM D5918, which will be discussed in Chapter 5, is overlaid on the applicable compaction curves.

## 160TH STREET

A well graded sand with silt and gravel material was sampled from the ditch along 160th Street along with a poorly graded sand with silt and gravel material from the roadway of 160th Street. Both materials were used as low volume unpaved granular surfacing material. A summary of the soil index properties for both materials is provided in Table 19. The grain size distributions for the two materials are displayed in Figure 56 and Figure 57.

**Table 19. Summary of 160th Street soil index properties**

| Soil index property | Well graded sand with silt and gravel | Poorly graded sand with silt and gravel |
|---|---|---|
| USCS classification | SW-SM | SP-SM |
| AASHTO classification | A-1-b | A-1-b |
| Coefficient of uniformity ($c_u$) | 39.6 | 13.5 |
| Coefficient of curvature ($c_c$) | 2.27 | 0.87 |
| $D_{10}$ (mm) | 0.074 | 0.179 |
| $D_{30}$ (mm) | 0.704 | 0.611 |
| $D_{60}$ (mm) | 2.94 | 2.42 |
| Gravel size (%) (> 4.75 mm) | 31.0 | 27.0 |
| Sand size (%) (4.75 – 0.074 mm) | 59.0 | 66.0 |
| Silt size (%) (0.074 – 0.002 mm) | 7.0 | 4.0 |
| Clay size (%) (≤ 0.002 mm) | 3.0 | 3.0 |
| Passing 0.074 mm (%) | 10.0 | 6.8 |
| Passing 0.02 mm (%) | 6.1 | 5.6 |
| Liquid limit (LL) | NP | NP |
| Plasticity index (PI) | NP | NP |
| Specific gravity ($G_s$) | 2.70 | 2.72 |
| Optimum moisture content (%) standard Proctor | 8.7 | 8.2 |
| Maximum dry unit weight (kN/m$^3$) standard Proctor | 20.9 | 21.1 |
| Minimum dry unit weight (kN/m$^3$) relative density | — | — |
| Maximum dry unit weight (kN/m$^3$) relative density | — | — |

NP—not plastic

The compaction curves are shown in Figure 58 and Figure 59. The maximum dry densities, of both materials, approached the zero air voids curve and were high compared to other materials investigated. One possibility for the ASTM D5918 samples to be above the zero air voids line is a slightly larger sample height than what is being used in the dry unit weight calculations. The increase in height was observed to be a result of the rings spreading apart in the compaction mold during sample compaction.

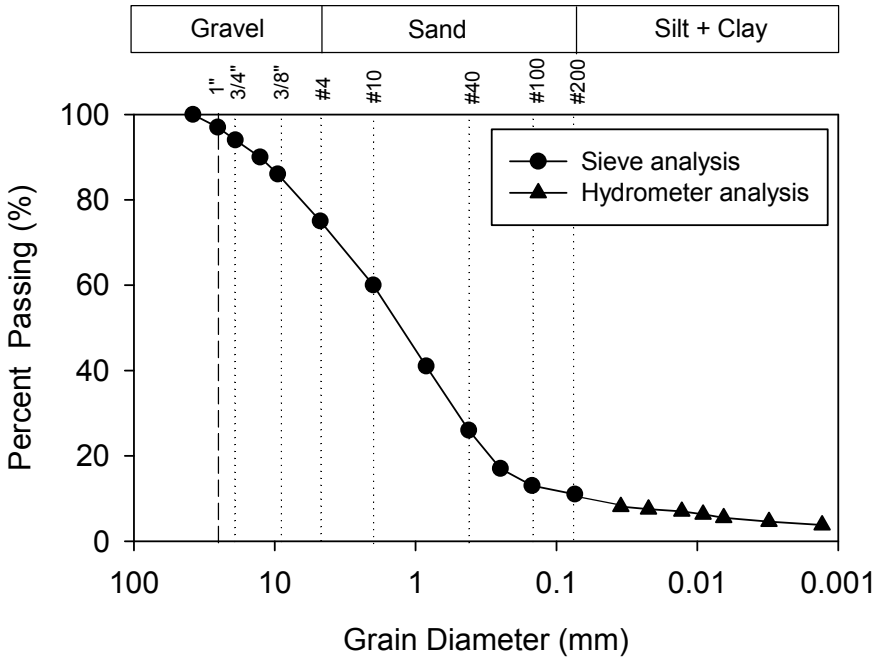


**Figure 56. 160th Street well graded sand with silt and gravel grain size distribution**

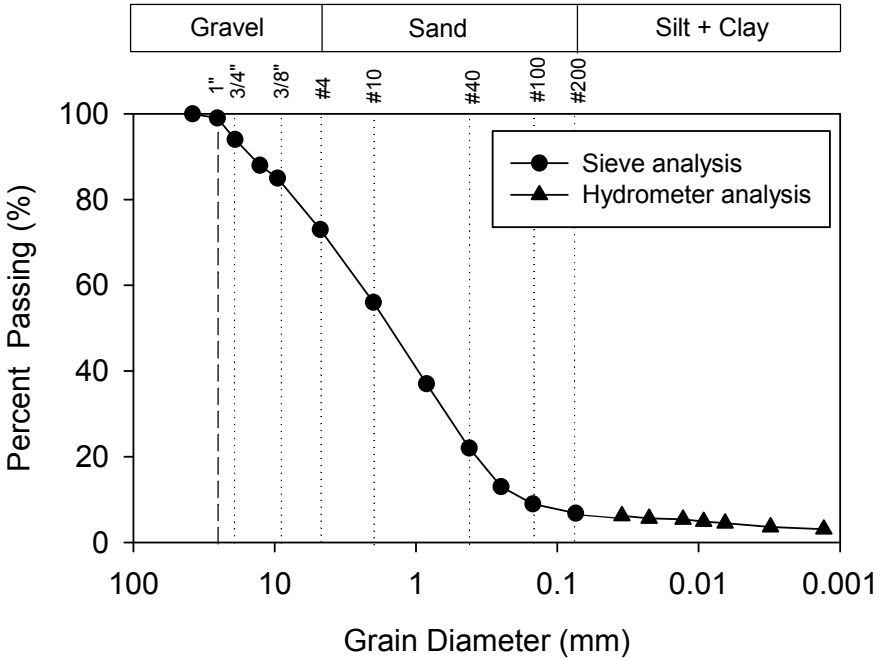


**Figure 57. 160th Street poorly graded sand with silt and gravel grain size distribution**

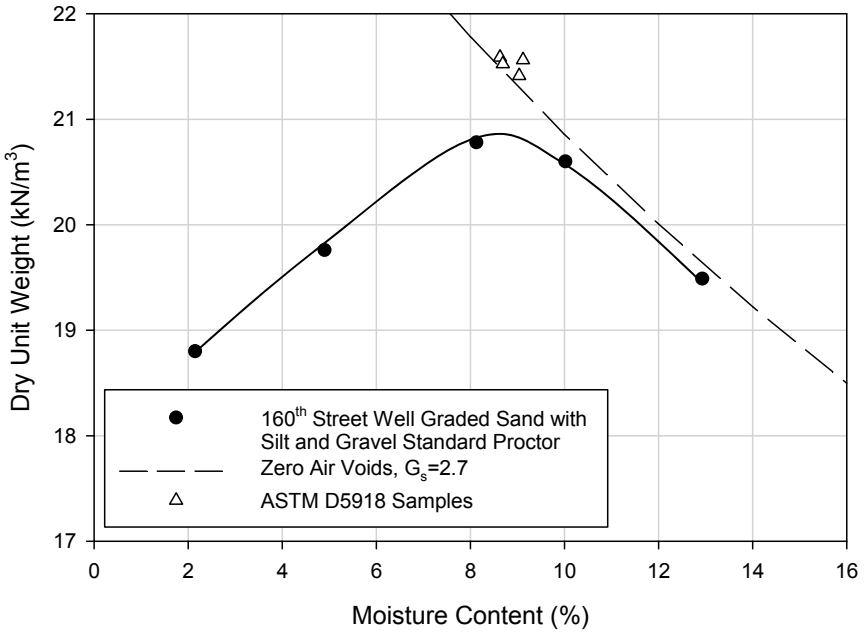


**Figure 58. 160th Street well graded sand with silt and gravel compaction data**

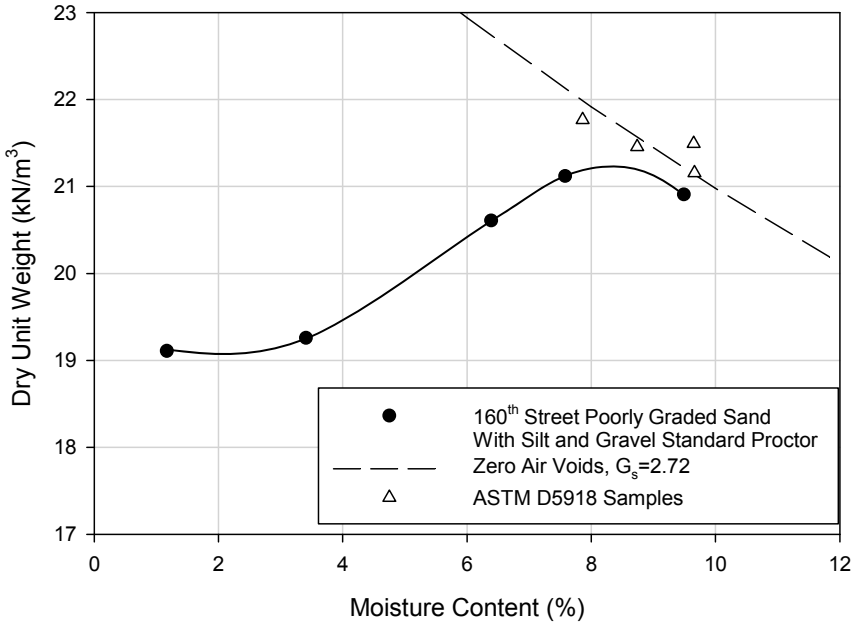


**Figure 59. 160th Street poorly graded sand with silt and gravel compaction data**

## IA I-29

Lean clay and silt with sand subgrades were sampled as part of an investigation of Interstate 29. Table 20 summarizes the soil index properties for the materials investigated.

**Table 20. Summary of IA I-29 soil index properties**

| Soil index property | Lean clay subgrade | Silt with sand subgrade |
|---|---|---|
| USCS classification | CL | ML |
| AASHTO classification | A-7-6(19) | A-4(2) |
| Coefficient of uniformity ($c_u$) | — | — |
| Coefficient of curvature ($c_c$) | — | — |
| $D_{10}$ (mm) | — | — |
| $D_{30}$ (mm) | 0.003 | 0.019 |
| $D_{60}$ (mm) | 0.018 | 0.058 |
| Gravel size (%) (> 4.75 mm) | 2.6 | 6.2 |
| Sand size (%) (4.75 – 0.074 mm) | 4.9 | 20.5 |
| Silt size (%) (0.074 – 0.002 mm) | 65.3 | 58.5 |
| Clay size (%) (≤ 0.002 mm) | 27.2 | 14.8 |
| Passing 0.074 mm (%) | 92.5 | 73.3 |
| Passing 0.02 mm (%) | 68.4 | 31.5 |
| Liquid limit (LL) | 41 | 27 |
| Plasticity index (PI) | 20 | 4 |
| Specific gravity ($G_s$) | 2.69 | 2.65 |
| Optimum moisture content (%) standard Proctor | 17.4 | 14.3 |
| Maximum dry unit weight ($kN/m^3$) standard Proctor | 16.4 | 17.8 |
| Minimum dry unit weight ($kN/m^3$) relative density | — | — |
| Maximum dry unit weight ($kN/m^3$) relative density | — | — |

The grain size distributions for the materials are presented in Figure 60 and Figure 61. The compaction curves are presented in Figure 62 and Figure 63.

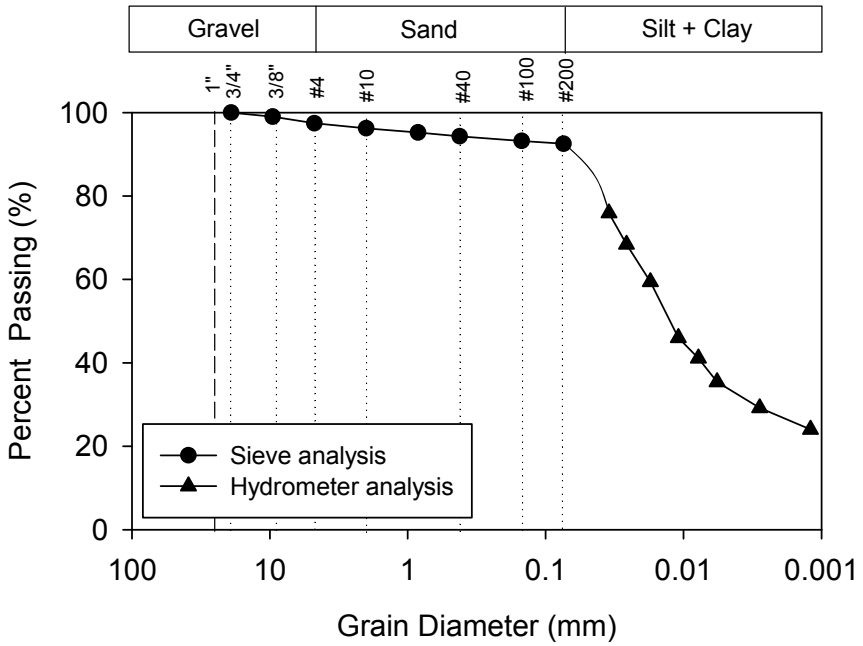


**Figure 60. IA I-29 lean clay subgrade grain size distribution**

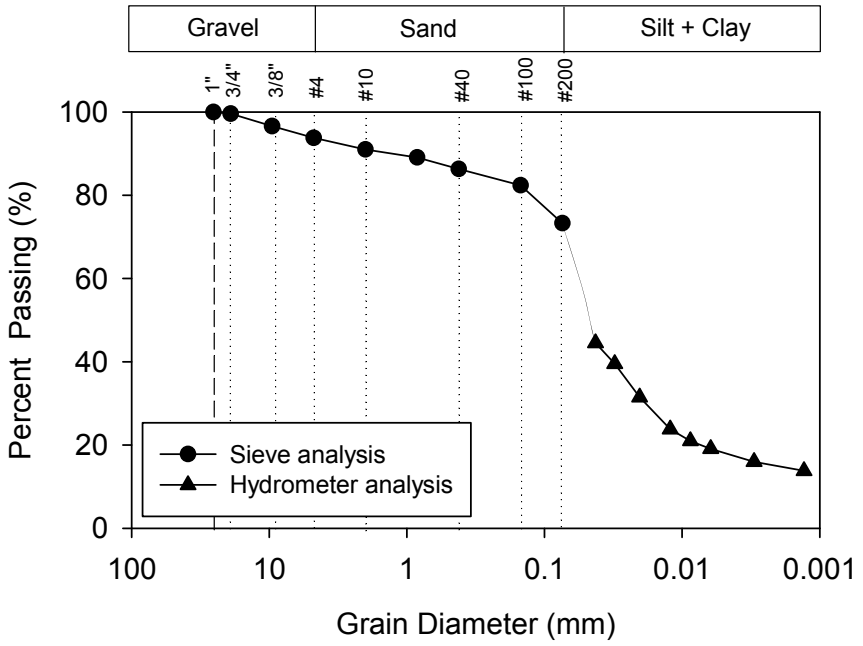


**Figure 61. IA I-29 silt with sand subgrade grain size distribution**

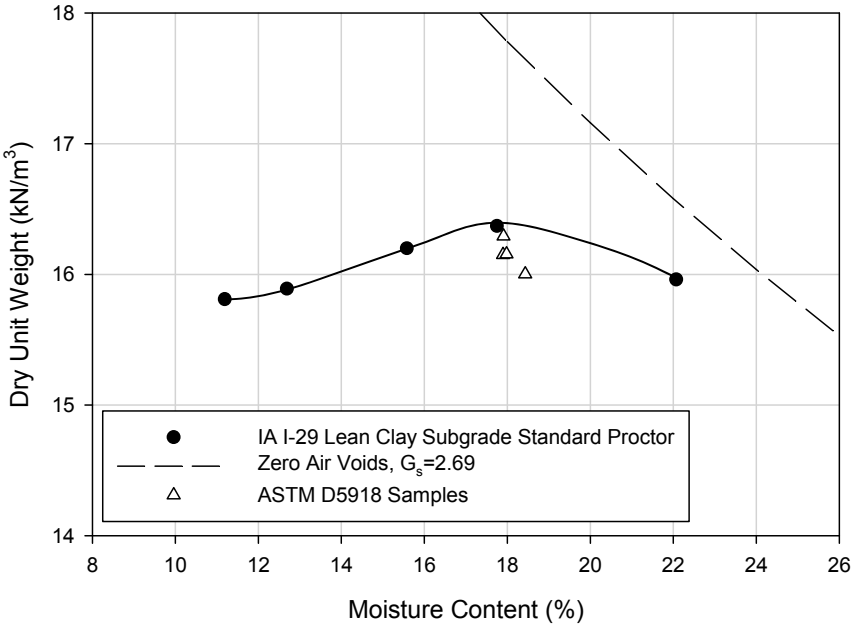


**Figure 62. IA I-29 lean clay subgrade compaction data**

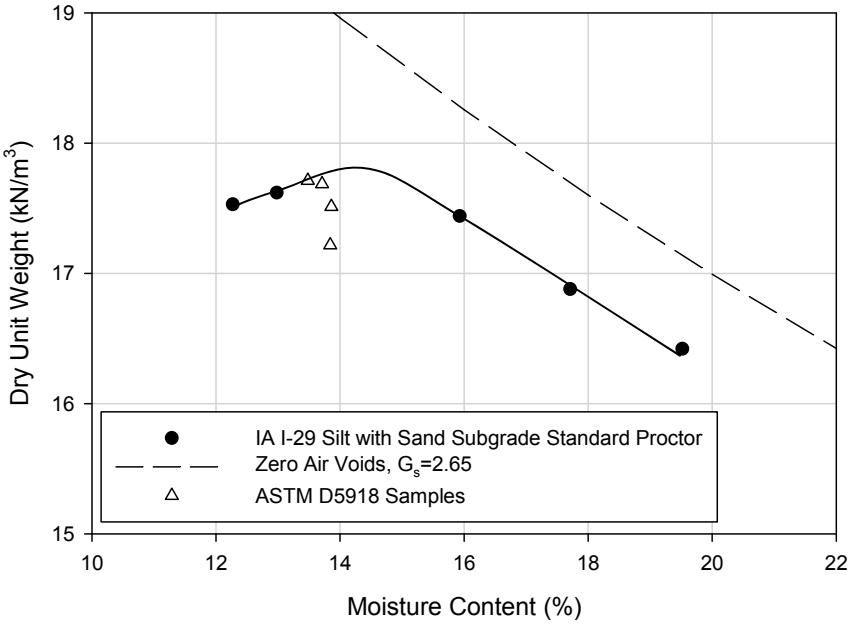


**Figure 63. IA I-29 silt with sand subgrade compaction data**

## IA US-30

The materials were collected as part of an investigation into a reconstructed portion of U.S. Highway 30. A summary of the soil index properties for the clayey sand subgrade, RPCC/RAP subbase, and limestone subbase is shown in Table 21.

**Table 21. Summary of IA US-30 soil index properties**

| Soil index property | Clayey sand subgrade | RPCC/RAP subbase | Limestone subbase |
|---|---|---|---|
| USCS classification | SC | GP-GM | GP-GM |
| AASHTO classification | A-6(2) | A-1-a | A-1-a |
| Coefficient of uniformity ($c_u$) | — | 34.3 | 20.1 |
| Coefficient of curvature ($c_c$) | — | 0.93 | 3.13 |
| $D_{10}$ (mm) | — | 0.232 | 0.539 |
| $D_{30}$ (mm) | 0.020 | 1.31 | 4.27 |
| $D_{60}$ (mm) | 0.286 | 7.97 | 10.8 |
| Gravel size (%) (> 4.75 mm) | 11.0 | 51.0 | 67.0 |
| Sand size (%) (4.75 – 0.074 mm) | 46.0 | 43.0 | 26.0 |
| Silt size (%) (0.074 – 0.002 mm) | 24.0 | 4.0 | 6.0 |
| Clay size (%) (≤ 0.002 mm) | 19.0 | 2.0 | 1.0 |
| Passing 0.074 mm (%) | 43.0 | 6.0 | 7.0 |
| Passing 0.02 mm (%) | 31.3 | 4.6 | 5.3 |
| Liquid limit (LL) | 27 | NP | NP |
| Plasticity index (PI) | 15 | NP | NP |
| Specific gravity ($G_s$) | 2.63 | 2.52 | 2.72 |
| Optimum moisture content (%) standard Proctor | 11.9 | 10.3 | — |
| Maximum dry unit weight ($kN/m^3$) standard Proctor | 18.7 | 19.3 | — |
| Minimum dry unit weight ($kN/m^3$) relative density | — | — | — |
| Maximum dry unit weight ($kN/m^3$) relative density | — | — | — |

NP—not plastic

The grain size distributions are shown in Figure 64 through Figure 66. The compaction curves for clayey sand subgrade and RPCC/RAP are presented in Figure 67 and Figure 68, respectively.

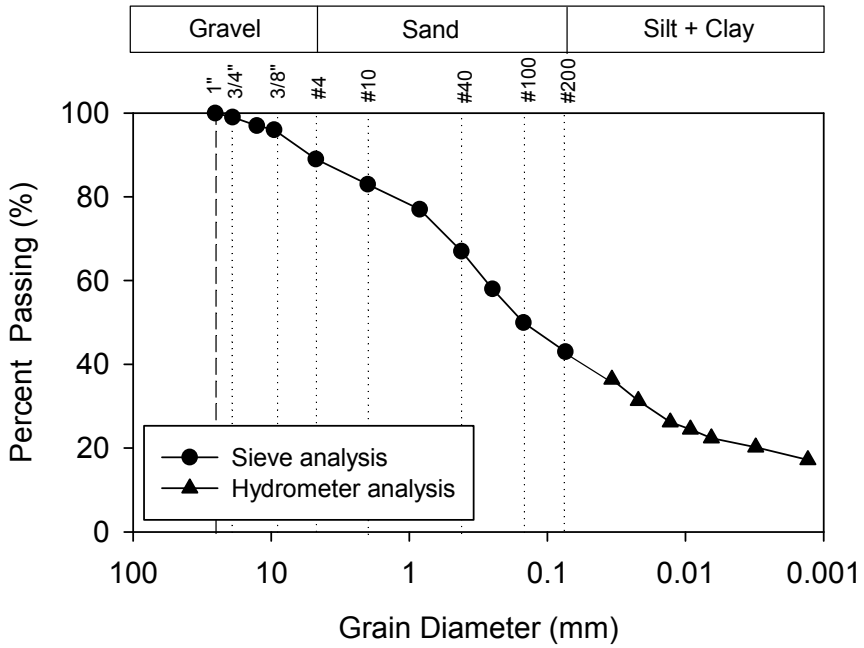


**Figure 64. IA US-30 clayey sand subgrade grain size distribution**

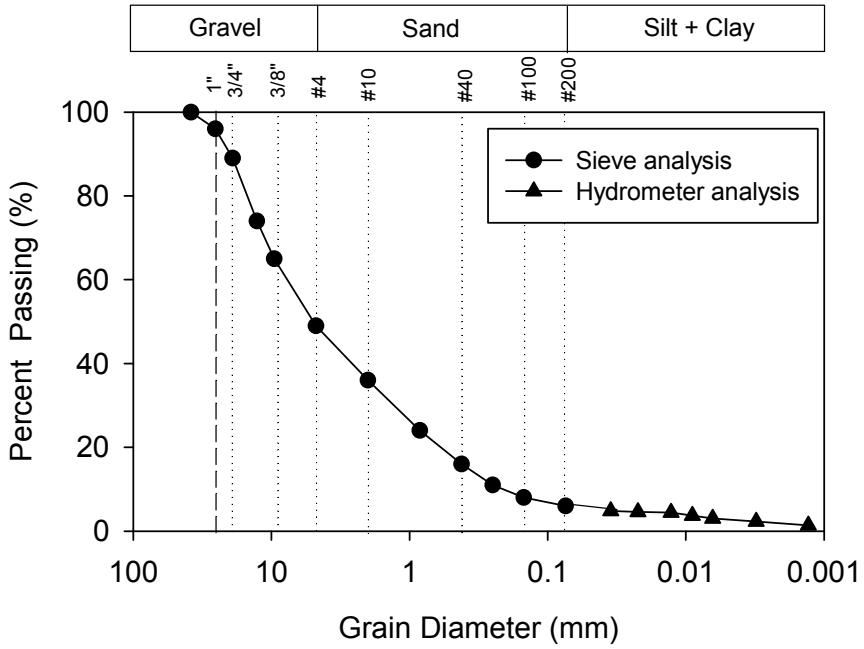


**Figure 65. IA US-30 RPCC/RAP subbase grain size distribution**

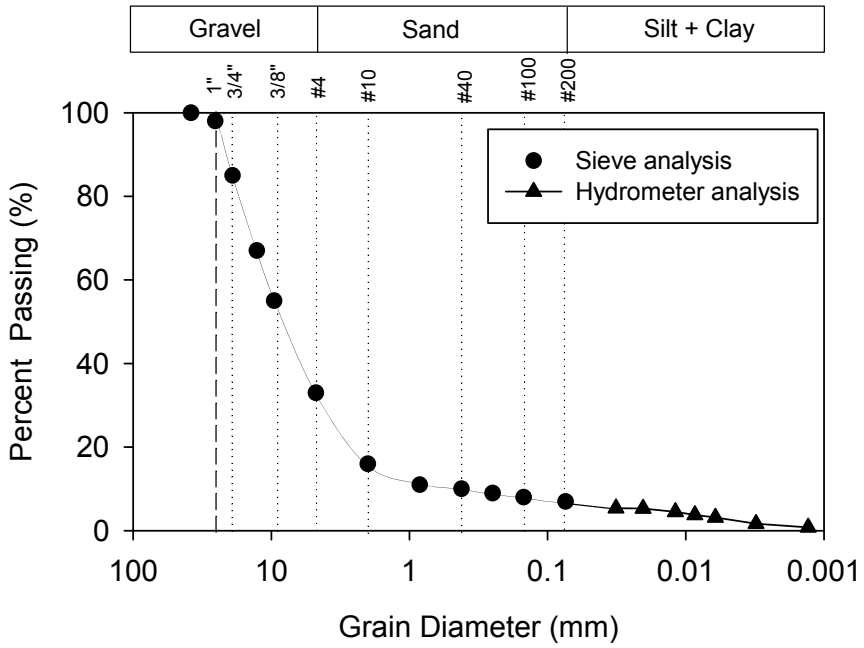


**Figure 66. IA US-30 limestone subbase grain size distribution**

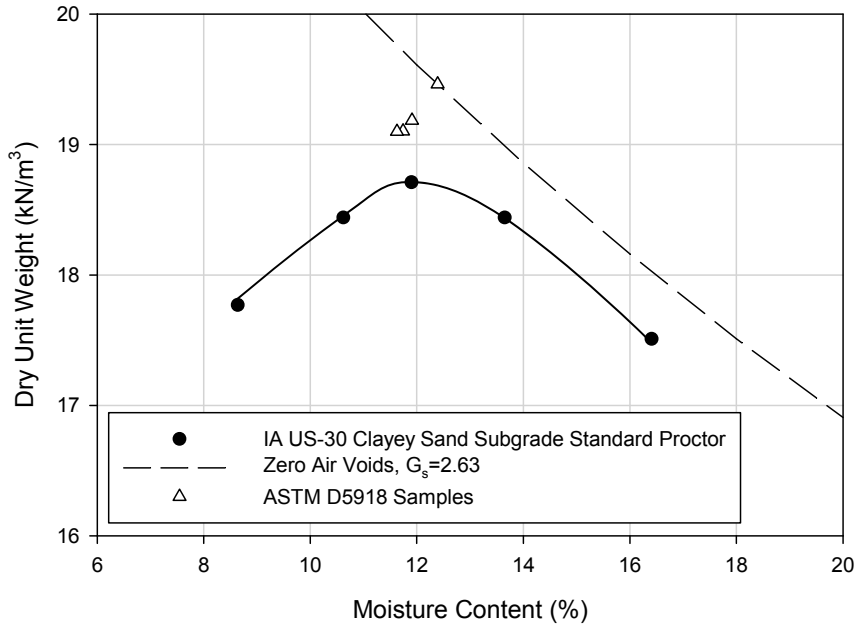


**Figure 67. IA US-30 clayey sand subgrade compaction data**

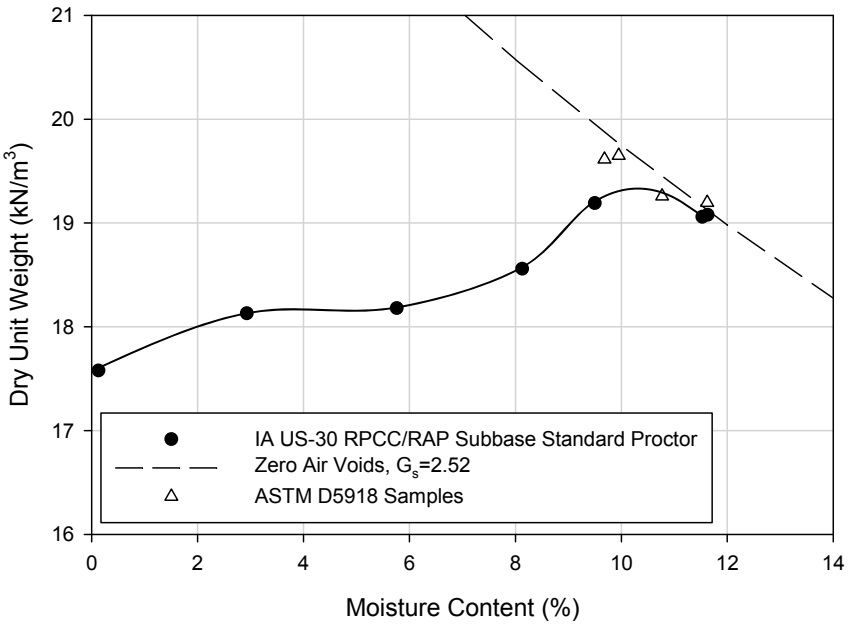


**Figure 68. IA US-30 RPCC/RAP subbase compaction data**

An RPCC material was also sampled as a part of the U.S. Highway 30 reconstruction project. The soil index properties are summarized in Table 22. Several grain size analyses were performed on the RPCC material. In addition to testing the original gradation of the RPCC, two additional samples were added to perform a study on the effects of varying fines content on frost susceptibility. One additional sample had half the fines removed and the other had all of the fines removed. In order to prepare the samples, samples with the original gradation were dry sieved over a 0.074 mm sieve to remove the fines. To create the sample with half of the original fines, half of the fines were added back to the original sample gradation and the other sample had all the fines removed. While performing this study, it was discovered that the second original gradation had a much lower fines content (5.2%) than the first original test sample did (13%). Figure 69 shows the grain size distribution of the first test sample and Figure 70 shows the grain size distribution for the second gradation, used as the original gradation in the fines content study. Figure 71 and Figure 72 show the grain size distributions of the samples with half and all of the fines removed, respectively. Figure 73 shows the compaction curve for the RPCC.

**Table 22. Summary of IA US-30 RPCC subbase soil index properties**

| Soil index property | RPCC subbase-sample 1 | RPCC subbase-sample 2 | RPCC subbase-sample 2 half of fines removed | RPCC subbase-Sample 2 all fines removed |
|---|---|---|---|---|
| USCS classification | GM | GP-GM | GP | GP |
| AASHTO classification | A-1-a | A-1-a | A-1-a | A-1-a |
| Coefficient of uniformity ($c_u$) | 176.4 | 44.3 | 39.4 | 31.7 |
| Coefficient of curvature ($c_c$) | 3.66 | 4.48 | 4.22 | 4.05 |
| $D_{10}$ (mm) | 0.057 | 0.273 | 0.323 | 0.452 |
| $D_{30}$ (mm) | 1.44 | 3.85 | 4.17 | 5.12 |
| $D_{60}$ (mm) | 9.99 | 12.1 | 12.7 | 14.3 |
| Gravel size (%) (> 4.75 mm) | 57.0 | 67.0 | 68.0 | 71.0 |
| Sand size (%) (4.75 – 0.074 mm) | 30.0 | 28.0 | 28.0 | 27.0 |
| Silt size (%) (0.074 – 0.002 mm) | 11.0 | 5.0 | 3.0 | 2.0 |
| Clay size (%) (≤ 0.002 mm) | 2.0 | 0.0 | 1.0 | 0.0 |
| Passing 0.074 mm (%) | 13.0 | 5.2 | 3.8 | 2.2 |
| Passing 0.02 mm (%) | 4.3 | 2.3 | 2.2 | 1.7 |
| Liquid limit (LL) | NP | — | — | — |
| Plasticity index (PI) | NP | — | — | — |
| Specific gravity ($G_s$) | 2.57 | — | — | — |
| Optimum moisture content (%) standard Proctor | — | — | — | — |
| Maximum dry unit weight (kN/m$^3$) standard Proctor | — | — | — | — |
| Minimum dry unit weight (kN/m$^3$) relative density | 13.2 | — | — | — |
| Maximum dry unit weight (kN/m$^3$) relative density | 16.7 | — | — | — |

NP—not plastic

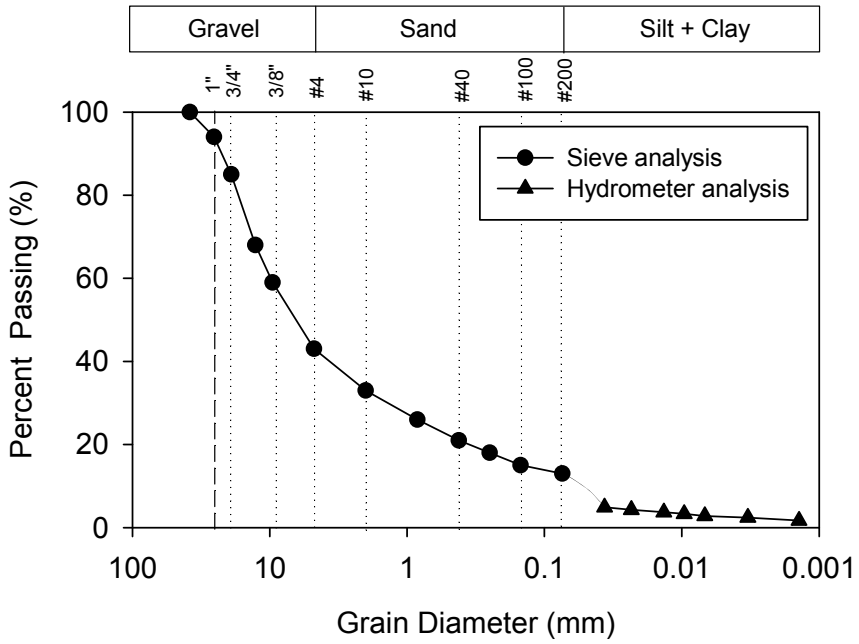


**Figure 69. IA US-30 RPCC subbase-sample 1 grain size distribution**

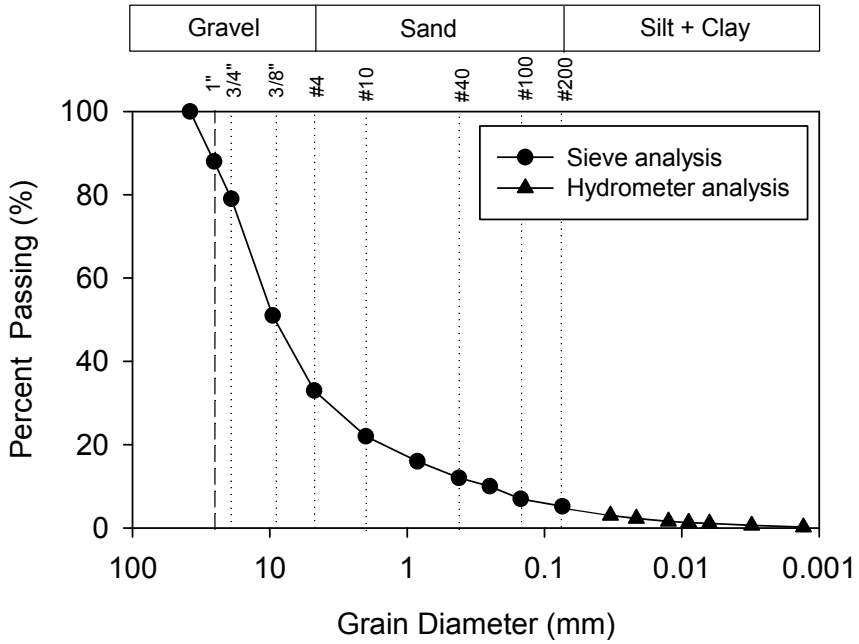


**Figure 70. IA US-30 RPCC subbase-sample 2 grain size distribution**

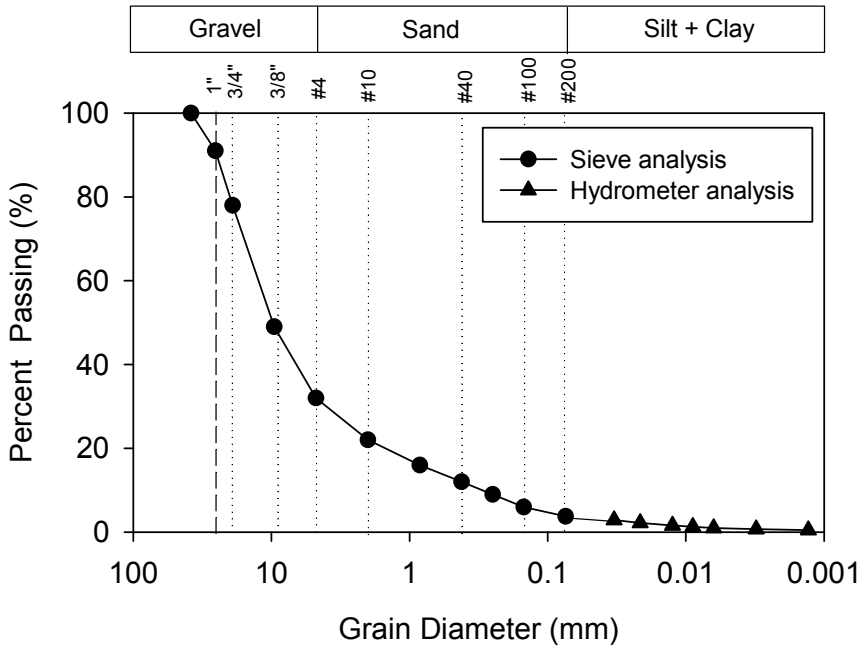


**Figure 71. IA US-30 RPCC subbase-sample 2 modified (half of fines removed) grain size distribution**

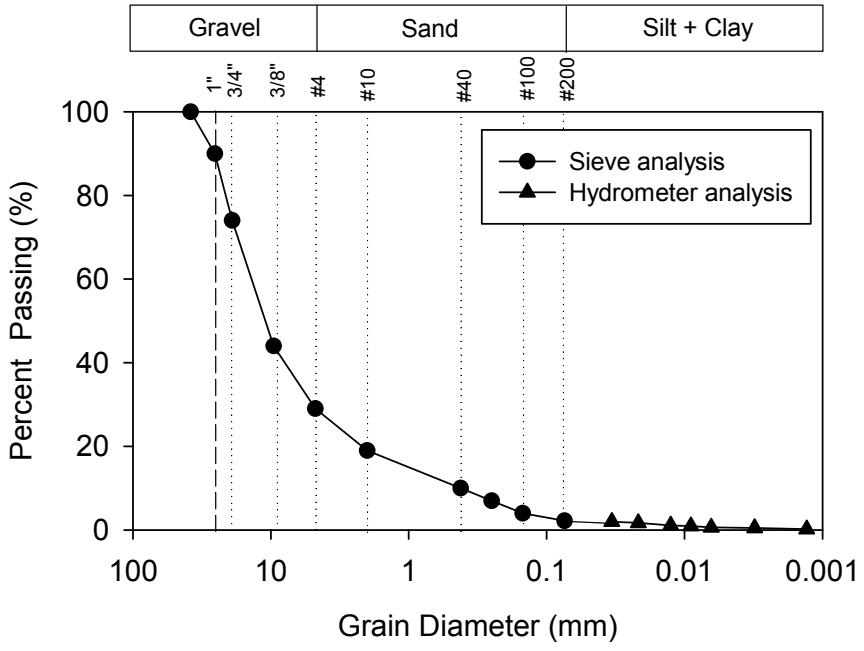


**Figure 72. IA US-30 RPCC subbase-sample 2 modified (all fines removed) grain size distribution**

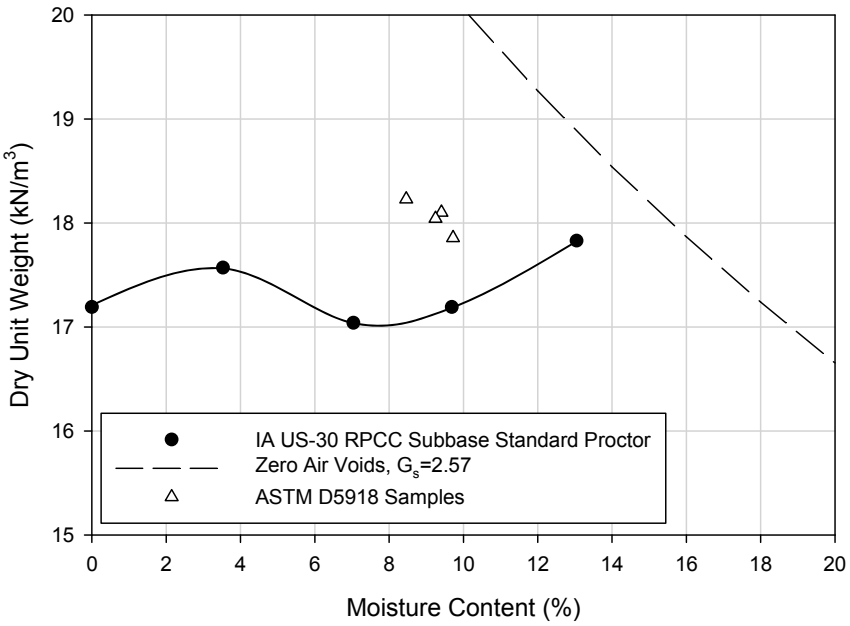


**Figure 73. IA US-30 RPCC subbase compaction data**

## MANATTS

Concrete sand subbase, RAP subbase, and RPCC/RAP subbase materials were collected from Manatts, a local material supplier. The soil index properties are summarized in Table 23. The grain size distributions are show in Figure 74 through Figure 76. The compaction curve for the concrete sand subbase is shown in Figure 77.

**Table 23. Summary of Manatts soil index properties**

| Soil index property | Concrete sand subbase | RAP Subbase | RPCC/RAP Subbase |
|---|---|---|---|
| USCS classification | SP | GW | GW |
| AASHTO classification | A-1-b | A-1-a | A-1-a |
| Coefficient of uniformity ($c_u$) | 3.27 | 13.3 | 10.7 |
| Coefficient of curvature ($c_c$) | 0.88 | 1.38 | 2.63 |
| $D_{10}$ (mm) | 0.318 | 0.507 | 1.39 |
| $D_{30}$ (mm) | 0.539 | 2.17 | 7.36 |
| $D_{60}$ (mm) | 1.04 | 6.73 | 14.8 |
| Gravel size (%) (> 4.75 mm) | 2.0 | 52.0 | 79.0 |
| Sand size (%) (4.75 – 0.074 mm) | 98.0 | 45.0 | 19.0 |
| Silt size (%) (0.074 – 0.002 mm) | 0.0 | 2.0 | 2.0 |
| Clay size (%) (≤ 0.002 mm) | 0.0 | 1.0 | 0.0 |
| Passing 0.074 mm (%) | 0.3 | 2.9 | 2.2 |
| Passing 0.02 mm (%) | — | 2.5 | 1.4 |
| Liquid limit (LL) | NP | NP | NP |
| Plasticity index (PI) | NP | NP | NP |
| Specific gravity ($G_s$) | 2.68 | 2.47 | 2.62 |
| Optimum moisture content (%) standard Proctor | — | — | — |
| Maximum dry unit weight ($kN/m^3$) standard Proctor | — | — | — |
| Minimum dry unit weight ($kN/m^3$) relative density | — | 13.7 | 14.7 |
| Maximum dry unit weight ($kN/m^3$) relative density | — | 14.3 | 16.4 |

NP—not plastic

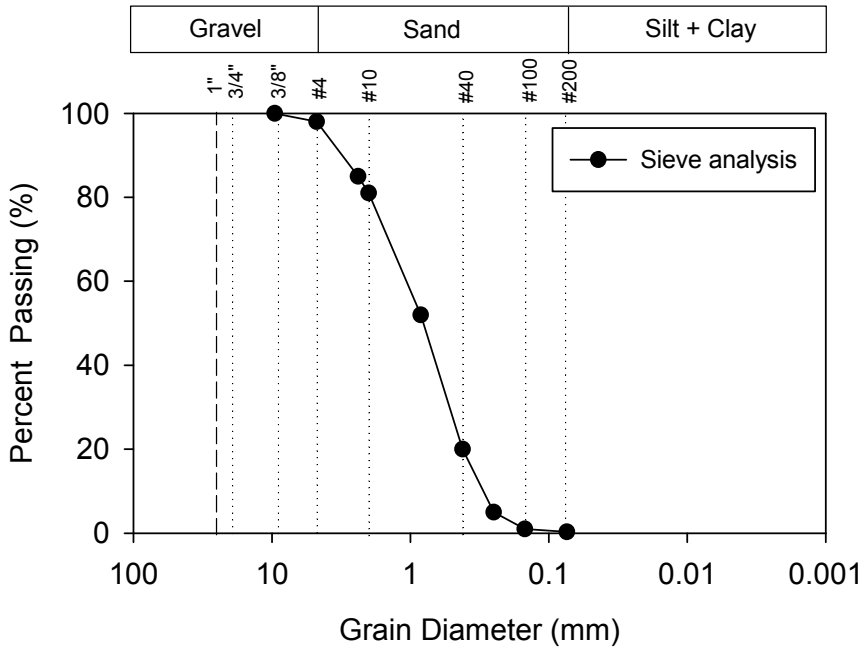


**Figure 74. Manatts concrete sand subbase grain size distribution**

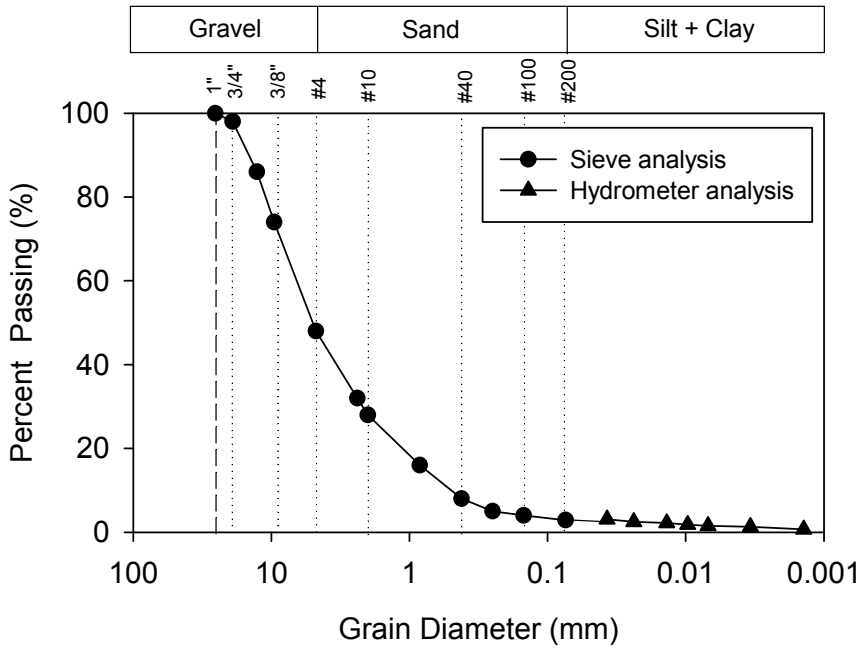


**Figure 75. Manatts RAP subbase grain size distribution**

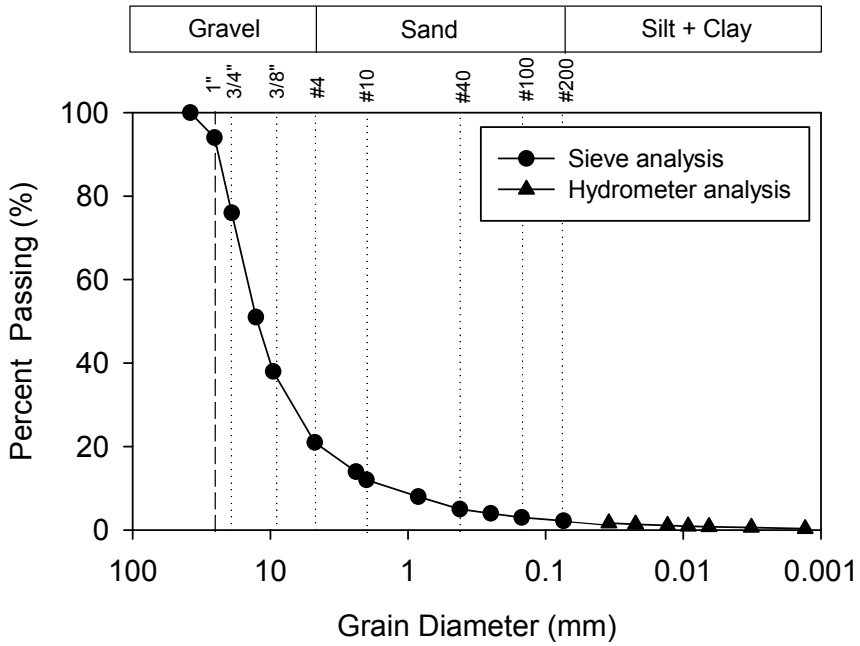


**Figure 76. Manatts RPCC/RAP subbase grain size distribution**

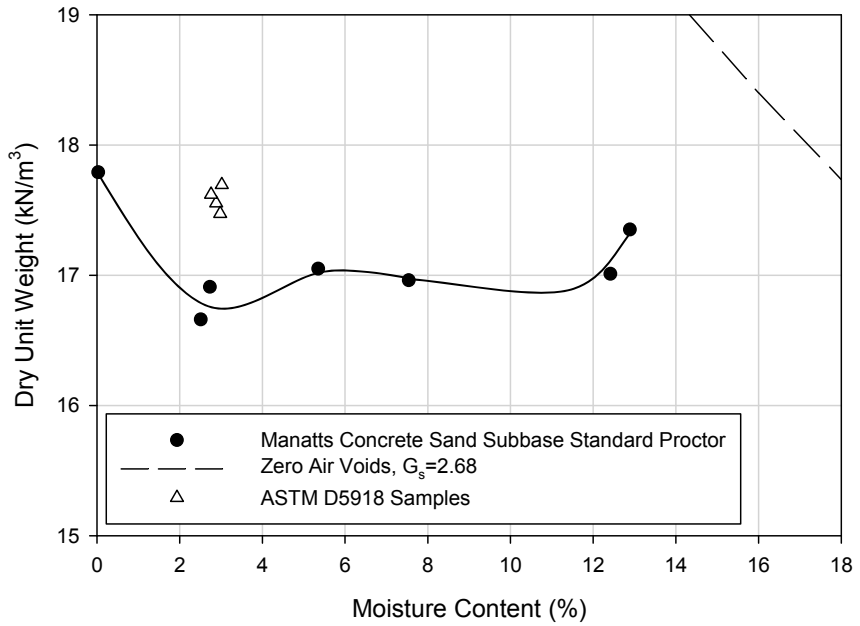


**Figure 77. Manatts concrete sand subbase compaction data**

## MARTIN MARIETTA MATERIALS

A Limestone subbase material was collected from Martin Marietta Materials. The soil index properties are summarized in Table 24 and the grain size distribution is shown in Figure 78.

**Table 24. Summary of Martin Marietta Materials soil index properties**

| Soil index property | Crushed limestone subbase |
|---|---|
| USCS classification | GP-GM |
| AASHTO classification | A-1-a |
| Coefficient of uniformity ($c_u$) | 61.9 |
| Coefficient of curvature ($c_c$) | 11.4 |
| $D_{10}$ (mm) | 0.171 |
| $D_{30}$ (mm) | 4.54 |
| $D_{60}$ (mm) | 10.6 |
| Gravel size (%) (> 4.75 mm) | 59.0 |
| Sand size (%) (4.75 – 0.074 mm) | 23.0 |
| Silt size (%) (0.074 – 0.002 mm) | 7.0 |
| Clay size (%) (≤ 0.002 mm) | 1.0 |
| Passing 0.074 mm (%) | 7.8 |
| Passing 0.02 mm (%) | 5.8 |
| Liquid limit (LL) | NP |
| Plasticity index (PI) | NP |
| Specific gravity ($G_s$) | 2.71 |
| Optimum moisture content (%) standard Proctor | — |
| Maximum dry unit weight (kN/m$^3$) standard Proctor | — |
| Minimum dry unit weight (kN/m$^3$) relative density | 16.8 |
| Maximum dry unit weight (kN/m$^3$) relative density | 17.8 |

NP—not plastic

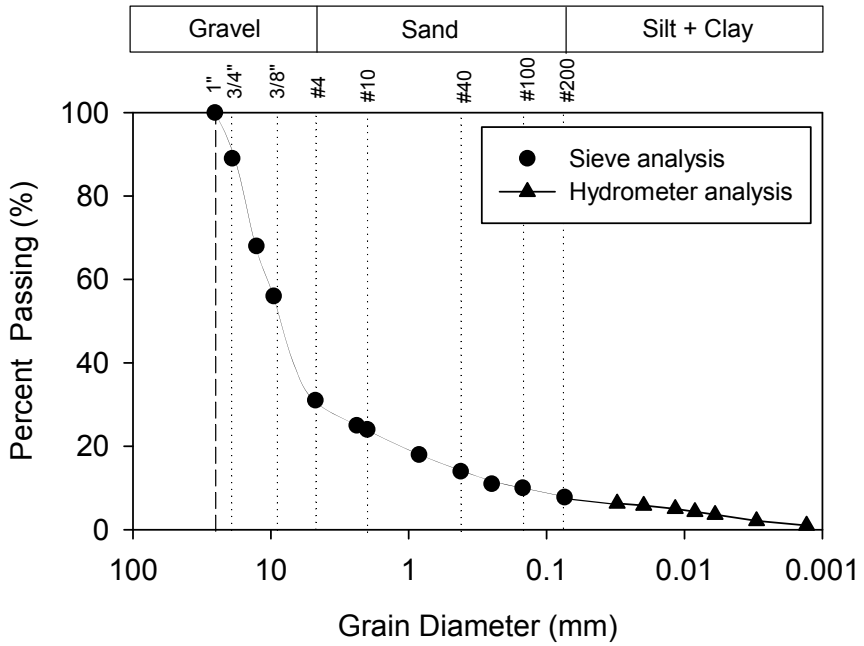


**Figure 78. Martin Marietta Materials crushed limestone subbase grain size distribution**

## MI I-96

A clayey sand subgrade and RPCC material used in a cement treated base were sampled as part of an investigation of Interstate 96. Table 25 summarizes the soil index properties. The grain size distributions for the materials are presented in Figure 79 and Figure 80. The compaction curve for the clayey sand subgrade is presented in Figure 81.

**Table 25. Summary of MI I-96 soil index properties**

| Soil index property | Clayey sand subgrade | CTB |
|---|---|---|
| USCS classification | SC | GP |
| AASHTO classification | A-4(1) | A-1-a |
| Coefficient of uniformity ($c_u$) | 41.1 | 1.93 |
| Coefficient of curvature ($c_c$) | 2.85 | 1.07 |
| $D_{10}$ (mm) | 0.004 | 9.75 |
| $D_{30}$ (mm) | 0.042 | 14.0 |
| $D_{60}$ (mm) | 0.158 | 18.9 |
| Gravel size (%) (> 4.75 mm) | 4.4 | 99.3 |
| Sand size (%) (4.75 – 0.074 mm) | 52.0 | 0.5.0 |
| Silt size (%) (0.074 – 0.002 mm) | 38.3 | 0.2 |
| Clay size (%) (≤ 0.002 mm) | 5.3 | |
| Passing 0.074 mm (%) | 43.6 | 0.2 |
| Passing 0.02 mm (%) | 20.0 | — |
| Liquid limit (LL) | 21 | NP |
| Plasticity index (PI) | 10 | NP |
| Specific gravity ($G_s$) | 2.66 | — |
| Optimum moisture content (%) standard Proctor | 9.5 | — |
| Maximum dry unit weight (kN/m$^3$) standard Proctor | 20.1 | — |
| Minimum dry unit weight (kN/m$^3$) relative density | — | 12.3 |
| Maximum dry unit weight (kN/m$^3$) relative density | — | 13.6 |

NP—not plastic

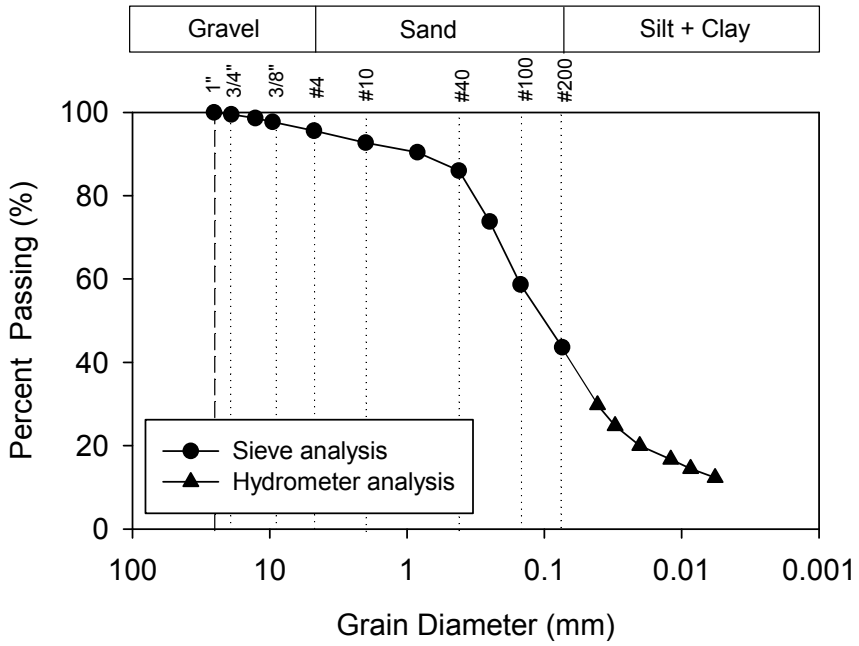


**Figure 79. MI I-96 clayey sand subgrade grain size distribution**

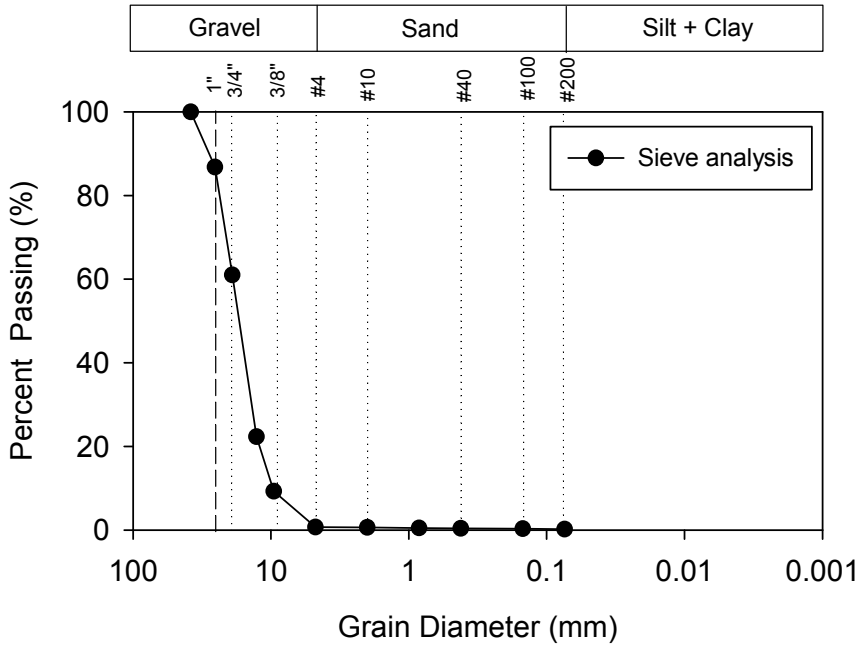


**Figure 80. MI I-96 CTB grain size distribution**

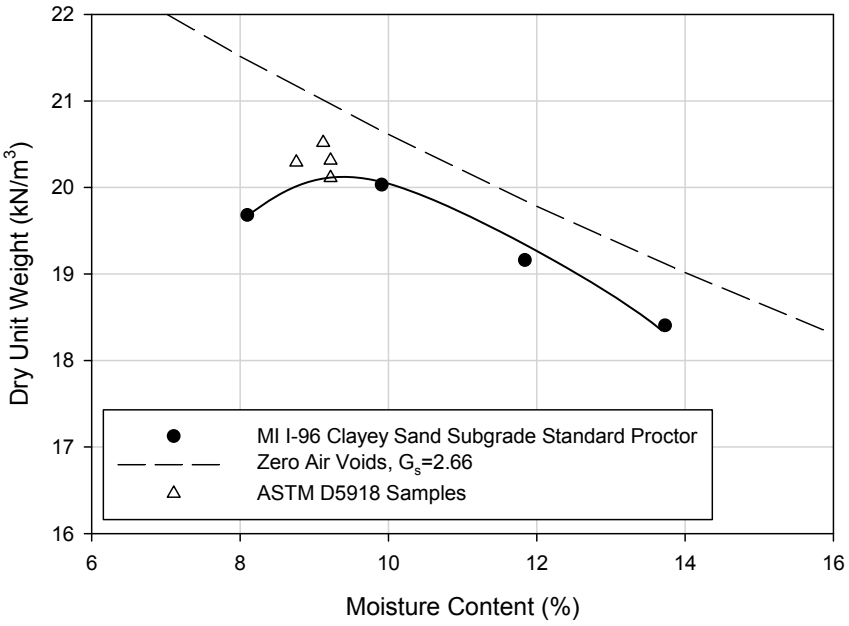


**Figure 81. MI I-96 clayey sand subgrade compaction data**

## PA US-22

A sandy lean clay subgrade material was sampled as part of an investigation of U.S. Highway 22. Table 26 summarizes the soil index properties..

**Table 26. Summary of PA US-22 soil index properties**

| Soil index property | Sandy lean clay subgrade |
|---|---|
| USCS classification | CL |
| AASHTO classification | A-6(6) |
| Coefficient of uniformity ($c_u$) | — |
| Coefficient of curvature ($c_c$) | — |
| $D_{10}$ (mm) | — |
| $D_{30}$ (mm) | 0.005 |
| $D_{60}$ (mm) | 0.089 |
| Gravel size (%) (> 4.75 mm) | 10.6 |
| Sand size (%) (4.75 – 0.074 mm) | 31.0 |
| Silt size (%) (0.074 – 0.002 mm) | 36.2 |
| Clay size (%) (≤ 0.002 mm) | 22.2 |
| Passing 0.074 mm (%) | 58.4 |
| Passing 0.02 mm (%) | 43.8 |
| Liquid limit (LL) | 37 |
| Plasticity index (PI) | 15 |
| Specific gravity ($G_s$) | 2.72 |
| Optimum moisture content (%) standard Proctor | 16.3 |
| Maximum dry unit weight ($kN/m^3$) standard Proctor | 17.7 |
| Minimum dry unit weight ($kN/m^3$) relative density | — |
| Maximum dry unit weight ($kN/m^3$) relative density | — |

The grain size distribution is presented in Figure 82 and the compaction curve is presented in Figure 83

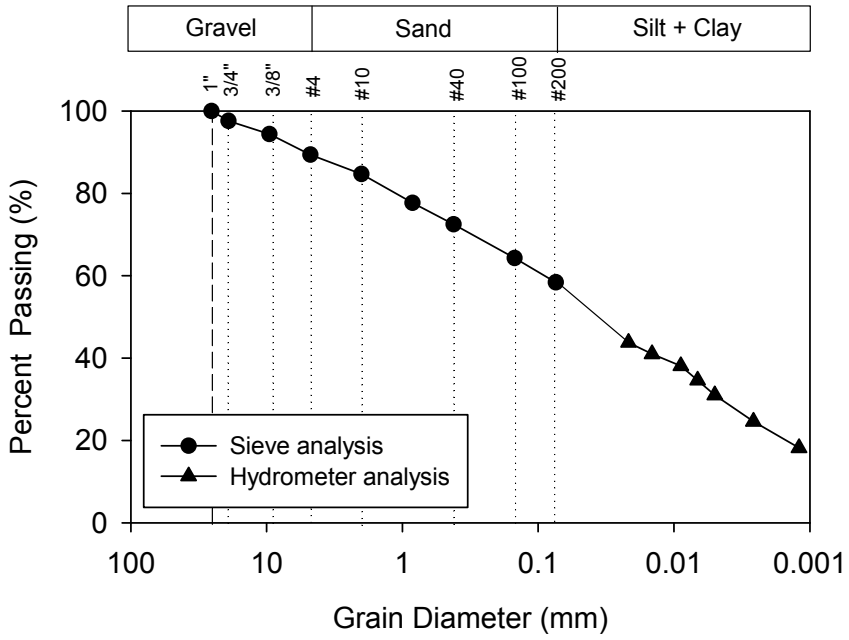


**Figure 82. PA US-22 sandy lean clay subgrade grain size distribution**

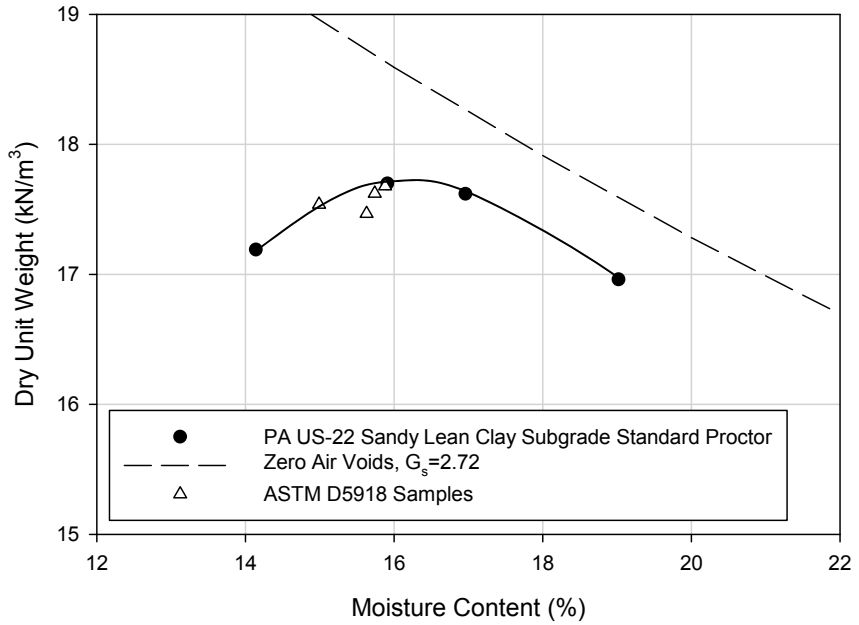


**Figure 83. PA US-22 sandy lean clay subgrade compaction data**

## LOESS

A loess material was sampled from the large deposits in western Iowa. The soil was used in a stabilization study to observe the effects of using portland cement and fly ash as stabilizers. The fly ash was from the Municipal Power Plant in Ames, Iowa. Appendix F contains X-ray diffraction, X-ray fluorescence, and set time test results for the fly ash. The soil index properties are shown in Table 27.

**Table 27. Summary of Loess soil index properties**

| Soil index property | Loess | Cement-stabilized loess | Fly ash-stabilized loess |
|---|---|---|---|
| USCS classification | ML | ML | ML |
| AASHTO classification | A-4(0) | A-4(0) | A-4(2) |
| Coefficient of uniformity ($c_u$) | — | 15.0 | — |
| Coefficient of curvature ($c_c$) | — | 3.86 | — |
| $D_{10}$ (mm) | — | 0.002 | — |
| $D_{30}$ (mm) | 0.013 | 0.017 | 0.011 |
| $D_{60}$ (mm) | 0.0281 | 0.335 | 0.0301 |
| Gravel size (%) (> 4.75 mm) | 0.0 | 0.0 | 0.0 |
| Sand size (%) (4.75 – 0.074 mm) | 0.0 | 15.0 | 3.0 |
| Silt size (%) (0.074 – 0.002 mm) | 82.0 | 75.0 | 82.0 |
| Clay size (%) (≤ 0.002 mm) | 18.0 | 10.0 | 15.0 |
| Passing 0.074 mm (%) | 100.0 | 85.0 | 97.0 |
| Passing 0.02 mm (%) | 43.3 | 37.2 | 42.6 |
| Liquid limit (LL) | 29 | — | — |
| Plasticity index (PI) | 6 | — | — |
| Specific gravity ($G_s$) | 2.7 | 2.74 | 2.68 |
| Optimum moisture content (%) standard Proctor | 16.7 | 18.6 | 16.7 |
| Maximum dry unit weight ($kN/m^3$) standard Proctor | 16.2 | 16.6 | 16.9 |
| Minimum dry unit weight ($kN/m^3$) relative density | — | — | — |
| Maximum dry unit weight ($kN/m^3$) relative density | — | — | — |

The grain size distributions are shown in Figure 84 through Figure 86. The compaction curves are shown in Figure 87 through Figure 89.

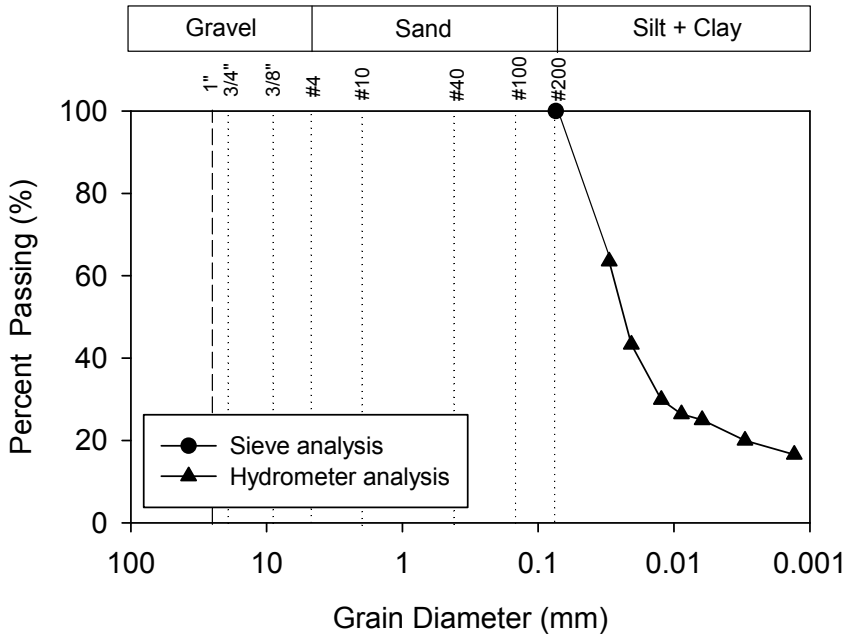


**Figure 84. Loess grain size distribution**

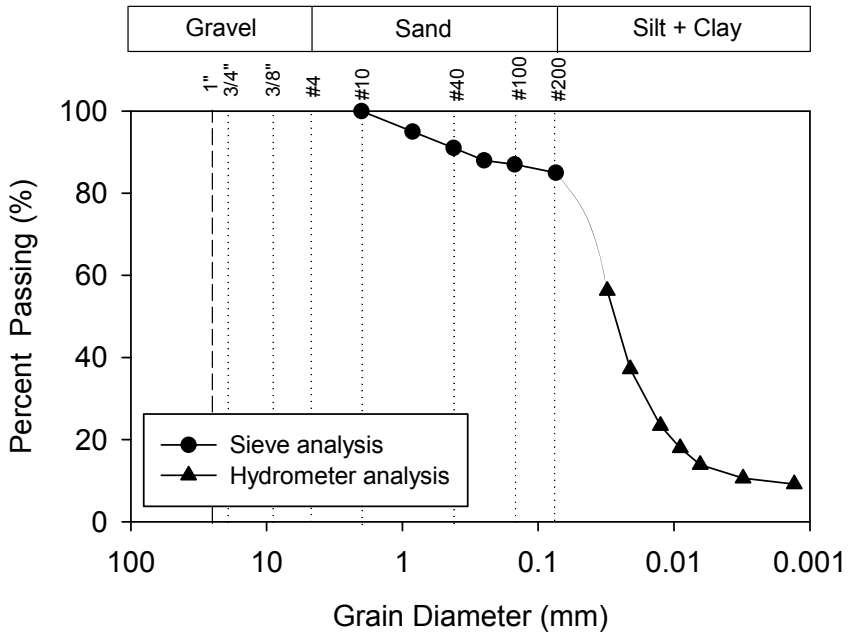


**Figure 85. Cement-stabilized loess grain size distribution**

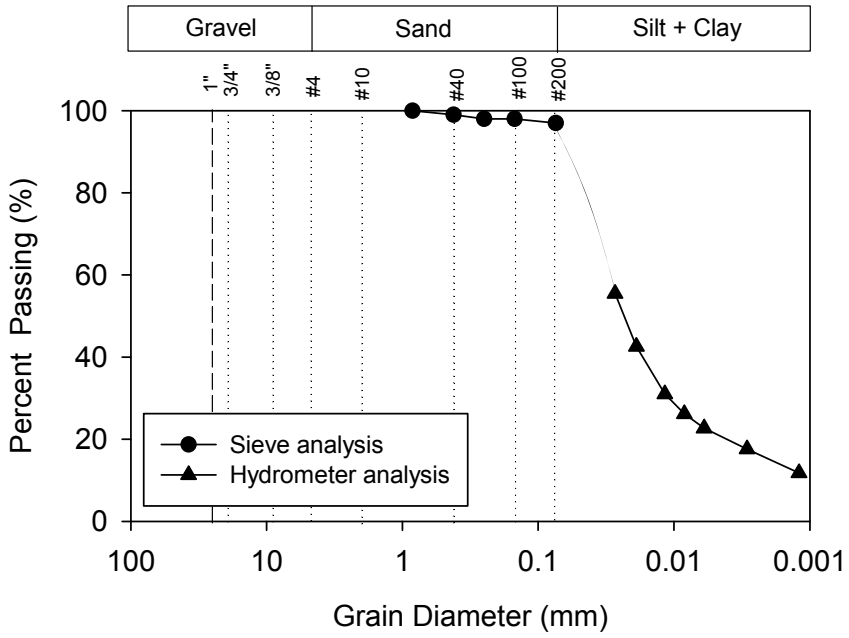


**Figure 86. Fly ash-stabilized loess grain size distribution**

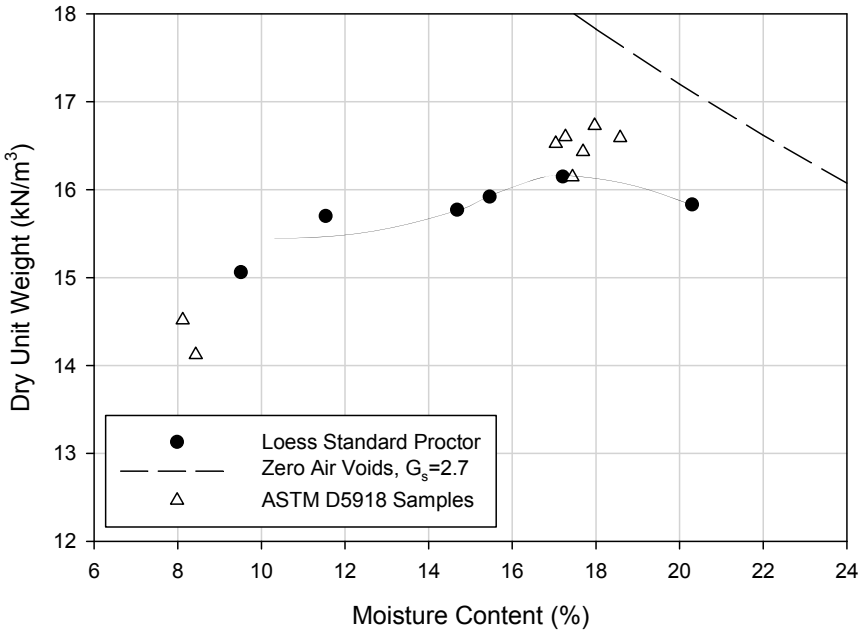


**Figure 87. Loess compaction data**

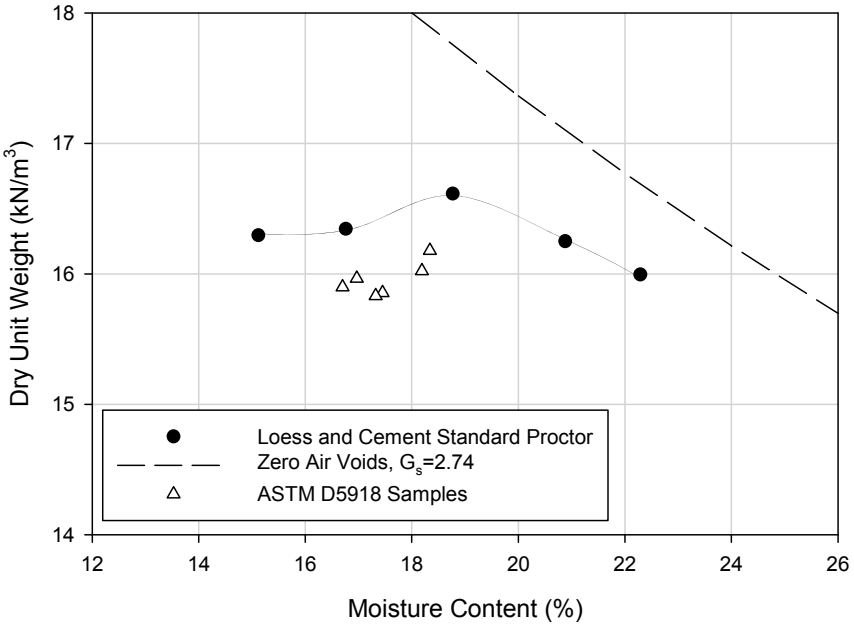


**Figure 88. Cement-stabilized loess compaction data**

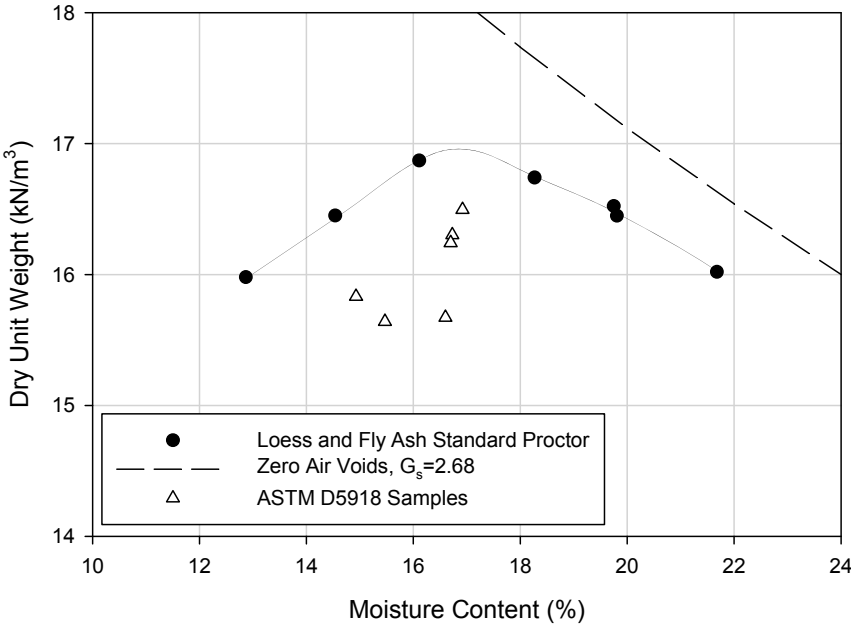


**Figure 89. Fly ash-stabilized loess compaction data**

## WI US-10

A sandy lean clay was sampled as part of an investigation of U.S. Highway 10. Table 28 summarizes the soil index properties. The grain size distribution is presented in Figure 90 and the compaction curve is presented in Figure 91.

**Table 28. Summary of WI US-10 soil index properties**

| Soil index property | Sandy lean clay subgrade |
|---|---|
| USCS classification | CL |
| AASHTO classification | A-6(8) |
| Coefficient of uniformity ($c_u$) | — |
| Coefficient of curvature ($c_c$) | — |
| $D_{10}$ (mm) | — |
| $D_{30}$ (mm) | 0.014 |
| $D_{60}$ (mm) | 0.081 |
| Gravel size (%) (> 4.75 mm) | 13.0 |
| Sand size (%) (4.75 – 0.074 mm) | 28.0 |
| Silt size (%) (0.074 – 0.002 mm) | 46.0 |
| Clay size (%) (≤ 0.002 mm) | 13.0 |
| Passing 0.074 mm (%) | 59.0 |
| Passing 0.02 mm (%) | 38.9 |
| Liquid limit (LL) | 38 |
| Plasticity index (PI) | 18 |
| Specific gravity ($G_s$) | 2.69 |
| Optimum moisture content (%) standard Proctor | 12.0 |
| Maximum dry unit weight (kN/m$^3$) standard Proctor | 18.6 |
| Minimum dry unit weight (kN/m$^3$) relative density | — |
| Maximum dry unit weight (kN/m$^3$) relative density | — |

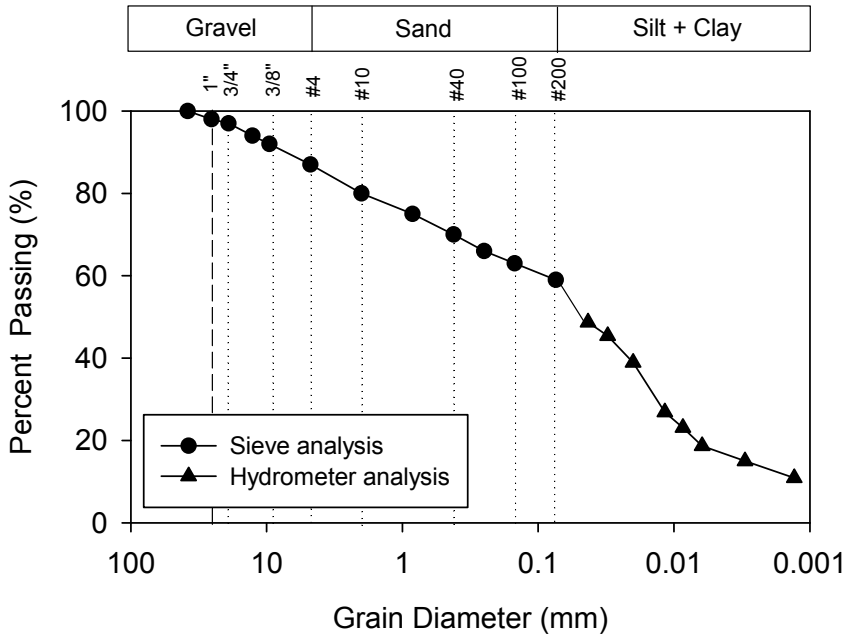


**Figure 90. WI US-10 sand lean clay subgrade grain size distribution**

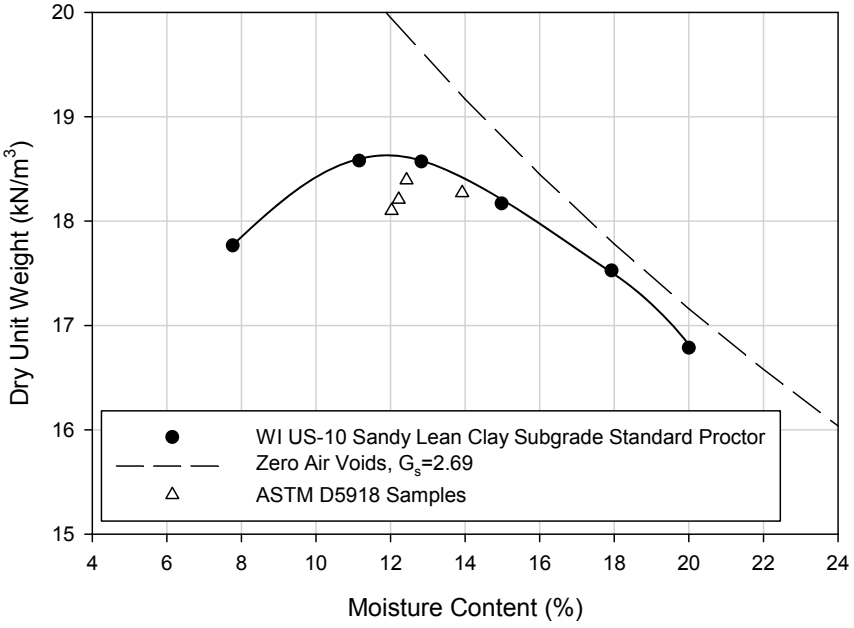


**Figure 91. WI US-10 sandy lean clay subgrade compaction data**

# CHAPTER 5. RESULTS AND DISCUSSION

This chapter presents and discusses laboratory and in situ test results. The laboratory investigations included durability and frost-heave and thaw-weakening results. The laboratory tests were performed on materials presented in Chapter 4. The in situ tests were performed at various times of the year across Iowa to observe seasonal variability.

## DURABILITY TESTS

Results related to the durability of pavement foundation materials are presented in the following two sections, 2-in. x 2-in. compressive strength and wet-dry and freeze-thaw durability.

### 2-in. x 2-in. Compressive Strength

The unconfined compressive strength (UCS) of cement and fly ash stabilized loess was determined at different mix proportions and moisture contents to target stabilization and moisture contents for freeze-thaw durability and frost-heave and thaw-weakening tests. Two sets of three 2-in. x 2-in. samples were made for each stabilizer/initial moisture content. The samples were cured at 38°C for 7 days before UCS testing. One set was vacuum saturated after curing. The results of the three samples were averaged to determine more representative results. The average results of the cement and fly ash treated samples are shown in Table 29 through Table 32.

Dempsey and Thompson (1973) performed UCS tests on samples that had been exposed to 10 freeze-thaw cycles and compared them to vacuum saturated samples. They found that there is a linear relationship between the UCS after freeze-thaw cycling and the UCS after vacuum saturation. They also found that the moisture content after freeze-thaw cycling showed a near 1:1 relationship with the moisture content after vacuum saturation.

**Table 29. Average 2-in. x 2-in. cement stabilized loess summary**

| Stabilizer content (%) | Initial moisture content (%) | Moisture content with cement (%) | Dry unit weight with cement (kN/m$^3$) | Failure stress (kPa) |
|---|---|---|---|---|
| 0 | 17.6 | 17.9 | 15.8 | 200 |
| 3 | 12.8 | 11.3 | 15.9 | 1342 |
| | 17.6 | 16.2 | 15.8 | 1337 |
| | 18.3 | 16.4 | 16.0 | 1270 |
| | 21.0 | 19.5 | 16.4 | 1379 |
| | 22.6 | 21.2 | 16.4 | 1203 |
| 5 | 12.8 | 11.6 | 15.8 | 1889 |
| | 17.6 | 15.3 | 15.7 | 2095 |
| | 18.3 | 16.1 | 15.9 | 2584 |
| | 21.0 | 18.7 | 16.4 | 2141 |
| | 22.6 | 20.8 | 16.5 | 2054 |
| 7 | 12.8 | 11.3 | 15.8 | 2587 |
| | 17.6 | 15.4 | 15.8 | 3027 |
| | 18.3 | 15.5 | 15.9 | 2975 |
| | 21.0 | 17.5 | 16.5 | 2942 |
| | 22.6 | 20.0 | 16.7 | 2741 |
| 9 | 13.4 | 11.8 | 15.3 | 3121 |
| | 16.3 | 14.5 | 15.4 | 3417 |
| | 18.6 | 16.4 | 15.9 | 3889 |
| | 20.2 | 17.8 | 16.3 | 3960 |
| | 22.2 | 19.9 | 16.6 | 3881 |
| 11 | 13.3 | 11.7 | 15.2 | 3346 |
| | 16.4 | 14.3 | 15.5 | 4484 |
| | 18.6 | 15.8 | 15.9 | 4537 |
| | 20.3 | 17.5 | 16.3 | 4330 |
| | 22.4 | 19.6 | 16.6 | 4379 |
| 13 | 13.5 | 11.3 | 15.3 | 3956 |
| | 16.4 | 14.1 | 15.5 | 4651 |
| | 18.6 | 15.7 | 16.0 | 4878 |
| | 20.3 | 17.4 | 16.2 | 5406 |
| | 22.3 | 19.2 | 16.5 | 5363 |
| | 23.1 | 20.5 | 16.5 | 4801 |
| | 25.7 | 22.2 | 16.3 | 3091 |

**Table 30. Average 2-in. x 2-in. vacuum saturated cement stabilized loess summary**

| Stabilizer content (%) | Initial moisture content (%) | Moisture content with cement (%) | Dry unit weight with cement (kN/m3) | Vacuum saturation moisture content (%) | Failure stress (kPa) | Change in moisture content (%) |
|---|---|---|---|---|---|---|
| 0 | 17.6 | 17.9 | 15.8 | Failed | Failed | — |
| 3 | 12.8 | 11.3 | 15.8 | 24.9 | 792 | 13.6 |
| | 17.6 | 16.2 | 15.7 | 25.9 | 873 | 9.7 |
| | 18.3 | 16.4 | 15.9 | 24.9 | 872 | 8.5 |
| | 21.0 | 19.5 | 16.3 | 23.5 | 1032 | 4 |
| | 22.6 | 21.2 | 16.4 | 23.0 | 664 | 1.8 |
| 5 | 12.8 | 11.6 | 15.8 | 24.0 | 1133 | 12.4 |
| | 17.6 | 15.3 | 15.7 | 25.9 | 1664 | 10.6 |
| | 18.3 | 16.1 | 15.8 | 25.8 | 1386 | 9.7 |
| | 21.0 | 18.7 | 16.4 | 23.9 | 1716 | 5.2 |
| | 22.6 | 20.8 | 16.4 | 22.3 | 1294 | 1.5 |
| 7 | 12.8 | 11.3 | 15.7 | 24.1 | 1789 | 12.8 |
| | 17.6 | 15.4 | 15.7 | 25.8 | 1980 | 10.4 |
| | 18.3 | 15.5 | 15.9 | 24.7 | 2037 | 9.2 |
| | 21.0 | 17.5 | 16.2 | 24.2 | 2318 | 6.7 |
| | 22.6 | 20.0 | 16.6 | 21.5 | 1924 | 1.5 |
| 9 | 13.4 | 11.8 | 15.2 | 27.3 | 1639 | 15.5 |
| | 16.3 | 14.5 | 15.3 | 26.3 | 2088 | 11.8 |
| | 18.6 | 16.4 | 15.7 | 24.6 | 2428 | 8.2 |
| | 20.2 | 17.8 | 16.1 | 23.1 | 2982 | 5.3 |
| | 22.2 | 19.9 | 16.3 | 22.0 | 2619 | 2.1 |
| 11 | 13.3 | 11.7 | 15.1 | 27.4 | 2035 | 15.7 |
| | 16.4 | 14.3 | 15.3 | 26.3 | 2374 | 12 |
| | 18.6 | 15.8 | 15.7 | 24.8 | 2544 | 9 |
| | 20.3 | 17.5 | 16.0 | 23.4 | 3247 | 5.9 |
| | 22.4 | 19.6 | 16.4 | 21.9 | 2732 | 2.3 |
| 13 | 13.5 | 11.3 | 15.2 | 27.4 | 2191 | 16.1 |
| | 16.4 | 14.1 | 15.4 | 25.8 | 2585 | 11.7 |
| | 18.6 | 15.7 | 11.8 | 24.7 | 2642 | 9 |
| | 20.3 | 17.4 | 16.1 | 23.0 | 3285 | 5.6 |
| | 22.3 | 19.2 | 16.5 | 21.5 | 3474 | 2.3 |
| | 23.1 | 20.5 | 16.4 | 22.6 | 3355 | 2.1 |
| | 25.7 | 22.2 | 16.5 | 22.6 | 2227 | 0.4 |

**Table 31. Average 2-in. x 2-in. fly ash stabilized loess summary**

| Stabilizer content (%) | Initial moisture content (%) | Moisture content with fly ash (%) | Dry unit weight with fly ash (kN/m$^3$) | Failure stress (kPa) |
|---|---|---|---|---|
| 10 | 10.1 | 8.5 | 15.4 | 734 |
| | 12.8 | 11.0 | 15.7 | 677 |
| | 15.5 | 14.5 | 15.9 | 669 |
| | 18.9 | 16.5 | 16.5 | 713 |
| | 21.7 | 19.3 | 16.8 | 656 |
| 15 | 9.8 | 8.2 | 15.2 | 551 |
| | 12.6 | 10.8 | 15.5 | 696 |
| | 15.5 | 13.2 | 15.8 | 694 |
| | 19.5 | 15.9 | 16.3 | 771 |
| | 21.8 | 18.3 | 16.6 | 696 |
| 20 | 10.1 | 8.0 | 15.2 | 728 |
| | 12.9 | 10.2 | 15.6 | 853 |
| | 16.0 | 12.1 | 15.9 | 923 |
| | 19.0 | 14.9 | 16.1 | 962 |
| | 21.8 | 17.5 | 16.5 | 960 |

**Table 32. Average 2-in. x 2-in. vacuum saturated fly ash stabilized loess summary**

| Stabilizer content (%) | Initial moisture content (%) | Moisture content with fly ash (%) | Dry unit weight with fly ash (kN/m3) | Vacuum saturation moisture content (%) | Failure stress (kPa) | Change in moisture content (%) |
|---|---|---|---|---|---|---|
| 10 | 10.1 | 8.5 | 15.1 | 27.9 | 204 | 19.4 |
| | 12.8 | 11.0 | 15.6 | 26.6 | 356 | 15.6 |
| | 15.5 | 14.5 | 16.0 | 24.9 | 371 | 10.4 |
| | 18.9 | 16.5 | 16.3 | 23.5 | 393 | 7 |
| | 21.7 | 19.3 | 16.6 | 22.3 | 360 | 3 |
| 15 | 9.8 | 8.2 | 15.1 | 28.5 | 253 | 20.3 |
| | 12.6 | 10.8 | 15.3 | 26.6 | 320 | 15.8 |
| | 15.5 | 13.2 | 15.8 | 24.9 | 399 | 11.7 |
| | 19.5 | 15.9 | 16.2 | 23.8 | 410 | 7.9 |
| | 21.8 | 18.3 | 16.5 | 22.9 | 380 | 4.6 |
| 20 | 10.1 | 8.0 | 15.0 | 28.0 | 320 | 20 |
| | 12.9 | 10.2 | 15.3 | 26.7 | 457 | 16.5 |
| | 16.0 | 12.1 | 15.6 | 25.7 | 480 | 13.6 |
| | 19.0 | 14.9 | 15.8 | 24.2 | 478 | 9.3 |
| | 21.8 | 17.5 | 16.1 | 23.4 | 522 | 5.9 |

During vacuum saturation, the samples with the lowest initial moisture showed the highest moisture content change between the initial moisture content with cement and the vacuum saturated moisture content (Table 30 and Table 32). Results indicated that the samples with the lowest initial moisture contents became the samples with the highest final moisture content for each stabilizer type and content except 3, 5, and 7% cement. This shows that the initial moisture content of the soil is very important in not only achieving the highest strength, but also for preventing a loss of strength from post-construction wetting. The lower the moisture content is during stabilization, the higher the moisture content could become after multiple freeze-thaw cycles and saturation.

The optimum cement content, based on weight, was estimated using the guidelines outlined by the Portland Cement Association (1992) which is based on the materials group index, the percentage of particles between 0.05 mm and 0.005 mm, and the dry density. Using that procedure, the optimum cement content for the loess material was found to be 11%. The fly ash contents were chosen to represent typically applied amounts, while meeting economic considerations.

The effect of moisture content on the UCS of cement treated samples is shown in Figure 92. The average of the non-vacuum saturated and vacuum saturated samples are presented to show how the compressive strength continues to decrease as the moisture content increases. There is a trend between the moisture content, UCS, and the stabilizer content. The maximum UCS of the 3% cement stabilized mixture is hardly affected by moisture content; however the 13% cement stabilized mixture is highly affected by the moisture content of the stabilized mixture. In order to reach the maximum strength for the 3% cement mixture, a moisture content of approximately 11% to 20% would be acceptable, However to achieve the maximum strength of the 13% cement stabilized mixture, the moisture content would need to approximately be between 17 and 19%. The effect of stabilizer content on the range of moisture contents required to achieve the maximum compressive strength increased as the stabilizer content increased. The vacuum saturated specimens continued to show a trend of decreasing strength with higher moisture contents. This effect shows that the initial soil moisture content becomes more important as the cement content increases.

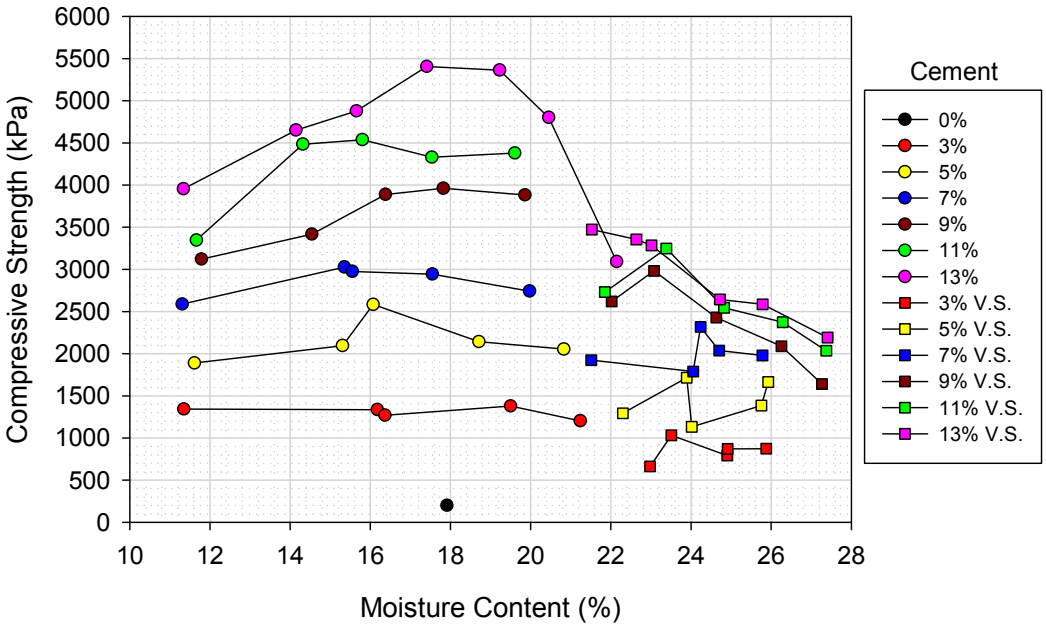


**Figure 92. Cement stabilized compressive strength and moisture content relationship**

The fly ash stabilized loess (Figure 93) shows the same trend as the cement stabilized loess material. The optimum moisture content, based on strength, for the 10% fly ash mixture is between 8 and 19%. The 20% fly ash mixture has an optimum strength between 15 to 18% moisture content. As the stabilizer content increased, the range of moisture contents needed to reach the maximum UCS decreased. As the moisture content increased because of vacuum saturation, the compressive strength decreased.

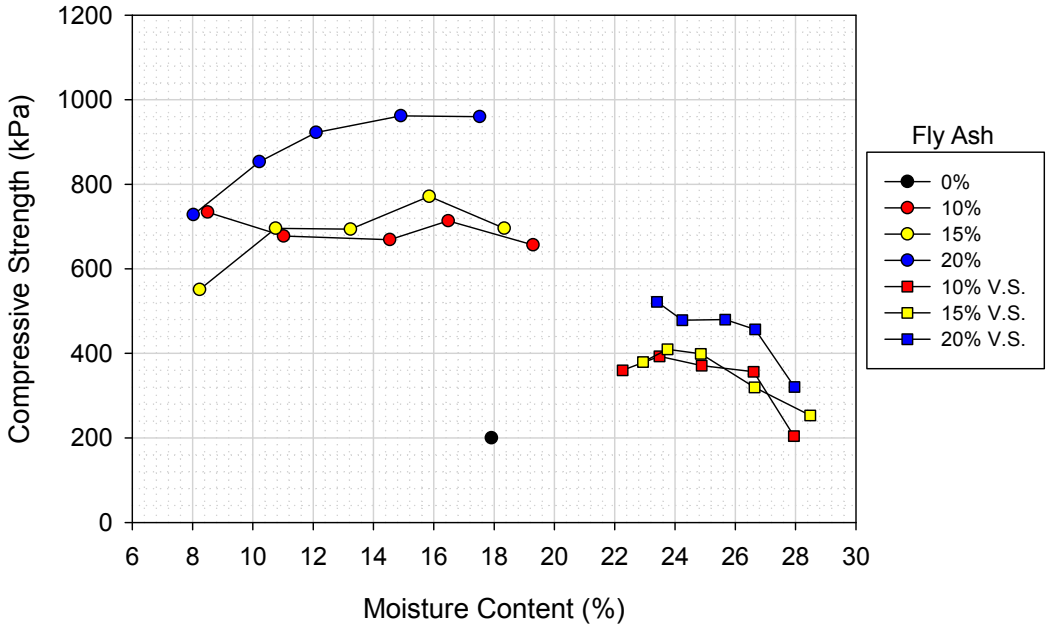


**Figure 93. Fly ash stabilized compressive strength and moisture content relationship**

The cement treated samples show a good trend with the exception of the samples that have moisture contents around 11.5%. The samples form two groups, with the upper samples being stabilized with 3, 5, and 7% cement and the lower group being stabilized with 9, 11, and 13% cement. Possible reasons for the formation of two groups could be compaction delay or lower dry unit weights caused by increased cement contents. The compaction delay for the cement and fly ash stabilized samples was generally less than 30 minutes. The remaining moisture contents showed no obvious grouping due to compaction delay or cement content. The maximum dry unit weight of the cement treated 2-in. x 2-in. samples is higher than the standard Proctor of the untreated loess, but it is approximately the same as the standard Proctor performed on 9% cement treated loess. The compaction data for the cement stabilized 2-in. x 2-in. specimens are shown in Figure 94.

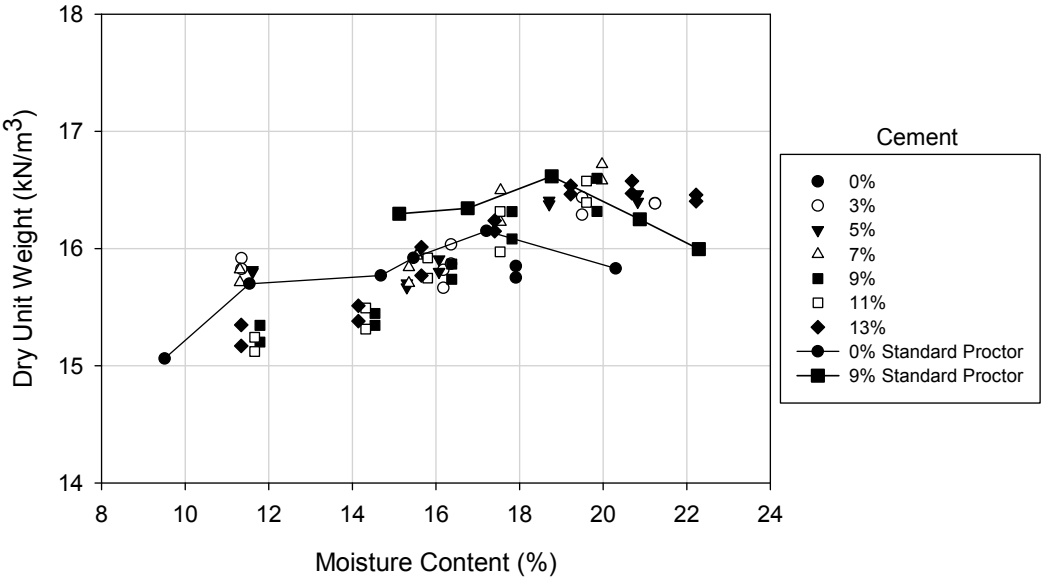


**Figure 94. Cement stabilized dry unit weight and moisture content relationship**

The compaction data shows a good trend between the fly ash treated samples. The 2-in. x 2-in. samples had approximately the same maximum dry unit weight as the 15% fly ash treated standard Proctor, however the optimum moisture content of the 2-in. x 2-in. samples is higher. The untreated loess standard Proctor shows a lower maximum dry unit weight and optimum moisture content compared to the 2-in. x 2-in. samples. The compaction data for the fly ash stabilized 2-in. x 2-in. samples are presented in Figure 95.

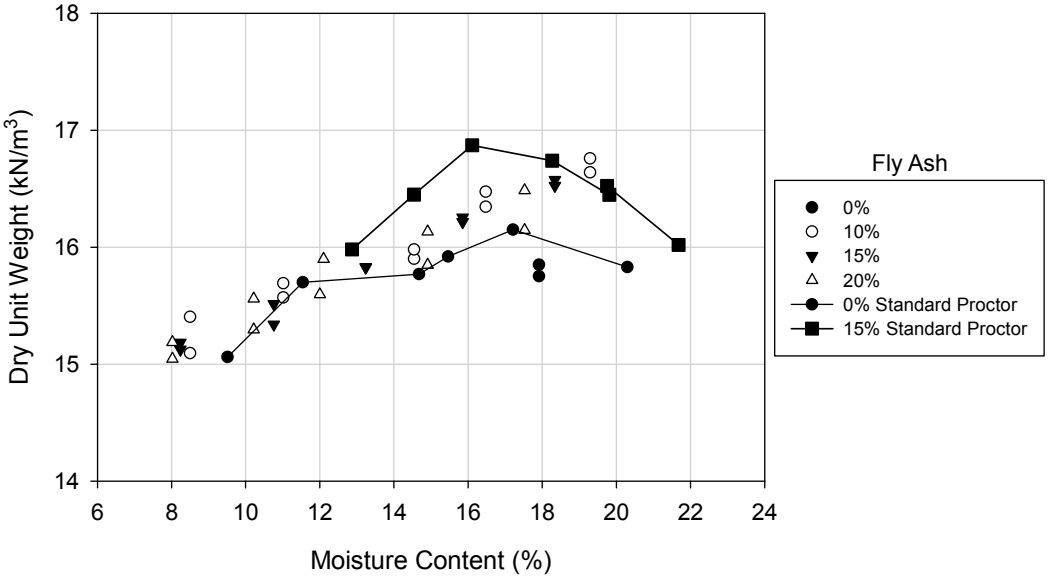


**Figure 95. Fly ash stabilized dry unit weight and moisture content relationship**

**Economic Analysis**

The decision to use cement or fly ash as a stabilizer can depend on many factors; however cost is among the most important. Table 33 compares the cost of using cement and fly ash to stabilize a square yard of soil. The average cement and fly ash costs were determined from the bids of six local contractors. The UCS values were determined from data presented in Table 29 through Table 32.

**Table 33. Economic comparison of cement and fly ash stabilization**

| UCS (kPa / psi) | Average cement cost ($/yd$^2$) | Approximate cement content (%) | Average fly ash cost ($/yd$^2$) | Approximate fly ash content (%) |
|---|---|---|---|---|
| 345 / 50 | — | — | — | — |
| 517 / 75 | — | — | 5.11 | 10 |
| 690 / 100 | — | — | 6.05 | 15 |
| 861 / 125 | — | — | 7.23 | 20 |
| 1034 / 150 | 3.31 | 3 | — | — |
| 2069 / 300 | 4.90 | 5 | — | — |
| 2758 / 400 | 6.50 | 7 | — | — |
| 3448 / 500 | 8.09 | 9 | — | — |
| 4137 / 600 | 9.69 | 11 | — | — |
| 4827 / 700 | 11.29 | 13 | — | — |
| 5516 / 800 | — | — | — | — |

The minimum UCS of cement treated loess is approximately 1380 kPa and the maximum is approximately 5400 kPa, for 3 to 13%fly ash. The minimum fly ash UCS is approximately 710 kPa and the maximum is 962 kPa, for 10 to 20% fly ash. Cement has a much higher range of possible compressive strengths compared to fly ash and is a more economical stabilization method compared to fly ash. The UCS of the 20% fly ash mixture is approximately 960 kPa compared to 1380 for the 3% cement mixture. The 20% fly ash mixture costs approximately $7.23 to place a square yard, whereas a 3% cement mixture costs approximately $3.31 to place a square yard.

**Statistical Analysis**

Several statistical analyses were performed on the data set generated from the 2-in. x 2-in. study. Linear regressions were used to predict the UCS based on the amount and type of stabilizer and to predict the vacuum saturated UCS from the UCS. A multiple linear regression was performed to more accurately predict the UCS based on several variables

(e.g., stabilizer content, moisture content, dry unit weight, compaction delay). The coefficient of determination ($R^2$) for the linear regression and adjusted $R^2$ for the multiple linear regressions are presented to measure how well the model represents the data. The adjusted $R^2$ is used in the multiple linear regressions because it relates to the $R^2$ from the linear regression.

Stabilizer content is one of the main contributors to increasing the UCS of the loess. Therefore, a simple linear regression can be used to estimate the stabilizer content needed to meet a specified UCS. The models presented are only valid for the range of stabilizer contents tested. The linear regression model used to predict UCS based on the stabilizer content is shown in Equation (2).

$$UCS\ (kPa) = b_0 + b_1 \bullet Stabilizer\ Content\ (\%) \quad (2)$$

where $b_0$ = intercept and

$b_1$ = regression parameter.

Figure 96 shows the linear regression analysis for the cement stabilizer and Figure 97 shows the analysis for the fly ash stabilizer. The cement stabilized model has a root mean square error (RMSE) of 752.09 kPa and the fly ash model has a RMSE equal to 93.50 kPa. The cement model has a higher $R^2$ (i.e., 0.69) value than the fly ash model (i.e., 0.42). This could be due to a larger amount of cement contents and samples observed (i.e., 6 stabilizer contents and 99 samples) compared to fly ash (i.e., 3 stabilizer contents and 45 samples). Figure 96 shows that there is more variability in the final compressive strength as the stabilizer content increases. This trend is related to the trends in Figure 92 where the range of moisture contents that will produce maximum compressive strengths decreases as the cement content increases.

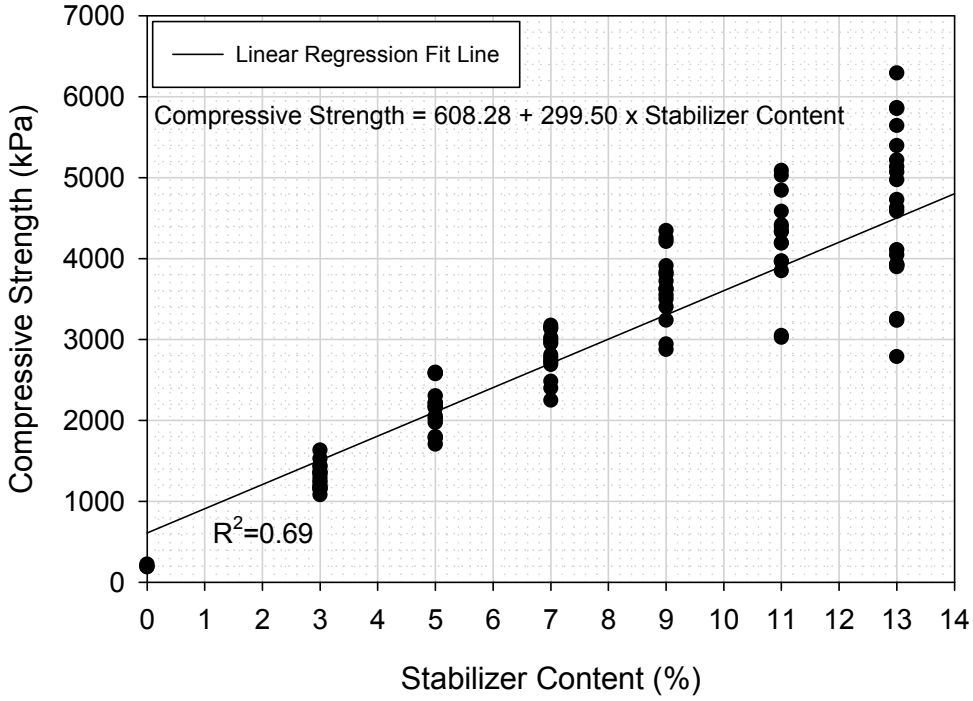


**Figure 96. Cement stabilized compressive strength and stabilizer content linear regression analysis**

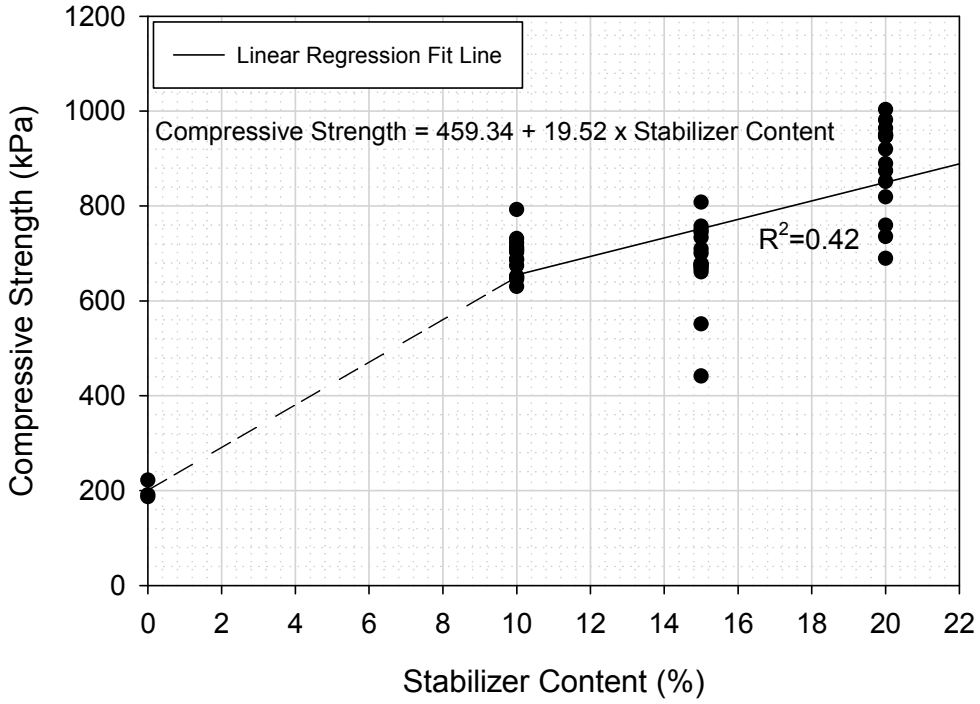


**Figure 97. Fly ash stabilized compressive strength and stabilizer content linear regression analysis**

The UCS can be used to estimate the vacuum saturated UCS. The linear regression model used to predict the vacuum saturated UCS from the UCS is presented in Equation (3).

$$Vacuum\ Saturated\ UCS\ (kPa) = b_0 + b_1 \bullet UCS\ (kPa) \quad (3)$$

where $b_0$ = intercept and

$b_1$ = regression parameter.

Figure 98 presents the statistical analysis for cement and Figure 99 shows the statistical analysis for fly ash. The RMSE of the cement model is 422.79 kPa and the RMSE of the fly ash model is 64.69 kPa. The $R^2$ of the cement model is 0.71, whereas it is 0.47 for the fly ash model. The cement model represents the cement treated samples better than the fly ash model represents the fly ash samples. Same as the UCS and stabilizer content analysis, this could be a result of the additional samples and cement contents tested compared to fly ash. Figure 100 presents a combined cement and fly ash model predicting the vacuum saturated UCS from UCS. The combined model has a RMSE equal to 375.61 kPa. The cement and fly ash combined model has an $R^2$ of 0.86, which is better than the models of either stabilizer individually.

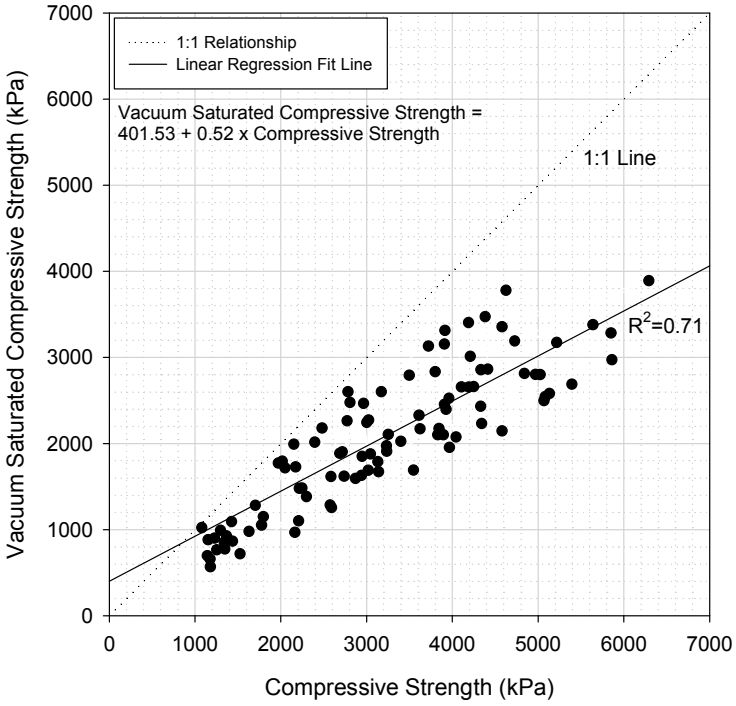


**Figure 98. Cement stabilized vacuum saturated compressive strength and compressive strength linear regression analysis**

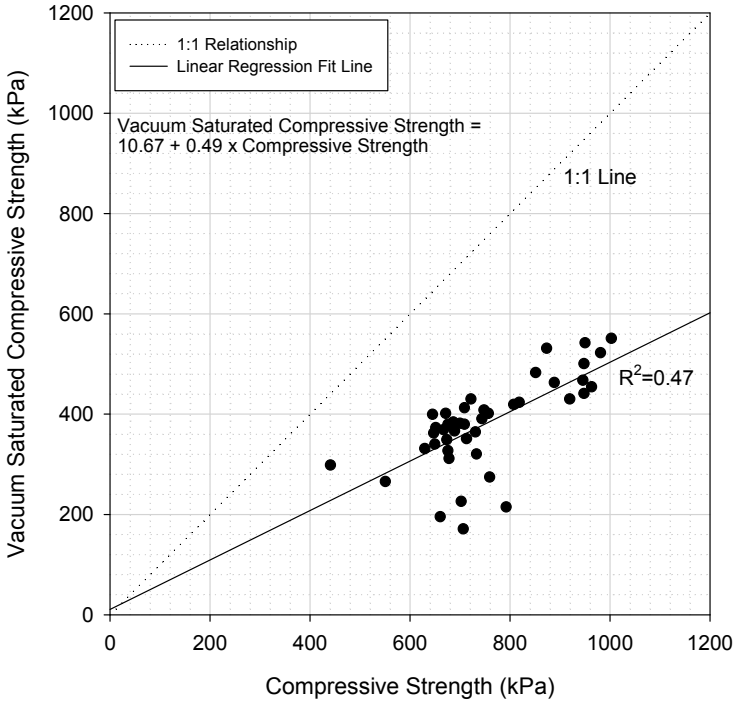


**Figure 99. Fly ash stabilized vacuum saturated compressive strength and compressive strength linear regression analysis**

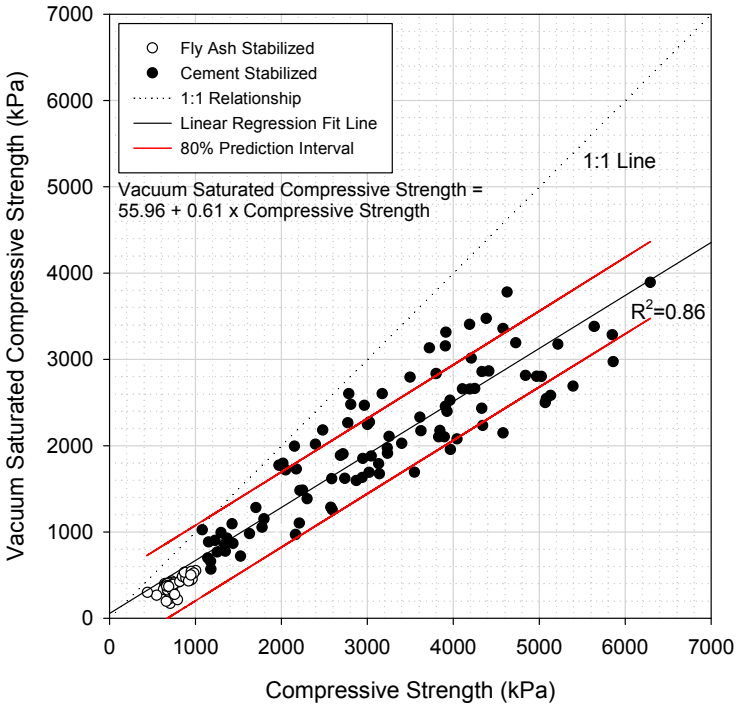


**Figure 100. Cement and fly ash stabilized vacuum saturated compressive strength and compressive strength design chart**

The 80% prediction interval in Figure 100 can be used to determine a range of target UCS values needed to achieve a desired vacuum saturated compressive strength. For example, if a vacuum saturated compressive strength of 2000 kPa is desired, a UCS approximately between 2500 and 3900 kPa would be required.

A multiple linear regression model was also investigated to determine whether additional variables could increase the accuracy of the linear model predicting UCS based on stabilizer content. In addition to stabilizer content, the moisture content, dry unit weight, and compaction delay were included in the model. The compaction delay is the time needed to add the stabilizer to the soil, mix it in, and compact the soil and stabilizer mixture. As the compaction delay increases, more energy is needed to overcome bonding forces.

The effect of compaction delay can be a decrease in dry unit weight and/or a decrease in compressive strength. Several other factors were investigated including void ratio, saturation, and many 2nd order variables. The additional variables increased the model fit, however a simple model that applied to both stabilizer types was chosen. More complex models for cement and fly ash stabilizers are presented in Appendix A.

The multiple linear regression model used to predict the UCS for cement and fly ash stabilized materials is presented in Equation (4).

$$UCS\ (kPa) = b_0 + b_1 \bullet s + b_2 \bullet w + b_3 \bullet \gamma_d + b_4 \bullet Delay \quad (4)$$

Where $b_0$ = intercept;

$b_1$, $b_2$, $b_3$, $b_4$ = regression parameters;

s = stabilizer content (%);

$w$ = moisture content (%);

$\gamma_d$ = dry unit weight (kN/m3); and

Delay = compaction delay (min).

The statistical significance of the variables was determined from p- and t-values. The p-value criteria used to determine if a variable is significant are: p-value < 0.05 = significant, <0.10 = possibly significant, >0.10 = not significant. The t-value criteria used to determine significance included: t-value < –2 or > +2 = significant. The p-value describes the significance of the variable and the t-ratio describes the relative importance compared to other variables (i.e., higher absolute values indicate more significance).

Equation (5) shows how the $R^2$ values have been adjusted for the number of regression parameters in the multiple linear regression. The adjusted $R^2$ allows for comparisons to be made with the $R^2$ from simple linear regressions, which allows for the model that better fits the data to be determined.

$$R^2\ (adjusted) = (R^2\ (n - 1)) / (n - p) \quad (5)$$

where n = the number of observations and

p = the number of regression parameters.

Collinearity should be avoided in a multiple linear regression analysis. Collinearity occurs when two or more variables that are closely related are used to predict the dependent variable. Collinearity can cause incorrect and inflated $R^2$ values. Variance inflation factors (VIF) can be used to detect collinearity and is defined in Equation (6).

$$VIF = 1 / (1 - R^2) \quad (6)$$

One indication that the variable is not contributing to collinearity is if the condition in Equation (7) is met (Freund et al. 2003).

$$VIF < 1 / (1 - R^2) \quad (7)$$

The results of the multiple linear regression analysis predicting the cement stabilized UCS are presented in Table 34. The RMSE of the cement model is 626.50 kPa. The $R^2$ of the cement model is 0.73, which is slightly higher than the 0.69 $R^2$ of the simple linear regression that predicted the UCS based on cement content. That shows that this multiple linear regression model does not significantly improve the fit of the data over the simple linear regression. The variables considered were all found to be statistically significant, based on the p-values. However, based on the t-value the stabilizer content is relatively much more important to model than the moisture content, dry unit weight, or compaction delay. The low VIF values show that collinearity is not a problem in the model. Figure 101 shows the actual UCS versus the predicted UCS for the multiple linear regression model.

**Table 34. Results of multiple linear regression analysis predicting cement stabilized UCS**

| Model | Parameter | Estimate | Standard error | t-ratio | p-value | R2 | VIF |
|---|---|---|---|---|---|---|---|
| $UCS = b_0 + b_1 \bullet s + b_2 \bullet w + b_3 \bullet \gamma_d + b_4 \bullet Delay$ | bo | -3710.50 | 1713.76 | -2.17 | 0.0320 | 0.73 | — |
| | b1 | 227.44 | 12.87 | 17.67 | <0.0001 | | 1.09 |
| | b2 | -72.30 | 12.11 | -5.97 | <0.0001 | | 1.58 |
| | b3 | 398.88 | 105.64 | 3.78 | 0.0002 | | 1.02 |
| | b4 | -41.79 | 8.37 | -4.99 | <0.0001 | | 1.67 |

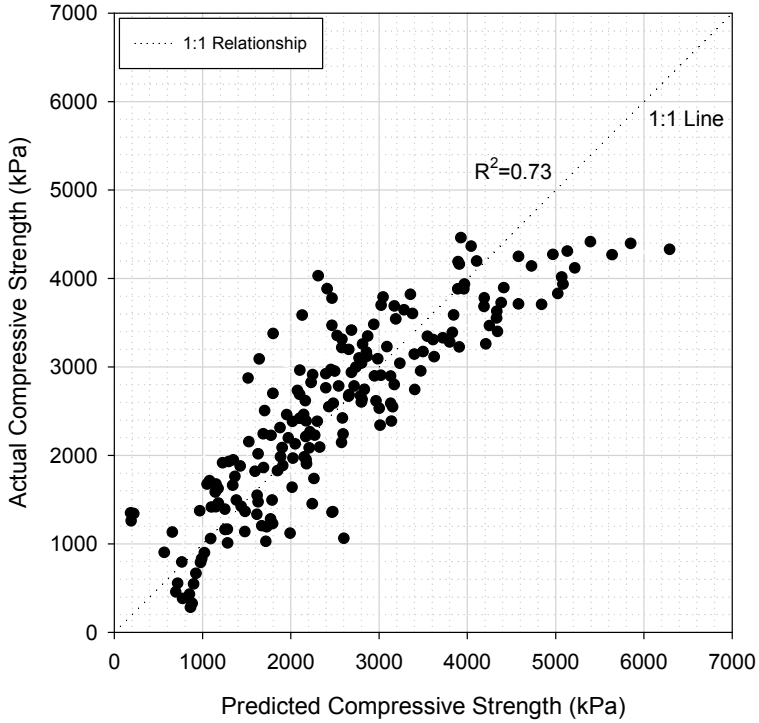


**Figure 101. Plot of actual versus predicted cement stabilized UCS**

The results of the multiple linear regression analysis predicting the fly ash stabilized UCS are presented in Table 35. The RMSE of the fly ash model was 96.95 kPa. The $R^2$ of the fly ash model is 0.80, which is significantly higher than the 0.42 $R^2$ value found from the linear regression analysis that predicted UCS from the fly ash content alone. The increase in $R^2$ shows that this multiple linear regression model significantly increases the fit of the data. The stabilizer content, moisture content, and dry unit weight were considered to be significant, based on the p-values. However, compaction delay was not found to be significant. The t-ratios show that the moisture content is the relatively most important variable in the model. The low VIF values of the fly ash model show that collinearity is not occurring in the model.

Figure 102 shows the actual versus predicted UCS values for this multiple linear regression model.

**Table 35. Results of multiple linear regression analysis predicting fly ash stabilized UCS**

| Model | Parameter | Estimate | Standard error | t-ratio | p-value | R2 | VIF |
|---|---|---|---|---|---|---|---|
| $UCS = b_0 + b_1 \bullet s + b_2 \bullet w + b_3 \bullet \gamma_d + b_4 \bullet Delay$ | bo | -1398.67 | 365.34 | -3.83 | 0.0002 | 0.80 | |
| | b1 | 18.73 | 2.66 | 7.04 | <0.0001 | | 1.11 |
| | b2 | -23.68 | 2.13 | -11.09 | <0.0001 | | 1.92 |
| | b3 | 136.23 | 22.66 | 6.01 | <0.0001 | | 1.26 |
| | b4 | -1.34 | 2.05 | -0.65 | 0.5154 | | 2.22 |

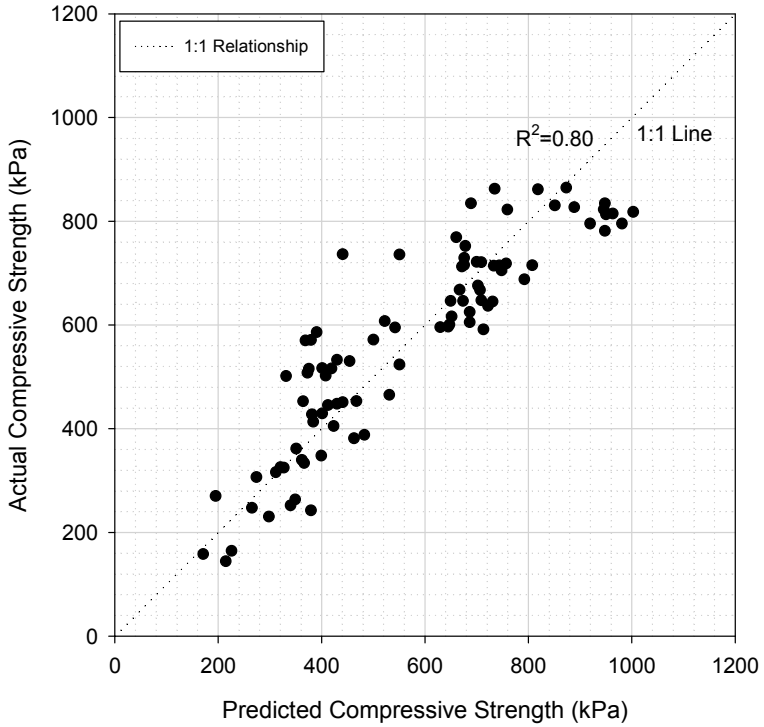


**Figure 102. Plot of actual versus predicted fly ash stabilized UCS**

## Freeze-Thaw and Wet-Dry Durability

This section discusses wet-dry and freeze-thaw durability test results of fly ash- and portland cement-stabilized materials. The tests were performed according to ASTM D559-03 and ASTM D560-03. The materials were sampled from the following project/source locations: IA I-29, MI I-96, PA US-22, and Pottawattamie, Iowa.

The durability of stabilized materials is important in determining how materials will perform when exposed to repeated wetting and drying or freezing and thawing cycles.

Laboratory test results are used to determine if the specified stabilization technique is adequate, which is determined by whether the soil loses strength and material as wet-dry or freeze-thaw cycles increase. The Soil-Cement Laboratory Handbook states "It has been amply demonstrated that cement contents that produce low soil-cement weight losses in the freeze-thaw and wet-dry tests resist volume changes or hydraulic pressures that could gradually break down bonds of cementation" (Portland Cement Association 1992, 7). The PCA and USACE specify minimum durability requirements (Table 36 and Table 37) that stabilized materials must meet.

**Table 36. PCA durability criteria for cement stabilized soils (Portland Cement Association 1992)**

| AASHTO soil group | Maximum allowable mass loss (%) |
|---|---|
| A-1, A-2-4, A-2-5, and A-3 | <14 |
| A-2-6, A-2-7, A-4, and A-5 | <10 |
| A-6 and A-7 | <7 |

**Table 37. USACE durability requirements for cement, lime, lime-cement, and lime-cement-fly ash stabilized soils (Joint Departments of the Army and Air Force 1994)**

| Type of soil stabilized | Maximum allowable weight loss after 12 wet-dry or freeze-thaw cycles percent of initial specimen weight |
|---|---|
| Granular, PI < 10 | 11 |
| Granular, PI > 10 | 8 |
| Silt | 8 |
| Clays | 6 |

ASTM D559-03 and D560-3 are not intended to be used to determine the durability of fly ash-stabilized materials; however they were applied to fly ash-stabilized materials in this research to provide a direct comparison to cement-stabilized materials.

A portion of the test methods require that the test specimens be brushed after each cycle. This results in a large source of error and has been criticized by Shihata and Baghdadi (2001). It is difficult to consistently brush the surface area of the test specimen with an equal pressure. The ASCE durability requirements omit the brushing portion of the durability tests (Joint Departments of the Army and Air Force 1994). ASTM D559-03 and ASTM D560-03 recommend that two samples be tested, with one being brushed to determine soil-cement loss (brushed specimen) and the second sample not being brushed (unbrushed specimen). The

unbrushed specimen is used to track moisture content and volume changes throughout the durability cycles.

The volume and moisture content changes are based off of the original dry mass of the sample, which causes inaccuracies in the calculations since the specimens typically loose material as they are exposed in more cycles. The volume calculations are based off of three diameter and three height measurements, taken at the same location on the sample during testing. A problem arises when the sample loses material, but not at the location where the measurements are taken. This was typical and resulted in the samples having a different volume than what the measurements would show. Equation (8) shows the calculation for determining the volume change and Equation (9) shows the calculation for the moisture content change.

$$Volume\ Change,\ \% = (A - B) / A \tag{8}$$

where: A = original volume and

B = volume after durability cycling.

$$Moisture\ Content,\ \% = (A - B) / B \tag{9}$$

where: A = mass after durability cycling and

B = original calculated oven-dry mass.

ASTM D559-03 and ASTM D560-03 use the same equations to calculate soil-cement loss. Equation (10) corrects the oven dry mass of the specimens to account for water that has reacted with the stabilizer during the test procedure.

$$Corrected\ oven\text{-}dry\ mass = (A / B) \bullet 100 \tag{10}$$

where: A = oven-dry mass after drying at 100°C and

B = percentage of water retained in specimen plus 100.

The corrected oven-dry mass is then used in Equation (11) to determine the soil-cement loss.

$$Soil\text{-}cement\ loss,\ \% = (A / B) \bullet 100 \tag{11}$$

where: A = original calculated oven-dry mass minus final corrected oven-dry mass and

B = original calculated oven-dry mass.

ASTM D559-03 and ASTM D560-03 contain average percentages of water that is retained in the specimens (i.e., has reacted with the stabilizer) (Table 38). The average values were used in the fly ash-stabilized and cement-stabilized calculations.

**Table 38. Average values of water retained in wet-dry and freeze-thaw durability specimens (ASTM D559-03 and ASTM D560-03)**

| AASHTO soil classification | Average water retained after drying at 230°F (110°C), % |
|---|---|
| A-1, A-3 | 1.5 |
| A-2 | 2.5 |
| A-4, A-5 | 3.0 |
| A-6, A-7 | 3.5 |

Through experience, the Soil-Cement Laboratory Handbook mentions that the freeze-thaw durability test is usually critical compared to the wet-dry tests, except when large amounts of silt or clay are present (Portland Cement Association 1992).

**IA I-29**

The lean clay subgrade collected from IA I-29 was stabilized with 15% fly ash. The stabilized material was tested for wet-dry and freeze-thaw durability. The results of the wet-dry durability test are summarized in Table 39. Before wet-dry durability testing pictures of sample 1 is shown in Figure 103. The specimen did not last the 12 test cycles, failing after the 10$^{th}$ cycle. The brushed specimen mass change during wet-dry cycling is shown in Figure 104 and the percent mass change in Figure 105. The total mass of the wet-dry samples is measured after brushing is performed, which takes place after the drying portion of the durability cycle. The unbrushed specimen volume decreased approximately 54.2% by the end the 12$^{th}$ cycle.

**Table 39. IA I-29 lean clay subgrade wet-dry durability results**

| Sample # | Design moisture content (%) | Design fly ash content (%) | Sample moisture content (%) | Sample dry unit weight (kN/m3) | Soil-cement loss (%) | Maximum volume change (%) | Maximum moisture content (%) |
|---|---|---|---|---|---|---|---|
| 1 | 19.8 | 15 | 20.1 | 17.1 | 100 | 54.2 | — |

**Figure 103. IA I-29 lean clay subgrade wet-dry durability sample #1 before testing**

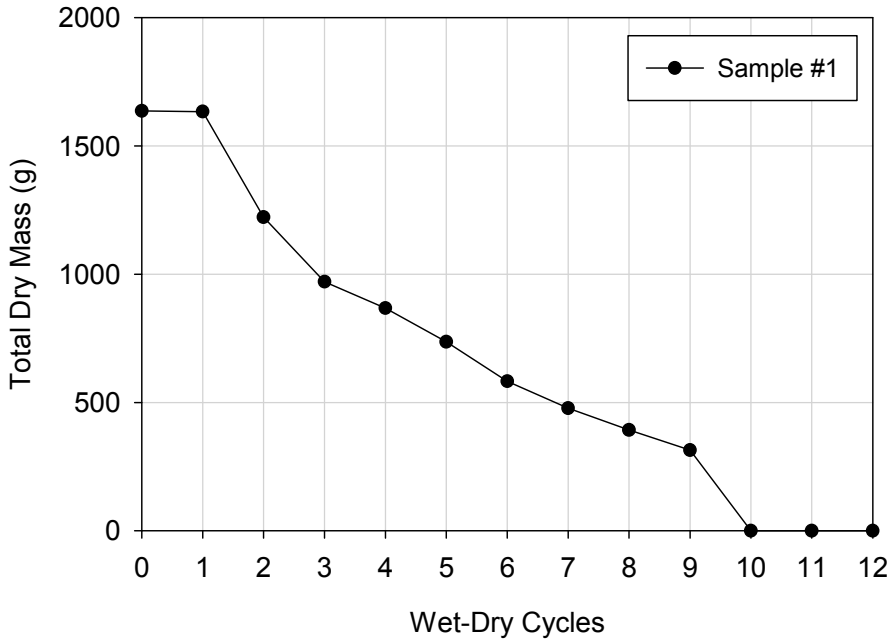


**Figure 104. IA I-29 lean clay subgrade mass change during wet-dry cycling**

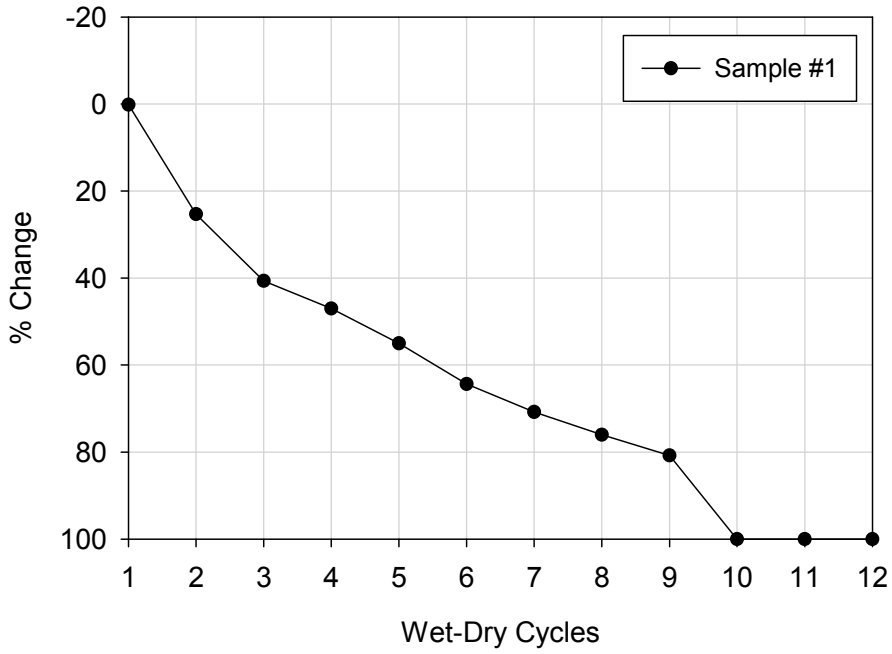


**Figure 105. IA I-29 lean clay subgrade percent mass change during wet-dry cycling**

Freeze-thaw durability was also tested for the lean clay subgrade with the same properties and stabilizer as the wet-dry specimen. The freeze-thaw durability results are summarized in Table 40 and pictures of sample 2 before testing is shown in Figure 106. The brushed freeze-thaw durability specimen also failed after the 10$^{th}$ cycle (Figure 107). The total mass of the freeze-thaw durability sample, in Figure 107, is measured after brushing, which takes place after the thawing portion of the durability cycle. The percent mass change of the freeze-thaw durability sample is presented in Figure 108. This results in a wet mass being measured, which makes it difficult to determine exact changes in the specimen weight between cycles due to water absorption. The unbrushed specimen had a maximum volume change of –5.9 %, which represents an increase in volume, after the 4$^{th}$ cycle. Sample 2 is an example of how the volume measurements can be incorrect. The mass has significantly decreased by the 4$^{th}$ cycle; however the volume measurements show an increase in volume. The maximum moisture content was 19.7%, after the 4$^{th}$ cycle for the unbrushed sample.

**Table 40. IA I-29 lean clay subgrade freeze-thaw durability results**

| Sample # | Design moisture content (%) | Design fly ash content (%) | Sample moisture content (%) | Sample dry unit weight (kN/m3) | Soil-cement loss (%) | Maximum volume change (%) | Maximum moisture content (%) |
|---|---|---|---|---|---|---|---|
| 2 | 19.8 | 15 | 19.3 | 17.3 | 100 | –5.9 | 19.7 |

**Figure 106. IA I-29 lean clay subgrade freeze-thaw durability sample #2 before testing**

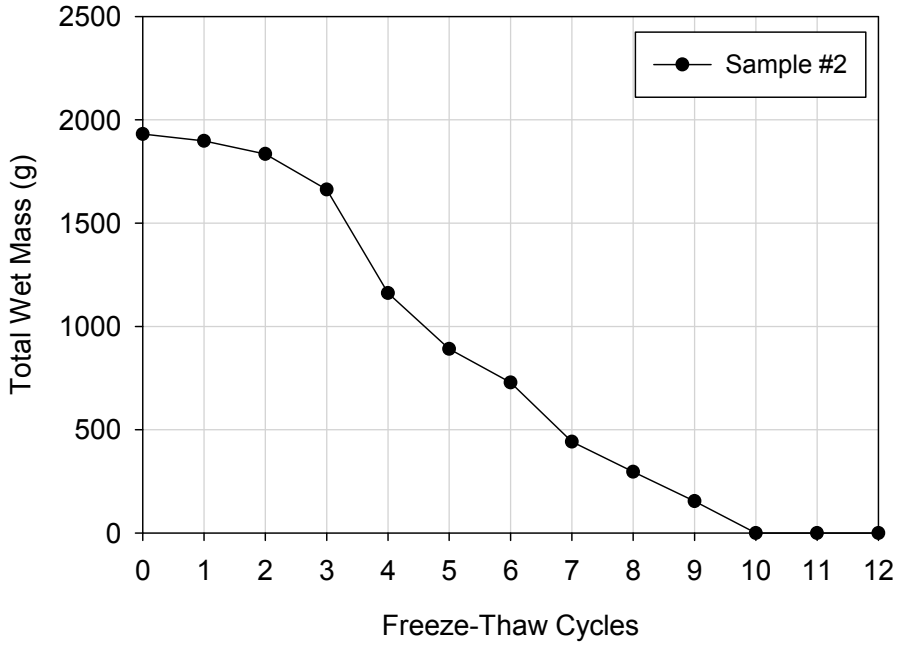


**Figure 107. IA I-29 lean clay subgrade mass change during freeze-thaw cycling**

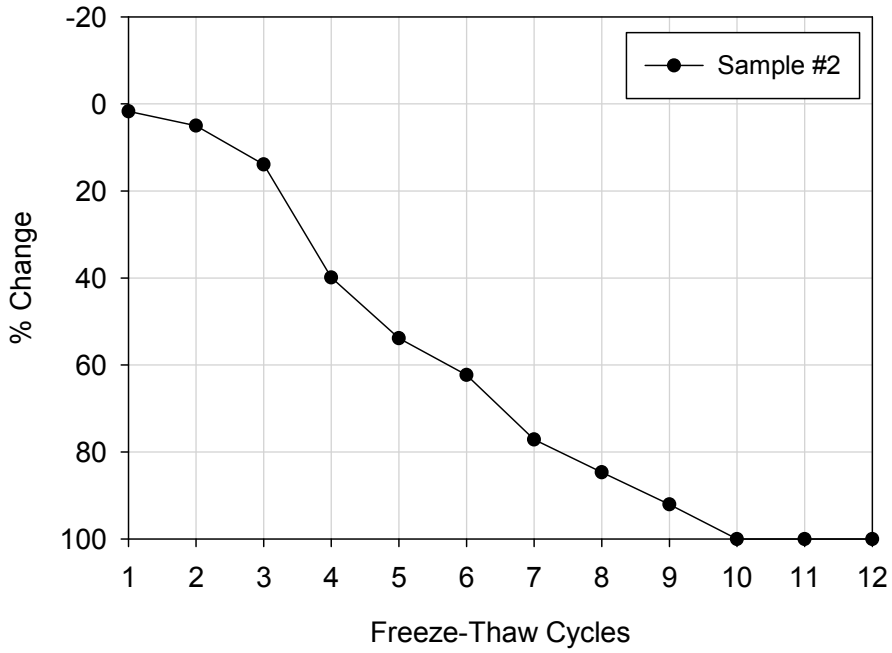


**Figure 108. IA I-29 lean clay subgrade percent mass change during freeze-thaw cycling**

The wet-dry and freeze-thaw durability tests of the fly ash-stabilized lean clay showed that the samples were not strong enough to endure the full 12 cycles. For a soil classified as an A-7, the acceptable loss, according to PCA, is 7% or less. The lean clay had approximately lost over 7% by the 2$^{nd}$ cycle of the wetting and drying and freezing and thawing tests.

**MI I-96**

The cement treated base (CTB) from MI I-96 consisted of recycle portland cement concrete (RPCC) from the existing pavement foundation. The mix design specified the mixture proportions to be 27 times the dry rodded unit weight of the aggregate (kN/m$^3$), 39.3 kN/m$^3$ of cement, 15.7–18.9 kN/m$^3$ water. This results in an approximate cement content of 10.7% The samples were made on-site, so the gradation of the material was not modified to meet the particle size requirement (i.e., all soil particles did not pass ¾ in.) of ASTM D559-03 and ASTM D560-03. A summary of the wet-dry durability results are shown in Table 41. The sample moisture content and dry unit weight could be accurately determined for this material. Before and after wet dry cycling pictures are shown for samples 1 through 3 in Figure 109 through Figure 111. The soil-cement loss of samples 1 through 3 were lower than the maximum loss of 14% allowed by PCA for a A-1 classified material, however, sample 3

had a considerably higher loss than samples 1 and 2. Sample 3 appeared to have a lower amount of fines in portions of the specimen (Figure 111), which could have decreased the strength of the cement bond. The brushed specimen mass change during wet-dry cycling for samples 1 through 3 can be seen in Figure 112. The percent mass change during wet-dry cycling is presented in Figure 113.

**Table 41. MI I-96 CTB wet-dry durability results**

| Sample # | Approximate cement content (%) | Soil-cement loss (%) |
|---|---|---|
| 1 | 10.7 | 4.2 |
| 2 | 10.7 | 4.3 |
| 3 | 10.7 | 12.9 |

**Figure 109. MI I-96 CTB wet-dry durability sample #1 before (left) and after (right) testing**

**Figure 110. MI I-96 CTB wet-dry durability sample #2 before (left) and after (right) testing**

**Figure 111. MI I-96 CTB wet-dry durability sample #3 before (left) and after (right) testing**

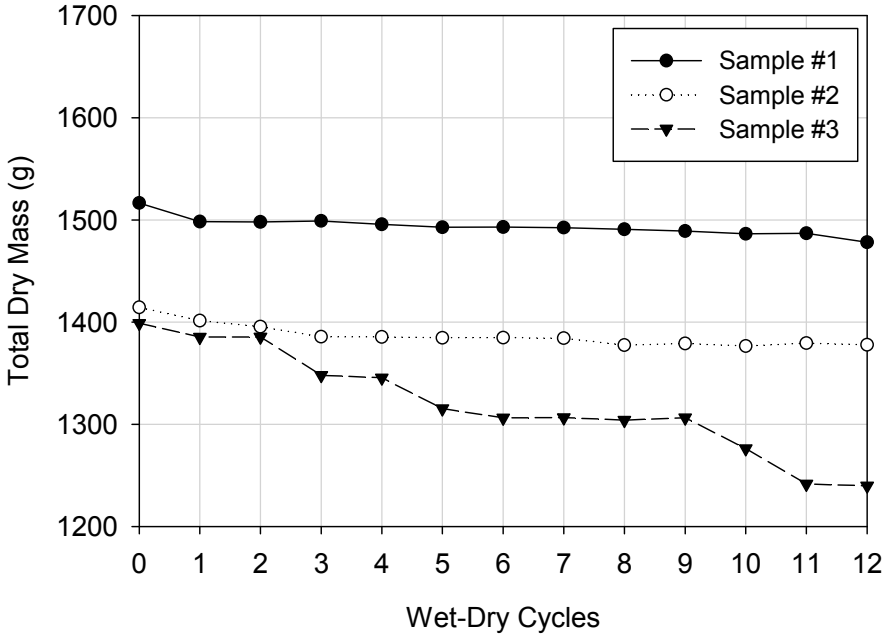


**Figure 112. MI I-96 CTB mass change during wet-dry cycling**

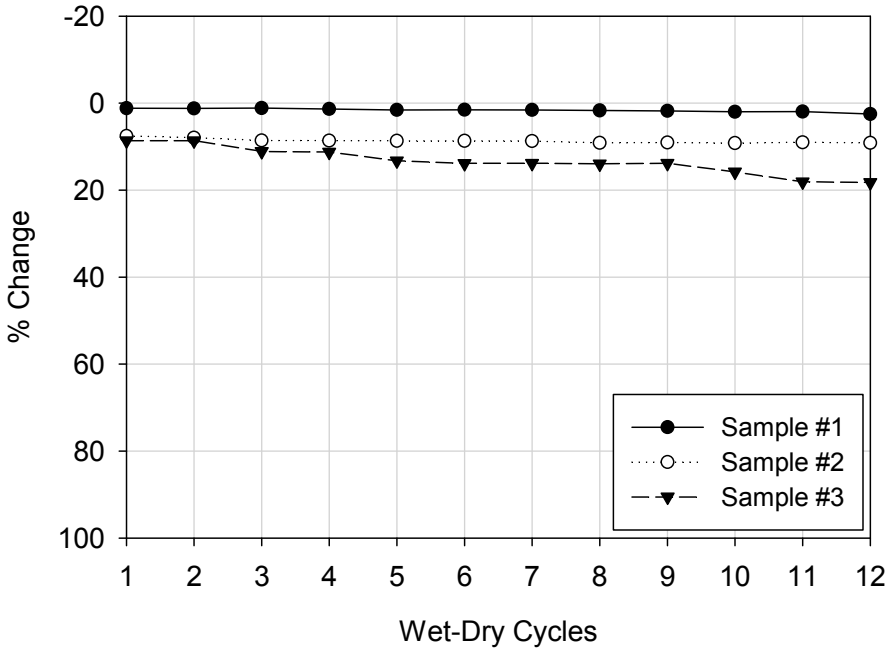


**Figure 113. MI I-96 CTB percent mass change during wet-dry cycling**

Freeze-thaw durability testing was performed on identical samples of MI I-96 CTB as the wet-dry durability testing. A summary of the freeze-thaw durability results is shown in Table 42. Samples 4 through 6 had relatively low and consistent soil-cement losses that met the

maximum soil-cement loss values specified by PCA (Table 36). Pictures of samples 4 through 6 before and after freeze-thaw cycling are shown in Figure 114 through Figure 116. Sample 5 (Figure 115) contained asphalt materials from the existing pavement foundation. Figure 117 shows the brushed specimen mass change during freeze-thaw cycling and Figure 118 shows the percent mass change.

**Table 42. MI I-96 CTB freeze-thaw durability results**

| Sample # | Approximate cement content (%) | Soil-cement loss (%) |
|---|---|---|
| 4 | 10.7 | 3.4 |
| 5 | 10.7 | 4.4 |
| 6 | 10.7 | 3.8 |

**Figure 114.MI I-96 CTB freeze-thaw durability sample #4 before (left) and after (right) testing**

**Figure 115. MI I-96 CTB freeze-thaw durability sample #5 before (left) and after (right) testing**

**Figure 116. MI I-96 CTB freeze-thaw durability sample #6 before (left) and after (right) testing**

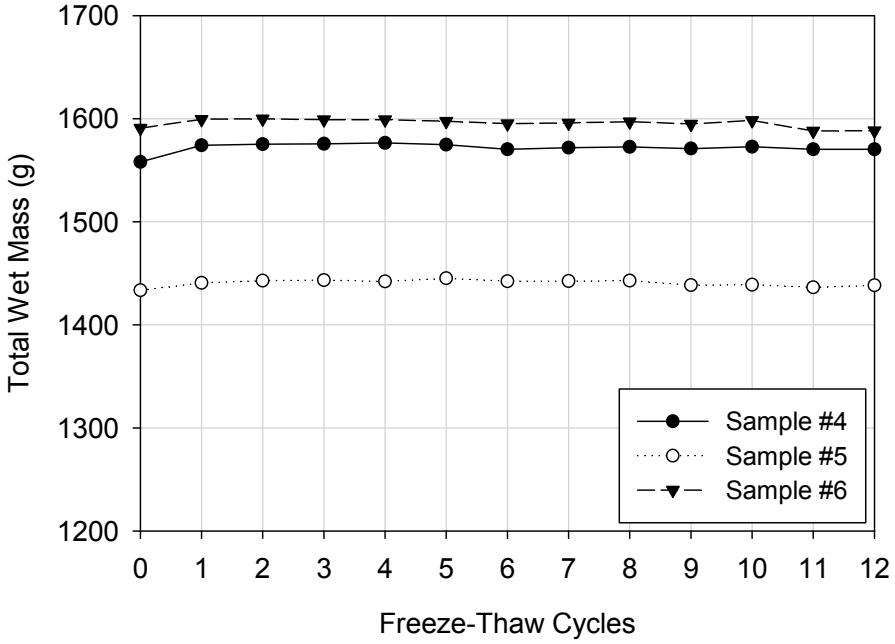


**Figure 117. MI I-96 CTB mass change during freeze-thaw cycling**

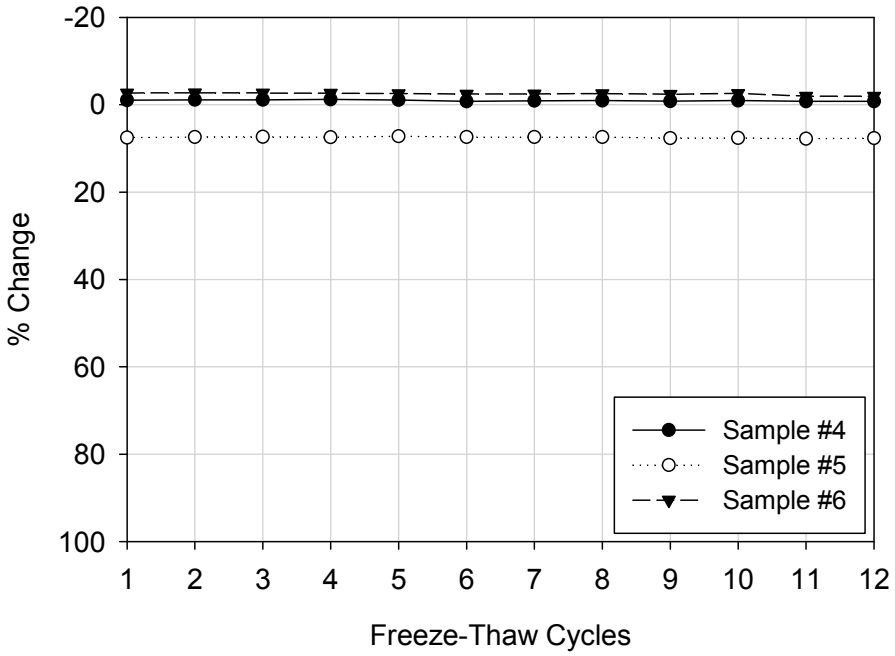


**Figure 118. MI I-96 CTB percent mass change during freeze-thaw cycling**

The CTB from MI I-96 proved to be strong enough to meet the wet-dry and freeze-thaw durability requirements set forth by PCA (Table 36) for an A-1 material.

**PA US-22**

The sandy lean clay subgrade from PA US-22 was subjected to wet-dry and freeze-thaw durability tests. The soil was stabilized with 10% portland cement. The wet-dry durability results are summarized in Table 43. The soil-cement loss, due to wet-dry cycling, was 11.4% which is above the acceptable limit of 7% for A-6 soil classification, according to PCA (Table 36). The maximum volume change of sample 1 was 2.6% after the 4$^{th}$ wet-dry cycle. The maximum moisture content during wet-dry cycling could not be reasonably determined, because the sample was losing mass as the wet-dry cycles increased. Figure 119 shows the brushed specimen before and after 12 wet-dry cycles. The mass change of the unbrushed specimen during wet-dry cycling is shown in Figure 120. The initial increase in mass during the first three cycles is due to cement reacting with water. The percent change in mass is presented in Figure 121.

**Table 43. PA US-22 sandy lean clay subgrade wet-dry durability results**

| Sample # | Design moisture content (%) | Design cement content (%) | Sample moisture content (%) | Sample dry unit weight (kN/m3) | Soil-cement loss (%) | Maximum volume change (%) | Maximum moisture content (%) |
|---|---|---|---|---|---|---|---|
| 1 | 21.2 | 10 | 21.2 | 17.3 | 11.4 | 2.6 | — |

**Figure 119. PA US-22 sandy lean clay subgrade wet-dry durability sample #1 before (left) and after (right) testing**

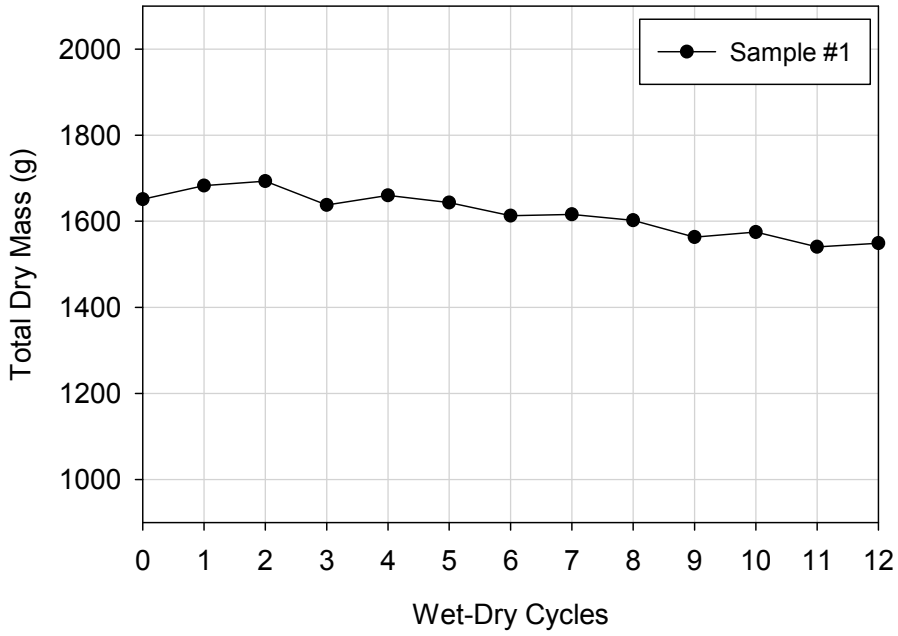


**Figure 120. PA US-22 sandy lean clay subgrade mass change during wet-dry cycling**

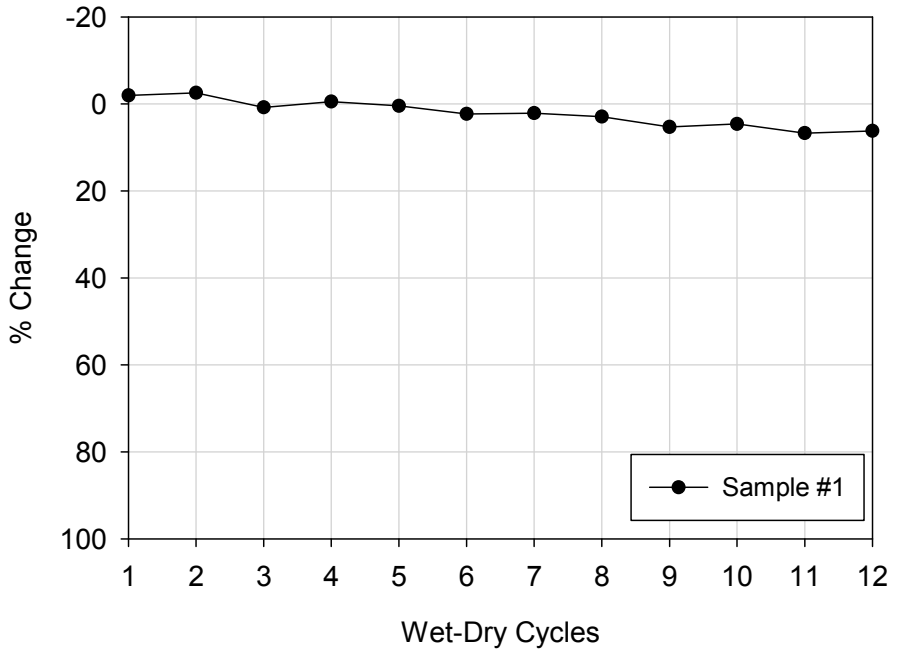


**Figure 121. PA US-22 sandy lean clay subgrade percent mass change during wet-dry cycling**

Freeze-thaw cycling was also performed on the sandy lean clay. A summary of the freeze-thaw durability results is shown in Table 44. The soil-cement loss was 53.3% which is does not satisfy the maximum requirement of 7%, set forth by PCA (Table 36). The

maximum volume change, of the unbrushed specimen, occurred after the 12th freeze-thaw cycle and was measured to be -7.7%, which indicates the sample expanded. The maximum moisture content of the unbrushed specimen was 20.9% and it occurred after the 4th cycle. Figure 122 shows the brushed sample 2 before and after 12 freeze-thaw cycles. The mass change of the brushed sample during freeze-thaw cycling is shown in Figure 123 and percent mass change is shown in Figure 124.

**Table 44. PA US-22 sandy lean clay subgrade freeze-thaw durability results**

| Sample # | Design moisture content (%) | Design cement content (%) | Sample moisture content (%) | Sample dry unit weight (kN/m3) | Soil-cement loss (%) | Maximum volume change (%) | Maximum moisture content (%) |
|---|---|---|---|---|---|---|---|
| 2 | 21.2 | 10 | 20.8 | 17.5 | 53.3 | -7.7 | 20.9 |

**Figure 122. PA US-22 sandy lean clay subgrade freeze-thaw durability sample #2 before (left) and after (right) testing**

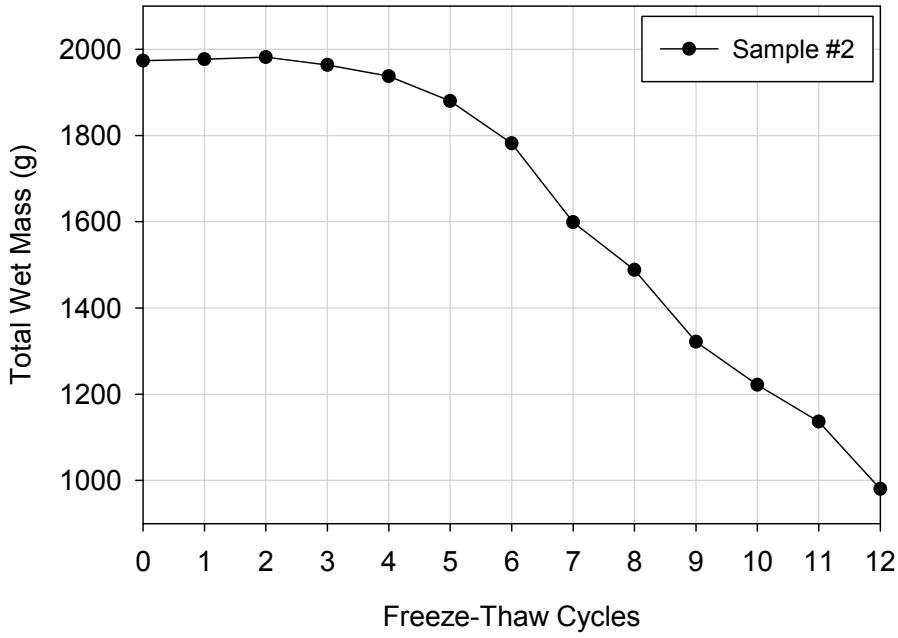


**Figure 123. PA US-22 sandy lean clay subgrade mass change during freeze-thaw cycling**

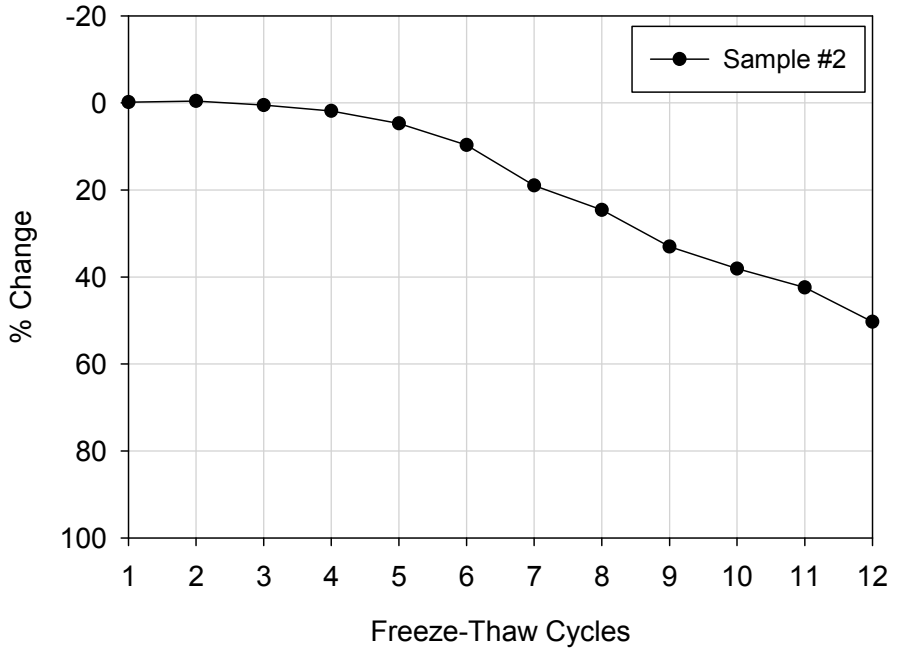


**Figure 124. PA US-22 sandy lean clay subgrade percent mass change during freeze-thaw cycling**

The sandy lean clay subgrade from PA US-22 did not meet the minimum soil-cement loss requirements of the wet-dry and freeze-thaw durability tests. Higher cement contents should be considered to produce a more durable soil matrix.

**Loess**

Loess was stabilized with cement and fly ash and subjected to freeze-thaw durability testing. Four specimens with varying moisture contents and stabilizer contents were tested for the cement and fly ash stabilizers. The cement, fly ash, and moisture content combinations were chosen from the 2-in. x 2-in. study. The cement contents between 9 and 13% were chosen to correlate with the optimum cement content of 11% that PCA recommended. The results of the cement-stabilized specimens are shown in Table 45. Samples 1 through 4 had soil-cement losses below the maximum of 10% allowed by PCA (Table 36). The maximum change in volume and moisture content, during freeze-thaw cycling, showed increases in volume and moisture contents. However the unbrushed samples showed significant loss of material so the values are not representative of the entire testing duration. Sample 1 had the highest approximate moisture content during testing even though it had the lowest initial moisture content of 13% versus 20% and 22% for Samples 2-4. Pictures of the brushed cement-stabilized samples before and after freeze-thaw cycling are shown in Figure 125 through Figure 128. The mass change of the brushed cement-stabilized samples is shown in Figure 129. The increase in mass after the first cycle is because the samples are absorbing water, which very evident for sample 1. The percent change in mass is presented in Figure 130.

**Table 45. Cement-treated loess freeze-thaw durability results**

| Sample # | Design moisture content (%) | Design cement content (%) | Sample moisture content (%) | Sample dry unit weight (kN/m3) | Soil-cement loss (%) | Maximum volume change (%) | Maximum moisture content (%) |
|---|---|---|---|---|---|---|---|
| Loess#1 | 13 | 9 | 13.63 | 15.6 | 4.7 | -0.3 | 24.6 |
| Loess#2 | 20 | 9 | 20.56 | 16.6 | 5.5 | -1.3 | 21.7 |
| Loess#3 | 20 | 11 | 20.38 | 16.6 | 2.7 | -1.2 | 22 |
| Loess#4 | 22 | 13 | 22.51 | 16.6 | 2.3 | -10.8 | 21.7 |

**Figure 125. Cement-treated loess freeze-thaw durability sample #1 before (left) and after (right) testing**

**Figure 126. Cement-treated loess freeze-thaw durability sample #2 before (left) and after (right) testing**


**Figure 127. Cement-treated loess freeze-thaw durability sample #3 before (left) and after (right) testing**


**Figure 128. Cement-treated loess freeze-thaw durability sample #4 before (left) and after (right) testing**

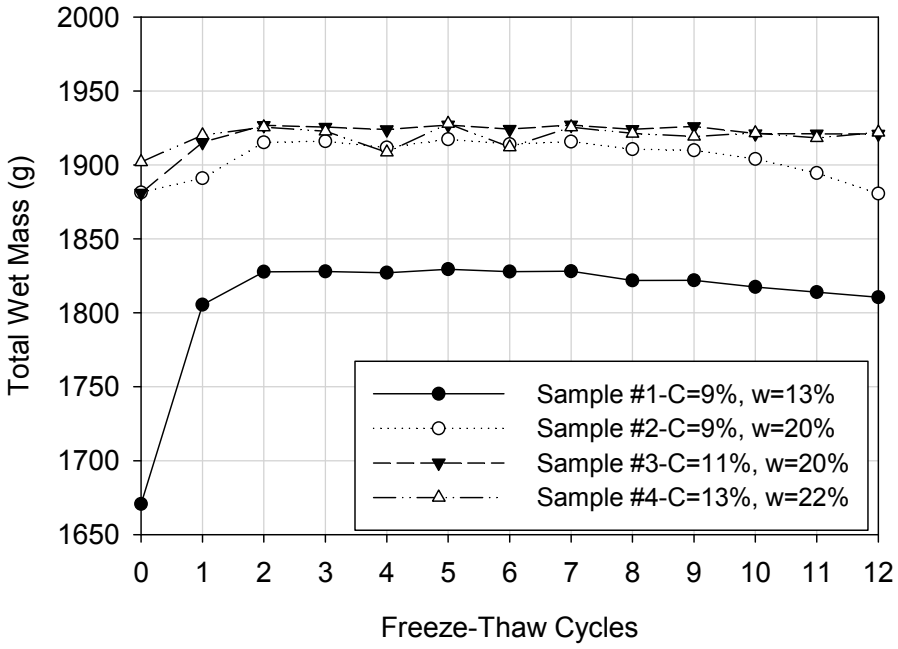


**Figure 129. Cement-treated loess mass change during freeze-thaw cycling**

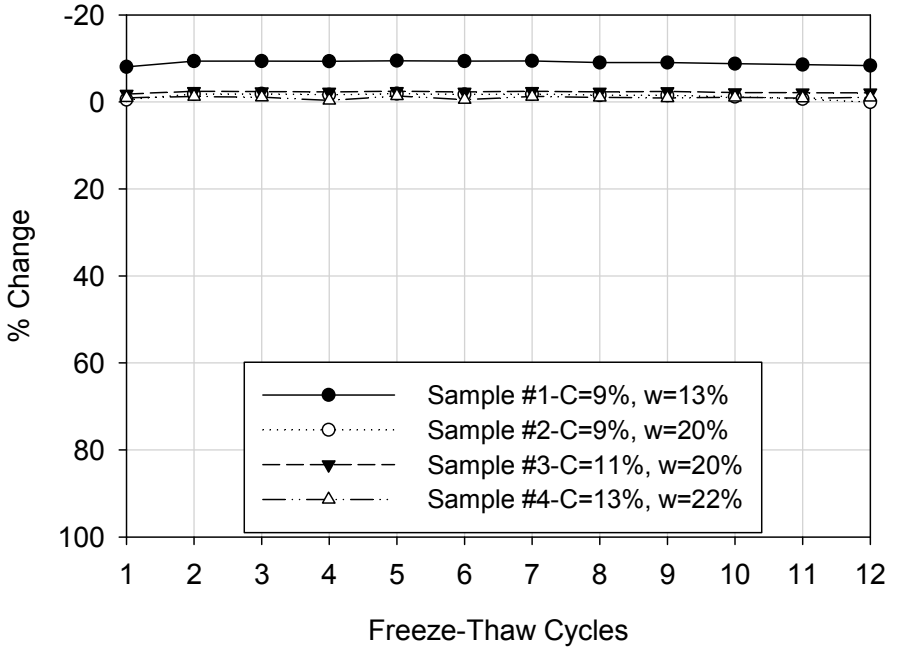


**Figure 130. Cement-treated loess percent mass change during freeze-thaw cycling**

The results of the fly-ash stabilized samples are shown in Table 46. All of the fly-ash stabilized samples failed before the end of the 12 freeze-thaw test cycles. The maximum volume change and moisture content of the unbrushed samples were measured within the first four cycles, after which there was significant material loss in each sample. The samples

before and after freeze-thaw durability testing are shown in Figure 131 through Figure 134. The mass change of the brushed samples is shown in Figure 135 and percent mass change is shown in Figure 136.

**Table 46. Fly ash-treated loess freeze-thaw durability results**

| Sample # | Design moisture content (%) | Design fly ash content (%) | Sample moisture content (%) | Sample dry unit weight (kN/m3) | Soil-cement loss (%) | Maximum volume change (%) | Maximum moisture content (%) |
|---|---|---|---|---|---|---|---|
| 5 | 10 | 10 | 10.7 | 15.3 | 100 | -5.1 | 31.2 |
| 6 | 19 | 10 | 18.7 | 16.4 | 100 | -0.3 | 21.5 |
| 7 | 19 | 15 | 19 | 16.6 | 100 | -5 | 26 |
| 8 | 22 | 20 | 21.7 | 16.8 | 100 | -0.8 | 21 |

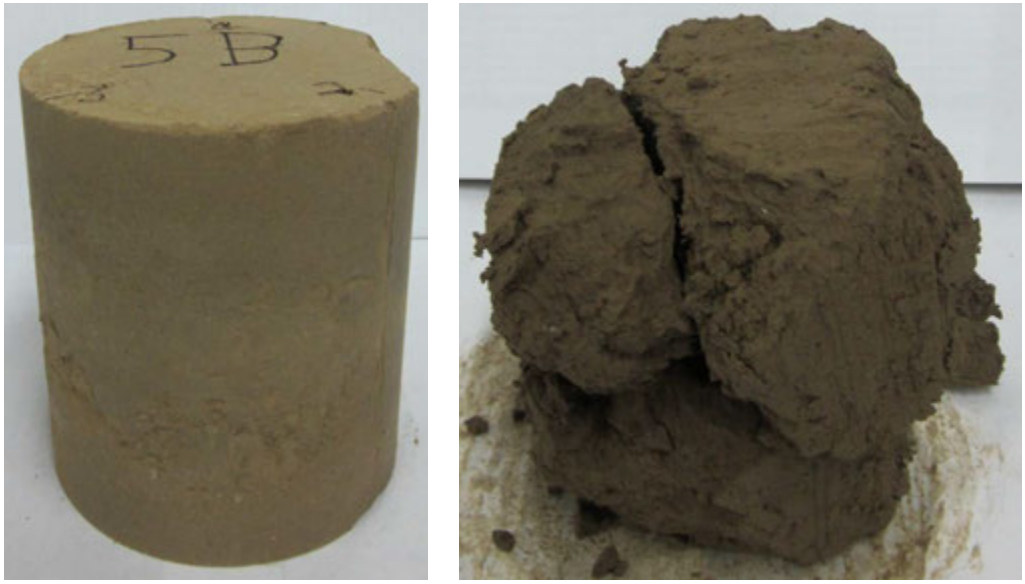


**Figure 131. Fly ash-treated loess freeze-thaw durability sample #5 before (left) and after 3rd cycle (right)**


**Figure 132. Fly ash-treated loess freeze-thaw durability sample #6 before (left) and after7th cycle (right)**


**Figure 133. Fly ash-treated loess freeze-thaw durability sample #7 before (left) and after 8th cycle (right)**

**Figure 134. Fly ash-treated loess freeze-thaw durability sample #8 before (left) and after 8th cycle (right) testing**

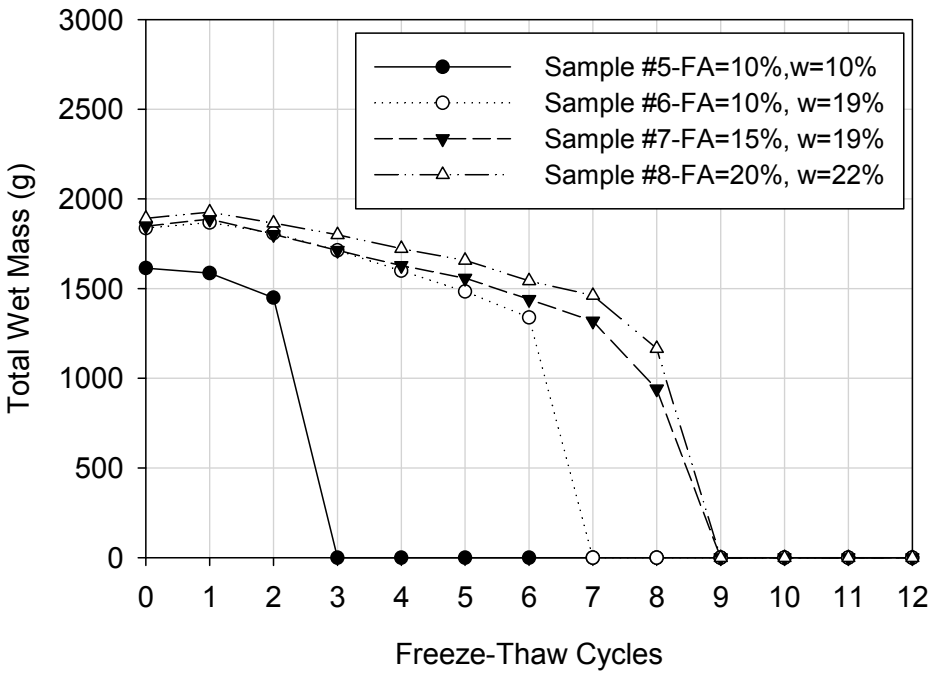


**Figure 135. Fly ash-treated loess mass change during freeze-thaw cycling**

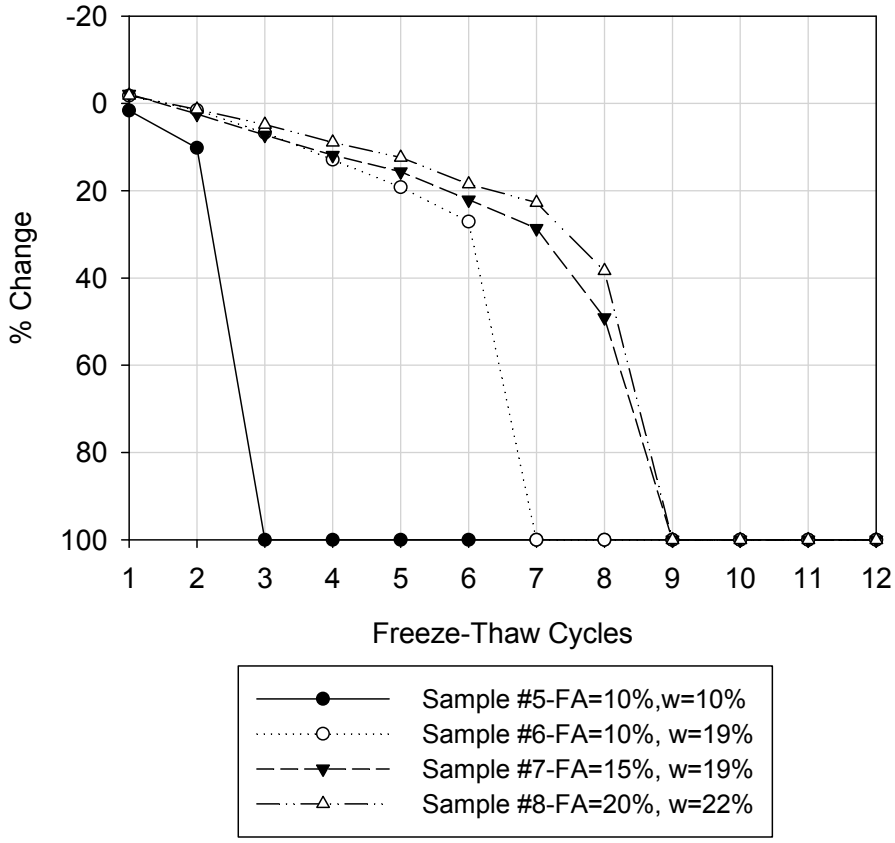


**Figure 136. Fly-ash treated loess percent mass change during freeze-thaw cycling**

The cement-stabilized loess samples met the maximum soil-cement loss requirements; however the fly ash-stabilized samples did not. The results show that the test methods are too harsh for fly ash stabilized materials. It is evident that cement-stabilization is much more effective at increasing the durability of this material.

**Summary**

Table 47 summarizes the results of the wet-dry durability tests and Table 48 summarizes the results of the freeze-thaw durability tests. All of the fly ash stabilized materials failed to meet the maximum soil-cement loss criteria set forth by PCA. However, the fly ash samples were cured under the same conditions as the cement samples and it could be possible that a longer curing period could result in better durability results. The cement stabilized materials from PA US-22 did not meet the criteria, however the loess samples and CTB samples from MI I-96 did. The durability tests outlined in ASTM D559-03 and 560-03 are rigorous tests that require the soil to have significant strength to meet the requirements.

**Table 47. Summary of wet-dry durability results**

| Sample # | Stabilizer | Design stabilizer content (%) | Sample Moisture content (%) | Soil-cement loss (%) | Met soil-cement loss requirements? |
|---|---|---|---|---|---|
| IA I-29 #1 | Fly ash | 15 | 20.1 | 100 | No |
| MI I-96#1 | Cement | 10.7 | — | 4.2 | Yes |
| MI I-96#2 | Cement | 10.7 | — | 4.3 | Yes |
| MI I-96#3 | Cement | 10.7 | — | 12.9 | Yes |
| PA US-22 #1 | Cement | 10 | 21.2 | 11.4 | No |

**Table 48. Summary of freeze-thaw durability results**

| Sample # | Stabilizer | Design stabilizer content (%) | Sample moisture content (%) | Soil-cement loss (%) | Met soil-cement loss requirements? |
|---|---|---|---|---|---|
| IA I-29 #2 | Fly ash | 15 | 19.3 | 100 | No |
| MI I-96 #4 | Cement | 10.7 | — | 3.4 | Yes |
| MI I-96 #5 | Cement | 10.7 | — | 4.4 | Yes |
| MI I-96 #6 | Cement | 10.7 | — | 3.8 | Yes |
| PA US-22 #2 | Cement | 10 | 20.8 | 53.3 | No |
| Loess #1 | Cement | 9 | 13.63 | 4.7 | Yes |
| Loess #2 | Cement | 9 | 20.56 | 5.5 | Yes |
| Loess #3 | Cement | 11 | 20.38 | 2.7 | Yes |
| Loess #4 | Cement | 13 | 22.51 | 2.3 | Yes |
| Loess #5 | Fly ash | 10 | 10.7 | 100 | No |
| Loess #6 | Fly ash | 10 | 18.7 | 100 | No |
| Loess #7 | Fly ash | 15 | 19 | 100 | No |
| Loess #8 | Fly ash | 20 | 21.7 | 100 | No |

## FROST HEAVE AND THAW WEAKENING TESTS

Frost-heave and thaw-weakening laboratory tests were performed on disturbed samples of typical pavement foundation materials to relatively classify the materials according to their frost-susceptibility. The tests were performed according to ASTM D5918-06, which specifies two freeze-thaw cycles and recommends that four samples be tested for each material. Testing was also performed on stabilized materials to determine if they are able to reduce the frost susceptibility of a naturally high frost-susceptible material. ASTM D5918-06 outlines frost-susceptibility criteria that classify materials based on the heave rate and post-test CBR (Table 49).

**Table 49. Frost-susceptibility classifications (ASTM D5918-06)**

| Frost Susceptibility Classification | 8-hr Heave Rate (mm/day) | Bearing Ratio After Thaw (%) |
|---|---|---|
| Negligible | <1 | >20 |
| Very low | 1 to 2 | 20 to 15 |
| Low | 2 to 4 | 15 to 10 |
| Medium | 4 to 8 | 10 to 5 |
| High | 8 to 16 | 5 to 2 |
| Very High | >16 | <2 |

The heave rate is determined from the slope of the heave versus time plot. ASTM D5918-06 specifies that the frost-heave rate should be determined during the first eight hours of each freeze thaw cycle, the boundary temperatures and test schedule is shown in Table 50. However, the samples did not always heave during the first 8 hours and because the heave rate determined from the first 8 hours is very similar to the 24 hour heave rate, the 24 hour heave rate is reported. The heave rate was determined from the time the sample began to heave until heaving had ceased and the temperature began to rise.

**Table 50. Boundary temperature conditions (ASTM D5918-06)**

| Day | Elapsed time (hr) | Top plate temperature (°C) | Bottom plate temperature (°C) | Comments |
|---|---|---|---|---|
| 1 | 0 | 3 | 3 | 24 hr conditioning |
| 2 | 24 | -3 | 3 | First 8 hr freeze |
| | 32 | -12 | 0 | Freeze to bottom |
| 3 | 48 | 12 | 3 | First thaw |
| | 64 | 3 | 3 | |
| 4 | 72 | -3 | 3 | Second 8 hr freeze |
| | 80 | -12 | 0 | Freeze to bottom |
| 5 | 96 | 12 | 3 | Second thaw |
| | 112 to 120 | 3 | 3 | |

The samples were compacted in 5 equal layers with 40 blows per layer from a standard 5.5 lb. Proctor hammer. The samples were saturated before testing began and an open system was used during testing. The elevation of the water supply was 0.5 in. above the sample bottom. The freezing point depression of the materials was not measured because the temperature measurement system did not meet accuracy requirements.

The following sections present the results of the frost-heave and thaw-weakening test. The frost-heave time plots and moisture content profiles for each of the samples are

presented along with the heave rates, bearing ratios, frost-heave susceptibility, and thaw-weakening susceptibility.

The first and second heave rates are provided to determine if the frost-susceptibility increases with additional freeze-thaw cycles. The first heave rate is recommended for use in areas where there is only one freeze-thaw cycle, whereas the second heave rate is recommended for areas that experience multiple freeze-thaw cycles. For each material, the properties are summarized by and average ($\mu$), standard deviation ($\sigma$), and coefficient of variation (COV). The individual sample properties for each material are presented in Appendix D along with the following average initial sample properties: dry unit weight ($\gamma_d$), moisture content ($w$%), saturation (S), void ratio (e), and porosity (n).

The materials are presented according to where they were sampled and in the same order as they were presented in chapter 4.

## 160th Street

### Well Graded Sand with Silt and Gravel

Heave began at different times for sample 1 compared to samples 2, 3, and 4. The total heave for sample 1 is higher than samples 2, 3, and 4; however the slopes of the lines are very similar so the heave rates are similar. It is evident from the frost heave time plots that the frost susceptibility of this material increases with an additional freeze-thaw cycle, because the total heave and slope of the heave versus time line are higher and steeper, respectively, for the second freeze-thaw cycle compared to the first. After the first and second freeze-thaw cycles, the samples consolidated to near their original height, which indicates that most of the water drawn into the soil drained during thawing. The frost heave time plot for the 160$^{th}$ Street ditch material is presented in Figure 137.

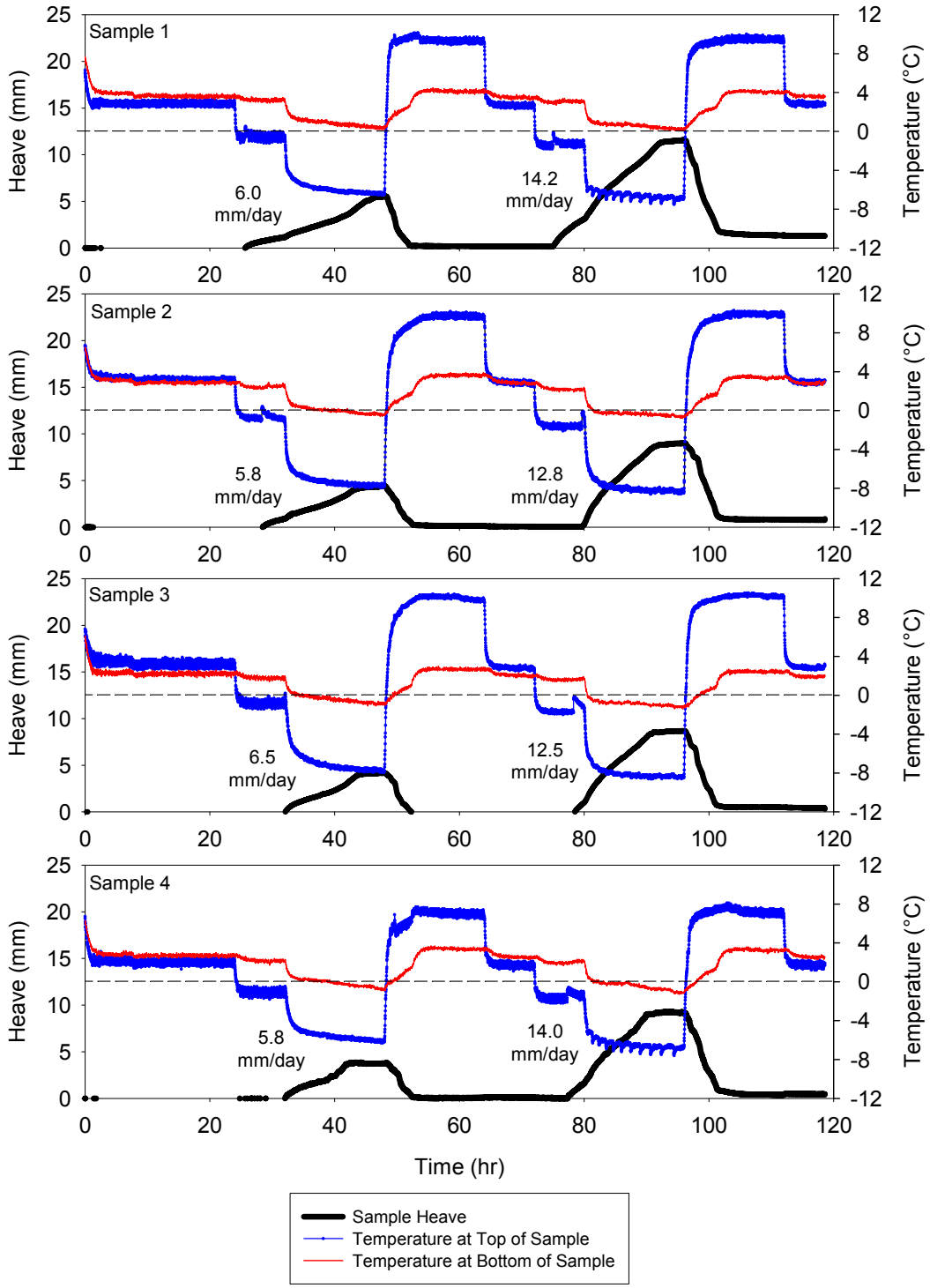


**Figure 137. 160th Street well graded sand with silt and gravel frost heave time plots**

The final moisture contents of the material do not significantly vary from the initial sample moisture contents. Figure 138 shows the moisture content profile of the four samples after freeze-thaw cycling.

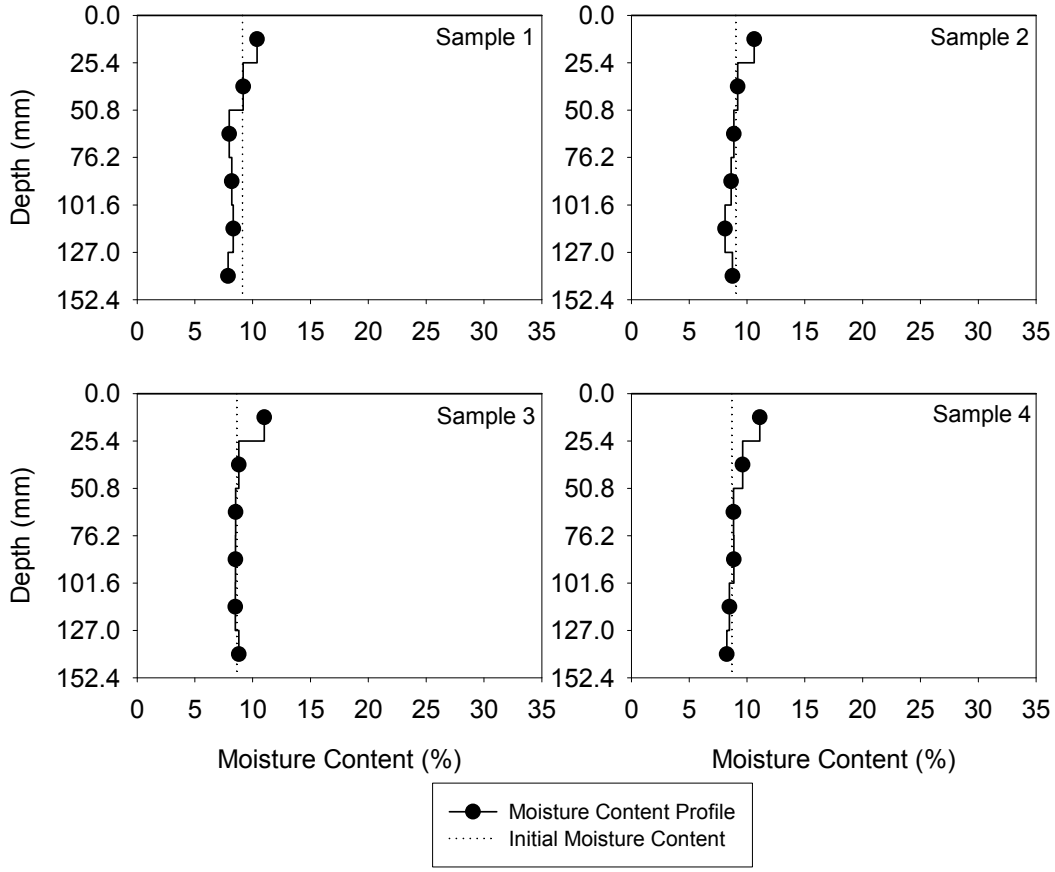


**Figure 138. 160th Street well graded sand with silt and gravel moisture content profiles**

The CBR of the material decreased after freeze-thaw cycling compared to the standard CBR test, which was performed at the initial moisture content and standard density. The thaw-weakening susceptibility of the material is rated as very low. The second frost-heave rate increased compared to the first frost-heave rate, which resulted in the frost-susceptibility increasing from medium to high. Table 51 summarizes the average frost-heave and thaw-weakening test results.

**Table 51. 160th Street well graded sand with silt and gravel frost-heave and thaw-weakening test results**

| | μ | σ | COV (%) | # of samples |
|---|---|---|---|---|
| CBR (%) (standard test) | 39.7 | | | 1 |
| CBR (%) (after frost-susceptibility test) | 15.0 | 1.7 | 11.5 | 4 |
| 1st Frost-heave rate (mm/day) | 6.0 | 0.3 | 5.2 | |
| 2nd Frost-heave rate (mm/day) | 13.4 | 0.8 | 6.2 | |
| 1st Frost-heave susceptibility rating | Medium | — | — | |
| 2nd Frost-heave susceptibility rating | High | — | — | |
| Thaw-weakening susceptibility rating | Very Low | — | — | |

**Poorly Graded Sand with Silt and Gravel**

The frost-susceptibility of the roadway material increased after the second freeze-thaw cycle. The total heave and slopes of the heave versus time plots are very similar for all four samples. The height of the samples returned to their initial height after the first and second freeze-thaw cycles, which indicates most of the water drawn into the soil drained during thawing. The frost heave time plots for the 160th Street roadway material are presented in Figure 139.

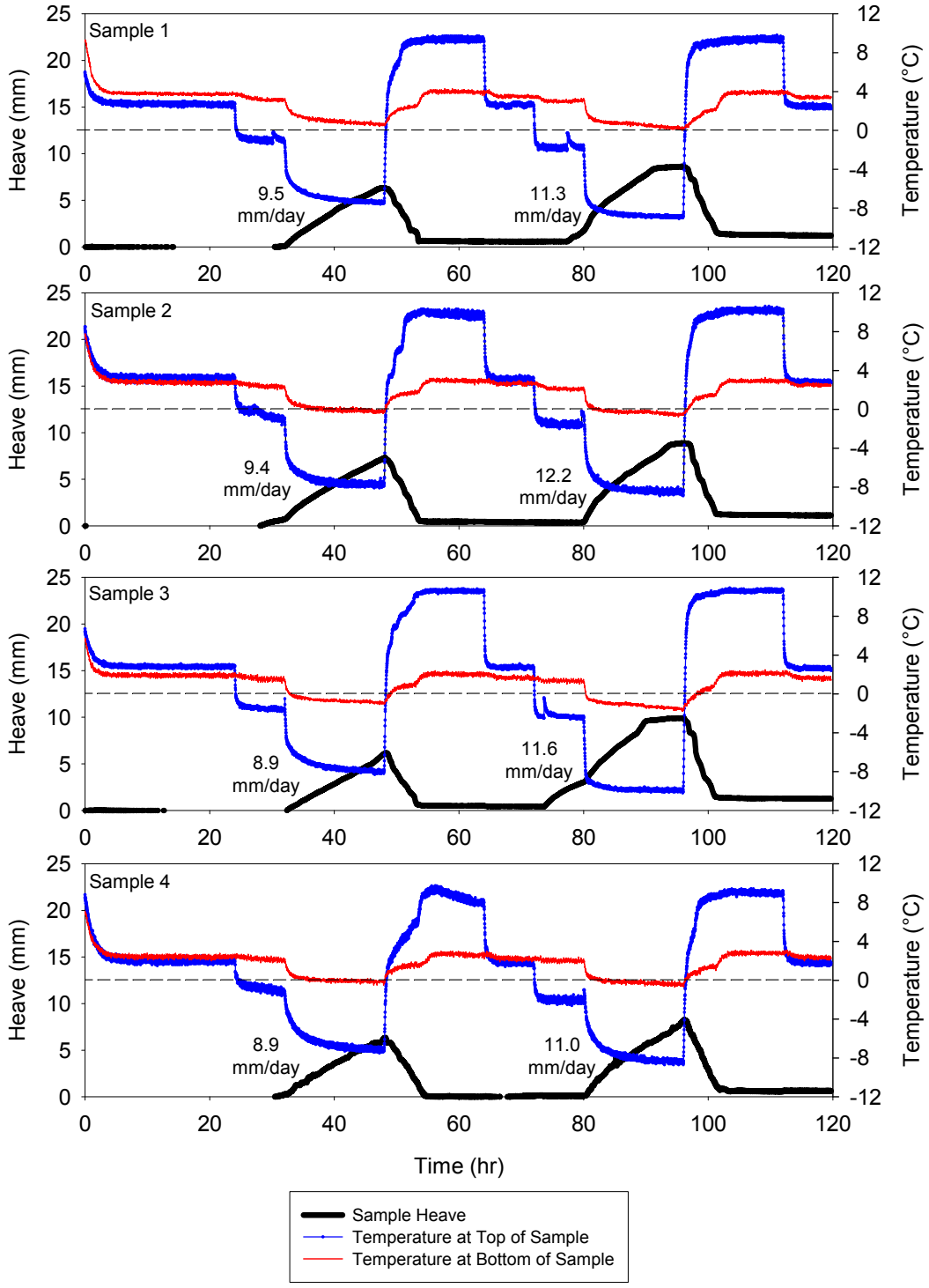


**Figure 139. 160th Street poorly graded sand with silt and gravel frost heave time plots**

The final moisture contents are very similar to the initial sample moisture contents and there is no sign of increased moisture at the top of the samples. The moisture content profiles for the roadway material are presented in Figure 140.

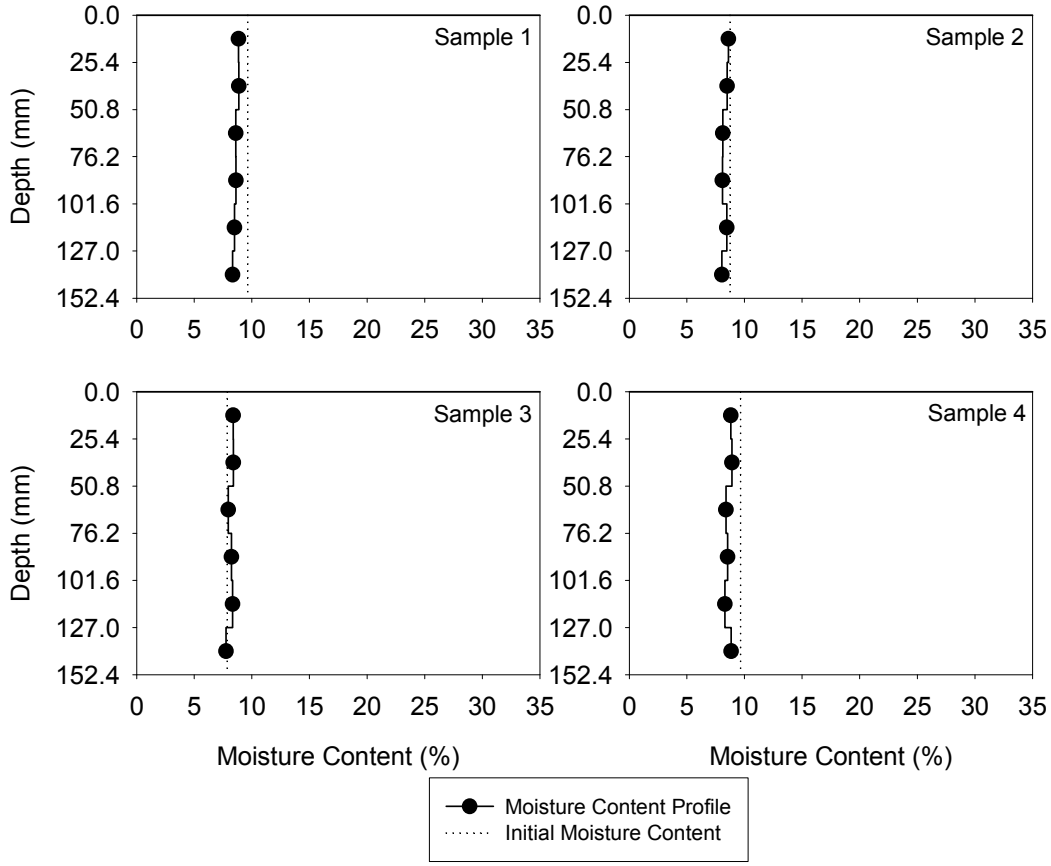


**Figure 140. 160th Street poorly graded sand with silt and gravel moisture content profiles**

There is a decrease in the CBR between the standard test and after freeze-thaw cycling. However, the thaw-weakening susceptibility of the material was rated as negligible. The frost-heave rate increased between the first and second freeze. Both frost-heave rates were rated as high. Table 52 summarizes the frost-heave and thaw-weakening test results.

**Table 52. 160th Street poorly graded sand with silt and gravel frost-heave and thaw-weakening test results**

| | μ | σ | COV (%) | # of samples |
|---|---|---|---|---|
| CBR (%) (standard test) | 65.1 | | | 1 |
| CBR (%) (after frost-susceptibility test) | 28.9 | 6.1 | 21.1 | 4 |
| 1st Frost-heave rate (mm/day) | 9.2 | 0.3 | 3.1 | |
| 2nd Frost-heave rate (mm/day) | 11.5 | 0.5 | 4.5 | |
| 1st Frost-heave susceptibility rating | High | — | — | |
| 2nd Frost-heave susceptibility rating | High | — | — | |
| Thaw-weakening susceptibility rating | Negligible | — | — | |

## IA I-29

### Lean Clay Subgrade

The slope of the heave versus time line increased between the first and second freeze. The height of the samples increased after both of the freeze-thaw cycles. This would show that the moisture drawn into the sample, by capillary action, did not drain from the soil during thawing. The frost-heave time plots are presented in Figure 141 for the lean clay subgrade from IA I-29.

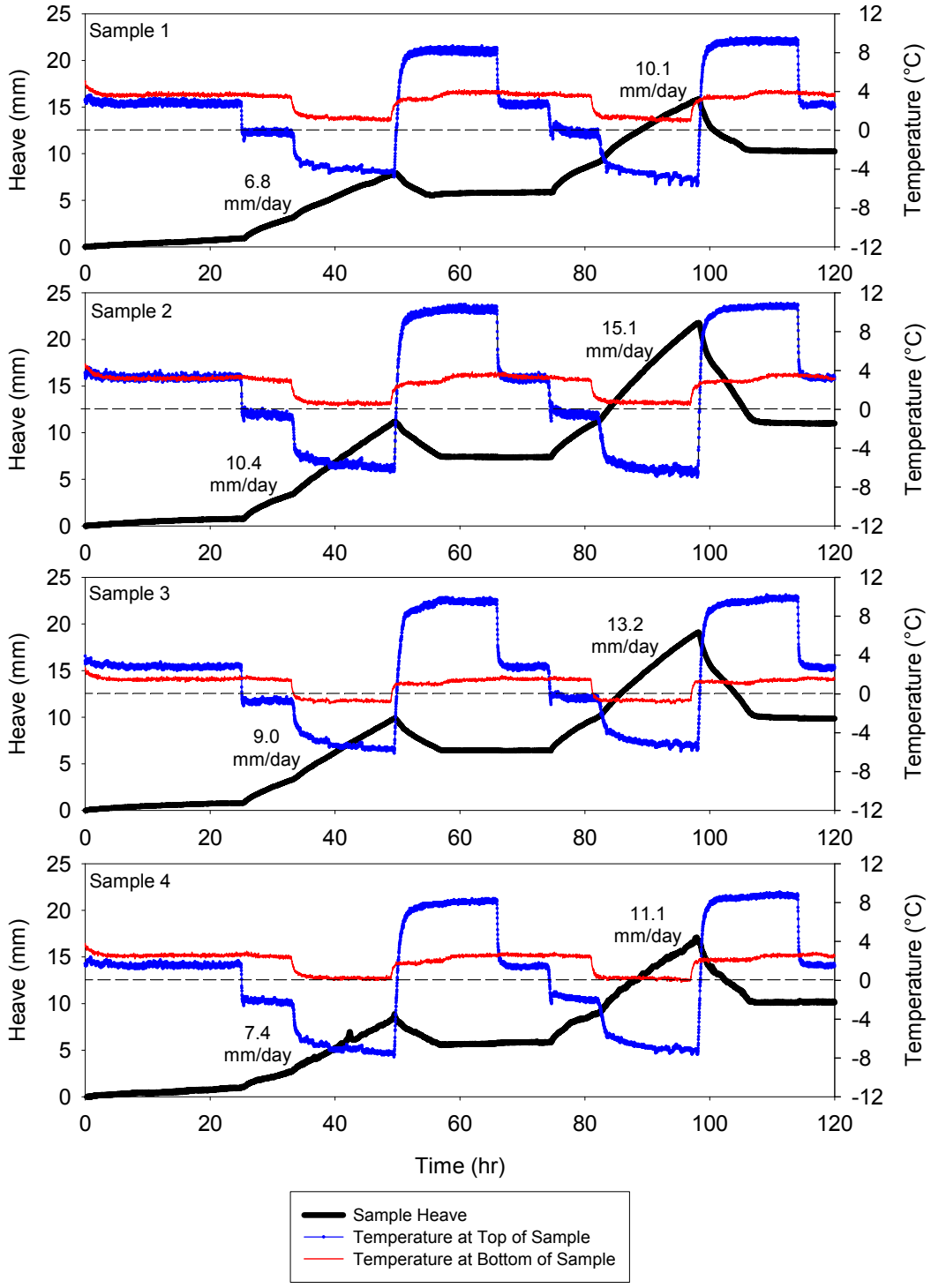


**Figure 141. IA I-29 lean clay subgrade frost heave time plots**

The moisture content after freeze-thaw cycling is higher at all depths in the samples compared to the initial moisture content. The moisture content at the top of the sample is also

higher than the middle or bottom the sample, which would indicate that water was drawn to the top cold plate through capillary action caused by the temperature gradient in the samples. Figure 142 presents the moisture content profiles of the four samples.

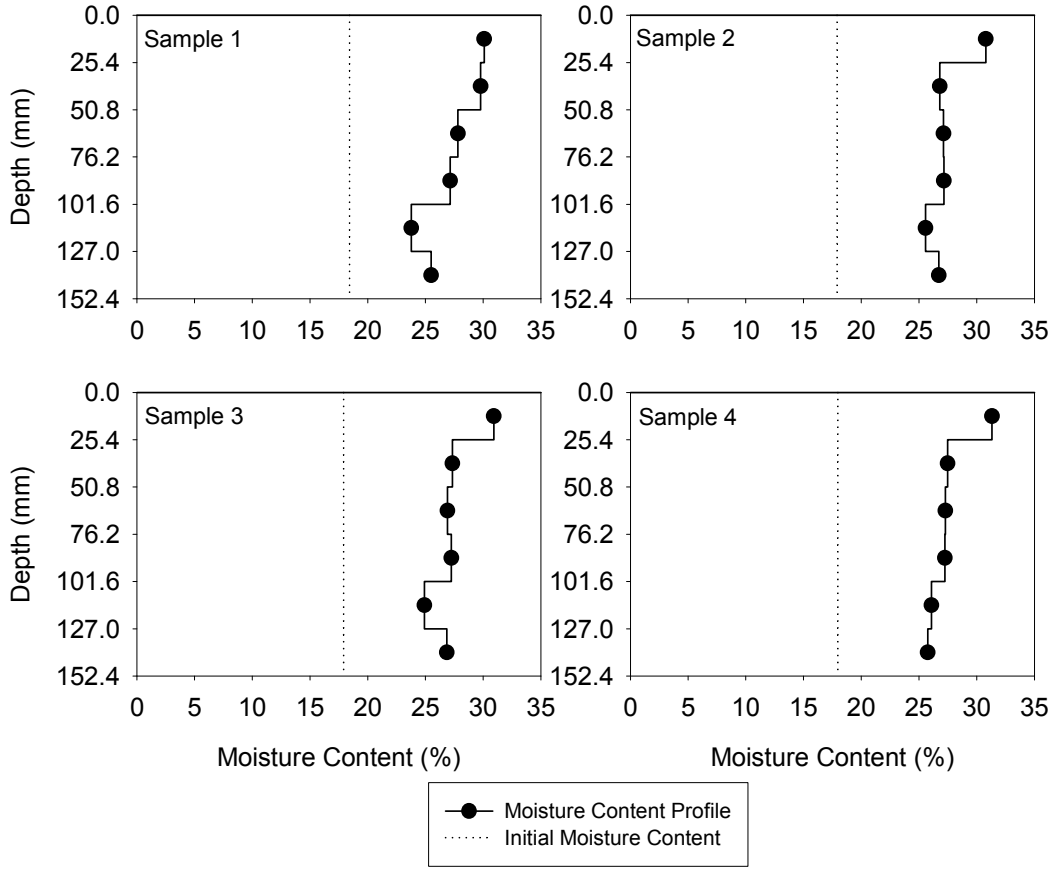


**Figure 142. IA I-29 lean clay subgrade moisture content profiles**

The CBR decreased after the frost-heave test compared to the standard CBR. The thaw-weakening susceptibility rating is very high for this material. The second frost-heave rate was higher than the first frost-heave rate, which indicates the material is sensitive to additional freeze-thaw cycles. The frost-heave susceptibility is rated as high for both the first and second freeze cycles. The frost-heave and thaw-weakening test results are presented in Table 53.

**Table 53. IA I-29 lean clay subgrade frost-heave and thaw-weakening test results**

| | μ | σ | COV (%) | # of samples |
|---|---|---|---|---|
| CBR (%) (standard test) | 21.8 | | | 1 |
| CBR (%) (after frost-susceptibility test) | 0.7 | 0.0 | 12.0 | 4 |
| 1st Frost-heave rate (mm/day) | 8.4 | 1.4 | 16.8 | |
| 2nd Frost-heave rate (mm/day) | 12.4 | 2.2 | 17.9 | |
| 1st Frost-heave susceptibility rating | High | — | — | |
| 2nd Frost-heave susceptibility rating | High | — | — | |
| Thaw-weakening susceptibility rating | Very high | — | — | |

**Silt with Sand Subgrade**

The slope of the first heave versus time line for samples 1, 2, and 3 are very similar, however sample 4 does not have as much total heave. The slope of the heave versus time lines during the second freeze for samples 1 and 2 are very similar, but are very different than samples 3 and 4. The height of the samples increased after the first and second freeze-thaw cycle. The frost-heave time plots for the silt with sand subgrade from IA I-29 are presented in Figure 143.

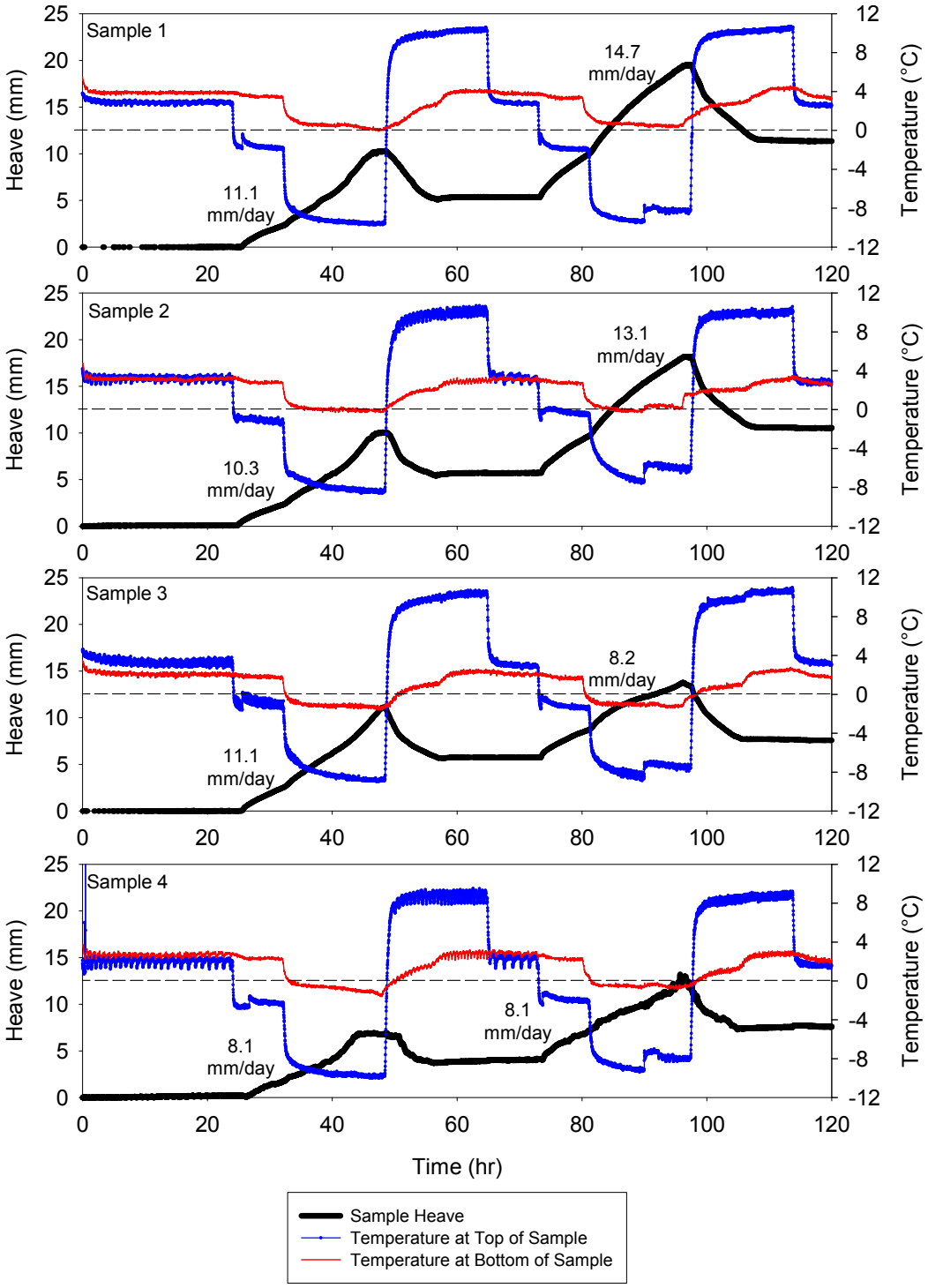


**Figure 143. IA I-29 silt with sand subgrade frost heave time plots**

The post-test moisture contents are higher than the initial moisture contents. The top of the four samples has higher moisture contents than the rest of the sample. The moisture content profiles for the silt with sand subgrade are presented in Figure 144.

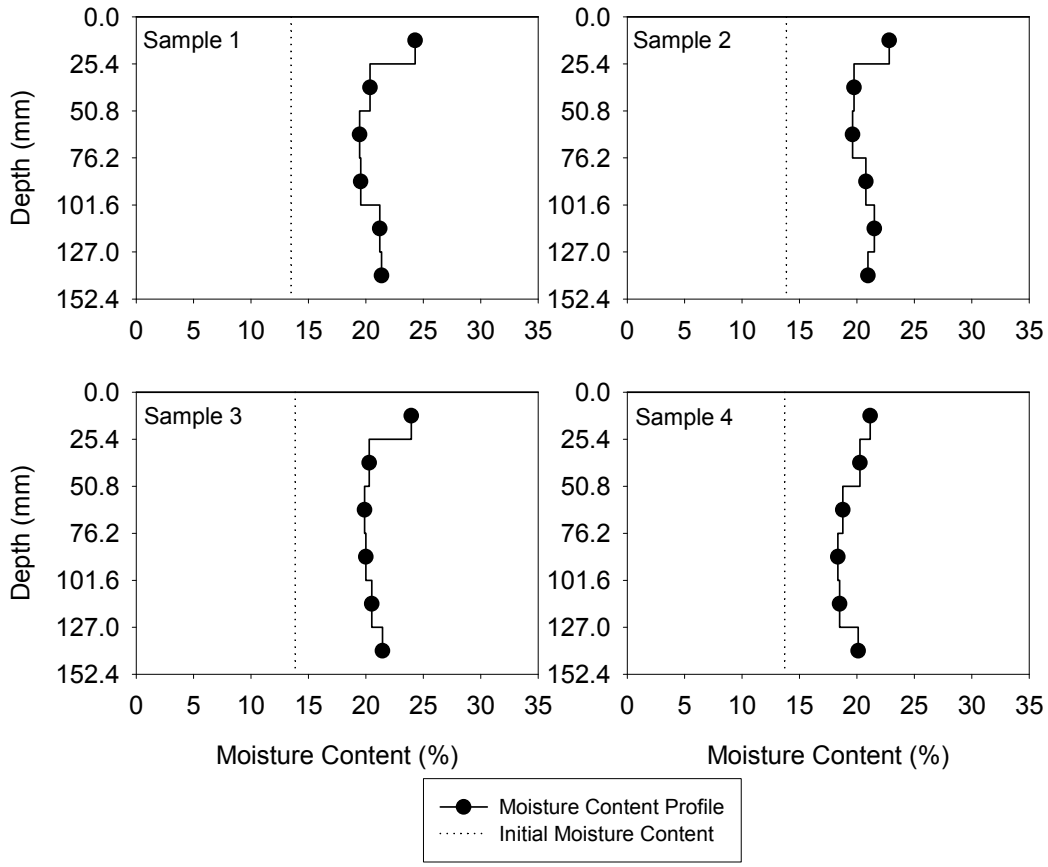


**Figure 144. IA I-29 silt with sand subgrade moisture content profiles**

The CBR of the material decreased after freeze-thaw cycling compared to the standard CBR performed at the initial moisture content. The thaw-weakening susceptibility of the material is very high. The average frost heave rate for the first freezing cycle is around 1 mm/day lower than that of the second freeze; however this average includes the differences between samples 1 and 2 compared to samples 3 and 4. The first and second frost-heave susceptibility ratings are high for the material. The results of the frost-heave and thaw weakening test is summarized in Table 54.

**Table 54. IA I-29 silt with sand subgrade frost-heave and thaw-weakening test results**

| | μ | σ | COV (%) | # of samples |
|---|---|---|---|---|
| CBR (%) (standard test) | 21.6 | | | 1 |
| CBR (%) (after frost-susceptibility test) | 1.4 | 0.4 | 25.9 | 4 |
| 1st Frost-heave rate (mm/day) | 10.2 | 1.3 | 12.4 | |
| 2nd Frost-heave rate (mm/day) | 11.0 | 3.4 | 30.4 | |
| 1st Frost-heave susceptibility rating | High | — | — | |
| 2nd Frost-heave susceptibility rating | High | — | — | |
| Thaw-weakening susceptibility rating | Very high | — | — | |

## IA US-30

### Clayey Sand Subgrade

All four samples heaved more during the second freeze compared to the first freeze, which also increased the slope of the heave versus time line. The temperature profiles for samples 1, 2, and 3 are similar; however sample 4 reached lower temperatures. The height of the samples slightly increased after the first freeze-thaw cycle, but increased more after the second freeze-thaw cycle. The frost-heave time plots for the clayey sand subgrade from IA US-30 are presented in Figure 145.

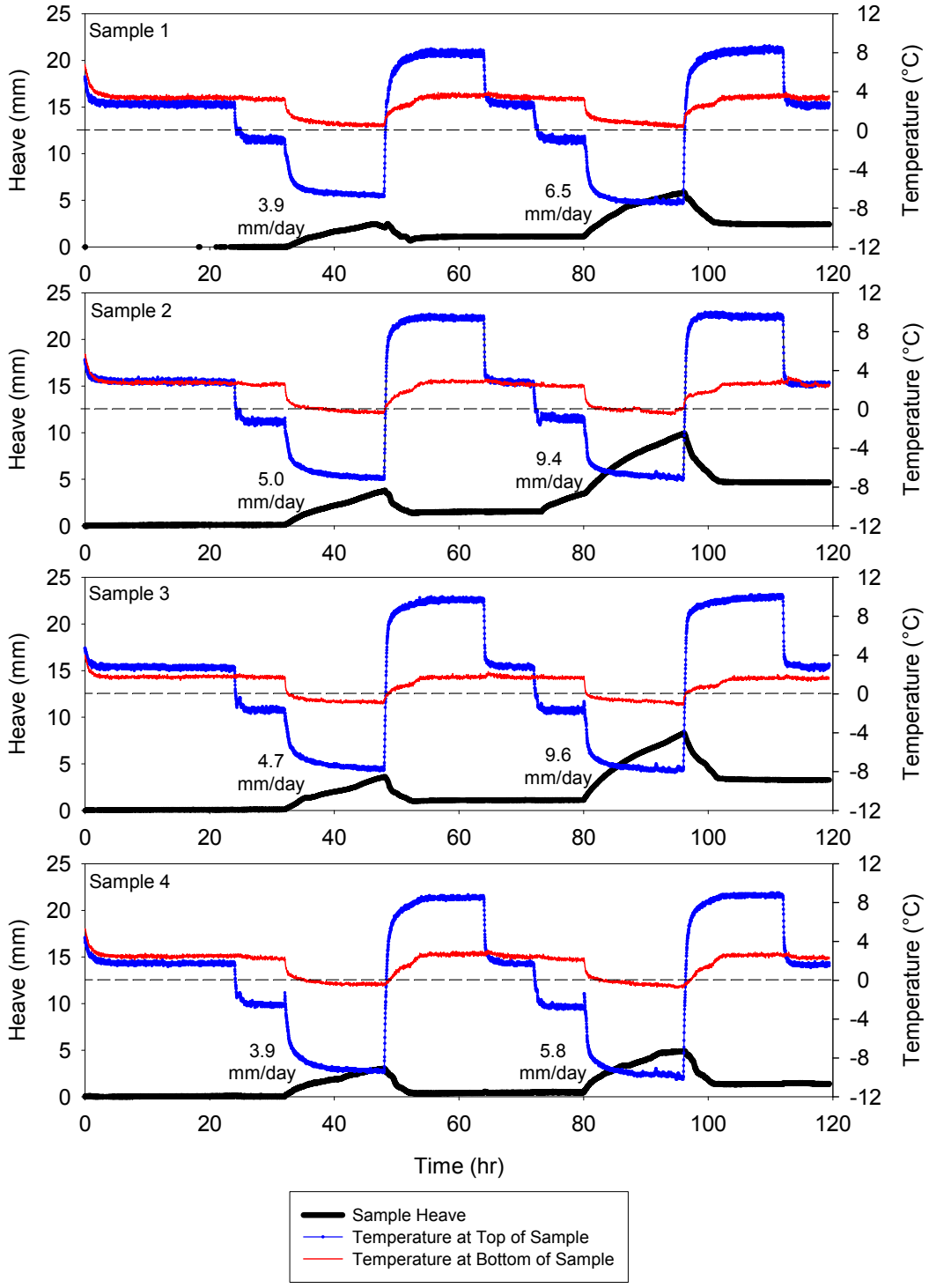


**Figure 145. IA US-30 clayey sand subgrade frost heave time plots**

The moisture contents in the soil profile are similar after freeze-thaw cycling compared to the initial moisture content; however the moisture content at the top of the sample did increase. The moisture content profiles are presented in Figure 146.

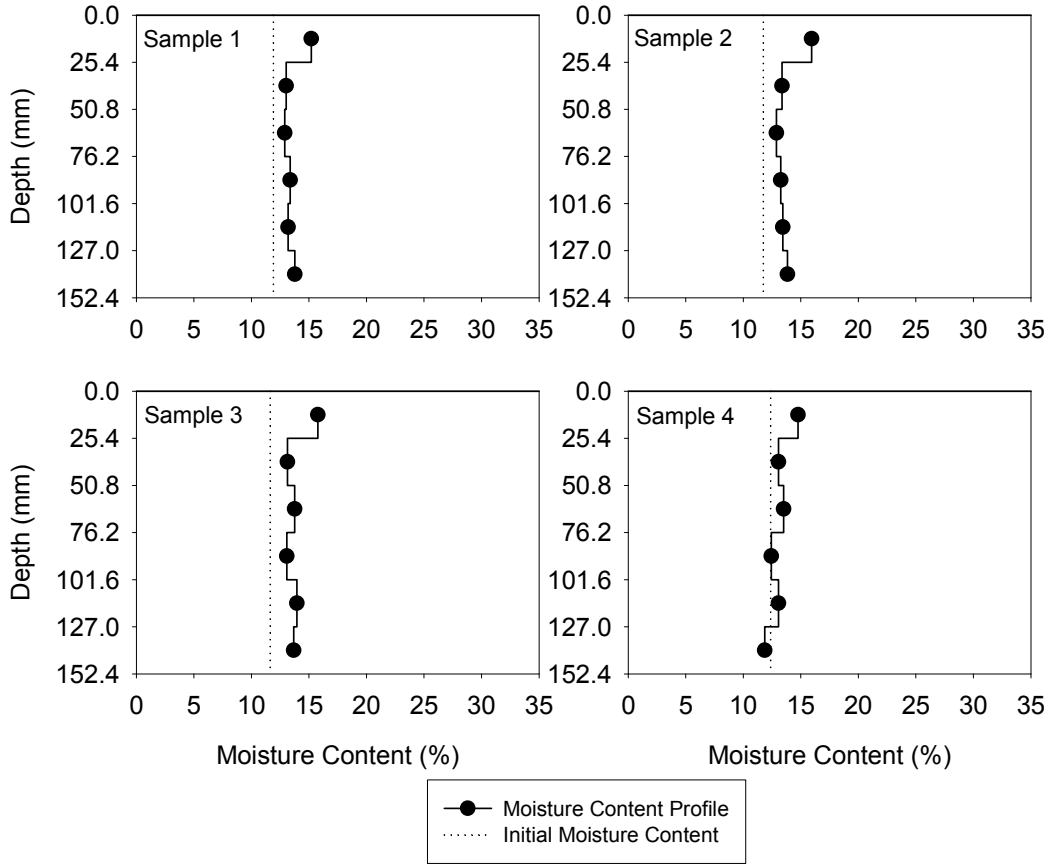


**Figure 146. IA US-30 clayey sand subgrade moisture content profiles**

The CBR from the standard test was low and the thaw-weakening susceptibility would be classified as medium. After freeze-thaw cycling, the thaw-weakening susceptibility increased to high. The frost-heave rate increased from the first freeze to the second; however the frost-heave susceptibility for both freezing periods is medium. The results of the frost-heave and thaw weakening test is summarized in Table 55.

**Table 55. IA US-30 clayey sand subgrade frost-heave and thaw-weakening test results**

| | μ | σ | COV (%) | # of samples |
|---|---|---|---|---|
| CBR (%) (standard test) | 8.4 | | | 1 |
| CBR (%) (after frost-susceptibility test) | 2.67 | 0.4 | 14.7 | 4 |
| 1st Frost-heave rate (mm/day) | 4.4 | 0.5 | 11.5 | |
| 2nd Frost-heave rate (mm/day) | 7.8 | 2.0 | 25.2 | |
| 1st Frost-heave susceptibility rating | Medium | — | — | |
| 2nd Frost-heave susceptibility rating | Medium | — | — | |
| Thaw-weakening susceptibility rating | High | — | — | |

**RPCC/RAP Subbase**

The frost heave time plots for all four samples are very similar. The slope heave versus time lines decreases during the second freeze even though the total heave is nearly the same for the first and second freeze. The height of the samples slightly increased after the first and second freeze-thaw cycles. The frost-heave time plots for the RPCC/RAP subbase from IA US-30 are presented in Figure 147.

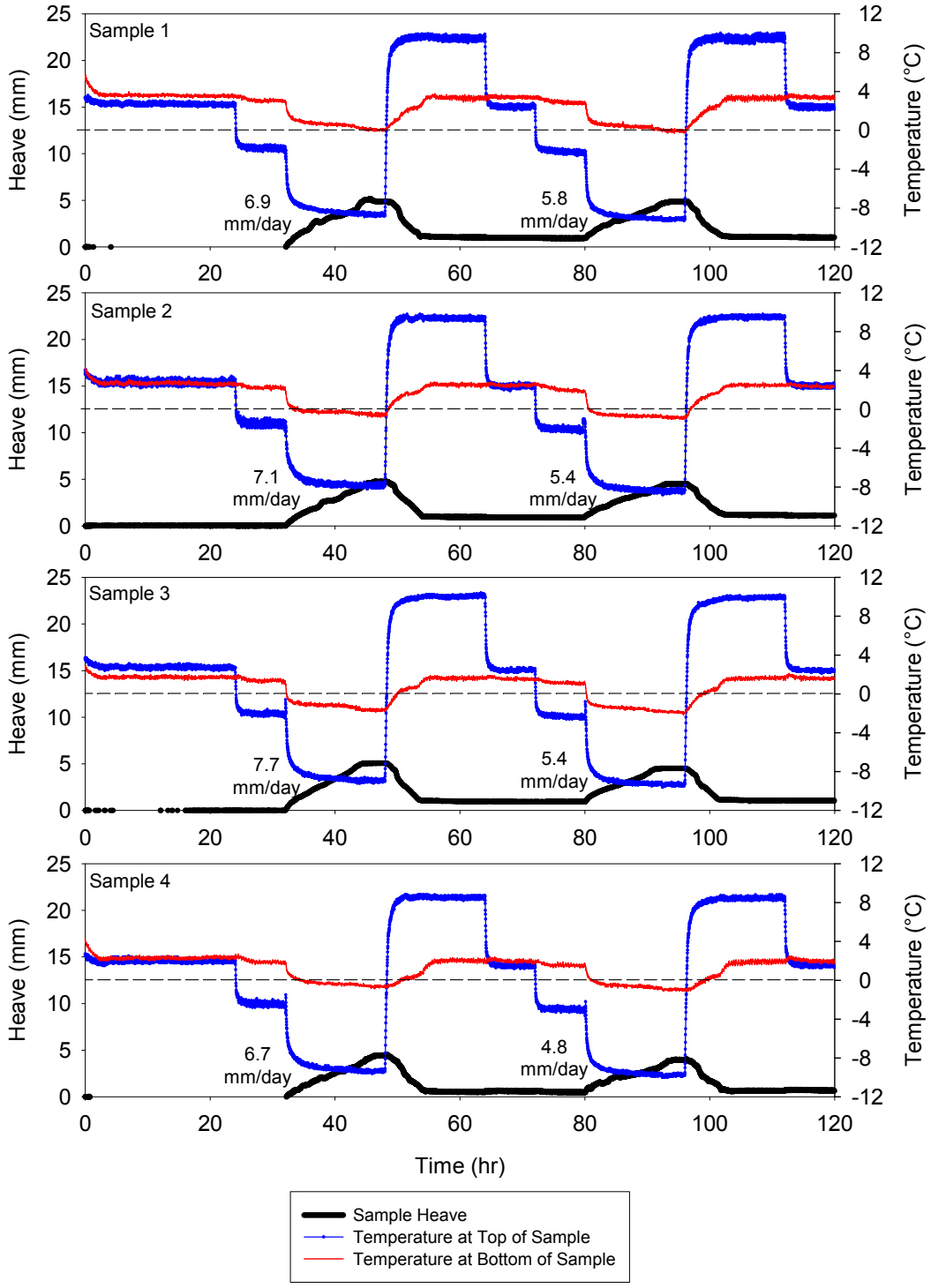


**Figure 147. IA US-30 RPCC/RAP subbase frost heave time plots**

The moisture contents after freeze-thaw cycling decreased from the initial moisture content. Samples 1, 2, and 4 do show higher moisture contents at the top of the samples

compared to the middle of the samples. Figure 148 shows the moisture content profiles after freeze-thaw cycling.

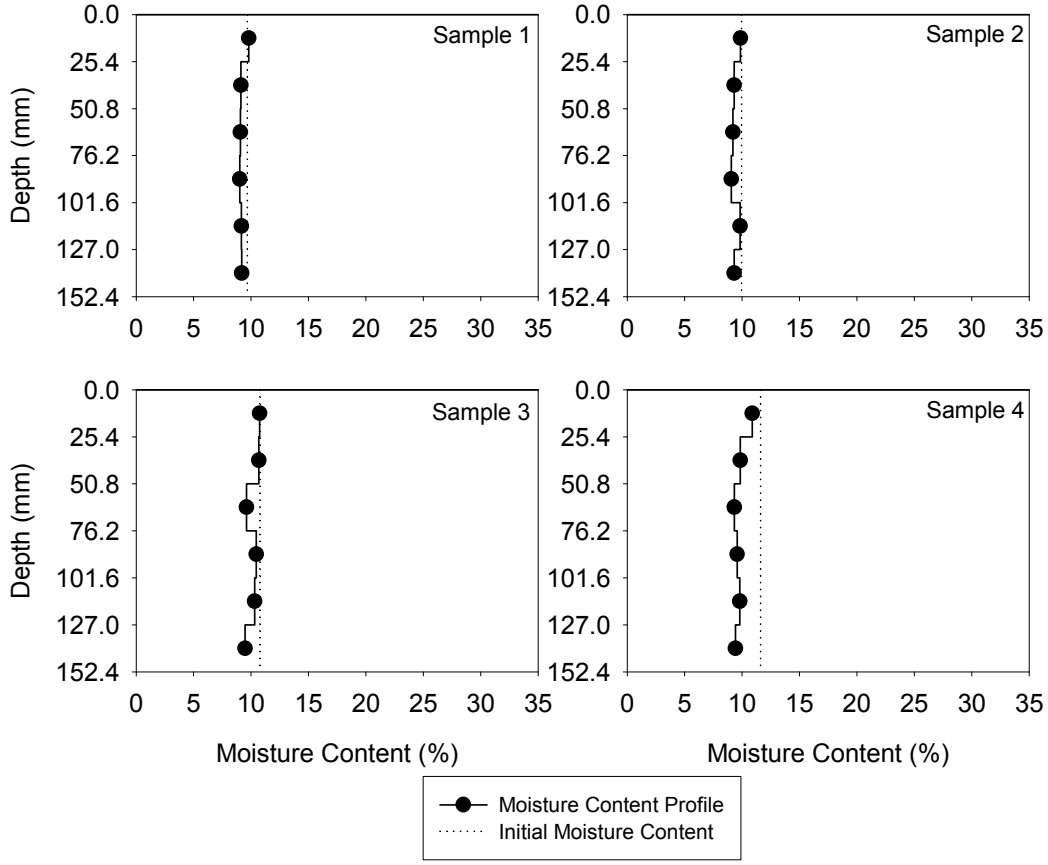


**Figure 148. IA US-30 RPCC/RAP subbase moisture content profiles**

The CBR after freeze-thaw cycling is very close to the standard CBR value. This shows that that the material is resistant to thaw-weakening. The thaw-weakening susceptibility is rated as negligible. The first freeze had a higher frost-heave rate compared to the second freeze. Therefore, the frost-heave susceptibility of this material does not decrease after the first freeze-thaw cycle. The frost-heave susceptibility rating for the first and second freezing periods is medium. The frost-heave and thaw-weakening test results are summarized in Table 56.

**Table 56. IA US-30 RPCC/RAP subbase frost-heave and thaw-weakening test results**

| | μ | σ | COV (%) | # of samples |
|---|---|---|---|---|
| CBR (%) (standard test) | 40.6 | | | 1 |
| CBR (%) (after frost-susceptibility test) | 37.6 | 10.3 | 27.5 | 4 |
| 1st Frost-heave rate (mm/day) | 7.1 | 0.4 | 5.3 | |
| 2nd Frost-heave rate (mm/day) | 5.4 | 0.4 | 7.5 | |
| 1st Frost-heave susceptibility rating | Medium | — | — | |
| 2nd Frost-heave susceptibility rating | Medium | — | — | |
| Thaw-weakening susceptibility rating | Negligible | — | — | |

**Limestone Subbase**

The heights of all four samples returned to the original height after the first and second freeze-thaw cycles, which shows the samples drained during thawing. In general, the total heave is higher after the second freeze compared to the first. The slope of the heave versus time line is very similar for both freezing periods. The frost-heave time plots for the limestone subbase from IA US-30 are presented in Figure 149.

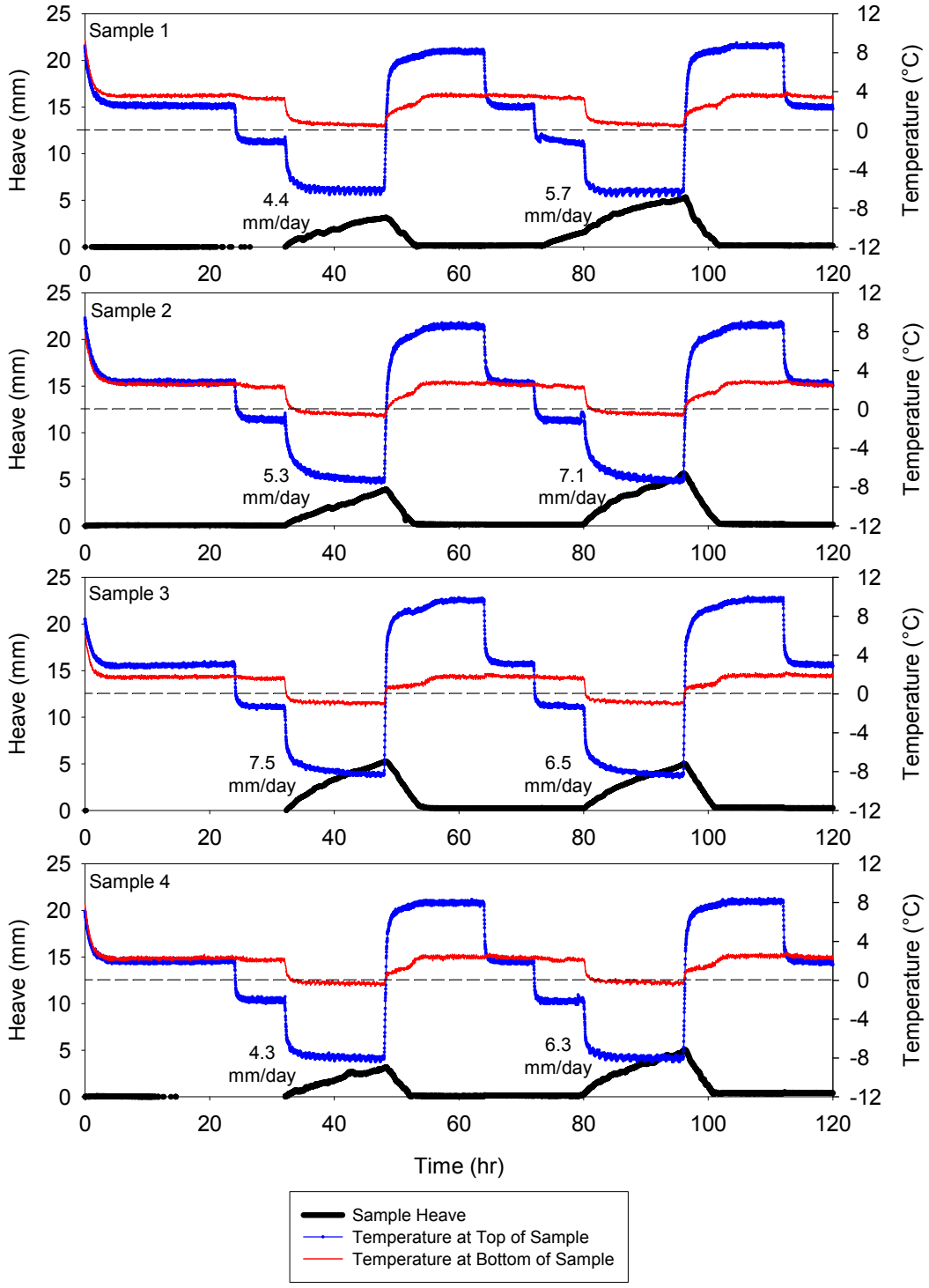


**Figure 149. IA US-30 limestone subbase frost heave time plots**

The sample moisture contents are very similar to the initial moisture contents, except the moisture content at the bottom of the samples is higher than the rest of the sample. The

material might drain fast enough for the water in the sample to move to the bottom during thawing. The moisture content profiles are presented in Figure 150.

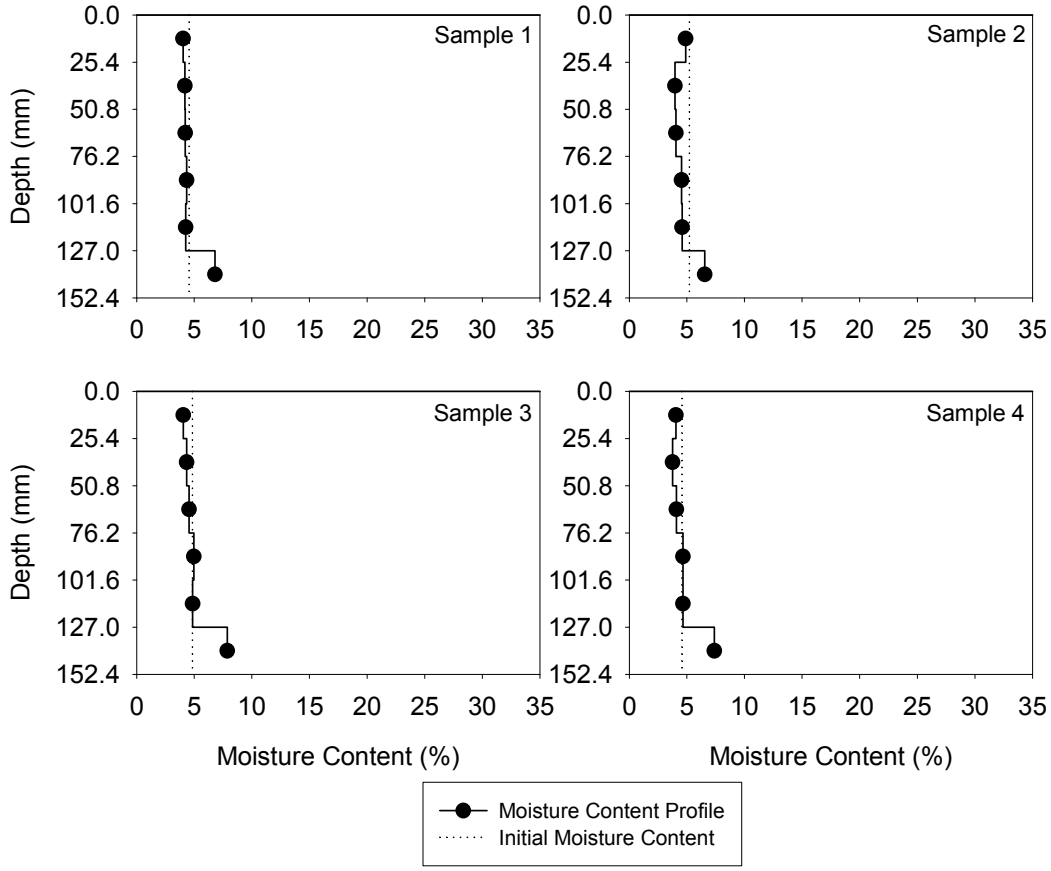


**Figure 150. IA US-30 limestone subbase moisture content profiles**

The post freeze-thaw CBR is lower than the standard CBR; however the thaw-weakening susceptibility is rated as negligible. The frost-heave rate increased during the second freeze compared to the first. The frost-heave susceptibility for the first and second freeze is medium. The results of the frost-heave and thaw weakening susceptibility tests are summarized in Table 57.

**Table 57. IA US-30 limestone subbase frost-heave and thaw-weakening test results**

| | μ | σ | COV (%) | # of samples |
|---|---|---|---|---|
| CBR (%) (standard test) | 70.5 | | | 1 |
| CBR (%) (after frost-susceptibility test) | 33.2 | 6.4 | 19.3 | 4 |
| 1st Frost-heave rate (mm/day) | 5.4 | 1.3 | 23.7 | |
| 2nd Frost-heave rate (mm/day) | 6.4 | 0.6 | 8.9 | |
| 1st Frost-heave susceptibility rating | Medium | — | — | |
| 2nd Frost-heave susceptibility rating | Medium | — | — | |
| Thaw-weakening susceptibility rating | Negligible | — | — | |

**RPCC Subbase**

The slope of the heave versus time line and the total heave decreases during the second freeze compared to the first freeze. The height of the samples increased after the first freeze, but remained nearly the same after the second freeze. The frost-heave time plots are nearly the same for the four samples. The frost-heave time plots are presented in Figure 151. This material is referred to as IA US-30 RPCC Sample 1 in Chapter 4.

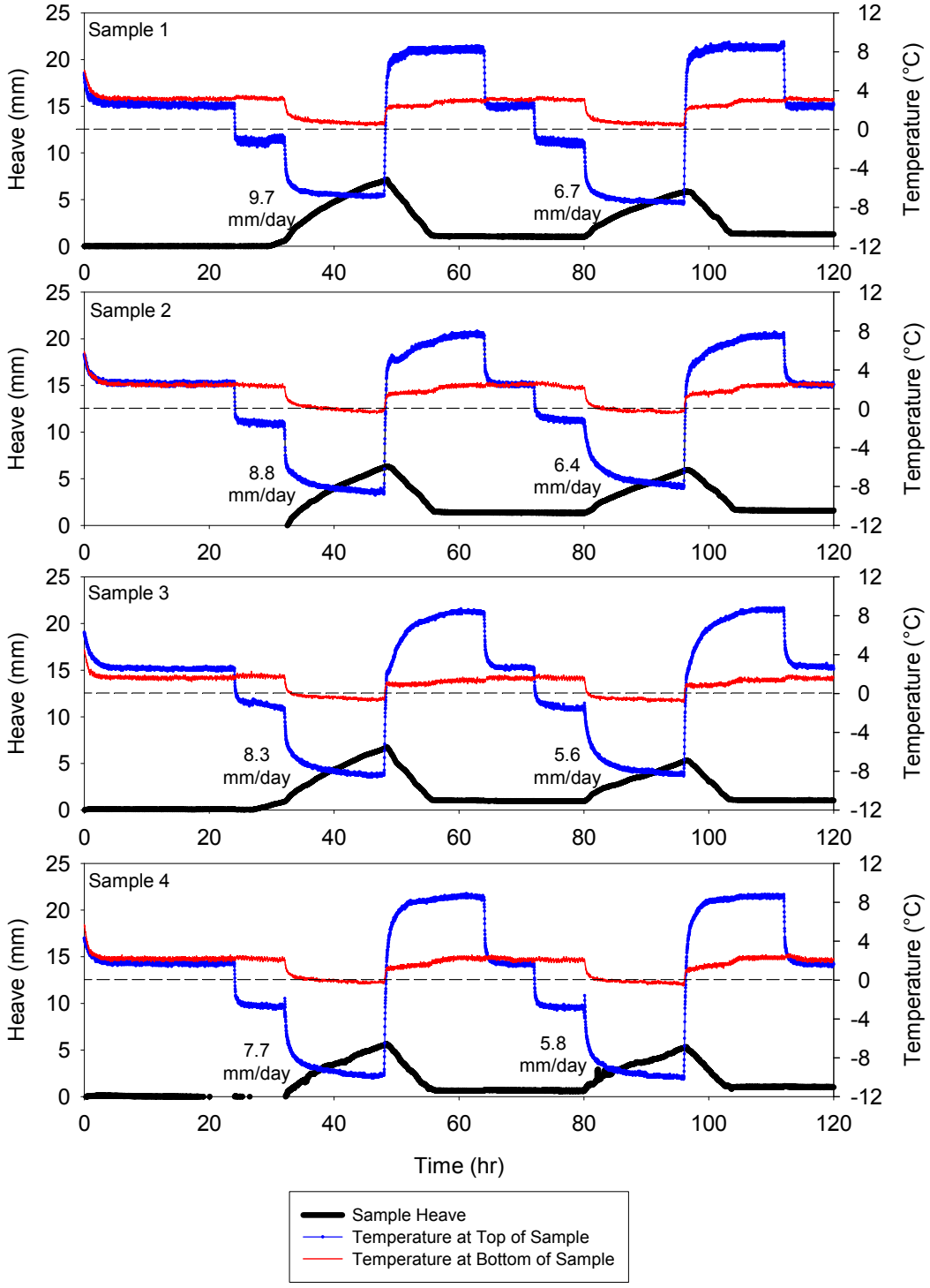


**Figure 151. IA US-30 RPCC subbase frost heave time plots**

The moisture content increased after freeze-thaw cycling compared to the initial moisture content. There moisture content profile shows no noticeable trend of moisture relocating to a certain location in the sample. The moisture content profiles are presented in Figure 152.

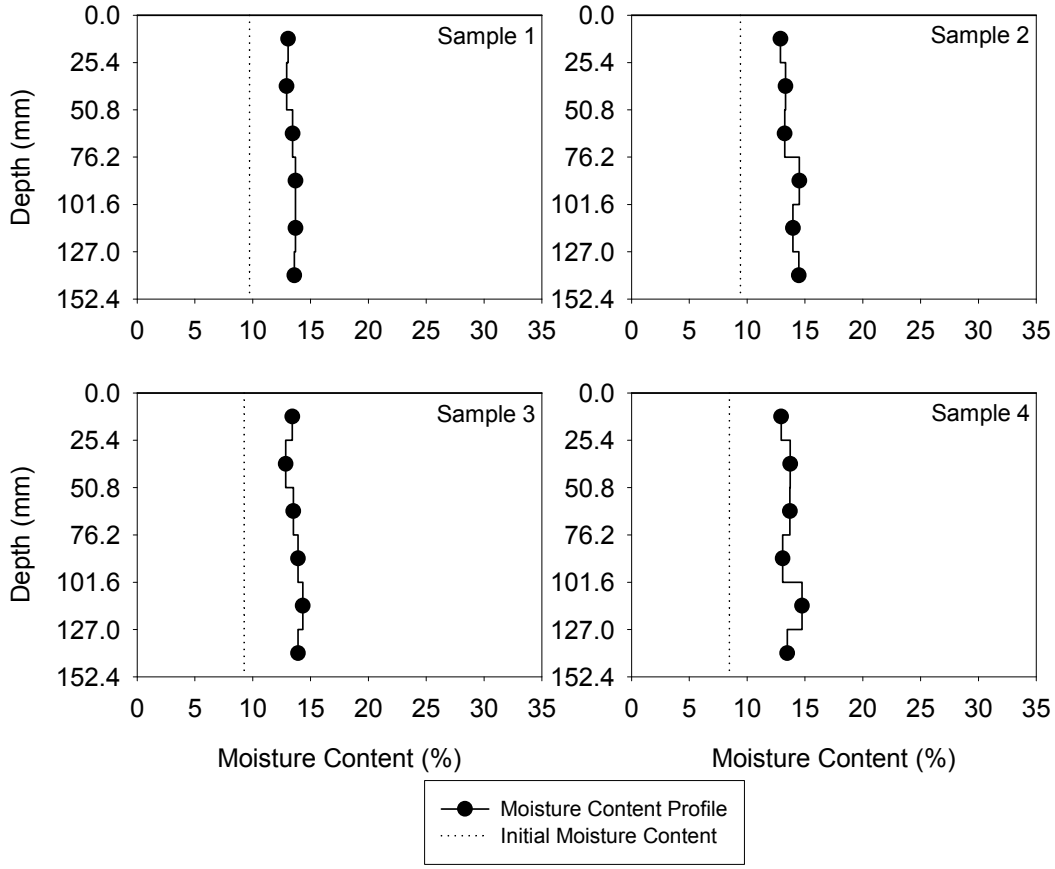


**Figure 152. IA US-30 RPCC subbase moisture content profiles**

The thaw-weakening susceptibility of the material is negligible, even though the post freeze-thaw CBR was significantly reduced compared to the standard CBR at the initial moisture content. The frost-heave rate for the first freeze was higher than the second freeze, which could mean that the soil structure may not be affected by additional freeze-thaw cycles. The frost-heave susceptibility of the first freeze is high, whereas it is medium for the second freeze. The frost-heave and thaw-weakening test results are presented in Table 58.

**Table 58. IA US-30 RPCC subbase frost-heave and thaw-weakening test results**

| | μ | σ | COV (%) | # of samples |
|---|---|---|---|---|
| CBR (%) (standard test) | 70.3 | | | 1 |
| CBR (%) (after frost-susceptibility test) | 33.3 | 4.3 | 12.8 | 4 |
| 1st Frost-heave rate (mm/day) | 8.6 | 0.7 | 8.4 | |
| 2nd Frost-heave rate (mm/day) | 6.1 | 0.5 | 8.0 | |
| 1st Frost-heave susceptibility rating | High | — | — | |
| 2nd Frost-heave susceptibility rating | Medium | — | — | |
| Thaw-weakening susceptibility rating | Negligible | — | — | |

In addition to the frost-heave and thaw-weakening tests performed on the IA US-30 RPCC, modified gradations of the RPCC were tested to determine if the fines content impacts the frost susceptibility of the material. Two samples were tested with half of the fines removed from the original gradation and two samples were tested with all of the fines removed from the original gradation. The fines were removed by dry sieving the samples. A problem appeared when the initial original RPCC gradation (Sample 1) was compared to the original gradation used for the modified samples (Sample 2), as was discussed in Chapter 4. Sample 1 had much higher fines content (13%) compared to Sample 2 (5.2%). The following results are for modified gradations of Sample 2.

The modified Sample 2 with half of the fines removed showed very similar trends between the two samples tested. The first and second heaves versus time plots are very similar. The samples returned to their original height after the first and second freeze-thaw cycles. The frost-heave time plots for the modified Sample 2 gradation with half of the fines removed is shown in Figure 153.

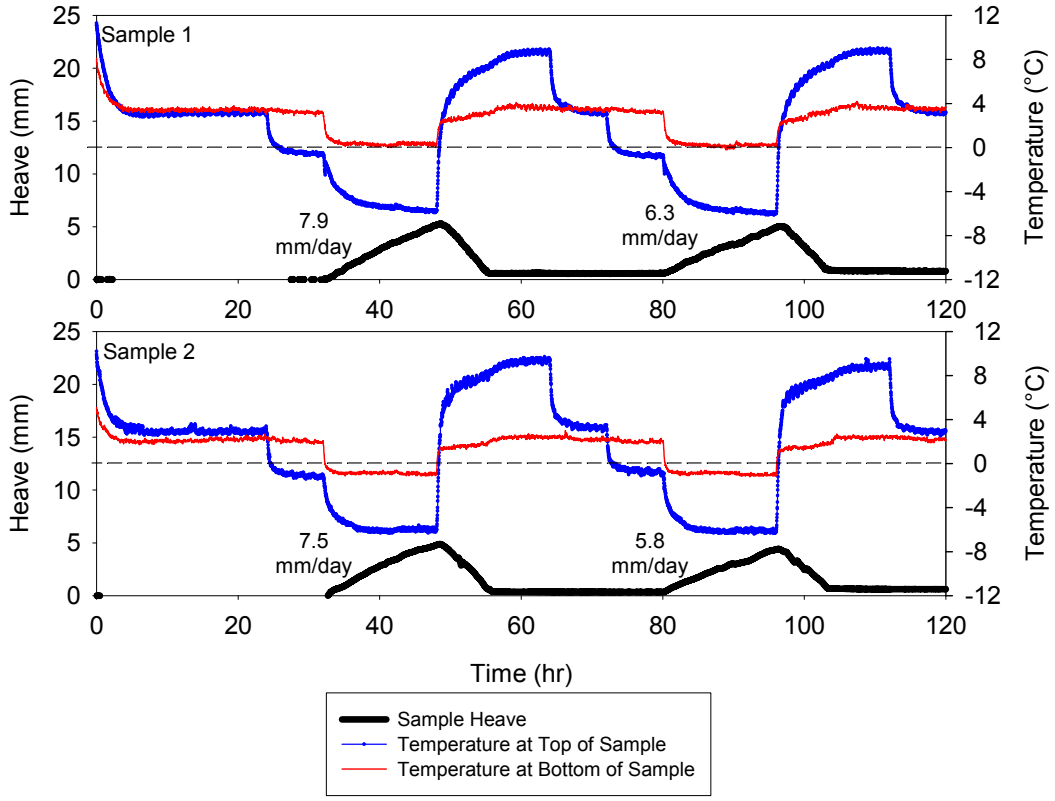


**Figure 153. IA US-30 RPCC subbase modified gradation (half of fines removed) frost heave time plots**

The moisture content profiles show that the moisture content increased after freeze-thaw cycling compared to the initial moisture content. Just as with the original Sample 1 moisture content profiles (Figure 152), there are no distinguishable trends in the moisture content profiles. The moisture content profiles of the Sample 2 modified gradation with half of the fines removed are shown in Figure 154.

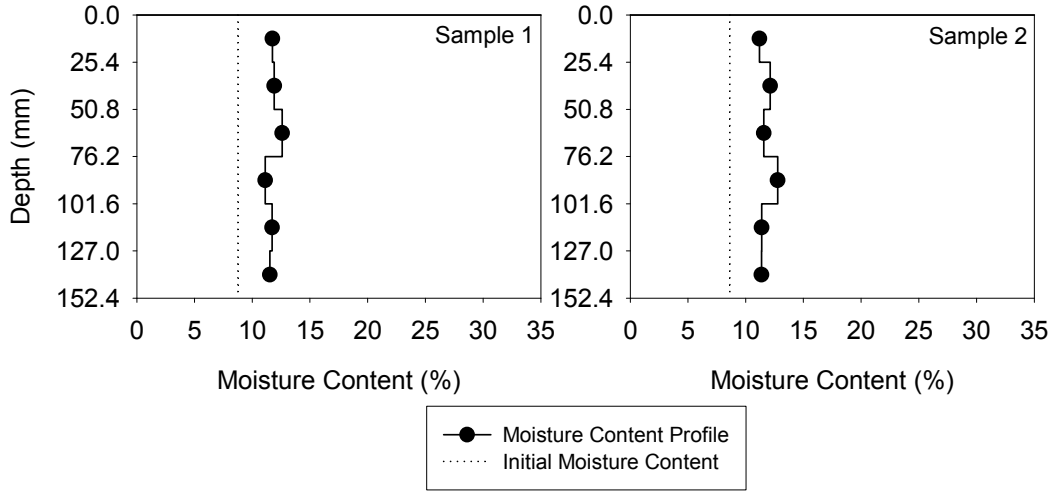


**Figure 154. IA US-30 RPCC subbase modified gradation (half of fines removed) moisture content profiles**

A standard CBR was not performed on the modified gradations. The thaw-weakening classification for the material is negligible and the post freeze-thaw CBR for the modified gradation is very similar to the original Sample 1 gradation. The frost-heave rate for the first freeze was higher than the second freeze, but both freeze cycles had a medium frost-heave susceptibility rating. The frost-heave rates for the first and second freeze cycles are very similar to the original Sample 1 gradation. The frost-heave and thaw-weakening test results are summarized in Figure 139.

**Table 59. IA US-30 RPCC subbase modified gradation (half of fines removed) frost-heave and thaw-weakening test results**

| | μ | σ | COV (%) | # of samples |
|---|---|---|---|---|
| CBR (%) (standard test) | | — | | 0 |
| CBR (%) (after frost-susceptibility test) | 39.2 | 8.3 | 21.1 | 2 |
| 1st Frost-heave rate (mm/day) | 7.7 | 0.2 | 2.7 | |
| 2nd Frost-heave rate (mm/day) | 6.1 | 0.3 | 5.7 | |
| 1st Frost-heave susceptibility rating | Medium | — | — | |
| 2nd Frost-heave susceptibility rating | Medium | — | — | |
| Thaw-weakening susceptibility rating | Negligible | — | — | |

A modified gradation was also made from RPCC Sample 2 where all of the fines were removed. The frost-heave time plots are similar to the original Sample 1 gradation and the modified Sample 2 gradation with half of the fines removed. The total heave for the first and second freeze cycles is very close for the two samples. After the two freeze-thaw cycles, the

samples returned to their original heights. Neither sample began heaving until after the first eight hours of freezing. The frost-heave time plots for the modified Sample 2 gradation with all of the fines removed is shown in Figure 155.

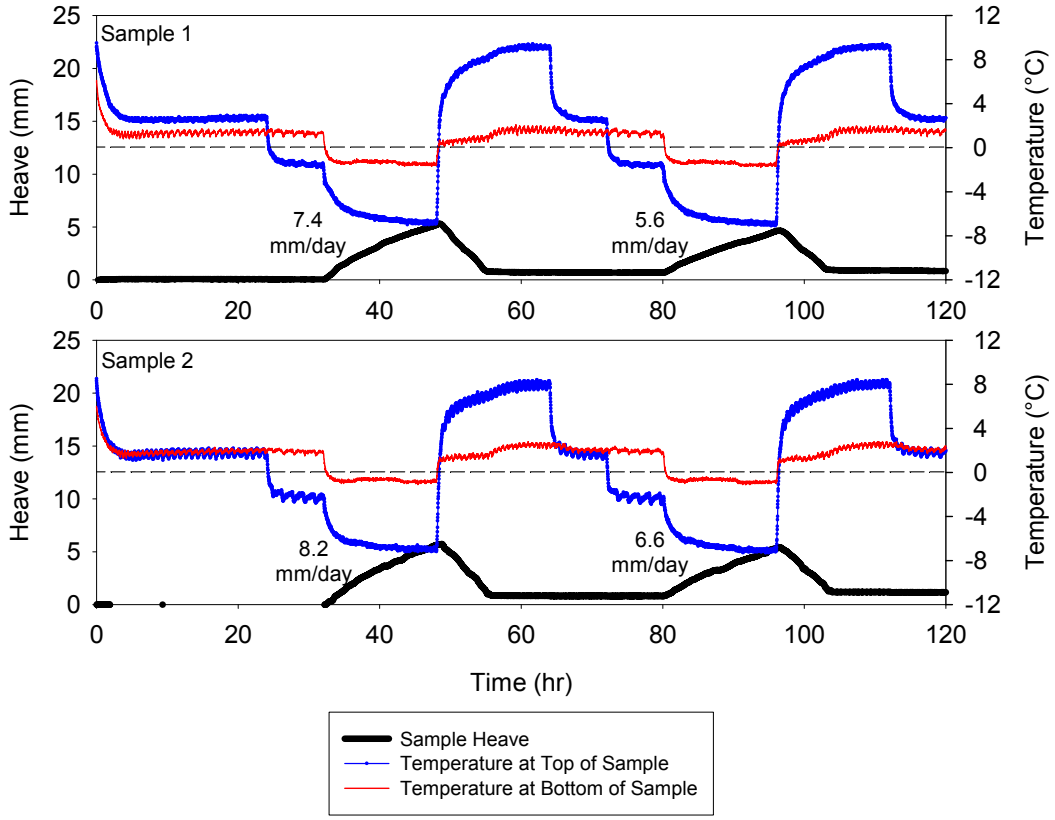


**Figure 155. IA US-30 RPCC subbase modified gradation (all fines removed) frost heave time plots**

The sample moisture contents increased after freeze-thaw cycling, compared to the initial moisture content. The modified samples with all of the fines removed showed no trends in the vertical moisture profile just as the original Sample 1 and modified Sample 2 with half of the fines removed. The moisture content profiles are presented in Figure 156.

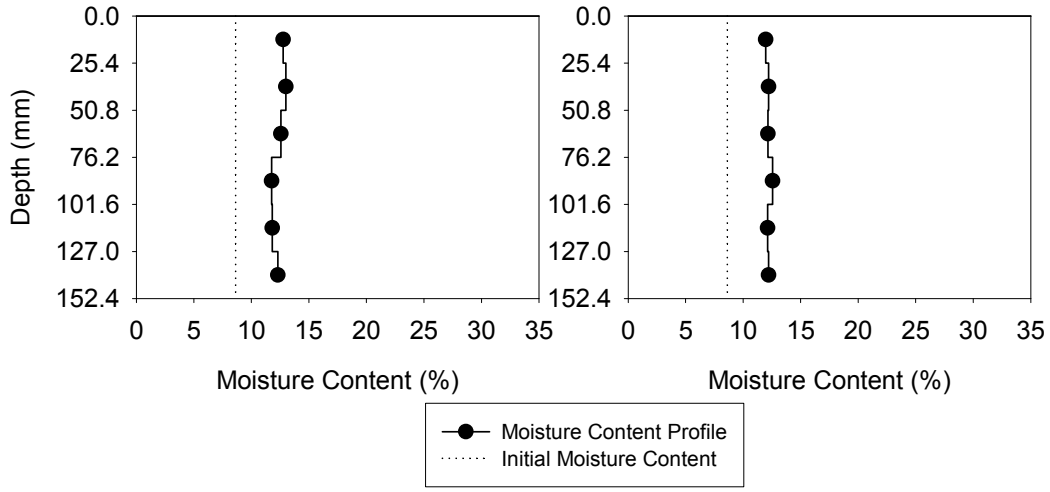


**Figure 156. IA US-30 RPCC subbase modified gradation (all fines removed) moisture content profiles**

The CBR after freeze thaw cycling is comparable to the original Sample 1 and the modified Sample 2 with half of the fines removed. The thaw-weakening susceptibility rating is negligible. The frost-heave susceptibility for the first freeze compared to the second freeze. The frost-heave rates are very similar to the original Sample 1 and the modified Sample 2 with half of the fines removed. The frost-heave susceptibility ratings for both freeze cycles are medium. The frost-heave and thaw-weakening test results are summarized in Table 60.

**Table 60. IA US-30 RPCC subbase modified gradation (all fines removed) frost-heave and thaw-weakening test results**

| | μ | σ | COV (%) | # of samples |
|---|---|---|---|---|
| CBR (%) (standard test) | | — | | 0 |
| CBR (%) (after frost-susceptibility test) | 35.5 | 4.0 | 11.3 | 2 |
| 1st Frost-heave rate (mm/day) | 7.8 | 0.4 | 5.4 | |
| 2nd Frost-heave rate (mm/day) | 6.1 | 0.7 | 10.8 | |
| 1st Frost-heave susceptibility rating | Medium | — | — | |
| 2nd Frost-heave susceptibility rating | Medium | — | — | |
| Thaw-weakening susceptibility rating | Negligible | — | — | |

Based on the results from the modified gradations of RPCC with half and all of the fines removed, the frost-heave rate for the first and second freeze cycles is not affected by the fines content. The post freeze-thaw CBR values are also not affected by the fines content. The frost-heave and thaw-weakening susceptibility ratings are nearly the same for all three

gradations. The exception is the frost-heave susceptibility rating of high for the original Sample 1 gradation.

## Manatts

### Concrete Sand Subbase

All four samples heaved small amounts during freezing. The samples returned to their original height after the freeze-thaw cycles were complete. The frost-heave time plots for the Manatts concrete sand subbase is shown in Figure 157.

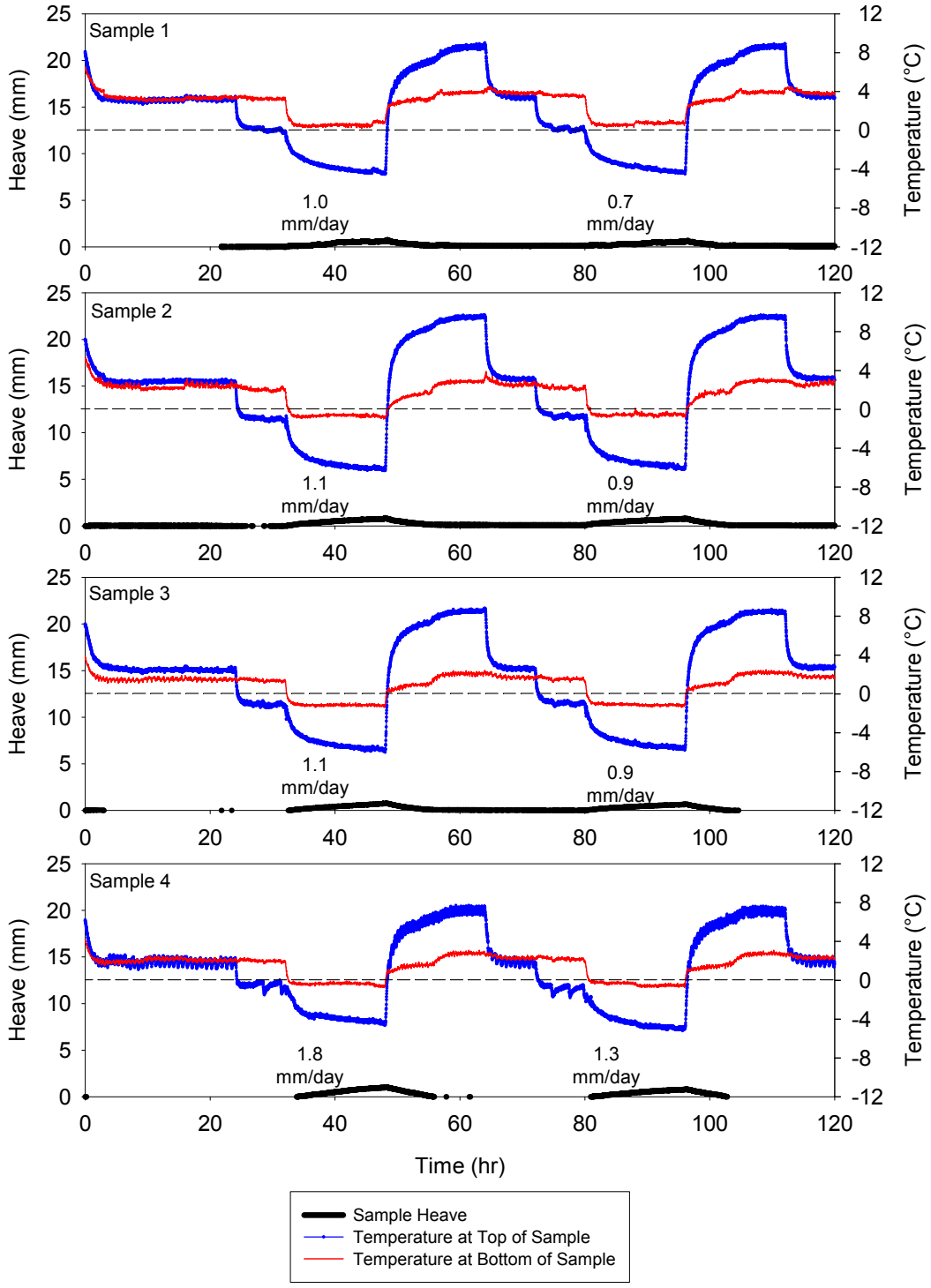


**Figure 157. Manatts concrete sand subbase frost heave time plots**

The moisture content profiles of all four samples are similar and show an increase from the initial moisture content. The moisture content that was measured when the material was

sampled was used as the initial moisture content. The lowest moisture content occurs at the top of the samples. The moisture content profiles are presented in Figure 158.

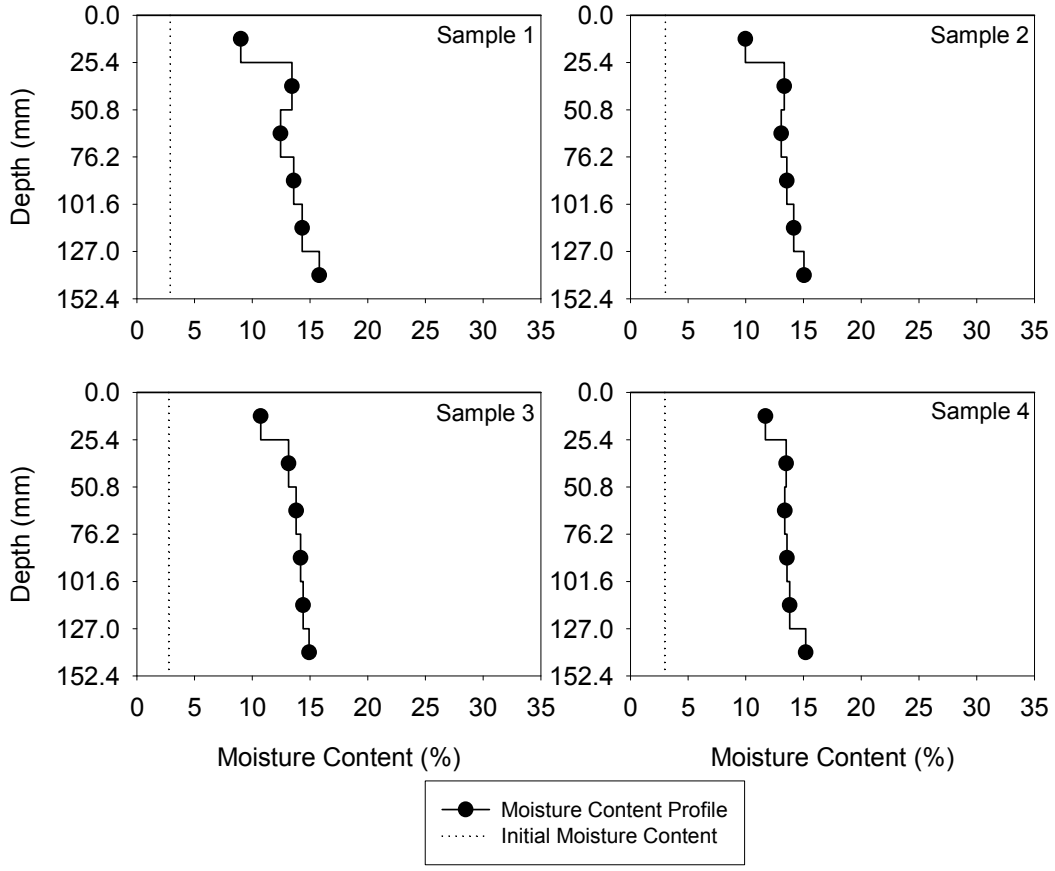


**Figure 158. Manatts concrete sand subbase moisture content profiles**

The CBR after freeze-thaw cycling was lower than the standard CBR performed at the initial moisture content. The thaw-weakening susceptibility of this material is rated as medium. The frost-heave rate was very low for the first and second freeze cycles. The frost-susceptibility of the first freeze was rated as very low and the second freeze was rated as negligible. Table 61 summarizes the frost-heave and thaw-weakening test results.

**Table 61. Manatts concrete sand subbase frost-heave and thaw-weakening test results**

| | μ | σ | COV (%) | # of samples |
|---|---|---|---|---|
| CBR (%) (standard test) | 9.4 | | | 1 |
| CBR (%) (after frost-susceptibility test) | 8.1 | 0.8 | 10.0 | 4 |
| 1st Frost-heave rate (mm/day) | 1.2 | 0.3 | 26.0 | |
| 2nd Frost-heave rate (mm/day) | 0.9 | 0.2 | 25.3 | |
| 1st Frost-heave susceptibility rating | Very low | — | — | |
| 2nd Frost-heave susceptibility rating | Negligible | — | — | |
| Thaw-weakening susceptibility rating | Medium | — | — | |

**RAP Subbase**

The frost-heave time plots of all four samples were similar and showed small amounts of total heave. All of the samples returned to their original height after the freeze-thaw cycling was complete. The frost-heave time plots are presented in Figure 159.

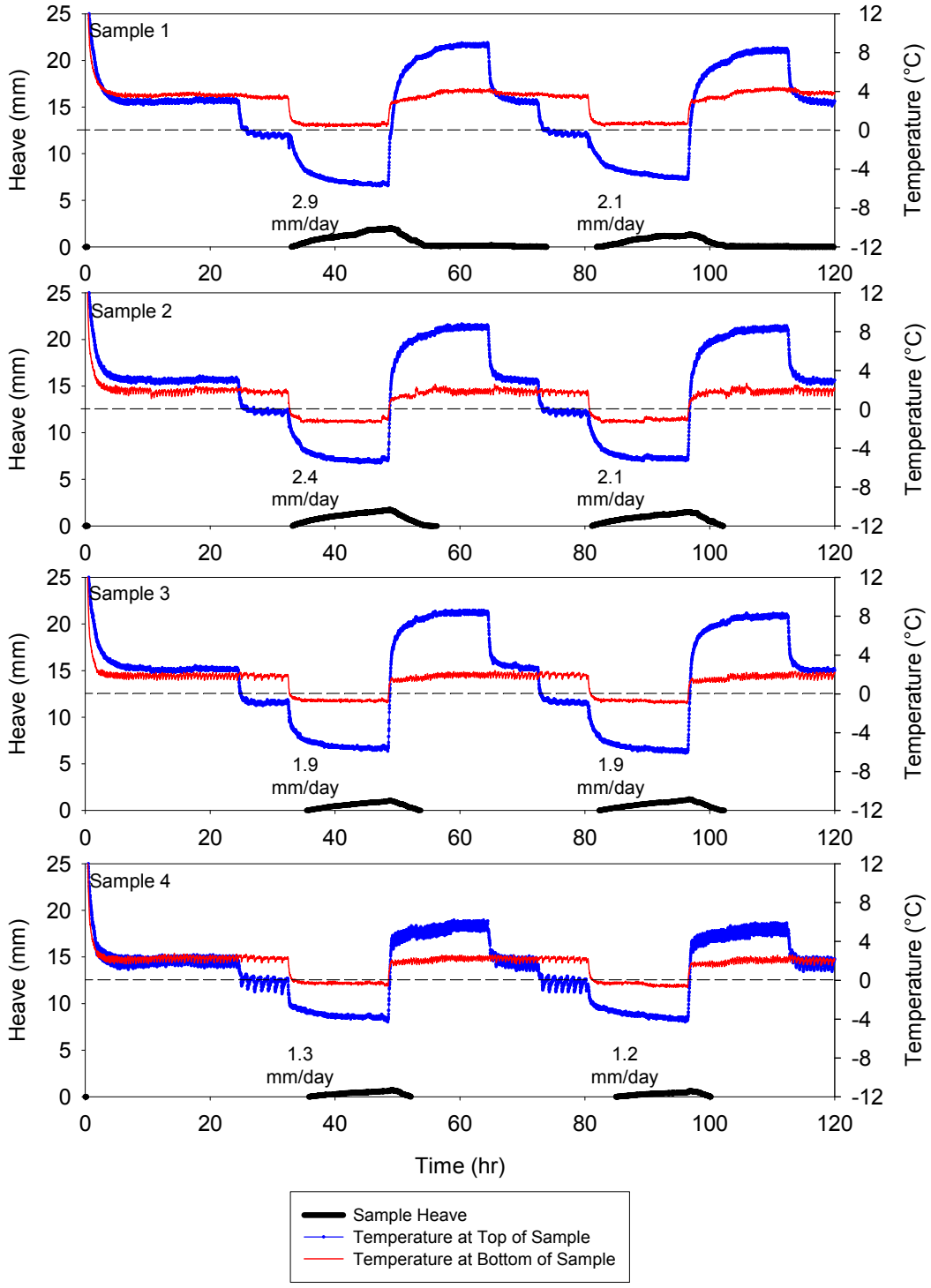


**Figure 159. Manatts RAP subbase frost heave time plots**

The moisture content of all four samples increased after freeze-thaw cycling. The lowest water contents are at the top of the samples and increase with increasing depth. The moisture

content of the sample during sampling was used when making the samples. The moisture content profiles are shown in Figure 160.

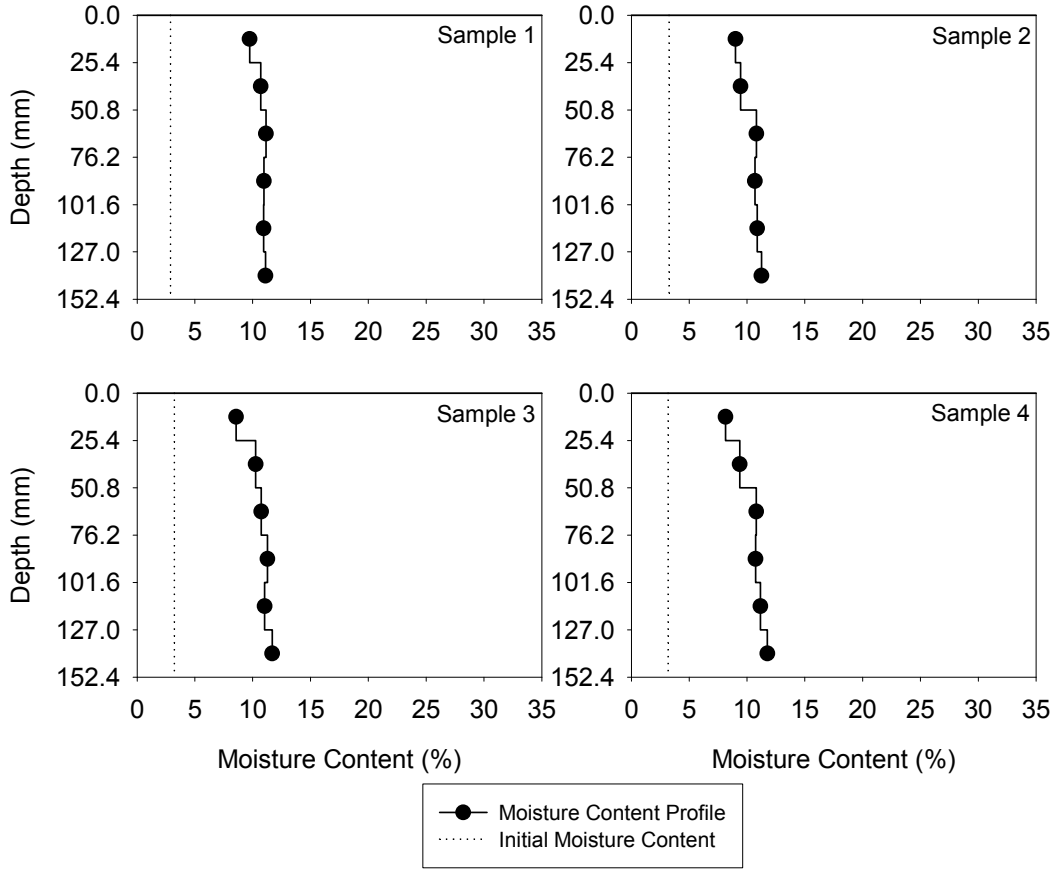


**Figure 160. Manatts RAP subbase moisture content profiles**

The CBR after freeze-thaw cycling was lower than the standard CBR. The thaw-weakening susceptibility rating for the material is medium. The frost-heave rate for the first and second freeze was low, with the first freeze cycle having a slightly higher heave rate. The frost-heave susceptibility rating for the first freeze was low and for the second freeze it was very low. The frost-heave and thaw-weakening test results are summarized in Table 62.

**Table 62. Manatts RAP subbase frost-heave and thaw-weakening test results**

| | μ | σ | COV (%) | # of samples |
|---|---|---|---|---|
| CBR (%) (standard test) | 11.6 | | | 1 |
| CBR (%) (after frost-susceptibility test) | 8.7 | 0.9 | 9.8 | 4 |
| 1st Frost-heave rate (mm/day) | 2.1 | 0.6 | 29.1 | |
| 2nd Frost-heave rate (mm/day) | 1.8 | 0.5 | 24.8 | |
| 1st Frost-heave susceptibility rating | Low | — | — | |
| 2nd Frost-heave susceptibility rating | Very low | — | — | |
| Thaw-weakening susceptibility rating | Medium | — | — | |

**RPCC/RAP Subbase**

All four frost-heave time plots show little heave. The frost-heave time plots are presented in Figure 161.

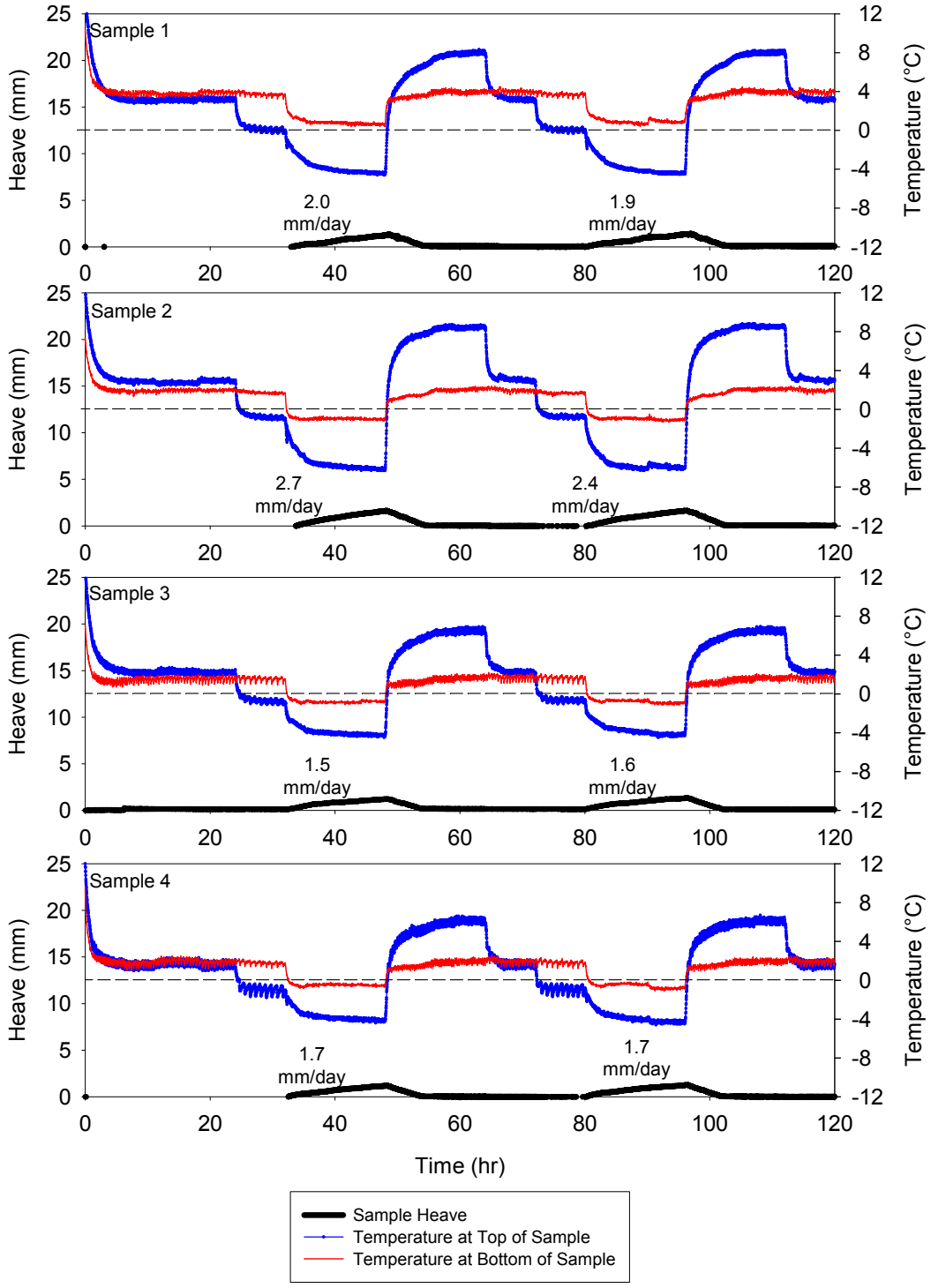


**Figure 161. Manatts RPCC/RAP subbase frost heave time plots**

The moisture contents of the material increased after freeze-thaw cycling compared to the initial moisture content. The initial moisture content was the same moisture content the

material was sampled at. The highest moisture contents in the soil profiles occurs at the top of the samples, which indicates that there may have been some capillary action drawing water to the coldest part of the samples. The moisture content profiles are presented in Figure 162.

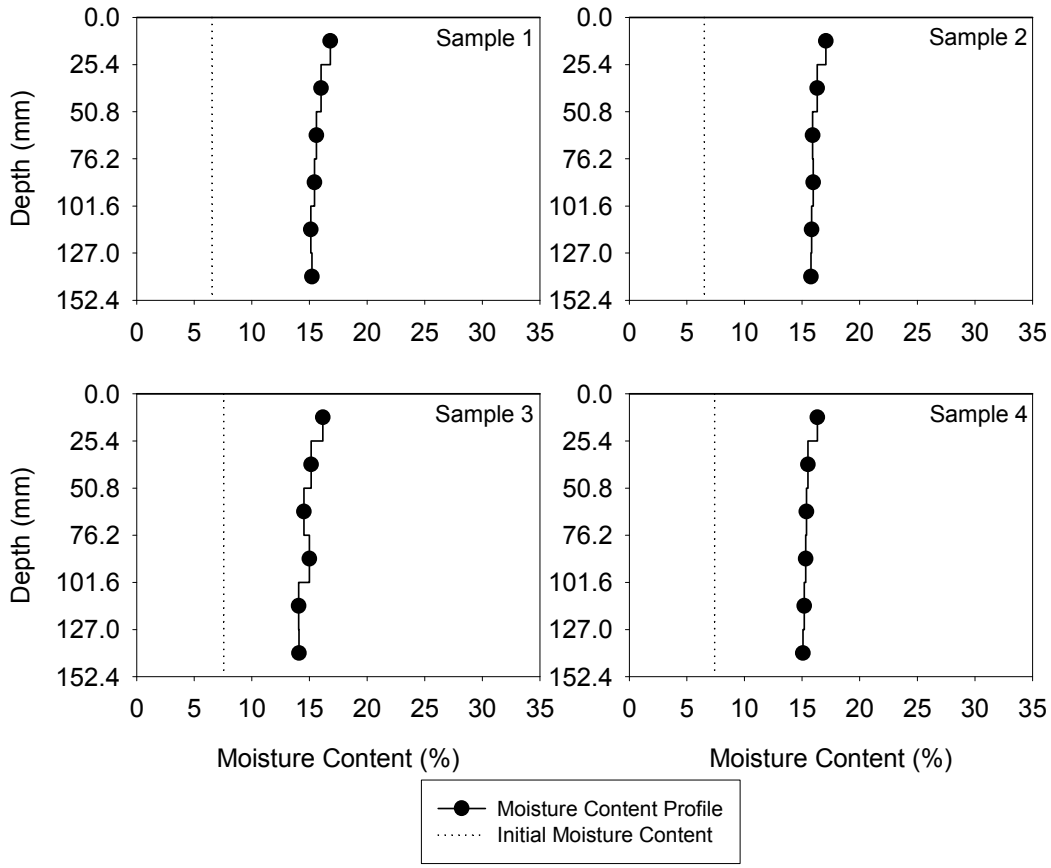


**Figure 162. Manatts RPCC/RAP subbase moisture content profiles**

The CBR after freeze-thaw cycling decreased compared to the standard CBR, however the thaw-weakening susceptibility rating is still negligible. The frost-heave rates for the first and second freeze cycles are very low. The first freeze is rated as having low frost-heave susceptibility and the second frost-heave rating is very low. The frost-heave and thaw-weakening test results are summarized in Table 63.

**Table 63. Manatts RPCC/RAP subbase frost-heave and thaw-weakening test results**

| | μ | σ | COV (%) | # of samples |
|---|---|---|---|---|
| CBR (%) (standard test) | 48.2 | | | 1 |
| CBR (%) (after frost-susceptibility test) | 33.2 | 5.8 | 17.4 | 4 |
| 1st Frost-heave rate (mm/day) | 2.0 | 0.4 | 23.0 | |
| 2nd Frost-heave rate (mm/day) | 1.9 | 0.4 | 19.1 | |
| 1st Frost-heave susceptibility rating | Low | — | — | |
| 2nd Frost-heave susceptibility rating | Very low | — | — | |
| Thaw-weakening susceptibility rating | Negligible | — | — | |

## Martin Marietta Materials

### Crushed Limestone Subbase

The total heave and slopes of the heave versus time lines are nearly the same for each sample, with the second freeze cycle being slightly higher. The sample heights returned to their original heights after freeze-thaw cycling was complete. The frost-heave time plots are presented in Figure 163.

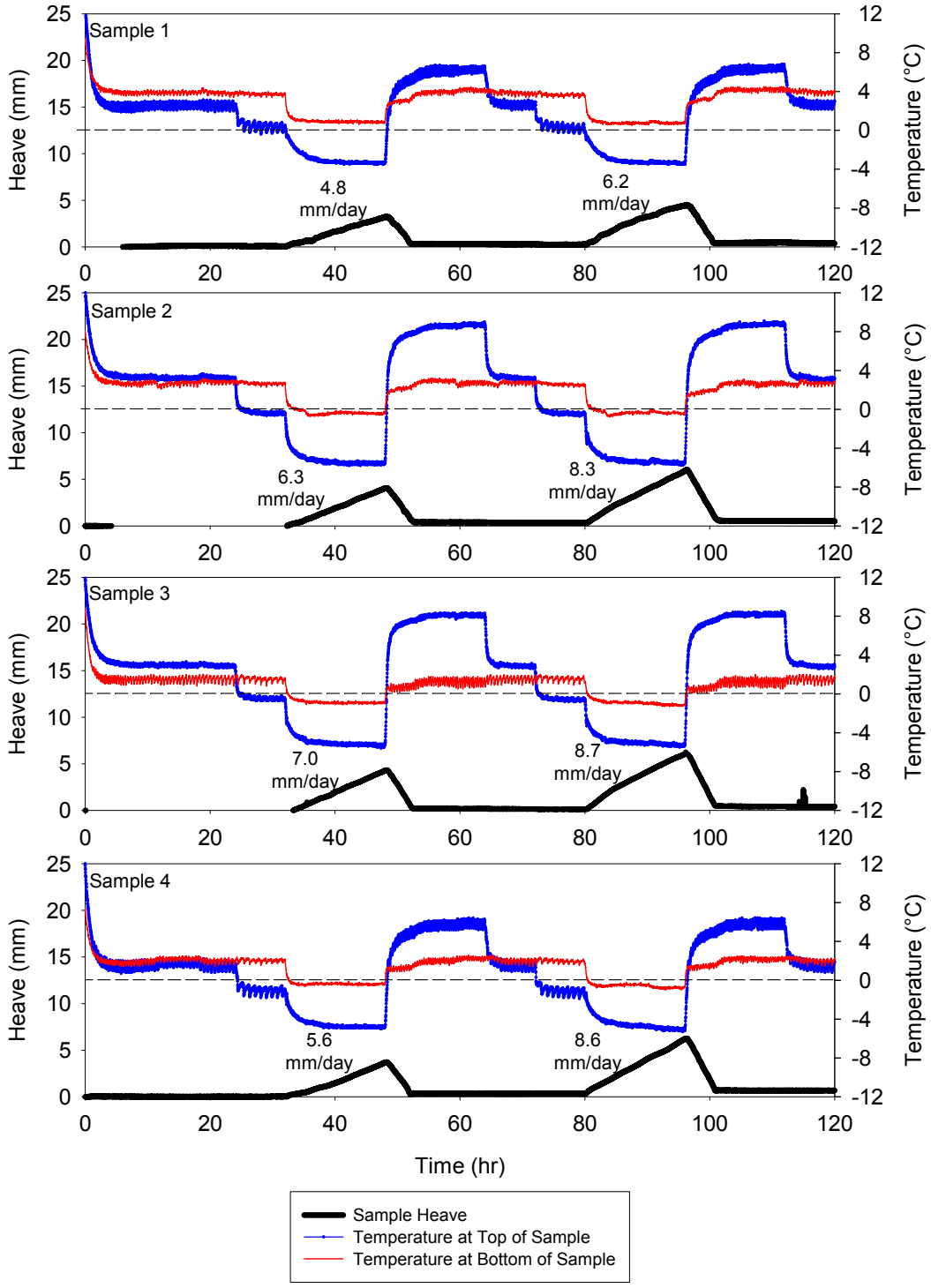


**Figure 163. Martin Marietta Materials crushed limestone subbase frost heave time plots**

The moisture content after freeze-thaw cycling is very close to the initial moisture content. The initial moisture content was the same as the moisture content at sampling.

Samples 1, 3, and 4 have the highest moisture contents at the bottom the samples, while sample 2 has the highest moisture content at the top of the sample. The moisture content profiles are presented in Figure 164.

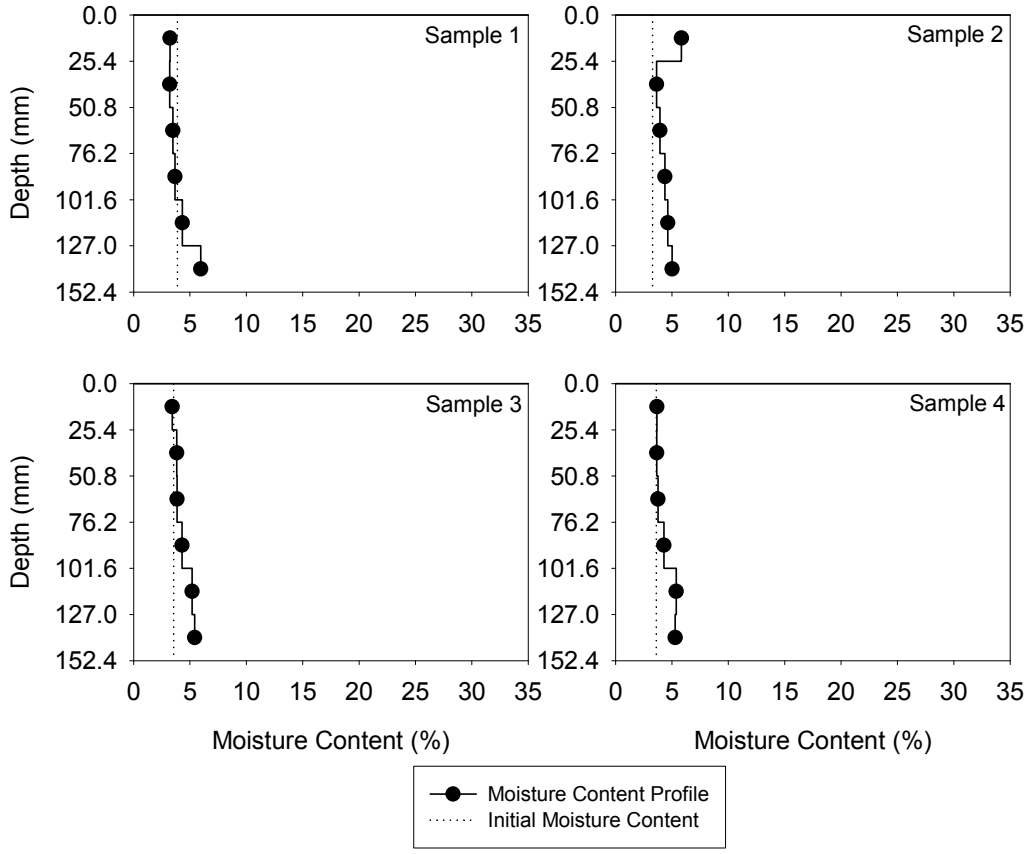


**Figure 164. Martin Marietta Materials crushed limestone subbase moisture content profiles**

The CBR after freeze-thaw cycling decreased from the standard CBR value, but the thaw-weakening susceptibility rating is still negligible. The frost-heave rate of the second freeze was higher compared to the first freeze. The frost-heave susceptibility for the first freeze was medium and high for second freeze. The results of the frost-heave and thaw-weakening test are summarized in Table 64.

**Table 64. Martin Marietta Materials crushed limestone frost-heave and thaw-weakening test results**

| | μ | σ | COV (%) | # of samples |
|---|---|---|---|---|
| CBR (%) (standard test) | 87.3 | | | 1 |
| CBR (%) (after frost-susceptibility test) | 47.5 | 8.1 | 17.0 | 4 |
| 1st Frost-heave rate (mm/day) | 5.9 | 0.8 | 13.5 | |
| 2nd Frost-heave rate (mm/day) | 8.0 | 1.2 | 14.6 | |
| 1st Frost-heave susceptibility rating | Medium | — | — | |
| 2nd Frost-heave susceptibility rating | High | — | — | |
| Thaw-weakening susceptibility rating | Negligible | — | — | |

## MI I-96

### Clayey Sand Subgrade

The frost-heave time plots show the same trends, however there are differences in the slope of the heave versus time line and the total heave. All four samples reach a peak amount of heave before flattening out for the remainder of the first and second freezing periods. One possibility or the plateau is the sample was completely frozen to the bottom and no ice lenses could be initiated or the material did not supply a sufficient amount of water to the growing ice lens. The slope of the heave versus time line increased during the second freeze compared to the first. The samples increased in height after the first and second freeze-thaw cycle. The frost-heave time plots are presented in Figure 165.

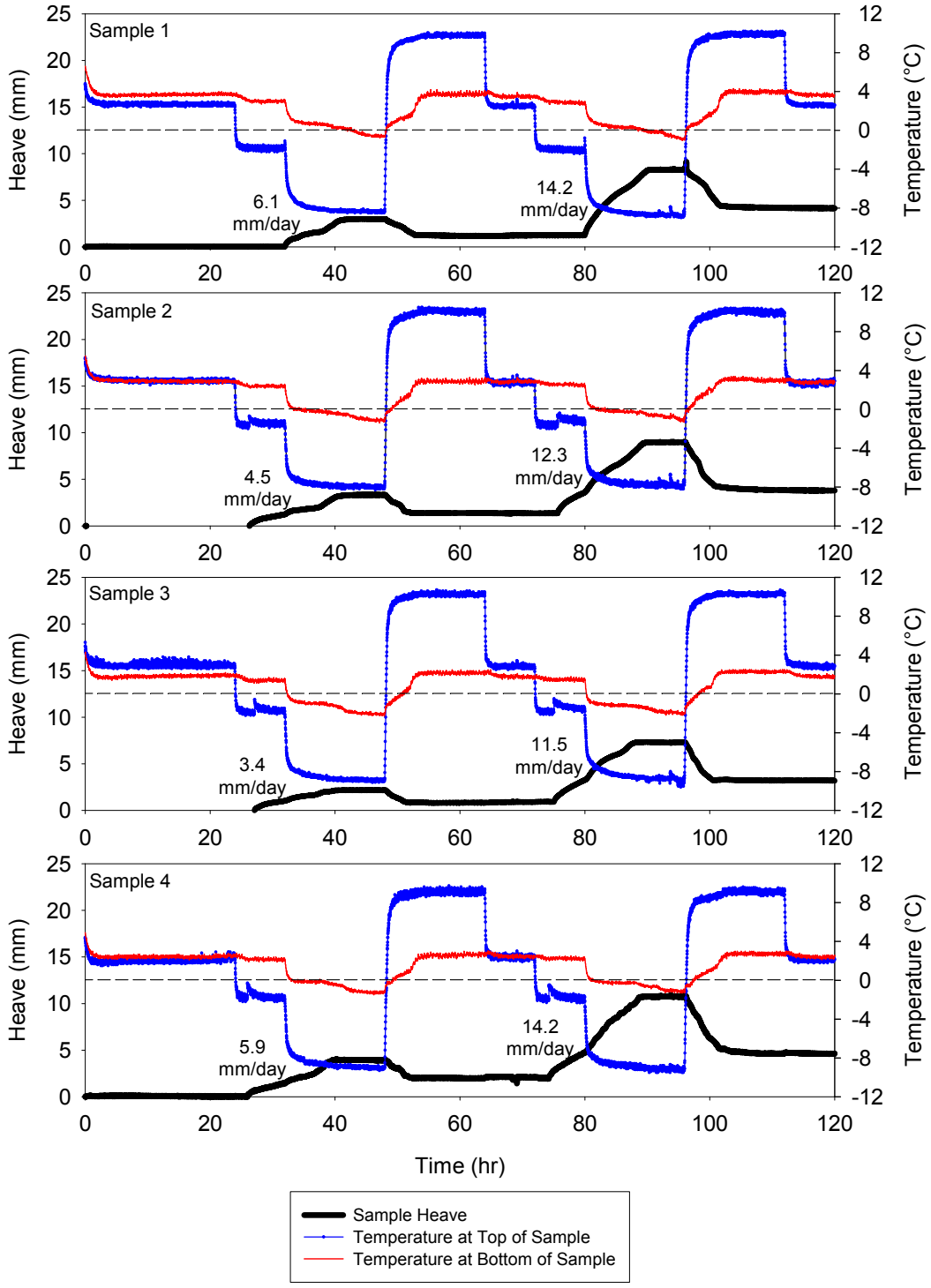


**Figure 165. MI I-96 clayey sand subgrade frost heave time plots**

The moisture content after freeze-thaw cycling is close to the initial moisture content. However, there is a clear increase in moisture content at the top of the sample. The moisture content profiles are presented in Figure 166.

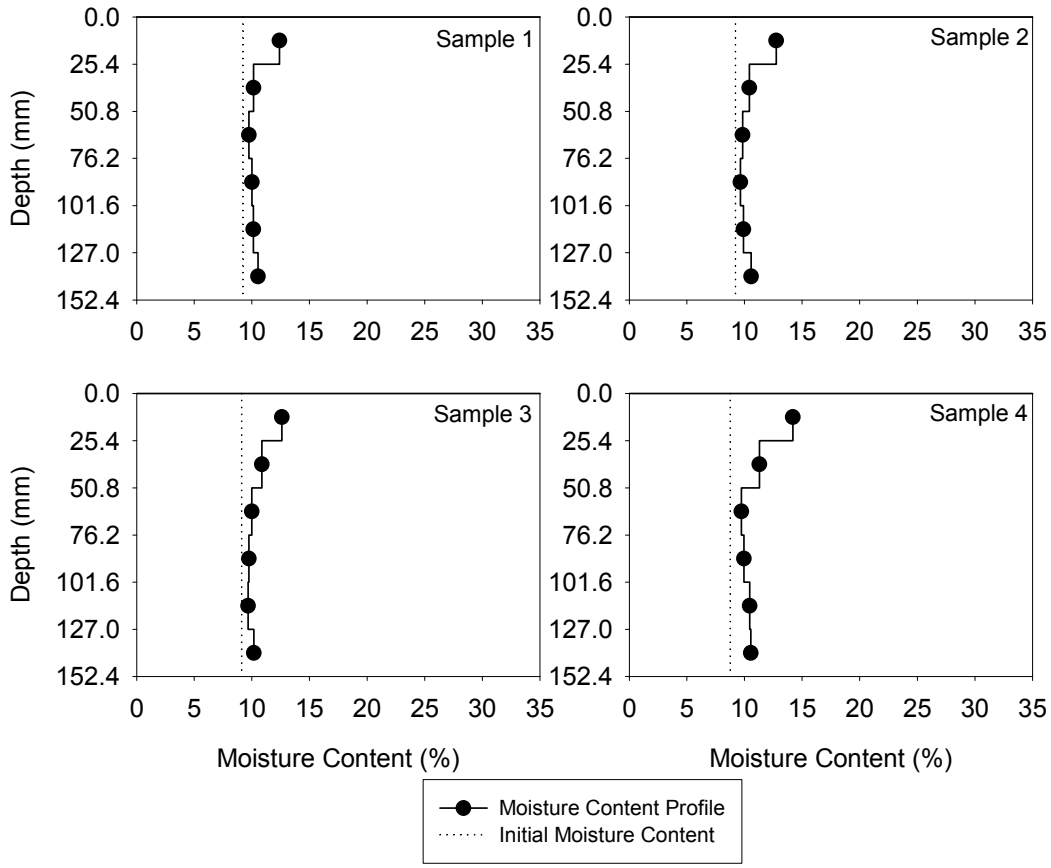


**Figure 166. MI I-96 clayey sand subgrade moisture content profiles**

The standard CBR value was higher than the post freeze-thaw CBR. The thaw-weakening susceptibility rating is medium. The frost-heave rate increased in the second freeze compared to the first. The frost-heave susceptibility rating for the first freeze was medium and it was high for the second freeze. The frost-heave and thaw-weakening test results are summarized in Table 65.

**Table 65. MI I-96 clayey sand subgrade frost-heave and thaw-weakening test results**

| | μ | σ | COV (%) | # of samples |
|---|---|---|---|---|
| CBR (%) (standard test) | 26.3 | | | 1 |
| CBR (%) (after frost-susceptibility test) | 5.8 | 0.7 | 12.6 | 4 |
| 1st Frost-heave rate (mm/day) | 4.9 | 1.1 | 22.3 | |
| 2nd Frost-heave rate (mm/day) | 13.1 | 1.4 | 10.6 | |
| 1st Frost-heave susceptibility rating | Medium | — | — | |
| 2nd Frost-heave susceptibility rating | High | — | — | |
| Thaw-weakening susceptibility rating | Medium | — | — | |

## PA US-22

### Sandy Lean Clay Subgrade

The frost-heave time plots for the four samples are very similar. The slope of the heave versus time line is approximately the same for the first and second freeze; however the total heave is higher during the second freeze, because the samples did not return to their original height after the first freeze-thaw cycle. The samples reach a peak heave after the first freeze and never consolidated during thawing. The sample height also increased after the second freeze-thaw cycle. The frost-heave time plots are presented in Figure 167.

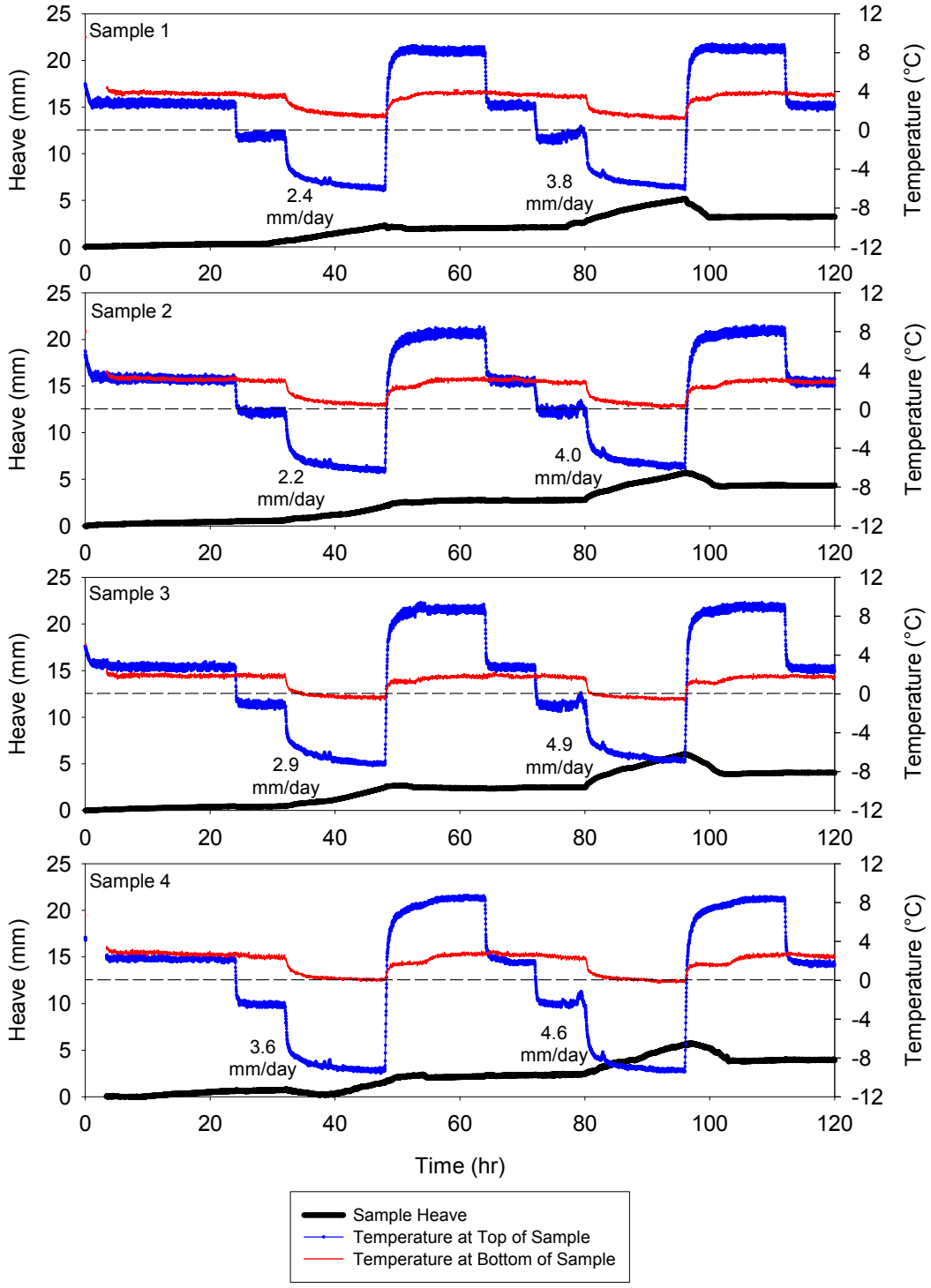


**Figure 167. PA US-22 sandy lean clay subgrade frost heave time plots**

The moisture content increased after freeze-thaw cycling compared to the initial moisture content. There are no trends showing redistribution of water in the samples, which would

indicate that there was not sufficient capillary action to draw water to the top of the sample. The moisture content profiles are presented in Figure 168.

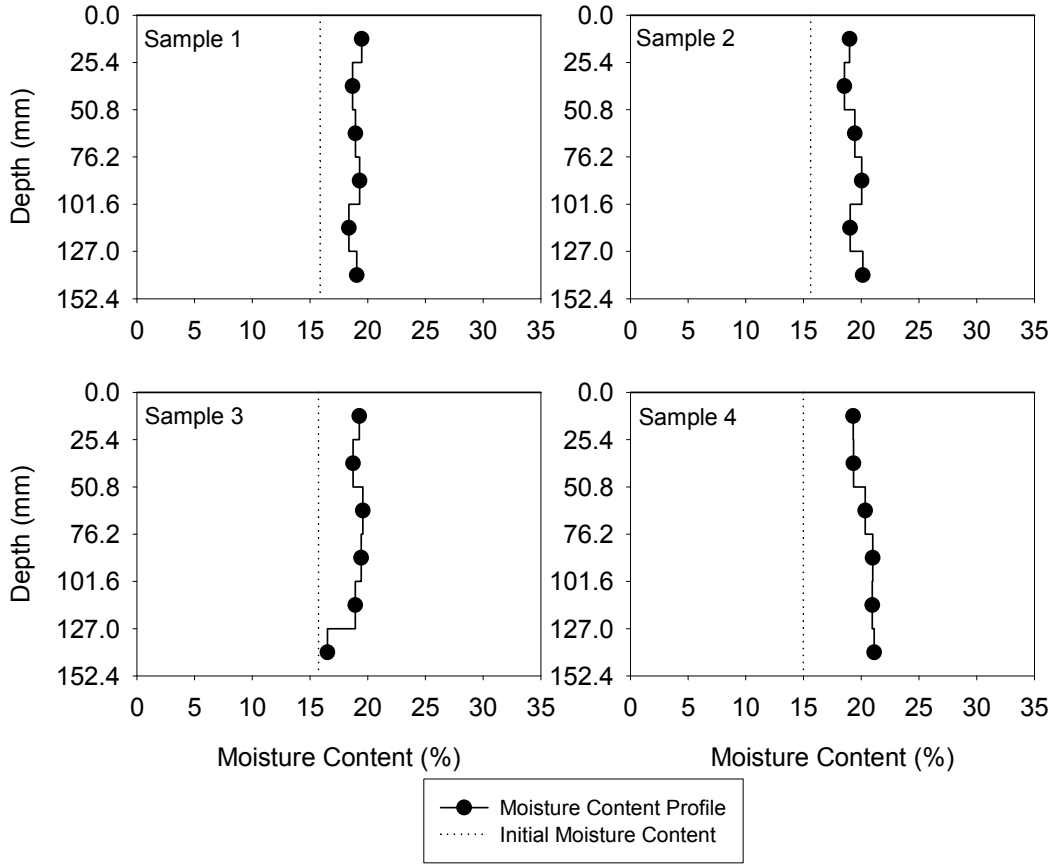


**Figure 168. PA US-22 sandy lean clay subgrade moisture content profiles**

The CBR after freeze-thaw cycling was lower than the standard CBR. The thaw-weakening susceptibility rating is high for the material. The frost-heave rate increased slightly from the first to the second freeze cycle. The frost-susceptibility rating for the first freeze is low and it medium for the second freeze. The frost-heave and thaw-weakening test results are summarized in Table 66.

**Table 66. PA US-22 sandy lean clay subgrade frost-heave and thaw-weakening test results**

| | μ | σ | COV (%) | # of samples |
|---|---|---|---|---|
| CBR (%) (standard test) | 21.1 | | | 1 |
| CBR (%) (after frost-susceptibility test) | 3.0 | 0.3 | 12.8 | 4 |
| 1st Frost-heave rate (mm/day) | 2.8 | 0.5 | 18.8 | |
| 2nd Frost-heave rate (mm/day) | 4.3 | 0.5 | 11.4 | |
| 1st Frost-heave susceptibility rating | Low | — | — | |
| 2nd Frost-heave susceptibility rating | Medium | — | — | |
| Thaw-weakening susceptibility rating | High | — | — | |

## Pottawattamie County, Iowa

### Loess

The frost-heave time plots have the same trends between the four samples. However, there are differences between samples 1 and 2 compared to samples 3 and 4. Samples 1 and 2 have very similar total heave values and heave versus time slopes. Samples 3 and 4 have lower total heave values and heave versus time slopes compared to samples 1 and 2. The heave versus time line is higher for the second freeze compared to the first freeze for all four samples. The height of all four samples increased after the first and second freeze-thaw cycle. The frost-heave time plots are presented in Figure 169.

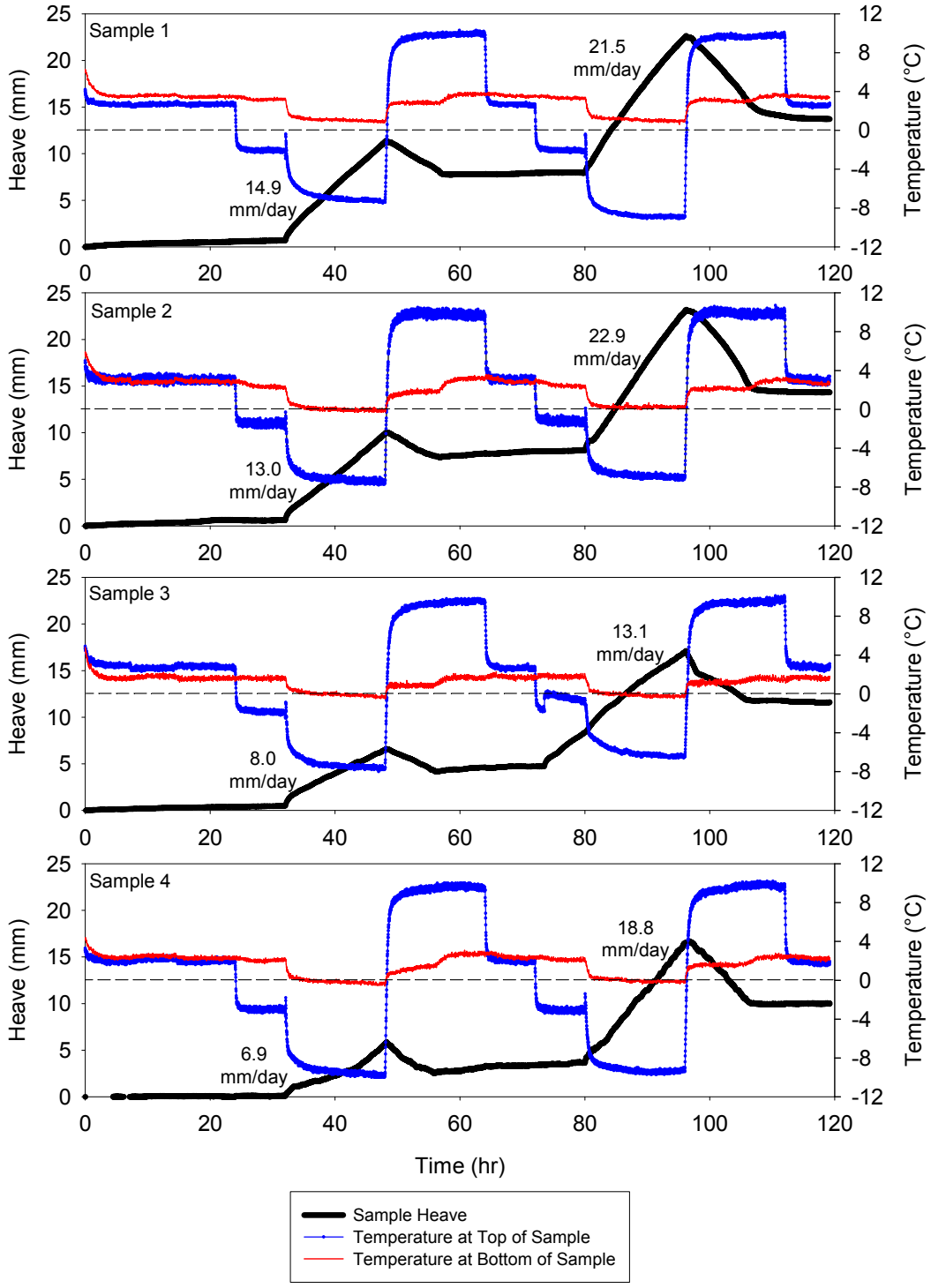


**Figure 169. Loess frost heave time plots**

The moisture content after freeze-thaw cycling increased compared to the initial moisture content. All four samples have higher moisture contents at the top of the samples. The

approximate saturation values are also presented for each moisture content that was measured. The dry unit weight of each 25.4 mm section was assumed to be the same as the initial dry unit weight of the sample. Approximate saturation values over 100% could indicate ice lensing at those locations. The moisture content profiles are presented in Figure 170.

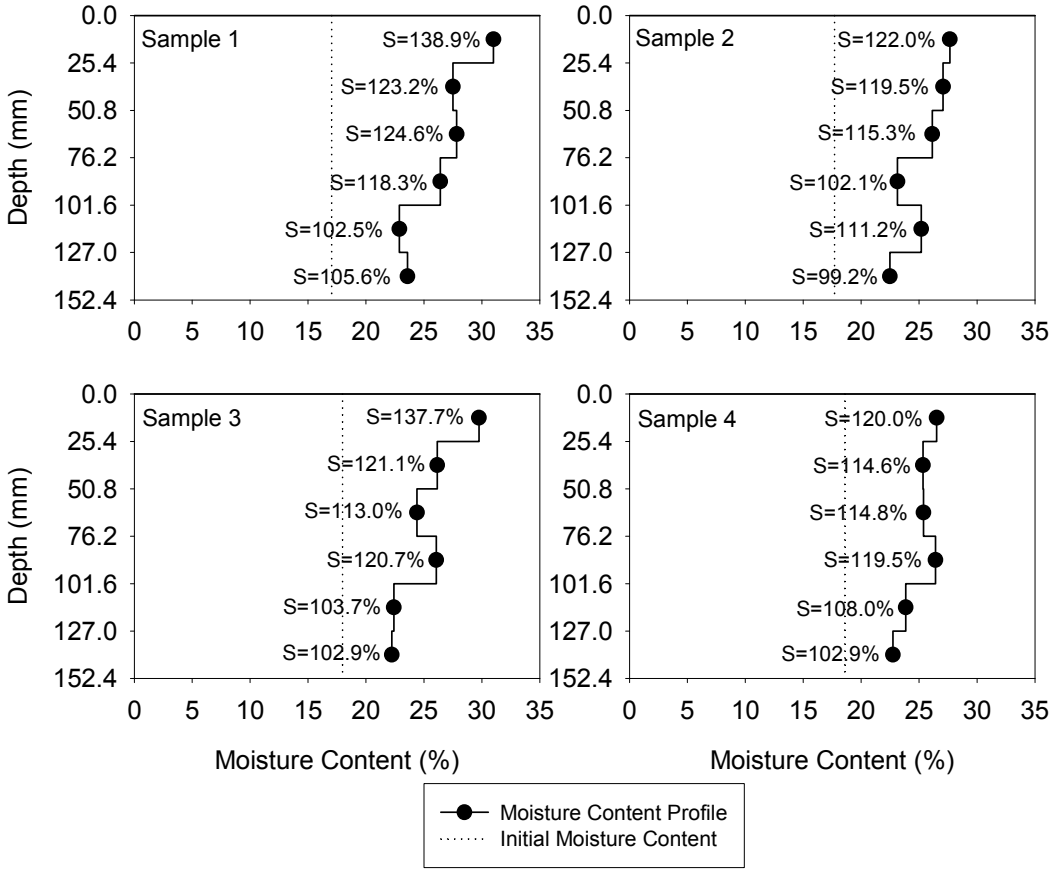


**Figure 170. Loess moisture content profiles**

The CBR after freeze-thaw cycling is low and justifies a thaw-weakening susceptibility rating of very high. The frost-heave rate increased from the first freeze to the second. The first freeze has a frost-heave susceptibility rating of high and the second freeze is rated as very high. The frost-heave and thaw-weakening test results are summarized Table 67.

**Table 67. Loess frost-heave and thaw-weakening test results**

| | μ | σ | COV (%) | # of samples |
|---|---|---|---|---|
| CBR (%) (standard test) | 10 | | | 1 |
| CBR (%) (after frost-susceptibility test) | 0.5 | 0.2 | 44 | 4 |
| 1st Frost-heave rate (mm/day) | 10.7 | 3.4 | 31.4 | |
| 2nd Frost-heave rate (mm/day) | 19.1 | 4.4 | 22.8 | |
| 1st Frost-heave susceptibility rating | High | — | — | |
| 2nd Frost-heave susceptibility rating | Very high | — | — | |
| Thaw-weakening susceptibility rating | Very high | — | — | |

**Cement-Treated Loess**

Several combinations of cement-treated loess were tested at different combinations of initial moisture contents and cement contents. The moisture content and cement content combinations were chosen from the 2-in. x 2-in. compressive strength results. Two samples were tested for each initial combination of moisture content and cement content. The 3% cement-treated samples will be presented in this chapter, while the rest of test results are presented in Appendix D. None of the cement-stabilized samples showed any frost-heave. The samples all had a post freeze-thaw CBR over 100 except for the samples with an initial moisture content of 13% and 3% cement. Even though the compressive strength study showed that they had the lowest compressive strength of any combinations investigated, those samples still had an average CBR of nearly 72. Table 68 shows the frost-heave and thaw-weakening results for the combinations of initial moisture contents and cement contents that were tested.

**Table 68. Cement-treated frost-heave and thaw-weakening test results summary**

| Initial *w* (%) | Cement content (%) | Average CBR (%) (after frost-susceptibility test) | Average 1st Frost-heave rate (mm/day) | Average 2nd Frost-heave rate (mm/day) |
|---|---|---|---|---|
| 13 | 3 | 71.6 | 0 | 0 |
| 20 | 3 | >100 | 0 | 0 |
| 20 | 5 | >100 | 0 | 0 |
| 20 | 7 | >100 | 0 | 0 |
| 13 | 9 | >100 | 0 | 0 |
| 20 | 9 | >100 | 0 | 0 |
| 20 | 11 | >100 | 0 | 0 |
| 22 | 13 | >100 | 0 | 0 |

The frost-heave time plots show that the soil structure of the cement-stabilized loess was strong enough to resist any forces due to frost heave. Representative frost-heave time plots for the cement-stabilized loess samples are presented in Figure 171 and Figure 173.

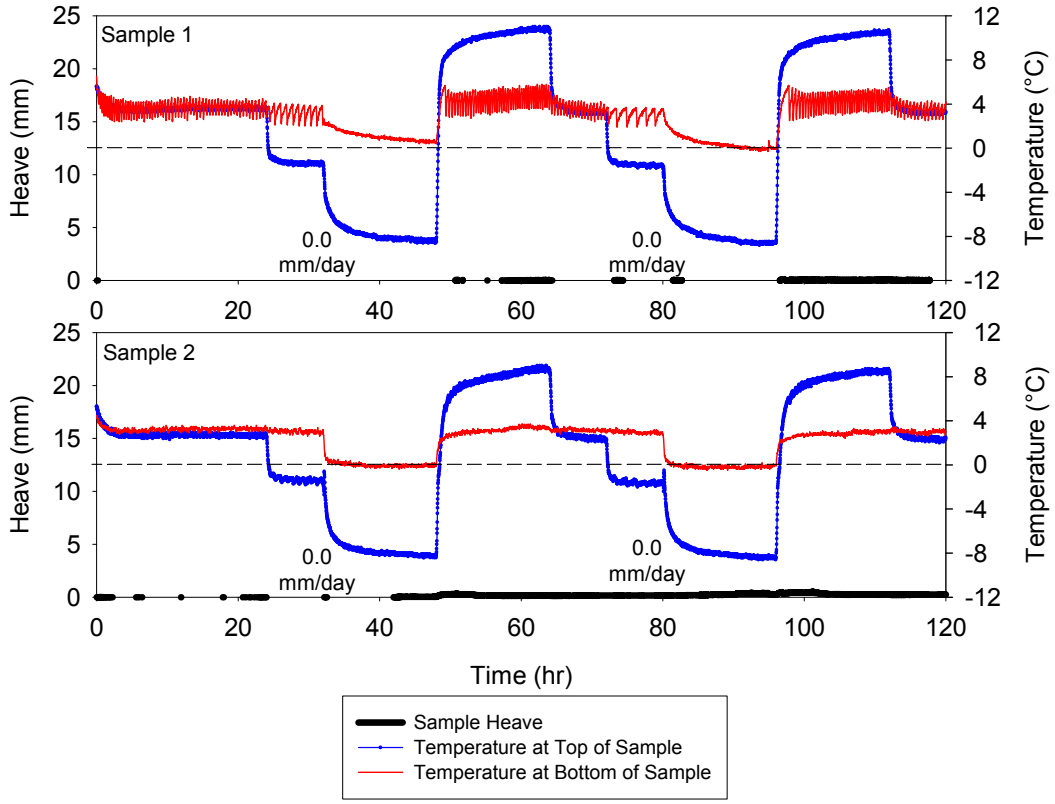


**Figure 171. Cement-treated loess frost heave time plots (13% initial moisture content and 3% cement content)**

The moisture content profile for the samples with an initial moisture content of 13% and cement content of 3% showed an increase in moisture content after freeze-thaw cycling compared to the initial moisture content. However, the samples that were initially at 20% moisture content and 3% cement content had lower increases in moisture content compared to the initial moisture content. One possibility for the samples with initial moisture contents of 13% to have such large increases in moisture content is the samples were hydrating and the soil structure had the ideal void structure to draw up water. The same trend occurred with the vacuum saturated 2-in. x 2-in. samples in compressive strength study. There were no distinguishable trends of higher moisture contents at any locations in the vertical profiles of

the cement-treated samples. Figure 172 and Figure 174 show typical moisture content profiles for the cement-treated loess samples.

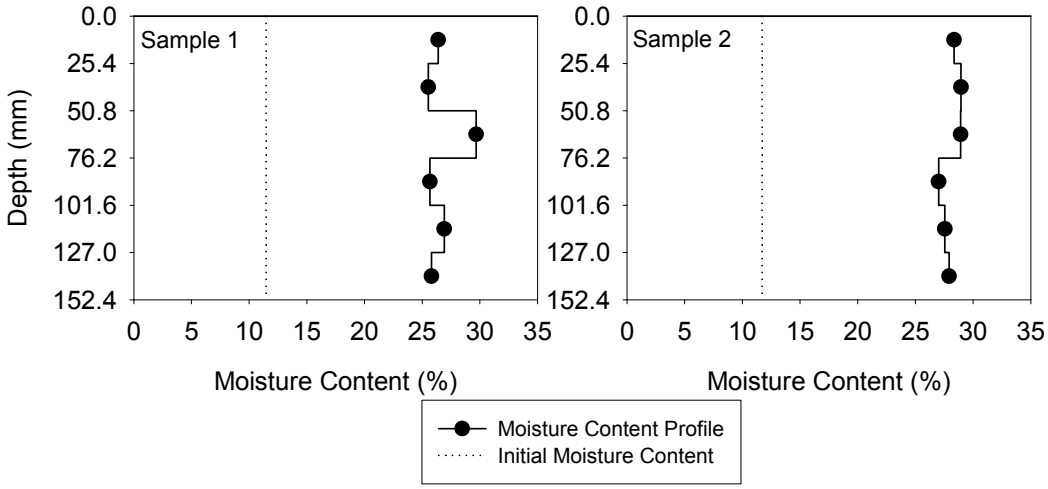


**Figure 172. Cement-treated loess moisture content profiles (13% initial moisture content and 3% cement content)**

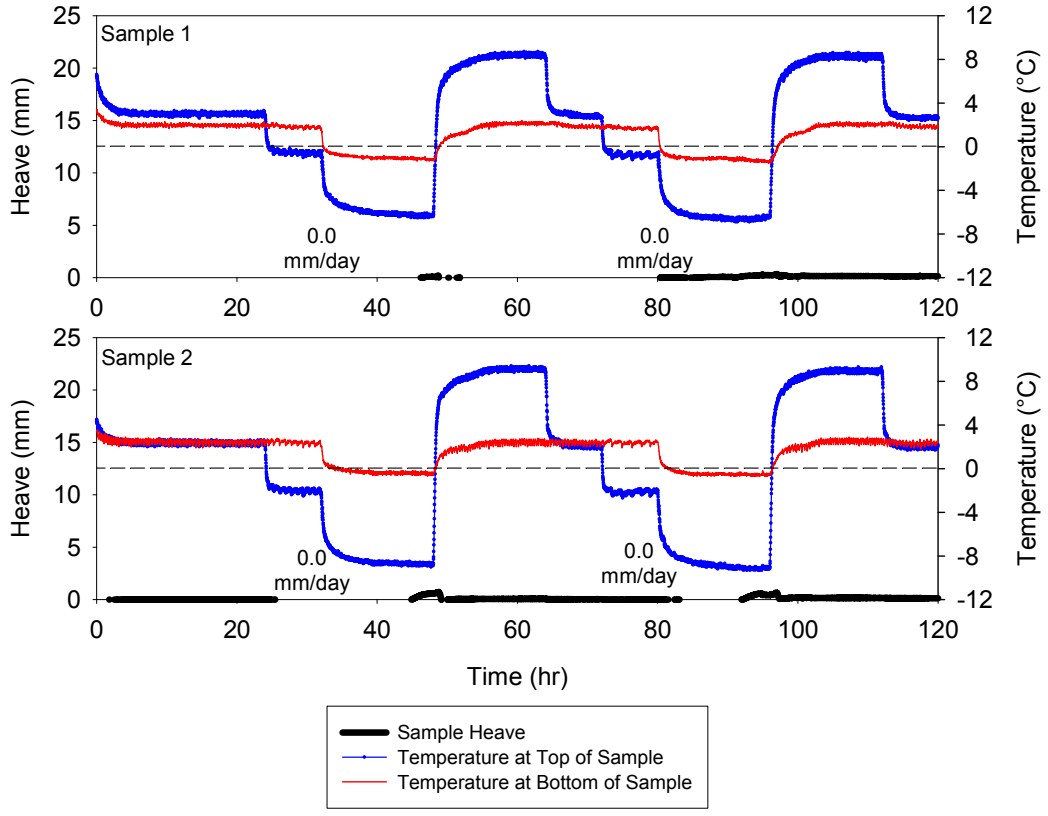


**Figure 173. Cement-treated loess frost heave time plots (20% initial moisture content and 3% cement content)**

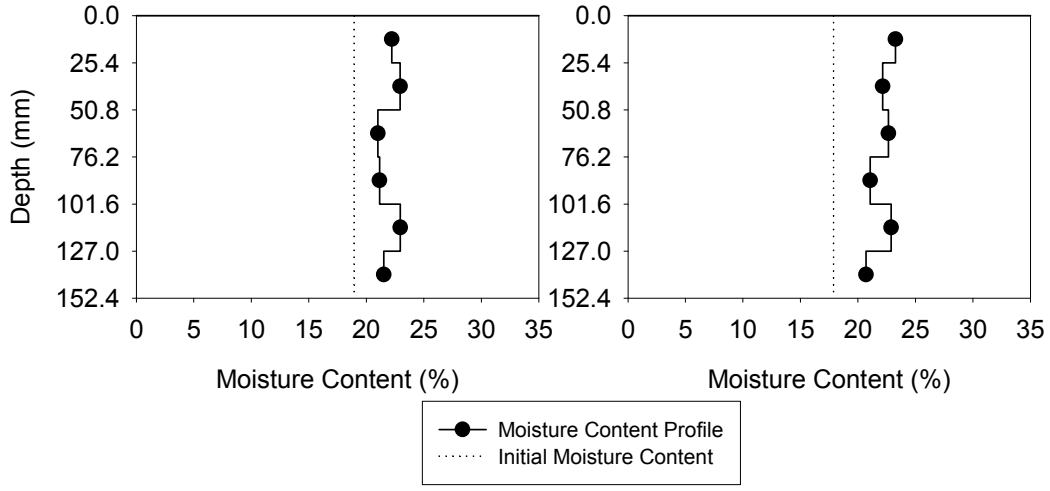


**Figure 174. Cement-treated loess moisture content profiles (20% initial moisture content and 3% cement content)**

**Fly Ash-Treated Loess**

Frost-heave and thaw-weakening tests were also performed on fly ash-treated samples. Several combinations of initial moisture contents and fly ash contents were chosen from the 2-in. x 2-in. compressive strength study. Two frost-heave and thaw-weakening samples were tested for each combination.

The frost-heave time plot for samples with an initial moisture content of 10% and fly ash content of 10%, showed unexpected results during the first freeze. The heave versus time line for the first freeze shows a steady increase in height until the second freeze begins. One possibility for this reaction is the samples were initially so dry that the samples could not heave, however water was pulled into the samples by capillary action, which resulted in the steady increase in height. Once the second freeze began, there was sufficient water in the samples for the samples to heave. The soil matrix of the fly ash-stabilized loess was not strong enough to resist heaving. The samples did not return to their initial height after first or second freeze-thaw cycle. The frost-heave time plots for the fly-ash treated samples with an initial moisture content of 10% and fly ash content of 10% is shown in Figure 175.

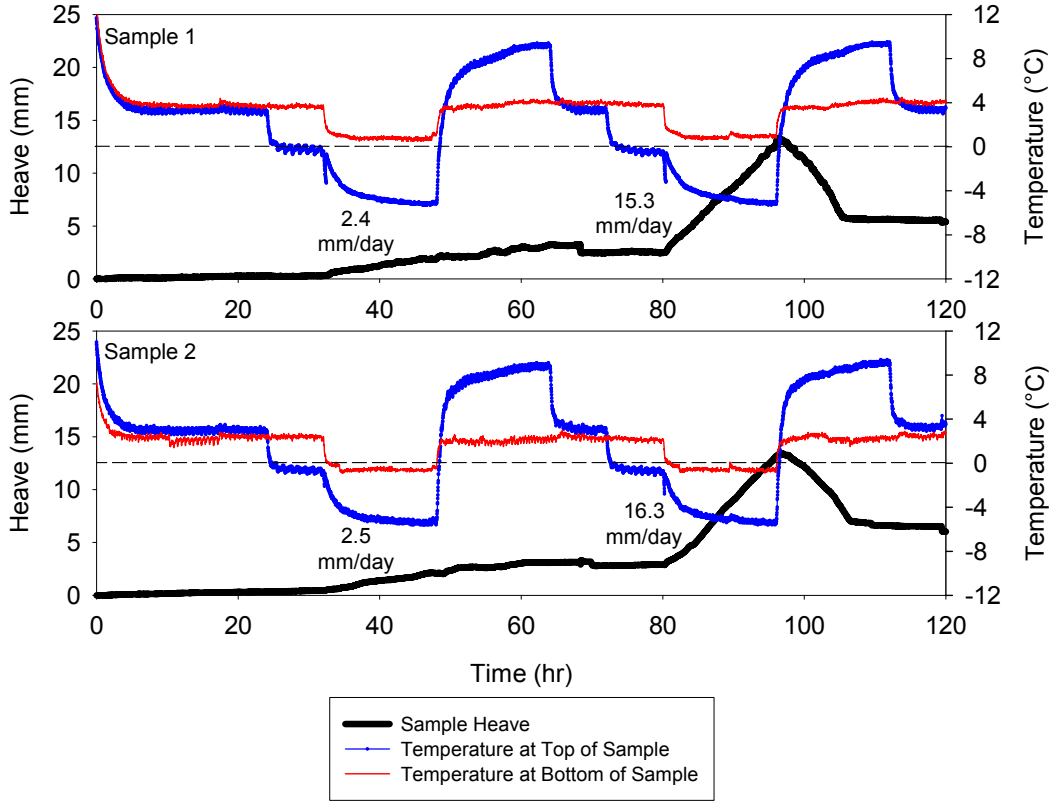


**Figure 175. Fly ash-treated loess frost heave time plots (10% initial moisture content and 10% fly ash content)**

The moisture content profiles show increases in moisture content after freeze-thaw cycling compared to the initial moisture content. The profiles also show that there is a higher concentration of water at the top of the samples compared to the rest of the profile. The moisture content profiles are shown in Figure 176.

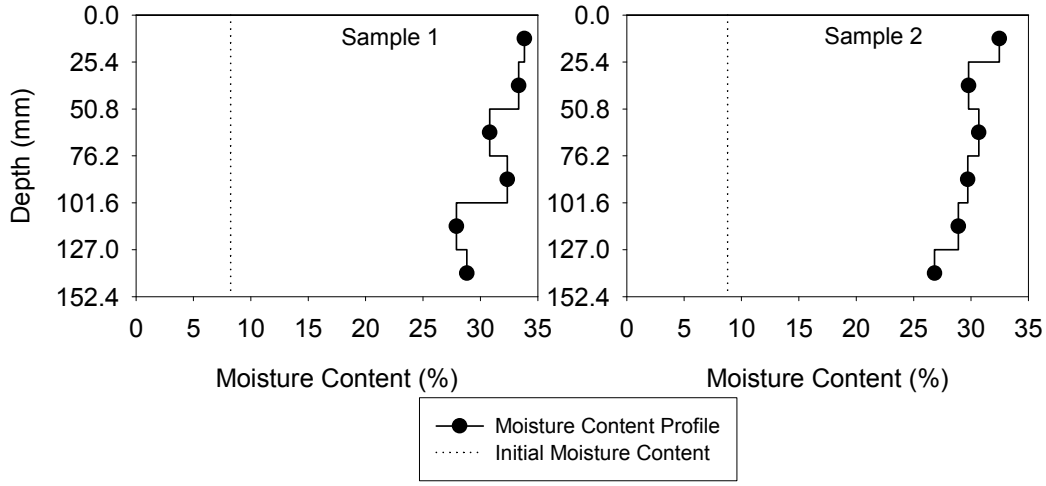


**Figure 176. Fly ash-treated loess moisture content profiles (10% initial moisture content and 10% fly ash content)**

The fly-ash treated samples had a low CBR value after freeze-thaw cycling. The thaw-weakening susceptibility rating is high for the fly ash-stabilized material. The frost-heave rate for the first freeze was low, but the second freeze had a higher frost-heave rate. The frost-heave susceptibility rating for the first freeze was low and high for the second freeze. The frost-heave and thaw-weakening test results for the loess with an initial moisture content of 10% and a fly ash content of 10% are shown in Table 69.

**Table 69. Fly ash-treated loess frost-heave and thaw-weakening test results (10% initial moisture content and 10% fly ash content)**

| | μ | σ | COV (%) | # of samples |
|---|---|---|---|---|
| CBR (%) (standard test) | | — | | 0 |
| CBR (%) (after frost-susceptibility test) | 3.8 | 0.3 | 8.2 | 2 |
| 1st Frost-heave rate (mm/day) | 2.5 | 0.1 | 2.0 | |
| 2nd Frost-heave rate (mm/day) | 15.83 | 0.7 | 4.5 | |
| 1st Frost-heave susceptibility rating | Low | — | — | |
| 2nd Frost-heave susceptibility rating | High | — | — | |
| Thaw-weakening susceptibility rating | High | — | — | |

The slope of the heave versus time line increased from the first freeze to the second for the samples with an initial moisture content of 19% and fly ash content of 10%. The total heave was higher during the second freeze than the first. However, that is mostly due to the height of the sample increasing after the first freeze-thaw cycle. The frost-heave time plots are shown in Figure 177.

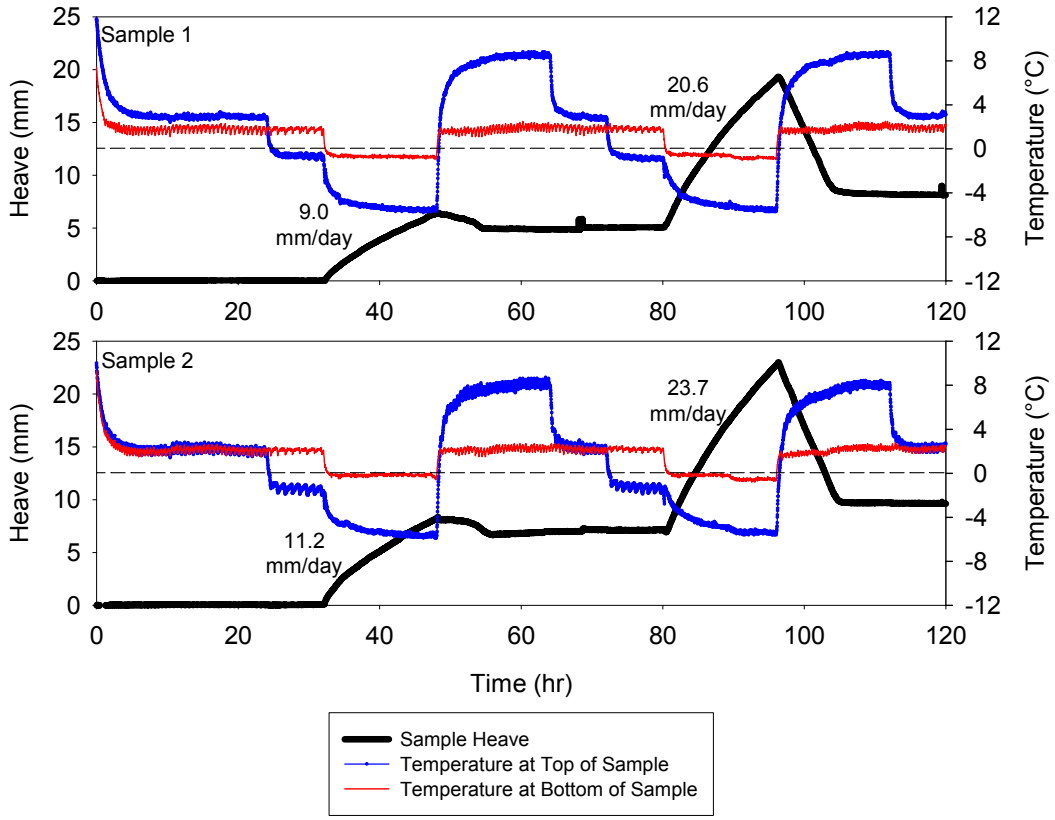


**Figure 177. Fly ash-treated loess frost heave time plots (19% initial moisture content and 10% fly ash content)**

The moisture contents increased after freeze-thaw cycling compared to the initial moisture content. There is a trend of decreasing moisture contents from the top to the bottom of the sample. The moisture content profiles are presented in Figure 178.

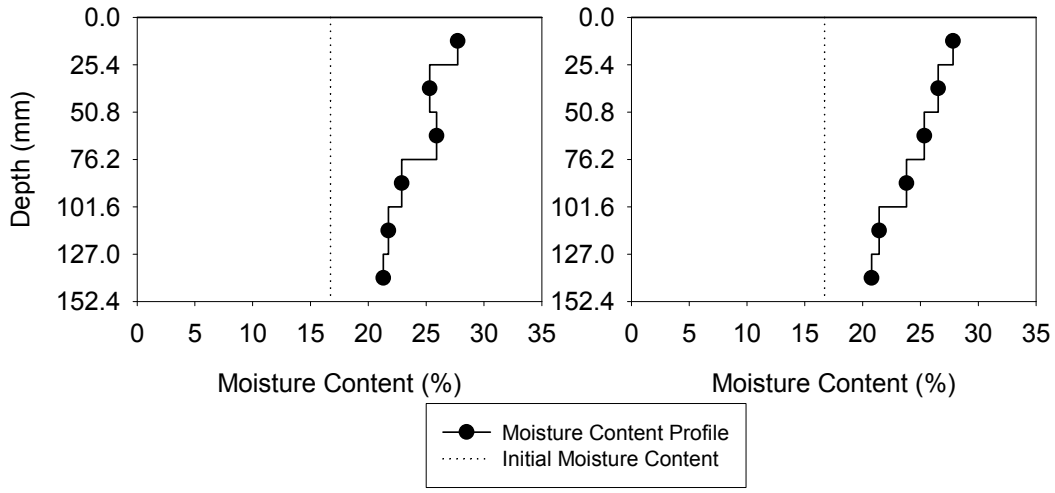


**Figure 178. Fly ash-treated loess moisture content profiles (19% initial moisture content and 10% fly ash content)**

The thaw-weakening susceptibility of the fly ash stabilized samples is rated as high. The frost-heave rate significantly increased from the first freeze to the second. The frost-heave susceptibility rating for the first and second freeze is high and very high, respectively. The frost-heave and thaw-weakening susceptibility ratings are summarized in Table 70.

**Table 70. Fly ash-treated loess frost-heave and thaw-weakening test results (19% initial moisture content and 10% fly ash content)**

| | μ | σ | COV (%) | # of samples |
|---|---|---|---|---|
| CBR (%) (standard test) | | — | | 0 |
| CBR (%) (after frost-susceptibility test) | 5.0 | 1.7 | 33.9 | 2 |
| 1st Frost-heave rate (mm/day) | 10.1 | 1.1 | 10.9 | |
| 2nd Frost-heave rate (mm/day) | 22.2 | 2.2 | 9.9 | |
| 1st Frost-heave susceptibility rating | High | — | — | |
| 2nd Frost-heave susceptibility rating | Very high | — | — | |
| Thaw-weakening susceptibility rating | High | — | — | |

The frost-heave time plot for the loess samples with an initial moisture content of 19% and fly ash content of 15% shows that the samples were not strong enough to resist heaving. The total heave and slope of the heave versus time line increased from the first freeze to the second. After the first and second freeze-thaw cycles, the height of the thawed samples increased. The frost-heave time plots are shown in Figure 179.

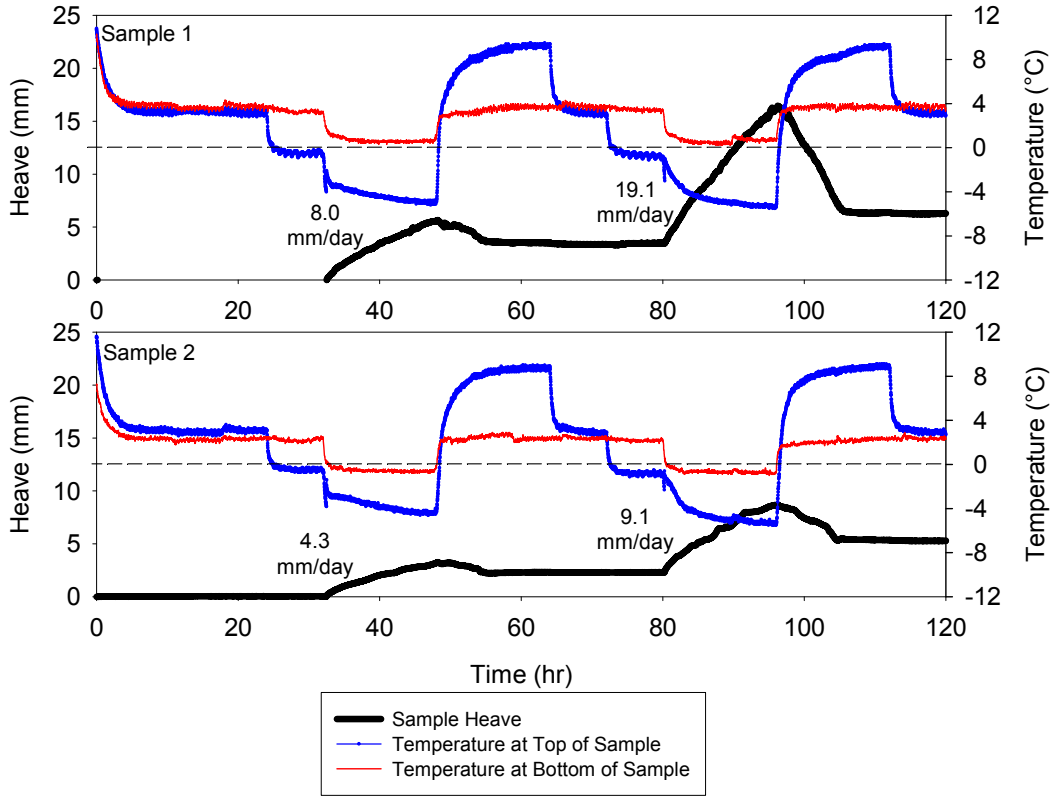


**Figure 179. Fly ash-treated loess frost heave time plots (19% initial moisture content and 15% fly ash content)**

The moisture content profiles show an increase in water content throughout the samples, with higher concentrations at the top of the samples. The moisture content profiles are shown in Figure 180.

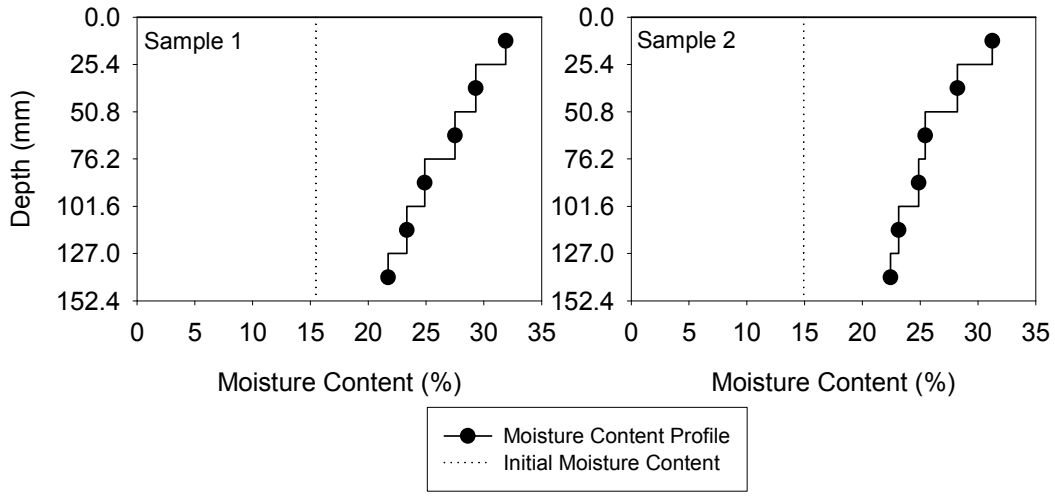


**Figure 180. Fly ash-treated loess moisture content profiles (19% initial moisture content and 15% fly ash content)**

The thaw-weakening susceptibility rating of samples is medium. The samples had a higher frost-heave rate during the second freeze compared to the first. The frost-susceptibility rating for the first freeze is medium and it is high for the second freeze. The frost-heave and thaw-weakening test results are summarized in Table 71.

**Table 71. Fly ash-treated loess frost-heave and thaw-weakening test results (19% initial moisture content and 15% fly ash content)**

| | μ | σ | COV (%) | # of samples |
|---|---|---|---|---|
| CBR (%) (standard test) | | — | | 0 |
| CBR (%) (after frost-susceptibility test) | 7.1 | 0.1 | 1.3 | 2 |
| 1st Frost-heave rate (mm/day) | 6.2 | 1.9 | 30.1 | |
| 2nd Frost-heave rate (mm/day) | 14.1 | 7.1 | 50.0 | |
| 1st Frost-heave susceptibility rating | Medium | — | — | |
| 2nd Frost-heave susceptibility rating | High | — | — | |
| Thaw-weakening susceptibility rating | Medium | — | — | |

The frost-heave plot for the loess with an initial moisture content of 22% and 20% fly ash content were similar. The heights of the thawed samples increased after the first and second freeze cycles. The slope of the heave versus time line increased during the second freeze compared to the first. The frost-heave time plots are shown in Figure 181.

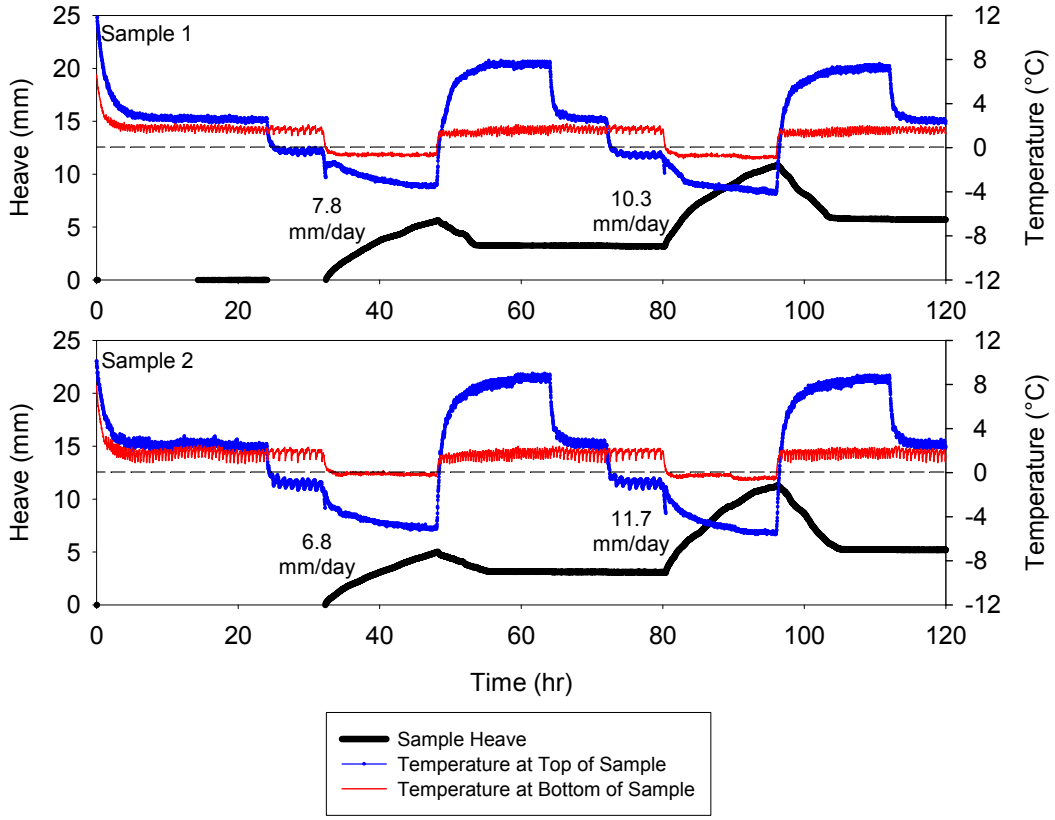


**Figure 181. Fly ash-treated loess frost heave time plots (22% initial moisture content and 20% fly ash content)**

The moisture content of the samples after freeze-thaw cycling increased compared to the initial moisture content. The moisture content is highest at the top of the samples. The moisture content profiles are presented in. Figure 182.

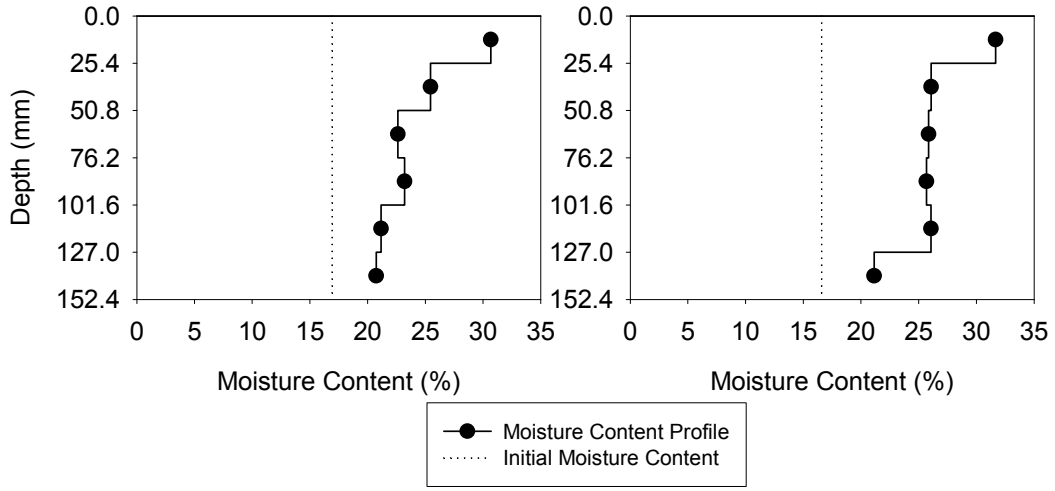


**Figure 182. Fly ash-treated loess moisture content profiles (22% initial moisture content and 20% fly ash content)**

The CBR after freeze-thaw cycling was high compared to the other fly ash-treated loess samples. The thaw-weakening susceptibility of the stabilized material is negligible. The frost-heave rate increased between the first and second freeze. The frost-susceptibility for the first freeze was medium and it was high for the second freeze. The frost-heave and thaw-weakening test results are summarized in Table 72.

**Table 72. Fly ash-treated loess frost-heave and thaw-weakening test results (22% initial moisture content and 20% fly ash content)**

| | μ | σ | COV (%) | # of samples |
|---|---|---|---|---|
| CBR (%) (standard test) | | — | | 0 |
| CBR (%) (after frost-susceptibility test) | 25.5 | 1.7 | 6.5 | 2 |
| 1st Frost-heave rate (mm/day) | 7.3 | 0.5 | 6.5 | |
| 2nd Frost-heave rate (mm/day) | 11.0 | 1.0 | 8.9 | |
| 1st Frost-heave susceptibility rating | Medium | — | — | |
| 2nd Frost-heave susceptibility rating | High | — | — | |
| Thaw-weakening susceptibility rating | Negligible | — | — | |

## WI US-10

### Sandy Lean Clay Subgrade

The frost-heave time plots are similar for the sandy lean clay subgrade. The height of all four samples increased after the first and second freeze-thaw cycle and began increasing

before freezing began, which could be because water was being drawn into the samples. The frost-heave time plots are presented in Figure 183.

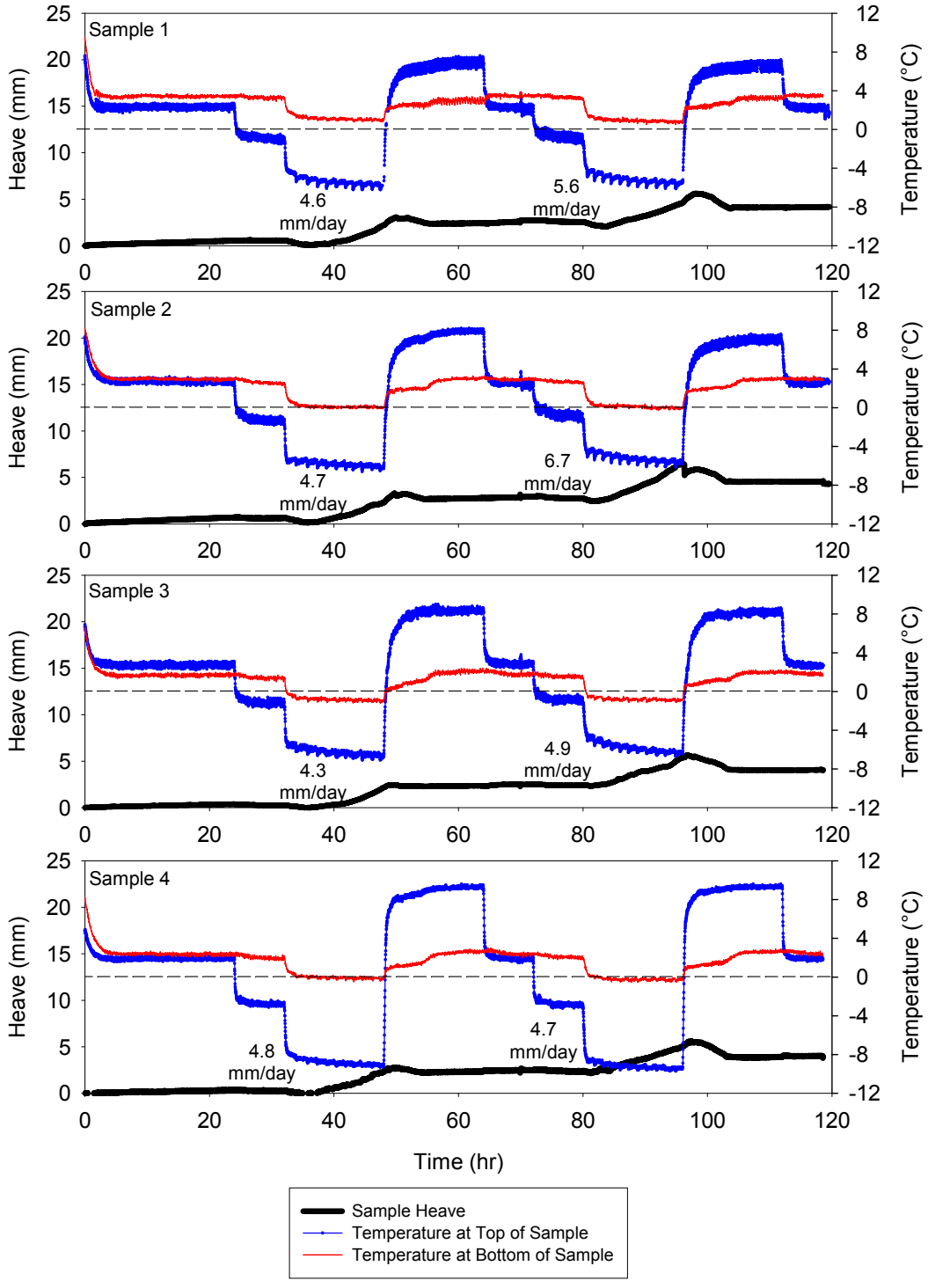


**Figure 183. WI US-10 sandy lean clay subgrade frost heave time plots**

The moisture content at the top of the samples and after freeze-thaw cycling is close to the initial moisture content. However, the moisture content increases as the depth increases. The moisture content profiles are presented in Figure 184.

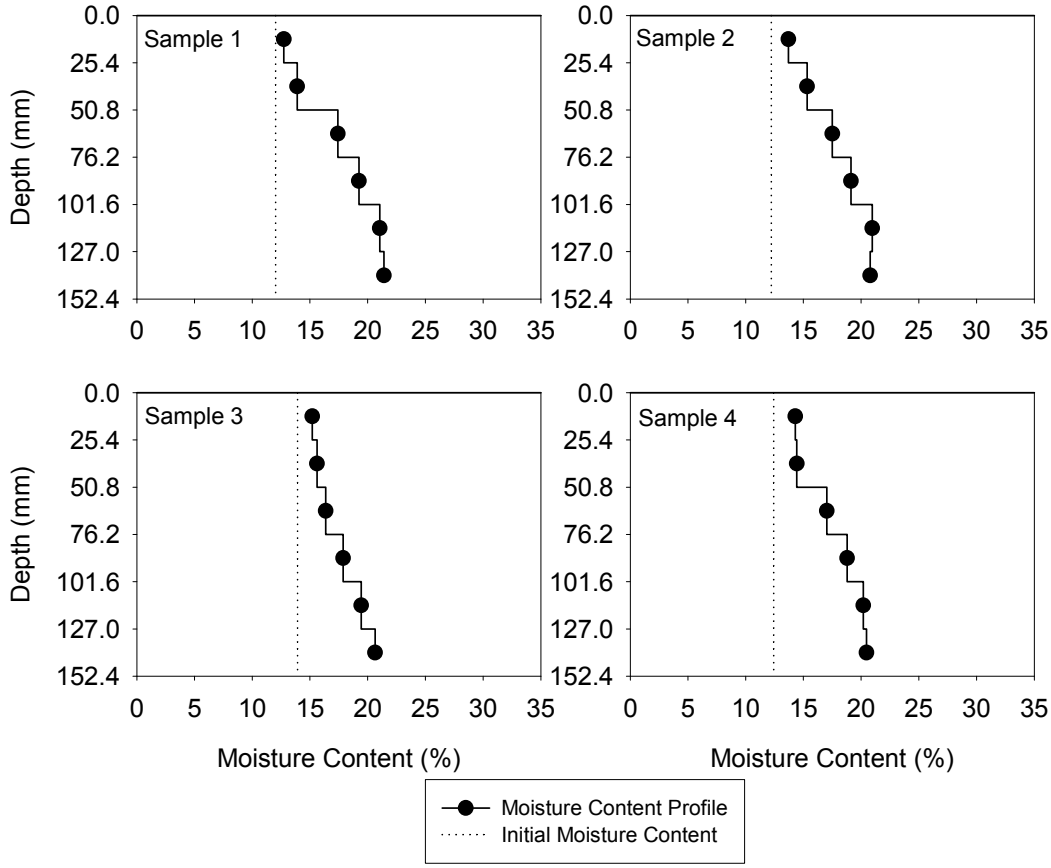


**Figure 184. WI US-10 sandy lean clay subgrade moisture content profiles**

The CBR after freeze-thaw cycling is much lower than the standard CBR. The thaw-weakening susceptibility rating for the material is medium. The frost-heave rate increased during the second freeze compared to the first. The frost-heave susceptibility rating for both freeze cycles is medium. The frost-heave and thaw-weakening test results are summarized in Table 73.

**Table 73. WI US-10 sandy lean clay subgrade frost-heave and thaw-weakening test results**

| | μ | σ | COV (%) | # of samples |
|---|---|---|---|---|
| CBR (%) (standard test) | 25.9 | | | 1 |
| CBR (%) (after frost-susceptibility test) | 7.2 | 4 | 5.5 | 4 |
| 1st Frost-heave rate (mm/day) | 4.6 | 0.2 | 4.2 | |
| 2nd Frost-heave rate (mm/day) | 5.5 | 0.9 | 17.2 | |
| 1st Frost-heave susceptibility rating | Medium | — | — | |
| 2nd Frost-heave susceptibility rating | Medium | — | — | |
| Thaw-weakening susceptibility rating | Medium | — | — | |

## Summary

The results of the frost-heave and thaw-weakening test provide a part of the data needed to select materials that will result in a good pavement foundation. The results of the frost-heave and thaw-weakening test are not a direct measurement of how much a material may heave or weakening in situ, but it can be used to relatively compare materials.

The frost-heave and thaw-weakening test results show variable results for materials with the same soil classifications. For example, the materials with a USCS classification of CL have similar standard CBR values, but the post-test CBR ranges from 0.7 to 7.2% and the frost-heave rate ranges from 4.3 mm/day to 12.4 mm/day. The thaw-weakening susceptibility ratings ranged from medium to very high and the frost-susceptibility ratings ranged from medium to high. For the CL classified materials, the general trend is the lower the post-test CBR, the higher the frost-heave rate. The average moisture content change is the difference between the initial moisture content of the four samples and the average of the moisture contents in the soil profile after the frost-susceptibility test. The average moisture content ($w$%) change can be used as an indication of higher frost-heave rates for the CL classified materials (Figure 185). However, the moisture content change is highly dependent on the initial moisture content of the samples.

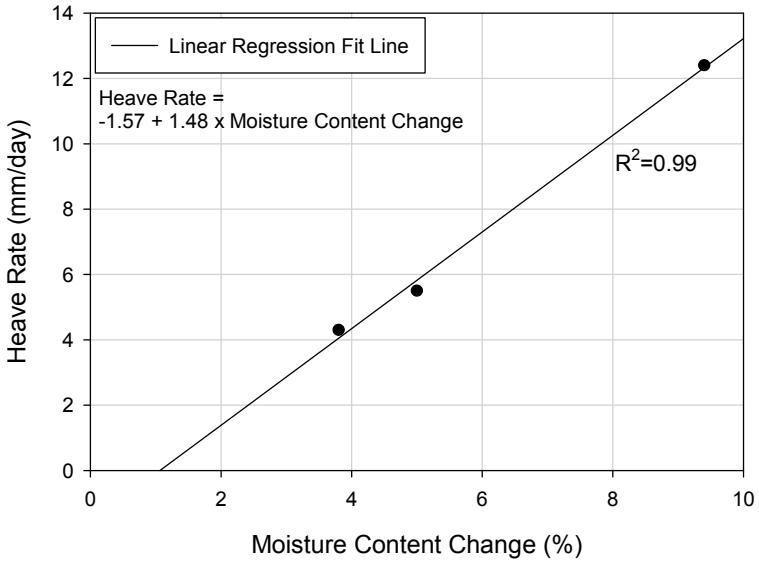


**Figure 185. Relationship between frost-heave rate and moisture content change for CL tested materials**

The two materials tested with a USCS classification of ML were susceptible to frost-heaving and thaw-weakening. The frost-heave rates ranged from 11.0 to 19.1 mm/day, which correlates to a frost-susceptibility rating of high to very high. The loess material had the highest measured frost-heave rate of any material tested with 19.1 mm/day. Both materials had a very high thaw-weakening susceptibility rating. The results of the tests performed on the ML materials are relatively similar to the CL material results, which is most likely due to the high fines content of the materials. The ML materials tended to have a higher heave-rate and lower post-test CBR values. The ML materials showed an increase of approximately 9 mm/day in the heave rate for an approximate 1% increase in the moisture content change, which is different from the relationship for CL classified materials. The difference in the water content change and heave rate relationship for the two materials could be because of the silt contents of the two materials. The IA I-29 silt with sand subgrade is 59% silt with 21% sand; whereas the loess is 82% silt with no sand sized particles. The clay contents of the two materials are similar.

The materials with a USCS classification of SC had relatively low post-test CBR values and high heave rates. The thaw-weakening susceptibility ratings ranged from medium to high for the two materials and the frost-heave susceptibility ratings ranged from medium to high. The IA US-30 clayey sand subgrade heaved less than the MI I-96 clayey sand subgrade

material, but had a lower average post-test CBR value compared to the MI I-96 clayey sand subgrade. The materials had similar frost-heave rates compared to the CL and ML materials; however the change in moisture content was lower than that observed for the CL and ML materials.

The two materials from 160th Street with USCS classifications of SP-SM and SW-SM showed high CBR values before and after the frost-susceptibility test compared to the CL, ML, and SC classified materials. The thaw-weakening susceptibility ratings ranged from negligible to very low. However, the frost-heave rate of both materials is very similar to the CL, ML, and SC classified materials. The frost-heave susceptibility rating for both materials was high. The moisture content change was nearly zero for both materials. The Manatts concrete sand subbase material had a low standard CBR compared to the 160th Street materials; however it was relatively unchanged after the frost-susceptibility test. The thaw-weakening susceptibility rating for the concrete sand is medium. The frost-heave rate of the concrete sand was the lowest measured value of the materials tested and had a frost-susceptibility rating of negligible. The concrete sand samples were compacted at low initial moisture contents, so the moisture content change value is not representable of the effects the frost-susceptibility test had on the material. A possible reason for differences between the frost-heave results of the 160th street materials and the Manatts concrete sand is the silt content in the 160th Street materials.

A total of six materials with gravel were tested. The USCS classifications ranged from GM to GW. The thaw-weakening susceptibility rating was negligible for all the materials with the exception of the Manatts RAP subbase, which had a rating of medium. The frost-heave rate ranged from 1.8 to 8.0 mm/day. The frost-heave susceptibility rating for the materials ranged from very low to high. The two materials classified as GW had a frost-heave rate of 1.8 and 1.9 mm/day compared to other four materials, which all contained silt sized particles, having a frost-heave rate between 5.4 and 8.0. The moisture content change of the materials cannot be considered to have an effect on the frost susceptibility of the material because the moisture content change is dependent on the initial moisture content, which varied between low of optimum and near optimum. An additional two samples of the IA US-30 RPCC subbase were tested with reduced fines content compared to the original

sample gradation. Samples with half of the fines removed and all of the fines removed showed almost no difference in the frost-susceptibility results compared to the original gradation. Tester and Gaskin (1992) also performed a fines content study, but they found that as the fines content of a limestone aggregate increased, the frost-heave rate increased.

Several of the gravel samples tested showed a decrease in the frost-heave rate between the first and second freeze cycles. This result was also found by Chamberlain (1986). The frost-susceptibility test results for the untreated materials are presented in Table 74.

The frost susceptibility of cement and fly ash-treated samples were also tested. The loess material was chosen, because it proved to be the most frost susceptible material. Eight moisture content and cement content combinations were tested. Four combinations of moisture content and fly ash content were also tested. The results of the cement-treated loess samples showed that the frost-susceptibility of the material becomes negligible after stabilization. All eight combinations of cement-stabilized loess samples had a thaw-weakening and frost-heave susceptibility rating of negligible. The moisture content change measurements showed that the cement-stabilized materials could absorb large amounts of water without increasing the frost susceptibility.

All of the fly ash-stabilized samples showed small improvements in the post-test CBR. However, only three of the four samples showed reduced frost-heave rates. The frost-heave rate of one sample increased compared to the unstabilized material. The post-test CBR of the fly ash-treated samples ranged from 3.8 to 25.5 and increased as the fly ash content increased. The thaw-weakening susceptibility ranged from negligible to high. The frost-heave rate of the fly ash-treated loess ranged from 11.0 to 22.2 mm/day. Compared to 19.1 mm/day for untreated loess, the frost-heave improvements are small. The frost-susceptibility of the samples ranged from high to very high. The frost-susceptibility test results for the stabilized materials are summarized in Table 75.

.

**Table 74. Summary of frost-heave and thaw-weakening tests performed on unstabilized materials**

| Material | USCS | Standard CBR (%) | Average CBR (%) after frost-susceptibility test | Average 2nd frost-heave rate (mm/day) | Average $w$% change | Thaw-weakening susceptibility rating | Frost-heave susceptibility rating |
|---|---|---|---|---|---|---|---|
| IA I-29 lean clay subgrade | CL | 21.8 | 0.7 | 12.4 | 9.4 [x] | Very high | High |
| PA US-22 sandy lean clay subgrade | CL | 21.1 | 3.0 | 4.3 | 3.8 [x] | High | Medium |
| WI US-10 sandy lean clay subgrade | CL | 25.9 | 7.2 | 5.5 | 5.0 [x] | Medium | Medium |
| IA I-29 silt with sand subgrade | ML | 21.6 | 1.4 | 11.0 | 6.9 [x] | Very high | High |
| Loess | ML | 10.0 | 0.5 | 19.1 | 7.7 [x] | Very high | Very high |
| IA US-30 clayey sand subgrade | SC | 8.4 | 2.7 | 7.8 | 1.7 [x] | High | Medium |
| MI I-96 clayey sand subgrade | SC | 26.3 | 5.8 | 13.1 | 1.6 [x] | Medium | High |
| 160th Street poorly graded sand with silt and gravel | SP-SM | 65.1 | 28.9 | 11.5 | -0.5 [x] | Negligible | High |
| 160th Street well graded sand with silt and gravel | SW-SM | 39.7 | 15.0 | 13.4 | 0.1 [x] | Very low | High |
| Manatts concrete sand subbase | SP | 9.4 | 8.1 | 0.9* | 10.4 | Medium | Negligible |
| IA US-30 RPCC subbase | GM | 70.3 | 33.3 | 6.1* | 4.4 | Negligible | Medium |
| IA US-30 RPCC/RAP subbase | GP-GM | 40.6 | 37.6 | 5.4* | -0.8 | Negligible | Medium |
| IA US-30 limestone subbase | GP-GM | 70.5 | 33.2 | 6.4 | 0.0 | Negligible | Medium |
| Martin Marietta crushed limestone subbase | GP-GM | 87.3 | 47.5 | 8.0 | 0.7 | Negligible | High |
| IA US-30 RPCC subbase modified (half of fines removed) | GP | — | 39.2 | 6.1* | 3.1 | Negligible | Medium |
| IA US-30 RPCC subbase modified (all fines removed) | GP | — | 35.5 | 6.1* | 3.7 | Negligible | Medium |
| Manatts RAP subbase | GW | 11.6 | 8.7 | 1.8* | 7.4 | Medium | Very low |
| Manatts RPCC/RAP subbase | GW | 48.2 | 33.2 | 1.9* | 8.5 | Negligible | Very low |

*Average 1st frost-heave rate is higher than 2nd
[x] Placed at optimum moisture content

**Table 75. Summary of frost-heave and thaw-weakening tests performed on stabilized materials**

| Material | Stabilizer type | Initial *w* (%) | Stabilizer content (%) | Average CBR (%) after frost-susceptibility test) | Average 2nd frost-heave rate (mm/day) | Moisture content change (%) | Thaw-weakening susceptibility rating | Frost-heave susceptibility rating |
|---|---|---|---|---|---|---|---|---|
| Loess | Cement | 13 | 3 | 71.6 | 0 | 15.8 | Negligible | Negligible |
| | Cement | 20 | 3 | >100 | 0 | 3.2 | Negligible | Negligible |
| | Cement | 20 | 5 | >100 | 0 | 5.6 | Negligible | Negligible |
| | Cement | 20 | 7 | >100 | 0 | 5.1 | Negligible | Negligible |
| | Cement | 13 | 9 | >100 | 0 | 14.9 | Negligible | Negligible |
| | Cement | 20 | 9 | >100 | 0 | 4.9 | Negligible | Negligible |
| | Cement | 20 | 11 | >100 | 0 | 5.4 | Negligible | Negligible |
| | Cement | 22 | 13 | >100 | 0 | 3.0 | Negligible | Negligible |
| | Fly ash | 10 | 10 | 3.8 | 15.8 | 21.9 | High | High |
| | Fly ash | 19 | 10 | 5.0 | 22.2 | 7.5 | High | Very high |
| | Fly ash | 19 | 15 | 7.1 | 14.1 | 12.2 | Medium | High |
| | Fly ash | 22 | 20 | 25.5 | 11.0 | 5.3 | Negligible | High |

Four samples were tested for each of the untreated materials, with the exception of the IA US-30 RPCC modified samples. The number of samples tested can be found the discussion of each material. The standard deviation and coefficient of variation are useful in determining the variation of the data set. The standard deviation (σ) is an indication of the variation of the data from the average and is in the same units as the average. The magnitude of the standard deviation depends on the magnitude of the average, whereas the coefficient of variation (COV) is normalized and expressed as a percentage. Equation (12) shows how the COV is calculated. The higher the COV, the more variation there is in the data.

$$COV\,(\%) = \sigma / \mu \tag{12}$$

where σ = standard deviation and

μ = average

The COV for the frost-heave results range from 4.5 to 30.4%. In general the frost-heave COV is higher for cohesive materials compared to cohesionless materials. The statistical parameters for the frost-heave test results are summarized in Table 76.

**Table 76. Summary of statistical parameters for frost-heave results of unstabilized materials**

| Material | USCS | Average 2nd frost-heave rate (mm/day) | σ | COV (%) | # of samples |
|---|---|---|---|---|---|
| IA I-29 lean clay subgrade | CL | 12.4 | 2.2 | 17.9 | 4 |
| PA US-22 sandy lean clay subgrade | CL | 4.3 | 0.5 | 11.4 | 4 |
| WI US-10 sandy lean clay subgrade | CL | 5.5 | 0.9 | 17.2 | 4 |
| IA I-29 silt with sand subgrade | ML | 11.0 | 3.4 | 30.4 | 4 |
| Loess | ML | 19.1 | 4.4 | 22.8 | 4 |
| IA US-30 clayey sand subgrade | SC | 7.8 | 2.0 | 25.2 | 4 |
| MI I-96 clayey sand subgrade | SC | 13.1 | 1.4 | 10.6 | 4 |
| 160th Street poorly graded sand with silt and gravel | SP-SM | 11.5 | 0.5 | 4.5 | 4 |
| 160th Street well graded sand with silt and gravel | SW-SM | 13.4 | 0.8 | 6.2 | 4 |
| Manatts concrete sand subbase | SP | 0.9 | 0.2 | 25.3 | 4 |
| IA US-30 RPCC subbase | GM | 6.1 | 0.5 | 8.0 | 4 |
| IA US-30 RPCC/RAP subbase | GP-GM | 5.4 | 0.4 | 7.5 | 4 |
| IA US-30 limestone subbase | GP-GM | 6.4 | 0.6 | 8.9 | 4 |
| Martin Marietta crushed limestone subbase | GP-GM | 8.0 | 1.2 | 14.6 | 4 |
| IA US-30 RPCC subbase modified (half of fines removed) | GP | 6.1 | 0.3 | 5.7 | 2 |
| IA US-30 RPCC subbase modified (all fines removed) | GP | 6.1 | 0.7 | 10.8 | 2 |
| Manatts RAP subbase | GW | 1.8 | 0.5 | 24.8 | 4 |
| Manatts RPCC/RAP subbase | GW | 1.9 | 0.4 | 19.1 | 4 |

For comparison, Table 77 presents the statistical parameters of frost-heave test results presented in Chamberlain (1986). The COV ranges from 0.8 to 31%, which is very similar to the range COV found in this research.

**Table 77. Summary of statistical parameters for frost-heave test results presented in Chamberlain (1986)**

| Material | USCS | Average 2nd frost-heave rate (mm/day) | σ | COV (%) | # of samples |
|---|---|---|---|---|---|
| Dense graded stone | GM-GP | 4.5 | 1.0 | 21.2 | 4 |
| Graves sand | SM | 6.4 | 2.0 | 31.0 | 4 |
| Hart Brothers sand | SM | 6.8 | 1.6 | 23.4 | 4 |
| Hyannis sand | SM | 1.4 | 0.4 | 26.4 | 4 |
| Ikalanian sand | SM-SP | 5.7 | 1.2 | 20.3 | 4 |
| Sibley till | SM-SC | 17.9 | 2.3 | 12.6 | 4 |
| Taxiway A base | SW-SM | 11.9 | 0.1 | 0.8 | 2 |
| Taxiway b subbase | GW-GM | 13.4 | 1.4 | 10.6 | 2 |
| Taxiway B subgrade | SM | 10.4 | 1.2 | 11.8 | 2 |

The COV for post-test CBR values range from 5.5 to 44%. Neither cohesive nor cohesionless materials appear to have higher or lower COV values. The statistical parameters for the thaw-weakening test results are summarized in Table 78.

Table 79 presents the statistical parameters for thaw-weakening results presented in Chamberlain (1986). The COV for the post-test CBR values range from 3.6 to 39.2%, which is very similar to the range of COV values found in this research.

**Table 78. Summary of statistical parameters for thaw-weakening results of unstabilized materials**

| Material | USCS | Average CBR (%) after frost-susceptibility test | σ | COV (%) | # of samples |
|---|---|---|---|---|---|
| IA I-29 lean clay subgrade | CL | 0.7 | 0.0 | 12.0 | 4 |
| PA US-22 sandy lean clay subgrade | CL | 3.0 | 0.3 | 12.8 | 4 |
| WI US-10 sandy lean clay subgrade | CL | 7.2 | 4 | 5.5 | 4 |
| IA I-29 silt with sand subgrade | ML | 1.4 | 0.4 | 25.9 | 4 |
| Loess | ML | 0.5 | 0.2 | 44 | 4 |
| IA US-30 clayey sand subgrade | SC | 2.67 | 0.4 | 14.7 | 4 |
| MI I-96 clayey sand subgrade | SC | 5.8 | 0.7 | 12.6 | 4 |
| 160th Street poorly graded sand with silt and gravel | SP-SM | 28.9 | 6.1 | 21.1 | 4 |
| 160th Street well graded sand with silt and gravel | SW-SM | 15.0 | 1.7 | 11.5 | 4 |
| Manatts concrete sand subbase | SP | 8.1 | 0.8 | 10.0 | 4 |
| IA US-30 RPCC subbase | GM | 33.3 | 4.3 | 12.8 | 4 |
| IA US-30 RPCC/RAP subbase | GP-GM | 37.6 | 10.3 | 27.5 | 4 |
| IA US-30 limestone subbase | GP-GM | 33.2 | 6.4 | 19.3 | 4 |
| Martin Marietta crushed limestone subbase | GP-GM | 47.5 | 8.1 | 17.0 | 4 |
| IA US-30 RPCC subbase modified (half of fines removed) | GP | 39.2 | 8.3 | 21.1 | 2 |
| IA US-30 RPCC subbase modified (all fines removed) | GP | 35.5 | 4.0 | 11.3 | 2 |
| Manatts RAP subbase | GW | 8.7 | 0.9 | 9.8 | 4 |
| Manatts RPCC/RAP subbase | GW | 33.2 | 5.8 | 17.4 | 4 |

**Table 79. Summary of statistical parameters for thaw-weakening test results presented in Chamberlain (1986)**

| Material | USCS | Average CBR (%) after frost-susceptibility test | σ | COV (%) | # of samples |
|---|---|---|---|---|---|
| Dense graded stone | GM-GP | 10.0 | 1.9 | 19.5 | 4 |
| Graves sand | SM | 1.7 | 0.2 | 9.1 | 4 |
| Hart Brothers sand | SM | 4.7 | 0.9 | 19.2 | 4 |
| Hyannis sand | SM | 8.1 | 0.9 | 11.6 | 4 |
| Ikalanian sand | SM-SP | 2.0 | 0.8 | 39.2 | 4 |
| Sibley till | SM-SC | 1.1 | 0.3 | 28.2 | 4 |
| Taxiway A base | SW-SM | 12.7 | 0.5 | 3.6 | 2 |
| Taxiway b subbase | GW-GM | 8.2 | 0.5 | 5.5 | 2 |
| Taxiway B subgrade | SM | 16.2 | 2.4 | 14.6 | 2 |

The average frost-heave rates can be compared to the percentage of particles smaller than 0.02 mm. Cassagrande (1931) found that the percentage of particle passing 0.02 mm can be used as an indication of frost-susceptibility. The untreated materials do show an increase in frost-heave rate as the percentage of particles passing 0.02 mm increases (Figure 186).

However, the relationship is not great, as there are several materials with lower percentages of particles passing 0.02 mm that have comparably high heave rates to materials with more particles passing 0.02 mm. For example, the materials from 160th Street have around 6% passing 0. 02 mm, but they have heave rates around 12 mm/day which is comparable fine grained materials with much higher percentages passing 0.02 mm.

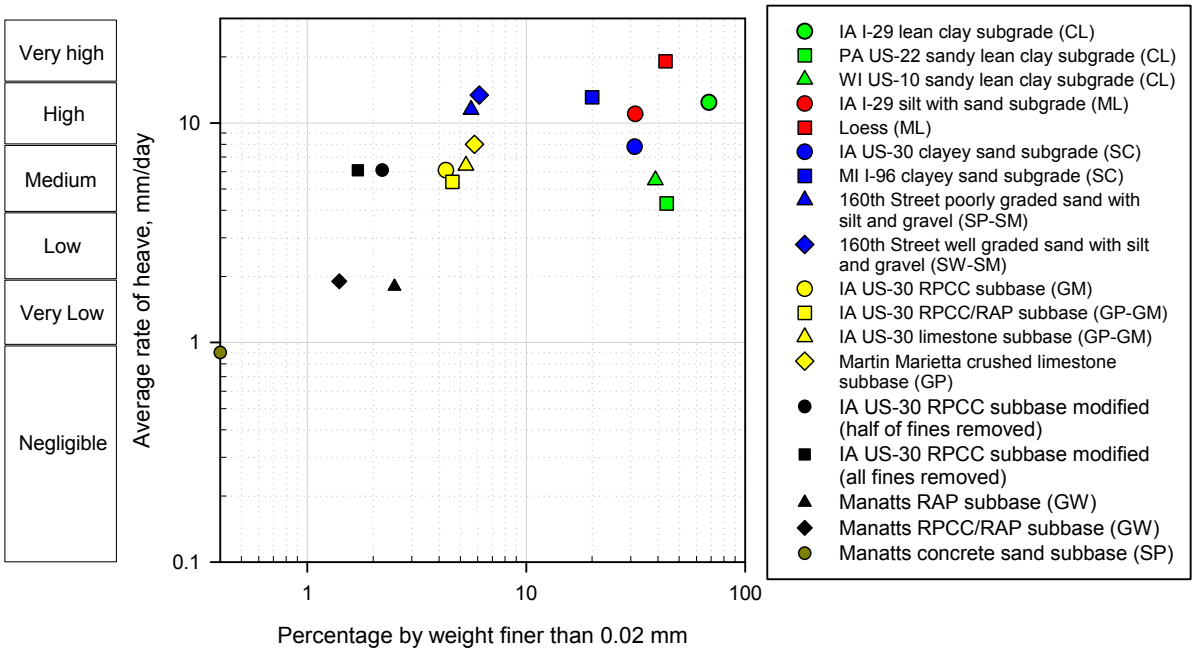


**Figure 186. Frost-heave rate versus percentage of particles finer than 0.02 mm for unstabilized materials**

The unstabilized and stabilized materials can also be compared to the percentage of particles passing 0.02 mm (Figure 187). The fly ash-stabilized samples have a high heave rate and a high percentage of particles passing 0.02 mm. One combination of fly ash-stabilized loess had the highest frost-heave rate of all the unstabilized and stabilized materials. In comparison, the cement-stabilized samples have a high percentage of particles passing 0.02 mm, but the heave rate is zero.

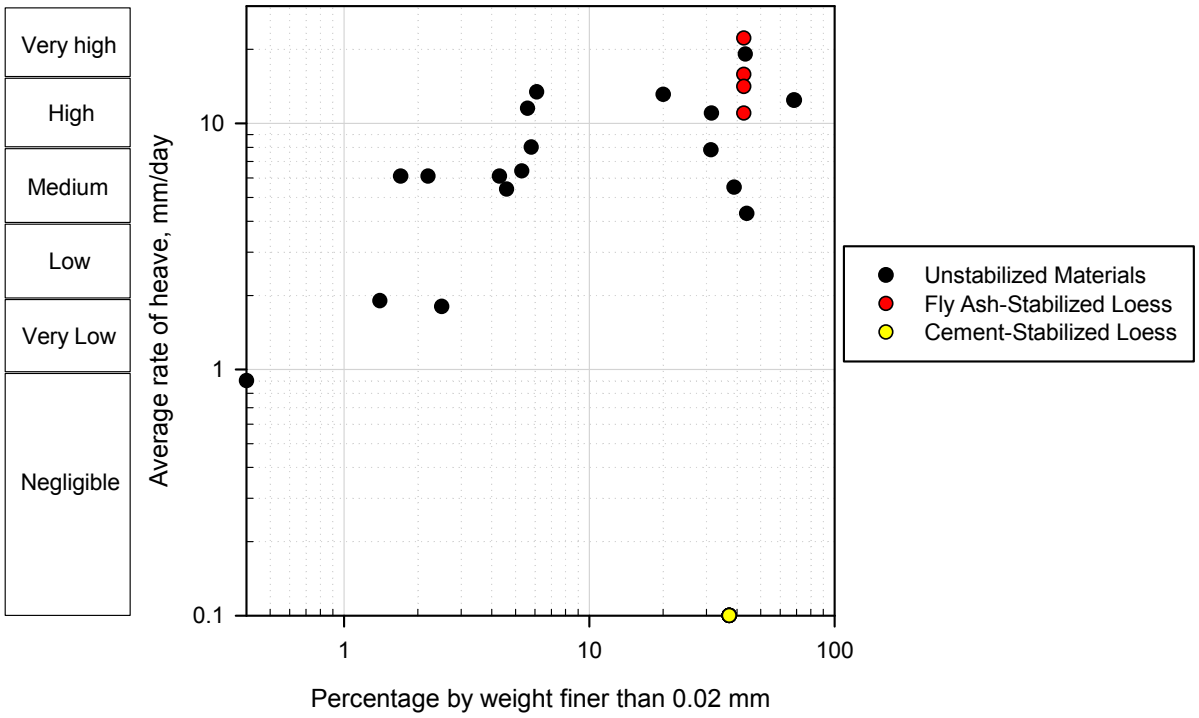


**Figure 187. Comparison of frost-heave rate for unstabilized and stabilized soils**

The frost-heave results for the untreated materials have been overlaid on the Army Corps of Engineers frost-susceptibility plot in Figure 188. This figure was developed by the Army Corps of Engineers from the results of the original CRREL frost-heave test, whereas the results of this research are based on the CRREL II frost-heave and thaw-weakening test (i.e., ASTM D5918). However, comparisons can be made between the results of both types of test. The general trend determined from the original CRREL frost-heave test is that the frost-heave rate increases as the percentage of particles passing 0.02 mm increases. The results of this study have the same trend, however the rate of heave is generally higher compared to the original CRREL test. For example, the materials from 160$^{th}$ Street are in the same percent passing 0.02 mm range for their soil classification, but the frost-heave rate of the 160$^{th}$ Street materials is higher than the range outlined in the plot for SP-SM and SW-SM classifications.

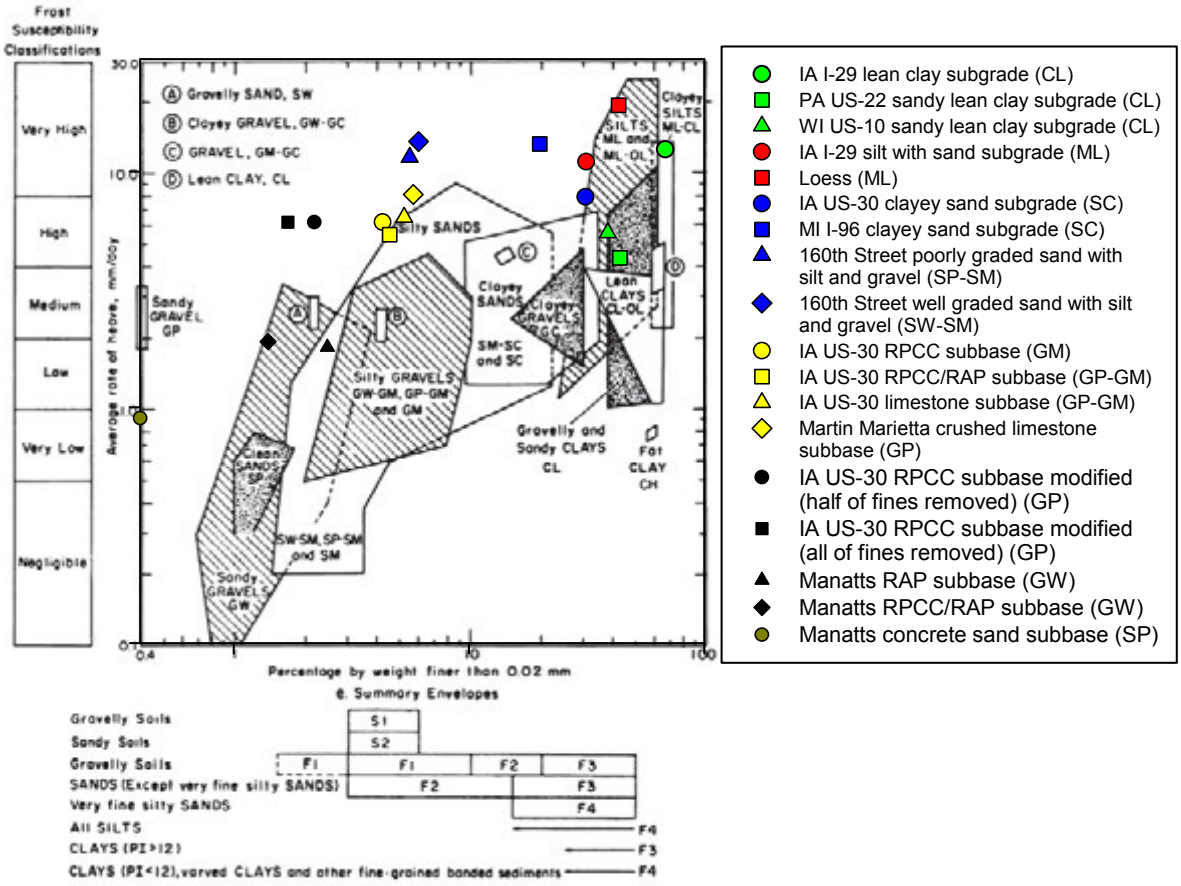


**Figure 188. Untreated frost-heave and thaw-weakening test results overlaid on U.S. Army Corps of Engineers frost susceptibility of soils plot (Joint Departments of the Army and Air Force 1985)**

## Statistical Analysis

Linear and multiple linear regression analyses were performed on the frost-heave and thaw-weakening test results. The linear and multiple linear regression models that included statistically significant variables were chosen and assessed based on the coefficient of determination ($R^2$) for the linear regression and adjusted $R^2$ for the multiple linear regressions. The adjusted $R^2$ is used for the multiple linear regressions because it relates to the $R^2$ from the linear regression. Equation (5) shows how the $R^2$ values were adjusted for the number of regression parameters in the multiple linear regression. The root mean square error (RMSE) was also used to determine the accuracy of the model for predicting the frost-heave rate or thawed CBR value. RMSE has the same units as the variable being predicted and is an indication of how accurately the model predicts the variable.

The statistical significance of the variables was determined from p- and t-values. The p-value criteria that were used to determine if a variable was significant were: p-value < 0.05 = significant, < 0.10 = possibly significant, > 0.10 = not significant. The t-value criteria used to determine significance included: t-value < –2 or > +2 = significant. The p-value describes the significance of the variable and the t-ratio describes the relative importance compared to other variables (i.e., higher absolute values indicate more significance).

Collinearity should be avoided in a multiple linear regression analysis. Collinearity occurs when two or more variables that are closely related are used to predict the dependent variable. Collinearity can cause incorrect and inflated $R^2$ values. Variance inflation factors (VIF) can be used to detect collinearity and is defined in Equation (6).

The 18 materials that were subjected to the frost-heave and thaw-weakening test were split into three categories, based on grain size, to predict the frost-heave rate. The first category was a combined model that included all 18 materials. The parameters considered in the combined model are summarized in Table 80. The second category considered was for fine grained materials, which is based on the USCS separation of 50% of the particles smaller 0.074 mm. The parameters considered in the fine grained category are shown in Table 82. The third category considered was for coarse grained materials, which is based on the USCS separation of 50% of the particles being larger 0.074 mm. The parameters considered in the coarse grained category are presented in Table 84. Selected models were chosen from the three categories considered, based on if the parameters were determined to be significant and if the collinearity was determined to not be a problem. The results of the selected models for the combined category are shown in Table 81. The results of the selected models for the fine grained category are shown in Table 83. The results of the selected models for the coarse grained category are shown in Table 85.

.

**Table 80. Summary of linear and multiple linear regression analyses predicting frost-heave rate from fine and coarse samples**

| No. | $C_u$ | $C_c$ | $D_{10}$ | $D_{30}$ | $D_{60}$ | Gravel content (%) | Sand content (%) | Silt content (%) | Clay content (%) | Passing 0.074 mm (%) | Passing 0.02 mm (%) | LL | PI | Activity Index | USCS | 1st frost-heave rate | 2nd frost-heave rate |
|---|---|---|---|---|---|---|---|---|---|---|---|---|---|---|---|---|---|
| 1 | — | — | — | x | x | x | x | x | x | x | x | — | — | — | | — | No |
| 2 | — | — | — | | x | x | x | x | x | x | x | — | — | — | | — | No |
| 3 | — | — | — | | x | x | | x | x | x | x | — | — | — | | — | No |
| 4 | — | — | — | | x | x | | x | x | x | | — | — | — | | — | No |
| 5 | — | — | — | | | x | | x | x | x | | — | — | — | | — | No |
| 6 | — | — | — | | | | | x | x | x | | — | — | — | | — | No |
| 7 | — | — | — | | | | | x | | x | | — | — | — | | — | No |
| 8 | — | — | — | | | | | x | | | | — | — | — | | — | Yes |
| 9 | — | — | — | x | | | | | | | | — | — | — | | — | No |
| 10 | — | — | — | | x | | | | | | | — | — | — | | — | No |
| 11 | — | — | — | | | x | | | | | | — | — | — | | — | Yes |
| 12 | — | — | — | | | | x | | | | | — | — | — | | — | No |
| 13 | — | — | — | | | | | | x | | | — | — | — | | — | No |
| 14 | — | — | — | | | | | | | x | | — | — | — | | — | Yes |
| 15 | — | — | — | | | | | | | | x | — | — | — | | — | No |
| 16 | — | — | — | | | | | | | | | — | — | — | x | — | No |

Yes – statistical significance exists
No – no statistical significance exists
— parameter not included in analysis

**Table 81. Linear and multiple linear regression analysis results for selected models of fine and coarse samples**

| Term | Estimate | Standard error | t ratio | Prob > t | VIF | $R^2$ | $R^2$ (adj.) | RMSE | Mean of response | Number of observations |
|---|---|---|---|---|---|---|---|---|---|---|
| **Model No. 8** | | | | | | | | | | |
| Intercept | 5.172 | 1.168 | 4.43 | 0.0004 | | 0.42 | 0.39 | 3.72 | 7.82 | 18 |
| Silt content (%) | 0.12 | 0.035 | 3.43 | 0.0034 | 1 | | | | | |
| **Model No. 11** | | | | | | | | | | |
| Intercept | 10.487 | 1.616 | 6.49 | <0.0001 | | 0.22 | 0.17 | 4.33 | 7.82 | 18 |
| Gravel content (%) | -0.078 | 0.037 | -2.13 | 0.0493 | 1 | | | | | |
| **Model No. 14** | | | | | | | | | | |
| Intercept | 5.283 | 1.233 | 4.28 | 0.0006 | | 0.37 | 0.33 | 3.89 | 7.82 | 18 |
| Passing 0.074 mm (%) | 0.086 | 0.028 | 3.08 | 0.0072 | 1 | | | | | |

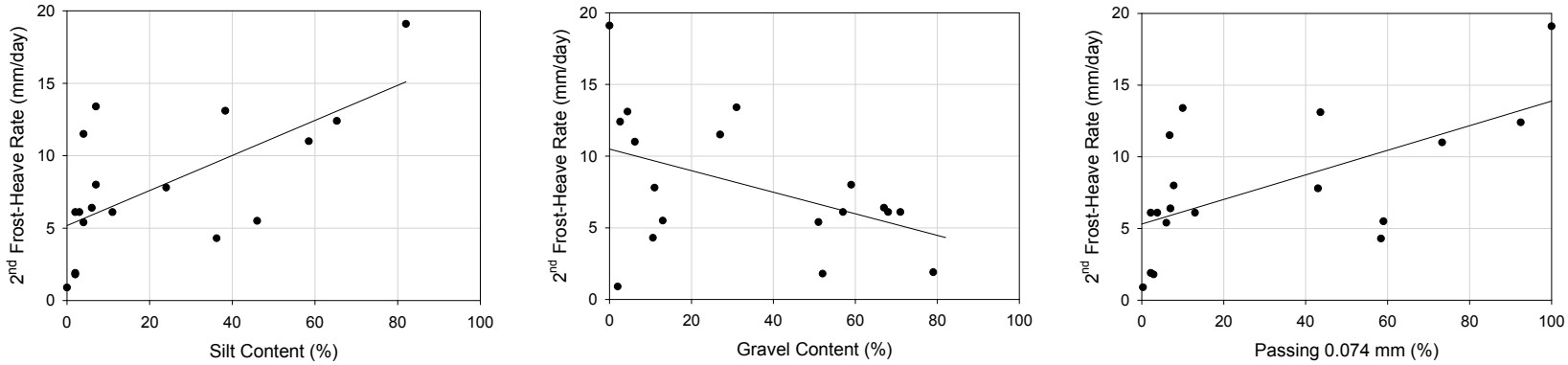


**Figure 189. Linear regression analysis results to predict 2nd frost-heave rate from fine and coarse samples for models**

**Table 82. Summary of linear and multiple linear regression analyses predicting frost-heave rate from fine samples**

| No. | $C_u$ | $C_c$ | $D_{10}$ | $D_{30}$ | $D_{60}$ | Gravel content (%) | Sand content (%) | Silt content (%) | Clay content (%) | Passing 0.074 mm (%) | Passing 0.02 mm (%) | LL | PI | Activity Index | USCS | 1st frost-heave rate | 2nd frost-heave rate |
|---|---|---|---|---|---|---|---|---|---|---|---|---|---|---|---|---|---|
| 1 | — | — | — | | x | | | x | x | x | x | x | | | — | — | No |
| 2 | — | — | — | | | | | x | x | x | x | x | | | — | — | No |
| 3 | — | — | — | | | | | x | | x | x | x | | | — | — | No |
| 4 | — | — | — | | | | | x | | | x | x | | | — | — | Yes |
| 5 | — | — | — | | | | | x | | | | x | | | — | — | Yes |
| 6 | — | — | — | x | | | | | | | | | | | — | — | No |
| 7 | — | — | — | | x | | | | | | | | | | — | — | No |
| 8 | — | — | — | | | x | | | | | | | | | — | — | Yes |
| 9 | — | — | — | | | | x | | | | | | | | — | — | No |
| 10 | — | — | — | | | | | x | | | | | | | — | — | No |
| 11 | — | — | — | | | | | | x | | | | | | — | — | No |
| 12 | — | — | — | | | | | | | x | | | | | — | — | No |
| 13 | — | — | — | | | | | | | | x | | | | — | — | No |
| 14 | — | — | — | | | | | | | | | x | | | — | — | No |
| 15 | — | — | — | | | | | | | | | | x | | — | — | No |
| 16 | — | — | — | | | | | | | | | | | x | — | — | No |

Yes – statistical significance exists
No – no statistical significance exists
— parameter not included in analysis

**Table 83. Linear and multiple linear regression analysis results for selected models of fine samples**

| Term | Estimate | Standard error | t ratio | Prob > t | VIF | $R^2$ | $R^2$ (adj.) | RMSE | Mean of response | Number of observations |
|---|---|---|---|---|---|---|---|---|---|---|
| **Model No. 4** | | | | | | | | | | |
| Intercept | 17.331 | 4.201 | 4.12 | 0.0259 | | 0.95 | 0.89 | 1.68 | 10.46 | 7 |
| Silt content (%) | 0.159 | 0.045 | 3.52 | 0.0389 | 1.71 | | | | | |
| Passing 0.02 mm (%) | 0.234 | 0.109 | 2.14 | 0.1215 | 5.83 | | | | | |
| LL | -0.767 | 0.201 | -3.81 | 0.0318 | 5.83 | | | | | |
| **Model No. 5** | | | | | | | | | | |
| Intercept | 11.603 | 4.47 | 2.6 | 0.0603 | | 0.86 | 0.79 | 2.31 | 10.46 | 7 |
| Silt content (%) | 0.22 | 0.049 | 4.54 | 0.0105 | 1.04 | | | | | |
| LL | -0.387 | 0.132 | -2.94 | 0.0424 | 1.04 | | | | | |
| **Model No. 8** | | | | | | | | | | |
| Intercept | 17.207 | 1.308 | 13.16 | <0.001 | | 0.88 | 0.86 | 1.9 | 10.46 | 7 |
| Gravel content (%) | -0.988 | 0.16 | -6.17 | 0.0016 | 1 | | | | | |

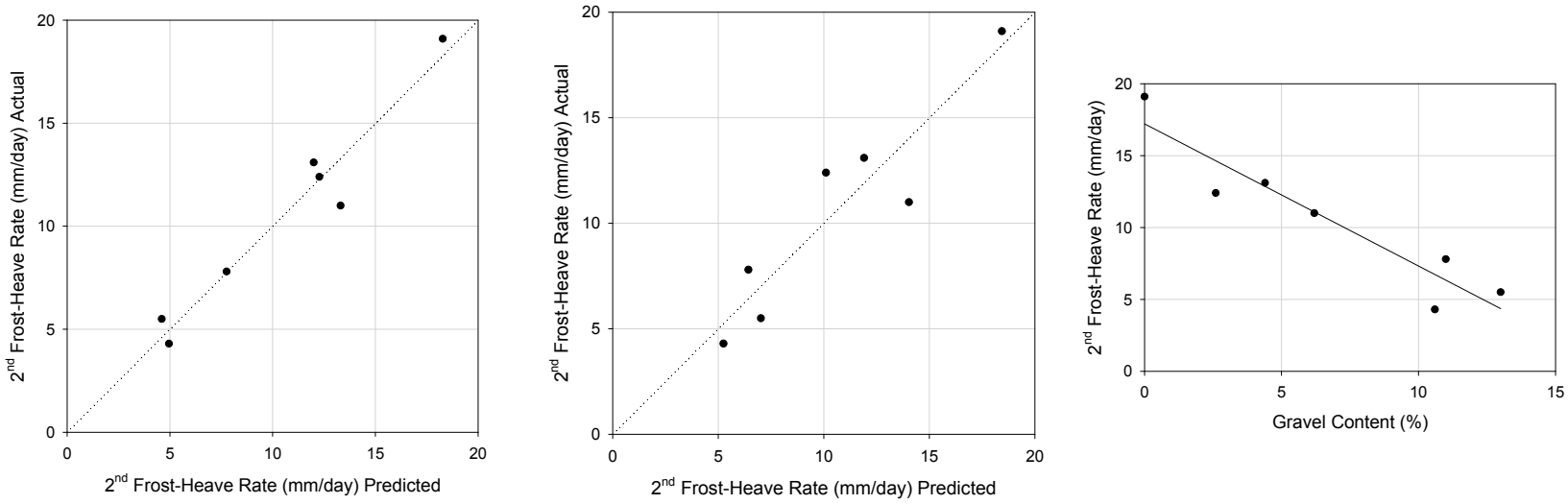


**Figure 190. Linear and multiple linear regression analysis results to predict 2nd frost-heave rate from fine samples for models 4, 5, and 8**

**Table 84. Summary of linear and multiple linear regression analyses predicting frost-heave rate from coarse samples**

| No. | $C_u$ | $C_c$ | $D_{10}$ | $D_{30}$ | $D_{60}$ | Gravel content (%) | Sand content (%) | Silt content (%) | Clay content (%) | Passing 0.074 mm (%) | Passing 0.02 mm (%) | LL | PI | Activity Index | USCS | 1st frost-heave rate | 2nd frost-heave rate |
|---|---|---|---|---|---|---|---|---|---|---|---|---|---|---|---|---|---|
| 1 | | | x | x | | x | x | x | x | x | x | — | — | — | — | No | No |
| 2 | | | x | x | | x | x | x | | x | x | — | — | — | — | No | No |
| 3 | | | x | x | | x | x | x | | x | | — | — | — | — | No | No |
| 4 | | | x | x | | x | | x | | x | | — | — | — | — | No | No |
| 5 | | | x | | | x | | x | | x | | — | — | — | — | No | No |
| 6 | | | x | | | x | | | | x | | — | — | — | — | No | No |
| 7 | | | x | | | x | | | | | | — | — | — | — | Yes | No |
| 8 | x | | | | | | | | | | | — | — | — | — | No | No |
| 9 | | x | | | | | | | | | | — | — | — | — | No | No |
| 10 | | | x | | | | | | | | | — | — | — | — | No | No |
| 11 | | | | x | | | | | | | | — | — | — | — | No | No |
| 12 | | | | | x | | | | | | | — | — | — | — | No | No |
| 13 | | | | | | x | | | | | | — | — | — | — | No | No |
| 14 | | | | | | | x | | | | | — | — | — | — | No | No |
| 15 | | | | | | | | x | | | | — | — | — | — | No | No |
| 16 | | | | | | | | | x | | | — | — | — | — | No | Yes |
| 17 | | | | | | | | | | x | | — | — | — | — | No | Yes |
| 18 | | | | | | | | | | | x | — | — | — | — | No | Yes |
| 19 | | | x | x | | | x | x | | x | | — | — | — | — | No | No |
| 20 | | | x | x | | | | x | | x | | — | — | — | — | No | No |
| 21 | | | | x | | | | x | | x | | — | — | — | — | No | No |
| 22 | | | | | | | | x | | x | | — | — | — | — | No | No |

Yes – statistical significance exists
No – no statistical significance exists
— parameter not included in analysis

**Table 85. Linear and multiple linear regression analysis results for selected models of coarse samples**

| Term | Estimate | Standard error | t ratio | Prob > t | VIF | $R^2$ | $R^2$ (adj.) | RMSE | Mean of response | Number of observations |
|---|---|---|---|---|---|---|---|---|---|---|
| **Model No. 7 (1st frost-heave rate)** | | | | | | | | | | |
| Intercept | 4.441 | 1.522 | 2.92 | 0.0193 | | 0.6 | 0.5 | 1.97 | 5.73 | 11 |
| $D_{10}$ | -6.543 | 1.93 | -3.39 | 0.0095 | 1.32 | | | | | |
| Gravel content (%) | 0.0743 | 0.031 | 2.37 | 0.0455 | 1.32 | | | | | |
| **Model No. 16 (2nd frost-heave rate)** | | | | | | | | | | |
| Intercept | 2.597 | 1.171 | 2.22 | 0.0537 | | 0.63 | 0.59 | 2.47 | 6.14 | 11 |
| Clay content (%) | 2.788 | 0.709 | 3.93 | 0.0034 | 1 | | | | | |
| **Model No. 17 (2nd frost-heave rate)** | | | | | | | | | | |
| Intercept | 2.381 | 1.719 | 1.39 | 0.1994 | | 0.43 | 0.37 | 3.08 | 6.15 | 11 |
| Passing 0.074 mm (%) | 0.668 | 0.257 | 2.6 | 0.0286 | 1 | | | | | |
| **Model No. 18 (2nd frost-heave rate)** | | | | | | | | | | |
| Intercept | 0.716 | 2.005 | 0.36 | 0.7302 | | 0.57 | 0.51 | 2.54 | 6.67 | 11 |
| Passing 0.02 mm (%) | 1.507 | 0.465 | 3.24 | 0.0119 | 1 | | | | | |

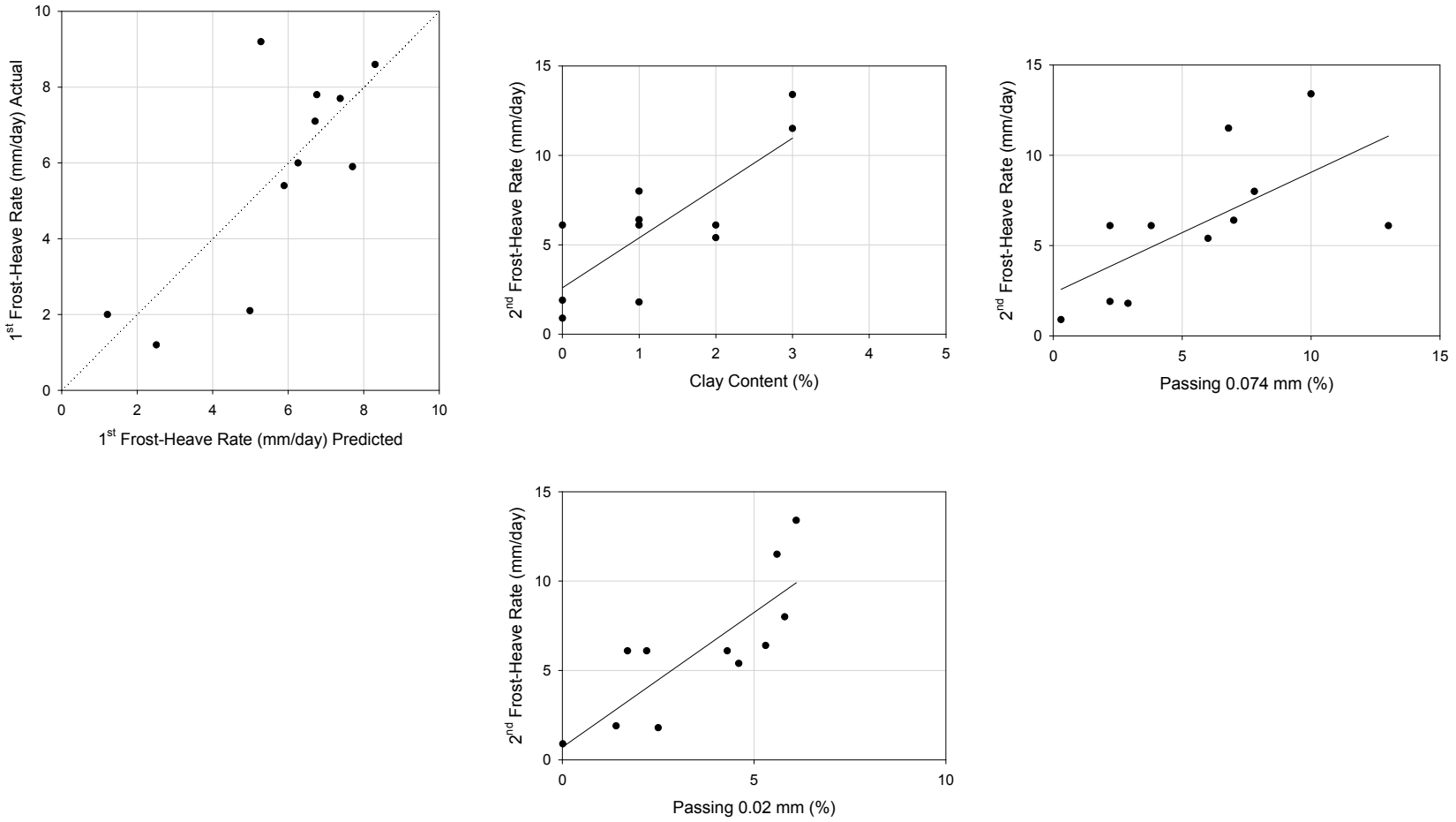


**Figure 191. Linear and multiple linear regression analysis results to predict 2nd frost-heave rate from coarse samples for models 7, 16, 17, and 18**

The results of the statistical analysis performed on the combined category show that the frost-heave rate of the 18 materials is best predicted by the silt content. The adjusted $R^2$ of the linear regression model predicting the frost-heave rate for the combined category from the silt content is 0.39 and the RMSE is 3.72.

The results of the fine grained category showed that the frost-heave rate is best predicted by the silt content and liquid limit of the materials. The model that included silt content, percentage passing 0.02 mm, and liquid limit had a higher adjusted $R^2$. However, the VIF values were also higher, which could indicate that collinearity is occurring. The gravel content was also found to be a good indicator of the frost-heave rate for fine grained materials, however it was not considered to be a good model because the gravel content was low and the materials larger than 19 mm were removed from the gradation. The gradation used in the statistical analysis was based on the full gradation rather than the gradation after the particles larger than 19 mm were removed, therefore the gravel content of the materials may be smaller than the gradation indicated from the particle size analysis. The adjusted $R^2$ of multiple linear regression model predicting the frost-heave rate for the fine grained category from the silt content and liquid limit is 0.79 and the RMSE is 2.31.

The results of the coarse grained category showed that the best predictor of the frost-heave rate is a linear regression based on the percentage of particles passing 0.02 mm. The percentage of particles passing 0.02 mm is the same parameter that the USACE used in Figure 188 to predict the frost-heave rate. Models that included $D_{10}$, gravel content, and clay content had comparable $R^2$ and RMSE values. However, as was discussed, the gravel content, in this study, is not true indication of the frost-heave rate because a portion of that material was removed. The clay content was very small for the coarse grained materials so it was not considered to be a good indication of the frost-heave rate. The adjusted $R^2$ of the linear regression model predicting the frost-heave rate for the coarse grained category from the percentage of particles passing 0.02 mm is 0.51 and the RMSE is 2.54.

There is a good correlation between the CBR after frost-susceptibility testing and the standard CBR value. A linear regression analysis shows the $R^2$ equals 0.81 with a RMSE of 7.3%. The model includes all of the untreated materials tested in this research. The linear regression model is shown in Figure 192.

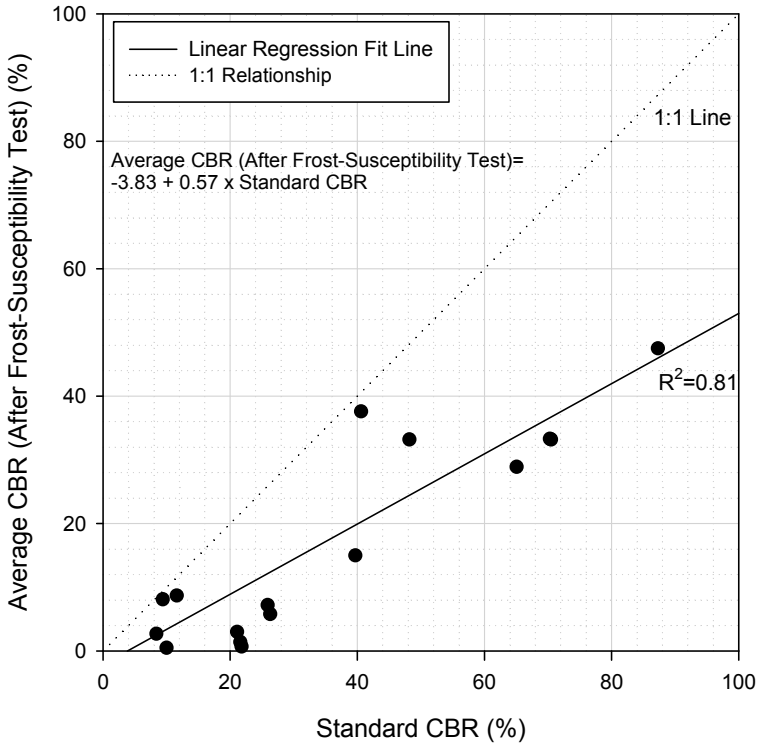


**Figure 192. Average CBR after frost-susceptibility testing and standard CBR linear regression analysis for unstabilized materials**

## IN SITU TESTS

In situ testing was performed on portland cement concrete (PCC) pavements at seven sites across Iowa (Figure 193). The test plan included measuring subsurface pavement temperatures (where available), performing falling weight deflectometer (FWD) tests, and dynamic cone penetration tests (DCP). The oldest pavement was constructed in 1958 and the newest in 2011, so there is a range of pavement ages between the seven sites. The International Roughness Index (IRI) and the Pavement Condition Index (PCI) is presented for most of the sites. The IRI indicates the smoothness of a pavement system. The IRI values have units of m/km. Smaller IRI values indicate smoother pavement conditions. The PCI indicates the condition of the pavement system on a scale of 0 to 100, with a value of 100 describing a pavement in excellent condition. Location and structural data for each site is presented in Table 86 (Iowa Department of Transportation Office of Materials 2010).

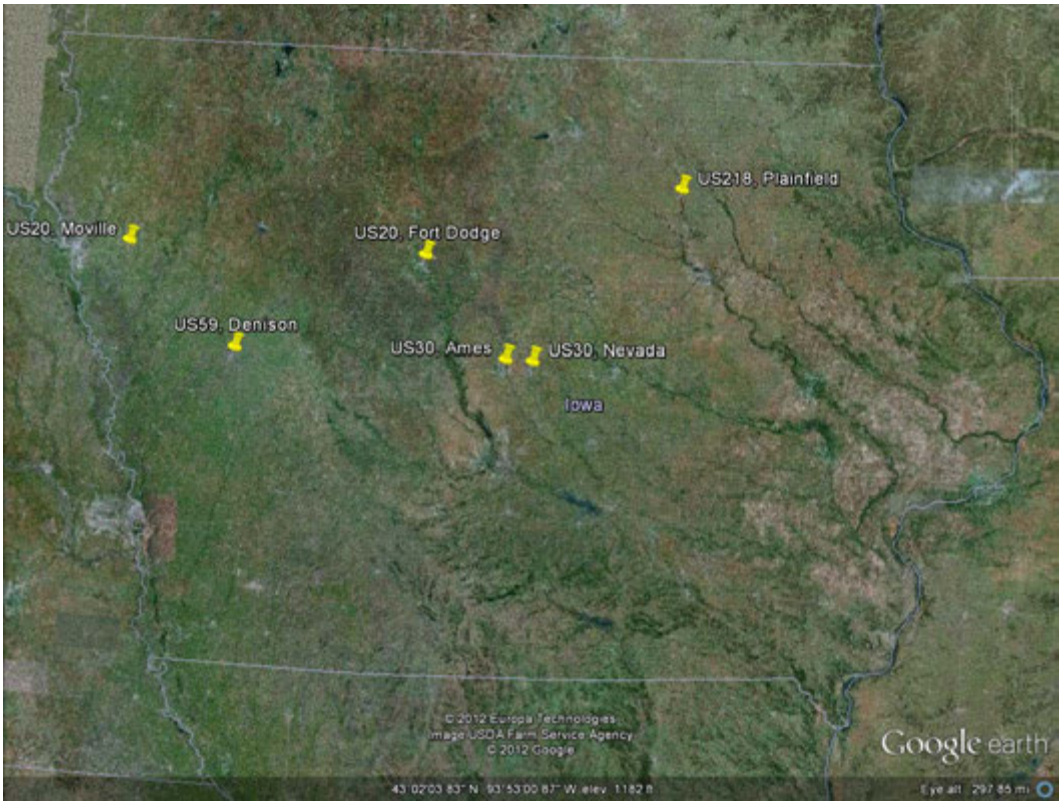


**Figure 193. In situ test sites**

**Table 86. Summary of in situ test sites**

| Site | Route | Direction | Mile marker | GPS location | Temperature array | Year constructed | Pavement surface (mm) | Base (mm) | IRI (m/km) | PCI |
|---|---|---|---|---|---|---|---|---|---|---|
| Moville | U.S. Highway 20 | EB | 18.5 | N42.48166, W96.06858 | Yes | 1958 | PCC (254) | — | 3.3 | 25 |
| Denison | U.S. Highway 59 | NB | 95.0 | N41.92349, W95.34414 | Yes | 1987<br>1971 | ACC (114)<br>PCC (203) | — | 1.5 | 61 |
| Fort Dodge | U.S. Highway 20 | WB | 119.8 | N42.44920, W94.21684 | No | 2005 | PCC (259) | GSB (259) | 1.4 | 99 |
| Ames | U.S. Highway 30 | EB | 142.40 | — | Yes | 2011 | PCC (254) | GSB (457) | — | — |
| West Nevada | U.S. Highway 30 | WB | 154.85 | N42.00893, W93.50358 | No | 1992 | PCC (254) | GSB (254) | 1.5 | 89 |
| East Nevada | U.S. Highway 30 | WB | 161.35 | N42.00773, W93.337796 | No | 1998 | PCC (254) | GSB (254) | 1.2 | 98 |
| Plainfield | U.S. Highway 218 | SB | 214.05 | N42.86990, W92.54476 | Yes | 2002 | PCC (241) | GSB (259) | 2 | 91 |

ACC-asphalt cement concrete
PCC-portland cement concrete
GSB-granular subbase

Temperature probe data from Moville, Denison, and Plainfield (Iowa State Environmental Mesonet 2012) were used to approximate the frost depth. The temperature probes begin at approximately 25 mm below the pavement and continue to a depth of 1830 mm. The frost depth was determined at 2 P.M. during freezing and thawing periods. The frost depth was chosen when the temperature was at or below 0°C during freezing and at or above 0°C during thawing. Several small freeze-thaw periods were observed in the top layers of the pavement foundation before and after the permanent freeze began; however only the permanent freeze depths will be presented.

At each site, FWD tests were performed on 10 to 16 points covering distances ranging from 116 m to 798 m. The center of the panels and joints were tested. The data collected from the center panels was used to determine how FWD measurements varied on a seasonal basis. The joint measurements were used to determine how the load transfer efficiency (LTE) changed seasonally. The LTE is determined by placing the loading plate on one side of a joint and the front displacement sensor on the other side of the joint. $D_0$ is then measured on the loaded slab and $D_1$ is measured on the unloaded slab. Equation (13) is used to determine the LTE.

$$LTE\,(\%) = (D_1 / D_0) \bullet 100 \tag{13}$$

where $D_0$ = deflection at center of loading plate and

$D_1$ = deflection 12 in. in front of loading plate.

By plotting the load applied to the loading plate versus the $D_0$ deflection, it is possible to estimate if there are voids under the pavement. The y-intercept value, determined from a linear regression analysis, is used as an indication of voids. McCracken (2008) reported that intercept values higher than 50 microns can indicate voids. An example calculation of the intercept value is shown in Figure 194.

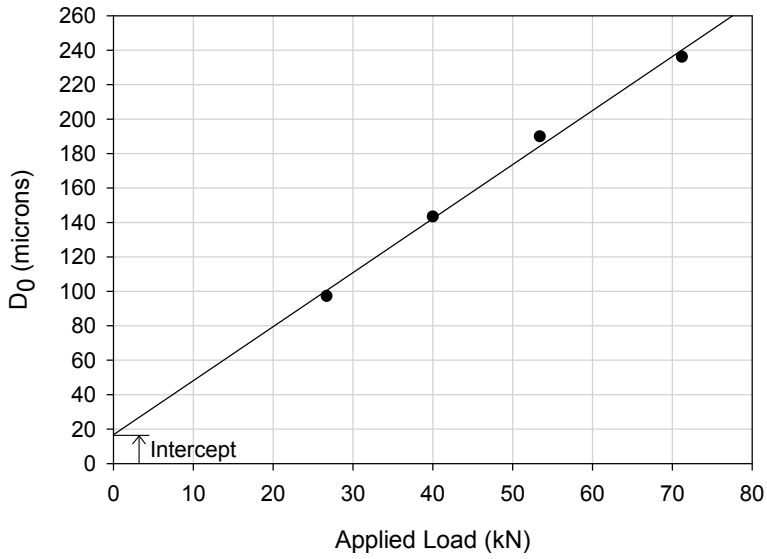


**Figure 194. Determination of intercept value used to predicted voids from FWD test**

Intercept values are affected by the temperature gradient in the PCC pavement (Vandenbossche 2005). Pavement temperatures were measured by filling drilled holes with temperature sensitive liquid at varying depths (Schmalzer 2006). The temperature gradient was determined by fitting a linear regression line to a depth versus temperature plot. Positive gradients occur when the pavement surface is warmer than the bottom, which results in negative intercept values (Vandenbossche 2005). Whereas, a negative gradient occurs when then the pavement surface is cooler than the bottom, which results in a positive intercept value.

The FWD measurements presented in this section include $D_0$, the backcalculated effective modulus of subgrade reaction (k), and LTE. $D_0$ is a direct measurement of pavement deflection and can be used to measure seasonal changes in pavement response. $D_0$ measurements were normalized to a load of 40 kN (AASHTO 1993). Lower $D_0$ values indicate a stiffer pavement.

The k value is a measure of support provided by the pavement foundation layers (e.g., subbase and subgrade layers). The k value was determined from an average FWD plate load of 43.3 kN and is a dynamic k value. The approximate static k value can be determined by dividing the dynamic k value by two. The dynamic k value was backcalculated using the methods described in AASHTO 1993. The backcalculation is performed by using $D_0$ and the AREA value on a design chart. The calculation of AREA is shown in Equation (14).

$$AREA = 6 \bullet [(D_0 / D_0) + (2 \bullet D_{305} / D_0) + (2 \bullet D_{610} / D_0) + (D_{914} / D_0)] \quad (14)$$

where $D_x$ = the surface deflection measured x mm from the loading plate.

The DCP values are presented as a CBR percentage based on the soil type. Equation (15) is used for all soils types except CL with CBR values less than 10 and CH soils. For CL soils with a CBR less than 10 use Equation (16) and for CH soils use Equation (17).

$$CBR \text{ (all soils except CL with CBR<10 and CH)} = 292 / DCP^{1.12} \quad (15)$$

where CBR = California Bearing Ratio and

DCP = DCP index (penetration per blow)

$$CBR \text{ (CL with CBR<10)} = 1 / (0.017019 \bullet DCP)^2 \quad (16)$$

$$CBR \text{ (CH soils)} = 1 / (0.002871 \bullet DCP) \quad (17)$$

## Moville

The permanent freeze began around November 23rd of 2010 and ended around February 29th 2011. The maximum frost depth during the 2010-2011 winter was around 1 m. The permanent freeze in the winter of 2011-2012 began around November 3, 2011 and ended around March 9th 2012. The maximum frost depth for the 2011-2012 winter was close to 0.5 m. The 2011-2012 winter was mild compared to the 2010-2011 winter. The frost penetration profiles are presented in Figure 195.

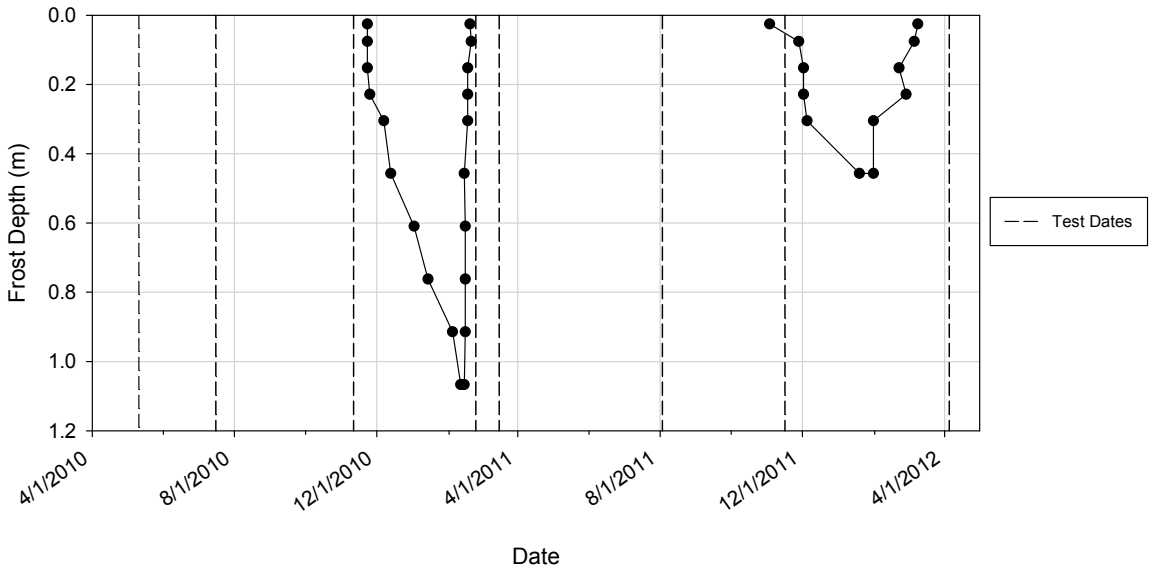


**Figure 195. U.S. Highway 20 Moville, IA frost penetration**

FWD tests were performed at 8 locations over a distance of approximately 555 m (Figure 196). There is variation in the $D_0$ values collected at the 8 test locations. The lowest D0 measurements were taken on February 24, 2011. However, due to poor weather conditions, all 8 locations were not able to be tested on February 24, 2011. The points at distances of 476.8 and 552.1 m were not tested as often as the remaining points. The highest and most variable $D_0$ values were measured on July 16th 2010, March 16th 2011, and August 3rd 2011. The variation in $D_0$ over the distance tested is shown in Figure 197.

**Figure 196. U.S. Highway 20 Moville, IA**

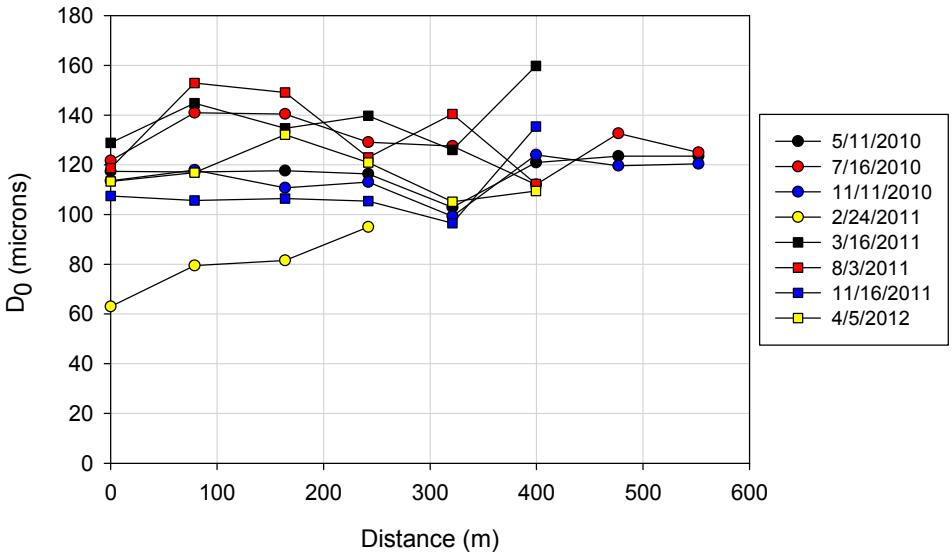


**Figure 197. U.S. Highway 20 Moville, IA distance variations in $D_0$**

The variation of $D_0$ with time shows a decrease in $D_0$ on February 24th 2011 followed by an increase on March 16th 2011. This represents the effect of thaw weakening on the pavement system. However, the $D_0$ values on Mach 16th 2011 are not lower than measurements taken on July 16th 2010 or August 3rd 2011. This could indicate that testing was not performed often enough to capture the full effects of thaw weakening. The subsurface temperatures indicate the pavement foundation was thawed on February 29th 2011. The changes in $D_0$ versus time are presented in Figure 198.

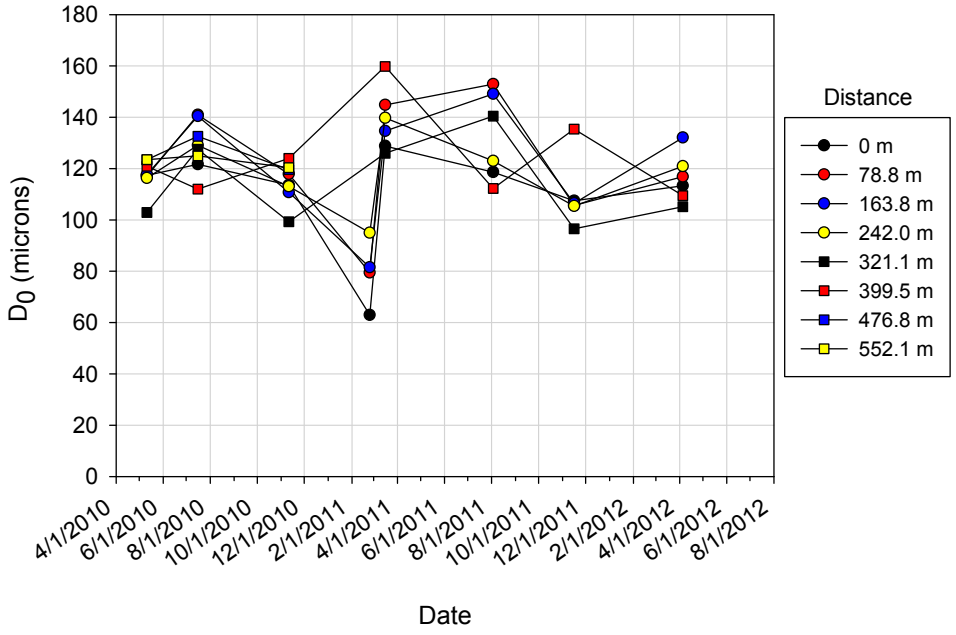


**Figure 198. U.S. Highway 20 Moville, IA seasonal $D_0$ variations**

The variation of k over time shows the stiffest conditions occurred on February 24th 2011 and the weakest conditions occurred on March 16th 2011. The variation of k with time is shown in Figure 199.

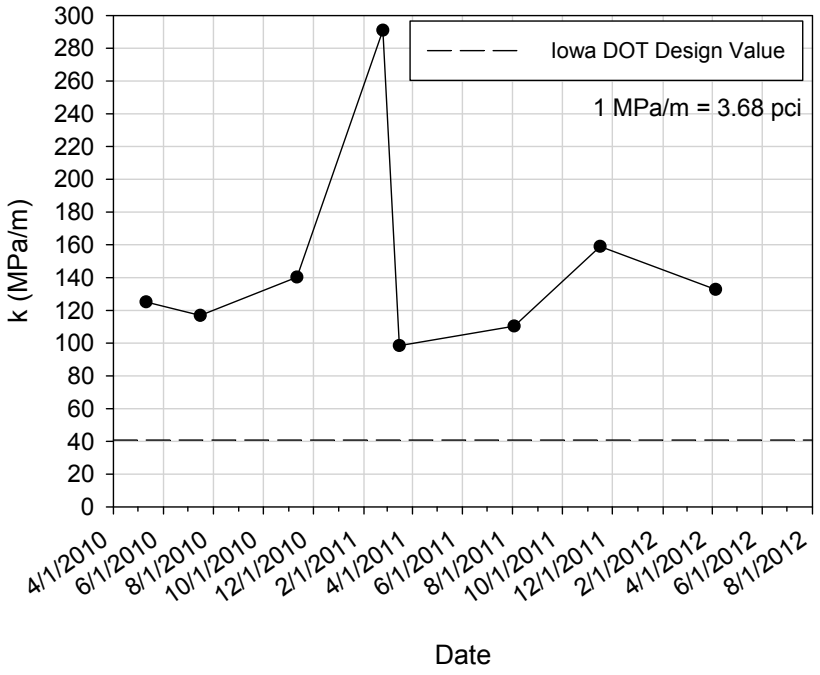


**Figure 199. U.S. Highway 20 Moville, IA average seasonal k values**

The lowest LTE values occurred on November 11th 2010 and November 16th 2011. High LTE values were recorded on February 24th 2011 and March 16th 2011, which indicates that LTE values were not affected by freeze-thaw processes. The one exception is at a distance of 164.2 m, the LTE increased between February 24th 2011 and March 16th 2011. The dates with the highest $D_0$ values (July 16th 2010 and August 3rd 2011) showed high LTE values. These measurements indicate that the LTE may be negatively affected by a stiffer subgrade. The variation of LTE over time is presented in Figure 200.

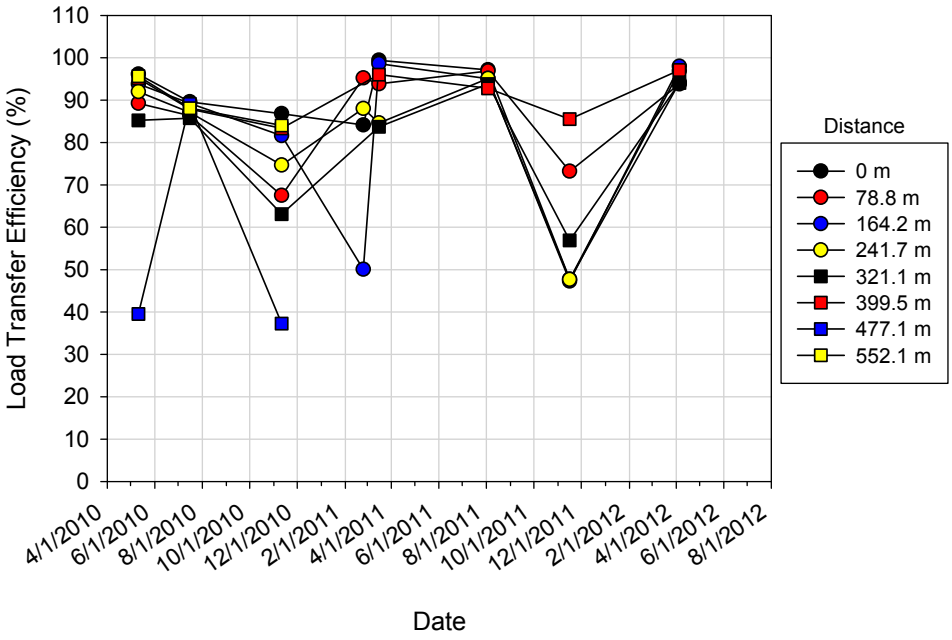


**Figure 200. U.S. Highway 20 Moville, IA seasonal LTE variations**

The intercept values are similar with the exception of November 16th 2011, which has the highest measured intercept values. The temperature gradient values are all positive, which indicates that the intercept values would be expected to be negative. The lowest temperature gradient was measured on November 16th 2011, which relates to the highest intercept values. The intercept values are presented in Figure 201 and the temperature gradients are presented in Table 87.

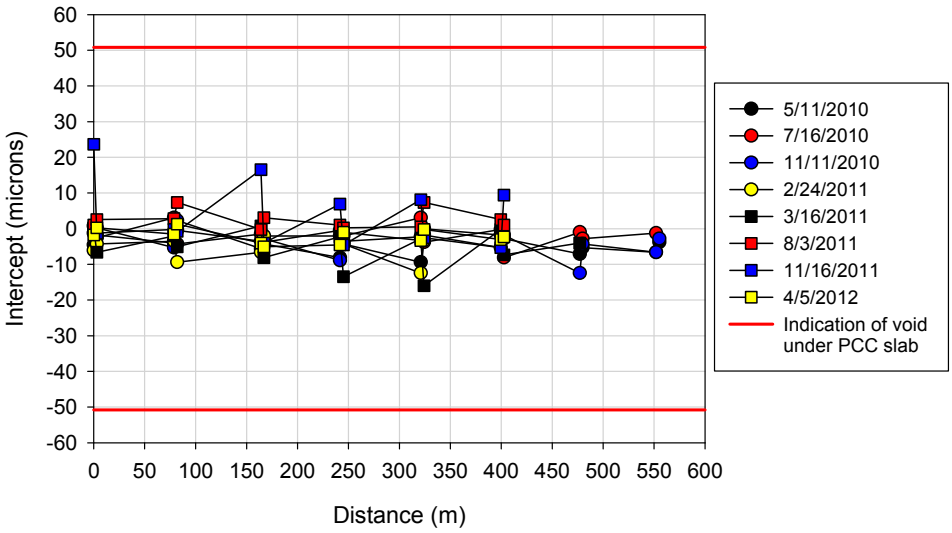


**Figure 201. U.S. Highway 20 Moville, IA FWD intercept values at center panels and joints**

**Table 87. U.S. Highway 20 Moville, IA PCC temperature gradients**

| Date | Temperature gradient (°C/mm) |
|---|---|
| 11/11/2010 | 0.017 |
| 3/16/2011 | 0.039 |
| 8/3/2011 | 0.010 |
| 11/16/2011 | 0.009 |
| 4/5/2012 | 0.023 |

The DCP profiles are similar and do not include any dates that are noticeably stronger or weaker than the typical profile. However, a DCP test was not able to be performed on February 24th 2011 due poor weather conditions, so no tests were performed in frozen conditions. The DCP profile is presented in Figure 202.

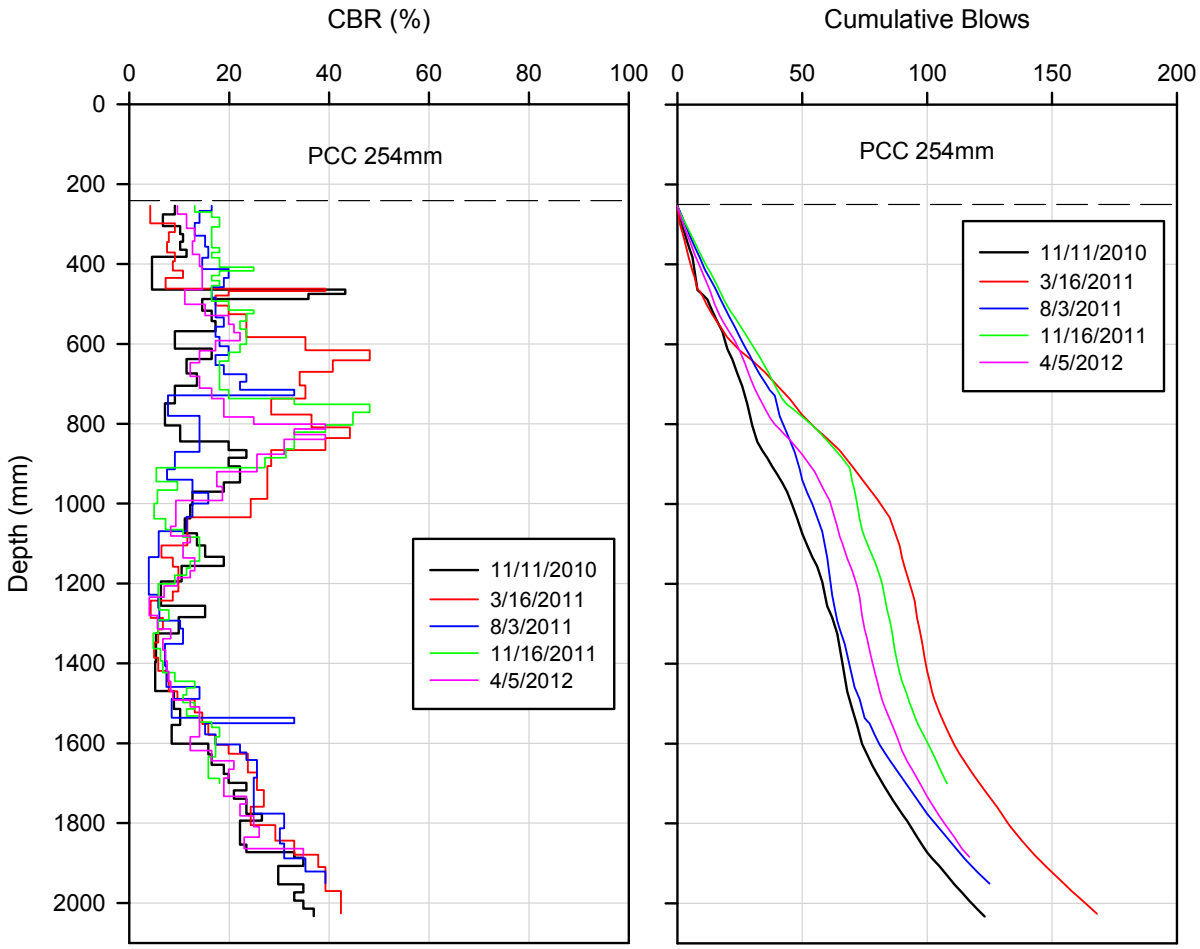


**Figure 202. U.S. Highway 20 Moville, IA seasonal DCP variations**

## Denison

The permanent freeze for the 2010-2011 winter began around November 14th 2010 and ended around March 16th 2011. The frost depth reached just over 1 m. The permanent freeze for the 2011-2012 winter began around November 28th 2011 and ended around March 6th 2012. The frost depth reached about 0.6 m. Like the frost depth for Moville, the 2011-2012 winter was milder than the 2010-2011 winter. The frost penetration profiles for the 2008-2009 and 2009-2010 winters are also presented in Figure 203 with the 2010-2011 and 2011-2012 winters.

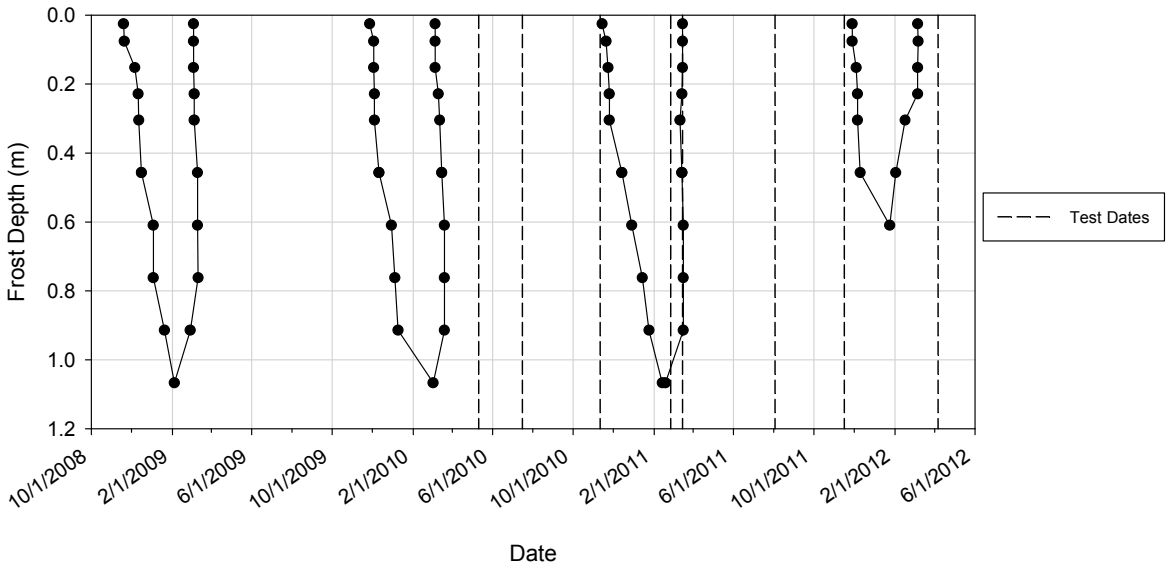


**Figure 203. U.S. Highway 59 Denison, IA frost penetration**

FWD tests were performed at 7 locations over an approximate distance of 145 m (Figure 204). The variation of $D_0$ collected at the 8 locations show consistent trends for the dates tested. The lowest $D_0$ values were measured on February 26$^{th}$ 2011 while the pavement foundation was frozen. The highest $D_0$ values were measured on August 3$^{rd}$ 2011. The approximate thaw date of March 16$^{th}$ 2011 coincided with the FWD tests, however the $D_0$ values were not higher compared to the rest of the year.

**Figure 204. U.S. Highway 59 Denison, IA**

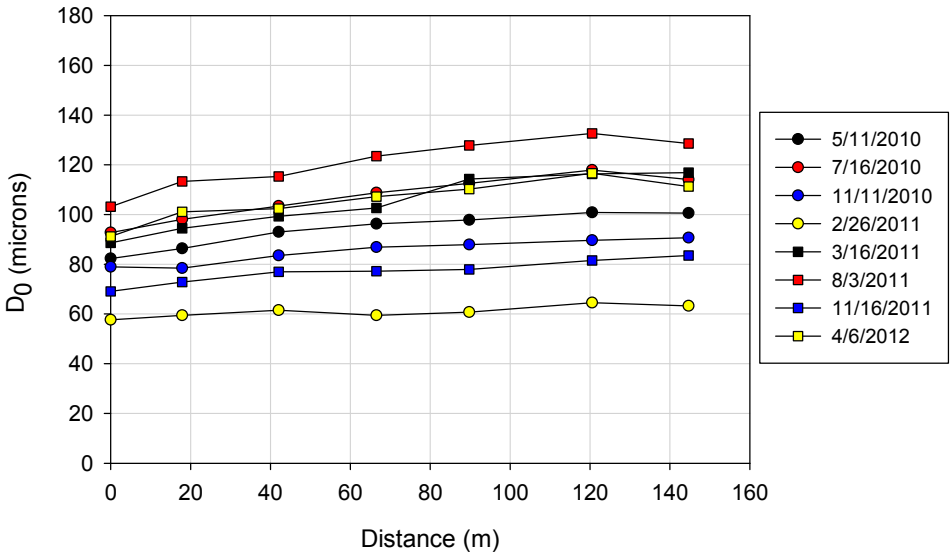


**Figure 205. U.S. Highway 59 Denison, IA distance variations in $D_0$**

The $D_0$ measurements over time are similar and show consistent trends. The pavement foundation stiffness increased from August to February, decreased from February to March, and decreased from March to August. There is a definite increase in $D_0$ between February 26th 2011 and March 16th 2011. The variations of $D_0$ with time are presented in Figure 206.

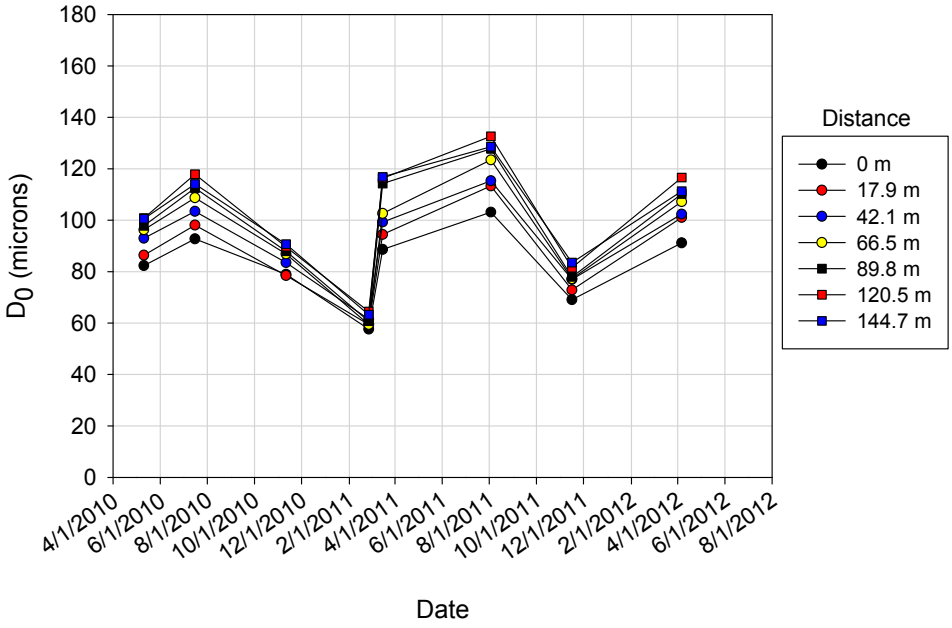


**Figure 206. U.S. Highway 59 Denison, IA seasonal $D_0$ variations**

The variations of k over time show that the stiffest conditions were measured on February 26th 2011 and the lowest k values were measured on March 16th 2011. The variation of k with time is presented in Figure 207.

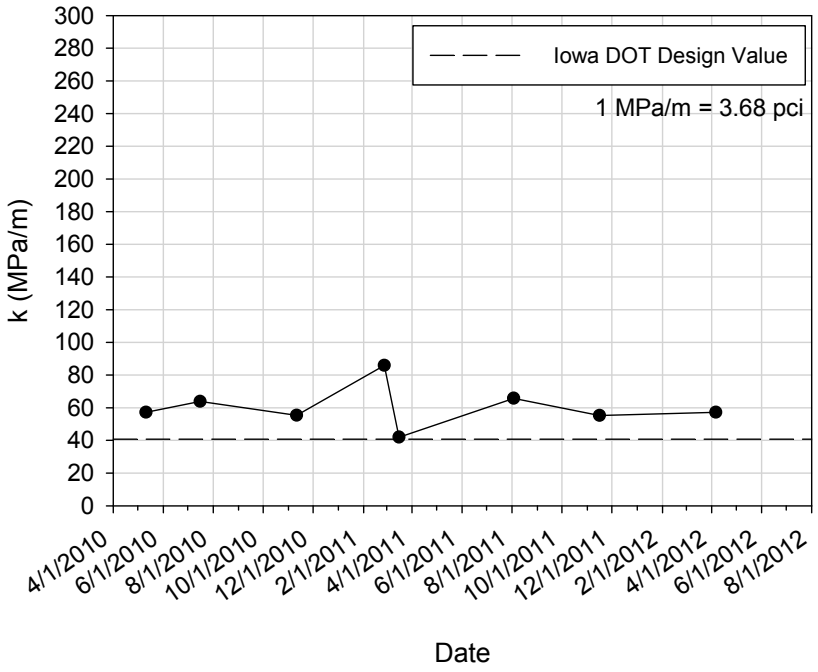


**Figure 207. U.S. Highway 59 Denison, IA average seasonal k values**

The DCP profiles show similar trends for most of the year, with the exceptions including November 11th 2010, February 26th 2011, and April 5th 2012. A hard layer was reached on November 11th 2010 and it is possible that this was a large enough rock to affect the test results. The same thing could have occurred on April 5th 2012. However, the increase in CBR on February 26th 2011 is most likely due to an ice lens from approximately 600 to 1000 mm. The DCP profile from March 16th 2011 is among the lowest CBR measurements, especially to a depth near 650 mm. The DCP profiles are presented in Figure 208.

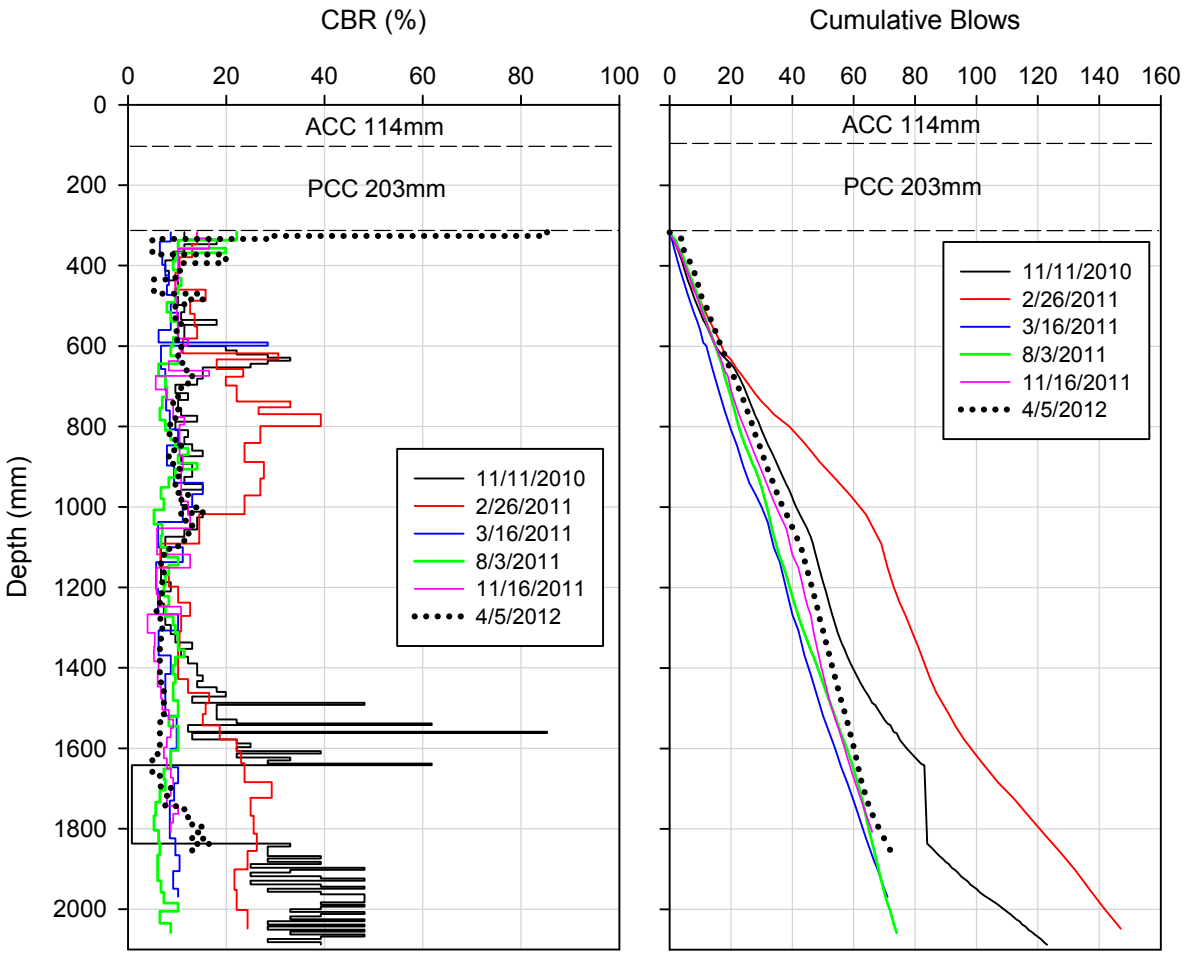


**Figure 208. U.S. Highway 59 Denison, IA seasonal DCP variations**

## Fort Dodge

FWD tests were performed at 7 points stretching over a distance of nearly 800 m (Figure 209). It is clear that the lowest $D_0$ values were measured on February 24th 2011. However, the measurements taken at other times throughout the year were very similar. There is a good trend between the distances and $D_0$ measured on different dates. The $D_0$ measurements versus distance are presented in Figure 210.

**Figure 209. U.S. Highway 20 Fort Dodge, IA**

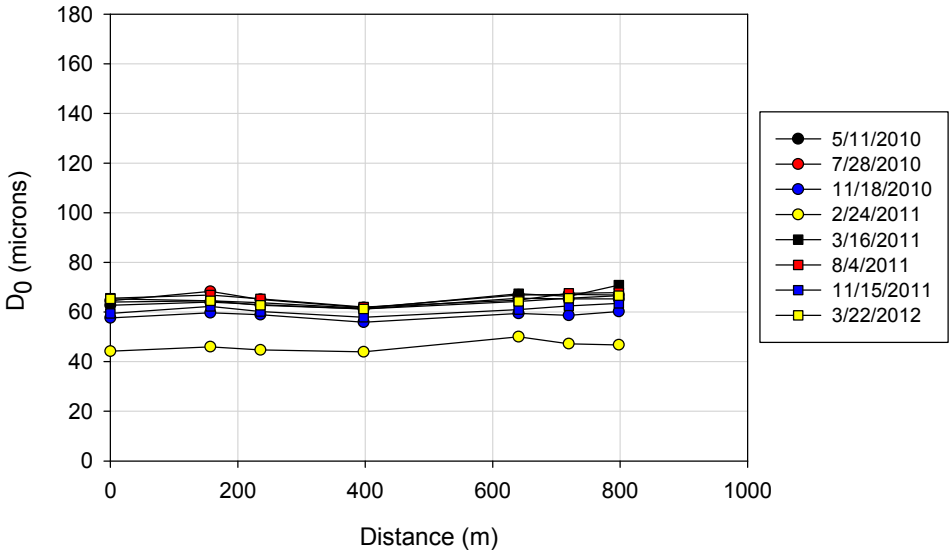


**Figure 210. U.S. Highway 20 Fort Dodge, IA distance variations in $D_0$**

There is a clear decrease in $D_0$ on February 24th 2011; however the remainder of the year had very similar $D_0$ values. There was a quick increase in $D_0$ between February 24th 2011 and March 16th 2011, which indicates the pavement foundation thawed between those dates. The variations of $D_0$ with time are presented in Figure 211.

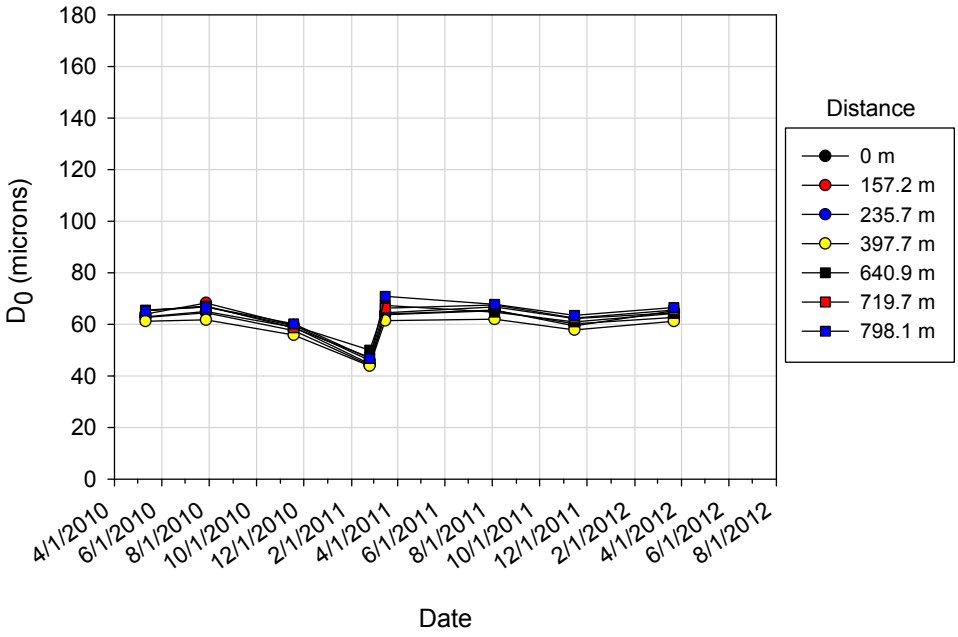


**Figure 211. U.S. Highway 20 Fort Dodge, IA seasonal $D_0$ variations**

The variation of k over time shows the highest k values occurred on February 24th 2011 and the lowest values of k were measured on March 16th 2011. The variations of k with time are presented in Figure 212.

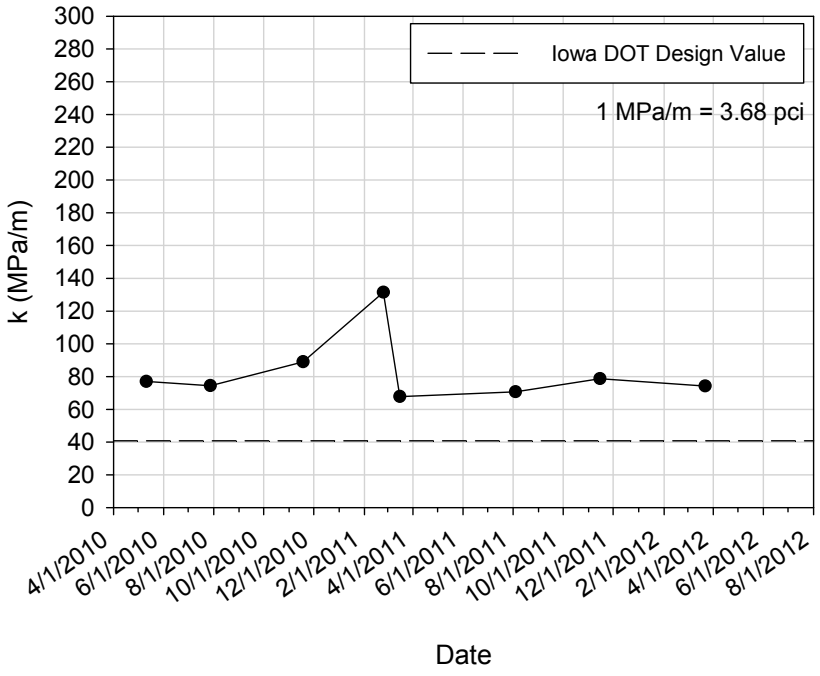


**Figure 212. U.S. Highway 20 Fort Dodge, IA average seasonal k values**

The LTE is similar over the testing period. Seasonal changes do not appear to have an effect on LTE. However, this could be associated with not capturing significant changes in $D_0$ during the thawing period. The variation of LTE over time is shown in Figure 213.

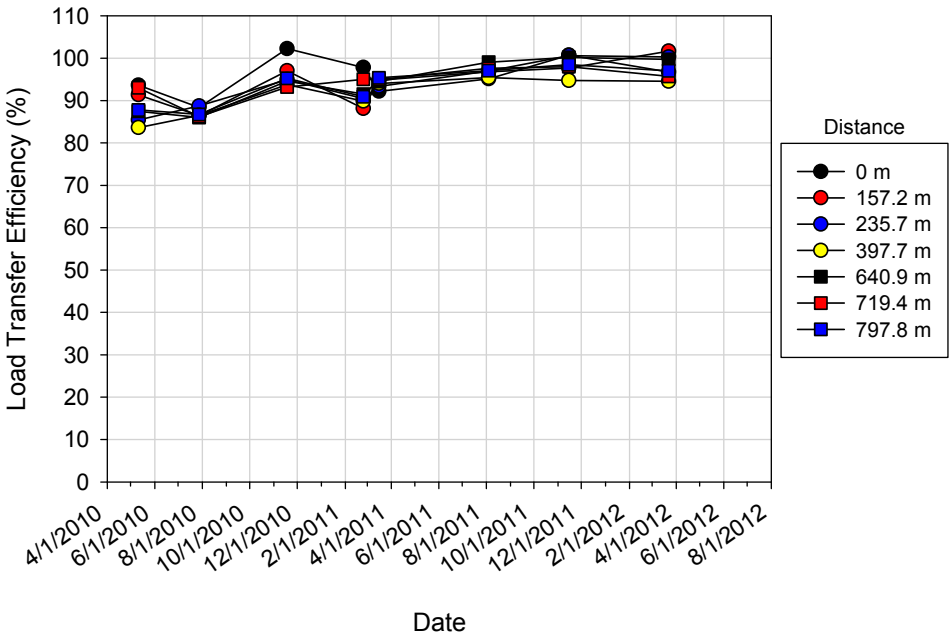


**Figure 213. U.S. Highway 20 Fort Dodge, IA seasonal LTE variations**

The intercept values are very close to zero with the exception of the measurements taken on November 18th 2010 and November 15th 2011. The temperature gradients are very small for all the test dates, with the exception of November 18th 2010, which is negative and indicates that the pavement surface temperature is cooler than the bottom of the pavement slab. According to Vandenbossche (2005) a positive intercept value would be expected to have negative temperature gradient. The intercept values are presented in Figure 214 and the temperature gradients are presented in Table 88

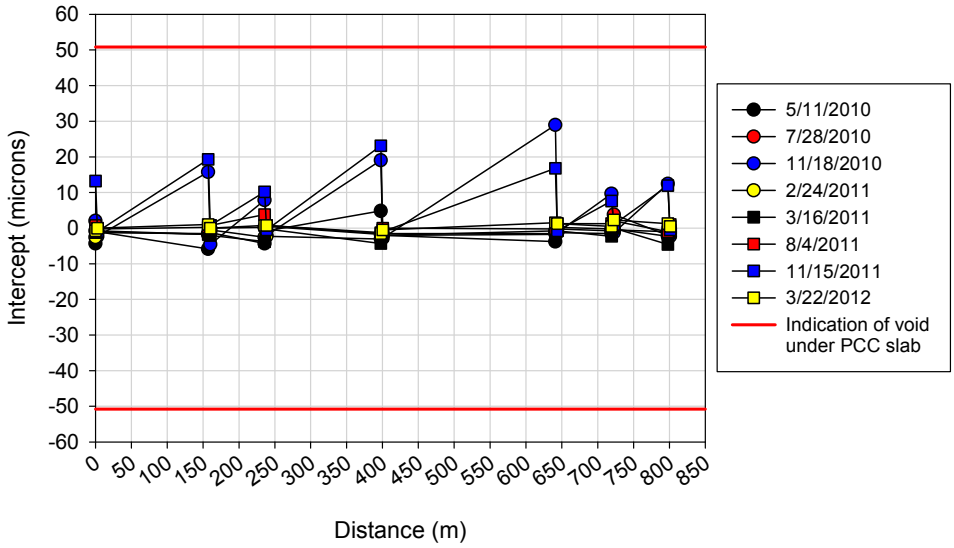


**Figure 214. U.S. Highway 20 Fort Dodge, IA FWD intercept values at center panels and joints**

**Table 88. U.S. Highway 20 Fort Dodge, IA PCC temperature gradients**

| Date | Temperature gradient (°C/mm) |
|---|---|
| 11/18/2010 | -0.017 |
| 3/16/2011 | -0.009 |
| 8/4/2011 | 0.004 |
| 11/15/2011 | -0.001 |
| 3/22/2012 | 0.004 |

The DCP profiles that represent the dates tested are very similar. The November 18th 2010 and November 15th 2011 profiles show some higher CBR values compared to the other profiles, however there is not a good explanation for them to be higher. A DCP was not performed on February 24th 2011 because of poor weather. The DCP profiles are presented in Figure 215.

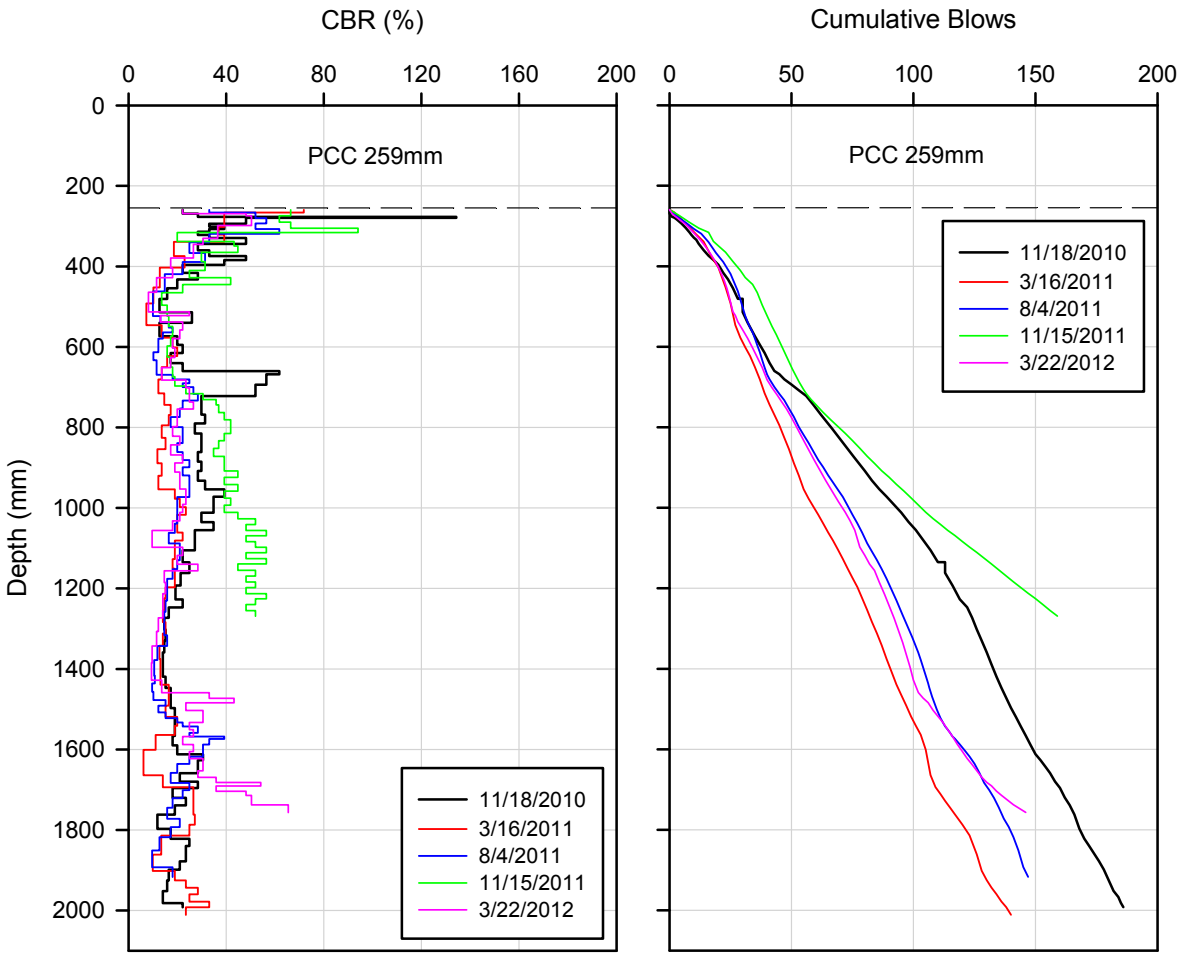


**Figure 215. U.S. Highway 20 Fort Dodge, IA seasonal DCP variations**

## Ames

The temperature probe near Ames, IA recorded 2 periods of freezing temperatures at an approximate depth of 0.15 m below the pavement surface during the 2011-2012 winter. No sustained frost penetration was measured. The frost penetration profile is presented in Figure 216.

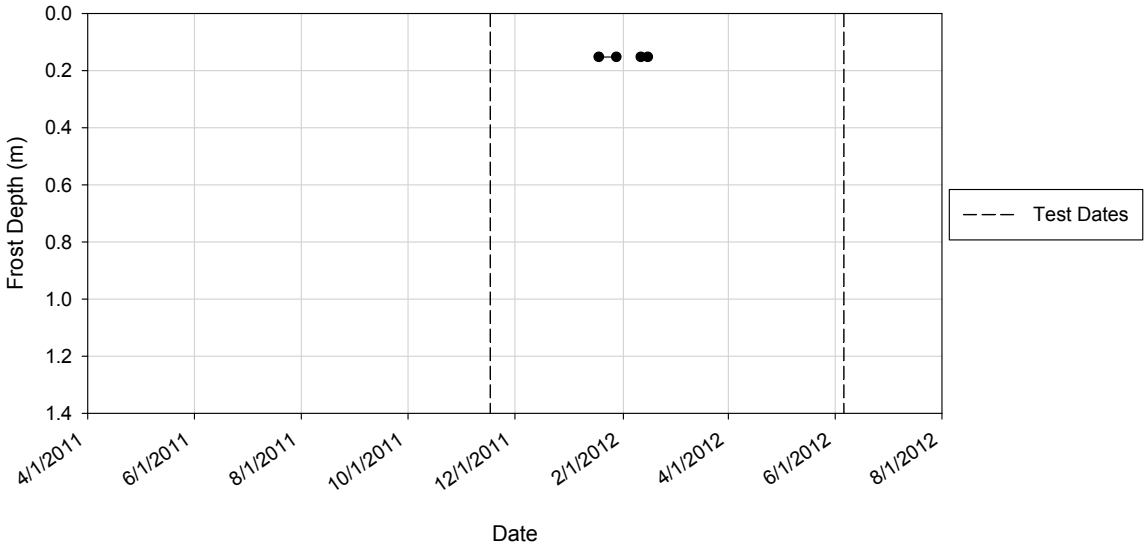


**Figure 216. U.S. Highway 30 Ames, IA frost penetration**

FWD tests were only performed twice at the Ames location. A total of 20 points were tested over an approximate distance of 116 m (Figure 217). The $D_0$ values and trends were similar for the tests performed on November 17$^{th}$ 2011 and June 6$^{th}$ 2011. The $D_0$ values versus distance are presentenced in Figure 218.

**Figure 217. U.S. Highway 30 Ames, IA**

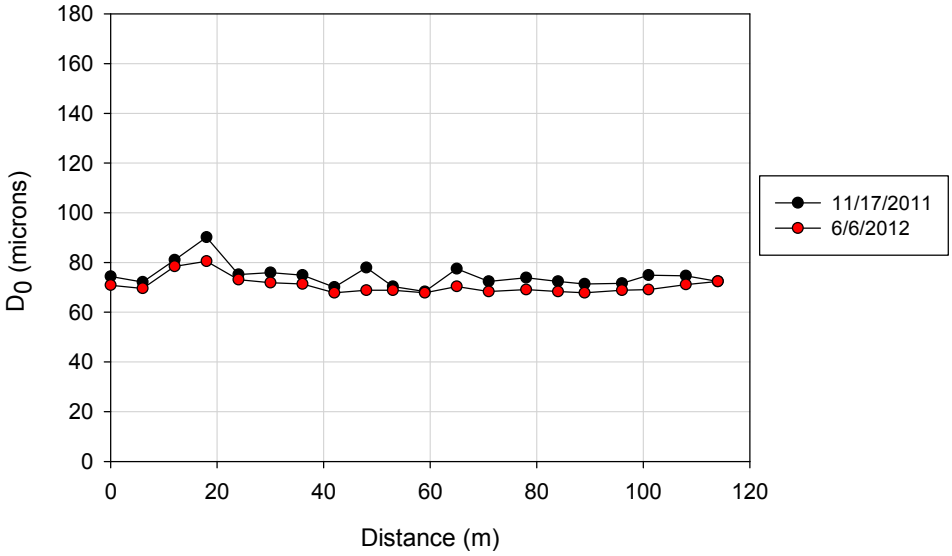


**Figure 218. U.S. Highway 30 Ames, IA distance variations in $D_0$**

The variation of k between the two test dates is presented in Figure 219.

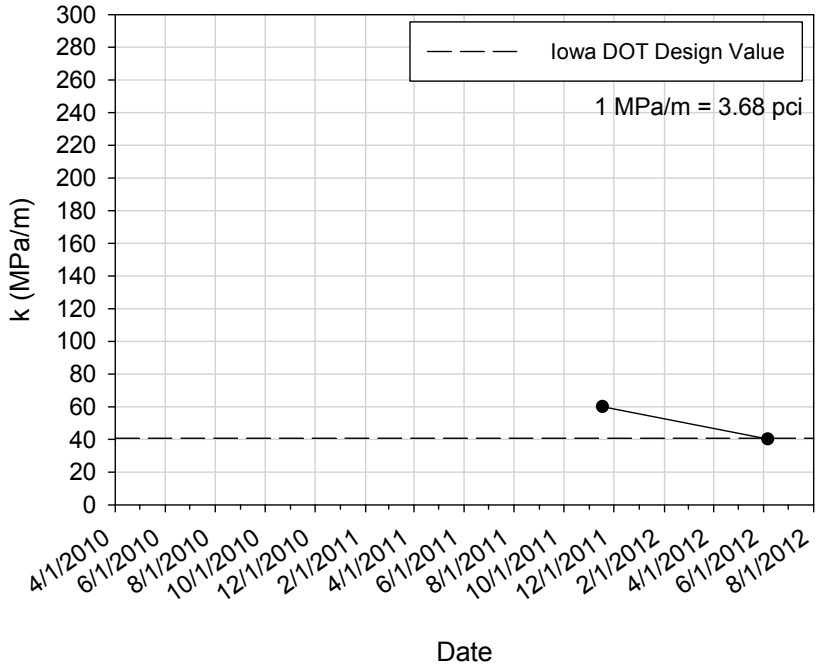


**Figure 219. U.S. Highway 30 Ames, IA average seasonal k values**

The LTE values for the two test dates show an improvement between November 17th 2011 and June 6th 2012. The results are presented in Figure 220.

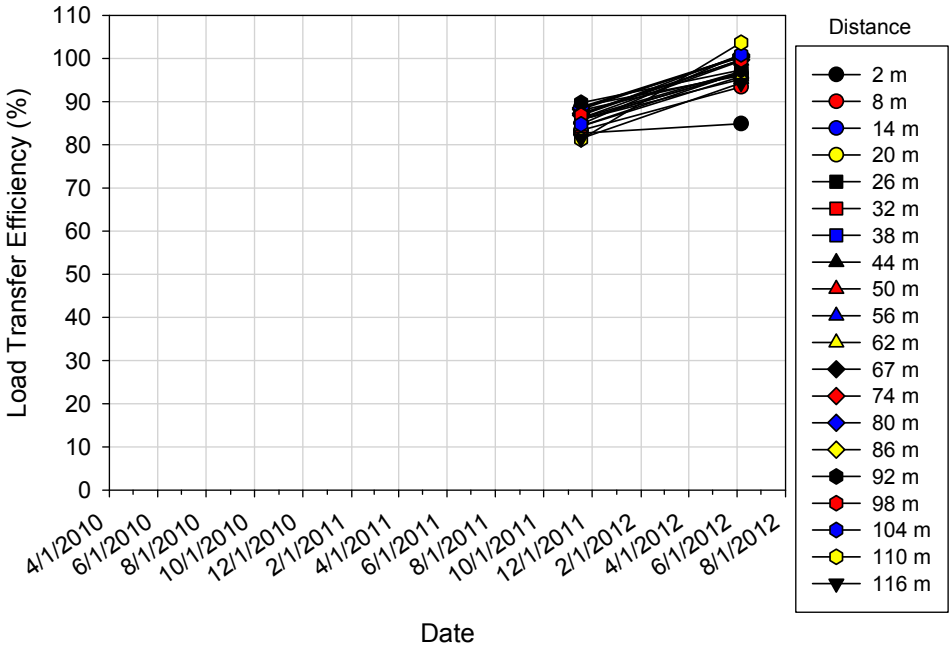


**Figure 220. U.S. Highway 30 Ames, IA seasonal LTE variations**

The intercept values for the two test dates are close to zero and have relatively small temperature gradients. The intercept values are presented in Figure 221 and the temperature gradients are presented in Table 89.

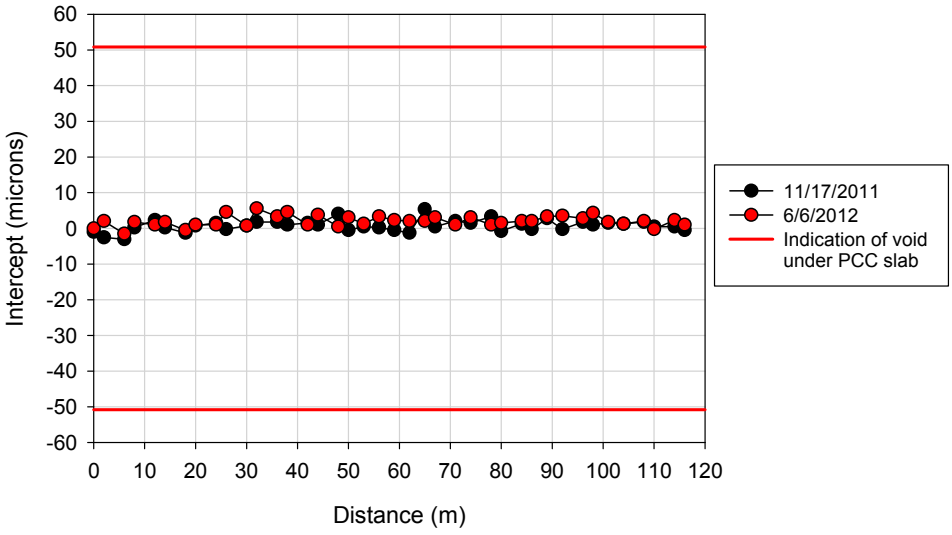


**Figure 221. U.S. Highway 30 Ames, IA FWD intercept values at center panels and joints**

**Table 89. U.S. Highway 30 Ames, IA PCC temperature gradients**

| Date | Temperature gradient (°C/mm) |
|---|---|
| 11/17/2011 | -0.002 |
| 6/6/2012 | 0.013 |

The DCP profile for June 6th 2012 is presented in Figure 222.

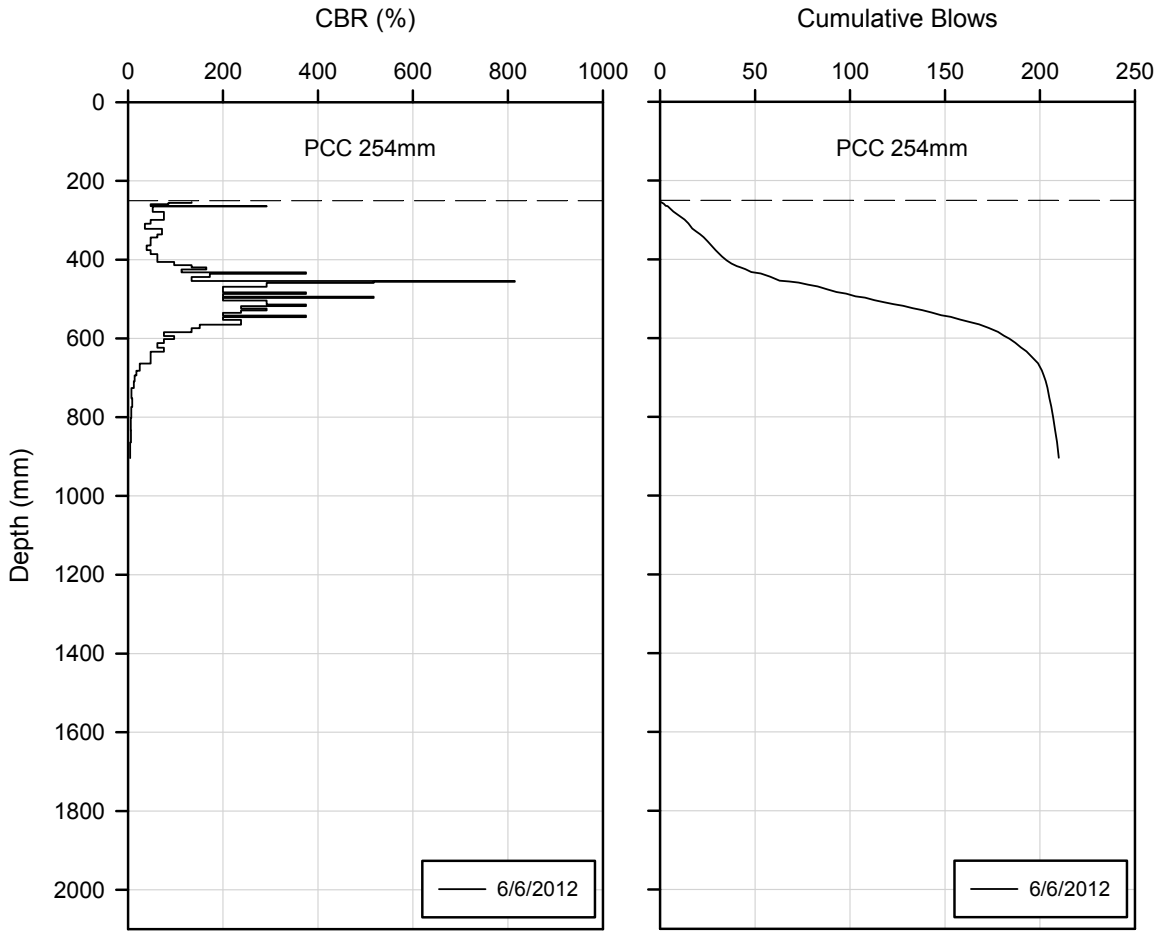


**Figure 222. U.S. Highway 30 Ames, IA seasonal DCP variations**

## West Nevada

FWD tests were performed at 5 locations over approximately 323 m (Figure 223). There is little variation of $D_0$ over the distance tested. None of the dates tested showed a significant decrease in $D_0$, which would indicate the pavement foundation materials were not frozen during any of the test dates. The variation of $D_0$ over the distance tested is presented in Figure 224.

**Figure 223. U.S. Highway 30 West Nevada, IA**

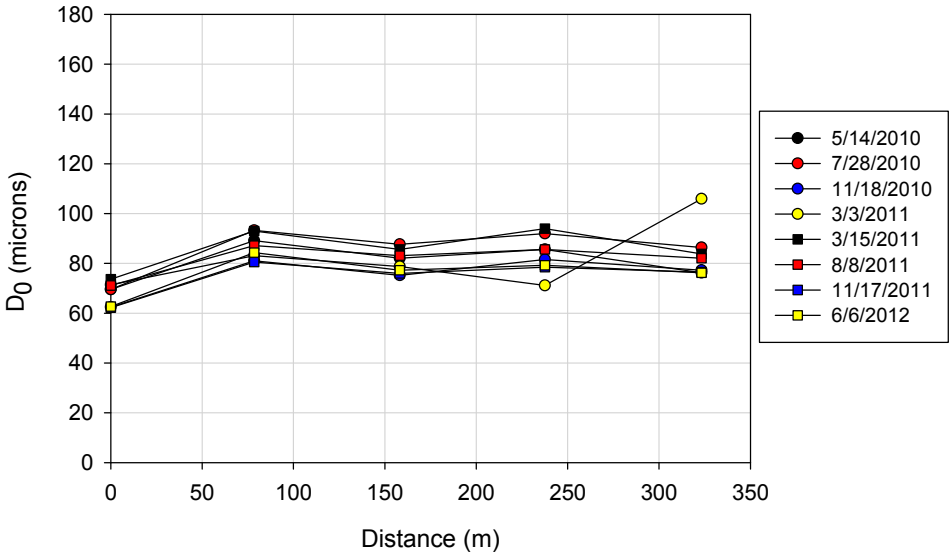


**Figure 224. U.S. Highway 30 West Nevada, IA distance variations in $D_0$**

The variation of $D_0$ over time is very similar at each distance for the dates tested. There is no indication of thaw weakening on March 3rd 2011 or March 15th 2011. The $D_0$ changes versus time are presented in Figure 225.

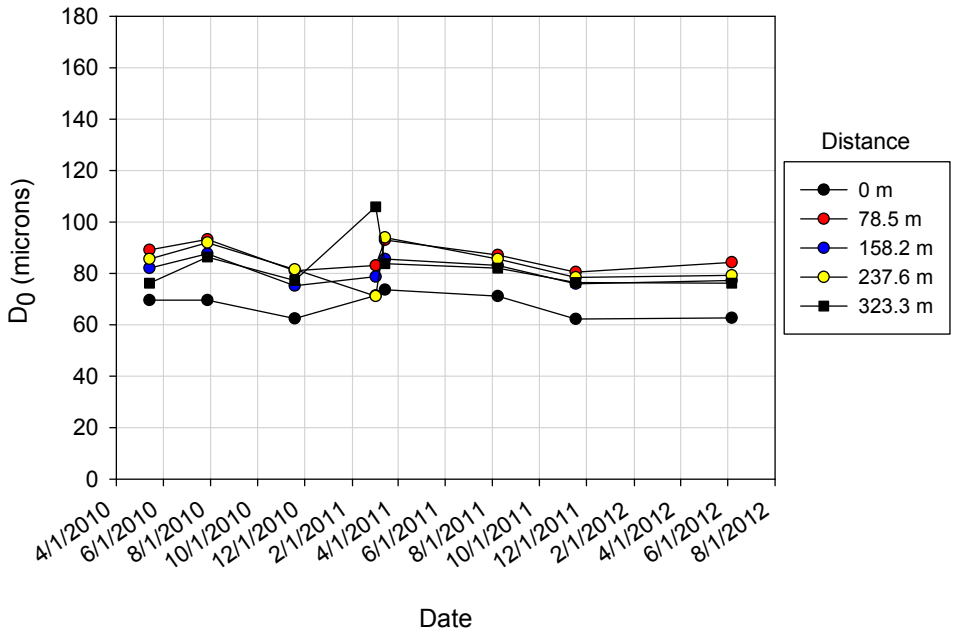


**Figure 225. U.S. Highway 30 West Nevada, IA seasonal $D_0$ variations**

The variations of k over time show similar results for the test dates. The lowest k values were measured on June 6th 2012. There was not an increase in k that would represent frozen conditions, compared to other test dates. However, there is evidence of thaw-weakening between March 3rd, 2011 and March 15th, 2011. The k values for the dates tested are presented in Figure 226.

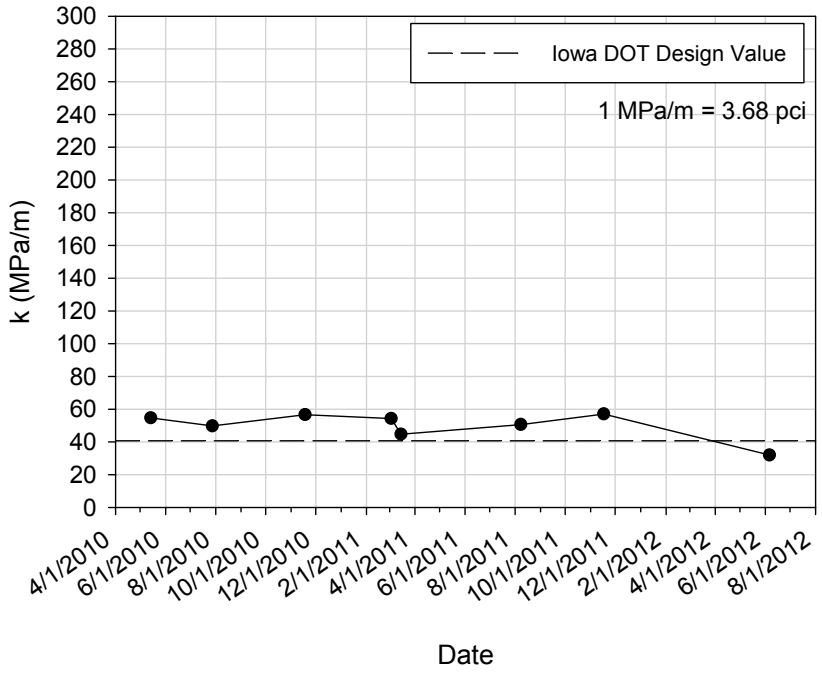


**Figure 226. U.S. Highway 30 West Nevada, IA average seasonal k values**

The variation of LTE over time show little variation, with the lowest values occurring on July 28th 2010. The LTE values were very close to 100, with the values for November 28th 2010 and June 6th 2012 being over 100. The changes in LTE values over time are presented in Figure 227.

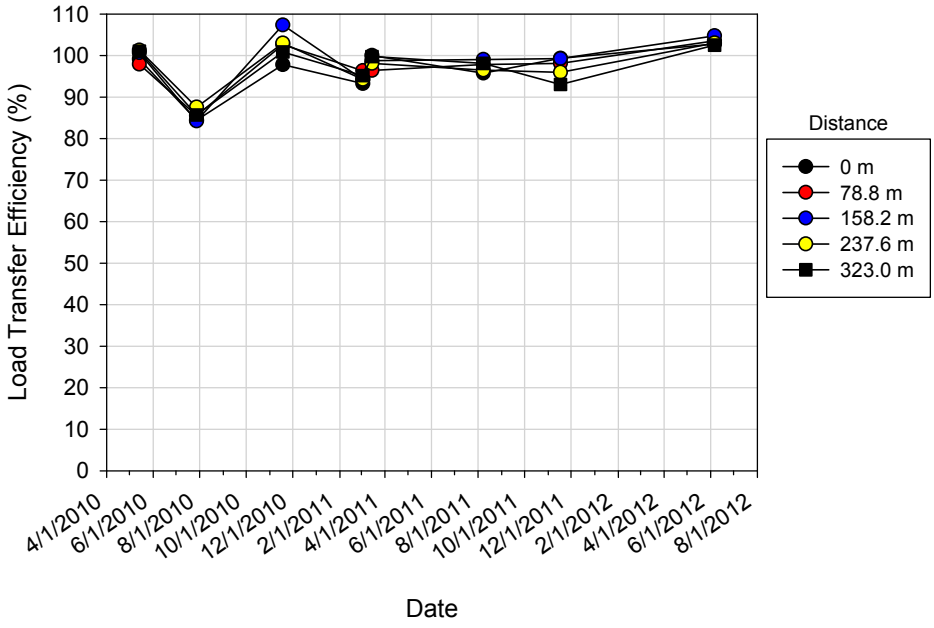


**Figure 227. U.S. Highway 30 West Nevada, IA seasonal LTE variations**

The intercept values are close to zero with the exception of the measurements taken on November 18th 2010 and November 17th 2011. The temperature gradients are positive with the exception of November 18th 2010 and November 17th 2011, which are negative and close to zero. The temperature gradients measured on March 3rd 2011, and March 15th are relatively high, however the intercept values are close to zero. The expected response for positive temperature gradients is negative intercept values. The intercept values are shown in Figure 228 and the temperature gradients are presented in Table 88.

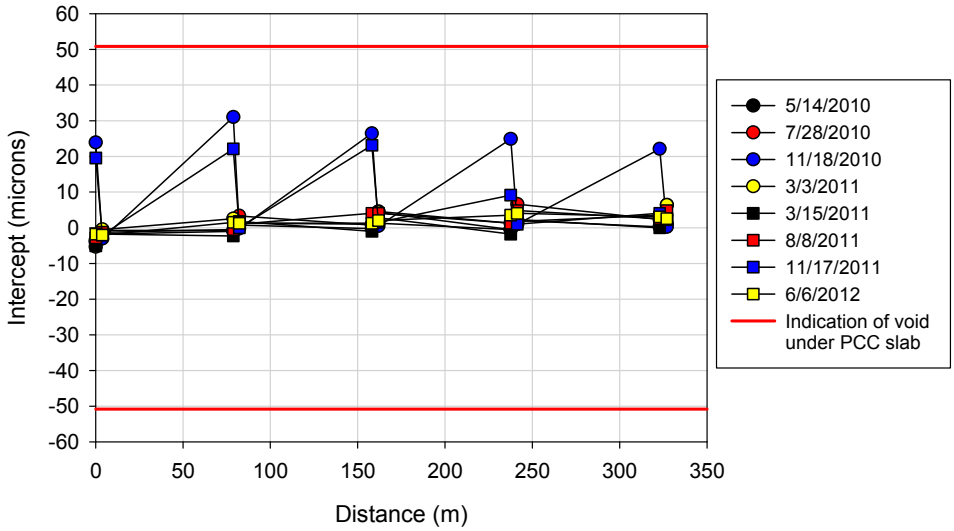


**Figure 228. U.S. Highway 30 West Nevada, IA FWD intercept values at center panels and joints**

**Table 90. U.S. Highway 30 West Nevada, IA PCC temperature gradients**

| Date | Temperature gradient (°C/mm) |
|---|---|
| 11/18/2010 | -0.003 |
| 3/3/2011 | 0.028 |
| 3/15/2011 | 0.043 |
| 8/8/2011 | 0.010 |
| 11/17/2011 | -0.002 |
| 6/6/2012 | 0.004 |

The DCP profiles show repeatable results and are presented in Figure 229.

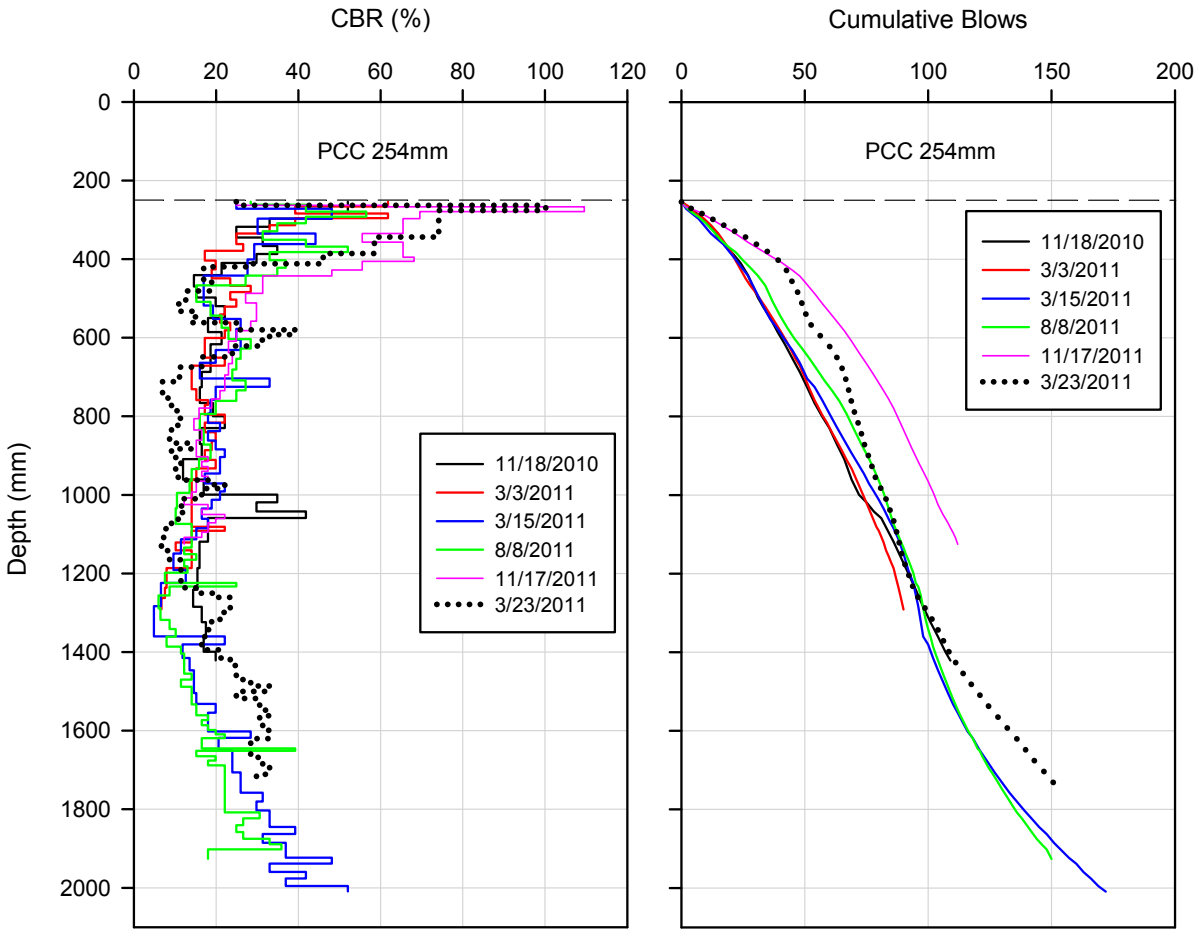


**Figure 229. U.S. Highway 30 West Nevada, IA seasonal DCP variations**

## East Nevada

FWD tests were performed at 6 locations over a distance of approximately 402 m (Figure 230). There is little variation over time in the $D_0$ values measured at the distances tested. The site was not tested during February 2011 and because the March 3rd 2011 test did not show a decrease in $D_0$ compared to the other dates, it is likely that the site was not tested during frozen conditions. The variations of $D_0$ with distance are shown in Figure 231.

**Figure 230. U.S. Highway 30 East Nevada, IA**

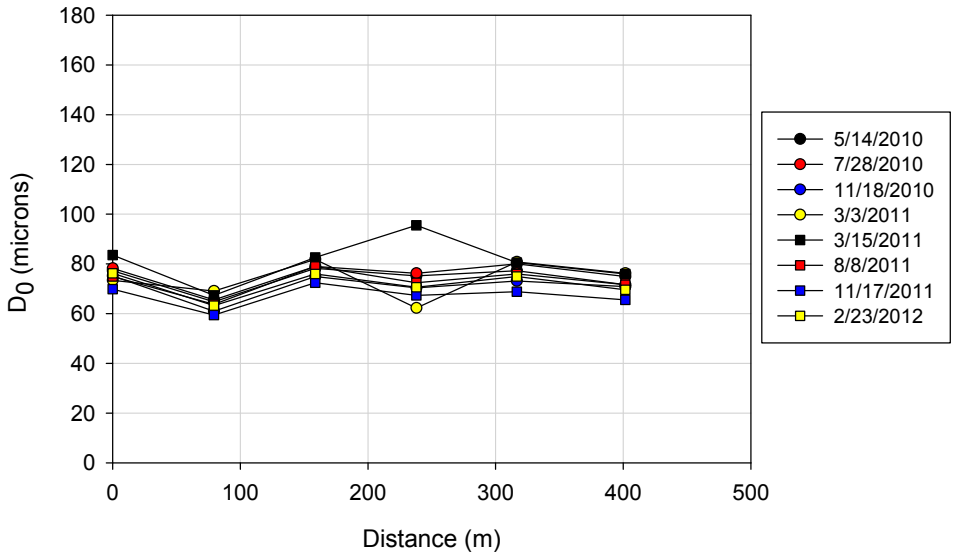


**Figure 231. U.S. Highway 30 East Nevada, IA distance variations in $D_0$**

The $D_0$ measurements are very similar with no low measurements that could indicate frozen conditions. The variation of $D_0$ with time is presented in Figure 232.

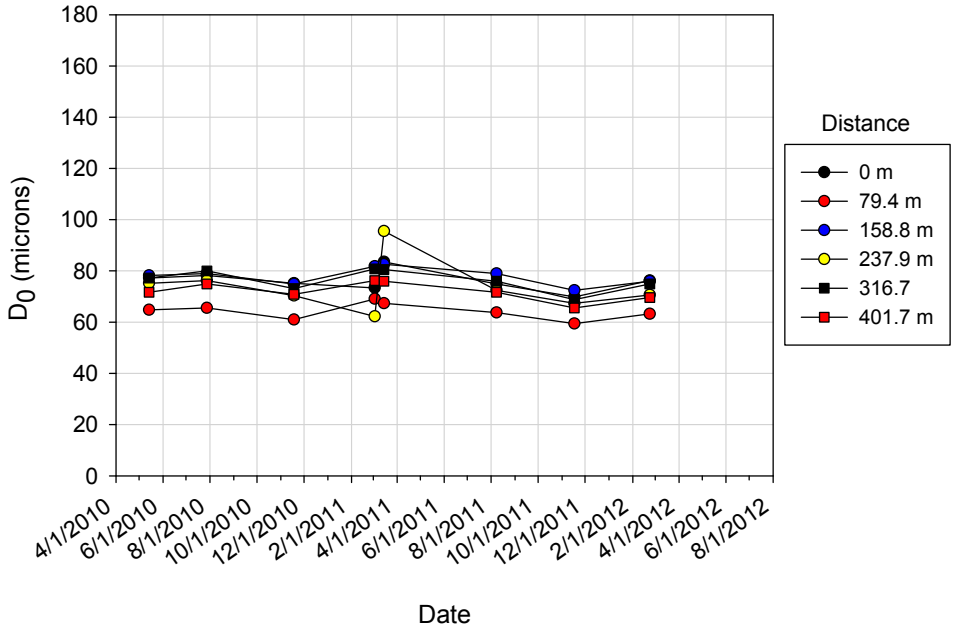


**Figure 232. U.S. Highway 30 East Nevada, IA seasonal $D_0$ variations**

The values of k are very similar for the dates tested. The lowest values occurred on March 15th 2011. The remaining test dates were very similar. The variation of k with time is presented in Figure 233.

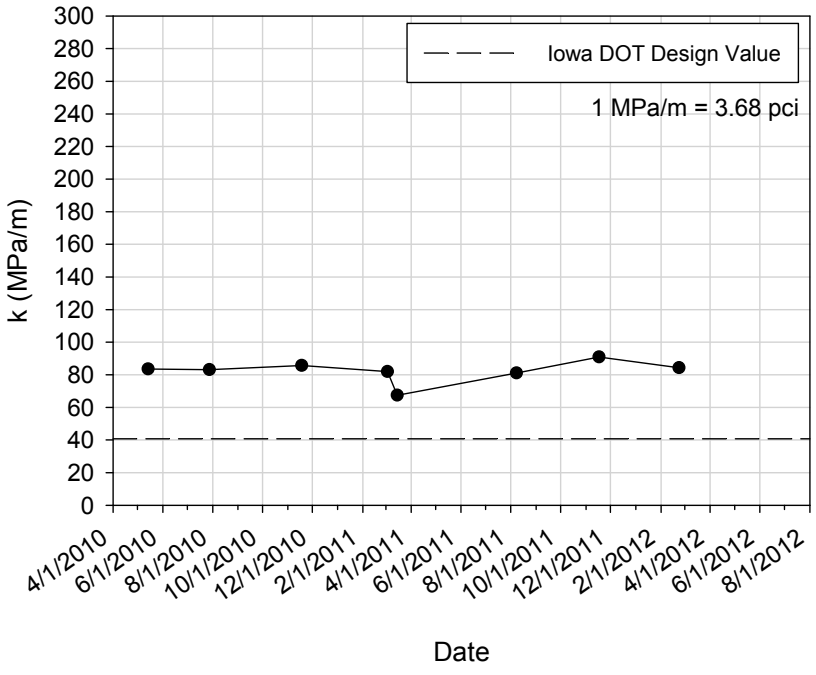


**Figure 233. U.S. Highway 30 East Nevada, IA average seasonal k values**

The LTE values are very similar for all the dates tested. The lowest LTE values were measured on July 28th 2010. The variation of LTE values versus time is shown in Figure 234.

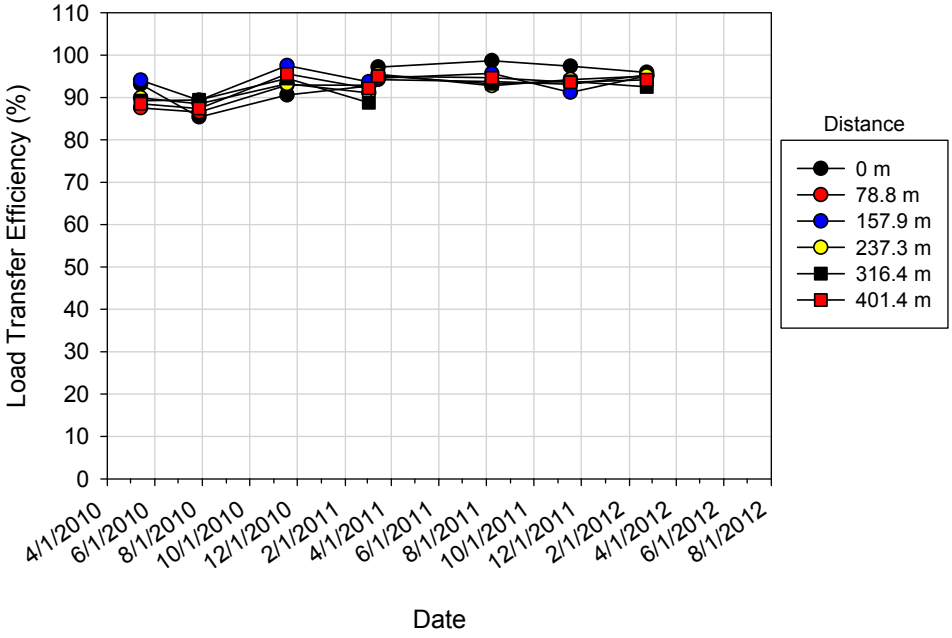


**Figure 234. U.S. Highway 30 East Nevada, IA seasonal LTE variations**

The intercept values are close to zero for all the test dates. The temperature gradients measured on March 3rd 2011 and March 15th 2011 were relatively high, but did not result in negative intercept values as would be expected (Vandenbossche 2005). The intercept values are presented in Figure 245 and the temperature gradients are presented in Table 91.

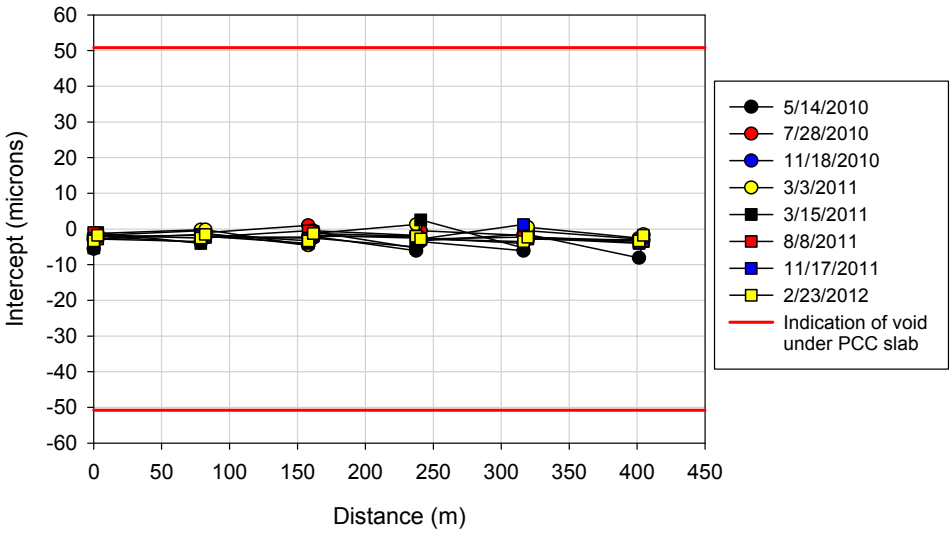


**Figure 235. U.S. Highway 30 East Nevada, IA FWD intercept values at center panels and joints**

**Table 91. U.S. Highway 30 East Nevada, IA PCC temperature gradients**

| Date | Temperature gradient (°C/mm) |
|---|---|
| 11/18/2010 | 0.000 |
| 3/3/2011 | 0.028 |
| 3/15/2011 | 0.042 |
| 8/8/2011 | -0.006 |
| 11/17/2011 | -0.015 |
| 2/23/2012 | 0.013 |

The DCP profiles are very similar with the exception of August 9th 2011. The DCP profile for August 9th 2011 shows higher CBR values between 1000 and 1900 mm compared to the other profiles. The DCP profiles are presented in Figure 236.

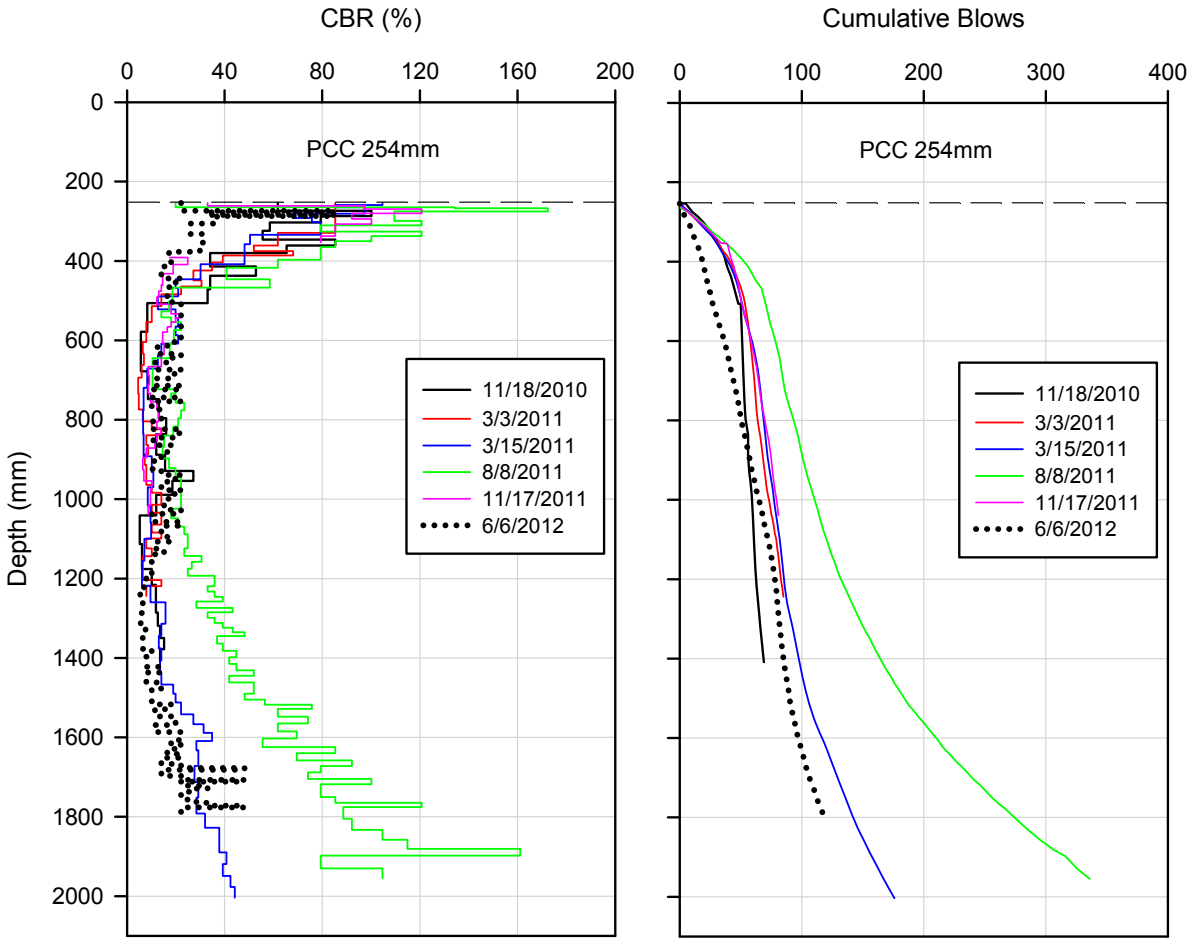


**Figure 236. U.S. Highway 30 East Nevada, IA seasonal DCP variations**

## Plainfield

The permanent freeze for the 2010-2011 winter approximately began on November 24th 2010 and ended on March 12th 2011. The maximum frost depth during the 2010-2011 winter was approximately 1.2 m. The permanent freeze in the winter of 2011-2012 began around December 4th 2011 and ended around February 29th 2012. The maximum frost depth was close 0.6 m. The 2011-2012 winter was mild compared to the 2008-2009, 2009-2010, and 2010-2011 winters. The frost depth profiles are presented in Figure 237.

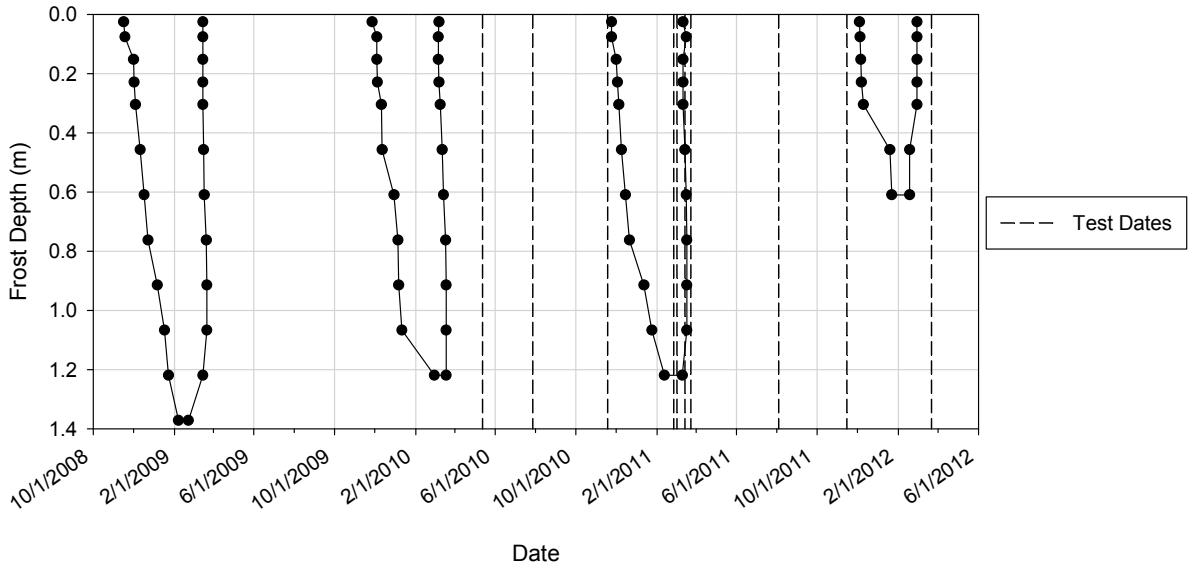


**Figure 237. U.S. Highway 218 Plainfield, IA frost penetration**

For the 2010-2011 winter, the number freeze-thaw cycles was determined from the temperature probe measurements in Plainfield (Figure 238). A freeze-thaw cycle was defined as a temperature drop below 0°C followed by a temperature increase above 0°C. At an approximate depth of 0.025 m below the pavement, 46 freeze-thaw cycles were observed, which decreased to 1 freeze-thaw cycle for depths approximately between 0.45 m and 1.2 m.

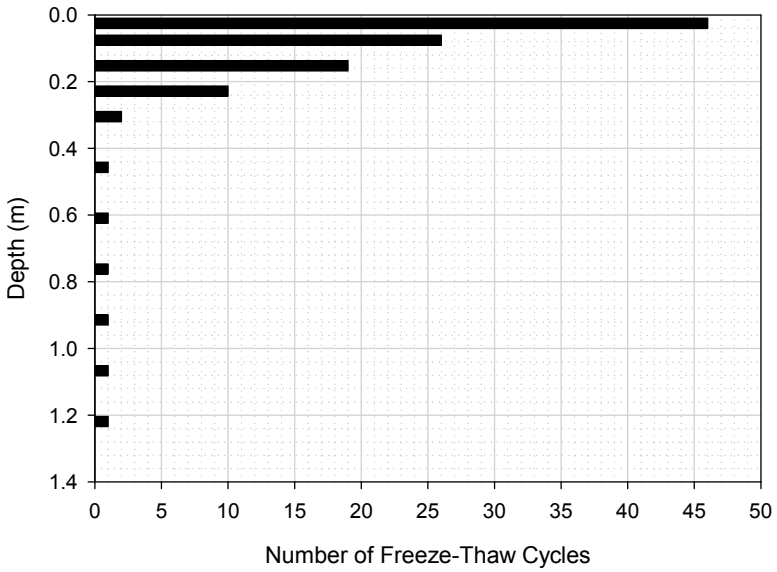


**Figure 238. U.S. Highway 218 Plainfield, IA freeze-thaw cycles during 2010-2011 winter**

Sustained cold air temperatures result in a subsurface temperature profile that is the coldest directly below the bottom of the pavement and becomes warmer as depth increases. Whereas, hot air temperatures result in a subsurface temperature profile that is warmest directly below the pavement and is decreasingly cooler as depth increases. Example temperature profiles measured on February 9th 2011 and July 19th 2011 are shown in Figure 239.

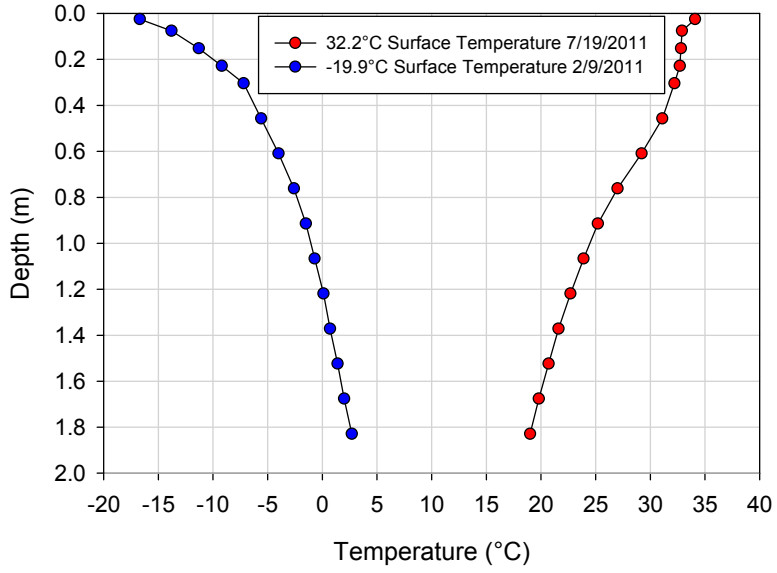


**Figure 239. U.S. Highway 218 Plainfield, IA hot and cold subsurface pavement temperature profiles**

FWD tests were performed at 7 locations over an approximate distance of 464 m (Figure 240). The trends in $D_0$ for the test locations are very similar for the dates tested. The lowest $D_0$ values were measured on February 26, 2011 and March 3rd 2011, which are both before the approximate thaw date of March 12th 2011. However, there is no indication that significant thaw weakening occurred from the $D_0$ measurements on March 15th 2011. The variation of $D_0$ over the test locations is presented in Figure 241.

**Figure 240. U.S. Highway 218 Plainfield, IA**

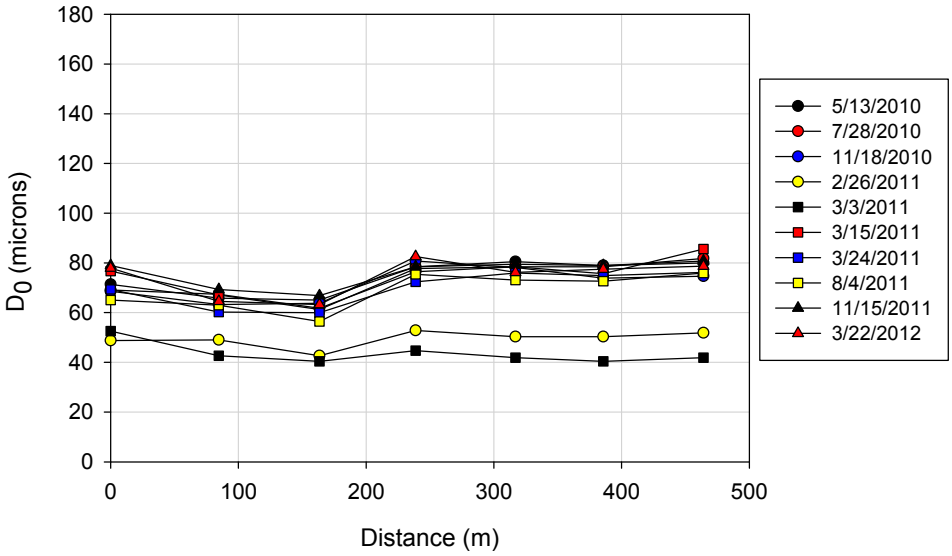


**Figure 241. U.S. Highway 218 Plainfield, IA distance variations in $D_0$**

There is a noticeable increase in $D_0$ between March 3rd 2011 and March 15th 2011. There is one point at a distance of 464.2 m that has a higher $D_0$ value than tests performed on other dates throughout the year. Otherwise, there is no indication of thaw weakening significantly decreasing the strength of the pavement system. The changes in $D_0$ over time are presented in Figure 242.

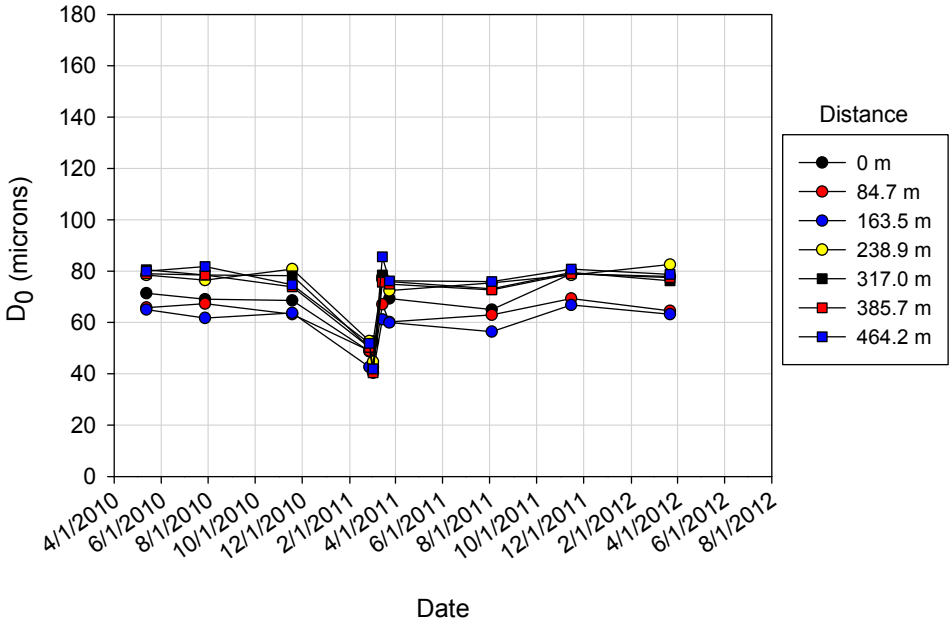


**Figure 242. U.S. Highway 218 Plainfield, IA seasonal $D_0$ variations**

The variations in the backcalculated k over time show high values measured on February 26th 2011 and March 3rd 2011. There is a large drop in the k value measured on March 15th 2011. However, the March 15th 2011 did not have the lowest backcalculated k value. The variation of k over time is presented in Figure 243.

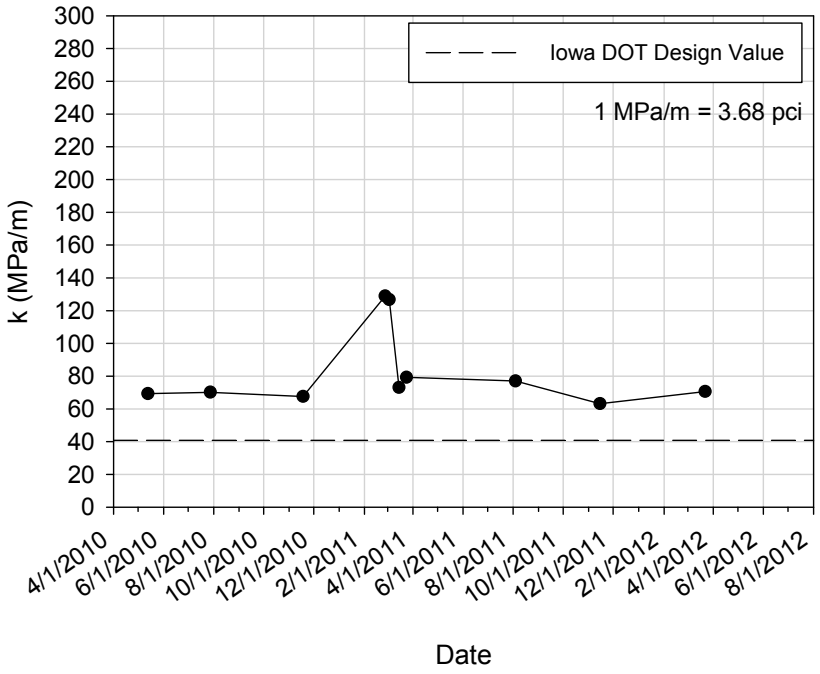


**Figure 243. U.S. Highway 218 Plainfield, IA average seasonal k values**

The LTE values vary over time. The lowest LTE values were measured on May 13th 2010, July 28th 2010, and March 3rd 2011. There was a decrease in LTE on March 3rd 2011 compared to February 26th 2011. The temperature data and $D_0$ values indicate the pavement foundation was still frozen on March 3rd 2011. The remaining dates had LTE values very close or over 100%. The variation of LTE with time is presented in Figure 244.

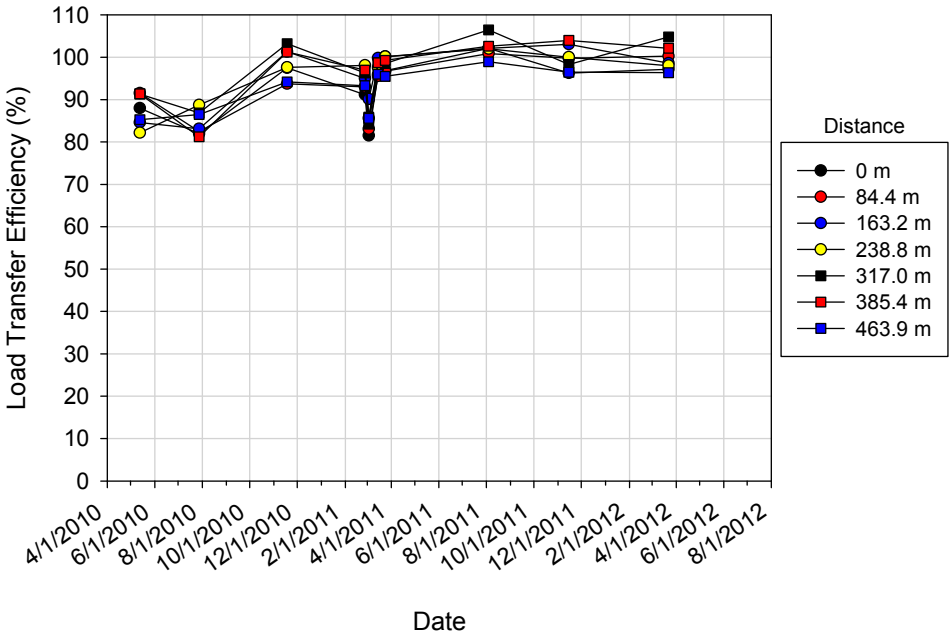


**Figure 244. U.S. Highway 218 Plainfield, IA seasonal LTE variations**

The measured intercept values are mostly positive. The highest intercept values were measured on August 4th 2011. The temperature gradients were close to zero for all the dates tested. The intercept values measured on November 18th 2010 and August 4th 2011 were close or over the void indicating intercept value of 50 microns reported by McCracken (2008). The intercept values are shown in Figure 245 and the temperature gradients are presented in Table 92.

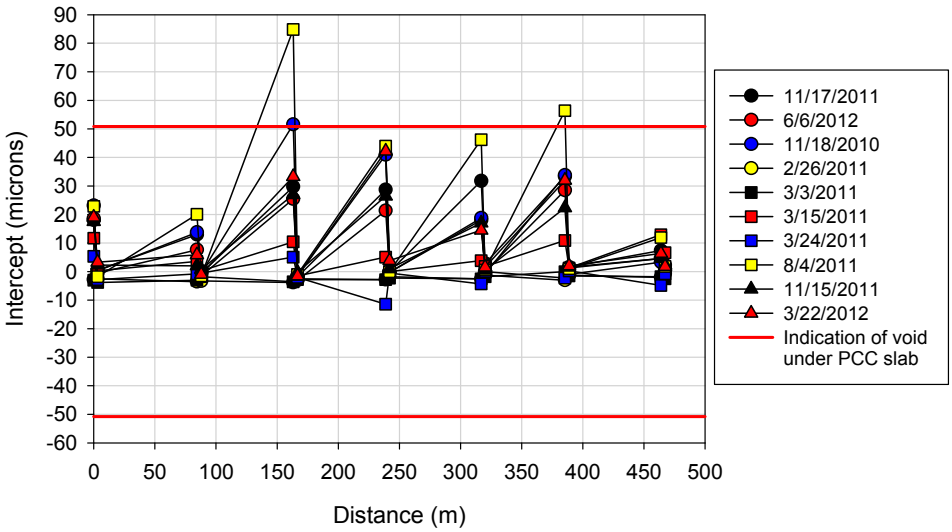


**Figure 245. U.S. Highway 218 Plainfield, IA FWD intercept values at center panels and joints**

**Table 92. U.S. Highway 218 Plainfield, IA PCC temperature gradients**

| Date | Temperature gradient (°C/mm) |
|---|---|
| 11/18/2010 | 0.001 |
| 2/26/2011 | -0.010 |
| 3/3/2011 | 0.002 |
| 3/15/2011 | -0.002 |
| 3/24/2011 | -0.004 |
| 8/4/2011 | 0.007 |
| 11/15/2011 | 0.002 |
| 3/22/2012 | 0.002 |

The DCP profiles are presented in Figure 246.

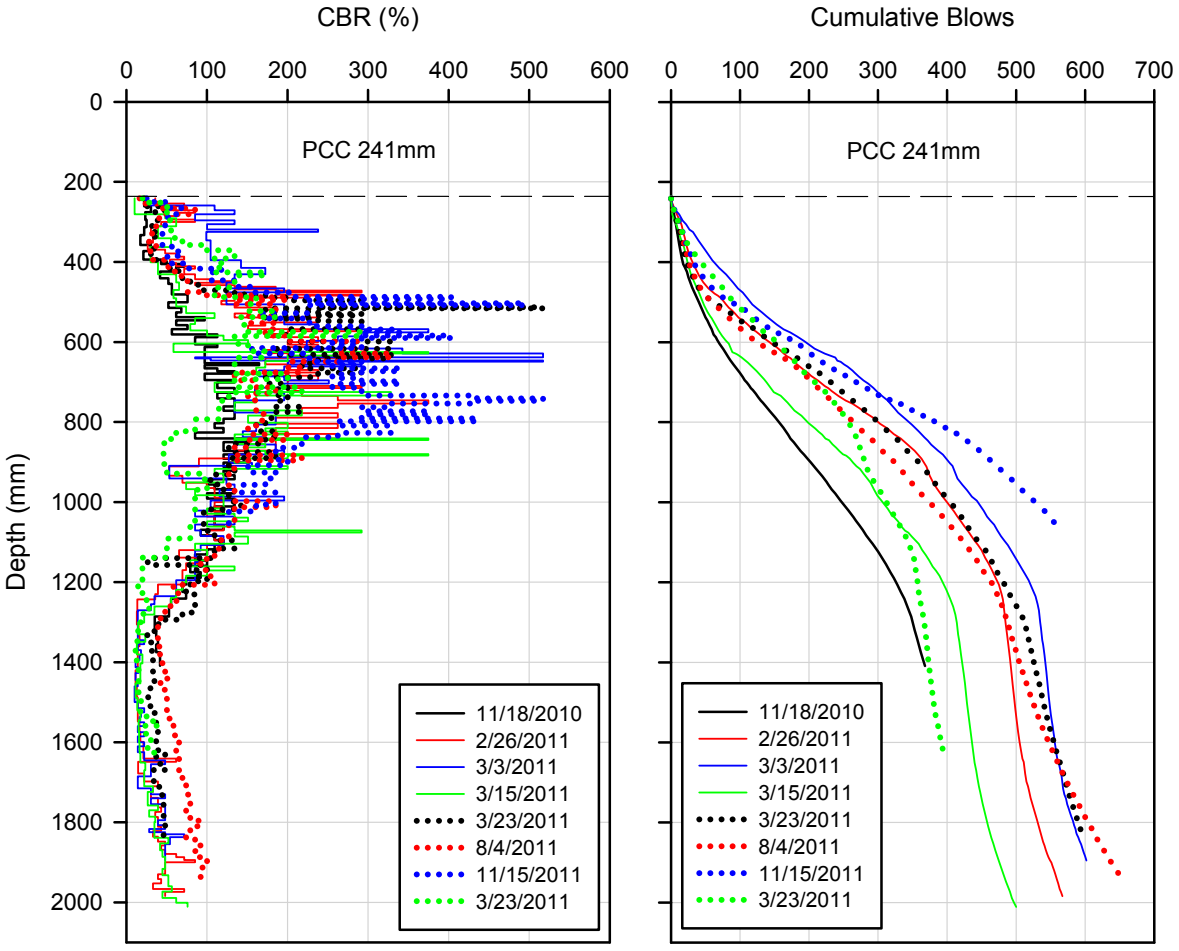


**Figure 246. U.S. Highway 218 Plainfield, IA seasonal DCP variations**

In addition to the $D_0$ values and backcalculated k values, the AREA index, deflection at 1524 mm ($D_{1524}$) behind the loading plate, base curvature index (BCI), surface curvature

index (SCI), basin damage index (BDI), partial area (PA) index, subgrade damage index (SDI), and subsurface index (SI) are presented for the U.S. Highway 218 site near Plainfield, IA. The parameters are FWD indices were presented in Drumm and Meier (2003). They recommended that BCI, SDI, SI, and PA be used to observe thaw-weakening. Lower index values indicate a stiffer response.

Table 93 shows how the FWD indices are calculated and Figure 247 through Figure 254 show the FWD indices.

**Table 93. FWD indices (Drumm and Meier 2003)**

| Parameter | Formula |
|---|---|
| AREA | $6 * [(D_0/D_0) + (2*D_{305}/D_0) + (2*D_{610}/D_0) + (D_{914}/D_0)]$ |
| Deflection at load plate ($D_0$) | $D_0$ |
| Deflection at 1524 mm ($D_{1524}$) | $D_{1524}$ |
| Base curvature index (BCI) | $D_{610} - D_{914}$ |
| Surface curvature index (SCI) | $D_0 - D_{305}$ |
| Basin damage index (BDI) | $D_{305} - D_{610}$ |
| Partial area (PA), $m^2$ | $[(D_{457}+D_{610})/2*0.153] + [(D_{610}+D_{914})/2*0.304] + [(D_{914}+D_{1524})/2*0.610]$ |
| Subgrade damage index (SDI) | $D_{610} - D_{1524}$ |
| Subsurface index (SI) | $D_{305} - D_{1524}$ |

$D_x$ is the surface deflection measured x mm from the loading plate.

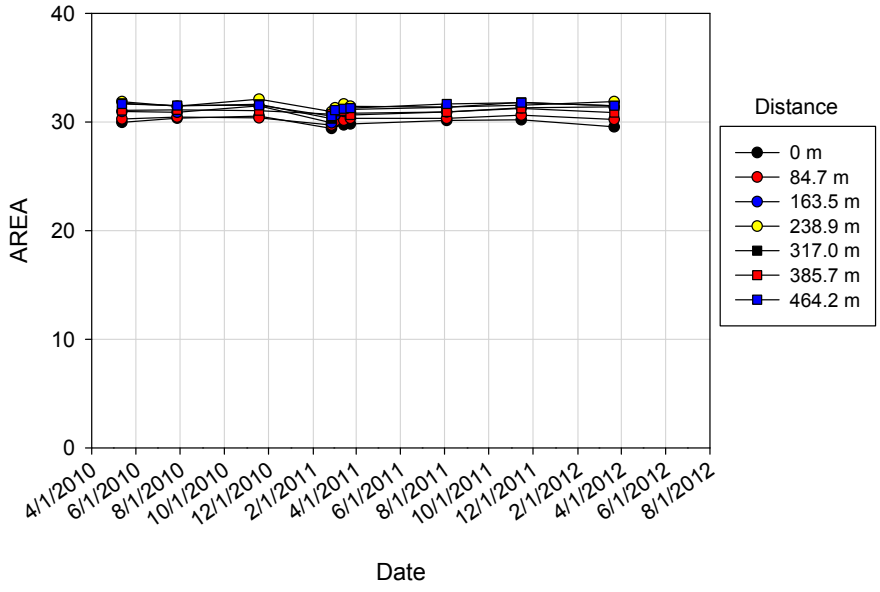


**Figure 247. U.S. Highway 218 Plainfield, IA seasonal AREA variations**

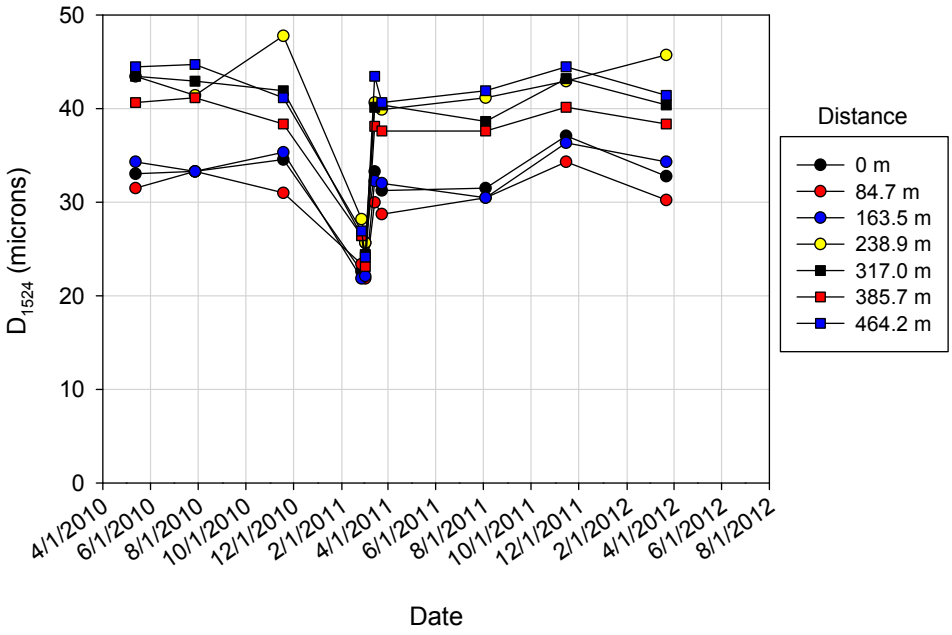


**Figure 248. U.S. Highway 218 Plainfield, IA seasonal $D_{1524}$ variations**

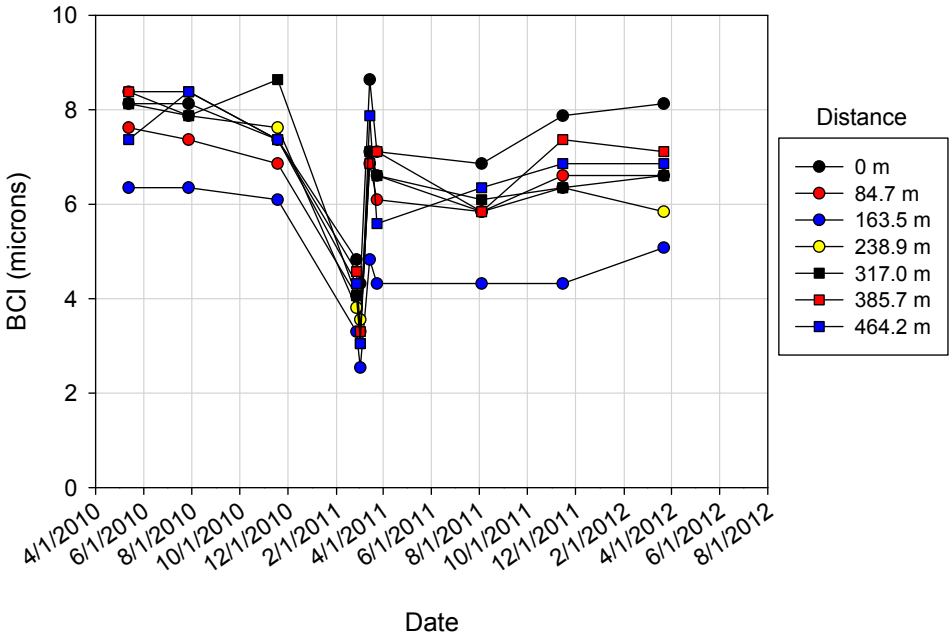


**Figure 249. U.S. Highway 218 Plainfield, IA seasonal BCI variations**

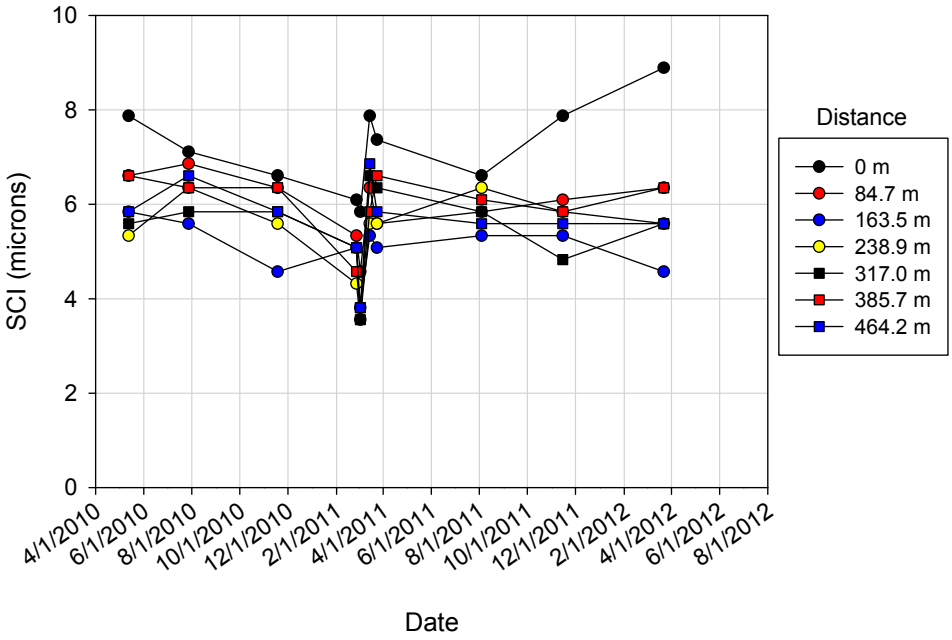


**Figure 250. U.S. Highway 218 Plainfield, IA seasonal SCI variations**

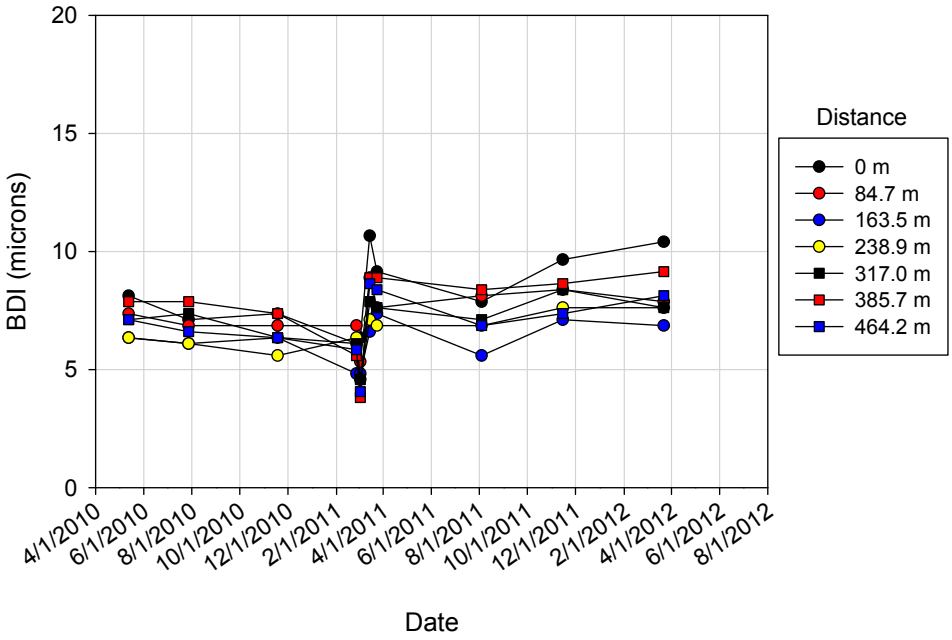


**Figure 251. U.S. Highway 218 Plainfield, IA seasonal BDI variations**

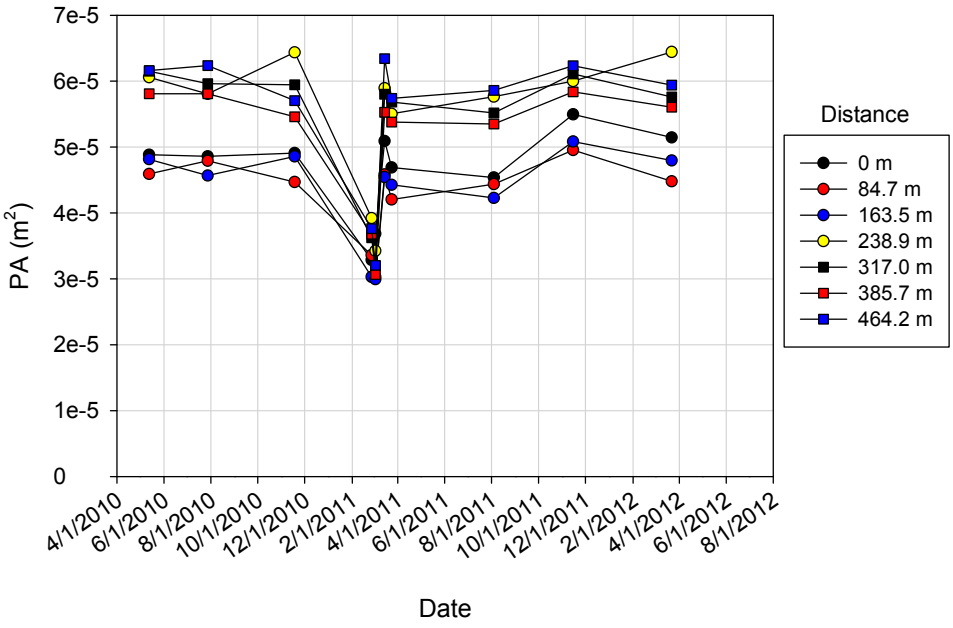


**Figure 252. U.S. Highway 218 Plainfield, IA seasonal PA variations**

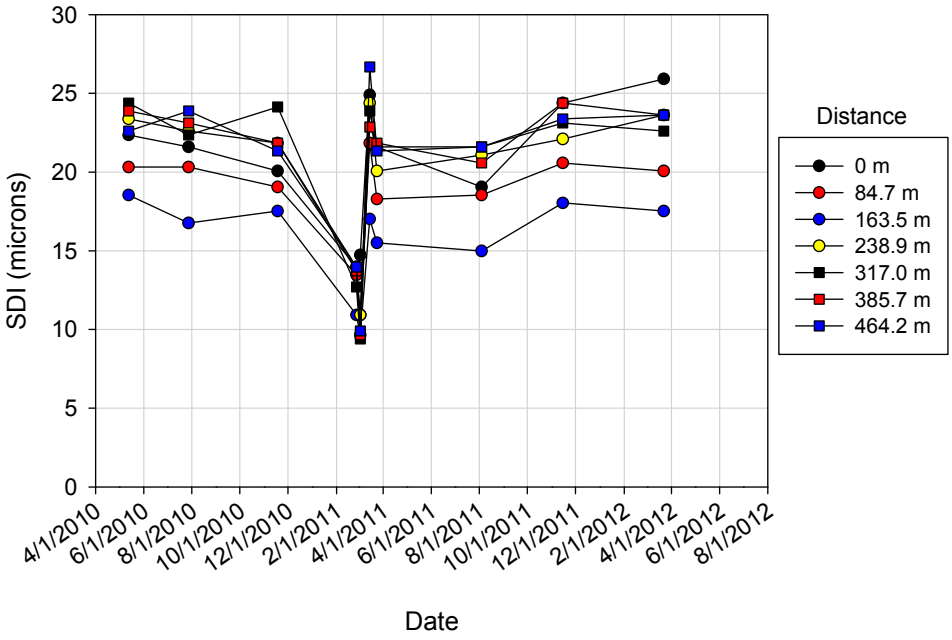


**Figure 253. U.S. Highway 218 Plainfield, IA seasonal SDI variations**

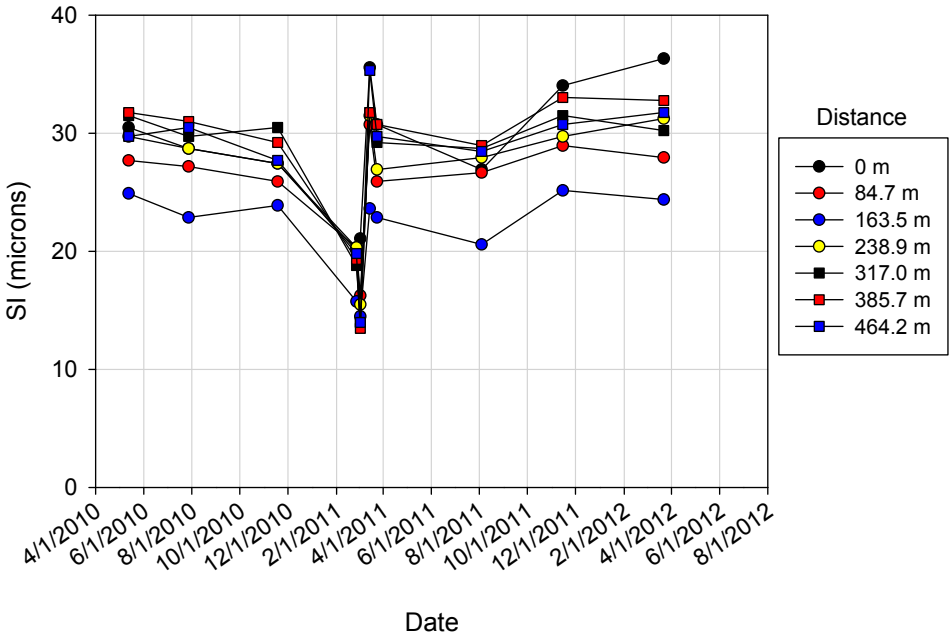


**Figure 254. U.S. Highway 218 Plainfield, IA seasonal SI variations**

The AREA, $D_{1524}$, BCI, SCI, BDI, PA, SDI, and SI FWD indices did not show significant signs of thaw-weakening, therefore they were only calculated for the U.S. Highway 218 site near Plainfield, IA.

## Summary

The seven pavement sites tested during thawing periods showed no indication of thaw-weakening behavior based on $D_0$ values. The expectation was for the pavement stiffness to be lowest during thawing periods, which would be represented by the highest $D_0$ values. Two possibilities for the pavement not having a lower stiffness during thawing are the pavement system was designed to not lose strength during thawing periods or the testing frequency was not high enough to measure the thaw-weakening period. However, there was a noticeable difference between the $D_0$ measured on frozen dates and thawed dates. The backcalculated k values measured at Moville, Denison, Fort Dodge, and East Nevada showed the weakest conditions of the year were during thawing periods. However, the decreases in the backcalculated k compared to other dates were small. The LTE values appeared to be unaffected by seasonal strength changes.

The 2011-2012 winter was less severe compared to the 2010-2011 winter based on the frost depths measure at Moville, Denison, and Plainfield. However, the $D_0$ values were not

significantly different in 2011-2012 compared to 2010-2011. Based on these results, the severity of the winter does not have a noticeable effect on the $D_0$ measurements after the pavement foundation has thawed.

# CHAPTER 6. CONCLUSIONS AND RECOMMENDATIONS

This chapter presents an overview of the conclusions found from the following three categories: durability tests, frost-heave and thaw-weakening tests, and in situ tests. The conclusions are then compared with the goal of the research. The last part of this chapter discusses recommendations for future research and practice.

## DURBILITY TEST CONCLUSIONS

### 2-in. x 2-in. Compressive Strength

The maximum dry unit weight of the loess samples increased when stabilized with cement and fly ash. The maximum dry unit weight of the cement-stabilized loess was approximately 0.5 kN/m$^3$ higher than the unstabilized loess and the maximum dry unit weight of the fly ash-stabilized loess was approximately 0.7 kN/m$^3$ higher than the unstabilized loess. The compaction delay for the cement and fly ash-stabilized samples was generally less than 30 minutes.

The moisture content limits to ensure achievement of the maximum compressive strength for cement stabilized loess decreased as the cement content increased. For example, the range of moisture contents needed to obtain the maximum compressive strength for a 3% cement loess mixture was about 9%, whereas a 13% cement loess mixture requires a moisture content range of about 2% to reach the maximum compressive strength. The compressive strength varied more for higher cement contents compared to lower cement contents, due to the differences in the target moisture content limits. For example, the coefficient of variation for the strength of a 3% cement loess mixture was 11.4% whereas it was 15.3% for a 13% cement loess mixture. Regression analysis showed that the compressive strength increased linearly as the stabilizer content increased, and is consistent with what others have found (e.g., Hausmann 1990). The compressive strength of vacuum saturated stabilized loess can be predicted from a linear relationship with the compressive strength of non-vacuum saturated samples. The vacuum saturated compressive strength was found to be approximately 60% of the non-vacuum saturated compressive strength, which shows that the stabilized loess mixtures are sensitive to saturation.

The loess 2-in. x 2-in. stabilized samples with the lowest initial moisture content before vacuum saturation showed the highest increase in moisture content after vacuum saturation. For example, cement and fly ash-stabilized samples showed increases in moisture content of up to 16.1% and 20.3%, respectively. Additionally, samples with the lowest initial moisture content typically had the highest final moisture content. Dempsey and Thompson (1973) found a 1:1 relationship between the moisture content measured after freeze-thaw cycling and the moisture content measured after vacuum saturation. The results found in this study along with those reported by Dempsey and Thompson (1973) show that the initial moisture content is important in determining how moisture conditions could change when exposed to frost action.

Bids were collected from local contractors to compare the costs associated with stabilizing soil with cement and fly ash. It was found that to reach a compressive strength of 850 kPa it would cost approximately $3.30 per square yard for cement versus $7.23 per square yard for fly ash. In addition to the cost difference, a larger amount of fly ash is needed compared to cement to meet the same compressive strength (e.g., 3% cement versus 20% fly ash).

### Freeze-Thaw and Wet-Dry Durability

Cement-stabilized loess samples that were tested according to ASTM D560-03 met the freeze-thaw durability criteria, which was provided by the Portland Cement Association (1992) and is based on the percent mass loss after 12 freeze-thaw cycles. Cement-stabilized samples from PA US-22 did not meet either the freeze-thaw or wet-dry criteria. Fly ash-stabilized loess samples and fly ash-stabilized IA I-29 samples did not endure the 12 cycle test duration.

## FROST-HEAVE AND THAW-WEAKENING TEST CONCLUSIONS

The results from this study show that the frost-heave rate is difficult to predict from the USCS classification. CL materials showed frost-heave rates between 4.3 and 12.4 mm/day; ML materials showed rates between 11.0 and 19.1 mm/day; SC materials showed rates between 7.9 and 13.1 mm/day; and samples with classifications from GM to GW had rates between 1.8 and 8.0 mm/day. The results show that not all granular materials are non-frost-susceptible. The frost-heave rate statistical analyses showed that the frost-heave rate of

untreated materials cannot be accurately predicted, but the accuracy does increase if the materials are divided into fine and coarse grained categories. However, the thawed CBR values of untreated materials can be predicted from the standard CBR values.

The frost-heave rates for 6 of the 8 samples with USCS classifications between GM and GW were higher during the first freeze than the second. A SP classified material also showed a decrease in heave-rate. The remaining 11 materials tested showed a higher heave rate during the second freeze compared to the first. Chamberlain (1986) also observed a decrease in heave rate from the first freeze to the second for granular materials.

Tester and Gaskin (1992) found that increased fines contents in limestone aggregate resulted in an increase in the frost- heave rate, but that was not found in this study. The fines content study performed on US-30 RPCC subbase included samples with 2.2% and 13.0% fines contents; however there was no change in the frost-heave rate with increasing fines contents.

The average frost-heave rate of cement-stabilized loess was 0 mm/day and seven of the eight cement-stabilized samples had CBR values over 100%. The cement-stabilized samples with low initial moisture contents showed moisture content changes of up to 15.8%, which shows that stabilized materials can become saturated and remain non-frost-susceptible. However, all four fly ash-stabilized loess samples heaved, with some samples heaving as much or more than unstabilized loess. Generally, the frost-heave rate decreased as the fly ash content increased and the CBR value increased as the fly ash content increased. Samples with a fly ash content of 10% had a frost-heave rate of 22.2 mm/day and a thawed CBR value of 5.0%. Whereas samples with a fly ash content of 20% had a frost-heave rate of 11.0 mm/day and a thawed CBR value of 25.5%.

The frost-heave rate COV values are between 4.5 and 30.4% and the post-test CBR COV values are between 5.5 and 44.0%. The COV values measured in this study are comparable to the results reported by Chamberlain (1986).

Of the 18 untreated materials, 16 showed an increase in moisture content after the frost-heave and thaw-weakening test. Of those 16 materials, 7 showed higher moisture contents at the top of the sample profiles. Of those 7 materials, 5 had a USCS classification between CL and SC, with the other two being SW-SM and GW classifications. So while materials with

higher fines contents are more likely to draw water to the top of the samples, it is possible for all material types.

## IN SITU TEST CONCLUSIONS

In situ tests were performed to observe seasonal stiffness changes of portland cement concrete (PCC) pavement systems. The k values that were backcalculated from FWD tests showed lower values during thawing periods compared to other times of the year. However, no signs of thaw-weakening were observed at the seven pavement sites, based on $D_0$ measurements. There was a noticeable difference in the $D_0$ measurements during frozen conditions compared to thawed conditions. The load transfer efficiency (LTE) values did not appear to be affected by seasonal stiffness changes.

Temperature probes beneath the bottom of the pavement were used to determine frost-penetration profiles. The frost-penetration profiles indicated whether the pavement foundation layers were frozen on the dates tested. It was found at the Plainfield, IA site that there were 46 freeze-thaw cycles at a depth of 0.025 m below the pavement bottom. The number of freeze-thaw cycles decreased until a depth of 0.45 m where there was only one freeze-thaw cycle measured.

## SUMMARY OF CONCLUSIONS

The first goal of the research was to provide guidance for the selection of pavement foundation materials based on their freeze-thaw durability. The second goal of the research was to better understand how pavement support conditions change on a seasonal basis. This research successfully addressed the two goals of the research. ASTM D5918-06 was found to be able to differentiate frost-susceptible materials from non-frost-susceptible materials and the in situ pavement testing results showed the variation in pavement stiffness throughout the year.

## RECOMMENDATIONS FOR FUTURE RESEARCH

- Perform frost-heave and thaw-weakening tests according to ASTM D5918 on more materials to better understand frost-heave variability.

- Compare laboratory frost-heave and thaw-weakening test results to in situ frost-heave and thaw-weakening measurements to validate the frost-susceptibility ratings found in ASTM D5918.
- Study the sensors and thermal boundary conditions used in the frost-heave and thaw-weakening test to determine what impact they have on the test results.
- Cure fly ash-stabilized samples for a longer period to determine if the compressive strength, freeze-thaw durability, wet-dry durability, or frost-susceptibility results improve.
- Perform frost-heave and thaw-weakening tests on cement-treated loess with cement contents lower than 3% to determine at what cement content/compressive strength the material will become susceptible to frost-heave.
- Determine the effectiveness of geofabric, fibers, and other chemical stabilizers, in addition to cement and fly ash, for decreasing frost-susceptibility.
- Expand the stabilization study to include materials from the base layer.
- Perform in situ testing more frequently during spring thawing periods, in an attempt to observe thaw-weakening behavior in PCC pavements and use sub-surface temperature probes to determine when in situ pavement tests should be performed.

## RECOMMENDATIONS FOR FUTURE PRACTICE

- Incorporate frost-heave and thaw-weakening tests early in the pavement design process to select materials with lower frost-susceptibility.

## WORKS CITED

AASHTO. (1993). AASHTO Guide for Design of Pavement Structures. American Association of State Highway and Transportation Officials, Washington, D.C.

American Concrete Pavement Association. (2008). Frost-susceptible soils. Concrete Pavement Technology Series.

Andersland, O.B., and Ladanyi, B. (2004). *Frozen ground engineering*, 2nd Ed., John Wiley and Sons, Inc., New Jersey.

ASTM. (2004). "Standard Test Method for Materials Finer than 75-µm (No. 200) Sieve in Mineral Aggregates by Washing." *Annual book of ASTM standards*, ASTM C117, West Conshohocken, PA.

ASTM. (2007). "Standard Test Method for Density, Relative Density (Specific Gravity) and Absorption of Coarse Aggregate." *Annual book of ASTM standards*, ASTM C127, West Conshohocken, PA.

ASTM. (2006). "Standard Test Method for Sieve Analysis of Fine and Coarse Aggregates." *Annual book of ASTM standards*, ASTM C136, West Conshohocken, PA.

ASTM. (1963). "Standard Test Method for Particle-Size Analysis of Soils." *Annual book of ASTM standards*, ASTM D422, West Conshohocken, PA.

ASTM. (2003). "Standard Test Methods for Wetting and Drying Compacted Soil-Cement Mixtures." *Annual book of ASTM standards*, ASTM D559, West Conshohocken, PA.

ASTM. (2003). "Standard Test Methods for Freezing and Thawing Compacted Soil-Cement Mixtures." *Annual book of ASTM standards*, ASTM D560, West Conshohocken, PA.

ASTM. (2007). "Standard Test Methods for Laboratory Compaction Characteristics of Soil Using Standard Effort." *Annual book of ASTM standards*, ASTM D698, West Conshohocken, PA.

ASTM. (2006). "Standard Test Methods for Specific Gravity of Soil Solids by Water Pycnometer." *Annual book of ASTM standards*, ASTM D854, West Conshohocken, PA.

ASTM. (2007). "Standard Test Method for CBR (California Bearing Ratio) of Laboratory-Compacted Soils." *Annual book of ASTM standards*, ASTM D1883, West Conshohocken, PA.

ASTM. (2006). "Standard Practice for Classification of Soils for Engineering Purposes (Unified Soil Classification System)." *Annual book of ASTM standards*, ASTM D2487, West Conshohocken, PA.

ASTM. (1993). "Standard Practice for Classification of Soils and Soil-Aggregate Mixtures for Highway Construction Purposes." *Annual book of ASTM standards*, ASTM D3282, West Conshohocken, PA.

ASTM. (2000). "Standard Test Methods for Maximum Index Density and Unit Weight of Soils Using a Vibratory Table." *Annual book of ASTM standards*, ASTM D4253, West Conshohocken, PA.

ASTM. (2000). "Standard test Methods for Minimum Index Density and Unit Weight of Soils and Calculation of Relative Density." *Annual book of ASTM standards*, ASTM D4254, West Conshohocken, PA.

ASTM. (2005). "Standard Test Methods for Liquid Limit, Plastic Limit, and Plasticity Index of Soils." *Annual book of ASTM standards*, ASTM D4318, West Conshohocken, PA.

ASTM. (2006). "Standard Test Methods for Frost Heave and Thaw Weakening Susceptibility of Soils." *Annual book of ASTM standards*, ASTM D5918, West Conshohocken, PA.

ASTM. (2003). "Standard Test Method for Use of the Dynamic Cone Penetrometer in Shallow Pavement Applications." *Annual book of ASTM standards*, ASTM D6951, West Conshohocken, PA.

Benkelman, A., and Olmstead, F. (1931). "A New Theory of Frost Heaving." *Highway Research Board, Proceedings*, Vol. 11, 152–165.

Beskow, G. (1935, 1991). "Soil Freezing and Frost Heaving with Special Applications to Roads and Railroads," in *Historical Perspectives in Frost Heave Research: The Early Works of S. Taber and G. Beskow*. Eds. Black, P.B., and Hardenberg, M.J. 37–158.

Bigl, S. R., and Berg, R. L. (1996). *Testing of materials from the Minnesota cold regions pavement research test facility*. CRREL Special Report 96–20, Hanover, NH.

Brandl,H. (2008). "Freezing-thawing behavior of soils and unbound road layers." Slovak Journal of Civil Engineering. 3. 4–12.

Cassagrande, A., Taber, S., and Watkins, W. (1931). "Discussion of Frost Heaving." *Highway Research Board, Proceedings*, Vol. 11, 165–177.

Chamberlain, E. J. (1986). Evaluation of selected frost-susceptibility test methods. U.S. Army Cold Regions Research and Engineering Laboratory Report 86–14.

Chamberlain, E. J. (1981). Frost Susceptibility of soil: Review of index tests. U.S. Army Cold Regions Research and Engineering Laboratory Monograph 81–02.

Chamberlain, E.J., Janoo, V.C., and Ketcham, S.A. (1996). "Material properties, specification and testing for pavements in cold regions," in *Roads and airfields in cold regions*. Ed. T.S. Vinson, J.W. Rooney, W.H. Haas. 289–318.

Christopher, B. R., Schwartz, C., and Boudreau, R. (2006). *Geotechnical aspects of pavement. FHWA NHI–05–037*. National Highway Institute, Federal Highway Administration, U.S. Department of Transportation, Washington, D.C.

Dempsey, B. J., and Thompson, M. R. (1973). Vacuum Saturation Method for Predicting Freeze-Thaw Durability of Stabilized Materials. University of Illinois, Urbana-Champaign, IL.

Drumm, E. C., and Meier, R. (2003). *LTPP data analysis: daily and seasonal variations in insitu material properties*. Prepared for National Cooperative Highway Research Program. Transportation Research Board. The University of Tennessee, Knoxville, TN.

Edgers, L., Bedingfield, L., and Bono, N. (1988). "Field evaluation of criteria for frost susceptibility of soils." Transportation Research Record. 1190. Transportation Research Board, Washington, D.C. 73–85.

FHWA. (2000). "LTPP Manual for Falling Weight Deflectometer Measurements Operational Field Guidelines: Version 3.1." Long Term Pavement Performance Program, Pavement Performance Division, U.S. Department of Transportation. McLean, VA.

Freund, R., R. Littell, and L. Creighton. (2003). Regression Using JMP®. SAS Institute and Wiley, Cary, NC.

Guthrie, W.S., Lay, R.D., and Birdsall, A.J. (2007). "Effect of reduced cement contents on frost heave of silty soil: laboratory testing and numerical modeling." Proceedings, Transportation Research Board 86th Annual Meeting. Paper No. 07-2999. Transportation Research Board, Washington, D.C.

Hausmann, M. R. (1990). *Engineering principles of ground modification*,: McGraw-Hill, New York.

Henry, K.S., and Holtz, R.D. (2003) "Simulating soil freezing conditions in the laboratory," in *Permafrost.* Ed. M. Phillips., S.M. Springman., L.U. Arenson. 377–382.

Iowa Department of Transportation Office of Materials (2010). Milepost Book. Iowa Department of Transportation. Accessed September 13, 2012. http://www.iowadot.gov/materials/MilepostBook.pdf

Iowa State Environmental Mesonet (2012). RWIS Soil Probe Download. Iowa State University Department of Agronomy. Accessed October 5, 2012. http://mesonet.agron.iastate.edu/request/rwis/soil.phtml.

Janoo, V. C., Barna, L. A., and Orchino, S. A. (1997). Frost-susceptibility testing and predictions for the Raymark superfund site. CRREL Special Report 97–31, Hanover, NH.

Janoo, V. C., and Berg, R. L. (1996). *PCC airfield pavement response during thaw-weakening periods, A field study.* CRREL Special Report 96–12, Hanover, NH.

Johnson, T. C., Berg, R. L., Chamberlain, E. J., and Cole, D. M. (1986). Frost action predictive techniques for roads and airfields: A comprehensive survey of research findings. U.S. Army Cold Regions Research and Engineering Laboratory Report 86–18.

Joint Departments of the Army and Air Force USA. (1994). Soil Stabilization for Pavements. Technical Manual TM 5–822–14/AFJMAN 32–1019. Washington, D.C. U.S. Government Printing Office.

Joint Departments of the Army and Air Force USA. (1985). Pavement Design for Seasonal Frost Conditions. Technical Manual TM 5–818–2/AFM 88–6, Chapter 4. Washington, D.C. U.S. Government Printing Office.

Jong, D. T., Bosscher, P.J., and Benson, C.H. (1998). "Field assessment of changes in pavement moduli caused by freezing and thawing." Transportation Research Record. 1615. Transportation Research Board, Washington, D.C. 275–284.

Kaplar, C. W. (1970). "Phenomenon and Mechanism of Frost Heaving." Highway Research Record. 304. Transportation Research Board, Washington, D.C. 1–13.

Kestler, M.A. (2003). "Techniques for extending the life of low-volume roads in seasonal frost areas." Transportation Research Record. 1819. Transportation Research Board, Washington, D.C. 275–284.

Konrad, J.M., and Lemieux, N. (2005). "Influence of fines on frost heave characteristics of a well-graded base-course material." *Canadian Geotechnical Journal*, 42(2), 515–527.

Lukanen, E. O., Worel, B. J., and Clyne, T. (2006). "MnROAD Environmental Factors that Affect Ride." Proceedings of the 13th International Conference on Cold Regions Engineering. Ed. M. Davies, J.E. Zufelt, July 23–26, Orono, Maine.

McCracken, J.K. (2008). "Seasonal analysis of the response of jointed plain concrete pavements to FWD and truck loads." M.S. Thesis, University of Pittsburg, Pittsburgh, Pennsylvania.

Miller, R. D. (1978). "Frost Heaving in Non-Colloidal Soils," in *Proceedings of the Third International Conference on Permafrost*. Edmonton, Alberta, Canada, July 10–13, 1978. Vol. 1. Ottawa: National Research Council of Canada, 708–713.

Miller, R. D. (1972). "Freezing and Heaving of Saturated and Unsaturated Soils." Highway Research Record. 393. Transportation Research Board, Washington, D.C. 1–11.

National Cooperative Highway Research Program (NCHRP). (2004). "Guide for Mechanistic-Empirical Design of New and Rehabilitated Pavement Structures." NCHRP Final Report for NCHRP 1–37A Project, Washington, D.C. http://onlinepubs.trb.org/onlinepubs/archive/mepdg/guide.htm (accessed August 24, 2012).

Newcomb, D. E., and Birgisson, B. (1999). *NCHRP Synthesis of Highway Practice 278: Measuring In Situ Mechanical Properties of Pavement Subgrade Soils*. Transportation Research Board, National Research Council, Washington D.C., 1999. 43–51.

O'Flaherty, C. A., Edgar, C. E., and Davidson, D. T. (1963). "The Iowa State Compaction Apparatus: A Small Sample Apparatus for Use in Obtaining Density and Strength Measurements of Soils and Soil-Additives." Presented at the 42nd Annual Meeting of the Highway Research Board, Washington, D.C., January.

Penner, E. (1966). "Frost-Heaving in Soils." National Research Council, Canada. Research Paper No. 295 of the Division of Building Research. Reprinted from Proceedings: Permafrost International Conference, November 1963, 197–202.

Penner, E. (1959). "The Mechanism of Frost Heaving in Soils." Highway Research Board Bulletin. 225. 1–22.

Portland Cement Association. (1992). Soil-Cement Laboratory Handbook. Portland Cement Association, Skokie, Ill.

Saarenketo, T., and Saara, A. (2005). *Managing spring thaw weakening on low volume roads – problem description, load restriction policies, monitoring and rehabilitation.* Final report 2_3 Roadex II Project. Roadscanners.

Salour, F., and Erlingsson, S. (2012). *Pavement structural behavior during spring thaw*. The Swedish National Road and Transport Research Institute, VTI Report 738A.

Schmalzer, P.N. (2006). *LTPP Manual for Falling Weight Deflectometer Measurements – Version 4.1.* Report No. FHWA-HRT-06-132, Federal Highway Administration, McLean, VA.

Shihata, S. A., and Baghdadi, Z. A. (2001). Simplified method to assess freeze-thaw durability of soil cement. Journal of Materials in Civil Engineering, 13(4), 243–247.

Simonsen, E., and Isacsson, U. (1999). "Thaw weakening of pavement structures in cold regions." Cold Regions Science and Technology. 29(2), 135–151.

Spizziri, M. (2012). "Boosting fuel economy where the rubber meets the road." Engineering News-Record.com. October 15, 2012. http://enr.construction.com/products/materials/2012/1015-boosting-fuel-economy-where-the-rubber-meets-the-road.asp (accessed October 30, 2012).

Svec, O.J. (1989). A new concept of frost-heave characteristics of soils. Cold Regions Science and Technology. 16(3), 271–279.

Taber, S. (1929). "Frost Heaving." *Journal of Geology*, Vol. 37, No. 5 (Jul.–Aug., 1929), 428–461.

Tester, R. E., and Gaskin, P. N. (1992). "The effect of fines content on the frost susceptibility of a crushed limestone." 45th Canadian Geotechnical Conference, Toronto, Ontario, October 26–28, 53.1–53.7.

Tighe, S.L., Mills, B., Haas, C.T., and Baiz, S. (2007). *Using road weather information systems (RWIS) to control load restrictions on gravel and surface-treated highways.* Ontario Ministry of Transportation Engineering Standards Branch Report, St. Catharines, Ontario, Canada.

Vandenbossche , J.M.(2005). "Effects of slab temperature profiles on the use of falling weight deflectometer data to monitor joint performance and detect voids." Transportation Research Record No. 2005, Transportation Research Board, Washington, D.C., 75-85.

Wolfe, A.J. (2011). "Behavior of composite pavement foundation materials subjected to cyclic loading." M.S. Thesis, Iowa State University, Ames, IA.

# APPENDIX A. ADDITIONAL 2-IN. X 2-IN. STATISTICAL ANALYSIS

This section presents detailed results of the linear and multiple linear regression analyses performed on the 2-in. x 2-in. stabilized loess samples.

## LINEAR REGRESSION ANALYSES

### Cement UCS and Stabilizer Content Linear Regression

#### Bivariate Fit of Shear Stress By Stabilizer Content

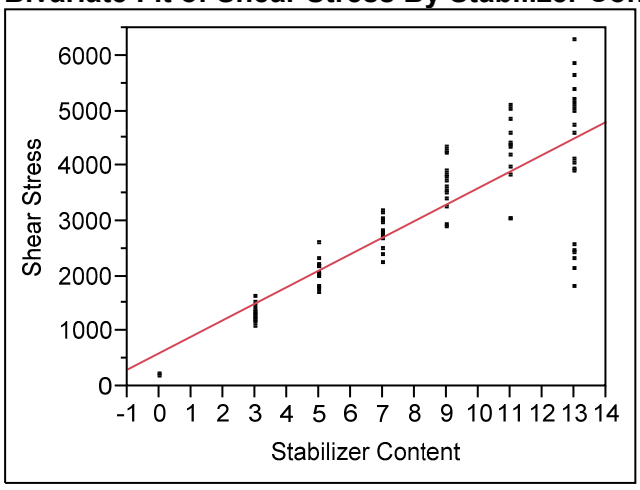


#### Linear Fit

Shear Stress = 608.27697 + 299.49771*Stabilizer Content

#### Summary of Fit

| | |
|---|---|
| RSquare | 0.694668 |
| RSquare Adj | 0.69152 |
| Root Mean Square Error | 752.0876 |
| Mean of Response | 3022.41 |
| Observations (or Sum Wgts) | 99 |

#### Analysis of Variance

| Source | DF | Sum of Squares | Mean Square | F Ratio |
|---|---|---|---|---|
| Model | 1 | 124828220 | 124828220 | 220.6866 |
| Error | 97 | 54866668 | 565635.75 | **Prob > F** |
| C. Total | 98 | 179694887 | | <.0001* |

#### Parameter Estimates

| Term | Estimate | Std Error | t Ratio | Prob>\|t\| |
|---|---|---|---|---|
| Intercept | 608.27697 | 179.2266 | 3.39 | 0.0010* |
| Stabilizer Content | 299.49771 | 20.1607 | 14.86 | <.0001* |

## Fly Ash UCS and Stabilizer Content Linear Regression

### Bivariate Fit of Shear Stress By Stabilizer Content

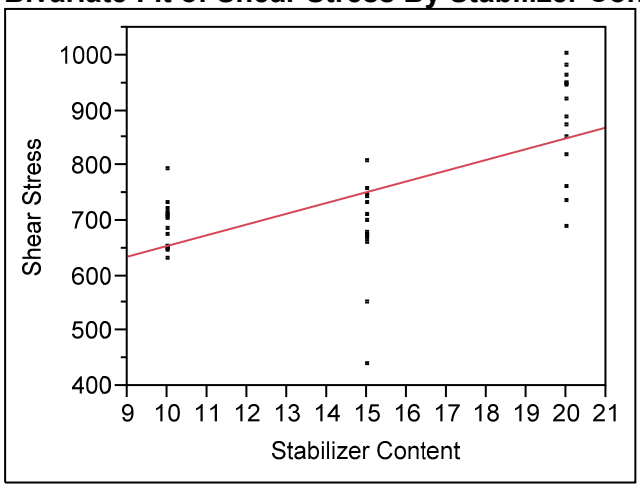


### Linear Fit

Shear Stress = 459.33609 + 19.518614*Stabilizer Content

### Summary of Fit

| | |
|---|---|
| RSquare | 0.431836 |
| RSquare Adj | 0.418623 |
| Root Mean Square Error | 93.50246 |
| Mean of Response | 752.1153 |
| Observations (or Sum Wgts) | 45 |

### Analysis of Variance

| Source | DF | Sum of Squares | Mean Square | F Ratio |
|---|---|---|---|---|
| Model | 1 | 285732.21 | 285732 | 32.6823 |
| Error | 43 | 375936.50 | 8743 | **Prob > F** |
| C. Total | 44 | 661668.71 | | <.0001* |

### Parameter Estimates

| Term | Estimate | Std Error | t Ratio | Prob>\|t\| |
|---|---|---|---|---|
| Intercept | 459.33609 | 53.07632 | 8.65 | <.0001* |
| Stabilizer Content | 19.518614 | 3.414227 | 5.72 | <.0001* |

## Cement Vacuum Saturated UCS and UCS Linear Regression

### Bivariate Fit of Cement V.S. UCS By Cement UCS

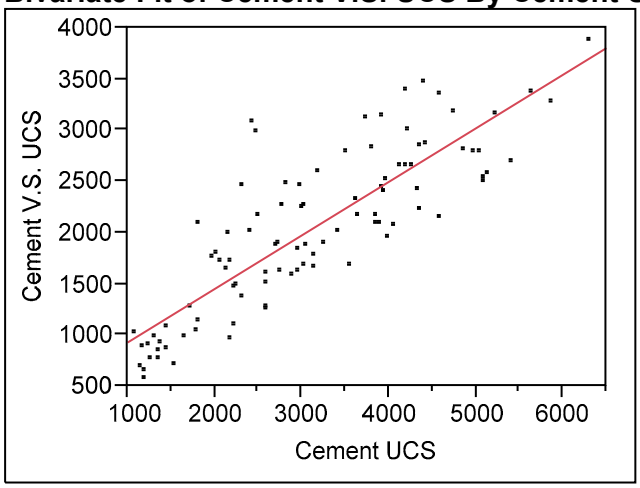


### Linear Fit

Cement V.S. UCS = 401.53269 + 0.523292*Cement UCS

### Summary of Fit

| | |
|---|---|
| RSquare | 0.716453 |
| RSquare Adj | 0.713437 |
| Root Mean Square Error | 422.7921 |
| Mean of Response | 2029.295 |
| Observations (or Sum Wgts) | 96 |

### Analysis of Variance

| Source | DF | Sum of Squares | Mean Square | F Ratio |
|---|---|---|---|---|
| Model | 1 | 42456535 | 42456535 | 237.5149 |
| Error | 94 | 16802798 | 178753.17 | **Prob > F** |
| C. Total | 95 | 59259334 | | <.0001* |

### Parameter Estimates

| Term | Estimate | Std Error | t Ratio | Prob>\|t\| |
|---|---|---|---|---|
| Intercept | 401.53269 | 114.0945 | 3.52 | 0.0007* |
| Cement UCS | 0.523292 | 0.033955 | 15.41 | <.0001* |

## Fly Ash Vacuum Saturated UCS and UCS Linear Regression

### Bivariate Fit of Fly Ash V.S. UCS By Fly Ash UCS

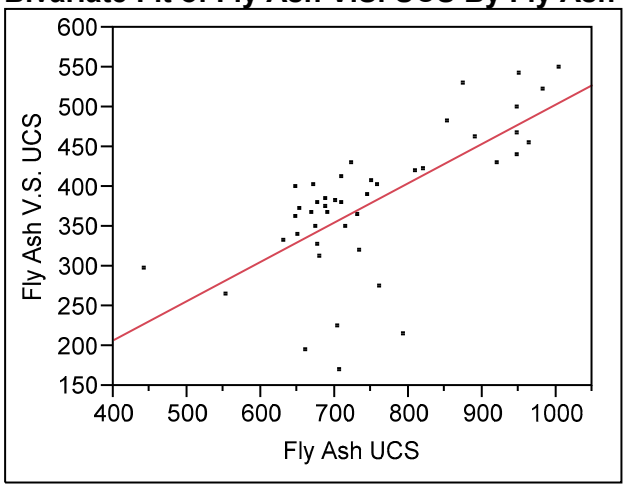


### Linear Fit

Fly Ash V.S. UCS = 10.67238 + 0.4927775*Fly Ash UCS

### Summary of Fit

| | |
|---|---|
| RSquare | 0.47746 |
| RSquare Adj | 0.465018 |
| Root Mean Square Error | 64.69076 |
| Mean of Response | 381.4869 |
| Observations (or Sum Wgts) | 44 |

### Analysis of Variance

| Source | DF | Sum of Squares | Mean Square | F Ratio |
|---|---|---|---|---|
| Model | 1 | 160602.07 | 160602 | 38.3766 |
| Error | 42 | 175765.58 | 4185 | **Prob > F** |
| C. Total | 43 | 336367.65 | | <.0001* |

### Parameter Estimates

| Term | Estimate | Std Error | t Ratio | Prob>\|t\| |
|---|---|---|---|---|
| Intercept | 10.67238 | 60.64743 | 0.18 | 0.8612 |
| Fly Ash UCS | 0.4927775 | 0.079546 | 6.19 | <.0001* |

## Combined Cement and Fly Ash Vacuum Saturated UCS and UCS Linear Regression

### Bivariate Fit of Cement and Fly Ash V.S. UCS By Cement and Fly Ash UCS

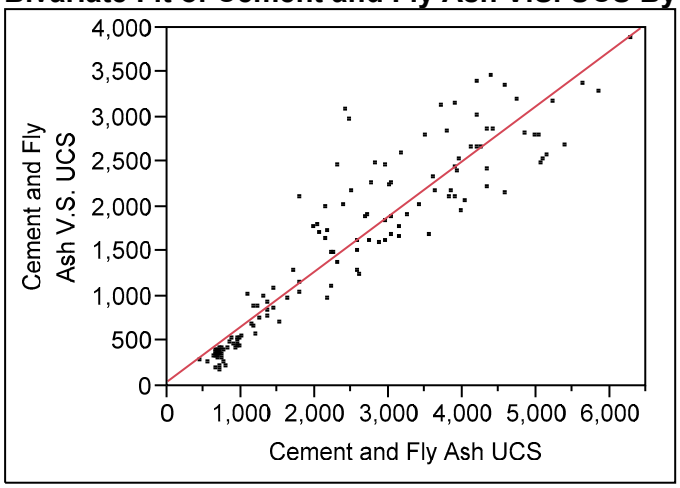


### Linear Fit

Cement and Fly Ash V.S. UCS = 55.955437 + 0.6142476*Cement and Fly Ash UCS

### Summary of Fit

| | |
|---|---|
| RSquare | 0.862422 |
| RSquare Adj | 0.861426 |
| Root Mean Square Error | 375.6142 |
| Mean of Response | 1511.412 |
| Observations (or Sum Wgts) | 140 |

### Analysis of Variance

| Source | DF | Sum of Squares | Mean Square | F Ratio |
|---|---|---|---|---|
| Model | 1 | 122049427 | 122049427 | 865.0707 |
| Error | 138 | 19469877 | 141086.06 | **Prob > F** |
| C. Total | 139 | 141519304 | | <.0001* |

### Parameter Estimates

| Term | Estimate | Std Error | t Ratio | Prob>\|t\| |
|---|---|---|---|---|
| Intercept | 55.955437 | 58.7922 | 0.95 | 0.3429 |
| Cement and Fly Ash UCS | 0.6142476 | 0.020884 | 29.41 | <.0001* |

## MULTIPLE LINEAR REGRESSION ANALYSES

The variables used in the simple multiple linear regression analysis for the cement and fly ash stabilizers were chosen to demonstrate which variables are important in predicting the

UCS. However, by adding more variables and including second order variables it is possible to increase the fit of the multiple linear regression model.

A stepwise regression was performed to choose variables that would be significant in predicting the UCS of cement and fly ash stabilized soils. A forward selection process was used, which starts with no variables in the model. Each variable is added one at a time to determine if it improves the fit of the model. The Bayesian information criterion was used. The variables considered in the cement and fly ash models were:

- Stabilizer content
- Moisture content
- Dry unit weight
- Void ratio
- Saturation
- Compaction delay
- Stabilizer content x moisture content
- Stabilizer content x dry unit weight
- Stabilizer content x void ratio
- Stabilizer content x saturation
- Stabilizer content x compaction delay
- Stabilizer content x stabilizer content
- Moisture content x moisture content
- Moisture content x dry unit weight
- Moisture content x saturation
- Moisture content x compaction delay
- Dry unit weight x dry unit weight
- Dry unit weight x void ratio
- Dry unit weight x saturation
- Dry unit weight x compaction delay
- Void ratio x void ratio
- Void ratio x saturation

- Void ratio x compaction delay
- Saturation x saturation
- Saturation x compaction delay
- Compaction delay x compaction delay

The following were determined to be important for predicting the cement UCS:

- Stabilizer contet
- Moisture content
- Void ratio
- Saturation
- Compaction delay
- Moisture content x moisture content
- Stabilizer content x moisture content
- Stabilizer content x stabilizer content
- Void ratio x saturation
- Stabilizer content x compaction delay
- Moisture content x compaction delay

These variables resulted in a high $R^2$ (0.89), however the VIF values were high. If the saturation variables were removed, the resulting $R^2$ was found to be 0.87 and all the VIF values below 4.09.

The following variables were determined to be important for predicting the fly ash UCS:

- Stabilizer content
- Moisture content
- Dry unit weight
- Saturation
- Compaction delay
- Moisture content x dry unit weight
- Dry unit weight x dry unit weight
- Saturation x saturation
- Moisture content x saturation

- Stabilizer content x stabilizer content
- Stabilizer content x compaction delay

The variables in this model resulted in a $R^2$ value of 0.97, however the VIF values were high. The saturation variables, void ratio variables, and moisture content x moisture content variables were removed. This resulted in a $R^2$ value of 0.95 with VIF values less than 5.6.

### Cement UCS Predicted by Simpler Multiple Linear Regression (model presented in results)

**Response Shear Stress**
**Whole Model**
**Actual by Predicted Plot**

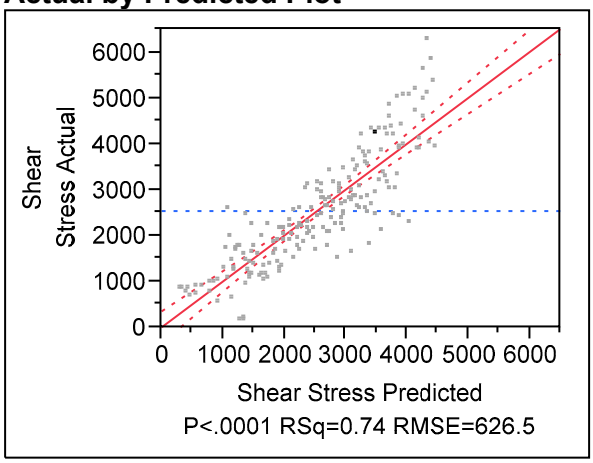


**Summary of Fit**

| | |
|---|---|
| RSquare | 0.740173 |
| RSquare Adj | 0.734703 |
| Root Mean Square Error | 626.5044 |
| Mean of Response | 2533.492 |
| Observations (or Sum Wgts) | 195 |

**Analysis of Variance**

| Source | DF | Sum of Squares | Mean Square | F Ratio |
|---|---|---|---|---|
| Model | 4 | 212447423 | 53111856 | 135.3142 |
| Error | 190 | 74576464 | 392507.71 | **Prob > F** |
| C. Total | 194 | 287023887 | | <.0001* |

**Parameter Estimates**

| Term | Estimate | Std Error | t Ratio | Prob>\|t\| | VIF |
|---|---|---|---|---|---|
| Intercept | -3710.504 | 1713.762 | -2.17 | 0.0316* | . |
| Stabilizer Content | 227.43523 | 12.87096 | 17.67 | <.0001* | 1.0911724 |
| Moisture Content | -72.30406 | 12.11396 | -5.97 | <.0001* | 1.5831753 |
| Dry Unit Weight | 398.8796 | 105.6393 | 3.78 | 0.0002* | 1.0184444 |
| Compaction Delay | -41.78607 | 8.36859 | -4.99 | <.0001* | 1.6740452 |

**Residual by Predicted Plot**

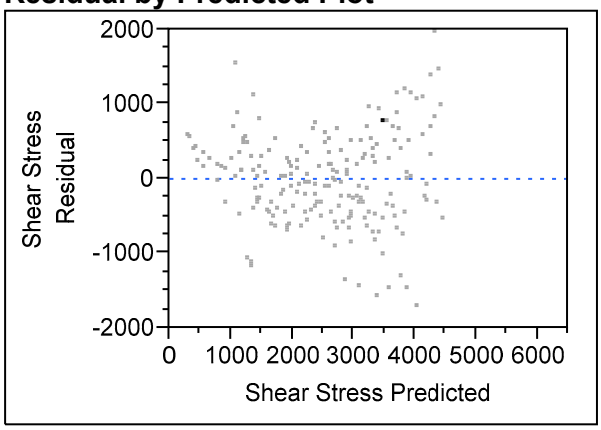


**Prediction Expression**

-3710.5043804388
+227.43523121757*Stabilizer Content
+-72.304056501926*Moisture Content
+398.879603291039*Dry Unit Weight
+-41.78607458012*Compaction Delay

## Cement UCS Predicted by Full Multiple Linear Regression

**Response Shear Stress**
**Whole Model**
**Actual by Predicted Plot**

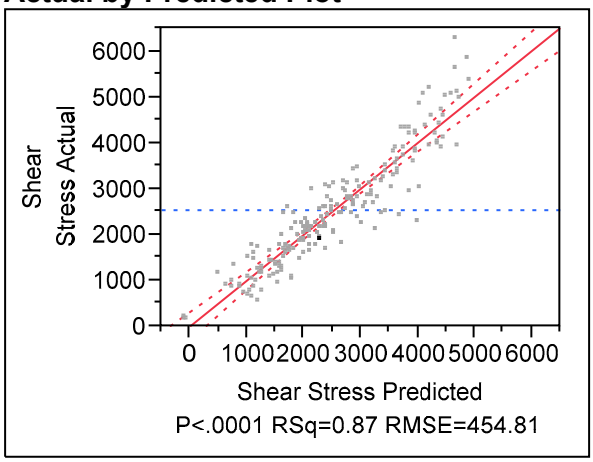


**Summary of Fit**

| | |
|---|---|
| RSquare | 0.866672 |
| RSquare Adj | 0.860186 |
| Root Mean Square Error | 454.8136 |
| Mean of Response | 2533.492 |
| Observations (or Sum Wgts) | 195 |

**Analysis of Variance**

| Source | DF | Sum of Squares | Mean Square | F Ratio |
|---|---|---|---|---|
| Model | 9 | 248755639 | 27639515 | 133.6176 |

| Source | DF | Sum of Squares | Mean Square | F Ratio |
|---|---|---|---|---|
| Error | 185 | 38268249 | 206855.4 | Prob > F |
| C. Total | 194 | 287023887 | | <.0001* |

## Lack Of Fit

| Source | DF | Sum of Squares | Mean Square | F Ratio |
|---|---|---|---|---|
| Lack Of Fit | 184 | 38267632 | 207976 | 337.3145 |
| Pure Error | 1 | 617 | 617 | Prob > F |
| Total Error | 185 | 38268249 | | 0.0434* |
| | | | | Max RSq |
| | | | | 1.0000 |

## Parameter Estimates

| Term | Estimate | Std Error | t Ratio | Prob>\|t\| |
|---|---|---|---|---|
| Intercept | 3350.843 | 744.4423 | 4.50 | <.0001* |
| Stabilizer Content | 216.89122 | 9.507542 | 22.81 | <.0001* |
| Moisture Content | -92.04846 | 12.0939 | -7.61 | <.0001* |
| Void Ratio | 487.64171 | 1293.667 | 0.38 | 0.7066 |
| (Moisture Content-20.3695)*(Moisture Content-20.3695) | -16.82488 | 2.964679 | -5.68 | <.0001* |
| (Moisture Content-20.3695)*(Stabilizer Content-8.18462) | 0.2691902 | 3.133224 | 0.09 | 0.9316 |
| (Stabilizer Content-8.18462)*(Stabilizer Content-8.18462) | -17.17209 | 2.796746 | -6.14 | <.0001* |
| Compaction Delay | -51.52499 | 6.956429 | -7.41 | <.0001* |
| (Stabilizer Content-8.18462)*(Compaction Delay-12.4032) | -10.71164 | 1.578857 | -6.78 | <.0001* |
| (Moisture Content-20.3695)*(Compaction Delay-12.4032) | 6.4549876 | 2.037931 | 3.17 | 0.0018* |

## Residual by Predicted Plot

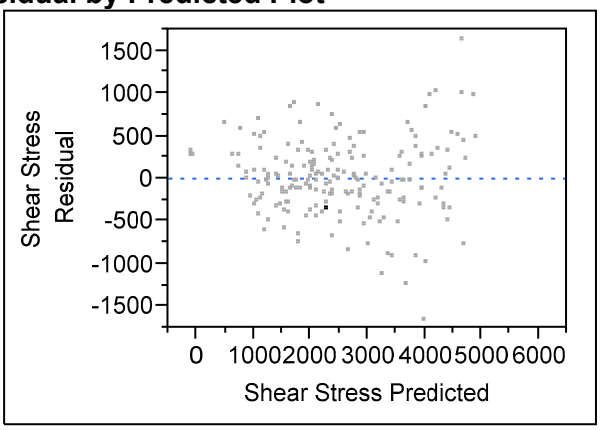

## Fly Ash UCS Predicted by Simpler Multiple Linear Regression (model presented in results)

**Response Shear Stress**
**Whole Model**
**Actual by Predicted Plot**

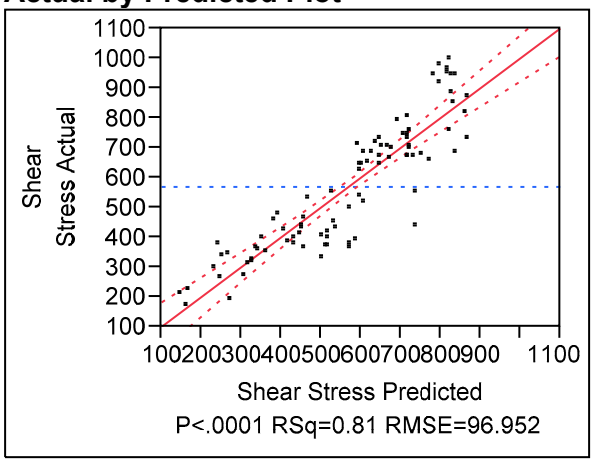


### Summary of Fit

| | |
|---|---|
| RSquare | 0.805238 |
| RSquare Adj | 0.795963 |
| Root Mean Square Error | 96.95189 |
| Mean of Response | 568.8833 |
| Observations (or Sum Wgts) | 89 |

### Analysis of Variance

| Source | DF | Sum of Squares | Mean Square | F Ratio |
|---|---|---|---|---|
| Model | 4 | 3264459.0 | 816115 | 86.8238 |
| Error | 84 | 789572.2 | 9400 | **Prob > F** |
| C. Total | 88 | 4054031.3 | | <.0001* |

### Parameter Estimates

| Term | Estimate | Std Error | t Ratio | Prob>\|t\| | VIF |
|---|---|---|---|---|---|
| Intercept | -1398.674 | 365.3395 | -3.83 | 0.0002* | . |
| Stabilizer Content | 18.729431 | 2.661502 | 7.04 | <.0001* | 1.1113487 |
| Moisture Content | -23.67774 | 2.134218 | -11.09 | <.0001* | 1.9164037 |
| Dry Unit Weight | 136.22623 | 22.6568 | 6.01 | <.0001* | 1.2598379 |
| Compaction Delay | -1.336093 | 2.045469 | -0.65 | 0.5154 | 2.2239209 |

**Residual by Predicted Plot**

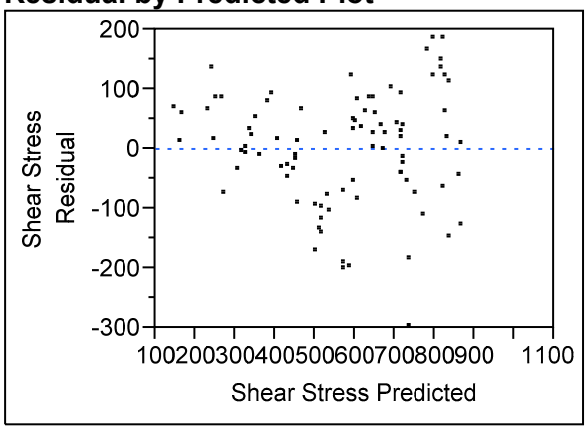


**Prediction Expression**

-1398.6742174283
+18.7294311413666*Stabilizer Content
+-23.677737814401*Moisture Content
+136.22622989422*Dry Unit Weight
+-1.3360927588604*Compaction Delay

## Fly Ash UCS Predicted by Full Multiple Linear Regression

**Response Shear Stress**
**Whole Model**
**Actual by Predicted Plot**

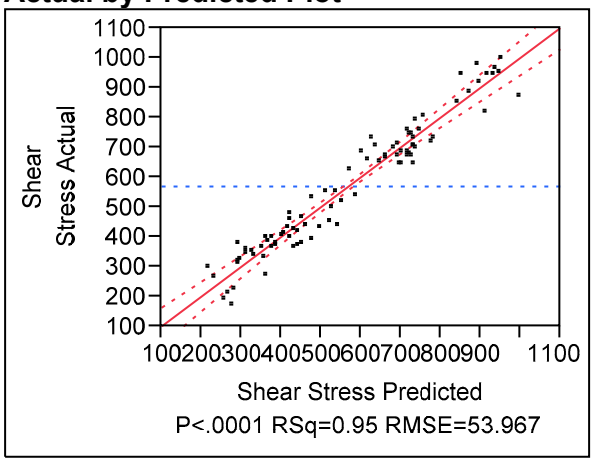


**Summary of Fit**

| | |
|---|---|
| RSquare | 0.945401 |
| RSquare Adj | 0.93678 |
| Root Mean Square Error | 53.96707 |
| Mean of Response | 568.8833 |
| Observations (or Sum Wgts) | 89 |

**Analysis of Variance**

| Source | DF | Sum of Squares | Mean Square | F Ratio |
|---|---|---|---|---|
| Model | 12 | 3832685.4 | 319390 | 109.6640 |

| Source | DF | Sum of Squares | Mean Square | F Ratio |
|---|---|---|---|---|
| Error | 76 | 221345.8 | 2912 | Prob > F |
| C. Total | 88 | 4054031.3 | | <.0001* |

## Parameter Estimates

| Term | Estimate | Std Error | t Ratio | Prob>\|t\| | VIF |
|---|---|---|---|---|---|
| Intercept | -1164.817 | 262.1988 | -4.44 | <.0001* | . |
| Stabilizer Content | 16.722817 | 1.675504 | 9.98 | <.0001* | 1.4214853 |
| Moisture Content | -28.56327 | 2.027894 | -14.09 | <.0001* | 5.5841199 |
| Dry Unit Weight | 130.08645 | 16.95955 | 7.67 | <.0001* | 2.2782494 |
| (Stabilizer Content-14.9438)*(Moisture Content-19.1965) | -0.217063 | 0.356786 | -0.61 | 0.5447 | 2.8549467 |
| (Stabilizer Content-14.9438)*(Dry Unit Weight-15.8555) | 9.1147529 | 3.747834 | 2.43 | 0.0174* | 1.7315138 |
| (Moisture Content-19.1965)*(Dry Unit Weight-15.8555) | -17.23991 | 3.443735 | -5.01 | <.0001* | 4.3294444 |
| (Dry Unit Weight-15.8555)*(Dry Unit Weight-15.8555) | -123.7104 | 31.08488 | -3.98 | 0.0002* | 1.8025734 |
| (Stabilizer Content-14.9438)*(Stabilizer Content-14.9438) | 3.6061309 | 0.652615 | 5.53 | <.0001* | 1.8190277 |
| Compaction Delay | -4.351555 | 1.693127 | -2.57 | 0.0121* | 4.9177602 |
| (Dry Unit Weight-15.8555)*(Compaction Delay-13.2734) | -8.354671 | 2.740162 | -3.05 | 0.0032* | 3.1366399 |
| (Stabilizer Content-14.9438)*(Compaction Delay-13.2734) | 0.2306975 | 0.336293 | 0.69 | 0.4948 | 3.8009948 |
| (Moisture Content-19.1965)*(Compaction Delay-13.2734) | -0.289358 | 0.192721 | -1.50 | 0.1374 | 1.6994608 |

## Residual by Predicted Plot

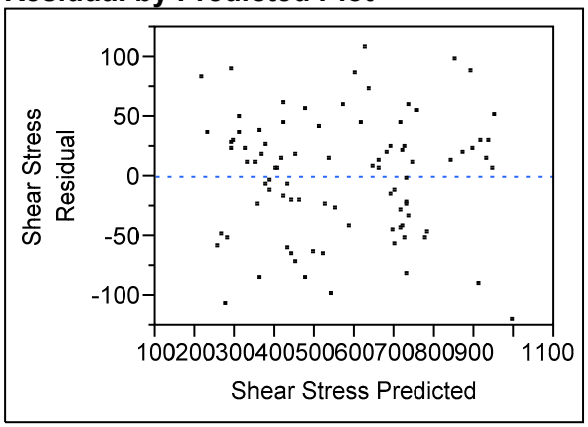

# APPENDIX B. FROST-HEAVE AND THAW-WEAKENING EQUIPMENT

The following section presents the measurement equipment used for the frost-heave and thaw-weakening test and the shop drawings used to manufacture the required components.

**Table 94. Frost-heave and thaw-weakening measurement equipment**

| Equipment | Quantity | Serial #s |
|---|---|---|
| Micro Epsilon optoNCDT1700 Tiggerbox ILD1700 | 3 | 0611030, 0611031, 0611011 |
| Micro Epsilon opto NCDT1700-50.0 mm Laser Optical Displacement Sensor | 3 | 0810055, 0807059, 0810054 |
| Micro Epsilon opto NCDT1302-50.0 Laser Optical Displacement Sensor | 1 | 1004153 |
| Wika Type A-10 Pressure Transducer, ¼" NPT connection, #13125983 | 4 | 110188O3, 1100W1I5, 110188O5, 110188O4 |
| Thermocouple wire, 24 gauge, Type-T, Polyvinyl insulation | — | — |
| A419 Johnson Controls Temperature Control Unit | 1 | — |
| PolyScience Model 9512 Water Bath with Programmable Temperature Controller | 2 | 1C1080033, 1C1080034 |
| iOtech Wavebook/516E-16-bit 1 MHz Data Acquisition System | 1 | 806438 |
| iOtech Personal DAQ/3000 series 16-bit/1-MHz USB Data Acquisition System | 1 | 330544 |
| iOtech PDQ30 Expansion Module | 1 | 347802 |
| DASYLab 9 Data Acquisition System | — | — |

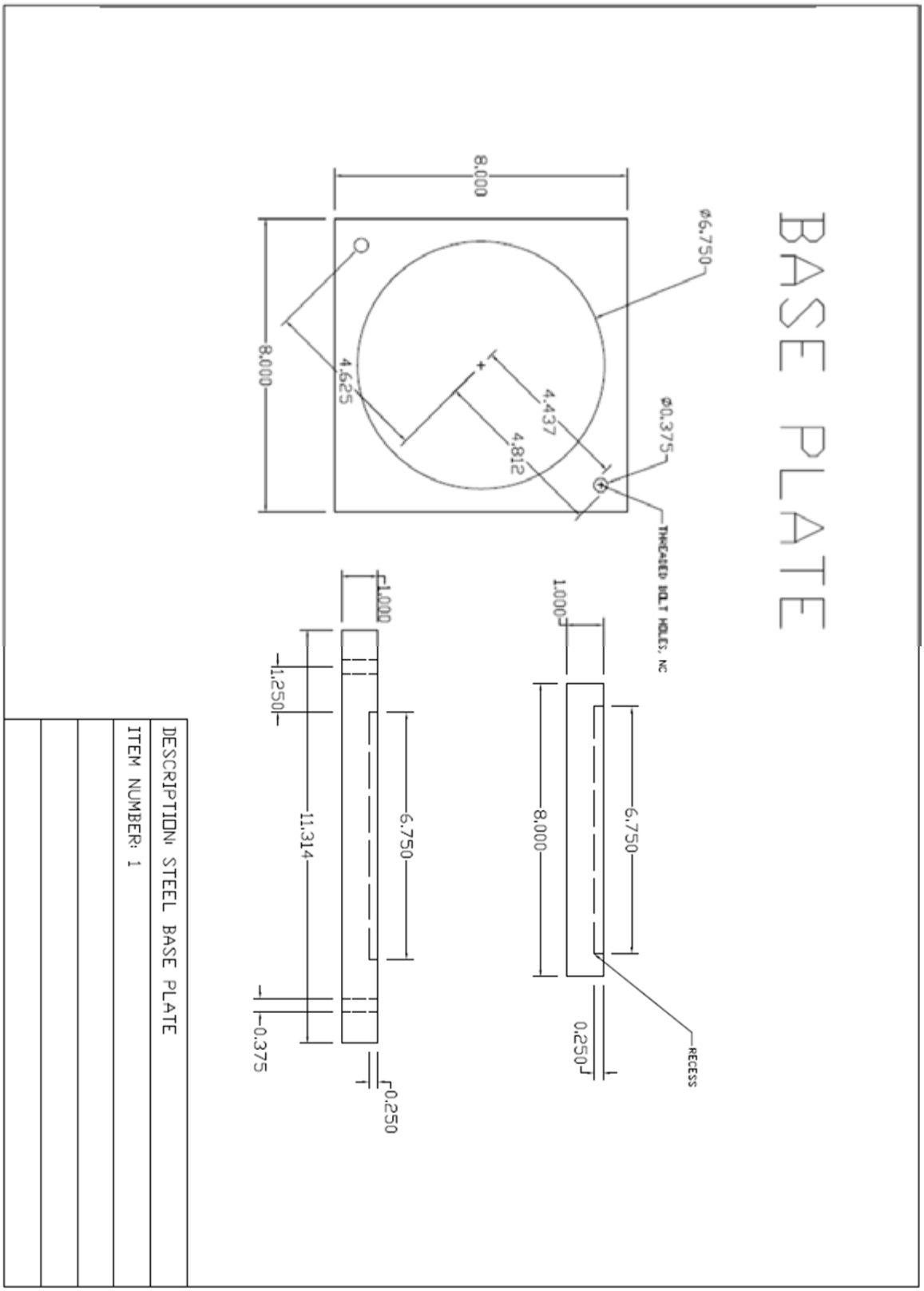


**Figure 255. Steel base plate for frost-heave and thaw-weakening test**

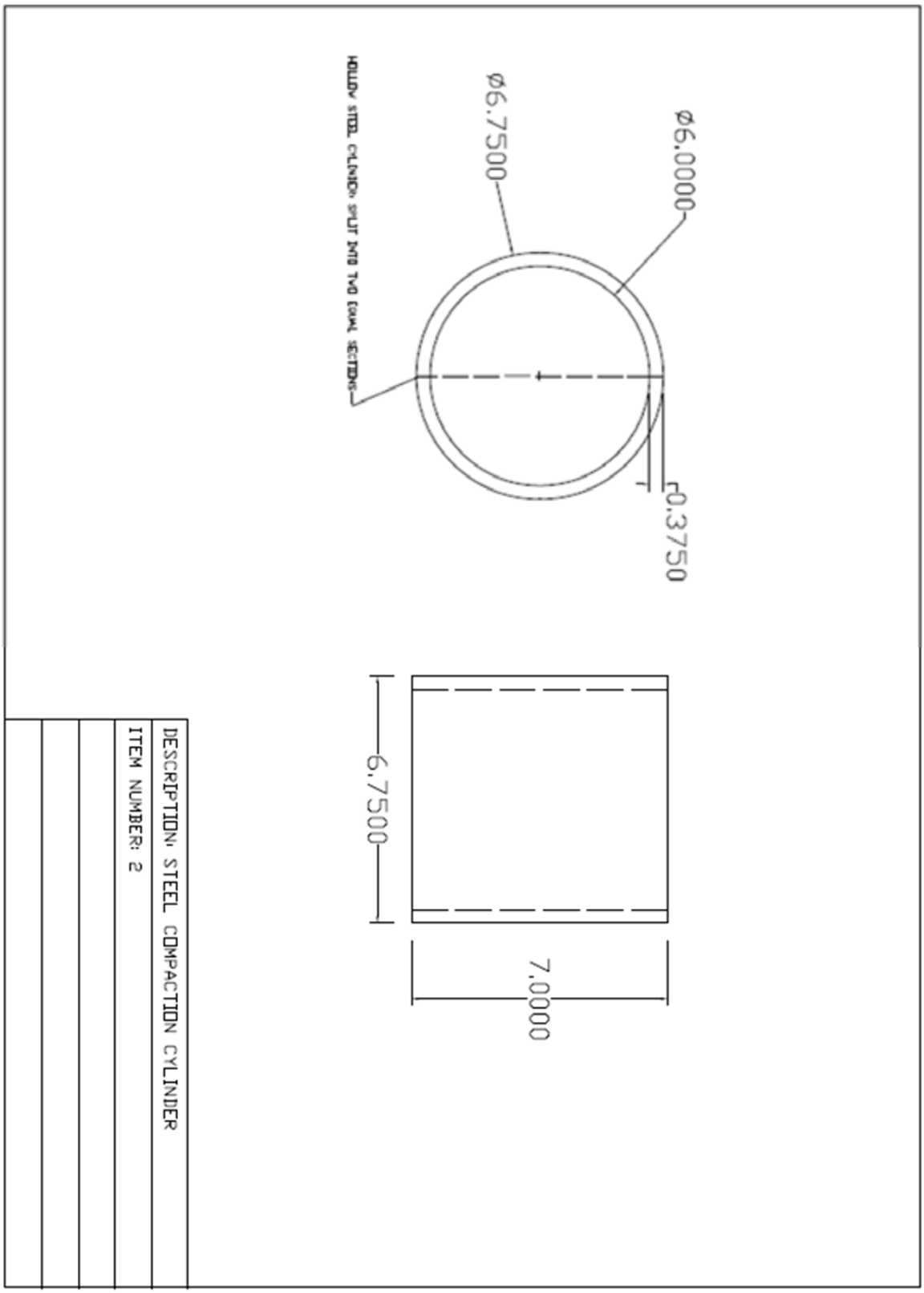


**Figure 256. Steel compaction cylinder for frost-heave and thaw-weakening test**

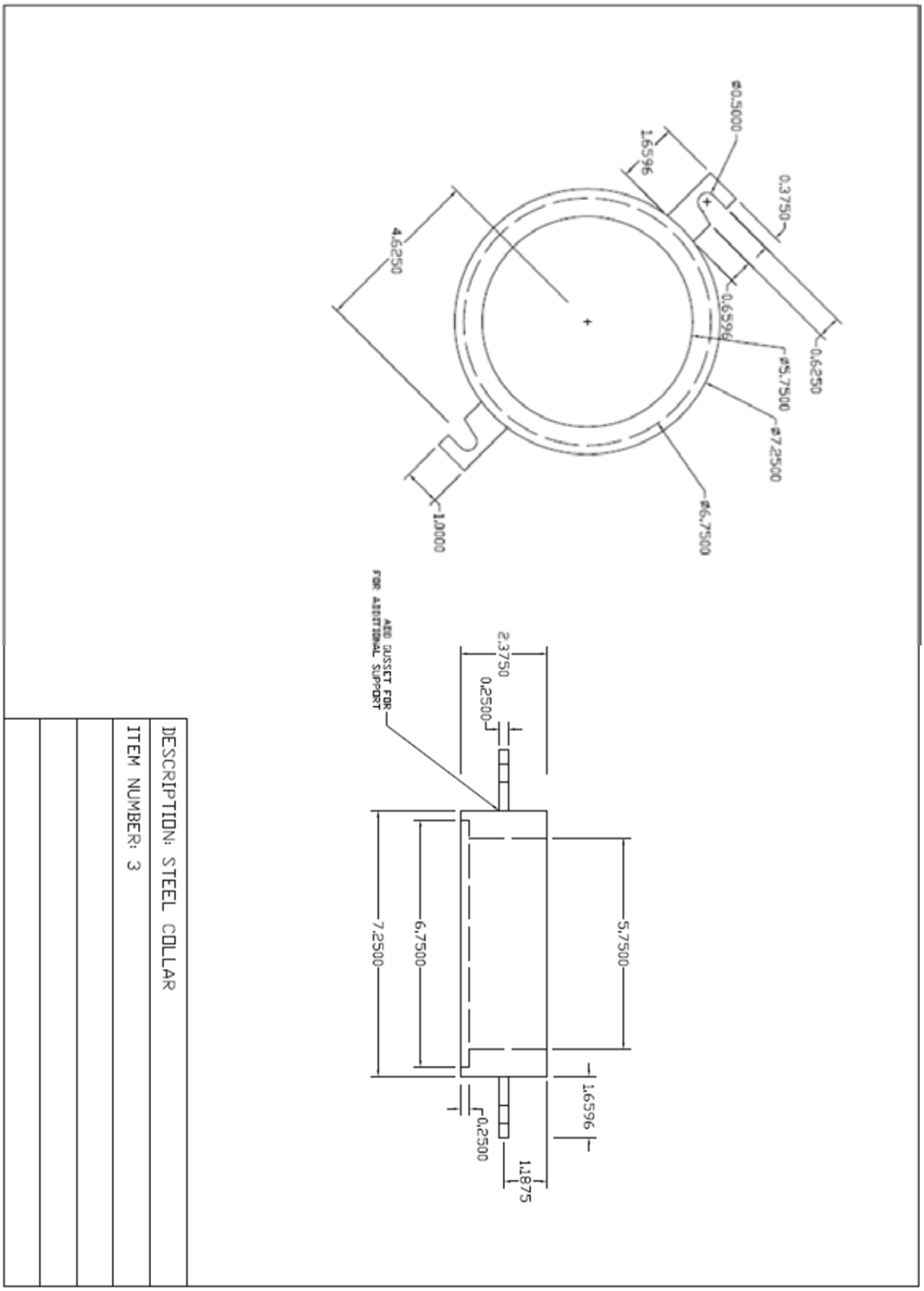


**Figure 257. Steel compaction collar for frost-heave and thaw-weakening test**

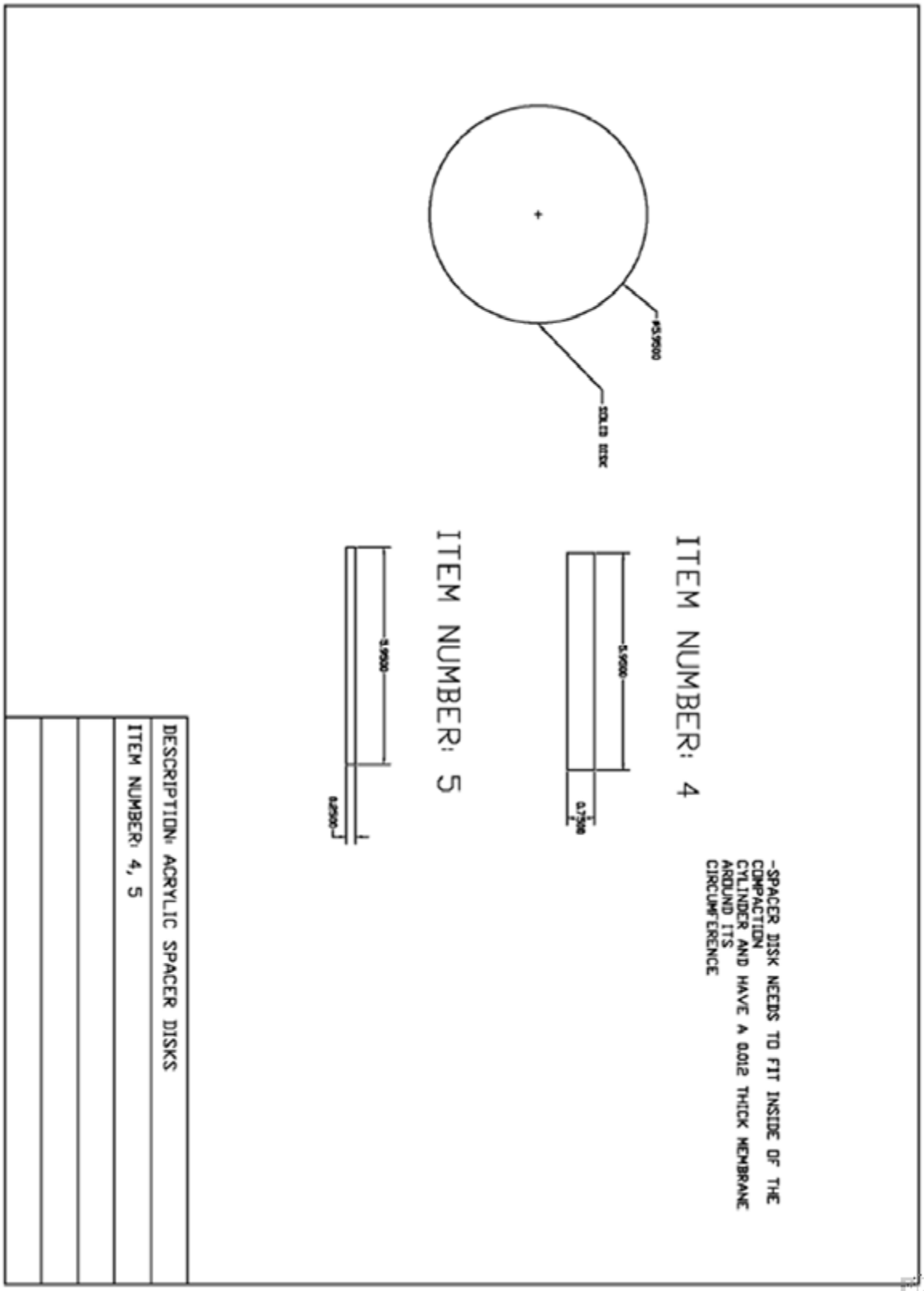


**Figure 258. Acrylic spacer disks for frost-heave and thaw-weakening test**

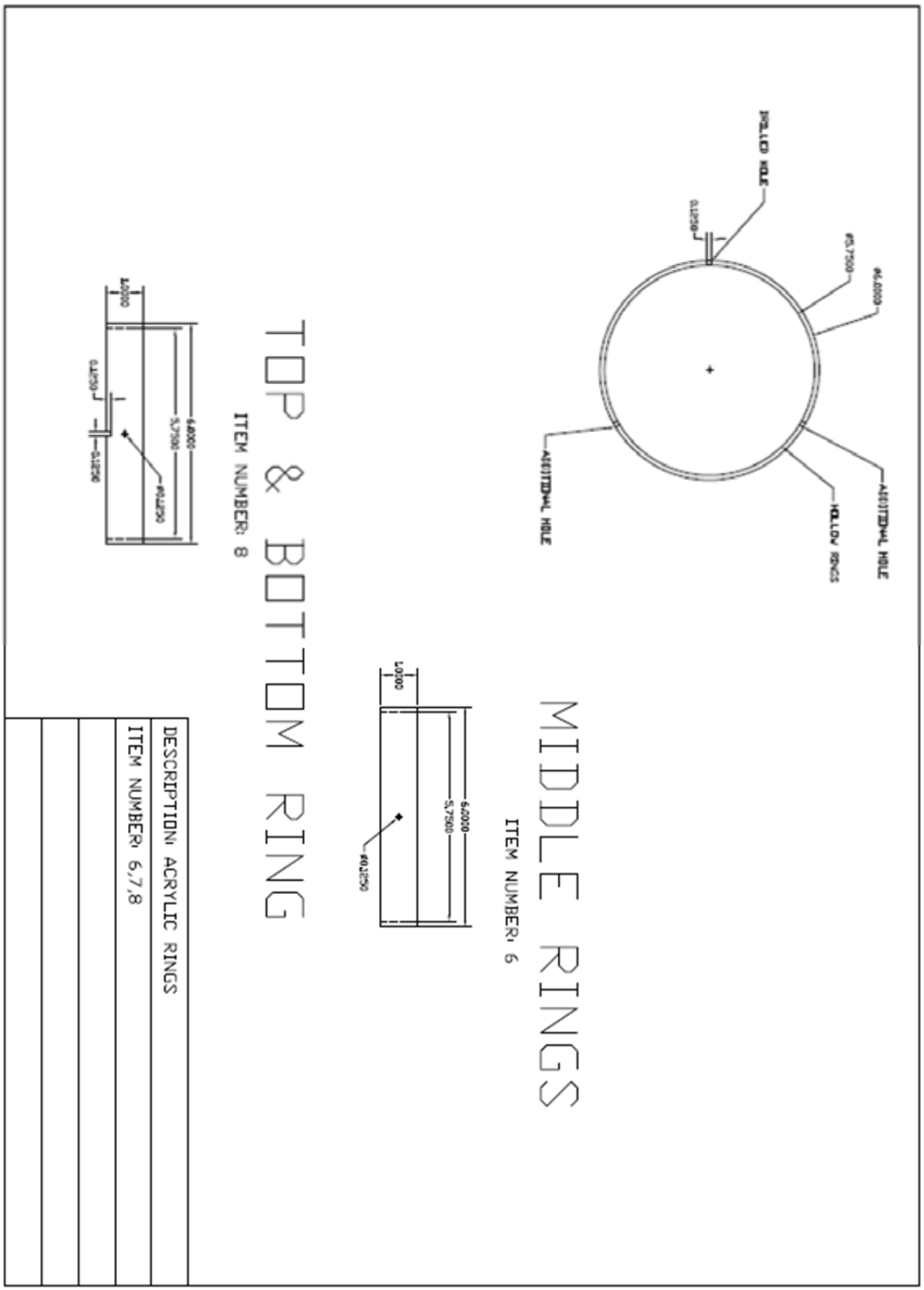


**Figure 259. Acrylic rings for frost-heave and thaw-weakening test**

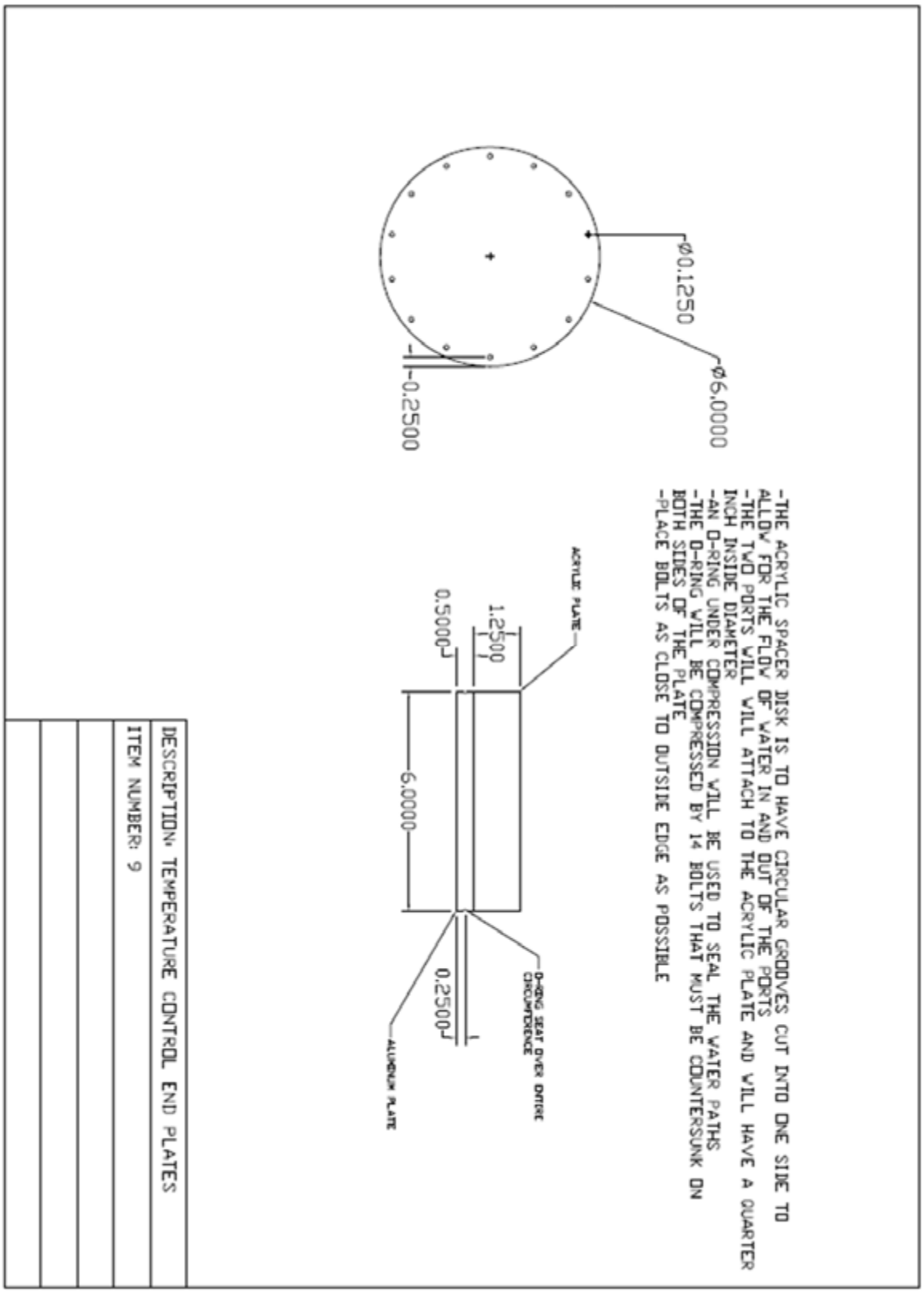


**Figure 260. Temperature control end plates for frost-heave and thaw-weakening test**

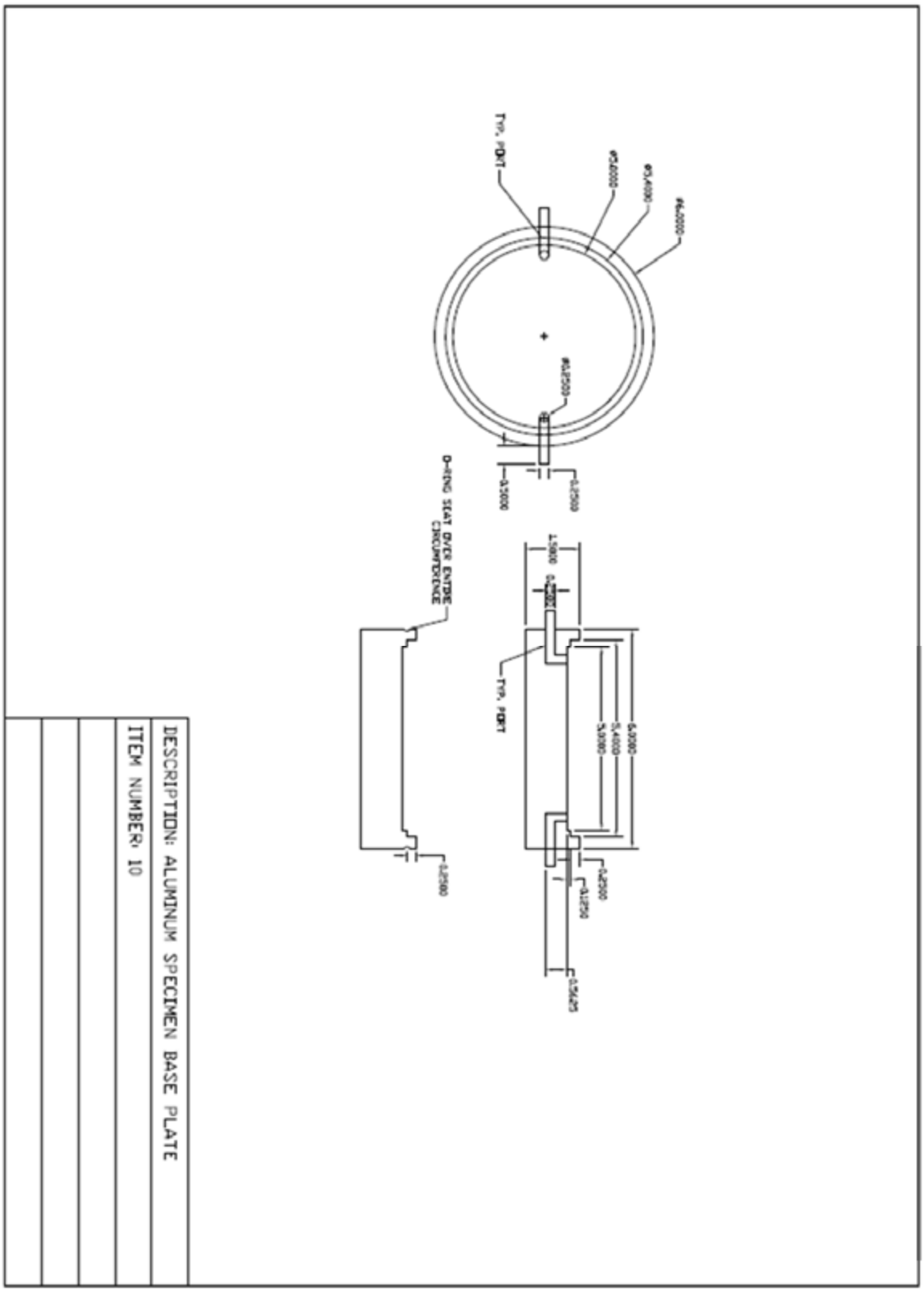


**Figure 261. Aluminum specimen base plate for frost-heave and thaw-weakening test**

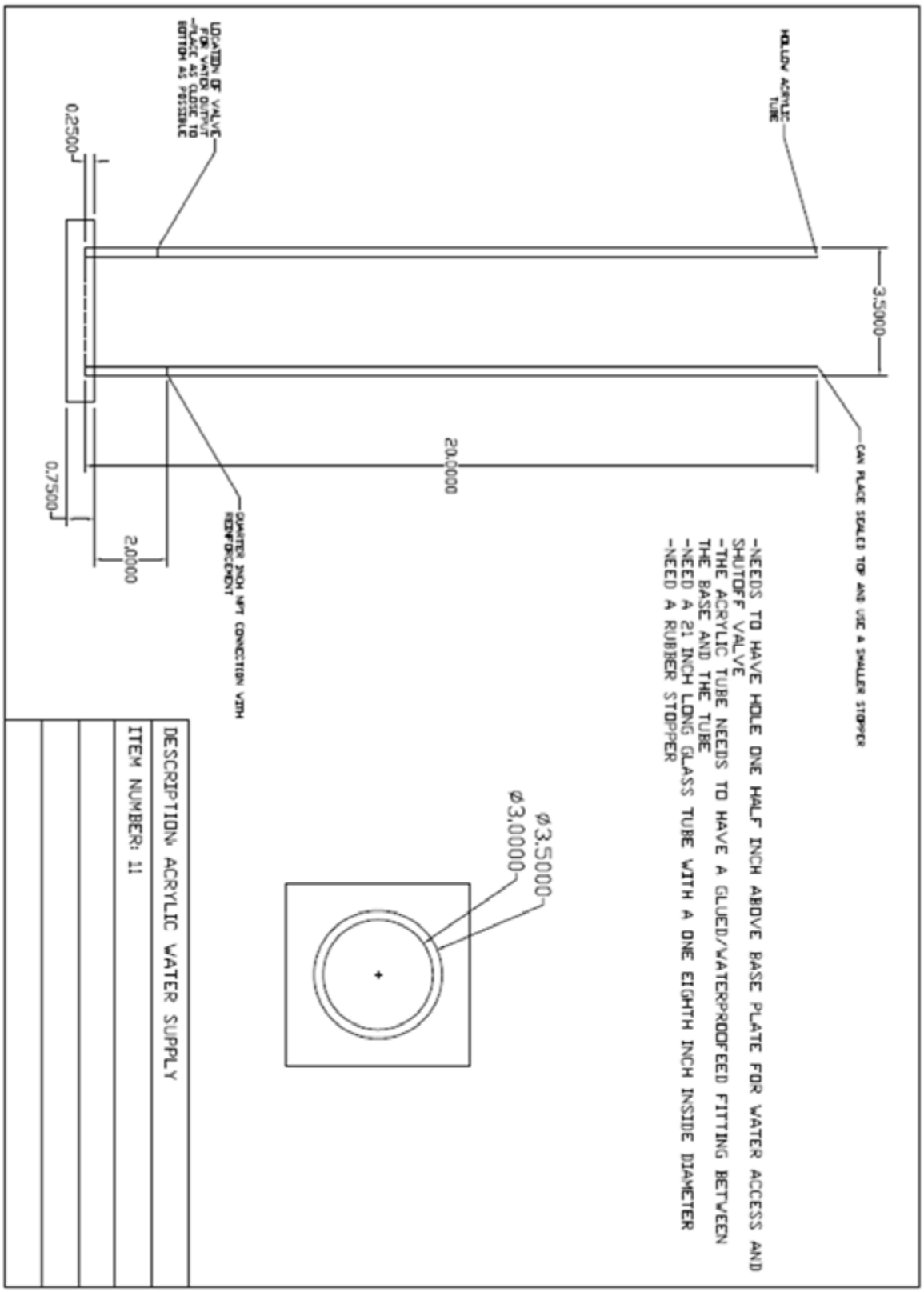


**Figure 262. Acrylic water supply for frost-heave and thaw-weakening test**

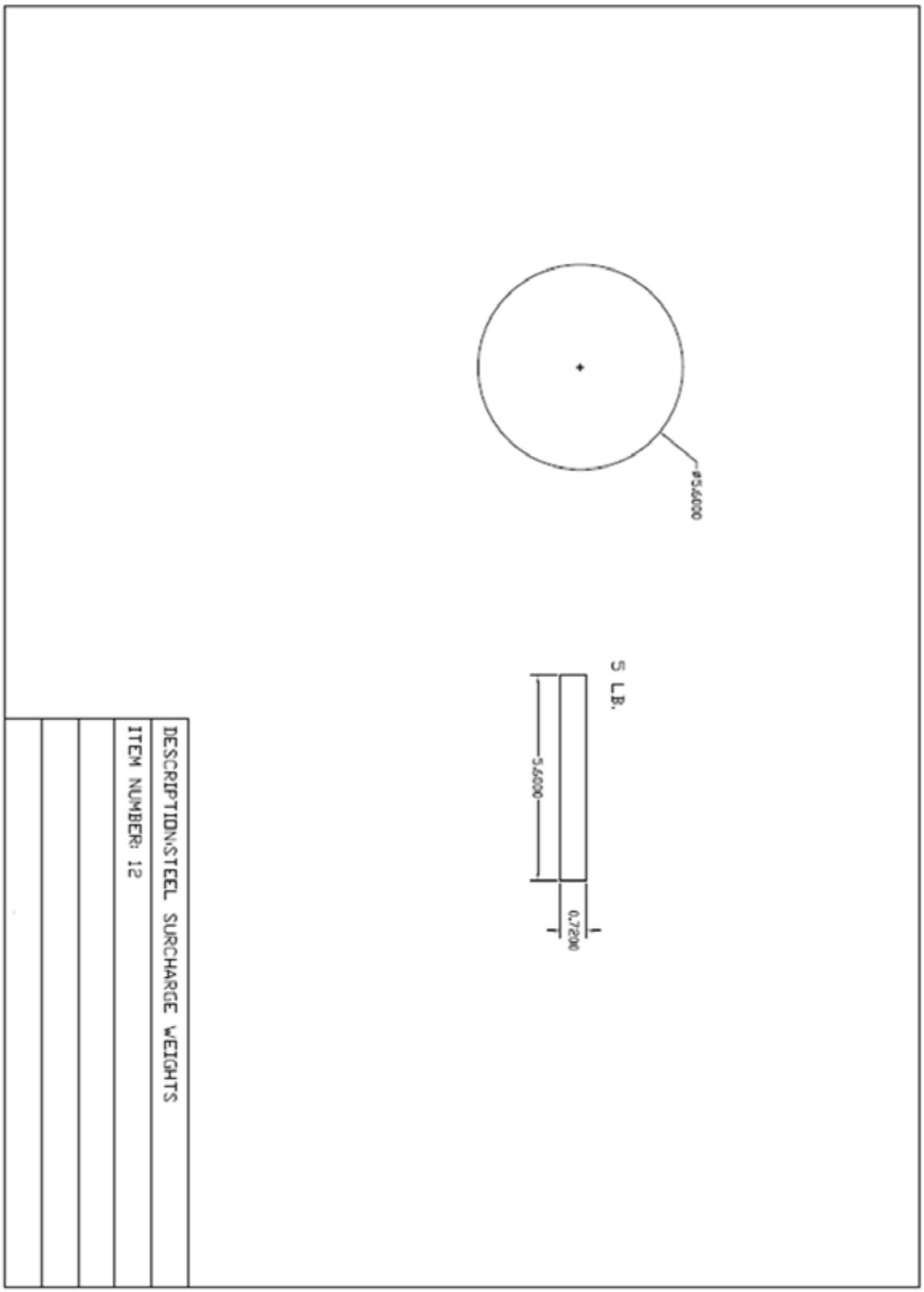


**Figure 263. Steel surcharge weights for frost-heave and thaw-weakening test**

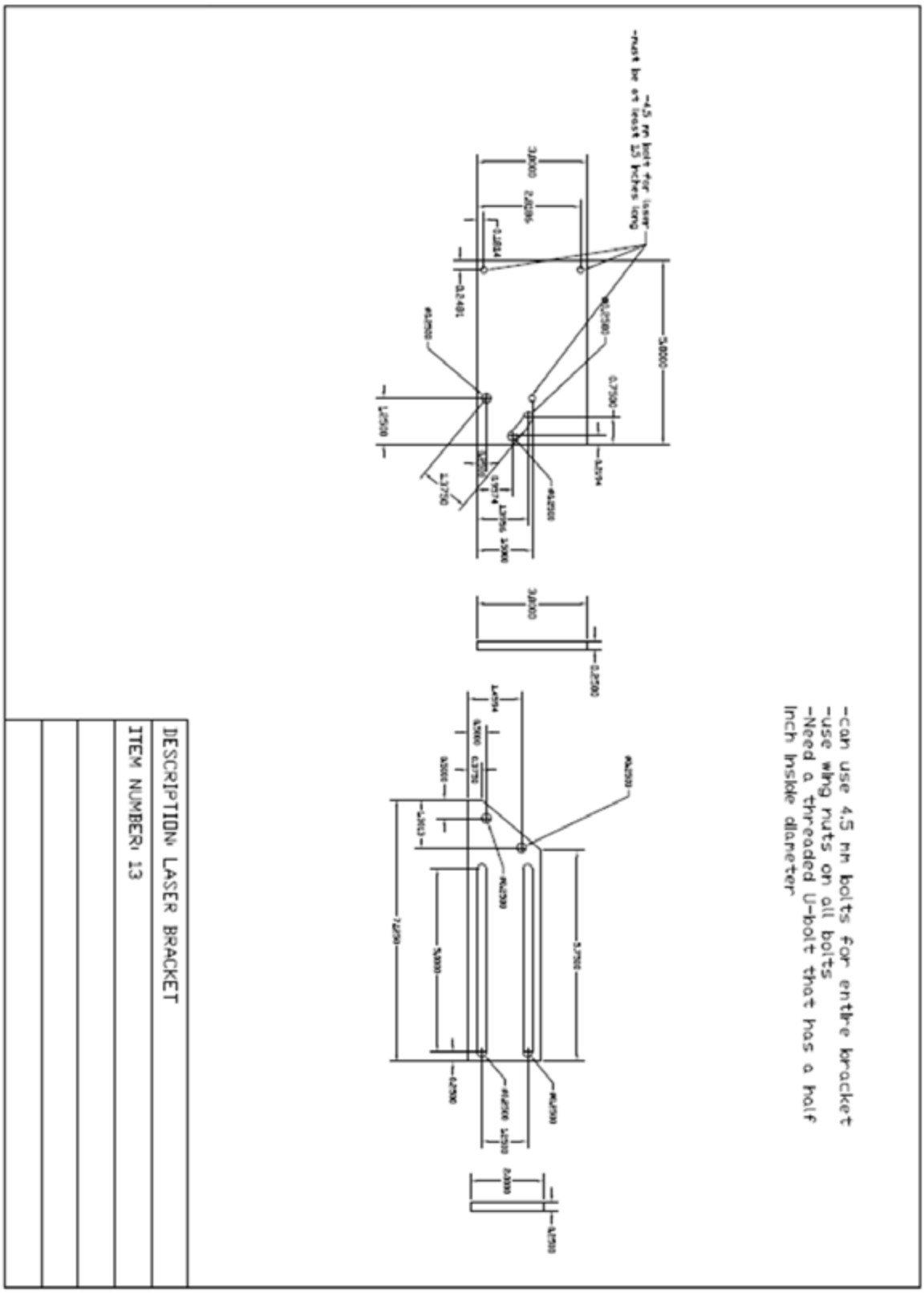


**Figure 264. Laser bracket for frost-heave and thaw-weakening test**

# APPENDIX C. FROST-HEAVE AND THAW-WEAKENING TEST PROCEDURAL MANUAL

## IOWA STATE UNIVERSITY

## ASTM D5918 PROCEDURAL MANUAL

### Material Preparation

7. Based on moisture-density tests, determine the optimum moisture content. Add sufficient water to the samples to reach the optimum moisture content.
8. Cohesive materials require approximately 6000g per sample and cohesionless materials require approximately 7000g per sample.
9. Separate into 4 samples and allow the samples to equilibrate overnight.
10. Take moisture content samples the day before compaction to verify accuracy and make any needed adjustments.

### Sample Preparation

11. Measure the mass of the top and bottom acrylic disks, the same mass can be used for all four samples.
12. Measure the mass of the rings, membrane, and disks that will be used for each of the 4 samples.

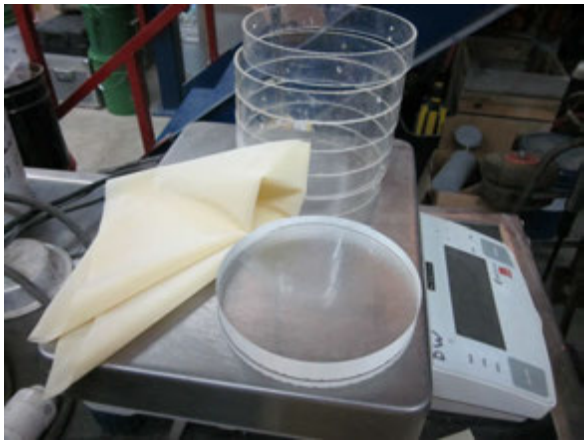

13. Wrap the membrane around bottom acrylic disk and place in the bottom of the sample mold with one half of the side walls removed.

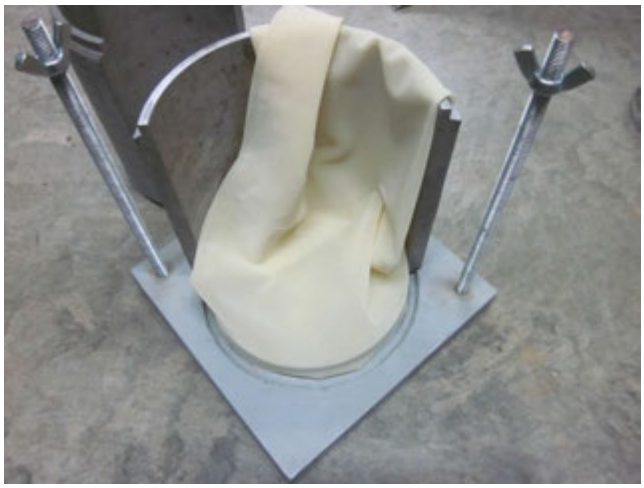

14. Place the 6 acrylic rings on the bottom acrylic disk, with the membrane inside of the rings. Align the thermocouple holes and notches vertically. The bottom ring should have a notch pointing down and the top ring should have a notch pointing up.

15. Place the other half of the side wall on the mold. Place 4 pipe clamps around the circumference of the side walls and tighten.

16. Place the collar on the mold and tighten the wing nuts

17. Stretch the membrane around the collar.

18. Compact material in 5 layers by applying 40 blows from a standard Proctor hammer to each layer. Each layer should be around 1.2 in. thick.
19. Remove the membrane from the collar and remove the pipe clamps and side walls.

20. Fold back the membrane and trim the sample.

21. Place the top acrylic disk on the sample and measure the mass of the sample, rings, membrane, and disks.
22. Measure the moisture content of each sample from the material that is remaining.

### Sample Setup and Saturation

23. Place the porous stone and filter paper on the specimen base.

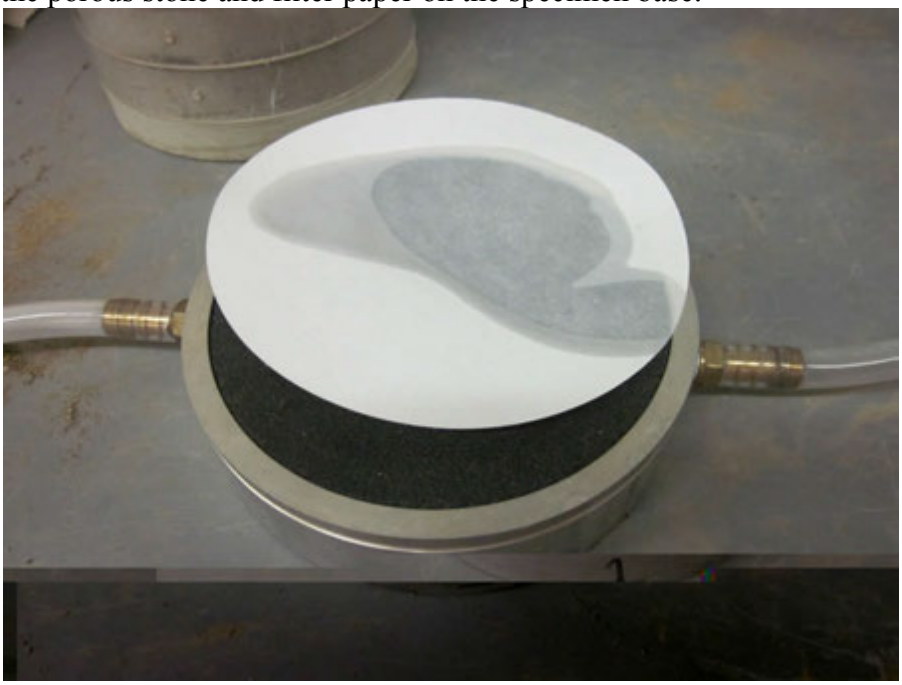

24. Remove the top and bottom acrylic disks from the sample and center the sample on the specimen base. For convenience, point the vertically aligned thermocouple holes and notches toward the tubing coming from the water supply.
25. Roll the membrane around the specimen base and slide an O-ring over the membrane onto the specimen base. The O-ring should fit into the grooves in the specimen base. Place a pipe clamp around the O-ring and tighten.

26. Roll the membrane around the top of the sample and place a sheet of plastic wrap over the sample, secure with a rubber band. Place the surcharge weight onto the samples.
27. Connect the specimen base to the water supply.
28. Flush the air out of the water lines and clamp the tubing shut. Fill the water supply and seal it. It may be easier to seal the water supply if after flushing the lines; the line is not completely closed. By allowing the water to flow while sealing the water supply, the water level should move to the bottom of the glass bubble tube. Clamp the tubing shut.

29. Set the water head level to 1 in. by placing the bottom of the glass bubble tube 1 in. above the bottom of the sample. Mark the initial water level and measure the change in water level at the end of the saturation period.
30. Raise the bubble tube at a rate of 1 in. per hour for 8 hrs., then set at 6 in. for 16 hrs.

### Setup in Freezer

31. Disconnect the samples from the water supplies and remove the surcharge weights.
32. Puncture the membrane at the locations where thermocouples will be placed.

33. Place the samples in the freezer on the bottom heat exchangers. Place the samples in the freezer according to the following arrangement:

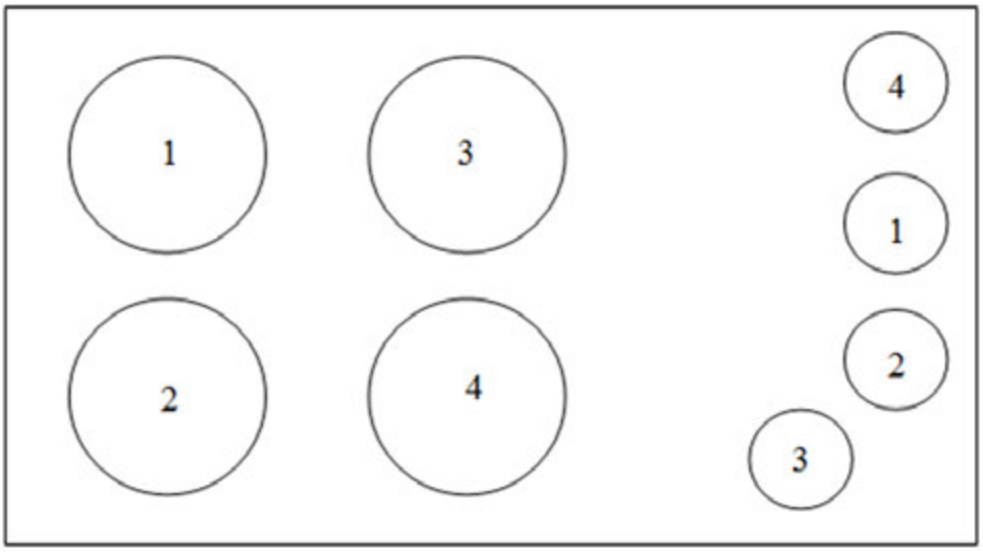


34. Place the top heat exchanger on the sample, seal with an O-ring, and reapply the surcharge weights.

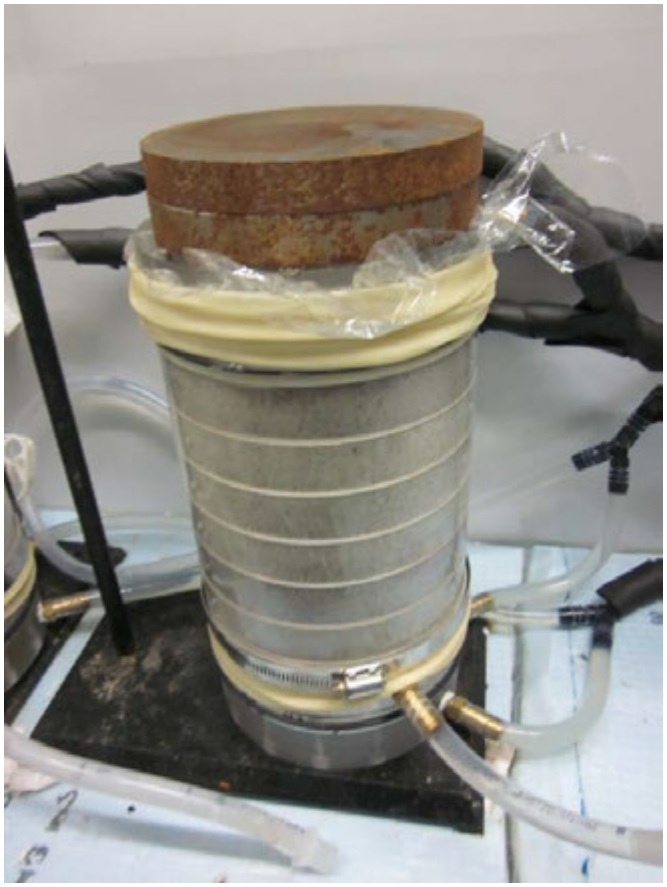

35. Place the water supplies in the freezer and re-connect to the specimen bases.

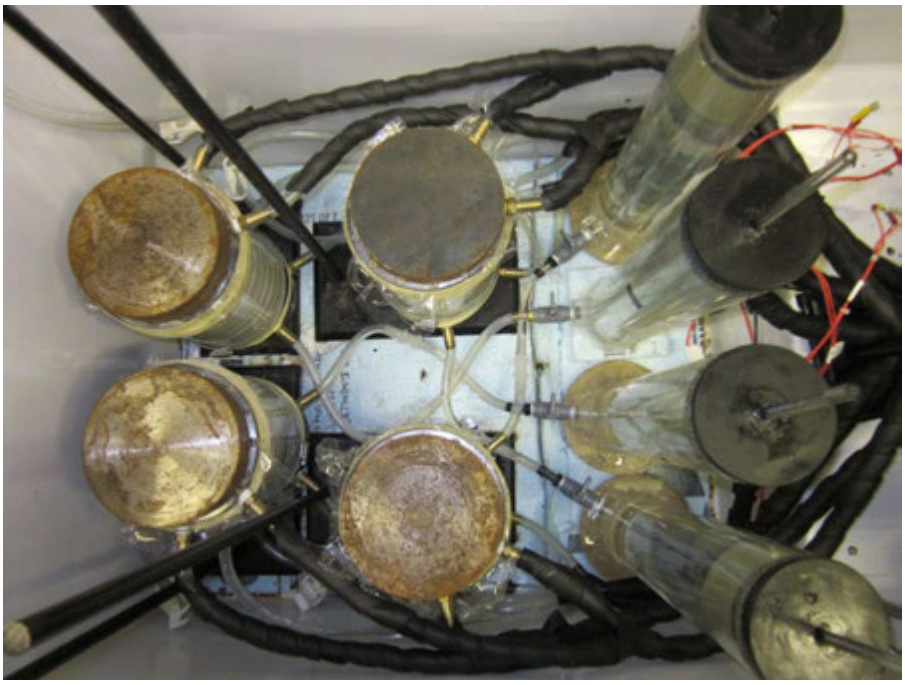

36. Purge the air from the water lines by allowing water to flow through the system. Set the head level 0.5 in. above the sample bottom, which is the same as setting the top of the bubble tube approximately 4.5 in. above the stopper. Mark the initial water level and measure the change in water level at the end of the testing period.
37. Connect the pressure transducer wires and wrap connections in electrical tape.
38. Dip the thermocouple tips in silicon adhesive and insert into sample. The numbers increase going down the sample (1 is on top and 8 is on bottom).

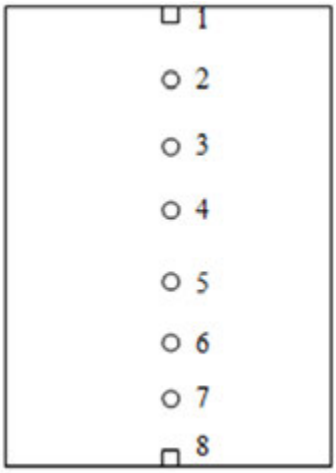

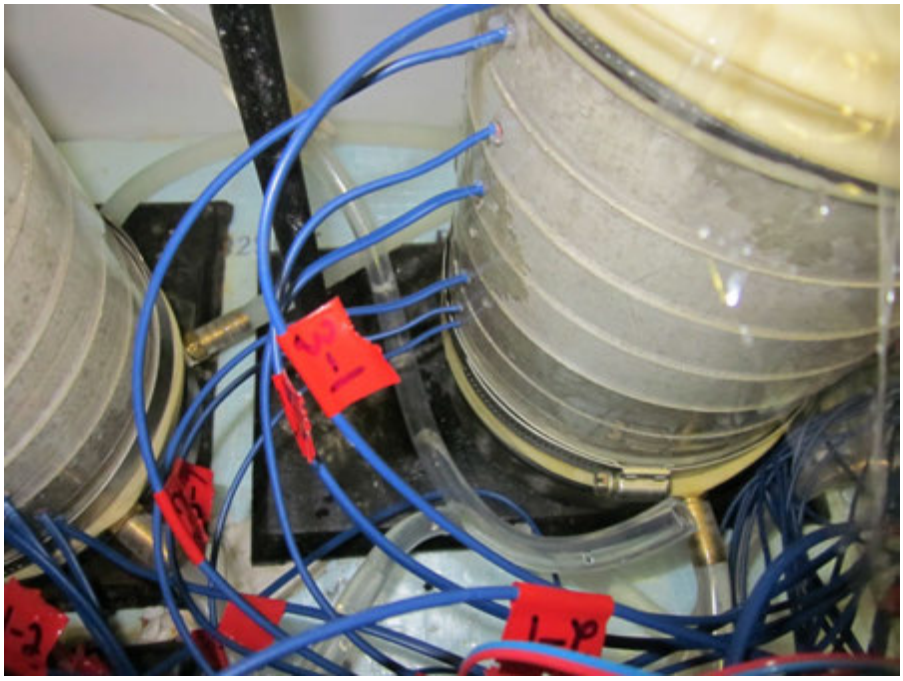

39. Turn on the water baths and set the target temperature to 3°C. Turn on the freezer and place the thermocouple connected to the temperature controller into the freezer. The following programs should be input into the top and bottom water baths:

| Top Heat Exchanger | | |
|---|---|---|
| **Program Step** | **Set Point (°C)** | **Duration** |
| 1 | 3 | 960 min |
| 2 | 3 | 480 min |
| 3 | 3 | 1 s |
| 4 | -3 | 480 min |
| 5 | -3 | 1 s |
| 6 | -12 | 960 min |
| 7 | -12 | 1 s |
| 8 | 12 | 960 min |
| 9 | 12 | 1 s |
| 10 | 3 | 480 min |
| 11 | 3 | 1 s |
| 12 | -3 | 480 min |
| 13 | -3 | 1 s |
| 14 | -12 | 960 min |
| 15 | -12 | 1 s |
| 16 | 12 | 960 min |
| 17 | 12 | 1 s |
| 18 | 3 | 480 min |
| 19 | 3 | 1 s |

| Bottom Heat Exchanger | | |
|---|---|---|
| **Program Step** | **Set Point (°C)** | **Duration** |
| 1 | 3 | 960 min |
| 2 | 3 | 480 min |
| 3 | 3 | 480 min |
| 4 | 3 | 1 s |
| 5 | 0 | 960 min |
| 6 | 0 | 1 s |
| 7 | 3 | 960 min |
| 8 | 3 | 960 min |
| 9 | 3 | 1 s |
| 10 | 0 | 960 min |
| 11 | 0 | 1 s |
| 12 | 3 | 960 min |
| 13 | 3 | 480 min |
| 14 | 3 | 1 s |

40. Place the displacement sensors above the samples. Place the sensors high enough that the expected range of heave can be measured. The light on the top of the laser gives an indication of where the laser is in the measuring range. The light on top of the lasers mean the following:
    - Red means the laser is out of the measurement range
    - Green means the laser is in the measurement range
    - Orange means the laser is at the midpoint of the measurement range

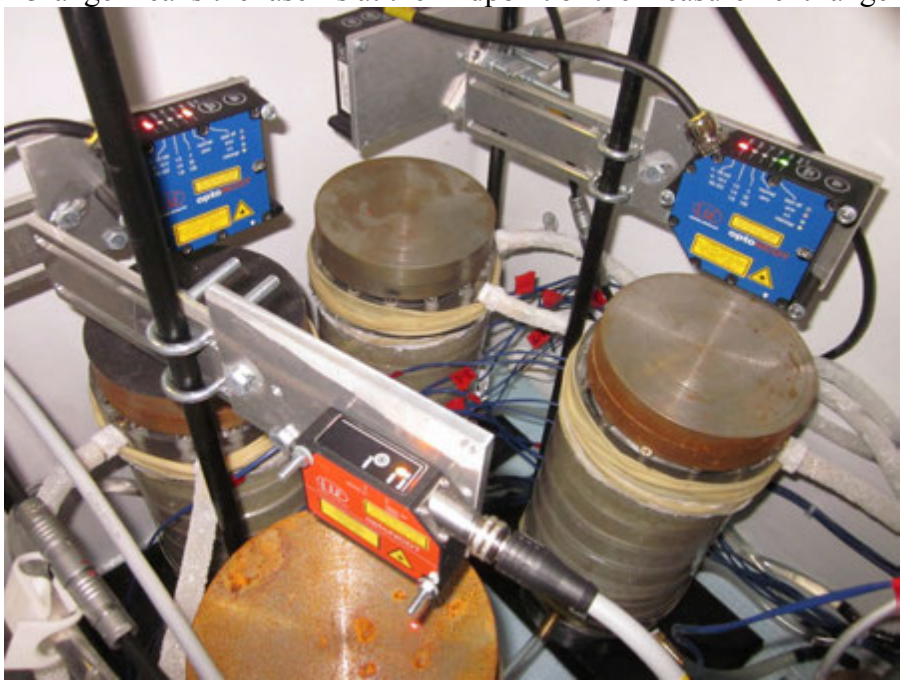

41. Observe the readings from the pressure transducers, thermocouples, and displacement transducers to make sure they are reasonable. Check the water supply connections, make sure the water supply valves are open, and check the thermocouple placement,
42. Fill with granular insulation.

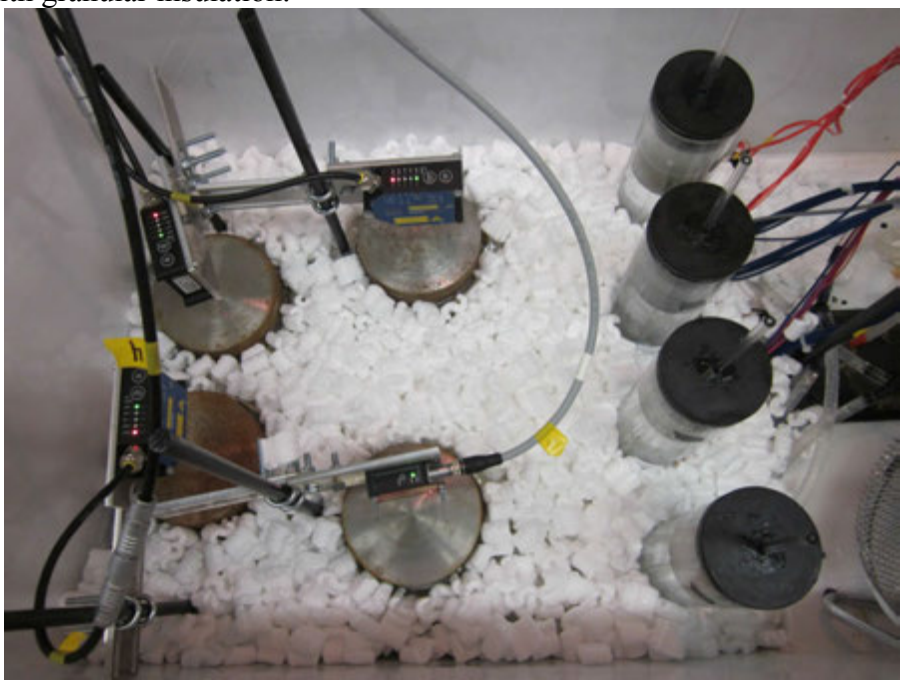

43. Place the thermocouple measuring the air temperature into the freezer. Make sure the air temperature and temperature control thermocouples are not in contact with anything that may give a false air temperature reading.
44. Restart the data acquisition system and start the water bath programs.

**Removal from Freezer and CBR**

45. Remove the displacement sensors, granular insulation, and thermocouples.
46. Disconnect the samples from the water supplies and remove from the freezer.
47. Remove the pipe clamp from the samples and both O-rings and measure the mass of the sample, rings, and membrane.
48. Place 4 pipe clamps around the top 4 acrylic rings and place the CBR surcharge weights on the sample. Perform the CBR test.

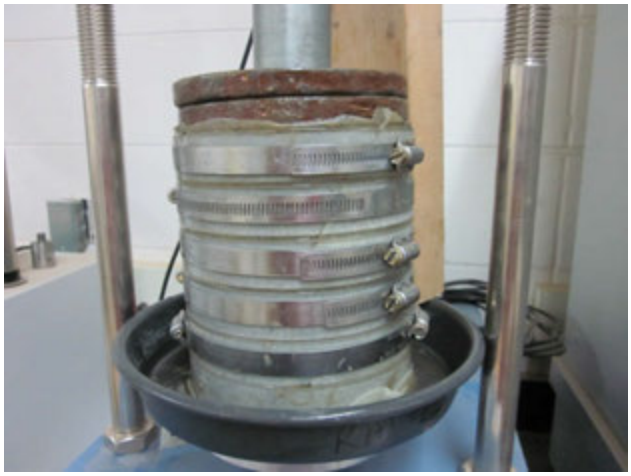

49. Take moisture content measurements from the samples on 1 in. centers in the vertical direction to develop a moisture content profile.

# APPENDIX D. ADDITIONAL FROST-HEAVE AND THAW WEAKENING TEST DATA

The following section presents the initial frost-heave and thaw-weakening sample properties, summaries of individual frost-heave and thaw-weakening test results, and cement-treated loess test results.

### 160th Street

## Well graded sand with silt and gravel

**Table 95. 160th Street well graded sand with silt and gravel frost-heave sample preparation properties**

| | 1 | 2 | 3 | 4 | μ | σ | COV (%) |
|---|---|---|---|---|---|---|---|
| $\gamma_d$ (kN/m$^3$) | 21.6 | 21.4 | 21.6 | 21.5 | 21.5 | 0.07 | 0.3 |
| *w (%)* | 9.1 | 9.0 | 8.6 | 8.7 | 8.9 | 0.2 | 2.4 |
| $G_s$ | 2.7 | | | | — | — | — |
| S (%) | 107.8 | 103.0 | 102.7 | 101.7 | 103.8 | 2.4 | 2.3 |
| e | 0.23 | 0.24 | 0.23 | 0.23 | 0.23 | 0.0 | 1.7 |
| n (%) | 18.6 | 19.2 | 18.5 | 18.7 | 18.7 | 0.3 | 1.3 |

**Table 96. 160th Street well graded sand with silt and gravel frost-heave and thaw-weakening test results**

| | 1 | 2 | 3 | 4 | μ | σ | COV (%) |
|---|---|---|---|---|---|---|---|
| CBR (%) (Standard Test) | 39.7* | | | | — | — | — |
| CBR (%) (After frost-heave test) | 15.8* | 12.4* | 15.7* | 16.1* | 15.0 | 1.7 | 11.5 |
| 1st Frost-Heave Rate (mm/day) | 6.0 | 5.8 | 6.5 | 5.8 | 6.0 | 0.3 | 5.2 |
| 2nd Frost-Heave Rate (mm/day) | 14.2 | 12.8 | 12.5 | 14 | 13.4 | 0.8 | 6.2 |
| 1st Frost-Heave Susceptibility Rating | Medium | Medium | Medium | Medium | Medium | — | — |
| 2nd Frost-Heave Susceptibility Rating | High | High | High | High | High | — | — |
| Thaw Weakening Susceptibility | Very low | Low | Very low | Very low | Very Low | — | — |

*CBR is higher at 0.2 in. penetration

**Poorly graded sand with silt and gravel**

**Table 97. 160th Street poorly graded sand with silt and gravel frost-heave sample preparation properties**

| | 1 | 2 | 3 | 4 | μ | σ | COV (%) |
|---|---|---|---|---|---|---|---|
| $\gamma_d$ (kN/m$^3$) | 21.5 | 21.5 | 21.8 | 21.2 | 21.5 | 0.2 | 1.0 |
| *w (%)* | 9.7 | 8.7 | 7.9 | 9.7 | 9.0 | 0.8 | 8.3 |
| $G_s$ | 2.72 | | | | — | — | — |
| S (%) | 108.7 | 97.6 | 94.7 | 100.6 | 100.4 | 5.2 | 5.2 |
| e | 0.24 | 0.24 | 0.23 | 0.26 | 0.24 | 0.01 | 5.16 |
| n (%) | 19.5 | 19.6 | 18.4 | 20.7 | 19.5 | 0.8 | 4.2 |

**Table 98. 160th Street poorly graded sand with silt and gravel frost-heave and thaw-weakening test results**

| | 1 | 2 | 3 | 4 | μ | σ | COV (%) |
|---|---|---|---|---|---|---|---|
| CBR (%) (Standard Test) | 65.1* | | | | — | — | — |
| CBR (%) (After frost-heave test) | 34.5* | 26.7* | 33.3* | 21.4* | 28.9 | 6.1 | 21.1 |
| 1st Frost-Heave Rate (mm/day) | 9.5 | 9.4 | 8.9 | 8.9 | 9.2 | 0.3 | 3.1 |
| 2nd Frost-Heave Rate (mm/day) | 11.3 | 12.2 | 11.6 | 11.0 | 11.5 | 0.5 | 4.5 |
| 1st Frost-Heave Susceptibility Rating | High | High | High | High | High | — | — |
| 2nd Frost-Heave Susceptibility Rating | High | High | High | High | High | — | — |
| Thaw Weakening Susceptibility | Negligible | Negligible | Negligible | Negligible | Negligible | — | — |

*CBR is higher at 0.2 in. penetration

## IA I-29

### Lean Clay Subgrade

**Table 99. IA I-29 lean clay subgrade frost-heave sample preparation properties**

| | 1 | 2 | 3 | 4 | μ | σ | COV (%) |
|---|---|---|---|---|---|---|---|
| $\gamma_d$ (kN/m$^3$) | 16.0 | 16.2 | 16.3 | 16.2 | 16.2 | 0.1 | 0.6 |
| *w (%)* | 18.4 | 17.9 | 17.9 | 18.0 | 18.1 | 0.2 | 1.2 |
| $G_s$ | 2.69 | | | | — | — | — |
| S (%) | 76.4 | 76.0 | 77.7 | 76.3 | 76.6 | 0.7 | 0.9 |
| e | 0.65 | 0.63 | 0.62 | 0.63 | 0.63 | 0.01 | 1.6 |
| n (%) | 39.4 | 38.8 | 38.3 | 38.8 | 38.8 | 0.4 | 1.0 |

**Table 100. IA I-29 lean clay subgrade frost-heave and thaw-weakening test results**

| | 1 | 2 | 3 | 4 | μ | σ | COV (%) |
|---|---|---|---|---|---|---|---|
| CBR (%) (Standard Test) | 21.8 | | | | — | — | — |
| CBR (%) (After frost-heave test) | 0.7* | 0.7* | 0.7* | 0.9* | 0.7 | 0.0 | 12.0 |
| 1$^{st}$ Frost-Heave Rate (mm/day) | 6.8 | 10.4 | 9.0 | 7.4 | 8.4 | 1.4 | 16.8 |
| 2$^{nd}$ Frost-Heave Rate (mm/day) | 10.1 | 15.1 | 13.2 | 11.1 | 12.4 | 2.2 | 17.9 |
| 1$^{st}$ Frost-Heave Susceptibility Rating | Medium | High | High | Medium | High | — | — |
| 2$^{nd}$ Frost-Heave Susceptibility Rating | High | High | High | High | High | — | — |
| Thaw Weakening Susceptibility | Very high | Very high | Very high | Very high | Very high | — | — |

*CBR is higher at 0.2 in. penetration

**Silt with Sand Subgrade**

**Table 101. IA I-29 silt with sand subgrade frost-heave sample preparation properties**

| | 1 | 2 | 3 | 4 | μ | σ | COV (%) |
|---|---|---|---|---|---|---|---|
| $\gamma_d$ (kN/m$^3$) | 17.7 | 17.5 | 17.2 | 17.7 | 17.5 | 0.2 | 1.1 |
| *w (%)* | 13.5 | 13.9 | 13.8 | 13.7 | 13.7 | 0.2 | 1.1 |
| $G_s$ | 2.65 | | | | — | — | — |
| S (%) | 76.4 | 75.8 | 71.9 | 77.3 | 75.3 | 2.0 | 2.7 |
| e | 0.47 | 0.48 | 0.51 | 0.47 | 0.48 | 0.02 | 3.5 |
| n (%) | 31.9 | 32.6 | 33.8 | 32.0 | 32.6 | 0.8 | 2.3 |

**Table 102. IA I-29 silt with sand subgrade frost-heave and thaw-weakening test results**

| | 1 | 2 | 3 | 4 | μ | σ | COV (%) |
|---|---|---|---|---|---|---|---|
| CBR (%) (Standard Test) | 21.6* | | | | — | — | — |
| CBR (%) (After frost-heave test) | 1.2* | 1.2* | 1.2* | 1.9* | 1.4 | 0.4 | 25.9 |
| 1$^{st}$ Frost-Heave Rate (mm/day) | 11.1 | 10.3 | 11.1 | 8.1 | 10.2 | 1.3 | 12.4 |
| 2$^{nd}$ Frost-Heave Rate (mm/day) | 14.7 | 13.1 | 8.2 | 8.1 | 11.0 | 3.4 | 30.4 |
| 1$^{st}$ Frost-Heave Susceptibility Rating | High | High | High | High | High | — | — |
| 2$^{nd}$ Frost-Heave Susceptibility Rating | High | High | High | High | High | — | — |
| Thaw Weakening Susceptibility | Very high | Very high | Very high | Very high | Very high | — | — |

*CBR is higher at 0.2 in. penetration

## IA US-30

### Clayey Sand Subgrade

**Table 103. IA US-30 clayey sand subgrade frost-heave sample preparation properties**

| | 1 | 2 | 3 | 4 | μ | σ | COV (%) |
|---|---|---|---|---|---|---|---|
| $\gamma_d$ (kN/m$^3$) | 19.2 | 19.1 | 19.1 | 19.5 | 19.2 | 0.2 | 0.8 |
| *w (%)* | 11.9 | 11.7 | 11.6 | 12.4 | 11.9 | 0.3 | 2.4 |
| $G_s$ | 2.63 | | | | — | — | — |
| S (%) | 90.8 | 88.1 | 87.2 | 100.0 | 91.5 | 5.1 | 5.6 |
| e | 0.34 | 0.35 | 0.35 | 0.33 | 0.34 | 0.01 | 3.0 |
| n (%) | 25.6 | 26.0 | 26.0 | 24.6 | 25.5 | 0.6 | 2.3 |

**Table 104. IA US-30 clayey sand subgrade frost-heave and thaw-weakening test results**

| | 1 | 2 | 3 | 4 | μ | σ | COV (%) |
|---|---|---|---|---|---|---|---|
| CBR (%) (Standard Test) | 8.4 | | | | — | — | — |
| CBR (%) (After frost-heave test) | 2.37* | 2.53* | 3.11* | 2.53* | 2.67 | 0.4 | 14.7 |
| 1$^{st}$ Frost-Heave Rate (mm/day) | 3.9 | 5.0 | 4.7 | 3.9 | 4.4 | 0.5 | 11.5 |
| 2$^{nd}$ Frost-Heave Rate (mm/day) | 6.5 | 9.4 | 9.6 | 5.8 | 7.8 | 2.0 | 25.2 |
| 1$^{st}$ Frost-Heave Susceptibility Rating | Low | Medium | Medium | Low | Medium | — | — |
| 2$^{nd}$ Frost-Heave Susceptibility Rating | Medium | High | High | Medium | Medium | — | — |
| Thaw Weakening Susceptibility | High | High | High | High | High | — | — |

*CBR is higher at 0.2 in. penetration

## RPCC/RAP Subbase

**Table 105. IA US-30 RPCC/RAP subbase frost-heave sample preparation properties**

| | 1 | 2 | 3 | 4 | μ | σ | COV (%) |
|---|---|---|---|---|---|---|---|
| $\gamma_d$ (kN/m$^3$) | 19.6 | 19.6 | 19.3 | 19.2 | 19.4 | 0.2 | 1.1 |
| *w (%)* | 9.7 | 9.9 | 10.8 | 11.6 | 10.5 | 0.8 | 7.2 |
| $G_s$ | 2.52 | | | | — | — | — |
| S (%) | 93.7 | 97.1 | 95.7 | 101.7 | 97.1 | 3.0 | 3.0 |
| e | 0.26 | 0.26 | 0.28 | 0.29 | 0.27 | 0.01 | 4.9 |
| n (%) | 20.7 | 20.5 | 22.1 | 22.4 | 21.4 | 0.8 | 3.9 |

**Table 106. IA US-30 RPCC/RAP subbase frost-heave and thaw-weakening test results**

| | 1 | 2 | 3 | 4 | μ | σ | COV (%) |
|---|---|---|---|---|---|---|---|
| CBR (%) (Standard Test) | 40.6* | | | | — | — | — |
| CBR (%) (After frost-heave test) | 60.0* | 48.0* | 27.3* | 37.3* | 37.6 | 10.3 | 27.5 |
| 1$^{st}$ Frost-Heave Rate (mm/day) | 6.9 | 7.1 | 7.7 | 6.7 | 7.1 | 0.4 | 5.3 |
| 2$^{nd}$ Frost-Heave Rate (mm/day) | 5.8 | 5.4 | 5.4 | 4.8 | 5.4 | 0.4 | 7.5 |
| 1$^{st}$ Frost-Heave Susceptibility Rating | Medium | Medium | Medium | Medium | Medium | — | — |
| 2$^{nd}$ Frost-Heave Susceptibility Rating | Medium | Medium | Medium | Medium | Medium | — | — |
| Thaw Weakening Susceptibility | Negligible | Negligible | Negligible | Negligible | Negligible | — | — |

*CBR is higher at 0.2 in. penetration

**Limestone Subbase**

**Table 107. IA US-30 limestone subbase frost-heave sample preparation properties**

| | 1 | 2 | 3 | 4 | μ | σ | COV (%) |
|---|---|---|---|---|---|---|---|
| $\gamma_d$ (kN/m$^3$) | 20.3 | 20.4 | 20.4 | 20.7 | 20.5 | 0.2 | 0.7 |
| *w (%)* | 4.6 | 5.2 | 4.9 | 4.6 | 4.8 | 0.3 | 5.5 |
| $G_s$ | 2.72 | | | | — | — | — |
| S (%) | 39.5 | 45.8 | 43.3 | 43.0 | 42.9 | 2.3 | 5.3 |
| e | 0.31 | 0.31 | 0.30 | 0.29 | 0.30 | 0.01 | 3.2 |
| n (%) | 23.9 | 23.6 | 23.4 | 22.4 | 23.3 | 0.6 | 2.5 |

**Table 108. IA US-30 limestone subbase frost-heave and thaw-weakening test results**

| | 1 | 2 | 3 | 4 | μ | σ | COV (%) |
|---|---|---|---|---|---|---|---|
| CBR (%) (Standard Test) | 70.5* | | | | — | — | — |
| CBR (%) (After frost-heave test) | 35.8* | — | 31.2* | 29.3* | 33.2 | 6.4 | 19.3 |
| 1$^{st}$ Frost-Heave Rate (mm/day) | 4.4 | 5.3 | 7.5 | 4.3 | 5.4 | 1.3 | 23.7 |
| 2$^{nd}$ Frost-Heave Rate (mm/day) | 5.7 | 7.1 | 6.5 | 6.3 | 6.4 | 0.6 | 8.9 |
| 1$^{st}$ Frost-Heave Susceptibility Rating | Medium | Medium | Medium | Medium | Medium | — | — |
| 2$^{nd}$ Frost-Heave Susceptibility Rating | Medium | Medium | Medium | Medium | Medium | — | — |
| Thaw Weakening Susceptibility | Negligible | — | Negligible | Negligible | Negligible | — | — |

*CBR is higher at 0.2 in. penetration

## RPCC Subbase

**Table 109. IA US-30 RPCC subbase frost-heave sample preparation properties**

| | 1 | 2 | 3 | 4 | μ | σ | COV (%) |
|---|---|---|---|---|---|---|---|
| $\gamma_d$ (kN/m$^3$) | 17.9 | 18.1 | 18.0 | 18.2 | 18.1 | 0.1 | 0.7 |
| *w (%)* | 9.7 | 9.4 | 9.3 | 8.5 | 9.2 | 0.5 | 5.1 |
| $G_s$ | 2.57 | | | | — | — | — |
| S (%) | 60.7 | 61.5 | 59.8 | 56.7 | 59.7 | 1.8 | 3.0 |
| e | 0.41 | 0.39 | 0.40 | 0.38 | 0.40 | 0.01 | 2.6 |
| n (%) | 29.2 | 28.2 | 28.4 | 27.7 | 28.4 | 0.5 | 1.9 |

**Table 110. IA US-30 RPCC subbase frost-heave and thaw-weakening test results**

| | 1 | 2 | 3 | 4 | μ | σ | COV (%) |
|---|---|---|---|---|---|---|---|
| CBR (%) (Standard Test) | 70.3* | | | | — | — | — |
| CBR (%) (After frost-heave test) | 36.7* | 30* | 29.3* | 37.3* | 33.3 | 4.3 | 12.8 |
| 1$^{st}$ Frost-Heave Rate (mm/day) | 9.7 | 8.8 | 8.3 | 7.7 | 8.6 | 0.7 | 8.4 |
| 2$^{nd}$ Frost-Heave Rate (mm/day) | 6.7 | 6.4 | 5.6 | 5.8 | 6.1 | 0.5 | 8.0 |
| 1$^{st}$ Frost-Heave Susceptibility Rating | High | High | High | Medium | High | — | — |
| 2$^{nd}$ Frost-Heave Susceptibility Rating | Medium | Medium | Medium | Medium | Medium | — | — |
| Thaw Weakening Susceptibility | Negligible | Negligible | Negligible | Negligible | Negligible | — | — |

*CBR is higher at 0.2 in. penetration

**Table 111. IA US-30 RPCC subbase modified gradation (half of fines removed) frost-heave sample preparation properties**

| | 1 | 2 | μ | σ | COV (%) |
|---|---|---|---|---|---|
| $\gamma_d$ (kN/m$^3$) | 17.9 | 17.6 | 17.7 | 0.2 | 0.9 |
| *w (%)* | 8.8 | 8.6 | 8.7 | 0.1 | 0.8 |
| $G_s$ | 2.57 | | — | — | — |
| S (%) | 55.1 | 51.0 | 53.1 | 2.1 | 3.9 |
| e | 0.41 | 0.43 | 0.42 | 0.0 | 3.2 |
| n (%) | 29.0 | 30.3 | 29.6 | 0.7 | 2.2 |

**Table 112. IA US-30 RPCC subbase modified gradation (half of fines removed) frost-heave and thaw-weakening test results**

| | 1 | 2 | μ | σ | COV (%) |
|---|---|---|---|---|---|
| CBR (%) (Standard Test) | — | | — | — | — |
| CBR (%) (After frost-heave test) | 45.0* | 33.3* | 39.2 | 8.3 | 21.1 |
| 1st Frost-Heave Rate (mm/day) | 7.9 | 7.5 | 7.7 | 0.2 | 2.7 |
| 2nd Frost-Heave Rate (mm/day) | 6.3 | 5.8 | 6.1 | 0.3 | 5.7 |
| 1st Frost-Heave Susceptibility Rating | Medium | Medium | Medium | — | — |
| 2nd Frost-Heave Susceptibility Rating | Medium | Medium | Medium | — | — |
| Thaw Weakening Susceptibility | Negligible | Negligible | Negligible | — | — |

*CBR is higher at 0.2 in. penetration

**Table 113. IA US-30 RPCC subbase modified gradation (all fines removed) frost-heave sample preparation properties**

| | 1 | 2 | μ | σ | COV (%) |
|---|---|---|---|---|---|
| $\gamma_d$ (kN/m$^3$) | 17.9 | 18.1 | 18.0 | 0.1 | 0.6 |
| *w (%)* | 8.6 | 8.6 | 8.6 | 0.0 | 0.0 |
| $G_s$ | 2.57 | | — | — | — |
| S (%) | 54.4 | 56.9 | 55.7 | 1.2 | 2.2 |
| e | 0.41 | 0.39 | 0.40 | 0.0 | 2.2 |
| n (%) | 28.9 | 28.0 | 28.5 | 0.5 | 1.6 |

**Table 114. IA US-30 RPCC subbase modified gradation (all fines removed) frost-heave and thaw-weakening test results**

| | 1 | 2 | μ | σ | COV (%) |
|---|---|---|---|---|---|
| CBR (%) (Standard Test) | — | | — | — | — |
| CBR (%) (After frost-heave test) | 38.3* | 32.7* | 35.5 | 4.0 | 11.3 |
| 1st Frost-Heave Rate (mm/day) | 7.4 | 8.2 | 7.8 | 0.4 | 5.4 |
| 2nd Frost-Heave Rate (mm/day) | 5.6 | 6.6 | 6.1 | 0.7 | 10.8 |
| 1st Frost-Heave Susceptibility Rating | Medium | High | Medium | — | — |
| 2nd Frost-Heave Susceptibility Rating | Medium | High | Medium | — | — |
| Thaw Weakening Susceptibility | Negligible | Negligible | Negligible | — | — |

*CBR is higher at 0.2 in. penetration

## Manatts

### Concrete Sand Subbase

**Table 115. Manatts concrete sand subbase frost-heave sample preparation properties**

| | 1 | 2 | 3 | 4 | μ | σ | COV (%) |
|---|---|---|---|---|---|---|---|
| $\gamma_d$ (kN/m$^3$) | 17.6 | 17.7 | 17.6 | 17.5 | 17.6 | 0.08 | 0.5 |
| *w (%)* | 2.9 | 3.0 | 2.8 | 3.0 | 2.9 | 0.1 | 3.4 |
| $G_s$ | 2.68 | | | | — | — | — |
| S (%) | 15.5 | 16.7 | 15.0 | 15.8 | 15.8 | 0.6 | 3.8 |
| e | 0.50 | 0.49 | 0.49 | 0.50 | 0.50 | 0.01 | 1.4 |
| n (%) | 33.2 | 32.7 | 33.0 | 33.5 | 33.1 | 0.3 | 0.9 |

**Table 116. Manatts concrete sand subbase frost-heave and thaw-weakening test results**

| | 1 | 2 | 3 | 4 | μ | σ | COV (%) |
|---|---|---|---|---|---|---|---|
| CBR (%) (Standard Test) | 9.4* | | | | — | — | — |
| CBR (%) (After frost-heave test) | 8.2 | 8.9* | 8.7* | 7.2* | 8.1 | 0.8 | 10.0 |
| 1st Frost-Heave Rate (mm/day) | 1.0 | 1.1 | 1.1 | 1.8 | 1.2 | 0.3 | 26.0 |
| 2nd Frost-Heave Rate (mm/day) | 0.7 | 0.9 | 0.9 | 1.3 | 0.9 | 0.2 | 25.3 |
| 1st Frost-Heave Susceptibility Rating | Very low | Very low | Very low | Very low | Very low | — | — |
| 2nd Frost-Heave Susceptibility Rating | Negligible | Negligible | Negligible | Very low | Negligible | — | — |
| Thaw Weakening Susceptibility | Medium | Medium | Medium | Medium | Medium | — | — |

*CBR is higher at 0.2 in. penetration

## RAP Subbase

**Table 117. Manatts RAP subbase frost-heave sample preparation properties**

| | 1 | 2 | 3 | 4 | μ | σ | COV (%) |
|---|---|---|---|---|---|---|---|
| $\gamma_d$ (kN/m$^3$) | 18.0 | 18.0 | 18.1 | 17.8 | 18.0 | 0.1 | 0.6 |
| *w (%)* | 2.9 | 3.3 | 3.2 | 3.2 | 3.1 | 0.2 | 4.7 |
| $G_s$ | 2.47 | | | | — | — | — |
| S (%) | 20.5 | 23.4 | 23.6 | 21.8 | 22.3 | 1.3 | 5.6 |
| e | 0.35 | 0.35 | .034 | 0.36 | 0.35 | 0.01 | 2.5 |
| n (%) | 25.8 | 25.7 | 25.1 | 26.5 | 25.8 | 0.5 | 1.8 |

**Table 118. Manatts RAP subbase frost-heave and thaw-weakening test results**

| | 1 | 2 | 3 | 4 | μ | σ | COV (%) |
|---|---|---|---|---|---|---|---|
| CBR (%) (Standard Test) | 11.6* | | | | — | — | — |
| CBR (%) (After frost-heave test) | 8.6* | 7.7* | 9.8* | 8.8* | 8.7 | 0.9 | 9.8 |
| 1st Frost-Heave Rate (mm/day) | 2.9 | 2.4 | 1.9 | 1.3 | 2.1 | 0.6 | 29.1 |
| 2nd Frost-Heave Rate (mm/day) | 2.1 | 2.1 | 1.9 | 1.2 | 1.8 | 0.5 | 24.8 |
| 1st Frost-Heave Susceptibility Rating | Low | Low | Very low | Very low | low | — | — |
| 2nd Frost-Heave Susceptibility Rating | Low | Low | Very low | Very low | Very low | — | — |
| Thaw Weakening Susceptibility | Medium | Medium | Medium | Medium | Medium | — | — |

*CBR is higher at 0.2 in. penetration

## RPCC/RAP Subbase

**Table 119. Manatts RPCC/RAP subbase frost-heave sample preparation properties**

| | 1 | 2 | 3 | 4 | μ | σ | COV (%) |
|---|---|---|---|---|---|---|---|
| $\gamma_d$ (kN/m$^3$) | 17.4 | 17.2 | 17.1 | 17.2 | 17.3 | 0.1 | 0.6 |
| *w (%)* | 6.5 | 6.5 | 7.6 | 7.4 | 7.0 | 0.5 | 6.9 |
| $G_s$ | 2.62 | | | | — | — | — |
| S (%) | 36.0 | 34.7 | 39.5 | 39.6 | 37.4 | 2.2 | 5.7 |
| e | 0.48 | 0.49 | 0.50 | 0.49 | 0.49 | 0.01 | 1.77 |
| n (%) | 32.3 | 32.9 | 33.4 | 32.9 | 32.9 | 0.4 | 1.2 |

**Table 120. Manatts RPCC/RAP subbase frost-heave and thaw-weakening test results**

| | 1 | 2 | 3 | 4 | μ | σ | COV (%) |
|---|---|---|---|---|---|---|---|
| CBR (%) (Standard Test) | 48.2* | | | | — | — | — |
| CBR (%) (After frost-heave test) | 38.7* | 25.3* | 32.7* | 36.0* | 33.2 | 5.8 | 17.4 |
| 1st Frost-Heave Rate (mm/day) | 2.0 | 2.7 | 1.5 | 1.7 | 2.0 | 0.4 | 23.0 |
| 2nd Frost-Heave Rate (mm/day) | 1.9 | 2.4 | 1.6 | 1.7 | 1.9 | 0.4 | 19.1 |
| 1st Frost-Heave Susceptibility Rating | Low | Low | Very low | Very low | Low | — | — |
| 2nd Frost-Heave Susceptibility Rating | Very low | Low | Very low | Very low | Very low | — | — |
| Thaw Weakening Susceptibility | Negligible | Negligible | Negligible | Negligible | Negligible | — | — |

*CBR is higher at 0.2 in. penetration

## Martin Marietta Materials

### Crushed Limestone Subbase

**Table 121. Martin Marietta Materials crushed limestone subbase frost-heave sample preparation properties**

| | 1 | 2 | 3 | 4 | μ | σ | COV (%) |
|---|---|---|---|---|---|---|---|
| $\gamma_d$ (kN/m$^3$) | 20.4 | 20.5 | 20.6 | 21.1 | 20.6 | 0.3 | 1.4 |
| *w (%)* | 3.9 | 3.3 | 3.6 | 3.6 | 3.6 | 0.2 | 6.1 |
| $G_s$ | 2.71 | | | | — | — | — |
| S (%) | 34.6 | 29.6 | 32.9 | 37.8 | 33.7 | 2.9 | 8.7 |
| e | 0.30 | 0.30 | 0.29 | 0.26 | 0.29 | 0.02 | 6.1 |
| n (%) | 23.3 | 23.0 | 22.6 | 20.6 | 22.4 | 1.1 | 4.8 |

**Table 122. Martin Marietta Materials crushed limestone frost-heave and thaw-weakening test results**

| | 1 | 2 | 3 | 4 | μ | σ | COV (%) |
|---|---|---|---|---|---|---|---|
| CBR (%) (Standard Test) | 87.3* | | | | — | — | — |
| CBR (%) (After frost-heave test) | 56.0* | 37.3* | 45.3* | 51.3* | 47.5 | 8.1 | 17.0 |
| 1st Frost-Heave Rate (mm/day) | 4.8 | 6.3 | 7.0 | 5.6 | 5.9 | 0.8 | 13.5 |
| 2nd Frost-Heave Rate (mm/day) | 6.2 | 8.3 | 8.7 | 8.6 | 8.0 | 1.2 | 14.6 |
| 1st Frost-Heave Susceptibility Rating | Medium | Medium | Medium | Medium | Medium | — | — |
| 2nd Frost-Heave Susceptibility Rating | Medium | High | High | High | High | — | — |
| Thaw Weakening Susceptibility | Negligible | Negligible | Negligible | Negligible | Negligible | — | — |

*CBR is higher at 0.2 in. penetration

## MI I-96

### Clayey Sand Subgrade

**Table 123. MI I-96 clayey sand subgrade frost-heave sample preparation properties**

| | 1 | 2 | 3 | 4 | μ | σ | COV (%) |
|---|---|---|---|---|---|---|---|
| $\gamma_d$ (kN/m$^3$) | 20.1 | 20.3 | 20.5 | 20.3 | 20.3 | 0.1 | 0.7 |
| *w (%)* | 9.2 | 9.2 | 9.1 | 8.8 | 9.1 | 0.2 | 2.1 |
| $G_s$ | 2.66 | | | | — | — | — |
| S (%) | 82.4 | 86.2 | 89.3 | 81.5 | 84.8 | 3.1 | 3.7 |
| e | 0.30 | 0.28 | 0.27 | 0.29 | 0.28 | 0.01 | 3.2 |
| n (%) | 22.9 | 22.2 | 21.4 | 22.2 | 22.2 | 0.6 | 2.5 |

**Table 124. MI I-96 clayey sand subgrade frost-heave and thaw-weakening test results**

| | 1 | 2 | 3 | 4 | μ | σ | COV (%) |
|---|---|---|---|---|---|---|---|
| CBR (%) (Standard Test) | 26.3* | | | | — | — | — |
| CBR (%) (After frost-heave test) | 4.7* | 6.3* | 5.2* | 7.0* | 5.8 | 0.7 | 12.6 |
| 1st Frost-Heave Rate (mm/day) | 6.1 | 4.5 | 3.4 | 5.9 | 4.9 | 1.1 | 22.3 |
| 2nd Frost-Heave Rate (mm/day) | 14.2 | 12.3 | 11.5 | 14.2 | 13.1 | 1.4 | 10.6 |
| 1st Frost-Heave Susceptibility Rating | Medium | Medium | Low | Medium | Medium | — | — |
| 2nd Frost-Heave Susceptibility Rating | High | High | High | High | High | — | — |
| Thaw Weakening Susceptibility | High | Medium | Medium | Medium | Medium | — | — |

*CBR is higher at 0.2 in. penetration

## PA US-22

### Sandy Lean Clay Subgrade

**Table 125. PA US-22 sandy lean clay subgrade frost-heave sample preparation properties**

| | 1 | 2 | 3 | 4 | μ | σ | COV (%) |
|---|---|---|---|---|---|---|---|
| $\gamma_d$ (kN/m$^3$) | 17.7 | 17.5 | 17.6 | 17.5 | 17.6 | 0.1 | 0.5 |
| *w (%)* | 15.9 | 15.6 | 15.7 | 15.0 | 15.6 | 0.3 | 2.2 |
| $G_s$ | 2.72 | | | | — | — | — |
| S (%) | 84.8 | 80.6 | 83.3 | 78.2 | 81.7 | 2.5 | 3.1 |
| e | 0.51 | 0.53 | 0.51 | 0.52 | 0.52 | 0.01 | 1.3 |
| n (%) | 33.7 | 34.5 | 34.0 | 34.3 | 34.1 | 0.3 | 0.9 |

**Table 126. PA US-22 sandy lean clay subgrade frost-heave and thaw-weakening test results**

| | 1 | 2 | 3 | 4 | μ | σ | COV (%) |
|---|---|---|---|---|---|---|---|
| CBR (%) (Standard Test) | 21.1 | | | | — | — | — |
| CBR (%) (After frost-heave test) | 3.1* | 3.5* | 2.8* | 2.6* | 3 | 0.3 | 12.8 |
| 1st Frost-Heave Rate (mm/day) | 2.4 | 2.2 | 2.9 | 3.6 | 2.8 | 0.5 | 18.8 |
| 2nd Frost-Heave Rate (mm/day) | 3.8 | 4.0 | 4.9 | 4.6 | 4.3 | 0.5 | 11.4 |
| 1st Frost-Heave Susceptibility Rating | Low | Low | Low | Low | Low | — | — |
| 2nd Frost-Heave Susceptibility Rating | Low | Medium | Medium | Medium | Medium | — | — |
| Thaw Weakening Susceptibility | High | High | High | High | High | — | — |

*CBR is higher at 0.2 in. penetration

## Pottawattamie County, Iowa

### Loess

**Table 127. Loess frost-heave sample preparation properties**

| | 1 | 2 | 3 | 4 | μ | σ | COV (%) |
|---|---|---|---|---|---|---|---|
| $\gamma_d$ (kN/m$^3$) | 16.5 | 16.4 | 16.7 | 16.6 | 16.6 | 0.1 | 0.7 |
| *w (%)* | 17.01 | 17.7 | 18.0 | 18.6 | 17.8 | 0.6 | 3.1 |
| $G_s$ | 2.7 | | | | — | — | — |
| S (%) | 76.3 | 78.0 | 83.2 | 84.1 | 80.4 | 3.3 | 4.1 |
| e | 0.60 | 0.61 | 0.58 | 0.60 | 0.60 | 0.01 | 1.74 |
| n (%) | 37.6 | 38.0 | 36.8 | 37.4 | 37.4 | 0.4 | 1.1 |

**Table 128. Loess frost-heave and thaw-weakening test results**

| | 1 | 2 | 3 | 4 | μ | σ | COV (%) |
|---|---|---|---|---|---|---|---|
| CBR (%) (Standard Test) | 10* | | | | — | — | — |
| CBR (%) (After frost-heave test) | 0.3* | — | 0.5* | 0.7* | 0.5 | 0.2 | 44 |
| 1st Frost-Heave Rate (mm/day) | 14.9 | 13.0 | 8.0 | 6.9 | 10.7 | 3.4 | 31.4 |
| 2nd Frost-Heave Rate (mm/day) | 21.5 | 22.9 | 13.1 | 18.8 | 19.1 | 4.4 | 22.8 |
| 1st Frost-Heave Susceptibility Rating | High | High | Medium | Medium | High | — | — |
| 2nd Frost-Heave Susceptibility Rating | Very high | Very high | High | Very high | Very high | — | — |
| Thaw Weakening Susceptibility | Very high | — | Very high | Very high | Very high | — | — |

*CBR is higher at 0.2 in. penetration

## Cement-Treated Loess

**Table 129. Cement-treated loess frost-heave sample preparation properties (13% initial moisture content and 3% cement content)**

| | 1 | 2 | μ | σ | COV (%) |
|---|---|---|---|---|---|
| $\gamma_d$ (kN/m$^3$) | 14.9 | 14.5 | 14.7 | 0.2 | 1.5 |
| Initial *w (%)* | 12.7 | 12.7 | 12.7 | 0.0 | 0.0 |
| *w (%)* with cement | 11.5 | 11.7 | 11.6 | 0.1 | 1.1 |
| $G_s$ | 2.74 | | — | — | — |
| S (%) | 39.1 | 37.5 | 38.3 | 0.8 | 2.1 |
| e | 0.80 | 0.86 | 0.83 | 0.03 | 3.2 |
| n (%) | 44.5 | 46.1 | 45.3 | 0.8 | 1.7 |

**Table 130. Cement-treated loess frost-heave and thaw-weakening test results (13% initial moisture content and 3% cement content)**

| | 1 | 2 | μ | σ | COV (%) |
|---|---|---|---|---|---|
| CBR (%) (Standard Test) | — | | — | — | — |
| CBR (%) (After frost-heave test) | 85.6 | 57.6 | 71.6 | 19.8 | 27.7 |
| 1st Frost-Heave Rate (mm/day) | 0 | 0 | 0 | — | — |
| 2nd Frost-Heave Rate (mm/day) | 0 | 0 | 0 | — | — |
| 1st Frost-Heave Susceptibility Rating | Negligible | Negligible | Negligible | — | — |
| 2nd Frost-Heave Susceptibility Rating | Negligible | Negligible | Negligible | — | — |
| Thaw Weakening Susceptibility | Negligible | Negligible | Negligible | — | — |

*CBR is higher at 0.2 in. penetration

**Table 131. Cement-treated loess frost-heave sample preparation properties (20% initial moisture content and 3% cement content)**

| | 1 | 2 | μ | σ | COV (%) |
|---|---|---|---|---|---|
| $\gamma_d$ (kN/m$^3$) | 16.2 | 16.4 | 16.3 | 0.1 | 0.6 |
| Initial *w (%)* | 21.2 | 20.1 | 20.6 | 0.5 | 2.5 |
| *w (%)* with cement | 18.9 | 17.9 | 18.4 | 0.5 | 2.9 |
| $G_s$ | 2.74 | | — | — | — |
| S (%) | 79.2 | 77.2 | 78.2 | 1.0 | 1.3 |
| e | 0.66 | 0.63 | 0.65 | 0.0 | 1.6 |
| n (%) | 39.6 | 38.8 | 39.2 | 0.4 | 1.0 |

**Table 132. Cement-treated loess frost-heave and thaw-weakening test results (20% initial moisture content and 3% cement content)**

| | 1 | 2 | μ | σ | COV (%) |
|---|---|---|---|---|---|
| CBR (%) (Standard Test) | — | | — | — | — |
| CBR (%) (After frost-heave test) | >100 | >100 | — | — | — |
| 1st Frost-Heave Rate (mm/day) | 0 | 0 | 0 | — | — |
| 2nd Frost-Heave Rate (mm/day) | 0 | 0 | 0 | — | — |
| 1st Frost-Heave Susceptibility Rating | Negligible | Negligible | Negligible | — | — |
| 2nd Frost-Heave Susceptibility Rating | Negligible | Negligible | Negligible | — | — |
| Thaw Weakening Susceptibility | Negligible | Negligible | Negligible | — | — |

*CBR is higher at 0.2 in. penetration

**Table 133. Cement-treated loess frost-heave sample preparation properties (20% initial moisture content and 5% cement content)**

| | 1 | 2 | μ | σ | COV (%) |
|---|---|---|---|---|---|
| $\gamma_d$ (kN/m$^3$) | 15.8 | 15.6 | 15.7 | 0.1 | 0.6 |
| Initial *w (%)* | 20.0 | 19.9 | 19.9 | 0.0 | 0.3 |
| *w (%)* with cement | 17.7 | 18.1 | 17.9 | 0.2 | 0.9 |
| $G_s$ | 2.74 | | — | — | — |
| S (%) | 69.0 | 68.2 | 68.6 | 0.4 | 0.6 |
| e | 0.71 | 0.73 | 0.72 | 0.0 | 1.4 |
| n (%) | 41.4 | 42.0 | 41.7 | 0.3 | 0.8 |

**Table 134. Cement-treated loess frost-heave and thaw-weakening test results (20% initial moisture content and 5% cement content)**

| | 1 | 2 | μ | σ | COV (%) |
|---|---|---|---|---|---|
| CBR (%) (Standard Test) | — | | — | — | — |
| CBR (%) (After frost-heave test) | >100 | >100 | — | — | — |
| 1st Frost-Heave Rate (mm/day) | 0 | 0 | 0 | — | — |
| 2nd Frost-Heave Rate (mm/day) | 0 | 0 | 0 | — | — |
| 1st Frost-Heave Susceptibility Rating | Negligible | Negligible | Negligible | — | — |
| 2nd Frost-Heave Susceptibility Rating | Negligible | Negligible | Negligible | — | — |
| Thaw Weakening Susceptibility | Negligible | Negligible | Negligible | — | — |

*CBR is higher at 0.2 in. penetration

**Table 135. Cement-treated loess frost-heave sample preparation properties (20% initial moisture content and 7% cement content)**

| | 1 | 2 | μ | σ | COV (%) |
|---|---|---|---|---|---|
| $\gamma_d$ (kN/m$^3$) | 15.9 | 15.9 | 15.9 | 0.0 | 0.1 |
| Initial *w (%)* | 20.3 | 20.2 | 20.2 | 0.0 | 0.1 |
| *w (%)* with cement | 17.7 | 17.9 | 17.8 | 0.1 | 0.7 |
| $G_s$ | 2.74 | | — | — | — |
| S (%) | 69.8 | 70.6 | 70.2 | 0.4 | 0.5 |
| e | 0.69 | 0.70 | 0.70 | 0 | 0.1 |
| n (%) | 41.0 | 41.0 | 41.0 | 0.0 | 0.1 |

**Table 136. Cement-treated loess frost-heave and thaw-weakening test results (20% initial moisture content and 7% cement content)**

| | 1 | 2 | μ | σ | COV (%) |
|---|---|---|---|---|---|
| CBR (%) (Standard Test) | — | | — | — | — |
| CBR (%) (After frost-heave test) | >100 | >100 | — | — | — |
| 1st Frost-Heave Rate (mm/day) | 0 | 0 | 0 | — | — |
| 2nd Frost-Heave Rate (mm/day) | 0 | 0 | 0 | — | — |
| 1st Frost-Heave Susceptibility Rating | Negligible | Negligible | Negligible | — | — |
| 2nd Frost-Heave Susceptibility Rating | Negligible | Negligible | Negligible | — | — |
| Thaw Weakening Susceptibility | Negligible | Negligible | Negligible | — | — |

*CBR is higher at 0.2 in. penetration

**Table 137. Cement-treated loess frost-heave sample preparation properties (13% initial moisture content and 9% cement content)**

| | 1 | 2 | μ | σ | COV (%) |
|---|---|---|---|---|---|
| $\gamma_d$ (kN/m$^3$) | 15.0 | 15.0 | 15.0 | 0.01 | 0.1 |
| Initial *w (%)* | 12.9 | 13.4 | 13.1 | 0.3 | 2.0 |
| *w (%)* with cement | 10.4 | 11.1 | 10.7 | 0.4 | 3.3 |
| $G_s$ | 2.74 | | — | — | — |
| S (%) | 36.1 | 38.4 | 37.2 | 1.2 | 3.1 |
| e | 0.79 | 0.79 | 0.79 | 0 | 0.2 |
| n (%) | 44.0 | 44.1 | 44.1 | 0.1 | 0.12 |

**Table 138. Cement-treated loess frost-heave and thaw-weakening test results (13% initial moisture content and 9% cement content)**

| | 1 | 2 | μ | σ | COV (%) |
|---|---|---|---|---|---|
| CBR (%) (Standard Test) | — | | — | — | — |
| CBR (%) (After frost-heave test) | >100 | >100 | — | — | — |
| 1st Frost-Heave Rate (mm/day) | 0 | 0 | 0 | — | — |
| 2nd Frost-Heave Rate (mm/day) | 0 | 0 | 0 | — | — |
| 1st Frost-Heave Susceptibility Rating | Negligible | Negligible | Negligible | — | — |
| 2nd Frost-Heave Susceptibility Rating | Negligible | Negligible | Negligible | — | — |
| Thaw Weakening Susceptibility | Negligible | Negligible | Negligible | — | — |

*CBR is higher at 0.2 in. penetration

**Table 139. Cement-treated loess frost-heave sample preparation properties (20% initial moisture content and 9% cement content)**

| | 1 | 2 | μ | σ | COV (%) |
|---|---|---|---|---|---|
| $\gamma_d$ (kN/m$^3$) | 15.9 | 15.8 | 15.8 | 0.01 | 0.0 |
| Initial *w (%)* | 20.3 | 20.1 | 20.2 | 0.1 | 0.5 |
| *w (%)* with cement | 17.5 | 17.3 | 17.4 | 0.1 | 0.1 |
| $G_s$ | 2.74 | | — | — | — |
| S (%) | 68.8 | 68.0 | 68.4 | 0.4 | 0.6 |
| e | 0.70 | 0.70 | 0.70 | 0 | 0.2 |
| n (%) | 41.0 | 41.1 | 41.1 | 0.0 | 0.1 |

**Table 140. Cement-treated loess frost-heave and thaw-weakening test results (20% initial moisture content and 9% cement content)**

| | 1 | 2 | μ | σ | COV (%) |
|---|---|---|---|---|---|
| CBR (%) (Standard Test) | — | | — | — | — |
| CBR (%) (After frost-heave test) | >100 | >100 | — | — | — |
| 1st Frost-Heave Rate (mm/day) | 0 | 0 | 0 | — | — |
| 2nd Frost-Heave Rate (mm/day) | 0 | 0 | 0 | — | — |
| 1st Frost-Heave Susceptibility Rating | Negligible | Negligible | Negligible | — | — |
| 2nd Frost-Heave Susceptibility Rating | Negligible | Negligible | Negligible | — | — |
| Thaw Weakening Susceptibility | Negligible | Negligible | Negligible | — | — |

*CBR is higher at 0.2 in. penetration

**Table 141. Cement-treated loess frost-heave sample preparation properties (20% initial moisture content and 11% cement content)**

| | 1 | 2 | μ | σ | COV (%) |
|---|---|---|---|---|---|
| $\gamma_d$ (kN/m$^3$) | 16.0 | 15.9 | 15.9 | 0.0 | 0.2 |
| Initial *w (%)* | 19.45 | 19.74 | 19.59 | 0.1 | 0.7 |
| *w (%)* with cement | 17.0 | 16.7 | 16.8 | 0.1 | 0.8 |
| $G_s$ | 2.74 | | — | — | — |
| S (%) | 68.0 | 66.3 | 67.1 | 0.9 | 1.3 |
| e | 0.68 | 0.69 | 0.69 | 0.0 | 0.5 |
| n (%) | 40.6 | 40.9 | 40.7 | 0.1 | 0.3 |

**Table 142. Cement-treated loess frost-heave and thaw-weakening test results (20% initial moisture content and 11% cement content)**

| | 1 | 2 | μ | σ | COV (%) |
|---|---|---|---|---|---|
| CBR (%) (Standard Test) | — | | — | — | — |
| CBR (%) (After frost-heave test) | >100 | >100 | — | — | — |
| 1st Frost-Heave Rate (mm/day) | 0 | 0 | 0 | — | — |
| 2nd Frost-Heave Rate (mm/day) | 0 | 0 | 0 | — | — |
| 1st Frost-Heave Susceptibility Rating | Negligible | Negligible | Negligible | — | — |
| 2nd Frost-Heave Susceptibility Rating | Negligible | Negligible | Negligible | — | — |
| Thaw Weakening Susceptibility | Negligible | Negligible | Negligible | — | — |

*CBR is higher at 0.2 in. penetration

**Table 143. Cement-treated loess frost-heave sample preparation properties (22% initial moisture content and 13% cement content)**

| | 1 | 2 | μ | σ | COV (%) |
|---|---|---|---|---|---|
| $\gamma_d$ (kN/m$^3$) | 16.2 | 16.0 | 16.1 | 0.1 | 0.5 |
| Initial *w (%)* | 21.8 | 21.8 | 21.8 | 0 | 0.0 |
| *w (%)* with cement | 18.3 | 18.2 | 18.3 | .01 | 0.4 |
| $G_s$ | 2.74 | | — | — | — |
| S (%) | 76.0 | 73.6 | 74.8 | 1.2 | 1.6 |
| e | 0.66 | 0.68 | 0.67 | 0.0 | 1.22 |
| n (%) | 39.8 | 40.4 | 40.1 | 0.3 | 0.7 |

**Table 144. Cement-treated loess frost-heave and thaw-weakening test results (22% initial moisture content and 13% cement content)**

| | 1 | 2 | μ | σ | COV (%) |
|---|---|---|---|---|---|
| CBR (%) (Standard Test) | — | | — | — | — |
| CBR (%) (After frost-heave test) | >100 | >100 | — | — | — |
| 1st Frost-Heave Rate (mm/day) | 0 | 0 | 0 | — | — |
| 2nd Frost-Heave Rate (mm/day) | 0 | 0 | 0 | — | — |
| 1st Frost-Heave Susceptibility Rating | Negligible | Negligible | Negligible | — | — |
| 2nd Frost-Heave Susceptibility Rating | Negligible | Negligible | Negligible | — | — |
| Thaw Weakening Susceptibility | Negligible | Negligible | Negligible | — | — |

## Fly Ash-Treated Loess

**Table 145. Fly ash-treated loess frost-heave sample preparation properties (10% initial moisture content and 10% fly ash content)**

| | 1 | 2 | μ | σ | COV (%) |
|---|---|---|---|---|---|
| $\gamma_d$ (kN/m$^3$) | 14.5 | 14.6 | 14.5 | 0.1 | 0.4 |
| Initial *w (%)* | 10.0 | 10.0 | 10.0 | 0.0 | 0.0 |
| *w (%)* with cement | 8.2 | 8.8 | 8.5 | 0.3 | 3.2 |
| $G_s$ | 2.68 | | — | — | — |
| S (%) | 27.0 | 29.2 | 28.1 | 1.1 | 4.0 |
| e | 0.82 | 0.81 | 0.81 | 0.0 | 0.8 |
| n (%) | 45.0 | 44.6 | 44.8 | 0.2 | 0.4 |

**Table 146. Fly ash-treated loess frost-heave and thaw-weakening test results (10% initial moisture content and 10% fly ash content)**

| | 1 | 2 | μ | σ | COV (%) |
|---|---|---|---|---|---|
| CBR (%) (Standard Test) | — | | — | — | — |
| CBR (%) (After frost-heave test) | 4.0* | 3.6* | 3.8 | 0.3 | 8.2 |
| 1st Frost-Heave Rate (mm/day) | 2.4 | 2.5 | 2.5 | 0.1 | 2.0 |
| 2nd Frost-Heave Rate (mm/day) | 15.3 | 16.3 | 15.83 | 0.7 | 4.5 |
| 1st Frost-Heave Susceptibility Rating | Low | Low | Low | — | — |
| 2nd Frost-Heave Susceptibility Rating | High | Very high | High | — | — |
| Thaw Weakening Susceptibility | High | High | High | — | — |

*CBR is higher at 0.2 in. penetration

**Table 147. Fly ash-treated loess frost-heave sample preparation properties (19% initial moisture content and 10% fly ash content)**

| | 1 | 2 | μ | σ | COV (%) |
|---|---|---|---|---|---|
| $\gamma_d$ (kN/m$^3$) | 16.3 | 16.2 | 16.3 | 0.0 | 0.2 |
| Initial *w (%)* | — | 19.0 | — | — | — |
| *w (%)* with cement | 16.7 | 16.7 | 16.7 | 0.0 | 0.2 |
| $G_s$ | 2.68 | | — | — | — |
| S (%) | 73.2 | 72.3 | 72.8 | 0.4 | 0.6 |
| e | 0.61 | 0.62 | 0.62 | 0.0 | 0.5 |
| n (%) | 38.0 | 38.2 | 38.1 | 0.1 | 0.3 |

**Table 148. Fly ash-treated loess frost-heave and thaw-weakening test results (19% initial moisture content and 10% fly ash content)**

| | 1 | 2 | μ | σ | COV (%) |
|---|---|---|---|---|---|
| CBR (%) (Standard Test) | — | | — | — | — |
| CBR (%) (After frost-heave test) | 3.8* | 6.2* | 5.0 | 1.7 | 33.9 |
| 1st Frost-Heave Rate (mm/day) | 9.0 | 11.2 | 10.1 | 1.1 | 10.9 |
| 2nd Frost-Heave Rate (mm/day) | 20.6 | 23.7 | 22.2 | 2.2 | 9.9 |
| 1st Frost-Heave Susceptibility Rating | High | High | High | — | — |
| 2nd Frost-Heave Susceptibility Rating | Very high | Very high | Very high | — | — |
| Thaw Weakening Susceptibility | High | Medium | High | — | — |

*CBR is higher at 0.2 in. penetration

**Table 149. Fly ash-treated loess frost-heave sample preparation properties (19% initial moisture content and 15% fly ash content)**

| | 1 | 2 | μ | σ | COV (%) |
|---|---|---|---|---|---|
| $\gamma_d$ (kN/m$^3$) | 15.6 | 15.8 | 15.7 | 0.1 | 0.6 |
| Initial *w (%)* | 18.7 | 18.6 | 18.7 | 0.1 | 0.4 |
| *w (%)* with cement | 15.5 | 14.9 | 15.2 | 0.3 | 1.8 |
| $G_s$ | 2.68 | | — | — | — |
| S (%) | 60.9 | 60.6 | 60.7 | 0.2 | 0.3 |
| e | 0.68 | 0.66 | 0.67 | 0.0 | 1.5 |
| n (%) | 40.5 | 39.8 | 40.1 | 0.4 | 0.9 |

**Table 150. Fly ash-treated loess frost-heave and thaw-weakening test results (19% initial moisture content and 15% fly ash content)**

| | 1 | 2 | μ | σ | COV (%) |
|---|---|---|---|---|---|
| CBR (%) (Standard Test) | — | | — | — | — |
| CBR (%) (After frost-heave test) | 7.1* | 7.2* | 7.1 | 0.1 | 1.3 |
| 1st Frost-Heave Rate (mm/day) | 8.0 | 4.3 | 6.2 | 1.9 | 30.1 |
| 2nd Frost-Heave Rate (mm/day) | 19.1 | 9.1 | 14.1 | 7.1 | 50.0 |
| 1st Frost-Heave Susceptibility Rating | High | Medium | Medium | — | — |
| 2nd Frost-Heave Susceptibility Rating | Very high | High | High | — | — |
| Thaw Weakening Susceptibility | Medium | Medium | Medium | — | — |

*CBR is higher at 0.2 in. penetration

**Table 151. Fly ash-treated loess frost-heave sample preparation properties (22% initial moisture content and 20% fly ash content)**

| | 1 | 2 | μ | σ | COV (%) |
|---|---|---|---|---|---|
| $\gamma_d$ (kN/m$^3$) | 16.5 | 15.7 | 16.1 | 0.4 | 2.6 |
| Initial *w (%)* | 20.6 | 21.0 | 20.8 | 0.2 | 0.9 |
| *w (%)* with cement | 16.9 | 16.6 | 16.8 | 0.2 | 1.0 |
| $G_s$ | 2.68 | | — | — | — |
| S (%) | 76.4 | 65.7 | 71.0 | 5.4 | 7.6 |
| e | 0.59 | 0.68 | 0.64 | 0.0 | 6.6 |
| n (%) | 37.3 | 40.4 | 38.8 | 1.6 | 4.0 |

**Table 152. Fly ash-treated loess frost-heave and thaw-weakening test results (22% initial moisture content and 20% fly ash content)**

| | 1 | 2 | μ | σ | COV (%) |
|---|---|---|---|---|---|
| CBR (%) (Standard Test) | — | | — | — | — |
| CBR (%) (After frost-heave test) | 24.3* | 26.7* | 25.5 | 1.7 | 6.5 |
| 1st Frost-Heave Rate (mm/day) | 7.8 | 6.8 | 7.3 | 0.5 | 6.5 |
| 2nd Frost-Heave Rate (mm/day) | 10.3 | 11.7 | 11.0 | 1.0 | 8.9 |
| 1st Frost-Heave Susceptibility Rating | Medium | Medium | Medium | — | — |
| 2nd Frost-Heave Susceptibility Rating | High | High | High | — | — |
| Thaw Weakening Susceptibility | Negligible | Negligible | Negligible | — | — |

*CBR is higher at 0.2 in. penetration

## WI US-10

### Sandy Lean Clay Subgrade

**Table 153. WI US-10 sandy lean clay subgrade frost-heave sample preparation properties**

| | 1 | 2 | 3 | 4 | μ | σ | COV (%) |
|---|---|---|---|---|---|---|---|
| $\gamma_d$ (kN/m$^3$) | 18.1 | 18.2 | 18.3 | 18.4 | 18.2 | 0.1 | 0.6 |
| *w (%)* | 12.0 | 12.2 | 13.9 | 12.4 | 12.7 | 0.8 | 5.9 |
| $G_s$ | 2.69 | | | | — | — | — |
| S (%) | 70.7 | 73.2 | 84.3 | 76.9 | 76.3 | 5.1 | 6.7 |
| e | 0.46 | 0.45 | 0.44 | 0.43 | 0.45 | 0.01 | 1.89 |
| n (%) | 31.4 | 31.0 | 30.8 | 30.3 | 30.9 | 0.4 | 1.3 |

**Table 154. WI US-10 sandy lean clay subgrade frost-heave and thaw-weakening test results**

| | 1 | 2 | 3 | 4 | μ | σ | COV (%) |
|---|---|---|---|---|---|---|---|
| CBR (%) (Standard Test) | 25.9 | | | | — | — | — |
| CBR (%) (After frost-heave test) | 7.0* | 7.6* | 6.7* | 7.5* | 7.2* | 0.4 | 5.5 |
| 1st Frost-Heave Rate (mm/day) | 4.6 | 4.7 | 4.3 | 4.8 | 4.6 | 0.2 | 4.2 |
| 2nd Frost-Heave Rate (mm/day) | 5.6 | 6.7 | 4.9 | 4.7 | 5.5 | 0.9 | 17.2 |
| 1st Frost-Heave Susceptibility Rating | Medium | Medium | Medium | Medium | Medium | — | — |
| 2nd Frost-Heave Susceptibility Rating | Medium | Medium | Medium | Medium | Medium | — | — |
| Thaw Weakening Susceptibility | Medium | Medium | Medium | Medium | Medium | — | — |

*CBR is higher at 0.2 in. penetration

## Cement-treated loess

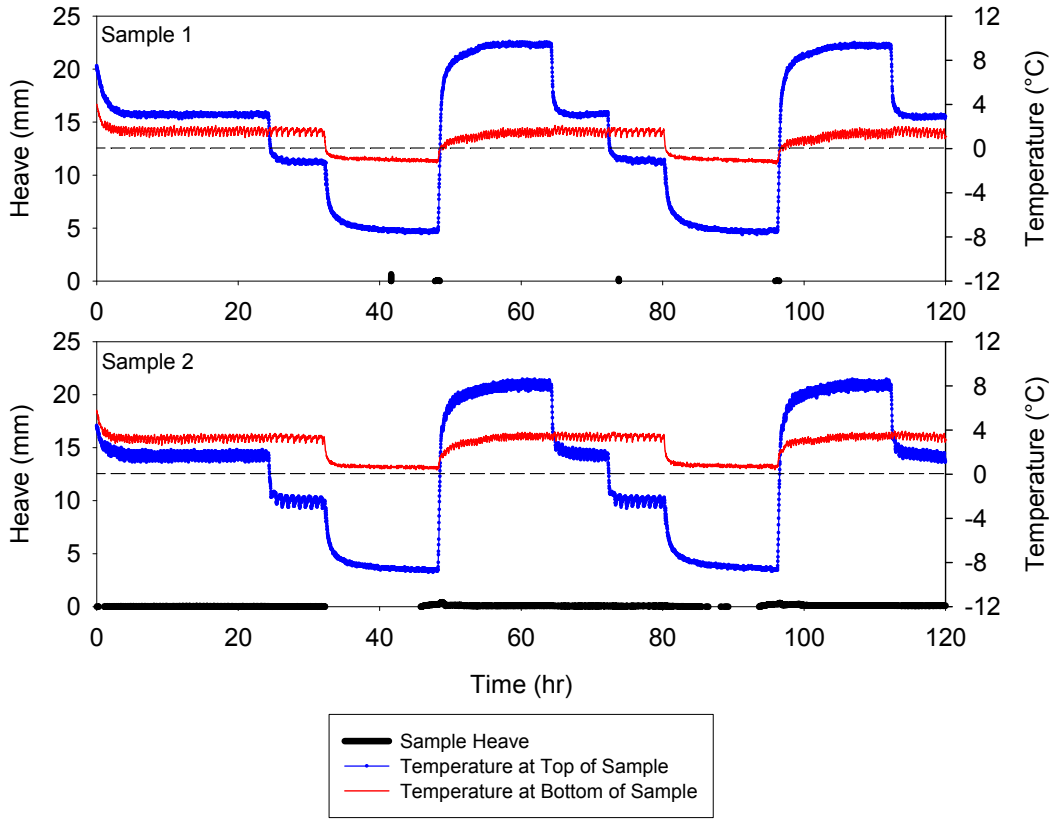


**Figure 265. Cement-treated loess frost heave time plots (20% initial moisture content and 5% cement content)**

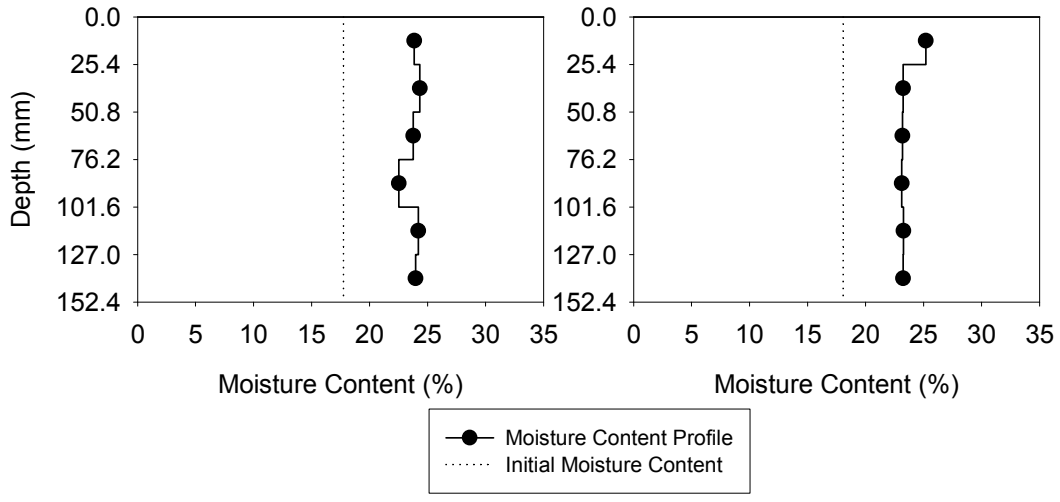


**Figure 266. Cement-treated loess moisture content profiles (20% initial moisture content and 5% cement content)**

**Table 155. Cement-treated loess frost-heave and thaw-weakening test results (20% initial moisture content and 5% cement content)**

| | μ | σ | COV (%) | # of samples |
|---|---|---|---|---|
| CBR (%) (standard test) | | — | | 0 |
| CBR (%) (after frost-susceptibility test) | >100 | — | — | 2 |
| 1st Frost-heave rate (mm/day) | 0 | — | — | |
| 2nd Frost-heave rate (mm/day) | 0 | — | — | |
| 1st Frost-heave susceptibility rating | Negligible | — | — | |
| 2nd Frost-heave susceptibility rating | Negligible | — | — | |
| Thaw-weakening susceptibility rating | Negligible | — | — | |

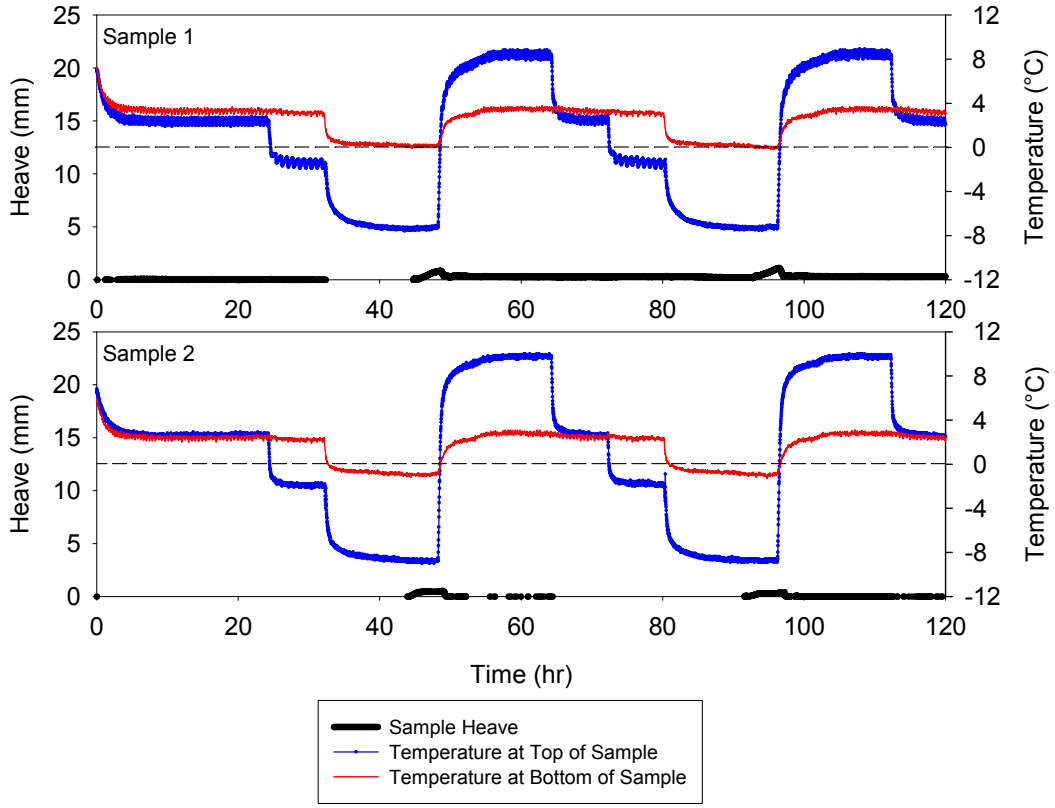


**Figure 267. Cement-treated loess frost heave time plots (20% initial moisture content and 7% cement content)**

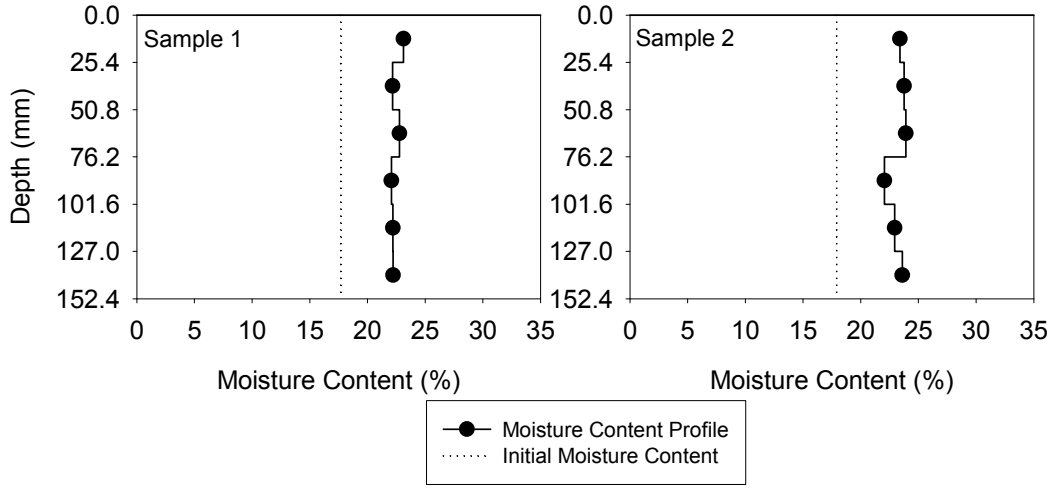


**Figure 268. Cement-treated loess moisture content profiles (20% initial moisture content and 7% cement content)**

**Table 156. Cement-treated loess frost-heave and thaw-weakening test results (20% initial moisture content and 7% cement content)**

| | μ | σ | COV (%) | # of samples |
|---|---|---|---|---|
| CBR (%) (standard test) | — | | | 0 |
| CBR (%) (after frost-susceptibility test) | >100 | — | — | 2 |
| 1st Frost-heave rate (mm/day) | 0 | — | — | |
| 2nd Frost-heave rate (mm/day) | 0 | — | — | |
| 1st Frost-heave susceptibility rating | Negligible | — | — | |
| 2nd Frost-heave susceptibility rating | Negligible | — | — | |
| Thaw-weakening susceptibility rating | Negligible | — | — | |

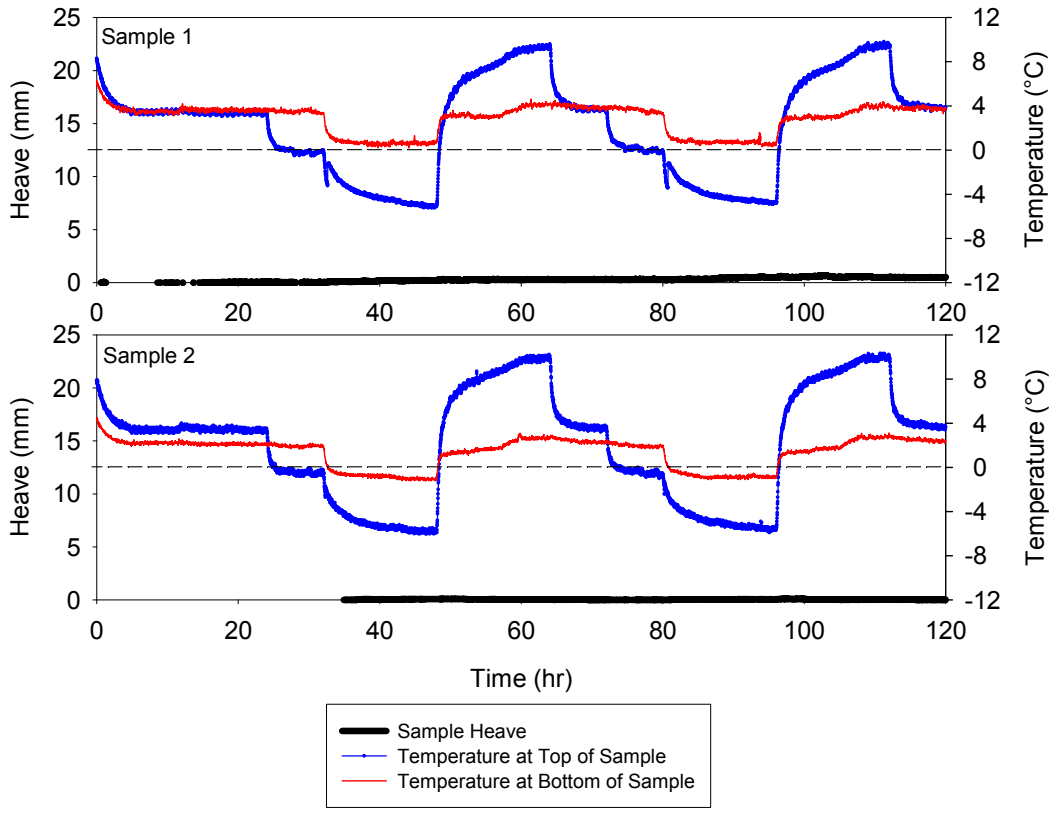


**Figure 269. Cement-treated loess frost heave time plots (13% initial moisture content and 9% cement content)**

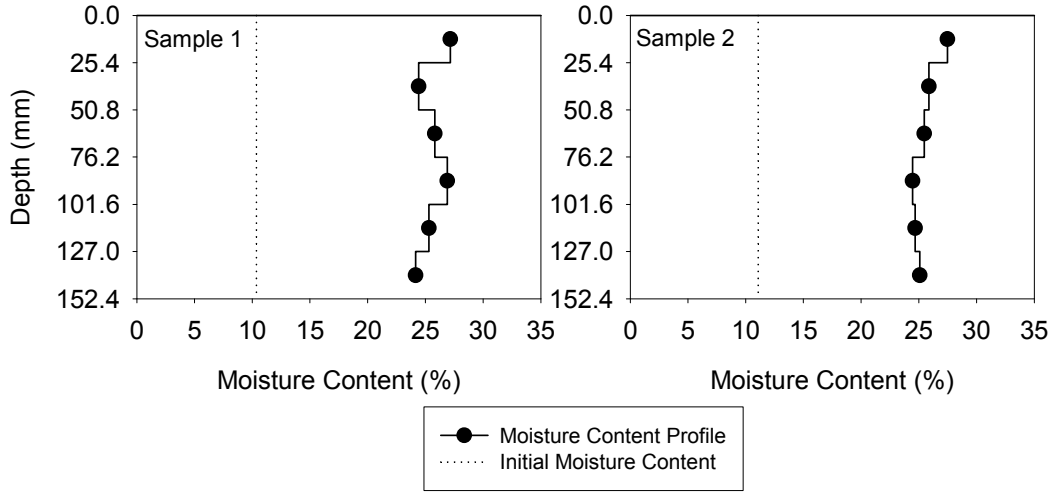


**Figure 270. Cement-treated loess moisture content profiles (13% initial moisture content and 9% cement content)**

**Table 157. Cement-treated loess frost-heave and thaw-weakening test results (13% initial moisture content and 9% cement content)**

| | μ | σ | COV (%) | # of samples |
|---|---|---|---|---|
| CBR (%) (standard test) | | — | | 0 |
| CBR (%) (after frost-susceptibility test) | >100 | — | — | 2 |
| 1st Frost-heave rate (mm/day) | 0 | — | — | |
| 2nd Frost-heave rate (mm/day) | 0 | — | — | |
| 1st Frost-heave susceptibility rating | Negligible | — | — | |
| 2nd Frost-heave susceptibility rating | Negligible | — | — | |
| Thaw-weakening susceptibility rating | Negligible | — | — | |

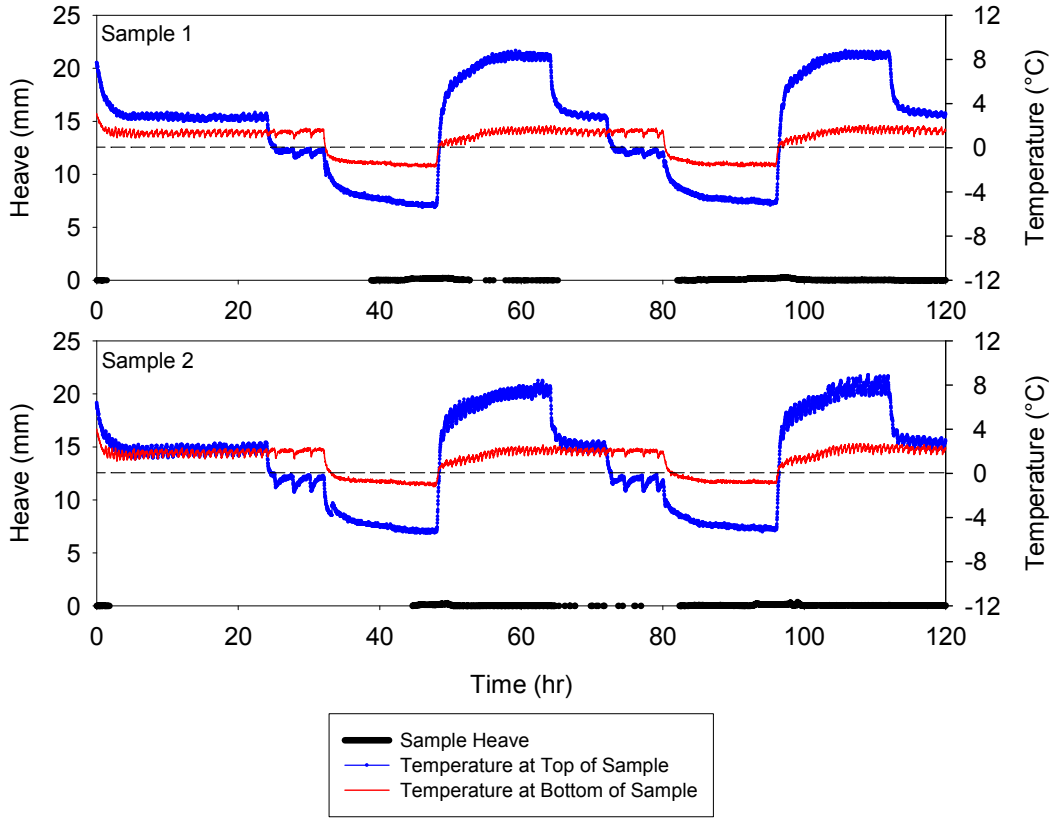


**Figure 271. Cement-treated loess frost heave time plots (20% initial moisture content and 9% cement content)**

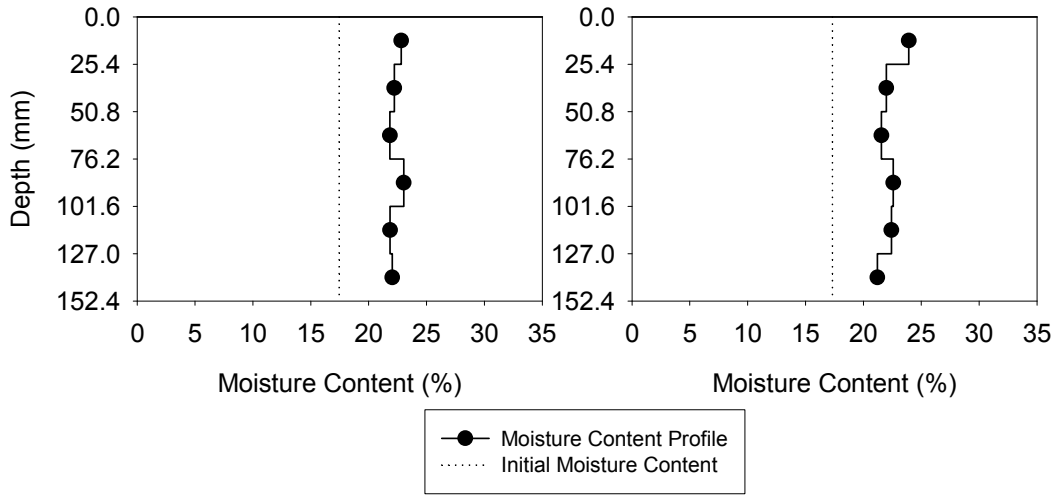


**Figure 272. Cement-treated loess moisture content profiles (20% initial moisture content and 9% cement content)**

**Table 158. Cement-treated loess frost-heave and thaw-weakening test results (20% initial moisture content and 9% cement content)**

| | μ | σ | COV (%) | # of samples |
|---|---|---|---|---|
| CBR (%) (standard test) | | — | | 0 |
| CBR (%) (after frost-susceptibility test) | >100 | — | — | 2 |
| 1st Frost-heave rate (mm/day) | 0 | — | — | |
| 2nd Frost-heave rate (mm/day) | 0 | — | — | |
| 1st Frost-heave susceptibility rating | Negligible | — | — | |
| 2nd Frost-heave susceptibility rating | Negligible | — | — | |
| Thaw-weakening susceptibility rating | Negligible | — | — | |

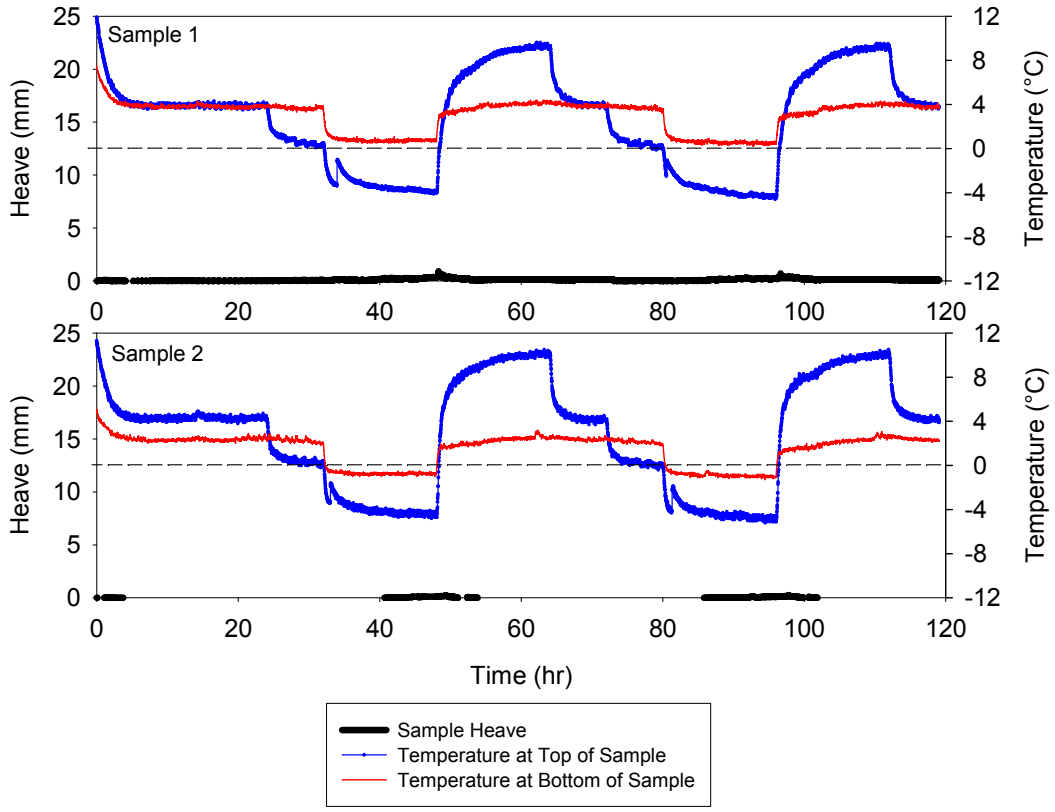


**Figure 273. Cement-treated loess frost heave time plots (20% initial moisture content and 11% cement content)**

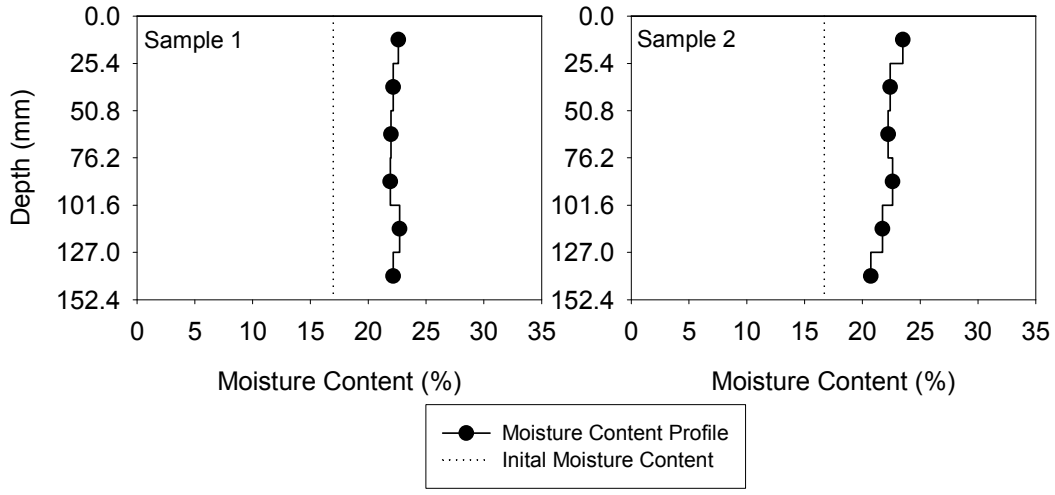


**Figure 274. Cement-treated loess moisture content profiles (20% initial moisture content and 11% cement content)**

**Table 159. Cement-treated loess frost-heave and thaw-weakening test results (20% initial moisture content and 11% cement content)**

| | μ | σ | COV (%) | # of samples |
|---|---|---|---|---|
| CBR (%) (standard test) | | — | | 0 |
| CBR (%) (after frost-susceptibility test) | >100 | — | — | 2 |
| 1st Frost-heave rate (mm/day) | 0 | — | — | |
| 2nd Frost-heave rate (mm/day) | 0 | — | — | |
| 1st Frost-heave susceptibility rating | Negligible | — | — | |
| 2nd Frost-heave susceptibility rating | Negligible | — | — | |
| Thaw-weakening susceptibility rating | Negligible | — | — | |

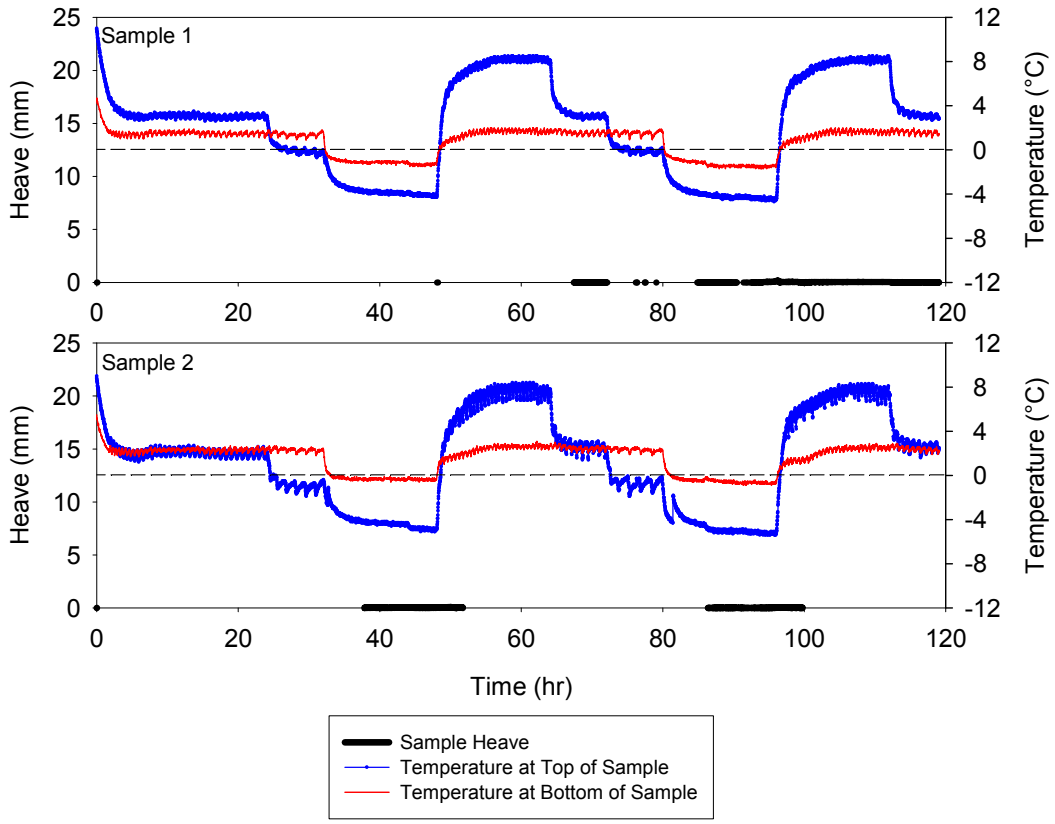


**Figure 275. Cement-treated loess frost heave time plots (22% initial moisture content and 13% cement content)**

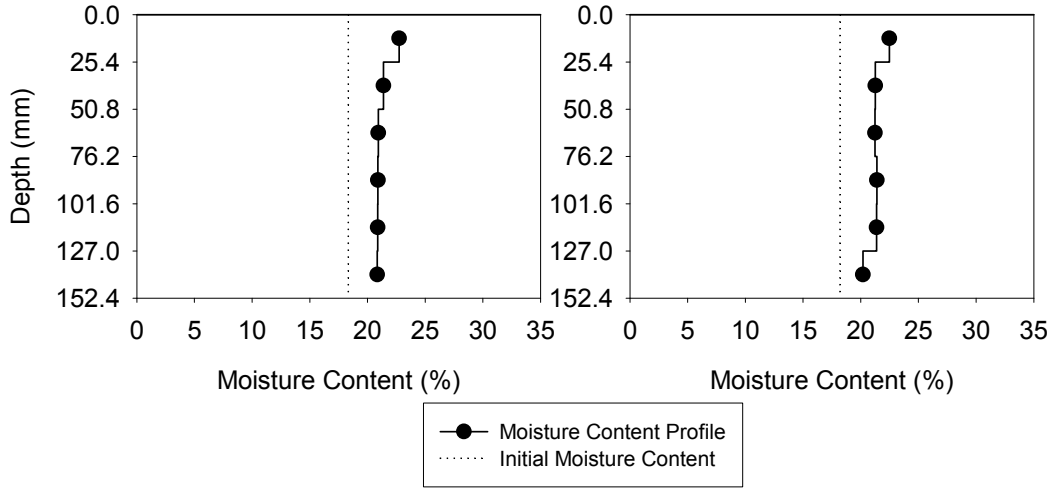


**Figure 276. Cement-treated loess moisture content profiles (22% initial moisture content and 13% cement content)**

**Table 160. Cement-treated loess frost-heave and thaw-weakening test results (22% initial moisture content and 13% cement content)**

| | μ | σ | COV (%) | # of samples |
|---|---|---|---|---|
| CBR (%) (standard test) | — | | | 0 |
| CBR (%) (after frost-susceptibility test) | >100 | — | — | 2 |
| 1st Frost-heave rate (mm/day) | 0 | — | — | |
| 2nd Frost-heave rate (mm/day) | 0 | — | — | |
| 1st Frost-heave susceptibility rating | Negligible | — | — | |
| 2nd Frost-heave susceptibility rating | Negligible | — | — | |
| Thaw-weakening susceptibility rating | Negligible | — | — | |

# APPENDIX E. FROST-HEAVE STATISTICAL ANALYSIS

**Fine and Coarse Materials 2nd Frost Heave Model**

## First Iteration

**Response 2nd Heave Rate**
**Whole Model**
**Actual by Predicted Plot**

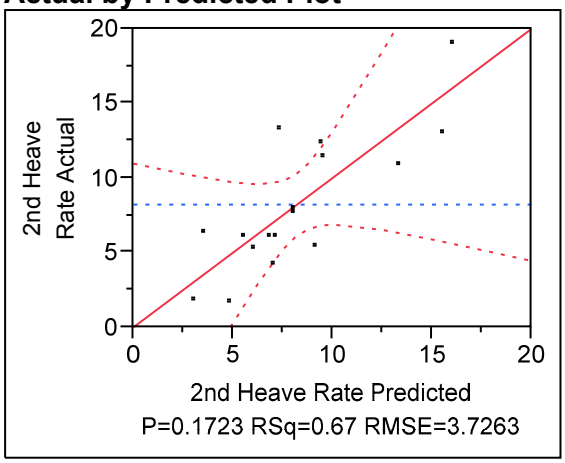


### Summary of Fit

| | |
|---|---|
| RSquare | 0.667295 |
| RSquare Adj | 0.33459 |
| Root Mean Square Error | 3.726292 |
| Mean of Response | 8.229412 |
| Observations (or Sum Wgts) | 17 |

### Analysis of Variance

| Source | DF | Sum of Squares | Mean Square | F Ratio |
|---|---|---|---|---|
| Model | 8 | 222.79326 | 27.8492 | 2.0057 |
| Error | 8 | 111.08203 | 13.8853 | **Prob > F** |
| C. Total | 16 | 333.87529 | | 0.1723 |

### Parameter Estimates

| Term | Estimate | Std Error | t Ratio | Prob>\|t\| | VIF |
|---|---|---|---|---|---|
| Intercept | 16.475538 | 50.33518 | 0.33 | 0.7518 | . |
| D30 | 0.0417378 | 1.226736 | 0.03 | 0.9737 | 9.3707382 |
| D60 | 1.3830968 | 1.254864 | 1.10 | 0.3024 | 58.704829 |
| Gravel Size | -0.418296 | 0.52216 | -0.80 | 0.4462 | 249.63294 |
| Sand Size | 0.0049467 | 0.50789 | 0.01 | 0.9925 | 93.045268 |
| Silt Size | 6.9397551 | 11.53439 | 0.60 | 0.5641 | 104014.61 |
| Clay Size | 6.6587856 | 11.5489 | 0.58 | 0.5801 | 12635.705 |
| Passing 0.074 mm | -6.853964 | 11.2333 | -0.61 | 0.5587 | 167644.22 |
| Passing 0.02 mm | -0.09247 | 0.248363 | -0.37 | 0.7193 | 29.51093 |

**Residual by Predicted Plot**

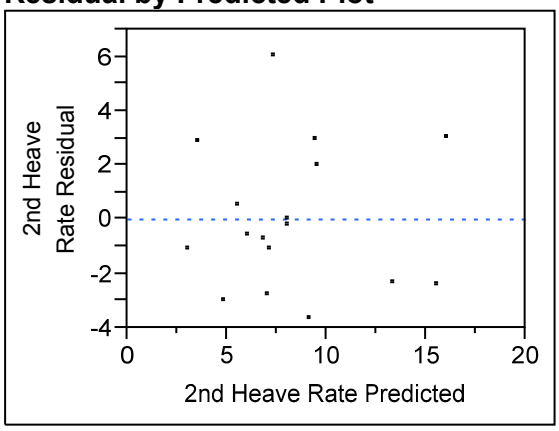


## Second Iteration

**Response 2nd Heave Rate**
**Whole Model**
**Actual by Predicted Plot**

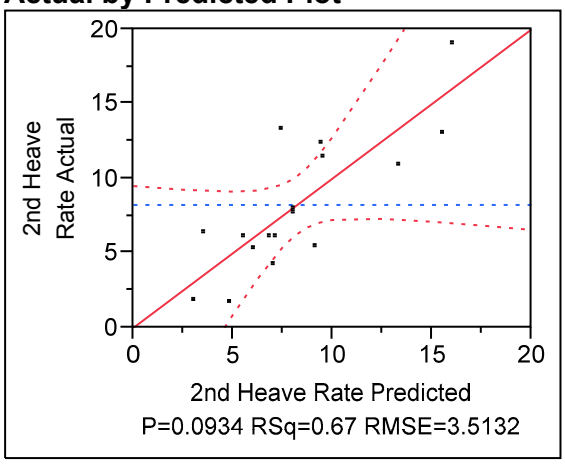


### Summary of Fit

| | |
|---|---|
| RSquare | 0.667291 |
| RSquare Adj | 0.408517 |
| Root Mean Square Error | 3.513203 |
| Mean of Response | 8.229412 |
| Observations (or Sum Wgts) | 17 |

### Analysis of Variance

| Source | DF | Sum of Squares | Mean Square | F Ratio |
|---|---|---|---|---|
| Model | 7 | 222.79194 | 31.8274 | 2.5787 |
| Error | 9 | 111.08335 | 12.3426 | **Prob > F** |
| C. Total | 16 | 333.87529 | | 0.0934 |

### Parameter Estimates

| Term | Estimate | Std Error | t Ratio | Prob>\|t\| | VIF |
|---|---|---|---|---|---|
| Intercept | 16.961739 | 6.089644 | 2.79 | 0.0212* | . |
| D60 | 1.3811396 | 1.167837 | 1.18 | 0.2672 | 57.199517 |
| Gravel Size | -0.422574 | 0.266198 | -1.59 | 0.1469 | 72.988073 |

| Term | Estimate | Std Error | t Ratio | Prob>\|t\| | VIF |
|---|---|---|---|---|---|
| Silt Size | 6.8711833 | 8.613998 | 0.80 | 0.4456 | 65262.288 |
| Clay Size | 6.5905922 | 8.659323 | 0.76 | 0.4661 | 7991.5905 |
| Passing 0.074 mm | -6.790206 | 8.606747 | -0.79 | 0.4504 | 110713.16 |
| Passing 0.02 mm | -0.092756 | 0.232514 | -0.40 | 0.6992 | 29.097454 |
| D30 | 0.03731 | 1.074233 | 0.03 | 0.9731 | 8.0838008 |

**Residual by Predicted Plot**

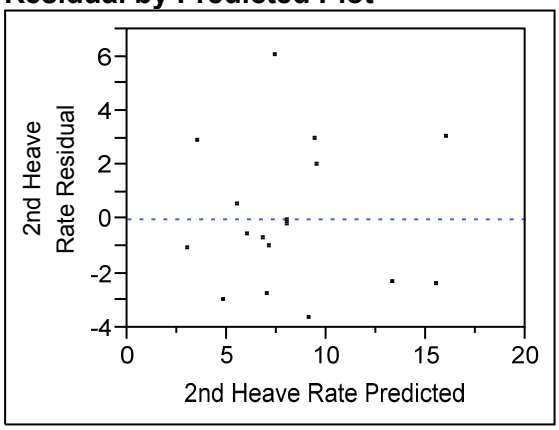


## Third Iteration

**Response 2nd Heave Rate**
**Whole Model**
**Actual by Predicted Plot**

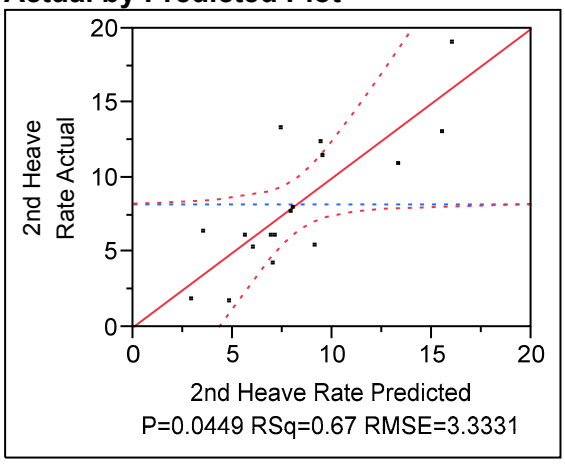


**Summary of Fit**

| | |
|---|---|
| RSquare | 0.667246 |
| RSquare Adj | 0.467594 |
| Root Mean Square Error | 3.33314 |
| Mean of Response | 8.229412 |
| Observations (or Sum Wgts) | 17 |

**Analysis of Variance**

| Source | DF | Sum of Squares | Mean Square | F Ratio |
|---|---|---|---|---|
| Model | 6 | 222.77705 | 37.1295 | 3.3420 |

| Source | DF | Sum of Squares | Mean Square | F Ratio |
|---|---|---|---|---|
| Error | 10 | 111.09824 | 11.1098 | Prob > F |
| C. Total | 16 | 333.87529 | | 0.0449* |

**Parameter Estimates**

| Term | Estimate | Std Error | t Ratio | Prob>\|t\| | VIF |
|---|---|---|---|---|---|
| Intercept | 16.933936 | 5.727397 | 2.96 | 0.0144* | . |
| D60 | 1.3951555 | 1.039731 | 1.34 | 0.2093 | 50.369642 |
| Gravel Size | -0.422281 | 0.252428 | -1.67 | 0.1253 | 72.915028 |
| Silt Size | 6.8235676 | 8.068334 | 0.85 | 0.4175 | 63609.182 |
| Clay Size | 6.5416219 | 8.105869 | 0.81 | 0.4384 | 7779.7162 |
| Passing 0.074 mm | -6.742561 | 8.061239 | -0.84 | 0.4225 | 107900.65 |
| Passing 0.02 mm | -0.09167 | 0.218593 | -0.42 | 0.6838 | 28.571142 |

**Residual by Predicted Plot**

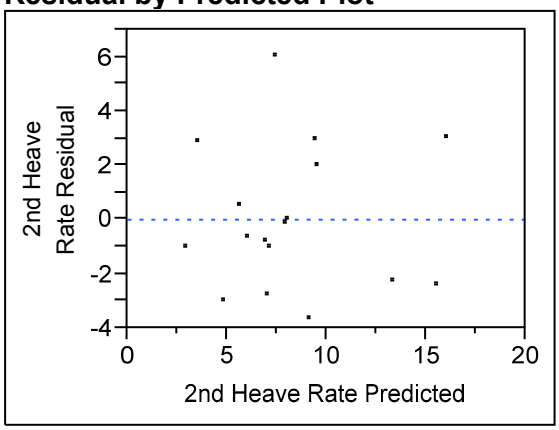


## Fourth Iteration

**Response 2nd Heave Rate**
**Whole Model**
**Actual by Predicted Plot**

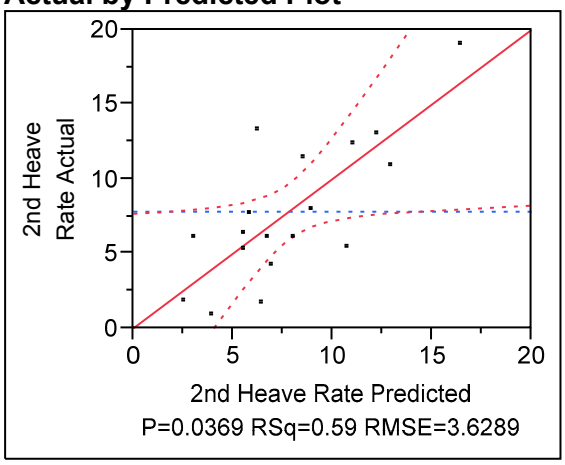


**Summary of Fit**

| | |
|---|---|
| RSquare | 0.589134 |
| RSquare Adj | 0.417939 |

| | |
|---|---|
| Root Mean Square Error | 3.628863 |
| Mean of Response | 7.822222 |
| Observations (or Sum Wgts) | 18 |

## Analysis of Variance

| Source | DF | Sum of Squares | Mean Square | F Ratio |
|---|---|---|---|---|
| Model | 5 | 226.58736 | 45.3175 | 3.4413 |
| Error | 12 | 158.02376 | 13.1686 | **Prob > F** |
| C. Total | 17 | 384.61111 | | 0.0369* |

## Parameter Estimates

| Term | Estimate | Std Error | t Ratio | Prob>\|t\| | VIF |
|---|---|---|---|---|---|
| Intercept | 7.6997067 | 3.319703 | 2.32 | 0.0388* | . |
| D60 | 0.2581134 | 0.928832 | 0.28 | 0.7858 | 35.159081 |
| Gravel Size | -0.085541 | 0.195523 | -0.44 | 0.6695 | 40.051942 |
| Silt Size | 13.170903 | 8.059851 | 1.63 | 0.1282 | 56109.035 |
| Clay Size | 12.746072 | 8.088581 | 1.58 | 0.1411 | 6824.8114 |
| Passing 0.074 mm | -13.00781 | 8.077624 | -1.61 | 0.1333 | 95888.376 |

## Residual by Predicted Plot

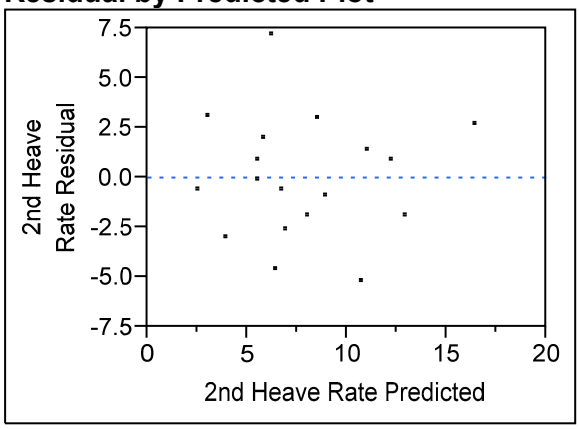

## Fifth Iteration

**Response 2nd Heave Rate**
**Whole Model**
**Actual by Predicted Plot**

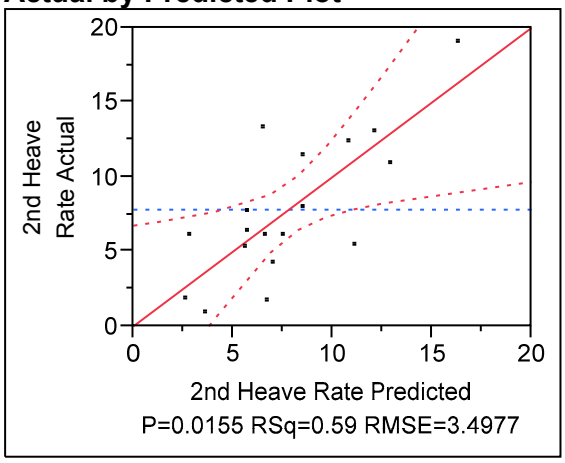


### Summary of Fit

| | |
|---|---|
| RSquare | 0.58649 |
| RSquare Adj | 0.459256 |
| Root Mean Square Error | 3.497699 |
| Mean of Response | 7.822222 |
| Observations (or Sum Wgts) | 18 |

### Analysis of Variance

| Source | DF | Sum of Squares | Mean Square | F Ratio |
|---|---|---|---|---|
| Model | 4 | 225.57043 | 56.3926 | 4.6095 |
| Error | 13 | 159.04068 | 12.2339 | **Prob > F** |
| C. Total | 17 | 384.61111 | | 0.0155* |

### Parameter Estimates

| Term | Estimate | Std Error | t Ratio | Prob>\|t\| | VIF |
|---|---|---|---|---|---|
| Intercept | 7.1830336 | 2.650786 | 2.71 | 0.0179* | . |
| Gravel Size | -0.032819 | 0.045563 | -0.72 | 0.4841 | 2.3411321 |
| Silt Size | 11.944117 | 6.499568 | 1.84 | 0.0891 | 39275.715 |
| Clay Size | 11.499648 | 6.487767 | 1.77 | 0.0997 | 4726.2077 |
| Passing 0.074 mm | -11.77315 | 6.502121 | -1.81 | 0.0934 | 66878.275 |

**Residual by Predicted Plot**

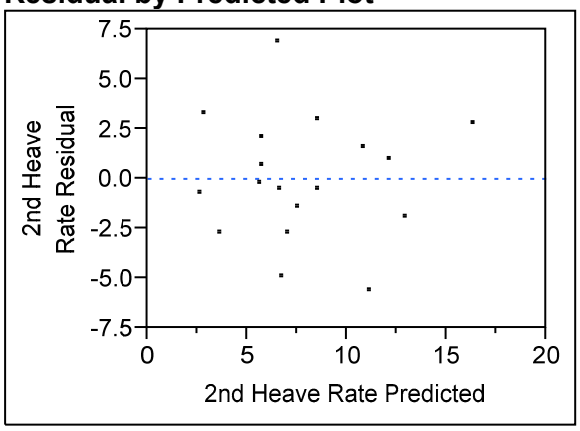


## Sixth Iteration

**Response 2nd Heave Rate**
**Whole Model**
**Actual by Predicted Plot**

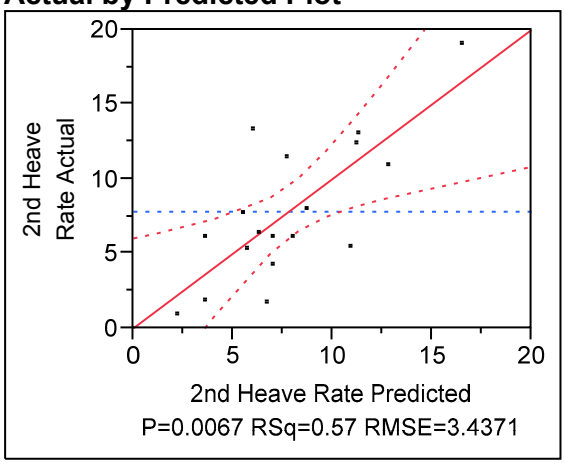


### Summary of Fit

| | |
|---|---|
| RSquare | 0.569986 |
| RSquare Adj | 0.47784 |
| Root Mean Square Error | 3.437068 |
| Mean of Response | 7.822222 |
| Observations (or Sum Wgts) | 18 |

### Analysis of Variance

| Source | DF | Sum of Squares | Mean Square | F Ratio |
|---|---|---|---|---|
| Model | 3 | 219.22304 | 73.0743 | 6.1857 |
| Error | 14 | 165.38807 | 11.8134 | **Prob > F** |
| C. Total | 17 | 384.61111 | | 0.0067* |

### Lack Of Fit

| Source | DF | Sum of Squares | Mean Square | F Ratio |
|---|---|---|---|---|
| Lack Of Fit | 13 | 156.56807 | 12.0437 | 1.3655 |
| Pure Error | 1 | 8.82000 | 8.8200 | **Prob > F** |

| Source | DF | Sum of Squares | Mean Square | F Ratio |
|---|---|---|---|---|
| Total Error | 14 | 165.38807 | | 0.5924 |
| | | | | **Max RSq** |
| | | | | 0.9771 |

**Parameter Estimates**

| Term | Estimate | Std Error | t Ratio | Prob>\|t\| | VIF |
|---|---|---|---|---|---|
| Intercept | 5.4497541 | 1.09261 | 4.99 | 0.0002* | . |
| Silt Size | 11.115806 | 6.286141 | 1.77 | 0.0988 | 38046.263 |
| Clay Size | 10.69595 | 6.280313 | 1.70 | 0.1106 | 4586.4171 |
| Passing 0.074 mm | -10.93011 | 6.285045 | -1.74 | 0.1040 | 64711.35 |

**Residual by Predicted Plot**

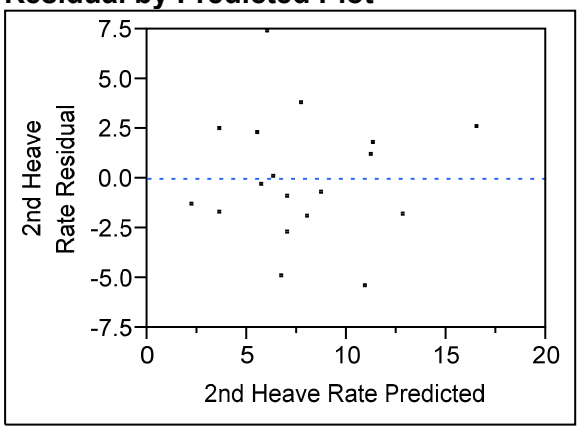


## Seventh Iteration

**Response 2nd Heave Rate**
**Whole Model**
**Actual by Predicted Plot**

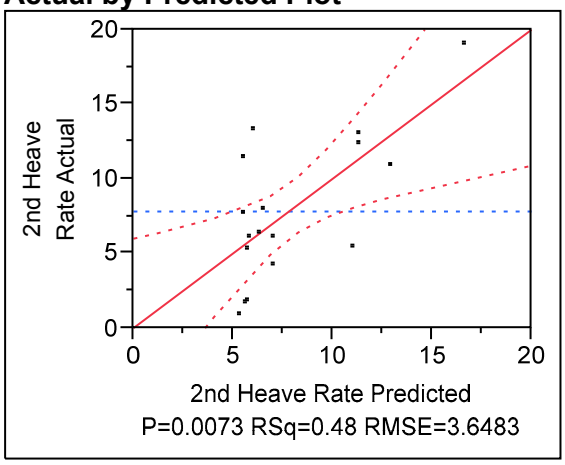


**Summary of Fit**

| | |
|---|---|
| RSquare | 0.480896 |
| RSquare Adj | 0.411682 |
| Root Mean Square Error | 3.648316 |
| Mean of Response | 7.822222 |

Observations (or Sum Wgts) 18

## Analysis of Variance

| Source | DF | Sum of Squares | Mean Square | F Ratio |
|---|---|---|---|---|
| Model | 2 | 184.95792 | 92.4790 | 6.9480 |
| Error | 15 | 199.65320 | 13.3102 | **Prob > F** |
| C. Total | 17 | 384.61111 | | 0.0073* |

## Lack Of Fit

| Source | DF | Sum of Squares | Mean Square | F Ratio |
|---|---|---|---|---|
| Lack Of Fit | 14 | 190.83320 | 13.6309 | 1.5455 |
| Pure Error | 1 | 8.82000 | 8.8200 | **Prob > F** |
| Total Error | 15 | 199.65320 | | 0.5654 |
| | | | | **Max RSq** |
| | | | | 0.9771 |

## Parameter Estimates

| Term | Estimate | Std Error | t Ratio | Prob>\|t\| | VIF |
|---|---|---|---|---|---|
| Intercept | 5.3998394 | 1.159346 | 4.66 | 0.0003* | . |
| Silt Size | 0.416534 | 0.234333 | 1.78 | 0.0958 | 46.92469 |
| Passing 0.074 mm | -0.229979 | 0.179648 | -1.28 | 0.2199 | 46.92469 |

## Residual by Predicted Plot

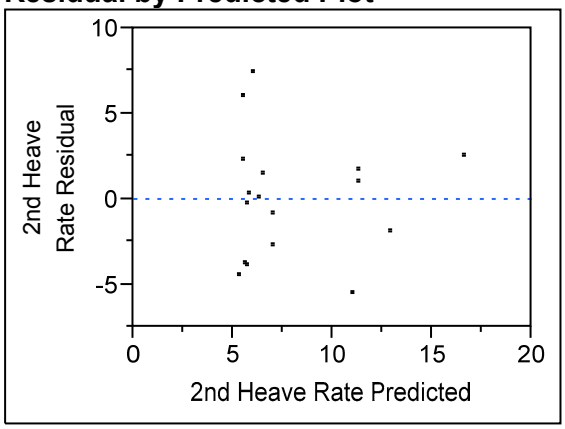

## Final Iteration

**Response 2nd Heave Rate**
**Whole Model**
**Regression Plot**

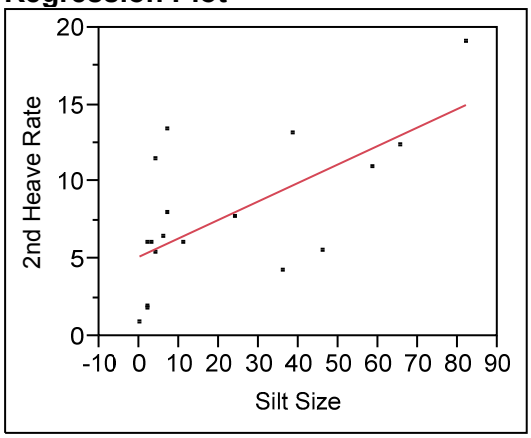


**Actual by Predicted Plot**

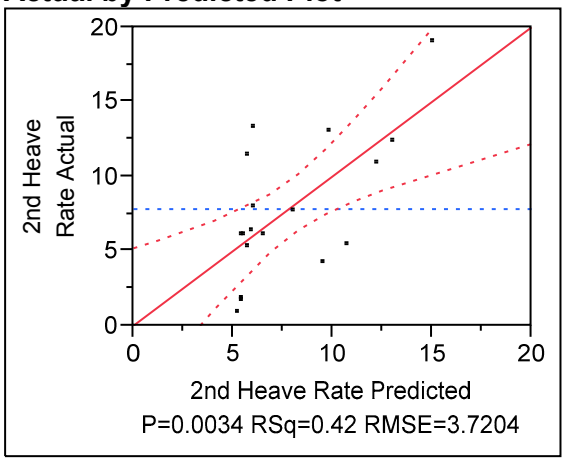


### Summary of Fit

| | |
|---|---|
| RSquare | 0.424182 |
| RSquare Adj | 0.388193 |
| Root Mean Square Error | 3.720434 |
| Mean of Response | 7.822222 |
| Observations (or Sum Wgts) | 18 |

### Analysis of Variance

| Source | DF | Sum of Squares | Mean Square | F Ratio |
|---|---|---|---|---|
| Model | 1 | 163.14503 | 163.145 | 11.7865 |
| Error | 16 | 221.46608 | 13.842 | **Prob > F** |
| C. Total | 17 | 384.61111 | | 0.0034* |

### Lack Of Fit

| Source | DF | Sum of Squares | Mean Square | F Ratio |
|---|---|---|---|---|
| Lack Of Fit | 12 | 176.23441 | 14.6862 | 1.2988 |
| Pure Error | 4 | 45.23167 | 11.3079 | **Prob > F** |
| Total Error | 16 | 221.46608 | | 0.4349 |

| Source | DF | Sum of Squares | Mean Square | F Ratio<br>Max RSq<br>0.8824 |
|---|---|---|---|---|

**Parameter Estimates**

| Term | Estimate | Std Error | t Ratio | Prob>\|t\| | VIF |
|---|---|---|---|---|---|
| Intercept | 5.172107 | 1.168263 | 4.43 | 0.0004* | . |
| Silt Size | 0.1197642 | 0.034885 | 3.43 | 0.0034* | 1 |

**Residual by Predicted Plot**

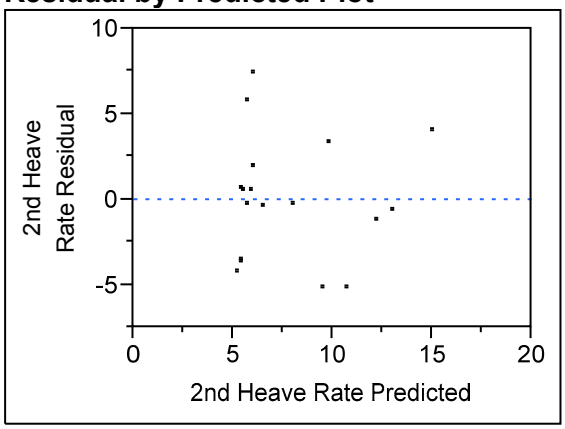


**Individual Parameter Analysis for Fine and Coarse Materials 2nd Frost Heave Model**

**$D_{30}$**

**Response 2nd Heave Rate**
**Whole Model**
**Regression Plot**

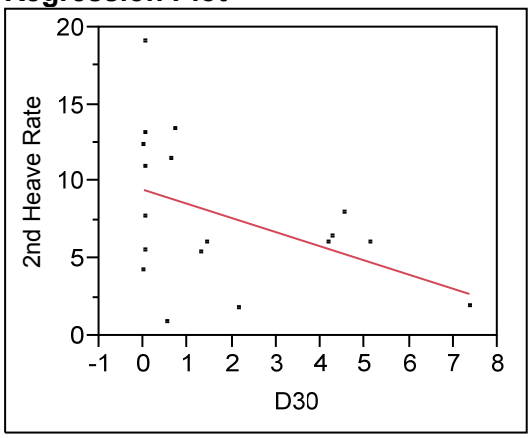

## Actual by Predicted Plot

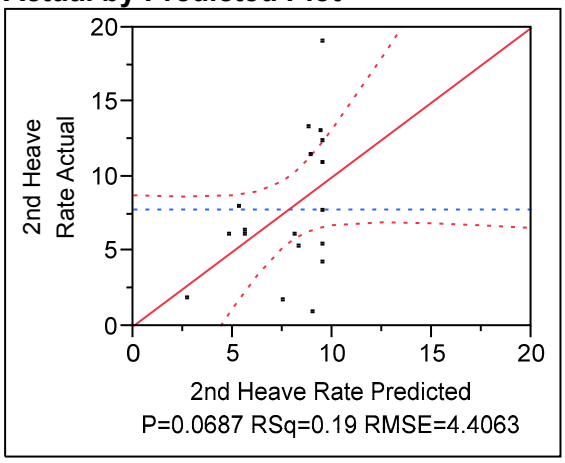


## Summary of Fit

| | |
|---|---|
| RSquare | 0.192303 |
| RSquare Adj | 0.141822 |
| Root Mean Square Error | 4.406311 |
| Mean of Response | 7.822222 |
| Observations (or Sum Wgts) | 18 |

## Analysis of Variance

| Source | DF | Sum of Squares | Mean Square | F Ratio |
|---|---|---|---|---|
| Model | 1 | 73.96182 | 73.9618 | 3.8094 |
| Error | 16 | 310.64929 | 19.4156 | **Prob > F** |
| C. Total | 17 | 384.61111 | | 0.0687 |

## Parameter Estimates

| Term | Estimate | Std Error | t Ratio | Prob>\|t\| | VIF |
|---|---|---|---|---|---|
| Intercept | 9.4685768 | 1.337971 | 7.08 | <.0001* | . |
| D30 | -0.916055 | 0.469346 | -1.95 | 0.0687 | 1 |

## Residual by Predicted Plot

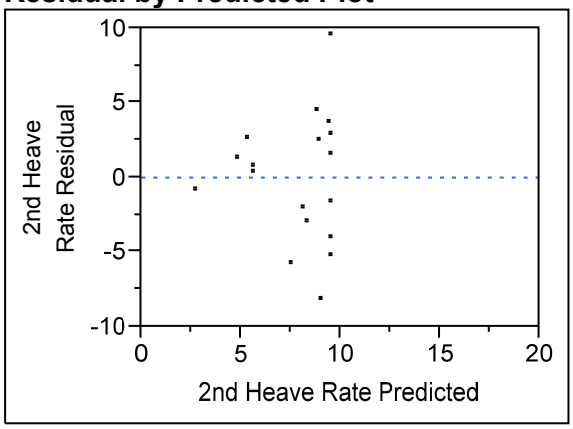

**$D_{60}$**

**Response 2nd Heave Rate**
**Whole Model**
**Regression Plot**

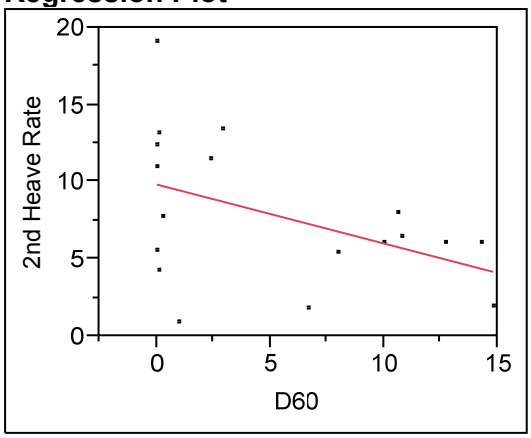


**Actual by Predicted Plot**

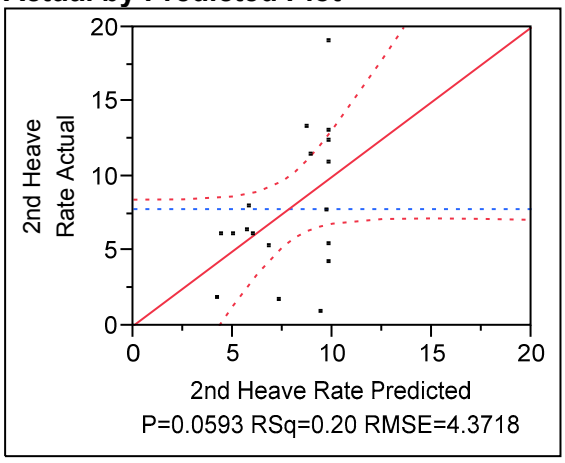


**Summary of Fit**

| | |
|---|---|
| RSquare | 0.204904 |
| RSquare Adj | 0.155211 |
| Root Mean Square Error | 4.371804 |
| Mean of Response | 7.822222 |
| Observations (or Sum Wgts) | 18 |

**Analysis of Variance**

| Source | DF | Sum of Squares | Mean Square | F Ratio |
|---|---|---|---|---|
| Model | 1 | 78.80845 | 78.8084 | 4.1234 |
| Error | 16 | 305.80266 | 19.1127 | **Prob > F** |
| C. Total | 17 | 384.61111 | | 0.0593 |

**Parameter Estimates**

| Term | Estimate | Std Error | t Ratio | Prob>\|t\| |
|---|---|---|---|---|
| Intercept | 9.8448788 | 1.433178 | 6.87 | <.0001* |
| D60 | -0.383208 | 0.188716 | -2.03 | 0.0593 |

**Residual by Predicted Plot**

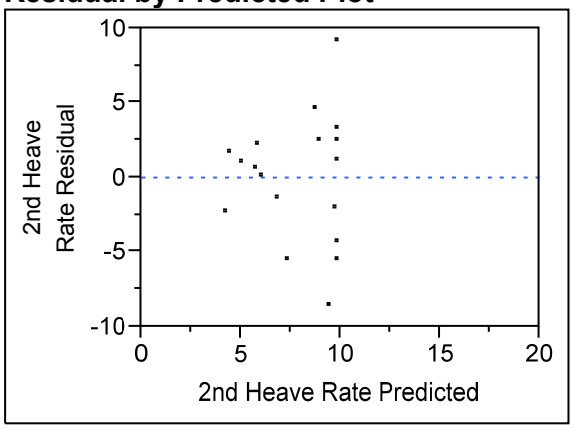


**Gravel Content**

**Response 2nd Heave Rate**
**Whole Model**
**Regression Plot**

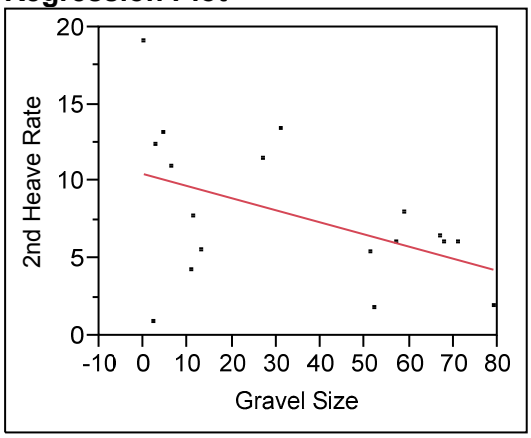


**Actual by Predicted Plot**

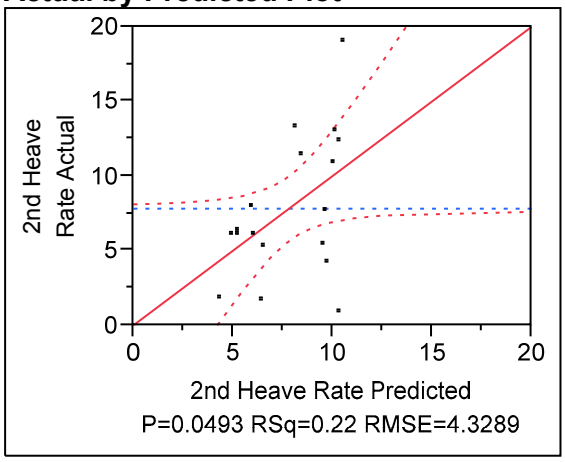

### Summary of Fit

| | |
|---|---|
| RSquare | 0.220415 |
| RSquare Adj | 0.171691 |
| Root Mean Square Error | 4.32895 |
| Mean of Response | 7.822222 |
| Observations (or Sum Wgts) | 18 |

### Analysis of Variance

| Source | DF | Sum of Squares | Mean Square | F Ratio |
|---|---|---|---|---|
| Model | 1 | 84.77424 | 84.7742 | 4.5238 |
| Error | 16 | 299.83687 | 18.7398 | **Prob > F** |
| C. Total | 17 | 384.61111 | | 0.0493* |

### Parameter Estimates

| Term | Estimate | Std Error | t Ratio | Prob>\|t\| | VIF |
|---|---|---|---|---|---|
| Intercept | 10.486529 | 1.615633 | 6.49 | <.0001* | . |
| Gravel Size | -0.078388 | 0.036855 | -2.13 | 0.0493* | 1 |

### Residual by Predicted Plot

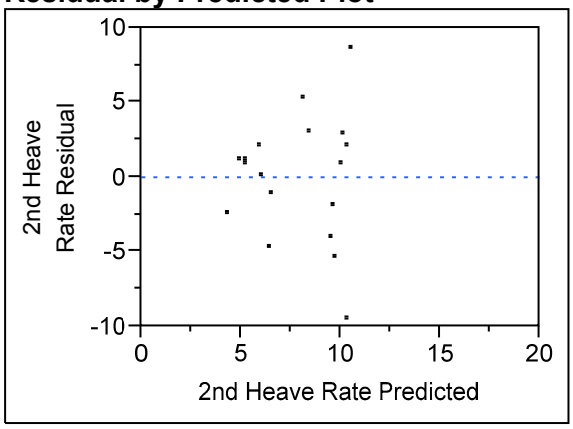


## Sand Content

### Response 2nd Heave Rate
### Whole Model
### Regression Plot

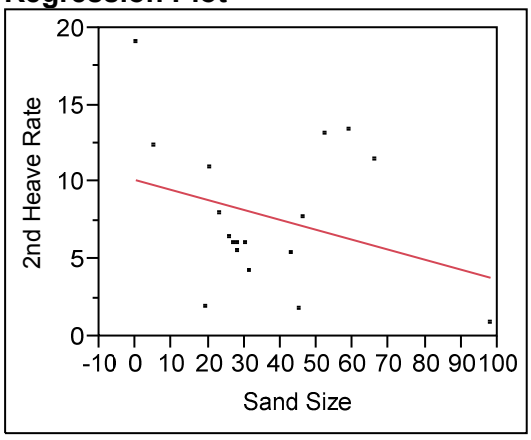

## Actual by Predicted Plot

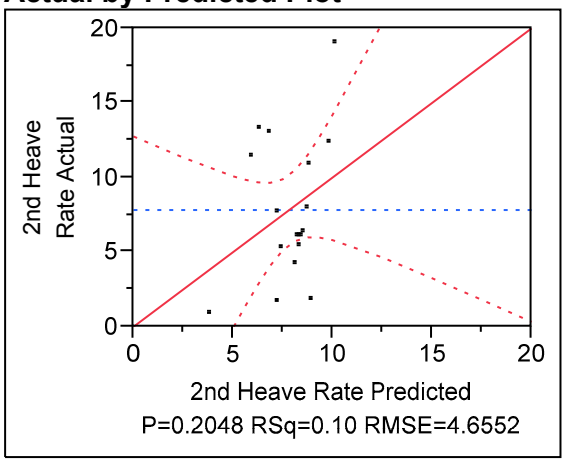


## Summary of Fit

| | |
|---|---|
| RSquare | 0.098462 |
| RSquare Adj | 0.042116 |
| Root Mean Square Error | 4.65525 |
| Mean of Response | 7.822222 |
| Observations (or Sum Wgts) | 18 |

## Analysis of Variance

| Source | DF | Sum of Squares | Mean Square | F Ratio |
|---|---|---|---|---|
| Model | 1 | 37.86948 | 37.8695 | 1.7474 |
| Error | 16 | 346.74163 | 21.6714 | **Prob > F** |
| C. Total | 17 | 384.61111 | | 0.2048 |

## Lack Of Fit

| Source | DF | Sum of Squares | Mean Square | F Ratio |
|---|---|---|---|---|
| Lack Of Fit | 15 | 346.56163 | 23.1041 | 128.3562 |
| Pure Error | 1 | 0.18000 | 0.1800 | **Prob > F** |
| Total Error | 16 | 346.74163 | | 0.0692 |
| | | | | **Max RSq** |
| | | | | 0.9995 |

## Parameter Estimates

| Term | Estimate | Std Error | t Ratio | Prob>\|t\| | VIF |
|---|---|---|---|---|---|
| Intercept | 10.140065 | 2.068428 | 4.90 | 0.0002* | . |
| Sand Size | -0.064544 | 0.048826 | -1.32 | 0.2048 | 1 |

**Residual by Predicted Plot**

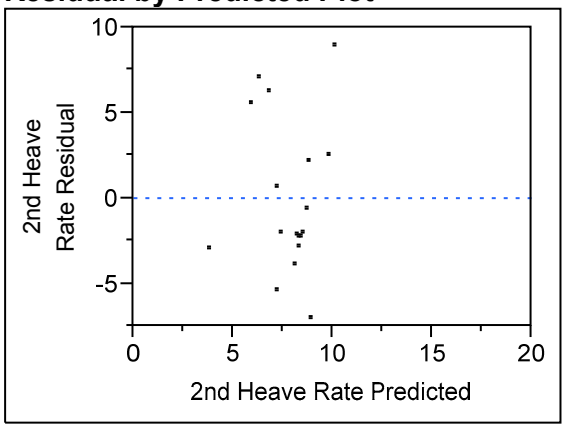


## Clay Content

**Response 2nd Heave Rate**
**Whole Model**
**Regression Plot**

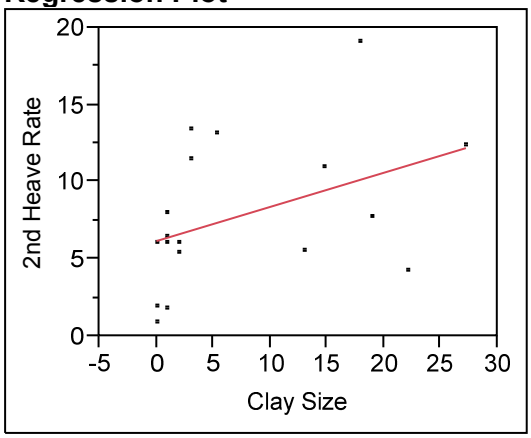


**Actual by Predicted Plot**

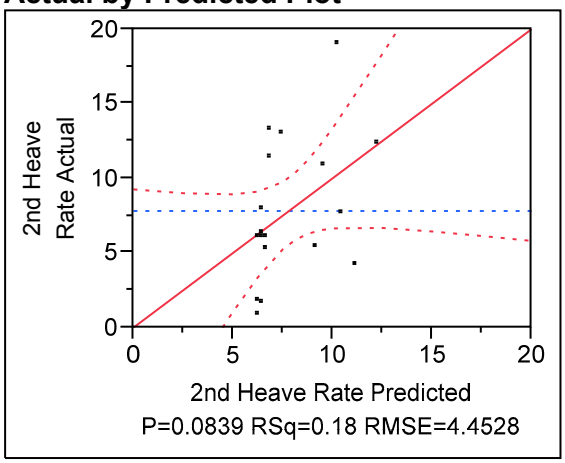

## Summary of Fit

| | |
|---|---|
| RSquare | 0.175154 |
| RSquare Adj | 0.123601 |
| Root Mean Square Error | 4.452844 |
| Mean of Response | 7.822222 |
| Observations (or Sum Wgts) | 18 |

## Analysis of Variance

| Source | DF | Sum of Squares | Mean Square | F Ratio |
|---|---|---|---|---|
| Model | 1 | 67.36600 | 67.3660 | 3.3975 |
| Error | 16 | 317.24511 | 19.8278 | **Prob > F** |
| C. Total | 17 | 384.61111 | | 0.0839 |

## Lack Of Fit

| Source | DF | Sum of Squares | Mean Square | F Ratio |
|---|---|---|---|---|
| Lack Of Fit | 9 | 278.88094 | 30.9868 | 5.6539 |
| Pure Error | 7 | 38.36417 | 5.4806 | **Prob > F** |
| Total Error | 16 | 317.24511 | | 0.0163* |
| | | | | **Max RSq** |
| | | | | 0.9003 |

## Parameter Estimates

| Term | Estimate | Std Error | t Ratio | Prob>\|t\| | VIF |
|---|---|---|---|---|---|
| Intercept | 6.1797971 | 1.376778 | 4.49 | 0.0004* | . |
| Clay Size | 0.2214506 | 0.120142 | 1.84 | 0.0839 | 1 |

## Residual by Predicted Plot

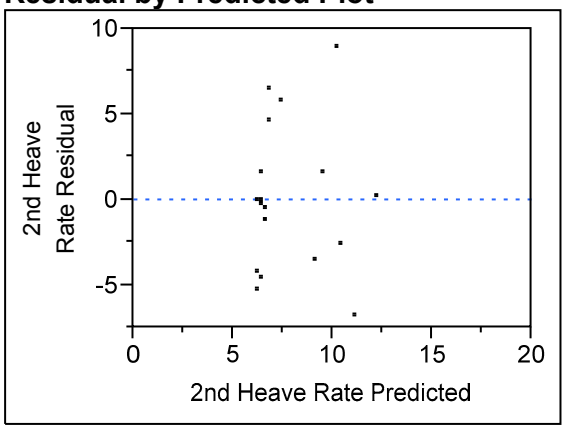

**Passing 0.074 mm**

**Response 2nd Heave Rate**

**Whole Model**

**Regression Plot**

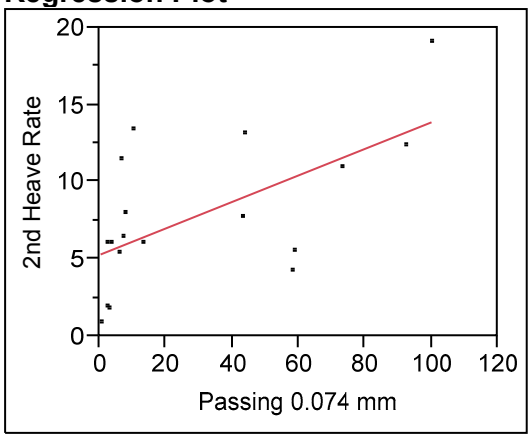


**Actual by Predicted Plot**

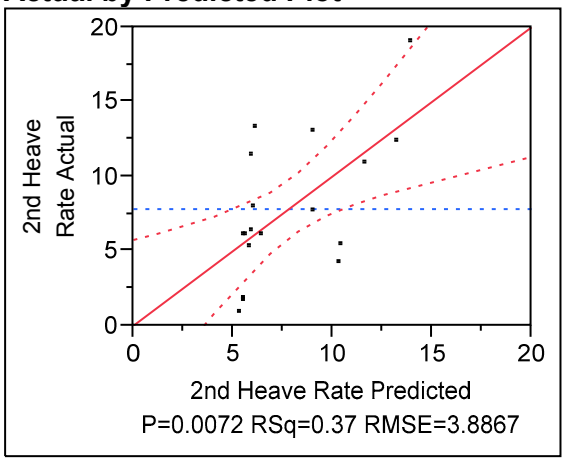


**Summary of Fit**

| | |
|---|---|
| RSquare | 0.371551 |
| RSquare Adj | 0.332273 |
| Root Mean Square Error | 3.886743 |
| Mean of Response | 7.822222 |
| Observations (or Sum Wgts) | 18 |

**Analysis of Variance**

| Source | DF | Sum of Squares | Mean Square | F Ratio |
|---|---|---|---|---|
| Model | 1 | 142.90274 | 142.903 | 9.4595 |
| Error | 16 | 241.70837 | 15.107 | **Prob > F** |
| C. Total | 17 | 384.61111 | | 0.0072* |

**Lack Of Fit**

| Source | DF | Sum of Squares | Mean Square | F Ratio |
|---|---|---|---|---|
| Lack Of Fit | 15 | 232.88837 | 15.5259 | 1.7603 |
| Pure Error | 1 | 8.82000 | 8.8200 | **Prob > F** |
| Total Error | 16 | 241.70837 | | 0.5373 |

| Source | DF | Sum of Squares | Mean Square | F Ratio<br>Max RSq<br>0.9771 |
|---|---|---|---|---|

**Parameter Estimates**

| Term | Estimate | Std Error | t Ratio | Prob>\|t\| | VIF |
|---|---|---|---|---|---|
| Intercept | 5.2834357 | 1.233141 | 4.28 | 0.0006* | . |
| Passing 0.074 mm | 0.0859311 | 0.027939 | 3.08 | 0.0072* | 1 |

**Residual by Predicted Plot**

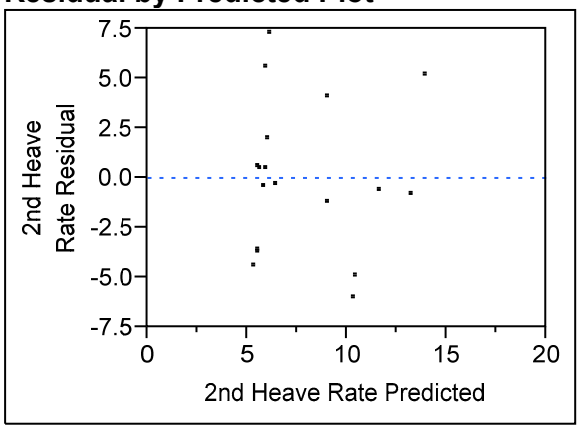


**Passing 0.02 mm**

**Response 2nd Heave Rate**
**Whole Model**
**Regression Plot**

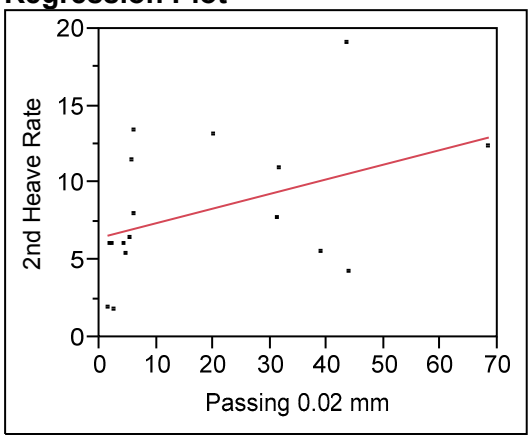

**Actual by Predicted Plot**

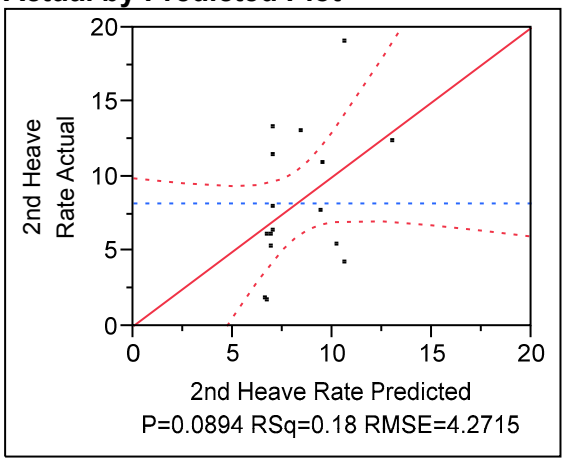


**Summary of Fit**

| | |
|---|---|
| RSquare | 0.180285 |
| RSquare Adj | 0.125638 |
| Root Mean Square Error | 4.271475 |
| Mean of Response | 8.229412 |
| Observations (or Sum Wgts) | 17 |

**Analysis of Variance**

| Source | DF | Sum of Squares | Mean Square | F Ratio |
|---|---|---|---|---|
| Model | 1 | 60.19281 | 60.1928 | 3.2990 |
| Error | 15 | 273.68248 | 18.2455 | **Prob > F** |
| C. Total | 16 | 333.87529 | | 0.0894 |

**Parameter Estimates**

| Term | Estimate | Std Error | t Ratio | Prob>\|t\| | VIF |
|---|---|---|---|---|---|
| Intercept | 6.4560821 | 1.423544 | 4.54 | 0.0004* | . |
| Passing 0.02 mm | 0.0951898 | 0.052408 | 1.82 | 0.0894 | 1 |

**Residual by Predicted Plot**

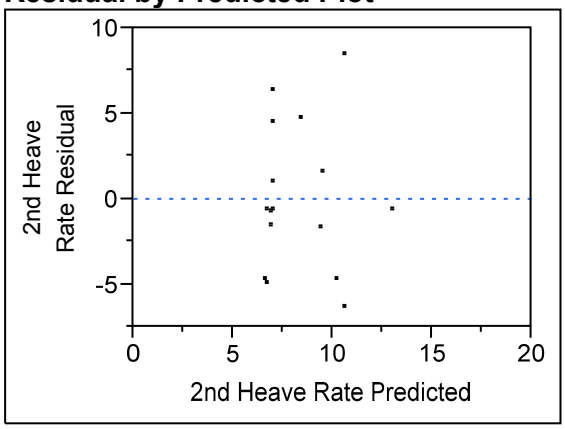

## USCS Classification

**Response 2nd Heave Rate**
**Whole Model**
**Actual by Predicted Plot**

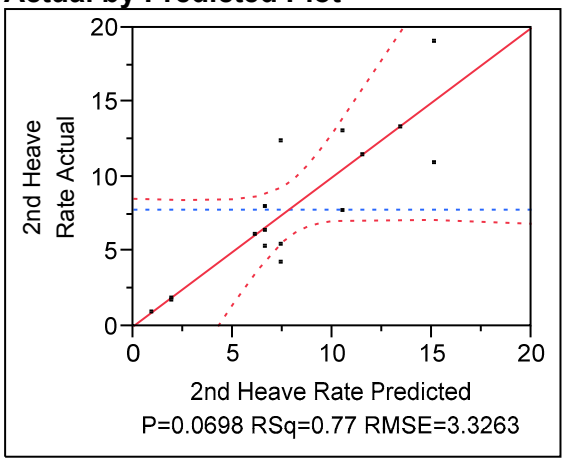


### Summary of Fit

| | |
|---|---|
| RSquare | 0.769858 |
| RSquare Adj | 0.510949 |
| Root Mean Square Error | 3.326316 |
| Mean of Response | 7.822222 |
| Observations (or Sum Wgts) | 18 |

### Analysis of Variance

| Source | DF | Sum of Squares | Mean Square | F Ratio |
|---|---|---|---|---|
| Model | 9 | 296.09611 | 32.8996 | 2.9735 |
| Error | 8 | 88.51500 | 11.0644 | **Prob > F** |
| C. Total | 17 | 384.61111 | | 0.0698 |

### Effect Tests

| Source | Nparm | DF | Sum of Squares | F Ratio | Prob > F |
|---|---|---|---|---|---|
| USCS Classification | 9 | 9 | 296.09611 | 2.9735 | 0.0698 |

**Residual by Predicted Plot**

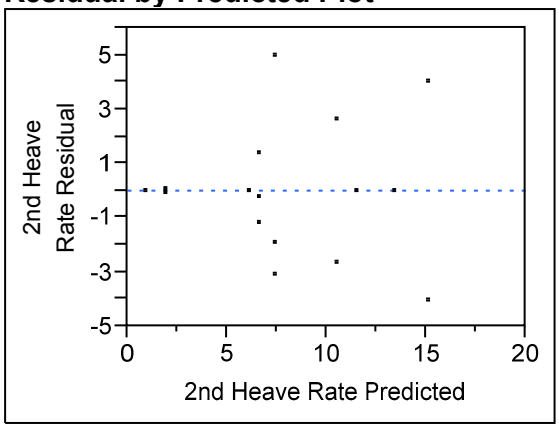

### Least Squares Means Table

| Level | Least Sq Mean | Std Error | Mean |
|---|---|---|---|
| CL | 7.400000 | 1.9204492 | 7.4000 |
| GM | 6.100000 | 3.3263155 | 6.1000 |
| GP | 6.100000 | 2.3520603 | 6.1000 |
| GP-GM | 6.600000 | 1.9204492 | 6.6000 |
| GW | 1.850000 | 2.3520603 | 1.8500 |
| ML | 15.050000 | 2.3520603 | 15.0500 |
| SC | 10.450000 | 2.3520603 | 10.4500 |
| SP | 0.900000 | 3.3263155 | 0.9000 |
| SP-SM | 11.500000 | 3.3263155 | 11.5000 |
| SW-SM | 13.400000 | 3.3263155 | 13.4000 |

**Fine Materials 2nd Frost Heave Model**

## First Iteration

### Response 2nd Heave Rate

### Singularity Details

Silt Size = - Clay Size + Passing 0.074 mm

### Whole Model

### Actual by Predicted Plot

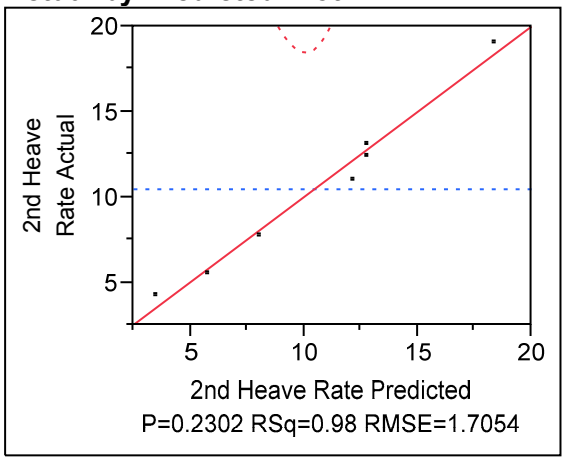


### Summary of Fit

| | |
|---|---|
| RSquare | 0.981272 |
| RSquare Adj | 0.88763 |
| Root Mean Square Error | 1.705417 |
| Mean of Response | 10.45714 |
| Observations (or Sum Wgts) | 7 |

### Analysis of Variance

| Source | DF | Sum of Squares | Mean Square | F Ratio |
|---|---|---|---|---|
| Model | 5 | 152.38870 | 30.4777 | 10.4790 |
| Error | 1 | 2.90845 | 2.9084 | **Prob > F** |
| C. Total | 6 | 155.29714 | | 0.2302 |

### Parameter Estimates

| Term | Estimate | Std Error | t Ratio | Prob>\|t\| | VIF |
|---|---|---|---|---|---|
| Intercept | 10.551641 | 10.65329 | 0.99 | 0.5031 | . |

| Term | | Estimate | Std Error | t Ratio | Prob>\|t\| | VIF |
|---|---|---|---|---|---|---|
| D60 | | 19.013278 | 20.39464 | 0.93 | 0.5223 | 7.4441503 |
| Silt Size | Biased | 0.2064211 | 0.097192 | 2.12 | 0.2801 | 7.6314579 |
| Clay Size | Biased | -0.304643 | 0.245131 | -1.24 | 0.4314 | 6.0694578 |
| Passing 0.074 mm | Zeroed | 0 | 0 | . | . | 0 |
| Passing 0.02 mm | | 0.3599124 | 0.18042 | 1.99 | 0.2958 | 15.444135 |
| LL | | -0.681759 | 0.275477 | -2.47 | 0.2445 | 8.3420055 |

**Residual by Predicted Plot**

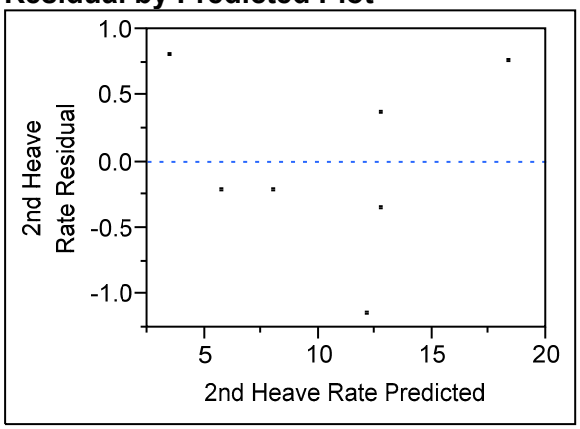


## Second Iteration

**Response 2nd Heave Rate**
**Singularity Details**
Silt Size = - Clay Size + Passing 0.074 mm

**Whole Model**
**Actual by Predicted Plot**

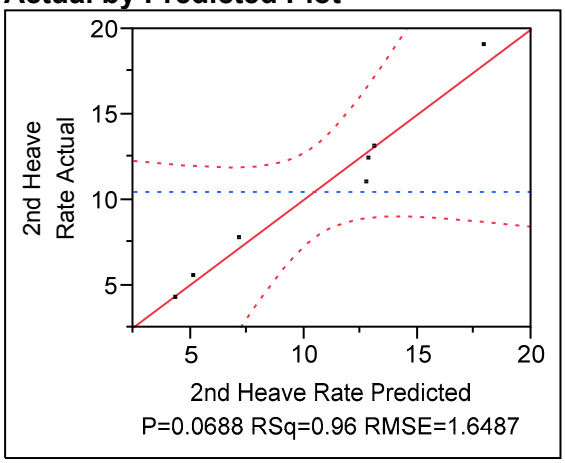


**Summary of Fit**

| | |
|---|---|
| RSquare | 0.964995 |
| RSquare Adj | 0.894984 |
| Root Mean Square Error | 1.648674 |
| Mean of Response | 10.45714 |
| Observations (or Sum Wgts) | 7 |

**Analysis of Variance**

| Source | DF | Sum of Squares | Mean Square | F Ratio |
|---|---|---|---|---|
| Model | 4 | 149.86089 | 37.4652 | 13.7835 |
| Error | 2 | 5.43625 | 2.7181 | **Prob > F** |
| C. Total | 6 | 155.29714 | | 0.0688 |

**Parameter Estimates**

| Term | | Estimate | Std Error | t Ratio | Prob>\|t\| | VIF |
|---|---|---|---|---|---|---|
| Intercept | | 19.442414 | 4.590052 | 4.24 | 0.0515 | . |
| Silt Size | Biased | 0.1309973 | 0.052069 | 2.52 | 0.1283 | 2.3436236 |
| Clay Size | Biased | -0.239182 | 0.227045 | -1.05 | 0.4026 | 5.5714447 |
| Passing 0.074 mm | Zeroed | 0 | 0 | . | . | 0 |
| Passing 0.02 mm | | 0.3774733 | 0.173464 | 2.18 | 0.1615 | 15.275788 |
| LL | | -0.840175 | 0.20961 | -4.01 | 0.0570 | 5.1679263 |

**Residual by Predicted Plot**

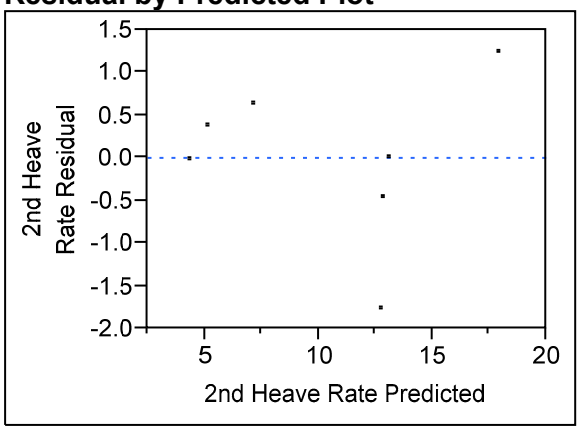


## Third Iteration

**Response 2nd Heave Rate**
**Whole Model**
**Actual by Predicted Plot**

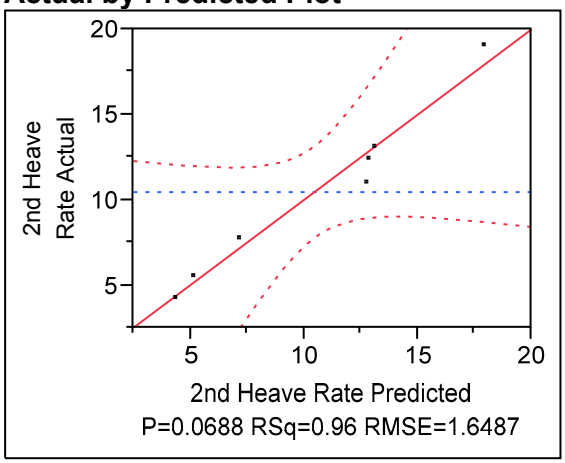

## Summary of Fit

| | |
|---|---|
| RSquare | 0.964995 |
| RSquare Adj | 0.894984 |
| Root Mean Square Error | 1.648674 |
| Mean of Response | 10.45714 |
| Observations (or Sum Wgts) | 7 |

## Analysis of Variance

| Source | DF | Sum of Squares | Mean Square | F Ratio |
|---|---|---|---|---|
| Model | 4 | 149.86089 | 37.4652 | 13.7835 |
| Error | 2 | 5.43625 | 2.7181 | Prob > F |
| C. Total | 6 | 155.29714 | | 0.0688 |

## Parameter Estimates

| Term | Estimate | Std Error | t Ratio | Prob>\|t\| | VIF |
|---|---|---|---|---|---|
| Intercept | 19.442414 | 4.590052 | 4.24 | 0.0515 | . |
| Silt Size | 0.3701793 | 0.20488 | 1.81 | 0.2125 | 36.285637 |
| Passing 0.074 mm | -0.239182 | 0.227045 | -1.05 | 0.4026 | 57.660749 |
| Passing 0.02 mm | 0.3774733 | 0.173464 | 2.18 | 0.1615 | 15.275788 |
| LL | -0.840175 | 0.20961 | -4.01 | 0.0570 | 5.1679263 |

## Residual by Predicted Plot

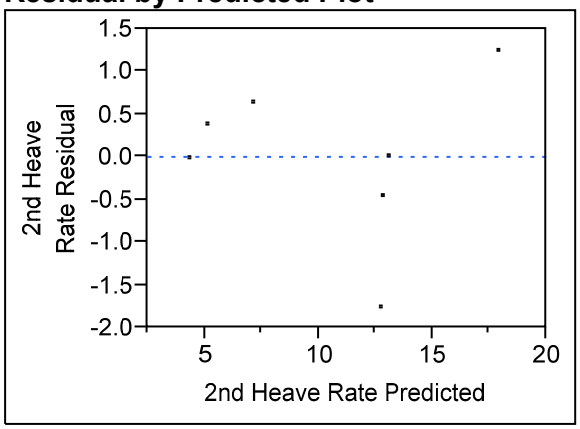

## Fourth Iteration

**Response 2nd Heave Rate**
**Whole Model**
**Actual by Predicted Plot**

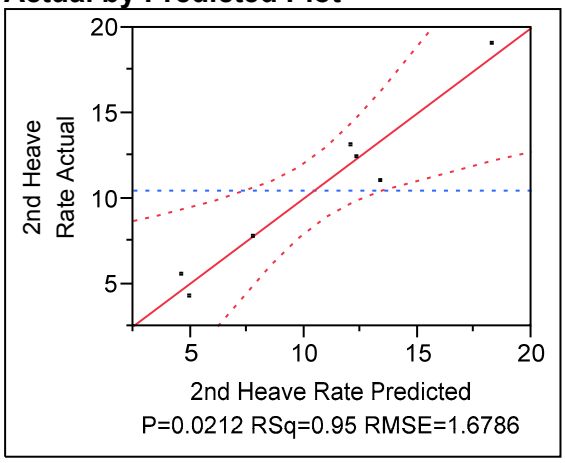


### Summary of Fit

| | |
|---|---|
| RSquare | 0.94557 |
| RSquare Adj | 0.891141 |
| Root Mean Square Error | 1.678566 |
| Mean of Response | 10.45714 |
| Observations (or Sum Wgts) | 7 |

### Analysis of Variance

| Source | DF | Sum of Squares | Mean Square | F Ratio |
|---|---|---|---|---|
| Model | 3 | 146.84440 | 48.9481 | 17.3724 |
| Error | 3 | 8.45275 | 2.8176 | **Prob > F** |
| C. Total | 6 | 155.29714 | | 0.0212* |

### Parameter Estimates

| Term | Estimate | Std Error | t Ratio | Prob>\|t\| | VIF |
|---|---|---|---|---|---|
| Intercept | 17.331362 | 4.204382 | 4.12 | 0.0259* | . |
| Silt Size | 0.1594969 | 0.045295 | 3.52 | 0.0389* | 1.7109526 |
| Passing 0.02 mm | 0.2337793 | 0.109107 | 2.14 | 0.1215 | 5.8302137 |
| LL | -0.76725 | 0.201436 | -3.81 | 0.0318* | 4.604259 |

**Residual by Predicted Plot**

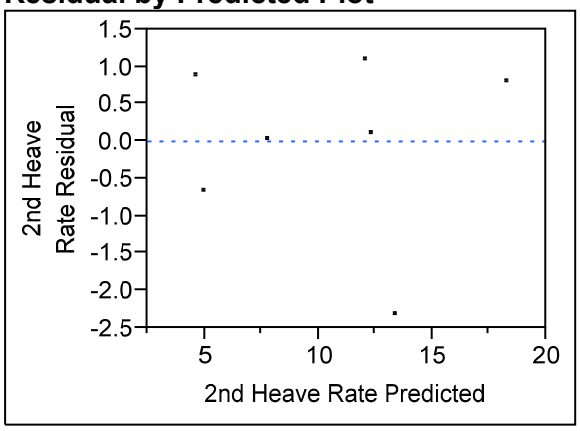


## Final Iteration

**Response 2nd Heave Rate**
**Whole Model**
**Actual by Predicted Plot**

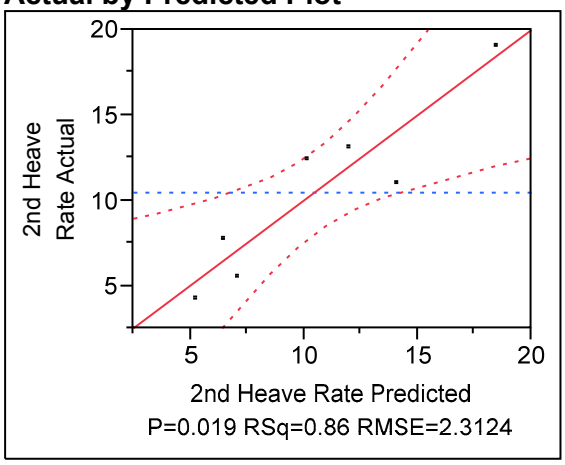


### Summary of Fit

| | |
|---|---|
| RSquare | 0.862276 |
| RSquare Adj | 0.793414 |
| Root Mean Square Error | 2.312369 |
| Mean of Response | 10.45714 |
| Observations (or Sum Wgts) | 7 |

### Analysis of Variance

| Source | DF | Sum of Squares | Mean Square | F Ratio |
|---|---|---|---|---|
| Model | 2 | 133.90895 | 66.9545 | 12.5218 |
| Error | 4 | 21.38819 | 5.3470 | **Prob > F** |
| C. Total | 6 | 155.29714 | | 0.0190* |

### Parameter Estimates

| Term | Estimate | Std Error | t Ratio | Prob>\|t\| | VIF |
|---|---|---|---|---|---|
| Intercept | 11.603391 | 4.47032 | 2.60 | 0.0603 | . |
| Silt Size | 0.2203801 | 0.048593 | 4.54 | 0.0105* | 1.0376377 |

| Term | Estimate | Std Error | t Ratio | Prob>\|t\| | VIF |
|---|---|---|---|---|---|
| LL | -0.387377 | 0.131734 | -2.94 | 0.0424* | 1.0376377 |

**Residual by Predicted Plot**

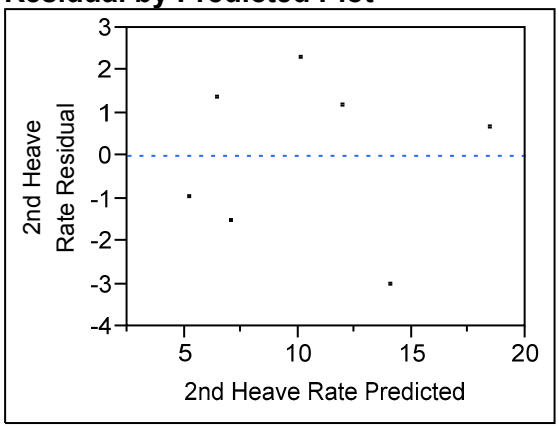


**Silt Size**
**Leverage Plot**

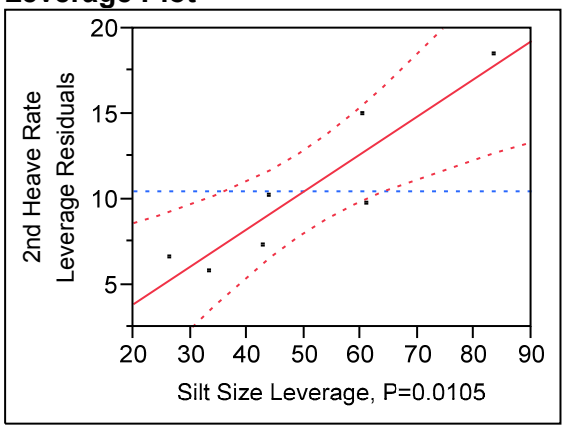

**Individual Parameter Analysis for Fine Materials 2nd Frost Heave Model**

$D_{30}$

**Response 2nd Heave Rate**
**Whole Model**
**Regression Plot**

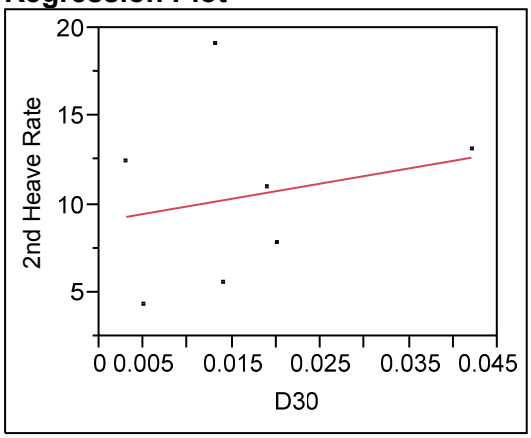


**Actual by Predicted Plot**

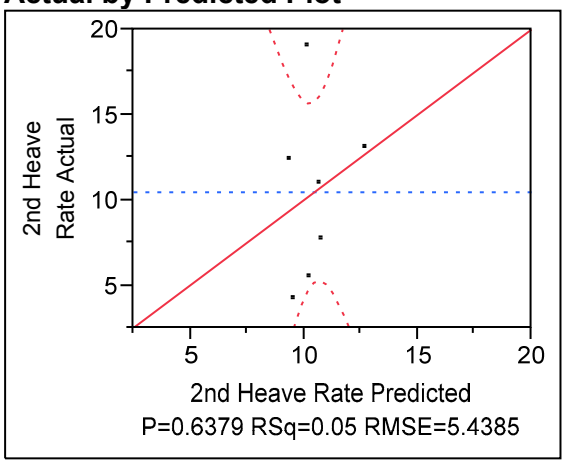


## Summary of Fit

| | |
|---|---|
| RSquare | 0.047733 |
| RSquare Adj | -0.14272 |
| Root Mean Square Error | 5.438462 |
| Mean of Response | 10.45714 |
| Observations (or Sum Wgts) | 7 |

## Analysis of Variance

| Source | DF | Sum of Squares | Mean Square | F Ratio |
|---|---|---|---|---|
| Model | 1 | 7.41281 | 7.4128 | 0.2506 |
| Error | 5 | 147.88434 | 29.5769 | **Prob > F** |
| C. Total | 6 | 155.29714 | | 0.6379 |

## Parameter Estimates

| Term | Estimate | Std Error | t Ratio | Prob>\|t\| |
|---|---|---|---|---|
| Intercept | 9.031603 | 3.511914 | 2.57 | 0.0499* |

| Term | Estimate | Std Error | t Ratio | Prob>\|t\| |
|---|---|---|---|---|
| D30 | 86.023959 | 171.832 | 0.50 | 0.6379 |

**Residual by Predicted Plot**

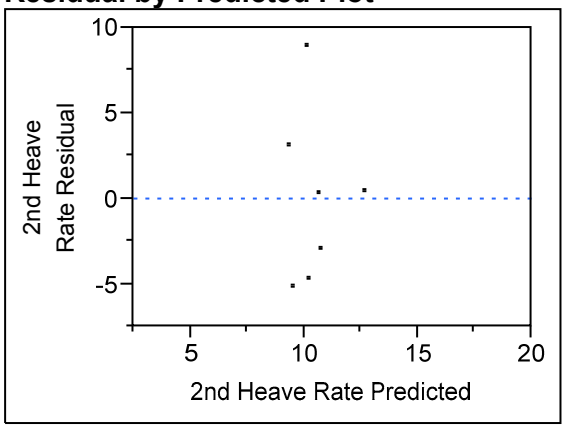


**$D_{60}$**

**Response 2nd Heave Rate**
**Whole Model**
**Regression Plot**

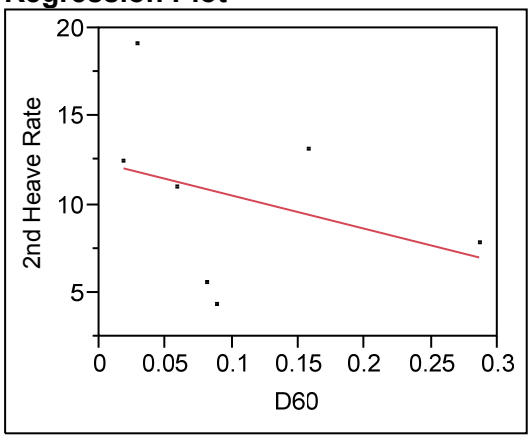

**Actual by Predicted Plot**

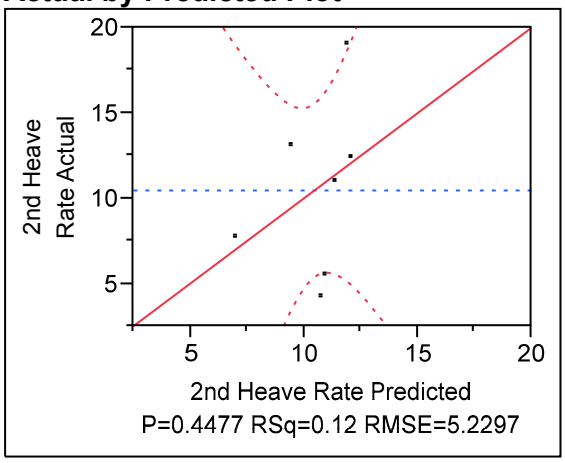


**Summary of Fit**

| | |
|---|---|
| RSquare | 0.11943 |
| RSquare Adj | -0.05668 |
| Root Mean Square Error | 5.229722 |
| Mean of Response | 10.45714 |
| Observations (or Sum Wgts) | 7 |

**Analysis of Variance**

| Source | DF | Sum of Squares | Mean Square | F Ratio |
|---|---|---|---|---|
| Model | 1 | 18.54718 | 18.5472 | 0.6781 |
| Error | 5 | 136.74997 | 27.3500 | **Prob > F** |
| C. Total | 6 | 155.29714 | | 0.4477 |

**Parameter Estimates**

| Term | Estimate | Std Error | t Ratio | Prob>\|t\| |
|---|---|---|---|---|
| Intercept | 12.393581 | 3.071914 | 4.03 | 0.0100* |
| D60 | -18.8763 | 22.92221 | -0.82 | 0.4477 |

**Residual by Predicted Plot**

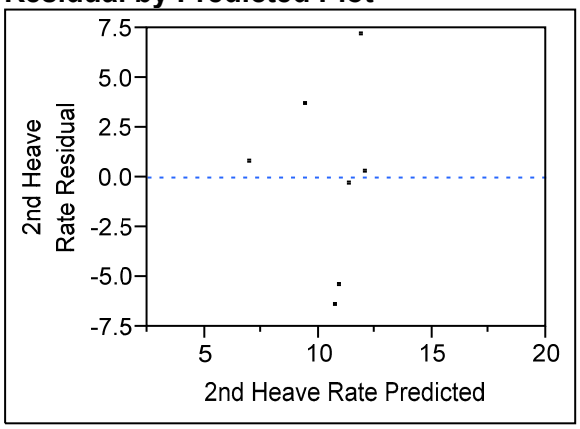

## Gravel Content

**Response 2nd Heave Rate**
**Whole Model**
**Regression Plot**


**Actual by Predicted Plot**

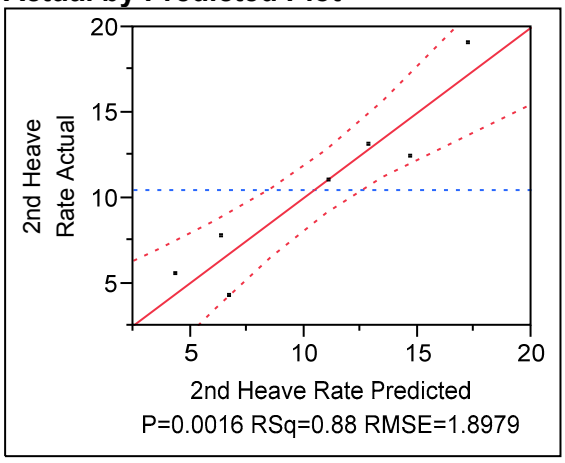


### Summary of Fit

| | |
|---|---|
| RSquare | 0.88403 |
| RSquare Adj | 0.860836 |
| Root Mean Square Error | 1.897885 |
| Mean of Response | 10.45714 |
| Observations (or Sum Wgts) | 7 |

### Analysis of Variance

| Source | DF | Sum of Squares | Mean Square | F Ratio |
|---|---|---|---|---|
| Model | 1 | 137.28731 | 137.287 | 38.1146 |
| Error | 5 | 18.00983 | 3.602 | **Prob > F** |
| C. Total | 6 | 155.29714 | | 0.0016* |

### Parameter Estimates

| Term | Estimate | Std Error | t Ratio | Prob>\|t\| |
|---|---|---|---|---|
| Intercept | 17.206848 | 1.307621 | 13.16 | <.0001* |
| Gravel Size | -0.988451 | 0.160107 | -6.17 | 0.0016* |

**Residual by Predicted Plot**

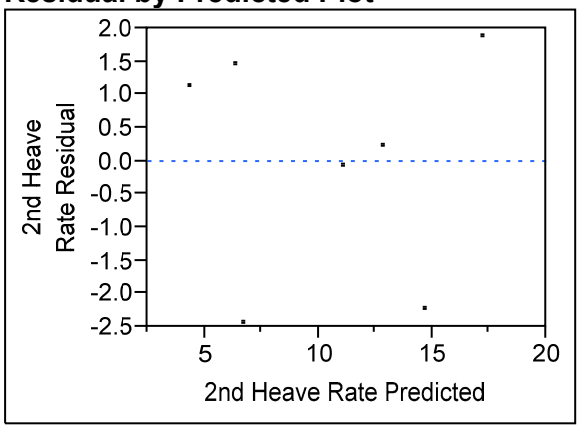


## Sand Content

**Response 2nd Heave Rate**
**Whole Model**
**Regression Plot**

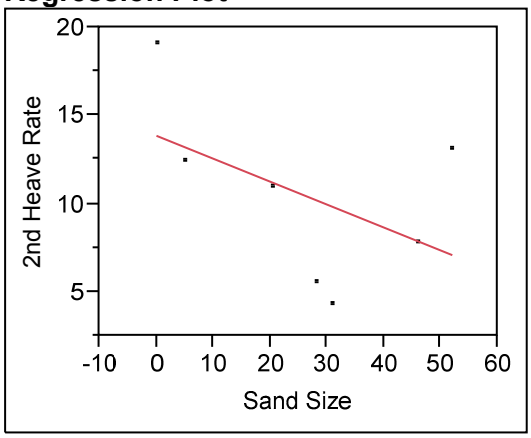


**Actual by Predicted Plot**

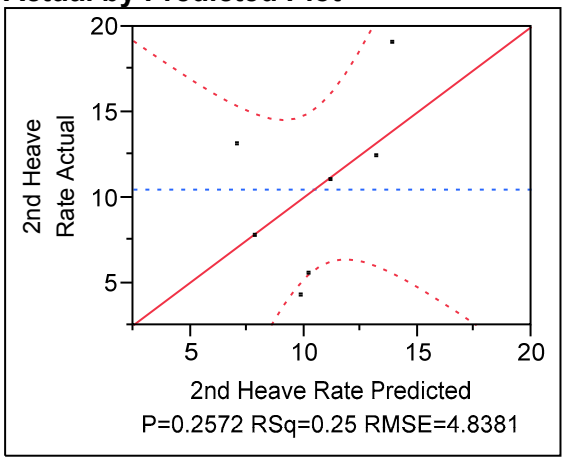

### Summary of Fit

| | |
|---|---|
| RSquare | 0.246368 |
| RSquare Adj | 0.095642 |
| Root Mean Square Error | 4.838117 |
| Mean of Response | 10.45714 |
| Observations (or Sum Wgts) | 7 |

### Analysis of Variance

| Source | DF | Sum of Squares | Mean Square | F Ratio |
|---|---|---|---|---|
| Model | 1 | 38.26026 | 38.2603 | 1.6345 |
| Error | 5 | 117.03688 | 23.4074 | **Prob > F** |
| C. Total | 6 | 155.29714 | | 0.2572 |

### Parameter Estimates

| Term | Estimate | Std Error | t Ratio | Prob>\|t\| |
|---|---|---|---|---|
| Intercept | 13.850184 | 3.222937 | 4.30 | 0.0077* |
| Sand Size | -0.130215 | 0.101851 | -1.28 | 0.2572 |

### Residual by Predicted Plot

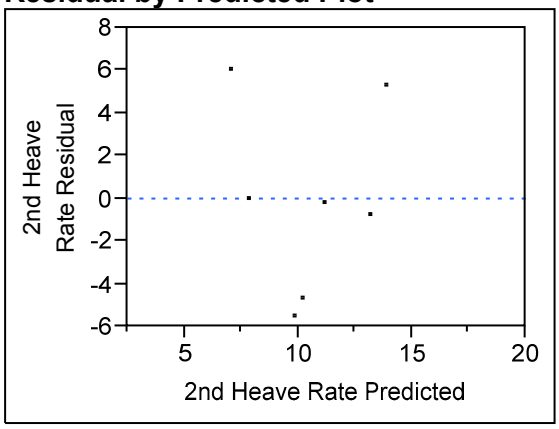


## Silt Content

### Response 2nd Heave Rate
### Whole Model
### Regression Plot

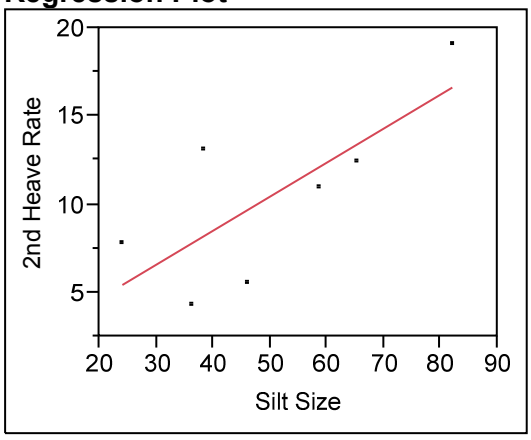

### Actual by Predicted Plot

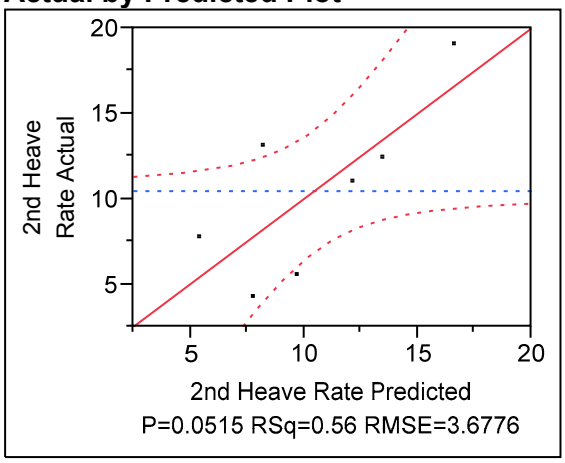


### Summary of Fit

| | |
|---|---|
| RSquare | 0.564547 |
| RSquare Adj | 0.477457 |
| Root Mean Square Error | 3.677622 |
| Mean of Response | 10.45714 |
| Observations (or Sum Wgts) | 7 |

### Analysis of Variance

| Source | DF | Sum of Squares | Mean Square | F Ratio |
|---|---|---|---|---|
| Model | 1 | 87.67261 | 87.6726 | 6.4823 |
| Error | 5 | 67.62453 | 13.5249 | **Prob > F** |
| C. Total | 6 | 155.29714 | | 0.0515 |

### Parameter Estimates

| Term | Estimate | Std Error | t Ratio | Prob>\|t\| |
|---|---|---|---|---|
| Intercept | 0.7905859 | 4.043156 | 0.20 | 0.8527 |
| Silt Size | 0.1931656 | 0.075869 | 2.55 | 0.0515 |

### Residual by Predicted Plot

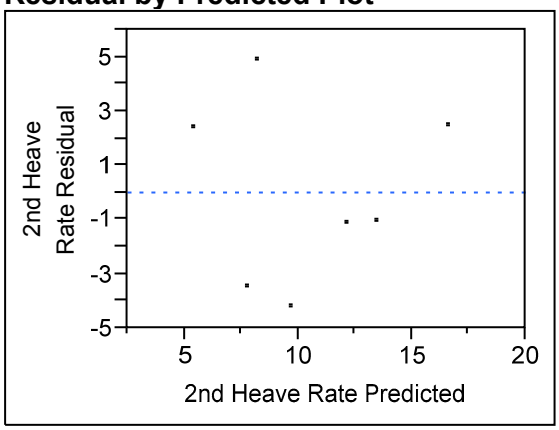

## Clay Content

**Response 2nd Heave Rate**
**Whole Model**
**Regression Plot**

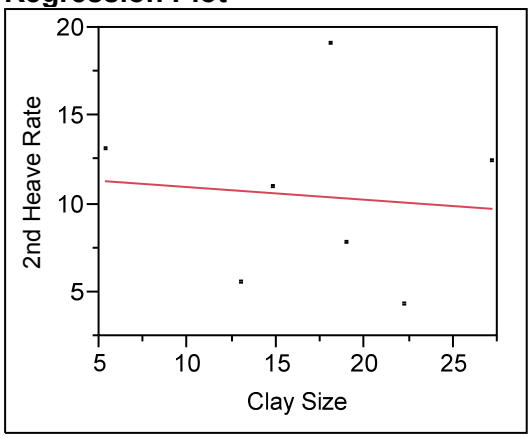


**Actual by Predicted Plot**

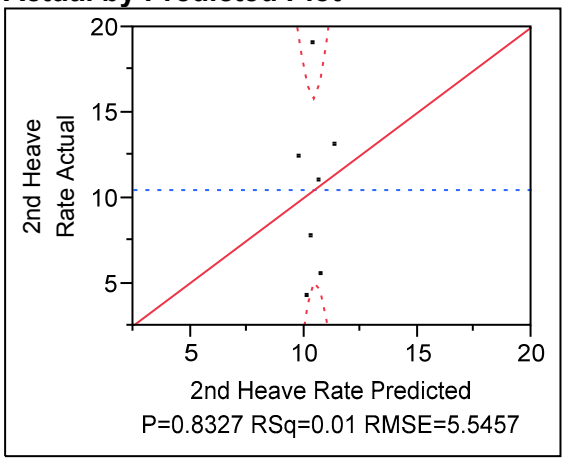


### Summary of Fit

| | |
|---|---|
| RSquare | 0.009813 |
| RSquare Adj | -0.18822 |
| Root Mean Square Error | 5.545687 |
| Mean of Response | 10.45714 |
| Observations (or Sum Wgts) | 7 |

### Analysis of Variance

| Source | DF | Sum of Squares | Mean Square | F Ratio |
|---|---|---|---|---|
| Model | 1 | 1.52391 | 1.5239 | 0.0496 |
| Error | 5 | 153.77323 | 30.7546 | **Prob > F** |
| C. Total | 6 | 155.29714 | | 0.8327 |

### Parameter Estimates

| Term | Estimate | Std Error | t Ratio | Prob>\|t\| |
|---|---|---|---|---|
| Intercept | 11.686682 | 5.907887 | 1.98 | 0.1048 |
| Clay Size | -0.072023 | 0.323555 | -0.22 | 0.8327 |

**Residual by Predicted Plot**

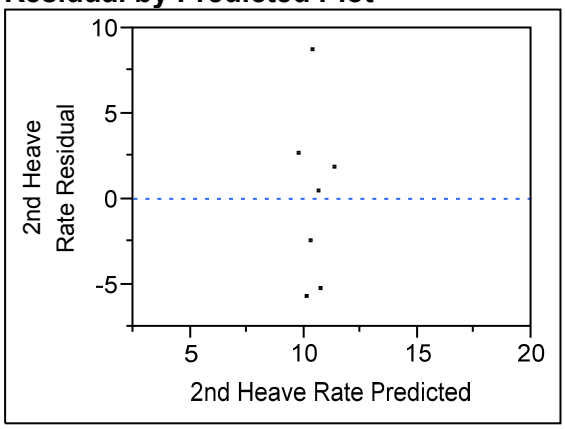


**Passing 0.074 mm**

**Response 2nd Heave Rate**
**Whole Model**
**Regression Plot**

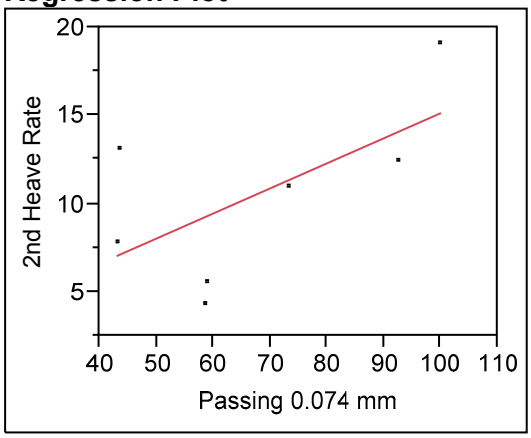


**Actual by Predicted Plot**

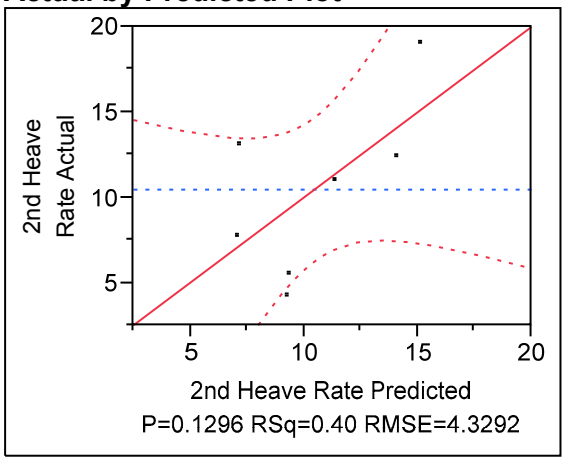

### Summary of Fit

| | |
|---|---|
| RSquare | 0.396564 |
| RSquare Adj | 0.275876 |
| Root Mean Square Error | 4.329248 |
| Mean of Response | 10.45714 |
| Observations (or Sum Wgts) | 7 |

### Analysis of Variance

| Source | DF | Sum of Squares | Mean Square | F Ratio |
|---|---|---|---|---|
| Model | 1 | 61.58518 | 61.5852 | 3.2859 |
| Error | 5 | 93.71196 | 18.7424 | **Prob > F** |
| C. Total | 6 | 155.29714 | | 0.1296 |

### Parameter Estimates

| Term | Estimate | Std Error | t Ratio | Prob>\|t\| |
|---|---|---|---|---|
| Intercept | 0.9052384 | 5.517651 | 0.16 | 0.8761 |
| Passing 0.074 mm | 0.142323 | 0.078514 | 1.81 | 0.1296 |

### Residual by Predicted Plot

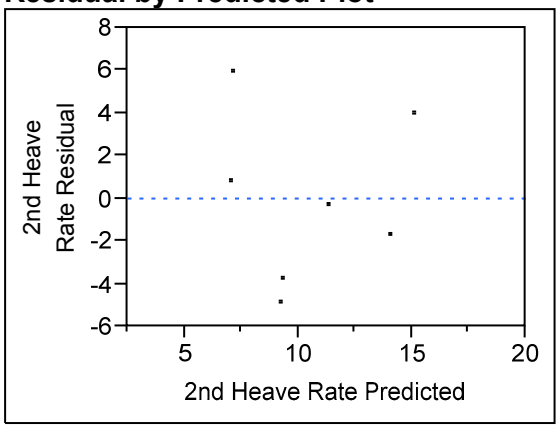


## Passing 0.02 mm

### Response 2nd Heave Rate
### Whole Model
### Regression Plot

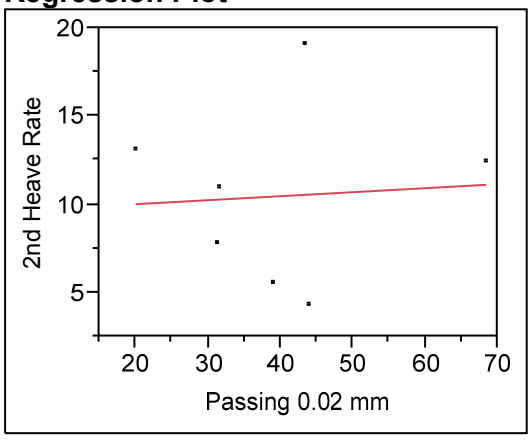

### Actual by Predicted Plot

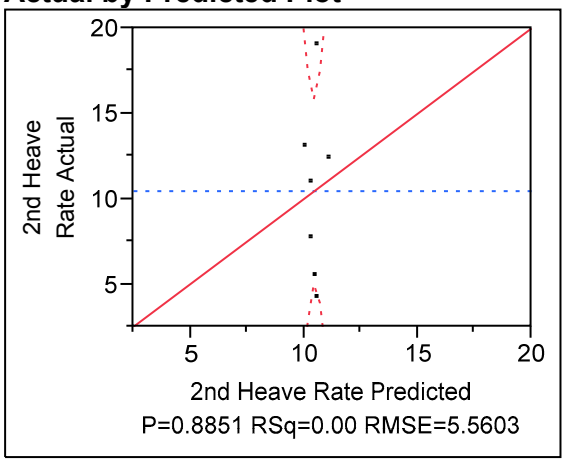


### Summary of Fit

| | |
|---|---|
| RSquare | 0.004601 |
| RSquare Adj | -0.19448 |
| Root Mean Square Error | 5.560263 |
| Mean of Response | 10.45714 |
| Observations (or Sum Wgts) | 7 |

### Analysis of Variance

| Source | DF | Sum of Squares | Mean Square | F Ratio |
|---|---|---|---|---|
| Model | 1 | 0.71451 | 0.7145 | 0.0231 |
| Error | 5 | 154.58264 | 30.9165 | **Prob > F** |
| C. Total | 6 | 155.29714 | | 0.8851 |

### Parameter Estimates

| Term | Estimate | Std Error | t Ratio | Prob>\|t\| |
|---|---|---|---|---|
| Intercept | 9.5560471 | 6.288928 | 1.52 | 0.1891 |
| Passing 0.02 mm | 0.0227549 | 0.149682 | 0.15 | 0.8851 |

### Residual by Predicted Plot

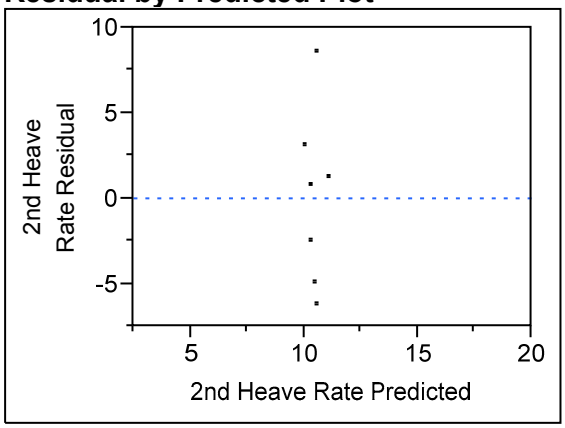

## Liquid Limit

**Response 2nd Heave Rate**
**Whole Model**
**Regression Plot**

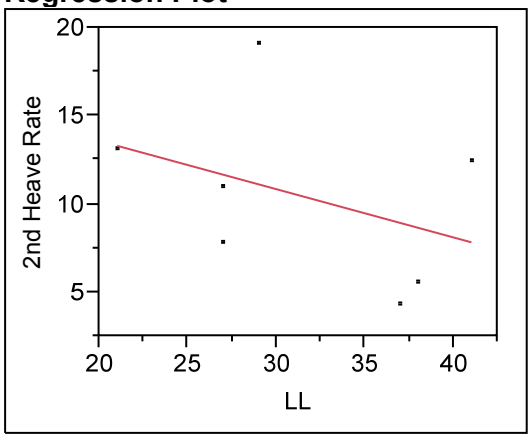


**Actual by Predicted Plot**

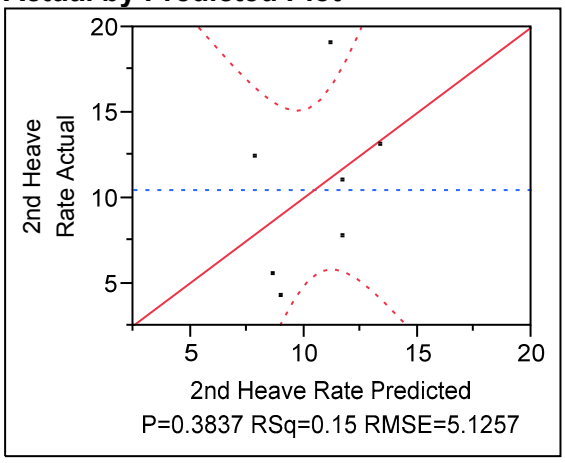


### Summary of Fit

| | |
|---|---|
| RSquare | 0.154102 |
| RSquare Adj | -0.01508 |
| Root Mean Square Error | 5.125731 |
| Mean of Response | 10.45714 |
| Observations (or Sum Wgts) | 7 |

### Analysis of Variance

| Source | DF | Sum of Squares | Mean Square | F Ratio |
|---|---|---|---|---|
| Model | 1 | 23.93153 | 23.9315 | 0.9109 |
| Error | 5 | 131.36562 | 26.2731 | **Prob > F** |
| C. Total | 6 | 155.29714 | | 0.3837 |

### Lack Of Fit

| Source | DF | Sum of Squares | Mean Square | F Ratio |
|---|---|---|---|---|
| Lack Of Fit | 4 | 126.24562 | 31.5614 | 6.1643 |
| Pure Error | 1 | 5.12000 | 5.1200 | **Prob > F** |
| Total Error | 5 | 131.36562 | | 0.2923 |

| Source | DF | Sum of Squares | Mean Square | F Ratio<br>Max RSq<br>0.9670 |
|---|---|---|---|---|

**Parameter Estimates**

| Term | Estimate | Std Error | t Ratio | Prob>\|t\| |
|---|---|---|---|---|
| Intercept | 19.055764 | 9.215419 | 2.07 | 0.0935 |
| LL | -0.273592 | 0.286665 | -0.95 | 0.3837 |

**Residual by Predicted Plot**

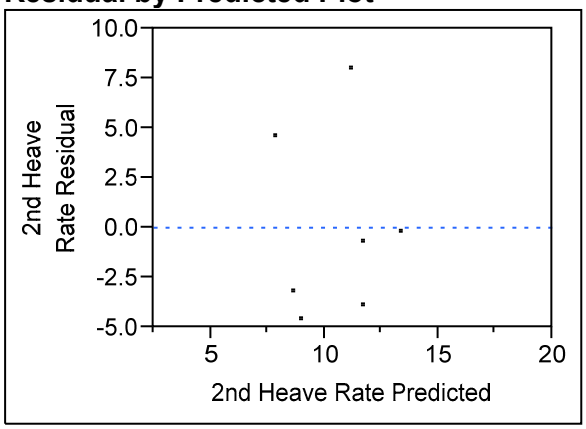


**Plasticity Index**

**Response 2nd Heave Rate**
**Whole Model**
**Regression Plot**

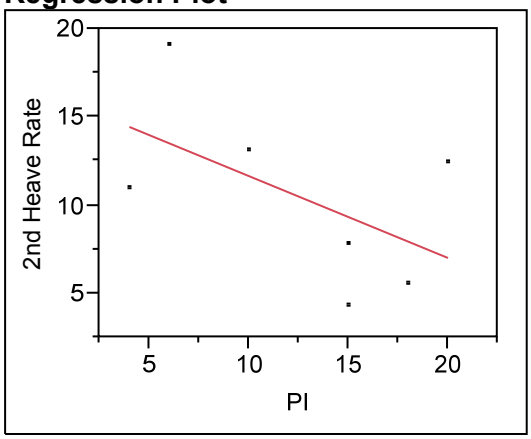

## Actual by Predicted Plot

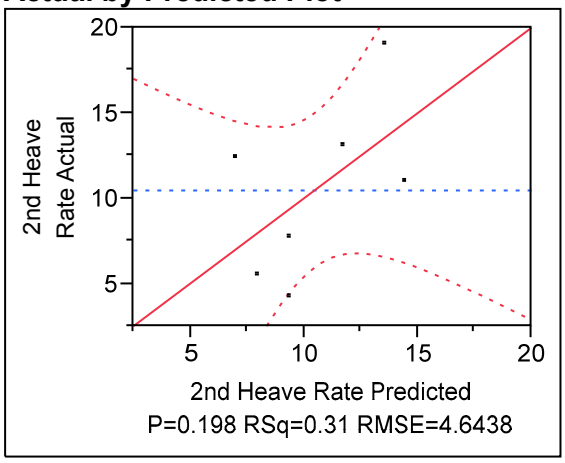


## Summary of Fit

| | |
|---|---|
| RSquare | 0.305684 |
| RSquare Adj | 0.166821 |
| Root Mean Square Error | 4.643819 |
| Mean of Response | 10.45714 |
| Observations (or Sum Wgts) | 7 |

## Analysis of Variance

| Source | DF | Sum of Squares | Mean Square | F Ratio |
|---|---|---|---|---|
| Model | 1 | 47.47186 | 47.4719 | 2.2013 |
| Error | 5 | 107.82529 | 21.5651 | **Prob > F** |
| C. Total | 6 | 155.29714 | | 0.1980 |

## Lack Of Fit

| Source | DF | Sum of Squares | Mean Square | F Ratio |
|---|---|---|---|---|
| Lack Of Fit | 4 | 101.70029 | 25.4251 | 4.1510 |
| Pure Error | 1 | 6.12500 | 6.1250 | **Prob > F** |
| Total Error | 5 | 107.82529 | | 0.3507 |
| | | | | **Max RSq** |
| | | | | 0.9606 |

## Parameter Estimates

| Term | Estimate | Std Error | t Ratio | Prob>\|t\| |
|---|---|---|---|---|
| Intercept | 16.30065 | 4.311902 | 3.78 | 0.0129* |
| PI | -0.464824 | 0.31329 | -1.48 | 0.1980 |

**Residual by Predicted Plot**

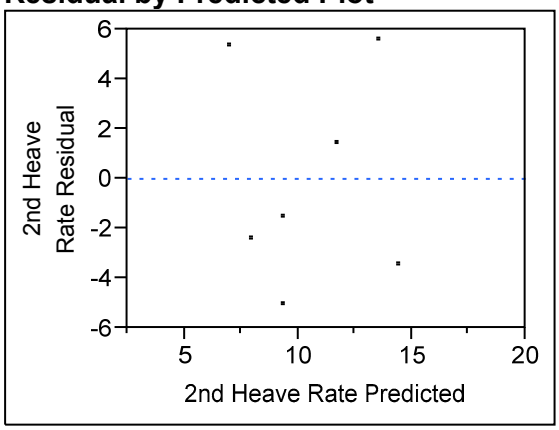


## Activity Index

**Response 2nd Heave Rate**
**Whole Model**
**Regression Plot**

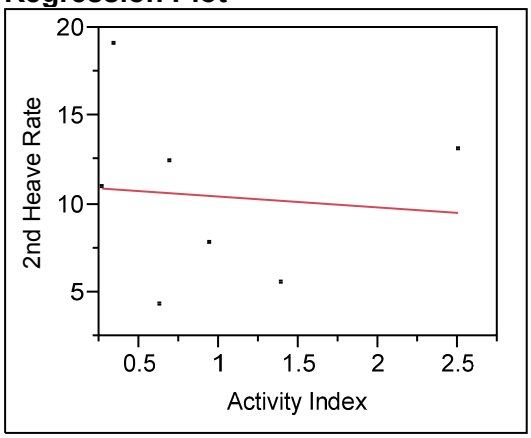


**Actual by Predicted Plot**

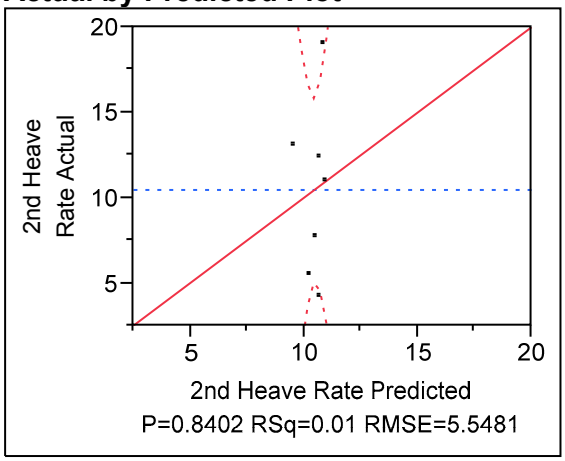

## Summary of Fit

| | |
|---|---|
| RSquare | 0.008936 |
| RSquare Adj | -0.18928 |
| Root Mean Square Error | 5.548141 |
| Mean of Response | 10.45714 |
| Observations (or Sum Wgts) | 7 |

## Analysis of Variance

| Source | DF | Sum of Squares | Mean Square | F Ratio |
|---|---|---|---|---|
| Model | 1 | 1.38780 | 1.3878 | 0.0451 |
| Error | 5 | 153.90934 | 30.7819 | **Prob > F** |
| C. Total | 6 | 155.29714 | | 0.8402 |

## Parameter Estimates

| Term | Estimate | Std Error | t Ratio | Prob>\|t\| |
|---|---|---|---|---|
| Intercept | 11.053131 | 3.503695 | 3.15 | 0.0252* |
| Activity Index | -0.61971 | 2.918581 | -0.21 | 0.8402 |

## Residual by Predicted Plot

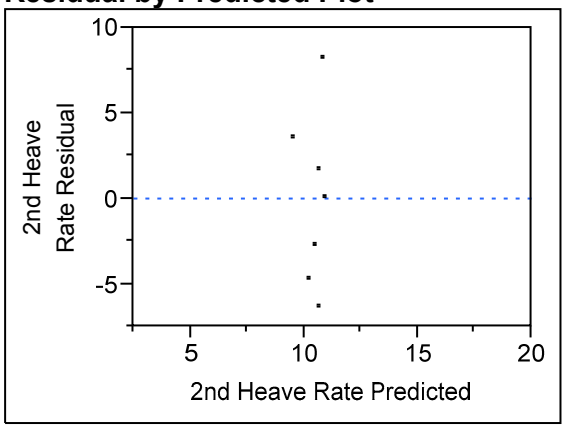

**Coarse Materials 1st Frost Heave Model**

## First Iteration

### Response 1st Heave Rate
### Whole Model
### Actual by Predicted Plot

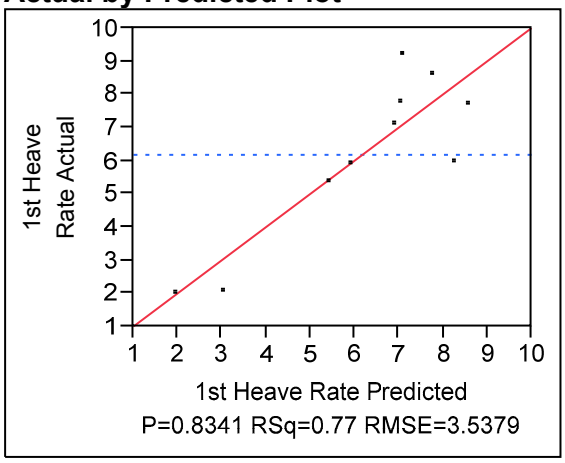


### Summary of Fit

| | |
|---|---|
| RSquare | 0.774868 |
| RSquare Adj | -1.02619 |
| Root Mean Square Error | 3.537859 |
| Mean of Response | 6.18 |
| Observations (or Sum Wgts) | 10 |

### Analysis of Variance

| Source | DF | Sum of Squares | Mean Square | F Ratio |
|---|---|---|---|---|
| Model | 8 | 43.079556 | 5.3849 | 0.4302 |
| Error | 1 | 12.516444 | 12.5164 | **Prob > F** |
| C. Total | 9 | 55.596000 | | 0.8341 |

### Parameter Estimates

| Term | Estimate | Std Error | t Ratio | Prob>\|t\| | VIF |
|---|---|---|---|---|---|
| Intercept | -20.62659 | 77.10558 | -0.27 | 0.8336 | . |
| D10 | -9.687927 | 6.938821 | -1.40 | 0.3957 | 5.2790687 |
| D30 | 1.4766364 | 2.120918 | 0.70 | 0.6128 | 16.362207 |
| Gravel Size | 0.2709512 | 0.700806 | 0.39 | 0.7651 | 99.493596 |
| Sand Size | 0.1953153 | 0.84196 | 0.23 | 0.8549 | 129.94857 |
| Silt Size | -2.778124 | 13.66838 | -0.20 | 0.8723 | 1158.284 |
| Clay Size | 0.8335627 | 11.73351 | 0.07 | 0.9548 | 114.39526 |
| Passing 0.074 mm | 2.7531068 | 12.73045 | 0.22 | 0.8644 | 1462.1146 |
| Passing 0.02 mm | -0.320691 | 1.559604 | -0.21 | 0.8709 | 5.8037712 |

**Residual by Predicted Plot**

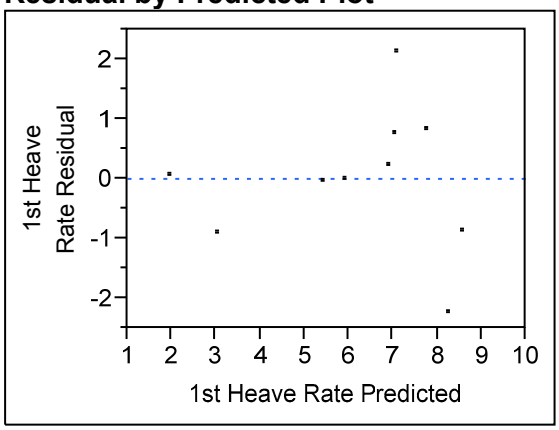


## Second Iteration

**Response 1st Heave Rate**
**Whole Model**
**Actual by Predicted Plot**

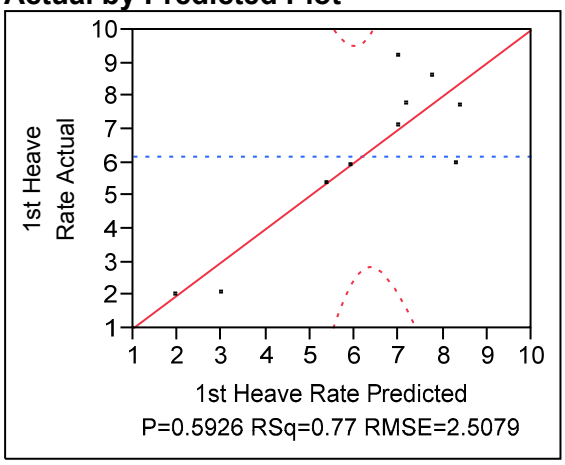


### Summary of Fit

| | |
|---|---|
| RSquare | 0.773732 |
| RSquare Adj | -0.01821 |
| Root Mean Square Error | 2.507949 |
| Mean of Response | 6.18 |
| Observations (or Sum Wgts) | 10 |

### Analysis of Variance

| Source | DF | Sum of Squares | Mean Square | F Ratio |
|---|---|---|---|---|
| Model | 7 | 43.016388 | 6.14520 | 0.9770 |
| Error | 2 | 12.579612 | 6.28981 | **Prob > F** |
| C. Total | 9 | 55.596000 | | 0.5926 |

### Parameter Estimates

| Term | Estimate | Std Error | t Ratio | Prob>\|t\| | VIF |
|---|---|---|---|---|---|
| Intercept | -18.17852 | 48.89684 | -0.37 | 0.7458 | . |
| D10 | -9.751215 | 4.878144 | -2.00 | 0.1836 | 5.1920512 |

| Term | Estimate | Std Error | t Ratio | Prob>\|t\| | VIF |
|---|---|---|---|---|---|
| D30 | 1.4421547 | 1.463594 | 0.99 | 0.4283 | 15.505269 |
| Gravel Size | 0.2489556 | 0.445679 | 0.56 | 0.6326 | 80.073442 |
| Sand Size | 0.1717624 | 0.548636 | 0.31 | 0.7839 | 109.79949 |
| Silt Size | -3.641354 | 4.436938 | -0.82 | 0.4981 | 242.87971 |
| Passing 0.074 mm | 3.5773755 | 3.713536 | 0.96 | 0.4370 | 247.57841 |
| Passing 0.02 mm | -0.318413 | 1.105352 | -0.29 | 0.8004 | 5.8013169 |

**Residual by Predicted Plot**

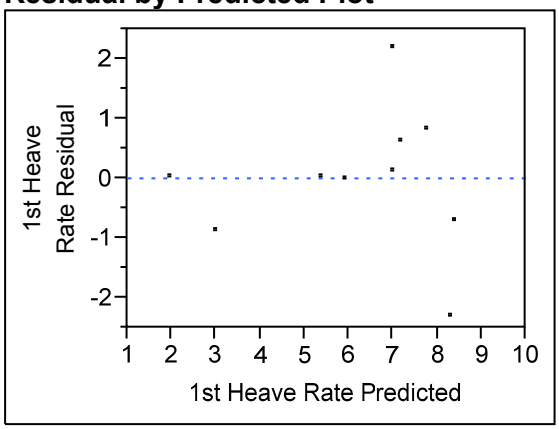


## Third Iteration

**Response 1st Heave Rate**
**Whole Model**
**Actual by Predicted Plot**

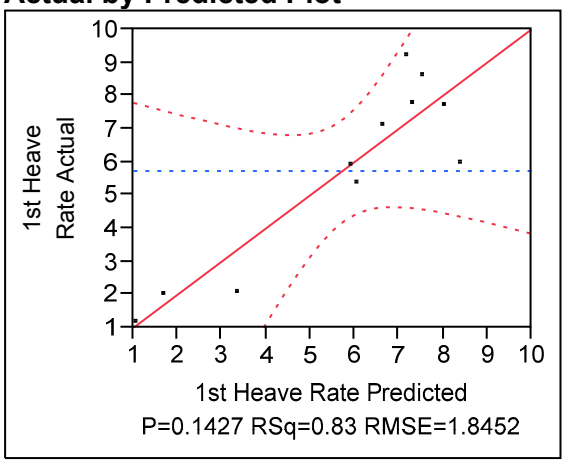


**Summary of Fit**

| | |
|---|---|
| RSquare | 0.825708 |
| RSquare Adj | 0.564269 |
| Root Mean Square Error | 1.845232 |
| Mean of Response | 5.727273 |
| Observations (or Sum Wgts) | 11 |

**Analysis of Variance**

| Source | DF | Sum of Squares | Mean Square | F Ratio |
|---|---|---|---|---|

| Source | DF | Sum of Squares | Mean Square | F Ratio |
|---|---|---|---|---|
| Model | 6 | 64.522291 | 10.7537 | 3.1583 |
| Error | 4 | 13.619527 | 3.4049 | **Prob > F** |
| C. Total | 10 | 78.141818 | | 0.1427 |

**Parameter Estimates**

| Term | Estimate | Std Error | t Ratio | Prob>\|t\| | VIF |
|---|---|---|---|---|---|
| Intercept | -30.37016 | 27.84138 | -1.09 | 0.3367 | . |
| D10 | -9.693813 | 3.584002 | -2.70 | 0.0538 | 5.1962615 |
| D30 | 1.4662065 | 1.041044 | 1.41 | 0.2318 | 16.493687 |
| Gravel Size | 0.3501203 | 0.255125 | 1.37 | 0.2419 | 99.522712 |
| Sand Size | 0.329987 | 0.283329 | 1.16 | 0.3089 | 134.89614 |
| Silt Size | -2.132121 | 1.23179 | -1.73 | 0.1585 | 43.914512 |
| Passing 0.074 mm | 2.30147 | 1.077889 | 2.14 | 0.0996 | 49.220791 |

**Residual by Predicted Plot**

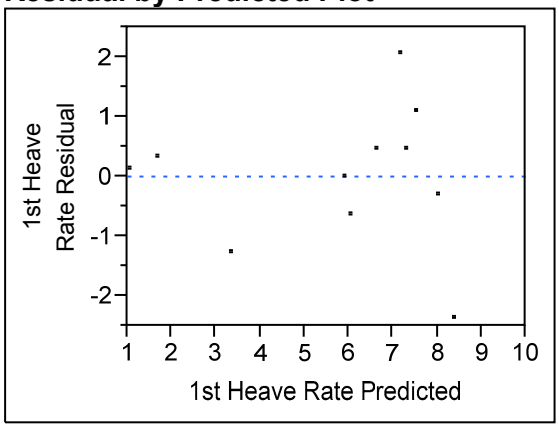


## Fourth Iteration

**Response 1st Heave Rate**
**Whole Model**
**Actual by Predicted Plot**

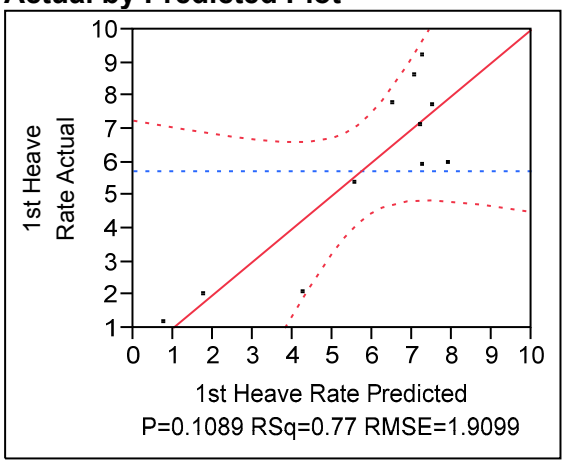


**Summary of Fit**

| | |
|---|---|
| RSquare | 0.766602 |

| | |
|---|---|
| RSquare Adj | 0.533203 |
| Root Mean Square Error | 1.909878 |
| Mean of Response | 5.727273 |
| Observations (or Sum Wgts) | 11 |

## Analysis of Variance

| Source | DF | Sum of Squares | Mean Square | F Ratio |
|---|---|---|---|---|
| Model | 5 | 59.903650 | 11.9807 | 3.2845 |
| Error | 5 | 18.238168 | 3.6476 | **Prob > F** |
| C. Total | 10 | 78.141818 | | 0.1089 |

## Parameter Estimates

| Term | Estimate | Std Error | t Ratio | Prob>\|t\| | VIF |
|---|---|---|---|---|---|
| Intercept | 1.9653424 | 2.154533 | 0.91 | 0.4035 | . |
| D10 | -7.282932 | 3.028281 | -2.40 | 0.0612 | 3.4628819 |
| D30 | 0.7162971 | 0.846703 | 0.85 | 0.4362 | 10.184333 |
| Gravel Size | 0.0606271 | 0.059514 | 1.02 | 0.3551 | 5.0553508 |
| Silt Size | -2.273149 | 1.26877 | -1.79 | 0.1332 | 43.49015 |
| Passing 0.074 mm | 2.0016737 | 1.083373 | 1.85 | 0.1239 | 46.413804 |

## Residual by Predicted Plot

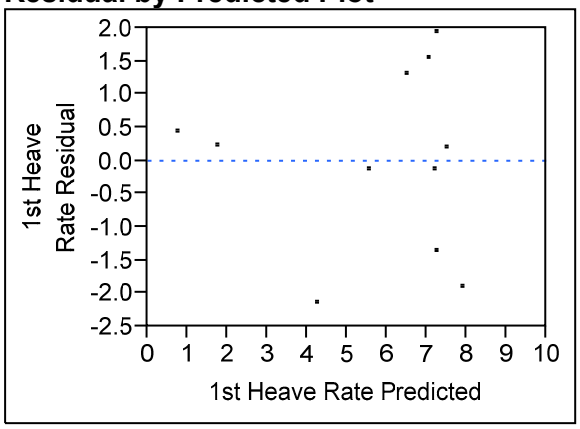

## Fifth Iteration

**Response 1st Heave Rate**
**Whole Model**
**Actual by Predicted Plot**

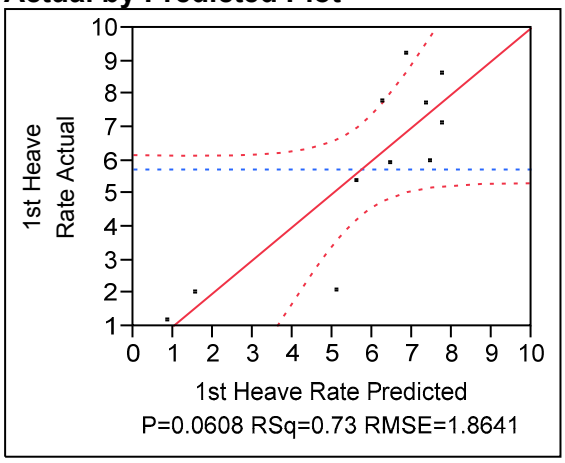


### Summary of Fit

| | |
|---|---|
| RSquare | 0.733194 |
| RSquare Adj | 0.555323 |
| Root Mean Square Error | 1.864079 |
| Mean of Response | 5.727273 |
| Observations (or Sum Wgts) | 11 |

### Analysis of Variance

| Source | DF | Sum of Squares | Mean Square | F Ratio |
|---|---|---|---|---|
| Model | 4 | 57.293079 | 14.3233 | 4.1221 |
| Error | 6 | 20.848739 | 3.4748 | **Prob > F** |
| C. Total | 10 | 78.141818 | | 0.0608 |

### Parameter Estimates

| Term | Estimate | Std Error | t Ratio | Prob>\|t\| | VIF |
|---|---|---|---|---|---|
| Intercept | 2.0778983 | 2.098854 | 0.99 | 0.3604 | . |
| D10 | -5.836092 | 2.439181 | -2.39 | 0.0538 | 2.3583924 |
| Gravel Size | 0.0984509 | 0.038339 | 2.57 | 0.0425* | 2.2022789 |
| Silt Size | -1.699021 | 1.046304 | -1.62 | 0.1555 | 31.047309 |
| Passing 0.074 mm | 1.4665568 | 0.85845 | 1.71 | 0.1384 | 30.591709 |

**Residual by Predicted Plot**

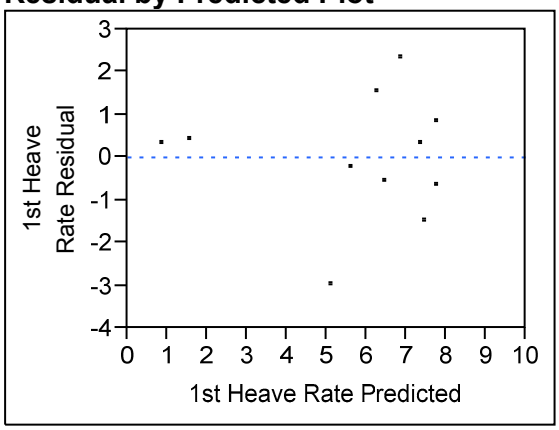


## Sixth Iteration

**Response 1st Heave Rate**
**Whole Model**
**Actual by Predicted Plot**

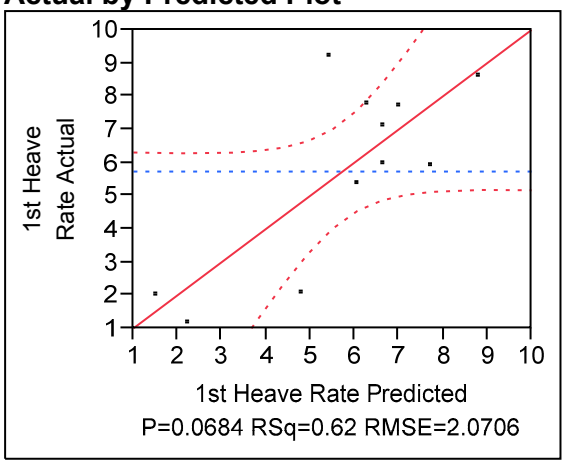


### Summary of Fit

| | |
|---|---|
| RSquare | 0.61594 |
| RSquare Adj | 0.451343 |
| Root Mean Square Error | 2.070582 |
| Mean of Response | 5.727273 |
| Observations (or Sum Wgts) | 11 |

### Analysis of Variance

| Source | DF | Sum of Squares | Mean Square | F Ratio |
|---|---|---|---|---|
| Model | 3 | 48.130663 | 16.0436 | 3.7421 |
| Error | 7 | 30.011155 | 4.2873 | **Prob > F** |
| C. Total | 10 | 78.141818 | | 0.0684 |

### Parameter Estimates

| Term | Estimate | Std Error | t Ratio | Prob>\|t\| | VIF |
|---|---|---|---|---|---|
| Intercept | 3.8572426 | 1.988413 | 1.94 | 0.0936 | . |
| D10 | -5.656722 | 2.706614 | -2.09 | 0.0750 | 2.3535557 |

| Term | Estimate | Std Error | t Ratio | Prob>\|t\| | VIF |
|---|---|---|---|---|---|
| Gravel Size | 0.0665068 | 0.036553 | 1.82 | 0.1117 | 1.6224638 |
| Passing 0.074 mm | 0.1138113 | 0.230204 | 0.49 | 0.6362 | 1.782963 |

**Residual by Predicted Plot**

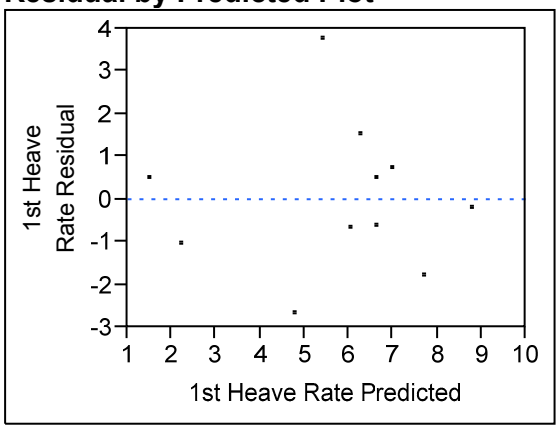


## Final Iteration

**Response 1st Heave Rate**
**Whole Model**
**Actual by Predicted Plot**

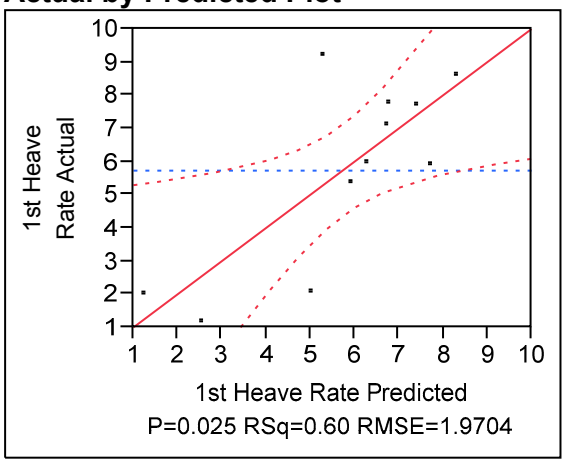


**Summary of Fit**

| | |
|---|---|
| RSquare | 0.602529 |
| RSquare Adj | 0.503162 |
| Root Mean Square Error | 1.970377 |
| Mean of Response | 5.727273 |
| Observations (or Sum Wgts) | 11 |

**Analysis of Variance**

| Source | DF | Sum of Squares | Mean Square | F Ratio |
|---|---|---|---|---|
| Model | 2 | 47.082738 | 23.5414 | 6.0636 |
| Error | 8 | 31.059081 | 3.8824 | Prob > F |
| C. Total | 10 | 78.141818 | | 0.0250* |

**Parameter Estimates**

| Term | Estimate | Std Error | t Ratio | Prob>\|t\| | VIF |
|---|---|---|---|---|---|
| Intercept | 4.4414622 | 1.521794 | 2.92 | 0.0193* | . |
| D10 | -6.542756 | 1.930122 | -3.39 | 0.0095* | 1.3216828 |
| Gravel Size | 0.0742877 | 0.031394 | 2.37 | 0.0455* | 1.3216828 |

**Residual by Predicted Plot**

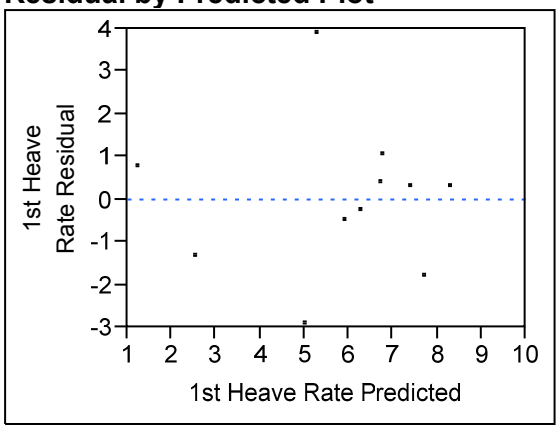


**Individual Parameter Analysis for Coarse Materials 1st Frost Heave Model**

**$C_c$**

**Response 1st Heave Rate**
**Whole Model**
**Regression Plot**

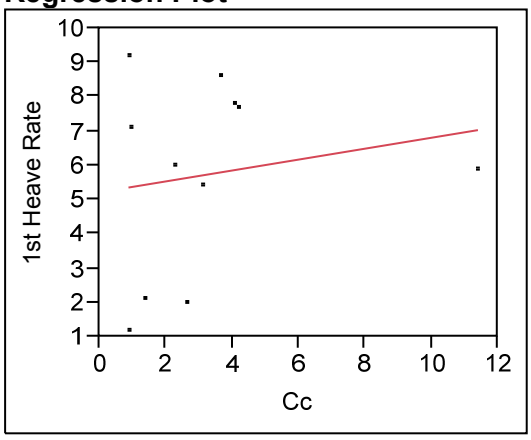

**Actual by Predicted Plot**

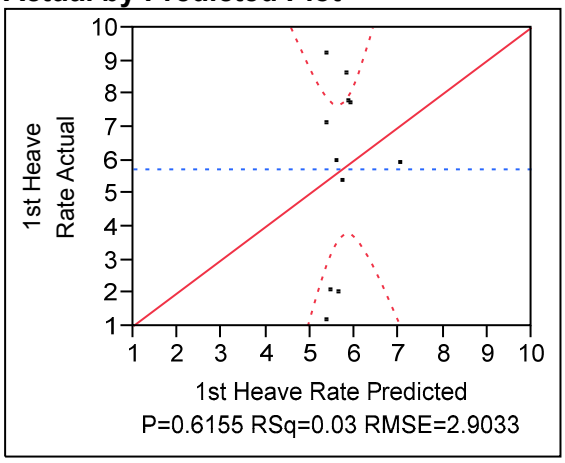


**Summary of Fit**

| | |
|---|---|
| RSquare | 0.029192 |
| RSquare Adj | -0.07868 |
| Root Mean Square Error | 2.903268 |
| Mean of Response | 5.727273 |
| Observations (or Sum Wgts) | 11 |

**Analysis of Variance**

| Source | DF | Sum of Squares | Mean Square | F Ratio |
|---|---|---|---|---|
| Model | 1 | 2.281140 | 2.28114 | 0.2706 |
| Error | 9 | 75.860678 | 8.42896 | **Prob > F** |
| C. Total | 10 | 78.141818 | | 0.6155 |

**Parameter Estimates**

| Term | Estimate | Std Error | t Ratio | Prob>\|t\| |
|---|---|---|---|---|
| Intercept | 5.2137252 | 1.319384 | 3.95 | 0.0033* |
| Cc | 0.1594868 | 0.306574 | 0.52 | 0.6155 |

**Residual by Predicted Plot**

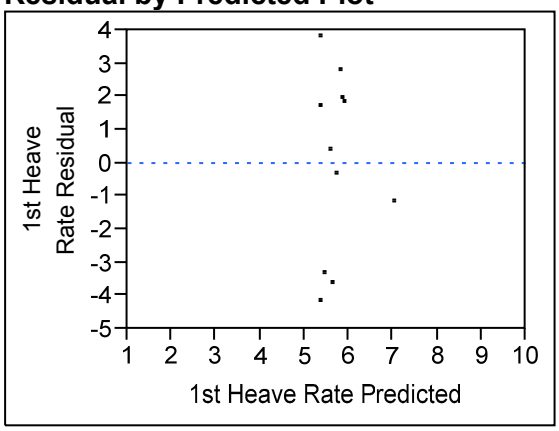

$C_u$

**Response 1st Heave Rate**
**Whole Model**
**Regression Plot**

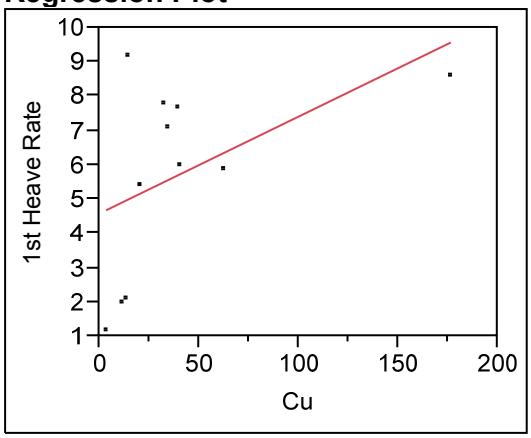


**Actual by Predicted Plot**

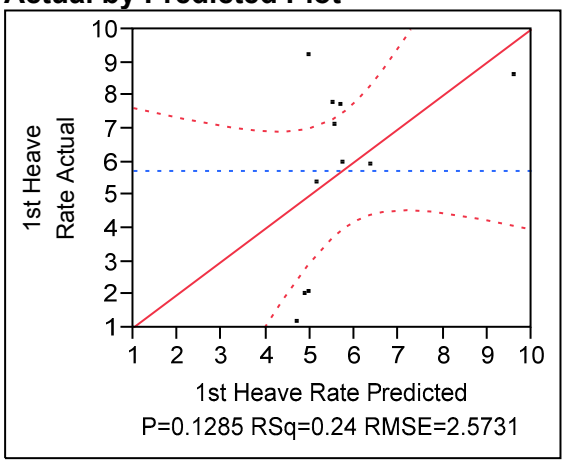


## Summary of Fit

| | |
|---|---|
| RSquare | 0.237434 |
| RSquare Adj | 0.152704 |
| Root Mean Square Error | 2.573116 |
| Mean of Response | 5.727273 |
| Observations (or Sum Wgts) | 11 |

## Analysis of Variance

| Source | DF | Sum of Squares | Mean Square | F Ratio |
|---|---|---|---|---|
| Model | 1 | 18.553493 | 18.5535 | 2.8023 |
| Error | 9 | 59.588325 | 6.6209 | **Prob > F** |
| C. Total | 10 | 78.141818 | | 0.1285 |

## Parameter Estimates

| Term | Estimate | Std Error | t Ratio | Prob>\|t\| |
|---|---|---|---|---|
| Intercept | 4.5854689 | 1.033025 | 4.44 | 0.0016* |
| Cu | 0.0282771 | 0.016892 | 1.67 | 0.1285 |

**Residual by Predicted Plot**

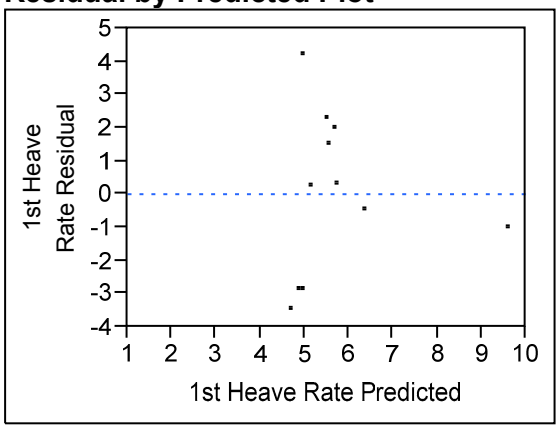


**$D_{10}$**

**Response 1st Heave Rate**
**Whole Model**
**Regression Plot**

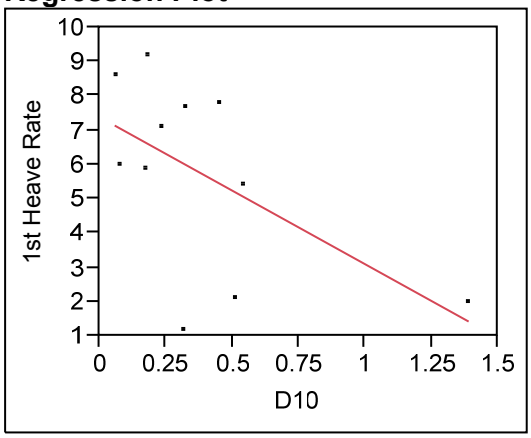


**Actual by Predicted Plot**

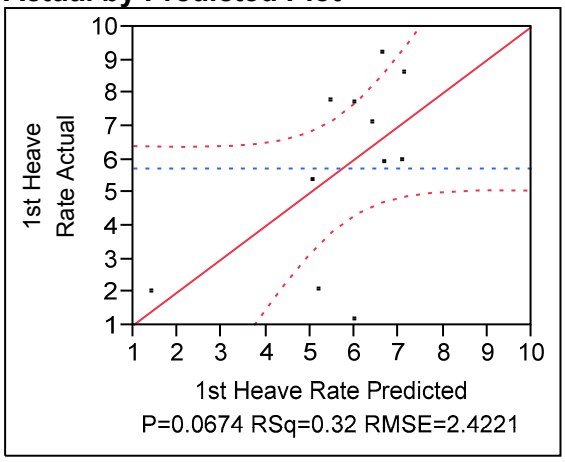

### Summary of Fit

| | |
|---|---|
| RSquare | 0.324338 |
| RSquare Adj | 0.249265 |
| Root Mean Square Error | 2.422061 |
| Mean of Response | 5.727273 |
| Observations (or Sum Wgts) | 11 |

### Analysis of Variance

| Source | DF | Sum of Squares | Mean Square | F Ratio |
|---|---|---|---|---|
| Model | 1 | 25.344398 | 25.3444 | 4.3203 |
| Error | 9 | 52.797420 | 5.8664 | **Prob > F** |
| C. Total | 10 | 78.141818 | | 0.0674 |

### Parameter Estimates

| Term | Estimate | Std Error | t Ratio | Prob>\|t\| |
|---|---|---|---|---|
| Intercept | 7.3814831 | 1.080137 | 6.83 | <.0001* |
| D10 | -4.28956 | 2.063749 | -2.08 | 0.0674 |

### Residual by Predicted Plot

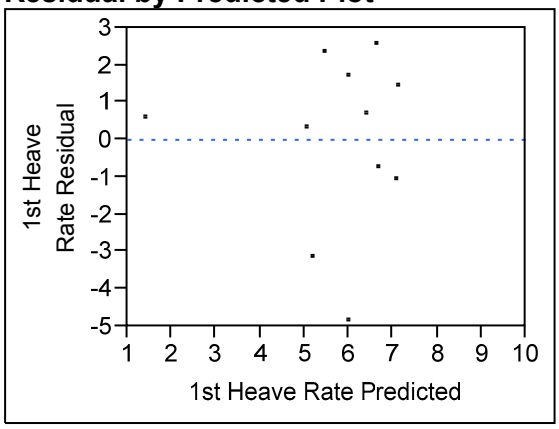


$D_{30}$

### Response 1st Heave Rate
### Whole Model
### Regression Plot

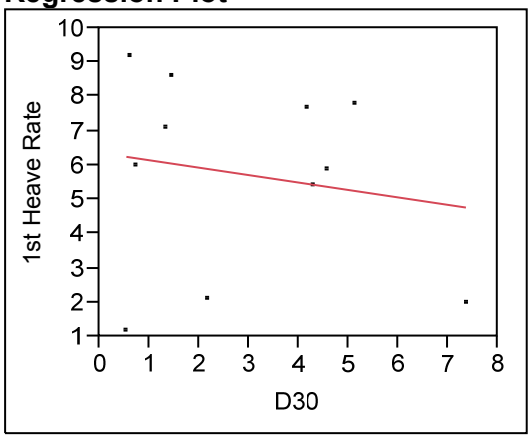

### Actual by Predicted Plot

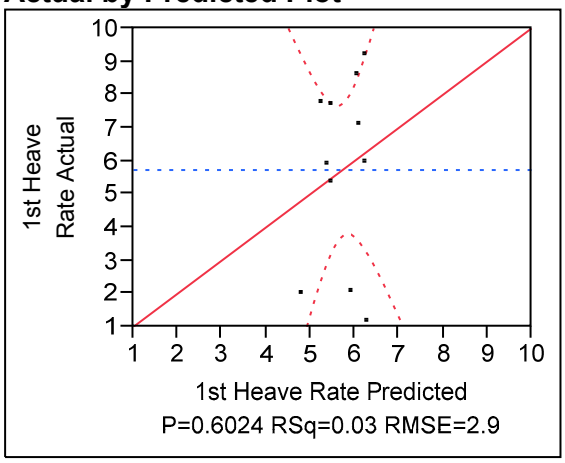


### Summary of Fit

| | |
|---|---|
| RSquare | 0.031367 |
| RSquare Adj | -0.07626 |
| Root Mean Square Error | 2.900014 |
| Mean of Response | 5.727273 |
| Observations (or Sum Wgts) | 11 |

### Analysis of Variance

| Source | DF | Sum of Squares | Mean Square | F Ratio |
|---|---|---|---|---|
| Model | 1 | 2.451090 | 2.45109 | 0.2914 |
| Error | 9 | 75.690728 | 8.41008 | **Prob > F** |
| C. Total | 10 | 78.141818 | | 0.6024 |

### Parameter Estimates

| Term | Estimate | Std Error | t Ratio | Prob>\|t\| |
|---|---|---|---|---|
| Intercept | 6.3645968 | 1.469091 | 4.33 | 0.0019* |
| D30 | -0.21749 | 0.402865 | -0.54 | 0.6024 |

### Residual by Predicted Plot

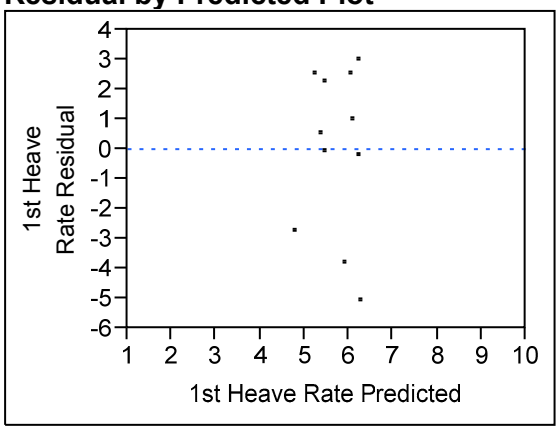

**$D_{60}$**

**Response 1st Heave Rate**
**Whole Model**
**Regression Plot**

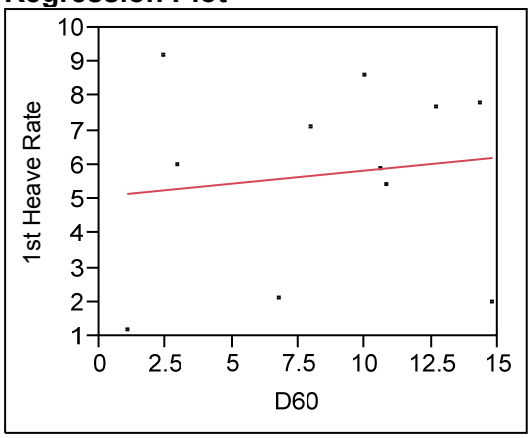


**Actual by Predicted Plot**

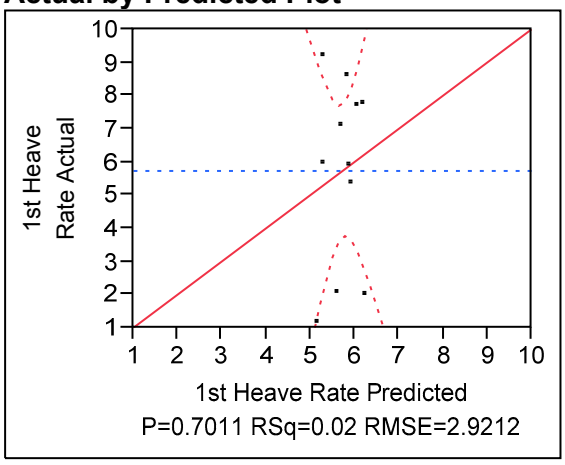


**Summary of Fit**

| | |
|---|---|
| RSquare | 0.017157 |
| RSquare Adj | -0.09205 |
| Root Mean Square Error | 2.921209 |
| Mean of Response | 5.727273 |
| Observations (or Sum Wgts) | 11 |

**Analysis of Variance**

| Source | DF | Sum of Squares | Mean Square | F Ratio |
|---|---|---|---|---|
| Model | 1 | 1.340653 | 1.34065 | 0.1571 |
| Error | 9 | 76.801165 | 8.53346 | **Prob > F** |
| C. Total | 10 | 78.141818 | | 0.7011 |

**Parameter Estimates**

| Term | Estimate | Std Error | t Ratio | Prob>\|t\| |
|---|---|---|---|---|
| Intercept | 5.0725217 | 1.872032 | 2.71 | 0.0240* |
| D60 | 0.0763841 | 0.192712 | 0.40 | 0.7011 |

**Residual by Predicted Plot**

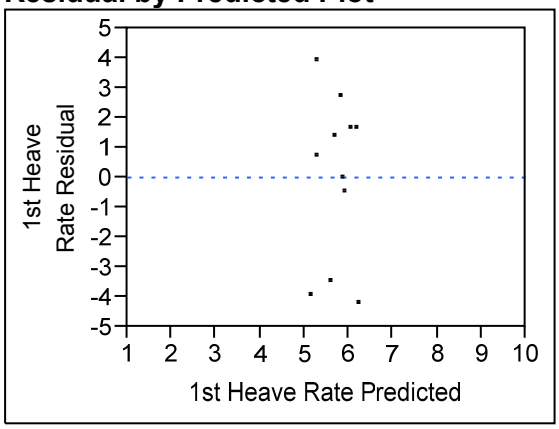


**Gravel Content**

**Response 1st Heave Rate**
**Whole Model**
**Regression Plot**

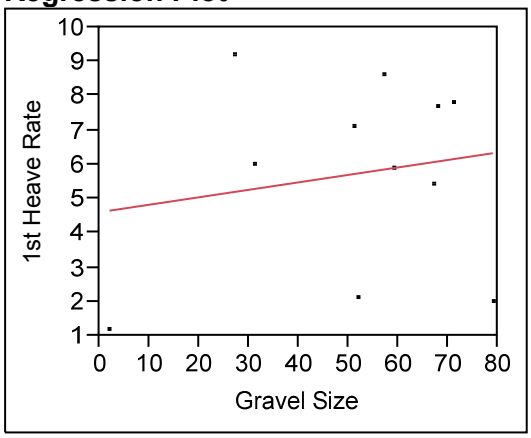


**Actual by Predicted Plot**

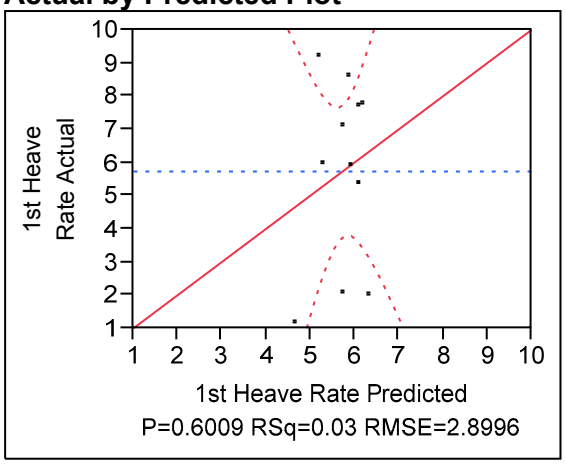

### Summary of Fit

| | |
|---|---|
| RSquare | 0.03162 |
| RSquare Adj | -0.07598 |
| Root Mean Square Error | 2.899635 |
| Mean of Response | 5.727273 |
| Observations (or Sum Wgts) | 11 |

### Analysis of Variance

| Source | DF | Sum of Squares | Mean Square | F Ratio |
|---|---|---|---|---|
| Model | 1 | 2.470848 | 2.47085 | 0.2939 |
| Error | 9 | 75.670970 | 8.40789 | **Prob > F** |
| C. Total | 10 | 78.141818 | | 0.6009 |

### Parameter Estimates

| Term | Estimate | Std Error | t Ratio | Prob>\|t\| |
|---|---|---|---|---|
| Intercept | 4.6102815 | 2.238295 | 2.06 | 0.0695 |
| Gravel Size | 0.0217853 | 0.040187 | 0.54 | 0.6009 |

### Residual by Predicted Plot

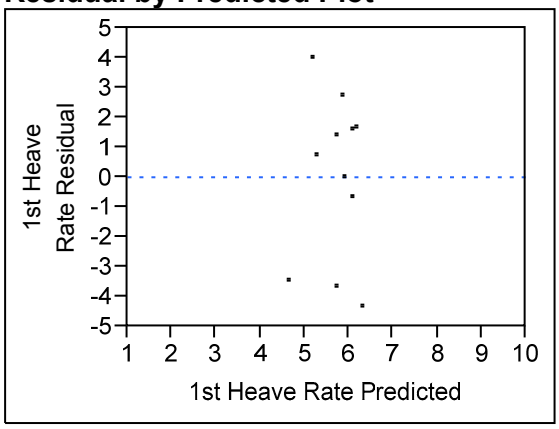


## Sand Content

### Response 1st Heave Rate
### Whole Model
### Regression Plot

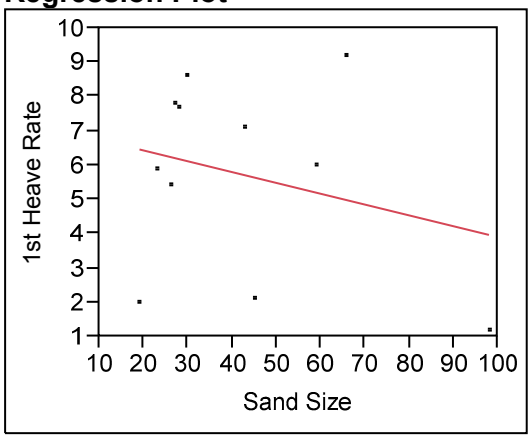

### Actual by Predicted Plot

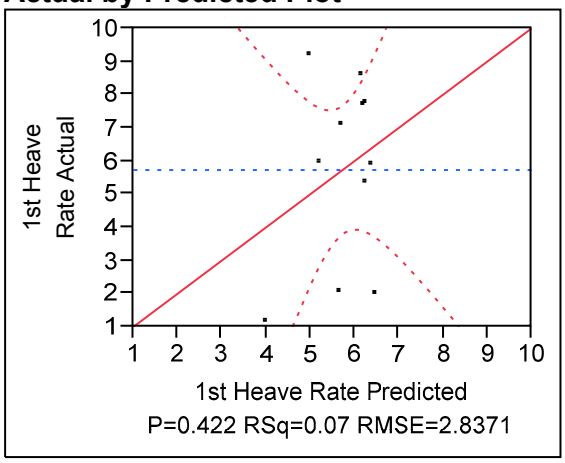


### Summary of Fit

| | |
|---|---|
| RSquare | 0.072914 |
| RSquare Adj | -0.0301 |
| Root Mean Square Error | 2.837138 |
| Mean of Response | 5.727273 |
| Observations (or Sum Wgts) | 11 |

### Analysis of Variance

| Source | DF | Sum of Squares | Mean Square | F Ratio |
|---|---|---|---|---|
| Model | 1 | 5.697661 | 5.69766 | 0.7078 |
| Error | 9 | 72.444157 | 8.04935 | **Prob > F** |
| C. Total | 10 | 78.141818 | | 0.4220 |

### Parameter Estimates

| Term | Estimate | Std Error | t Ratio | Prob>\|t\| |
|---|---|---|---|---|
| Intercept | 7.0583813 | 1.798592 | 3.92 | 0.0035* |
| Sand Size | -0.031556 | 0.037508 | -0.84 | 0.4220 |

### Residual by Predicted Plot

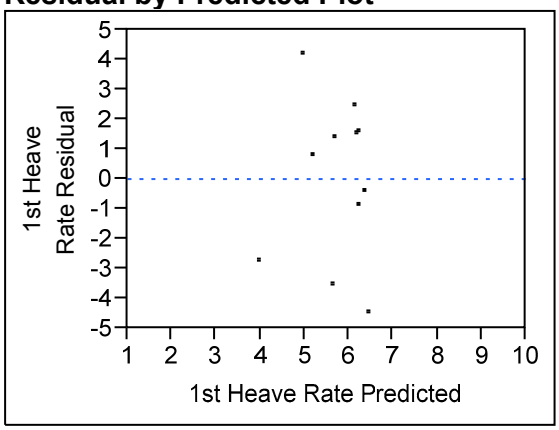

## Silt Content

**Response 1st Heave Rate**
**Whole Model**
**Regression Plot**

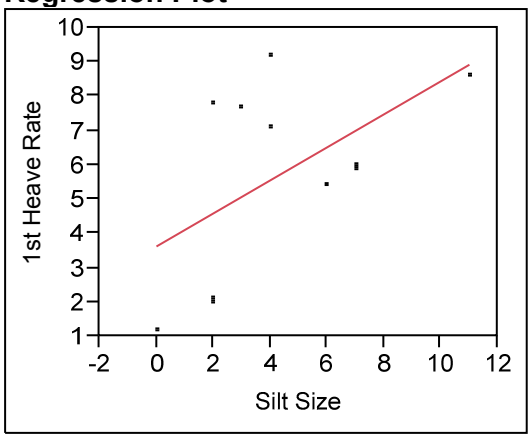


**Actual by Predicted Plot**

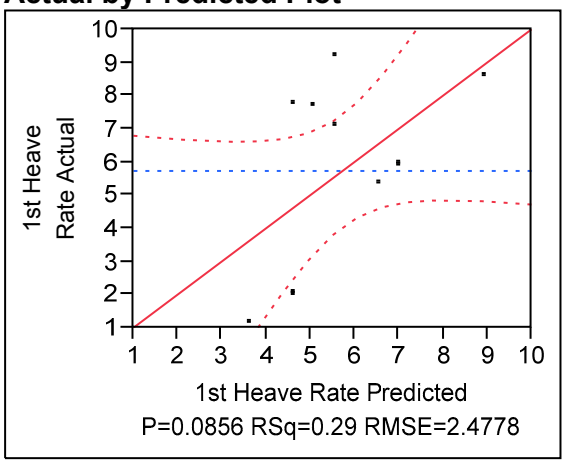


### Summary of Fit

| | |
|---|---|
| RSquare | 0.292888 |
| RSquare Adj | 0.214319 |
| Root Mean Square Error | 2.477791 |
| Mean of Response | 5.727273 |
| Observations (or Sum Wgts) | 11 |

### Analysis of Variance

| Source | DF | Sum of Squares | Mean Square | F Ratio |
|---|---|---|---|---|
| Model | 1 | 22.886763 | 22.8868 | 3.7278 |
| Error | 9 | 55.255055 | 6.1395 | **Prob > F** |
| C. Total | 10 | 78.141818 | | 0.0856 |

### Lack Of Fit

| Source | DF | Sum of Squares | Mean Square | F Ratio |
|---|---|---|---|---|
| Lack Of Fit | 5 | 30.998389 | 6.19968 | 1.0223 |
| Pure Error | 4 | 24.256667 | 6.06417 | **Prob > F** |
| Total Error | 9 | 55.255055 | | 0.5056 |

| Source | DF | Sum of Squares | Mean Square | F Ratio<br>Max RSq<br>0.6896 |
|---|---|---|---|---|

**Parameter Estimates**

| Term | Estimate | Std Error | t Ratio | Prob>\|t\| |
|---|---|---|---|---|
| Intercept | 3.6243542 | 1.320765 | 2.74 | 0.0227* |
| Silt Size | 0.4819188 | 0.249601 | 1.93 | 0.0856 |

**Residual by Predicted Plot**

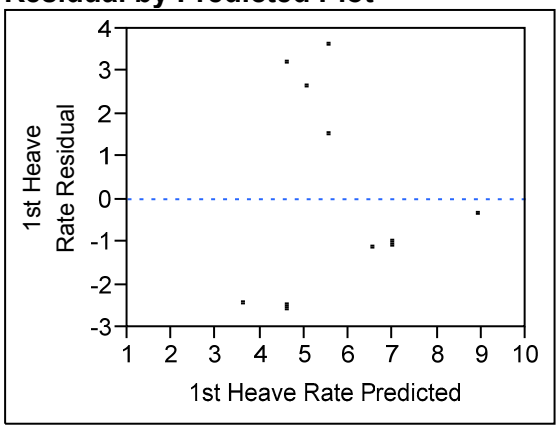


## Clay Content

**Response 1st Heave Rate**
**Whole Model**
**Regression Plot**

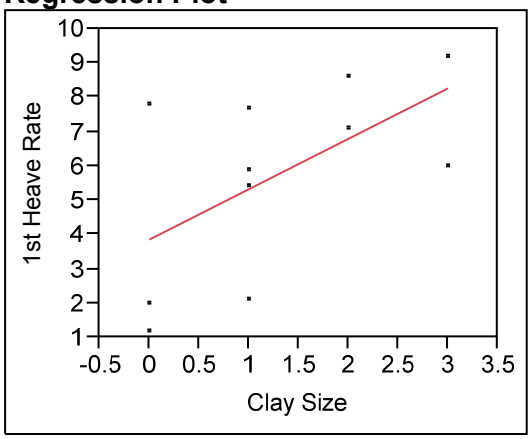

## Actual by Predicted Plot

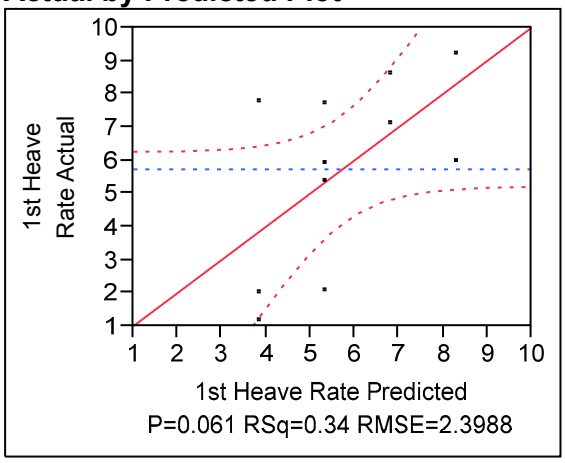


## Summary of Fit

| | |
|---|---|
| RSquare | 0.337281 |
| RSquare Adj | 0.263646 |
| Root Mean Square Error | 2.398751 |
| Mean of Response | 5.727273 |
| Observations (or Sum Wgts) | 11 |

## Analysis of Variance

| Source | DF | Sum of Squares | Mean Square | F Ratio |
|---|---|---|---|---|
| Model | 1 | 26.355773 | 26.3558 | 4.5804 |
| Error | 9 | 51.786045 | 5.7540 | **Prob > F** |
| C. Total | 10 | 78.141818 | | 0.0610 |

## Lack Of Fit

| Source | DF | Sum of Squares | Mean Square | F Ratio |
|---|---|---|---|---|
| Lack Of Fit | 2 | 3.226878 | 1.61344 | 0.2326 |
| Pure Error | 7 | 48.559167 | 6.93702 | **Prob > F** |
| Total Error | 9 | 51.786045 | | 0.7984 |
| | | | | **Max RSq** |
| | | | | 0.3786 |

## Parameter Estimates

| Term | Estimate | Std Error | t Ratio | Prob>\|t\| |
|---|---|---|---|---|
| Intercept | 3.8552239 | 1.134993 | 3.40 | 0.0079* |
| Clay Size | 1.4708955 | 0.687273 | 2.14 | 0.0610 |

**Residual by Predicted Plot**

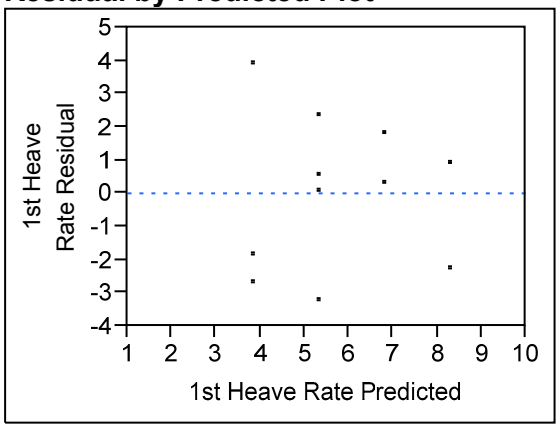


**Passing 0.074 mm**

**Response 1st Heave Rate**
**Whole Model**
**Regression Plot**

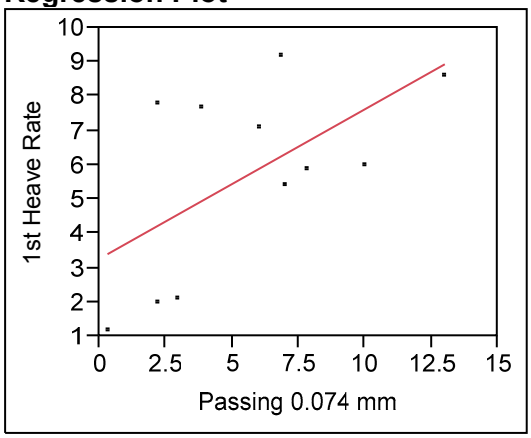


**Actual by Predicted Plot**

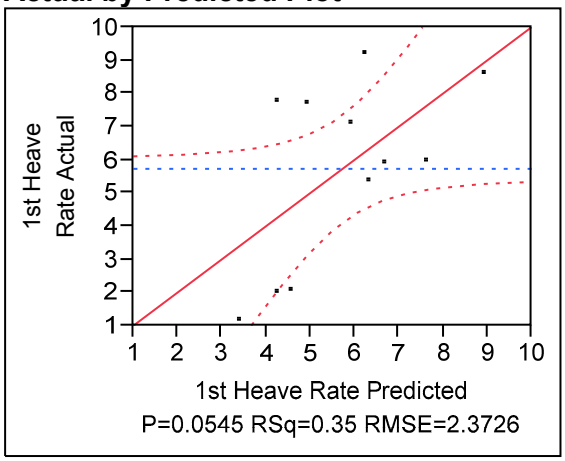

## Summary of Fit

| | |
|---|---|
| RSquare | 0.351667 |
| RSquare Adj | 0.27963 |
| Root Mean Square Error | 2.372573 |
| Mean of Response | 5.727273 |
| Observations (or Sum Wgts) | 11 |

## Analysis of Variance

| Source | DF | Sum of Squares | Mean Square | F Ratio |
|---|---|---|---|---|
| Model | 1 | 27.479875 | 27.4799 | 4.8817 |
| Error | 9 | 50.661943 | 5.6291 | **Prob > F** |
| C. Total | 10 | 78.141818 | | 0.0545 |

## Lack Of Fit

| Source | DF | Sum of Squares | Mean Square | F Ratio |
|---|---|---|---|---|
| Lack Of Fit | 8 | 33.841943 | 4.2302 | 0.2515 |
| Pure Error | 1 | 16.820000 | 16.8200 | **Prob > F** |
| Total Error | 9 | 50.661943 | | 0.9187 |
| | | | | **Max RSq** |
| | | | | 0.7848 |

## Parameter Estimates

| Term | Estimate | Std Error | t Ratio | Prob>\|t\| |
|---|---|---|---|---|
| Intercept | 3.2671583 | 1.323439 | 2.47 | 0.0356* |
| Passing 0.074 mm | 0.4364719 | 0.197546 | 2.21 | 0.0545 |

## Residual by Predicted Plot

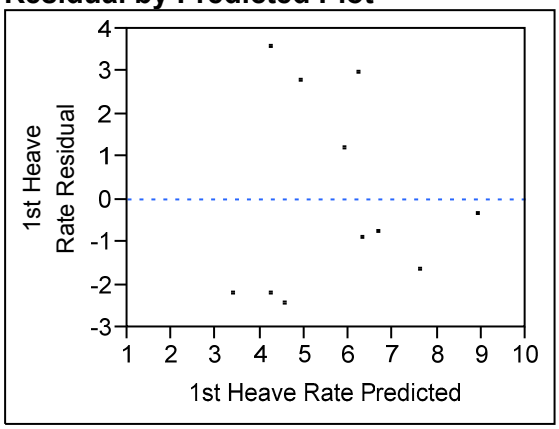

**Passing 0.02 mm**

**Response 1st Heave Rate**

**Whole Model**

**Regression Plot**

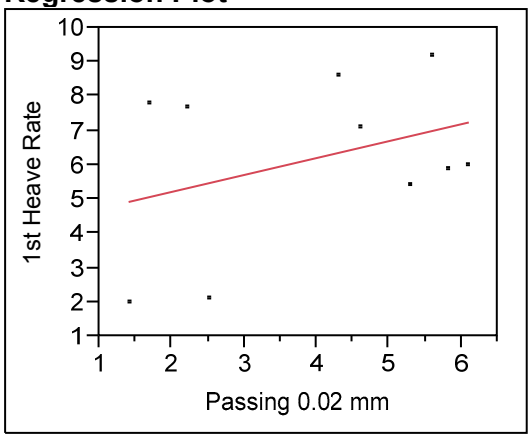


**Actual by Predicted Plot**

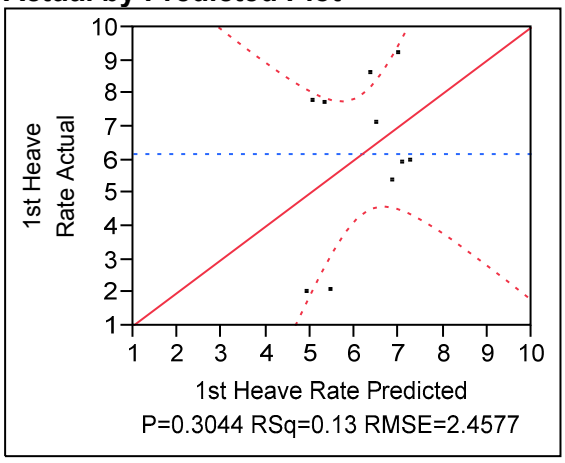


**Summary of Fit**

| | |
|---|---|
| RSquare | 0.130855 |
| RSquare Adj | 0.022211 |
| Root Mean Square Error | 2.457667 |
| Mean of Response | 6.18 |
| Observations (or Sum Wgts) | 10 |

**Analysis of Variance**

| Source | DF | Sum of Squares | Mean Square | F Ratio |
|---|---|---|---|---|
| Model | 1 | 7.274991 | 7.27499 | 1.2044 |
| Error | 8 | 48.321009 | 6.04013 | **Prob > F** |
| C. Total | 9 | 55.596000 | | 0.3044 |

**Parameter Estimates**

| Term | Estimate | Std Error | t Ratio | Prob>\|t\| |
|---|---|---|---|---|
| Intercept | 4.2304604 | 1.938964 | 2.18 | 0.0607 |
| Passing 0.02 mm | 0.4935543 | 0.44972 | 1.10 | 0.3044 |

**Residual by Predicted Plot**

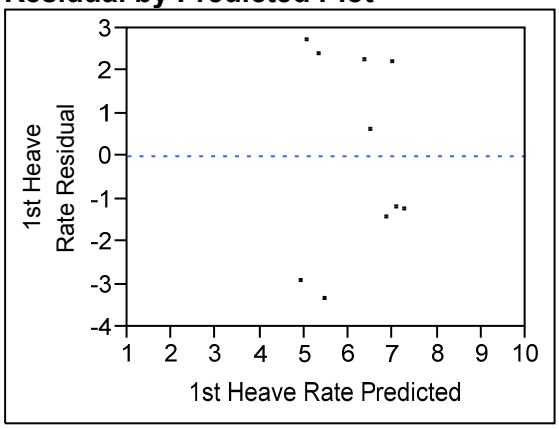


**Coarse Materials 2nd Frost Heave Model**

## First Iteration

**Response 2nd Heave Rate**
**Whole Model**
**Actual by Predicted Plot**

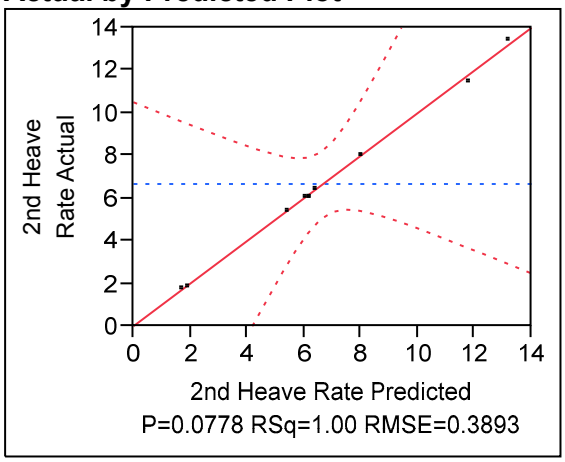


**Summary of Fit**

| | |
|---|---|
| RSquare | 0.998732 |
| RSquare Adj | 0.988589 |
| Root Mean Square Error | 0.389288 |
| Mean of Response | 6.67 |
| Observations (or Sum Wgts) | 10 |

**Analysis of Variance**

| Source | DF | Sum of Squares | Mean Square | F Ratio |
|---|---|---|---|---|
| Model | 8 | 119.36945 | 14.9212 | 98.4601 |
| Error | 1 | 0.15155 | 0.1515 | **Prob > F** |
| C. Total | 9 | 119.52100 | | 0.0778 |

**Parameter Estimates**

| Term | Estimate | Std Error | t Ratio | Prob>\|t\| | VIF |
|---|---|---|---|---|---|
| Intercept | -37.77478 | 8.484315 | -4.45 | 0.1407 | . |
| D10 | -10.58072 | 0.763513 | -13.86 | 0.0459* | 5.2790687 |
| D30 | 3.5047408 | 0.233375 | 15.02 | 0.0423* | 16.362207 |
| Gravel Size | 0.2175683 | 0.077113 | 2.82 | 0.2168 | 99.493596 |
| Sand Size | 0.478202 | 0.092645 | 5.16 | 0.1218 | 129.94857 |
| Silt Size | -3.30683 | 1.504001 | -2.20 | 0.2717 | 1158.284 |
| Clay Size | -1.02261 | 1.291097 | -0.79 | 0.5735 | 114.39526 |
| Passing 0.074 mm | 3.8055137 | 1.400796 | 2.72 | 0.2245 | 1462.1146 |
| Passing 0.02 mm | 0.4008278 | 0.171611 | 2.34 | 0.2575 | 5.8037712 |

**Residual by Predicted Plot**

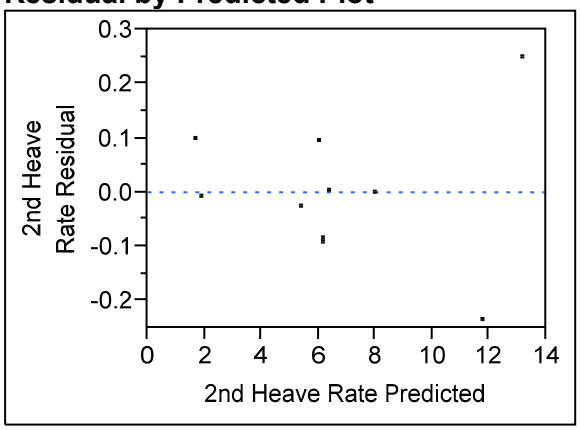


## Second Iteration

**Response 2nd Heave Rate**
**Whole Model**
**Actual by Predicted Plot**

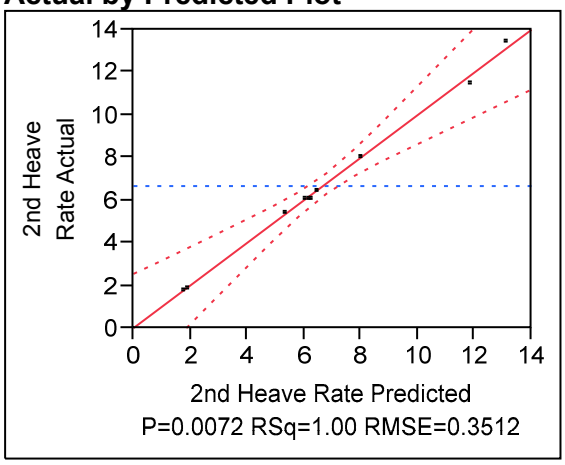


**Summary of Fit**

| | |
|---|---|
| RSquare | 0.997937 |
| RSquare Adj | 0.990715 |
| Root Mean Square Error | 0.351152 |
| Mean of Response | 6.67 |

Observations (or Sum Wgts) 10

## Analysis of Variance

| Source | DF | Sum of Squares | Mean Square | F Ratio |
|---|---|---|---|---|
| Model | 7 | 119.27438 | 17.0392 | 138.1841 |
| Error | 2 | 0.24662 | 0.1233 | **Prob > F** |
| C. Total | 9 | 119.52100 | | 0.0072* |

## Parameter Estimates

| Term | Estimate | Std Error | t Ratio | Prob>\|t\| | VIF |
|---|---|---|---|---|---|
| Intercept | -40.77806 | 6.846328 | -5.96 | 0.0270* | . |
| D10 | -10.50308 | 0.683017 | -15.38 | 0.0042* | 5.1920512 |
| D30 | 3.5470427 | 0.204926 | 17.31 | 0.0033* | 15.505269 |
| Gravel Size | 0.2445524 | 0.062402 | 3.92 | 0.0594 | 80.073442 |
| Sand Size | 0.5070965 | 0.076818 | 6.60 | 0.0222* | 109.79949 |
| Silt Size | -2.247824 | 0.621241 | -3.62 | 0.0686 | 242.87971 |
| Passing 0.074 mm | 2.7943055 | 0.519954 | 5.37 | 0.0329* | 247.57841 |
| Passing 0.02 mm | 0.3980326 | 0.154767 | 2.57 | 0.1237 | 5.8013169 |

## Residual by Predicted Plot

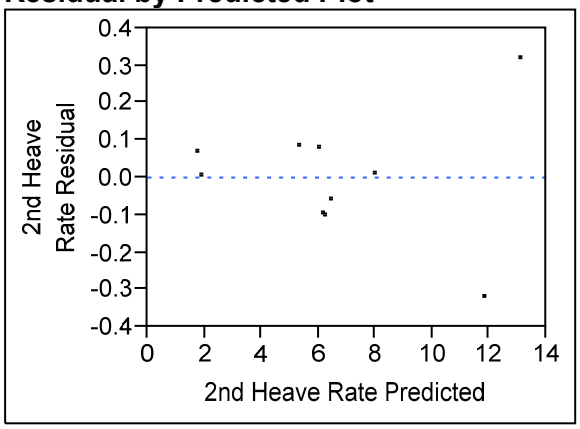

## Third Iteration

**Response 2nd Heave Rate**
**Whole Model**
**Actual by Predicted Plot**

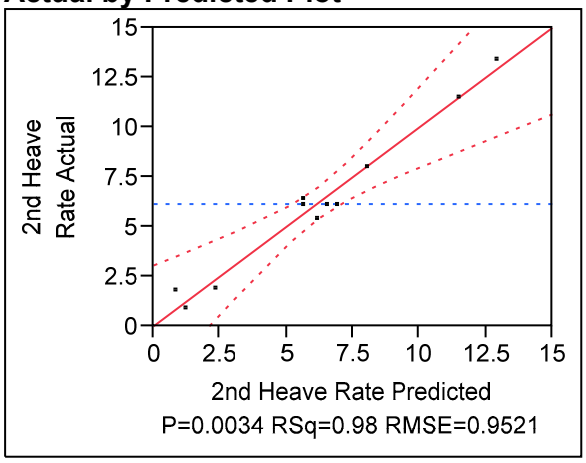


### Summary of Fit

| | |
|---|---|
| RSquare | 0.975791 |
| RSquare Adj | 0.939477 |
| Root Mean Square Error | 0.952135 |
| Mean of Response | 6.145455 |
| Observations (or Sum Wgts) | 11 |

### Analysis of Variance

| Source | DF | Sum of Squares | Mean Square | F Ratio |
|---|---|---|---|---|
| Model | 6 | 146.16103 | 24.3602 | 26.8710 |
| Error | 4 | 3.62624 | 0.9066 | **Prob > F** |
| C. Total | 10 | 149.78727 | | 0.0034* |

### Parameter Estimates

| Term | Estimate | Std Error | t Ratio | Prob>\|t\| | VIF |
|---|---|---|---|---|---|
| Intercept | -21.15303 | 14.36607 | -1.47 | 0.2149 | . |
| D10 | -10.55938 | 1.849335 | -5.71 | 0.0047* | 5.1962615 |
| D30 | 3.4320584 | 0.537176 | 6.39 | 0.0031* | 16.493687 |
| Gravel Size | 0.0944208 | 0.131644 | 0.72 | 0.5129 | 99.522712 |
| Sand Size | 0.225367 | 0.146197 | 1.54 | 0.1980 | 134.89614 |
| Silt Size | -5.216577 | 0.6356 | -8.21 | 0.0012* | 43.914512 |
| Passing 0.074 mm | 5.274504 | 0.556188 | 9.48 | 0.0007* | 49.220791 |

**Residual by Predicted Plot**

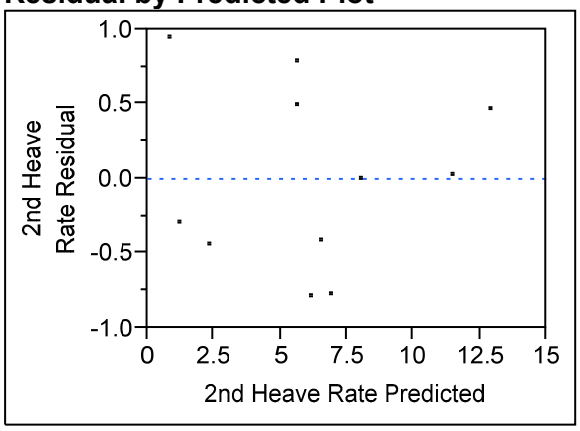


## Fourth Iteration

**Response 2nd Heave Rate**
**Whole Model**
**Actual by Predicted Plot**

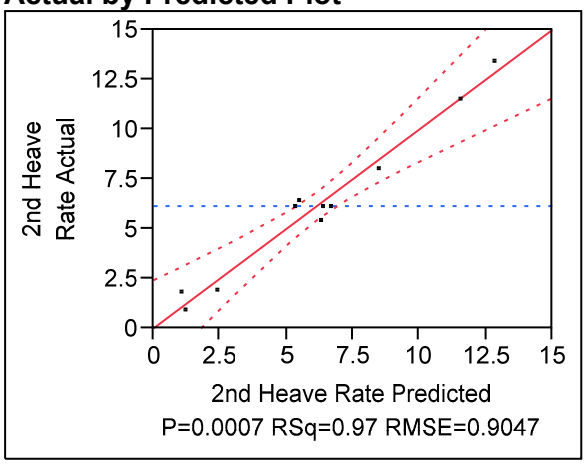


**Summary of Fit**

| | |
|---|---|
| RSquare | 0.972677 |
| RSquare Adj | 0.945354 |
| Root Mean Square Error | 0.904722 |
| Mean of Response | 6.145455 |
| Observations (or Sum Wgts) | 11 |

**Analysis of Variance**

| Source | DF | Sum of Squares | Mean Square | F Ratio |
|---|---|---|---|---|
| Model | 5 | 145.69466 | 29.1389 | 35.5994 |
| Error | 5 | 4.09261 | 0.8185 | **Prob > F** |
| C. Total | 10 | 149.78727 | | 0.0007* |

**Parameter Estimates**

| Term | Estimate | Std Error | t Ratio | Prob>\|t\| | VIF |
|---|---|---|---|---|---|
| Intercept | -11.09144 | 2.943643 | -3.77 | 0.0131* | . |
| D10 | -9.84292 | 1.478849 | -6.66 | 0.0012* | 3.6802194 |

| Term | Estimate | Std Error | t Ratio | Prob>\|t\| | VIF |
|---|---|---|---|---|---|
| D30 | 3.2511538 | 0.450664 | 7.21 | 0.0008* | 12.857486 |
| Sand Size | 0.1232058 | 0.031309 | 3.94 | 0.0110* | 6.8521776 |
| Silt Size | -5.272067 | 0.599459 | -8.79 | 0.0003* | 43.263879 |
| Passing 0.074 mm | 5.2008637 | 0.51941 | 10.01 | 0.0002* | 47.543531 |

**Residual by Predicted Plot**

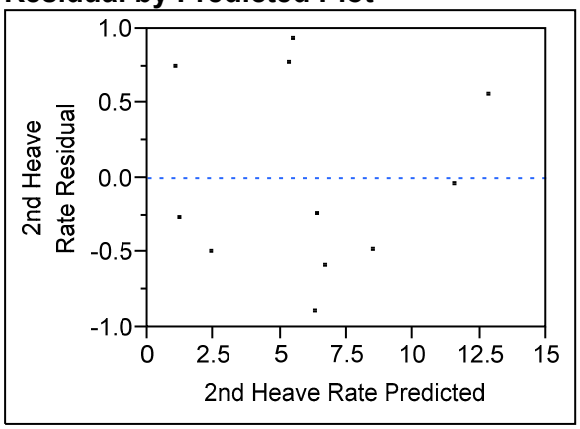


## Fifth Iteration

**Response 2nd Heave Rate**
**Whole Model**
**Actual by Predicted Plot**

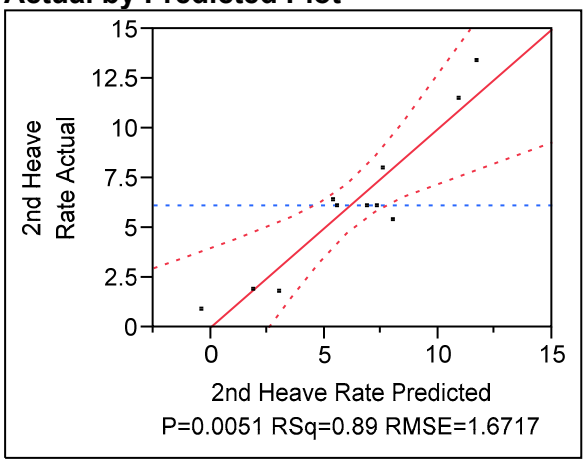


**Summary of Fit**

| | |
|---|---|
| RSquare | 0.888056 |
| RSquare Adj | 0.813427 |
| Root Mean Square Error | 1.671716 |
| Mean of Response | 6.145455 |
| Observations (or Sum Wgts) | 11 |

**Analysis of Variance**

| Source | DF | Sum of Squares | Mean Square | F Ratio |
|---|---|---|---|---|
| Model | 4 | 133.01948 | 33.2549 | 11.8995 |
| Error | 6 | 16.76780 | 2.7946 | **Prob > F** |

| Source | DF | Sum of Squares | Mean Square | F Ratio |
|---|---|---|---|---|
| C. Total | 10 | 149.78727 | | 0.0051* |

**Parameter Estimates**

| Term | Estimate | Std Error | t Ratio | Prob>\|t\| | VIF |
|---|---|---|---|---|---|
| Intercept | -0.162982 | 1.803389 | -0.09 | 0.9309 | . |
| D10 | -8.268386 | 2.630651 | -3.14 | 0.0200* | 3.4108141 |
| D30 | 1.8159475 | 0.489157 | 3.71 | 0.0099* | 4.436634 |
| Silt Size | -5.058146 | 1.103097 | -4.59 | 0.0037* | 42.908092 |
| Passing 0.074 mm | 4.6568231 | 0.925126 | 5.03 | 0.0024* | 44.175233 |

**Residual by Predicted Plot**

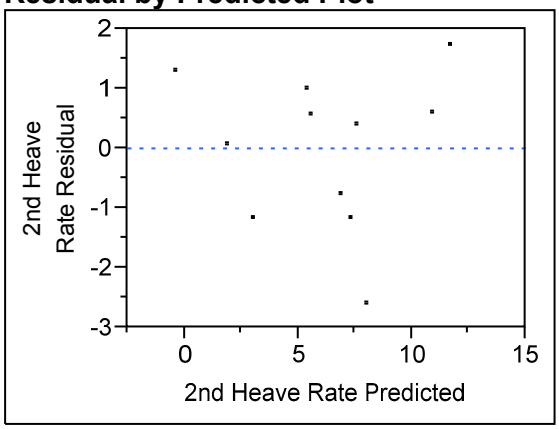


## Sixth Iteration

**Response 2nd Heave Rate**
**Whole Model**
**Actual by Predicted Plot**

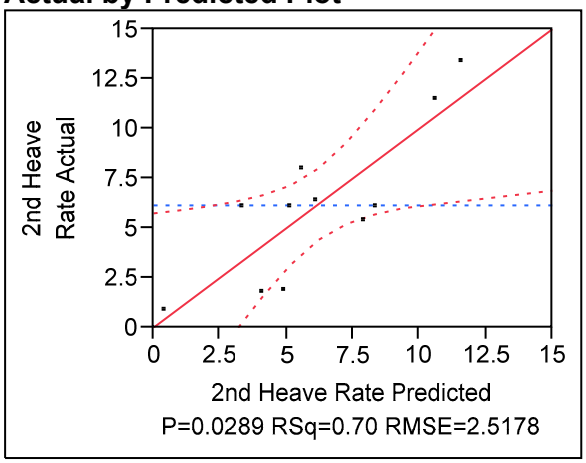


**Summary of Fit**

| | |
|---|---|
| RSquare | 0.703739 |
| RSquare Adj | 0.57677 |
| Root Mean Square Error | 2.517825 |
| Mean of Response | 6.145455 |
| Observations (or Sum Wgts) | 11 |

### Analysis of Variance

| Source | DF | Sum of Squares | Mean Square | F Ratio |
|---|---|---|---|---|
| Model | 3 | 105.41116 | 35.1371 | 5.5426 |
| Error | 7 | 44.37611 | 6.3394 | Prob > F |
| C. Total | 10 | 149.78727 | | 0.0289* |

### Parameter Estimates

| Term | Estimate | Std Error | t Ratio | Prob>\|t\| | VIF |
|---|---|---|---|---|---|
| Intercept | -1.190859 | 2.671111 | -0.45 | 0.6692 | . |
| D30 | 0.7066071 | 0.510098 | 1.39 | 0.2085 | 2.12685 |
| Silt Size | -3.934517 | 1.571744 | -2.50 | 0.0408* | 38.401562 |
| Passing 0.074 mm | 3.9803143 | 1.355127 | 2.94 | 0.0218* | 41.784071 |

### Residual by Predicted Plot

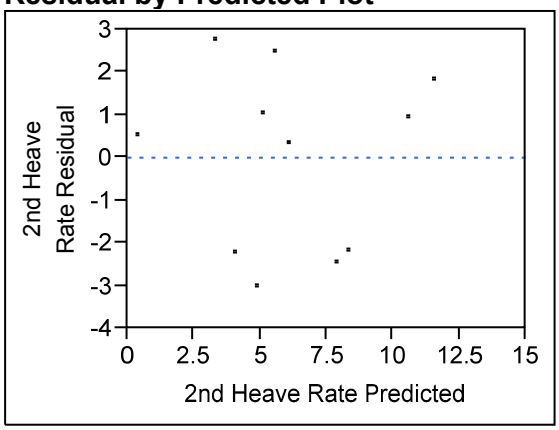


## Seventh Iteration

### Response 2nd Heave Rate
### Whole Model
### Actual by Predicted Plot

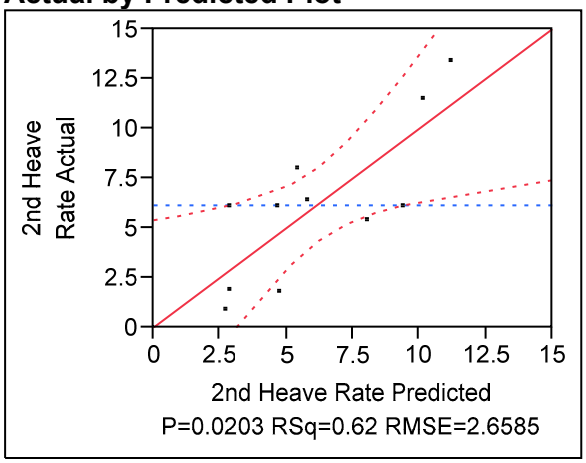


### Summary of Fit

| | |
|---|---|
| RSquare | 0.622526 |

| | |
|---|---|
| RSquare Adj | 0.528158 |
| Root Mean Square Error | 2.658496 |
| Mean of Response | 6.145455 |
| Observations (or Sum Wgts) | 11 |

## Analysis of Variance

| Source | DF | Sum of Squares | Mean Square | F Ratio |
|---|---|---|---|---|
| Model | 2 | 93.24648 | 46.6232 | 6.5968 |
| Error | 8 | 56.54079 | 7.0676 | **Prob > F** |
| C. Total | 10 | 149.78727 | | 0.0203* |

## Lack Of Fit

| Source | DF | Sum of Squares | Mean Square | F Ratio |
|---|---|---|---|---|
| Lack Of Fit | 7 | 47.720795 | 6.81726 | 0.7729 |
| Pure Error | 1 | 8.820000 | 8.82000 | **Prob > F** |
| Total Error | 8 | 56.540795 | | 0.7072 |
| | | | | **Max RSq** |
| | | | | 0.9411 |

## Parameter Estimates

| Term | Estimate | Std Error | t Ratio | Prob>\|t\| | VIF |
|---|---|---|---|---|---|
| Intercept | 1.9437176 | 1.498586 | 1.30 | 0.2308 | . |
| Silt Size | -2.440434 | 1.20714 | -2.02 | 0.0779 | 20.317951 |
| Passing 0.074 mm | 2.6348379 | 0.997757 | 2.64 | 0.0297* | 20.317951 |

## Residual by Predicted Plot

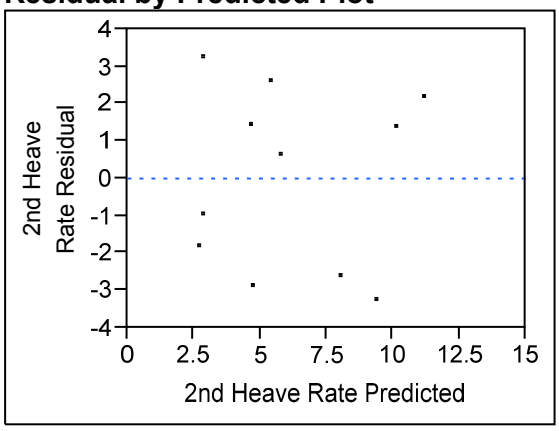

## Final Iteration

**Response 2nd Heave Rate**
**Whole Model**
**Regression Plot**

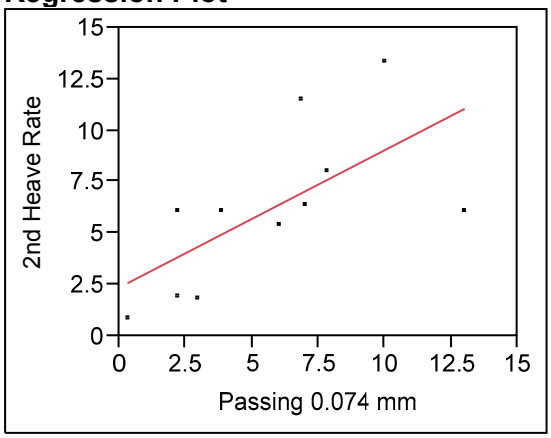


**Actual by Predicted Plot**

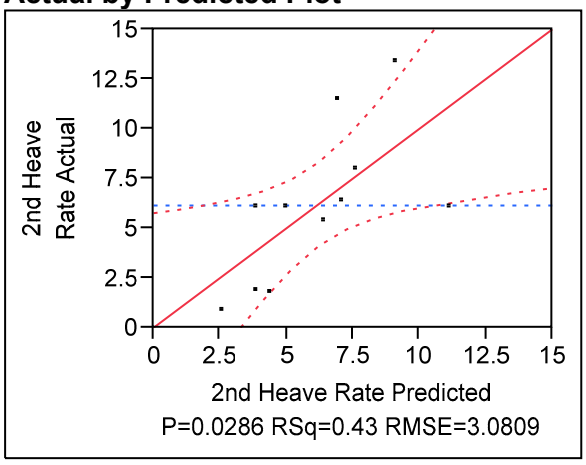


### Summary of Fit

| | |
|---|---|
| RSquare | 0.429678 |
| RSquare Adj | 0.366309 |
| Root Mean Square Error | 3.080891 |
| Mean of Response | 6.145455 |
| Observations (or Sum Wgts) | 11 |

### Analysis of Variance

| Source | DF | Sum of Squares | Mean Square | F Ratio |
|---|---|---|---|---|
| Model | 1 | 64.36025 | 64.3602 | 6.7805 |
| Error | 9 | 85.42703 | 9.4919 | **Prob > F** |
| C. Total | 10 | 149.78727 | | 0.0286* |

### Lack Of Fit

| Source | DF | Sum of Squares | Mean Square | F Ratio |
|---|---|---|---|---|
| Lack Of Fit | 8 | 76.607027 | 9.57588 | 1.0857 |
| Pure Error | 1 | 8.820000 | 8.82000 | **Prob > F** |
| Total Error | 9 | 85.427027 | | 0.6347 |

| Source | DF | Sum of Squares | Mean Square | F Ratio<br>Max RSq<br>0.9411 |
|---|---|---|---|---|

**Parameter Estimates**

| Term | Estimate | Std Error | t Ratio | Prob>\|t\| |
|---|---|---|---|---|
| Intercept | 2.3805256 | 1.718544 | 1.39 | 0.1994 |
| Passing 0.074 mm | 0.6679713 | 0.256522 | 2.60 | 0.0286* |

**Residual by Predicted Plot**

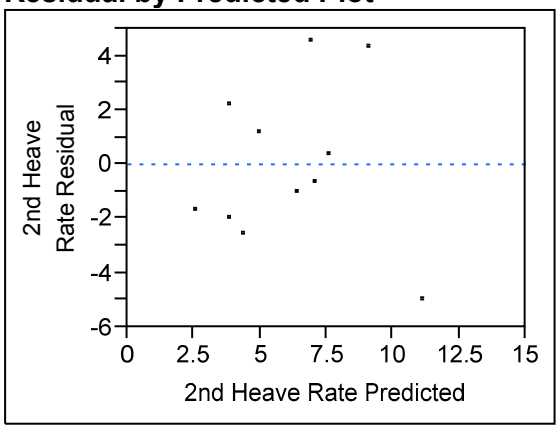


**Individual Parameter Analysis for Coarse Materials 2nd Frost Heave Model**

**$C_c$**

**Response 2nd Heave Rate**
**Whole Model**
**Regression Plot**

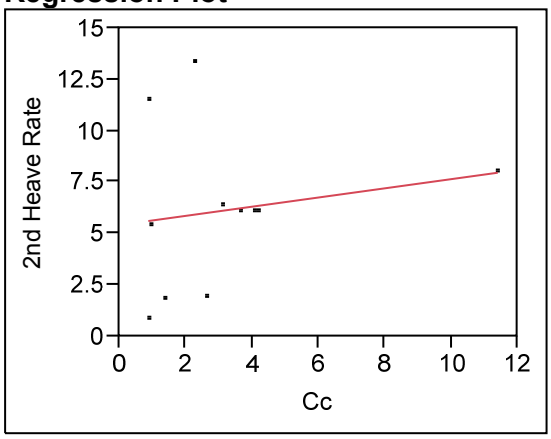

### Actual by Predicted Plot

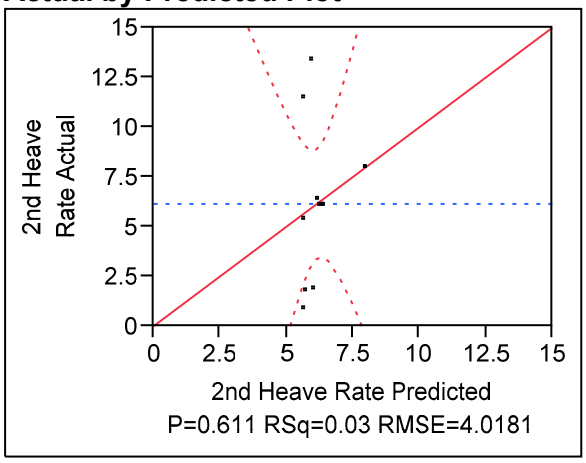


### Summary of Fit

| | |
|---|---|
| RSquare | 0.029929 |
| RSquare Adj | -0.07786 |
| Root Mean Square Error | 4.018074 |
| Mean of Response | 6.145455 |
| Observations (or Sum Wgts) | 11 |

### Analysis of Variance

| Source | DF | Sum of Squares | Mean Square | F Ratio |
|---|---|---|---|---|
| Model | 1 | 4.48301 | 4.4830 | 0.2777 |
| Error | 9 | 145.30426 | 16.1449 | **Prob > F** |
| C. Total | 10 | 149.78727 | | 0.6110 |

### Parameter Estimates

| Term | Estimate | Std Error | t Ratio | Prob>\|t\| |
|---|---|---|---|---|
| Intercept | 5.4255258 | 1.826005 | 2.97 | 0.0157* |
| Cc | 0.2235804 | 0.424294 | 0.53 | 0.6110 |

### Residual by Predicted Plot

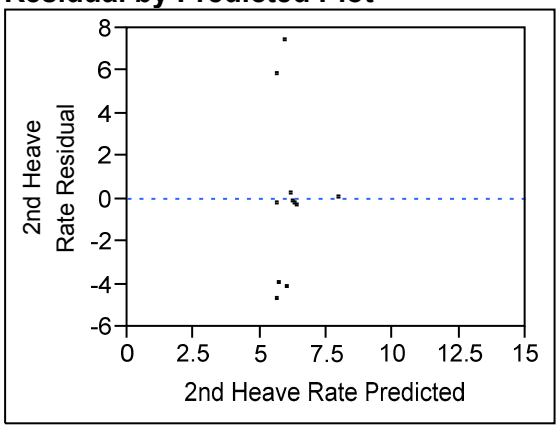

$C_u$

**Response 2nd Heave Rate**
**Whole Model**
**Regression Plot**

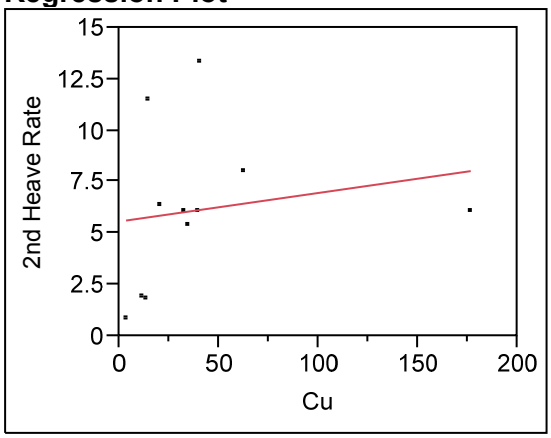


**Actual by Predicted Plot**

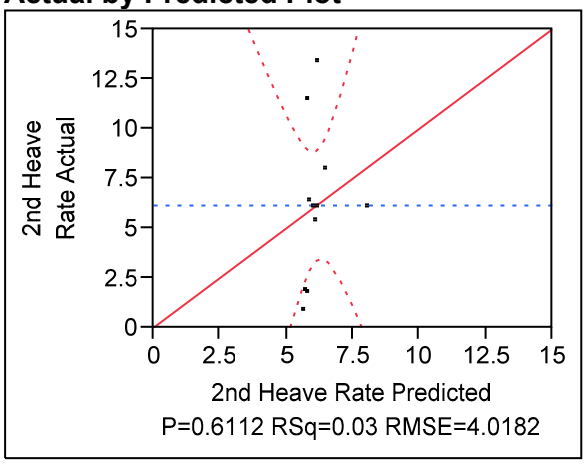


**Summary of Fit**

| | |
|---|---|
| RSquare | 0.029885 |
| RSquare Adj | -0.07791 |
| Root Mean Square Error | 4.018165 |
| Mean of Response | 6.145455 |
| Observations (or Sum Wgts) | 11 |

**Analysis of Variance**

| Source | DF | Sum of Squares | Mean Square | F Ratio |
|---|---|---|---|---|
| Model | 1 | 4.47639 | 4.4764 | 0.2773 |
| Error | 9 | 145.31088 | 16.1457 | **Prob > F** |
| C. Total | 10 | 149.78727 | | 0.6112 |

**Parameter Estimates**

| Term | Estimate | Std Error | t Ratio | Prob>\|t\| |
|---|---|---|---|---|
| Intercept | 5.5846096 | 1.613167 | 3.46 | 0.0071* |
| Cu | 0.0138895 | 0.026378 | 0.53 | 0.6112 |

**Residual by Predicted Plot**

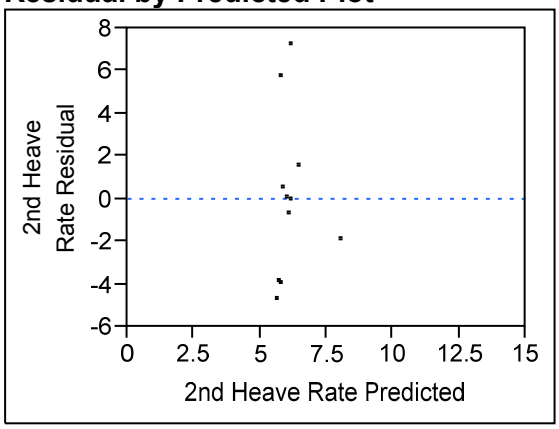


**$D_{10}$**

**Response 2nd Heave Rate**
**Whole Model**
**Regression Plot**

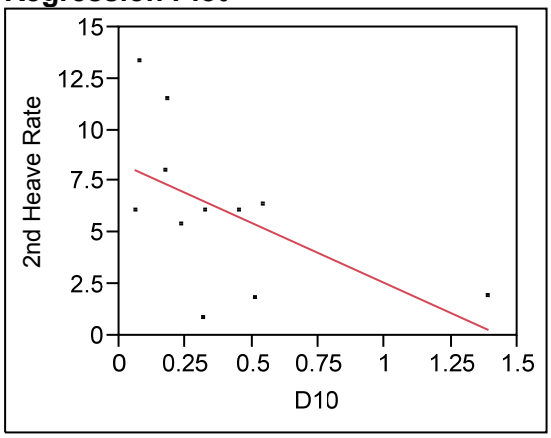


**Actual by Predicted Plot**

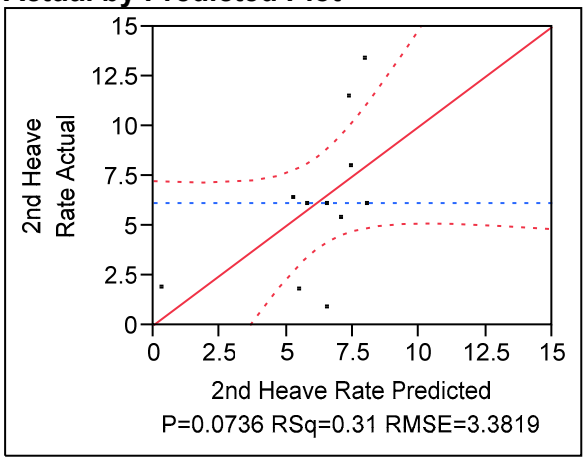

### Summary of Fit

| | |
|---|---|
| RSquare | 0.31281 |
| RSquare Adj | 0.236455 |
| Root Mean Square Error | 3.381853 |
| Mean of Response | 6.145455 |
| Observations (or Sum Wgts) | 11 |

### Analysis of Variance

| Source | DF | Sum of Squares | Mean Square | F Ratio |
|---|---|---|---|---|
| Model | 1 | 46.85491 | 46.8549 | 4.0968 |
| Error | 9 | 102.93236 | 11.4369 | **Prob > F** |
| C. Total | 10 | 149.78727 | | 0.0736 |

### Parameter Estimates

| Term | Estimate | Std Error | t Ratio | Prob>\|t\| |
|---|---|---|---|---|
| Intercept | 8.3946505 | 1.508163 | 5.57 | 0.0003* |
| D10 | -5.832427 | 2.881552 | -2.02 | 0.0736 |

### Residual by Predicted Plot

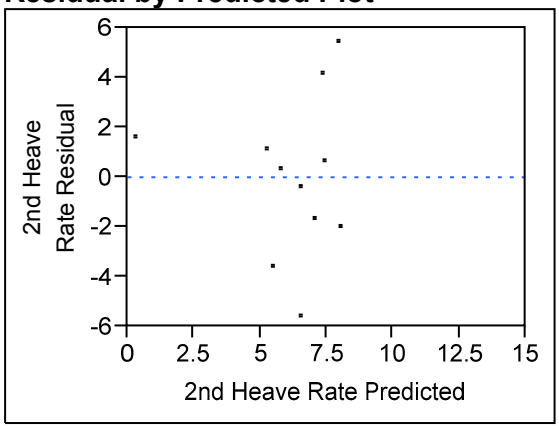


### $D_{30}$

### Response 2nd Heave Rate
### Whole Model
### Regression Plot

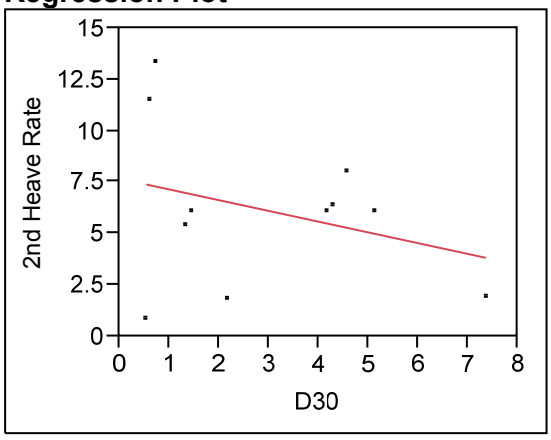

### Actual by Predicted Plot

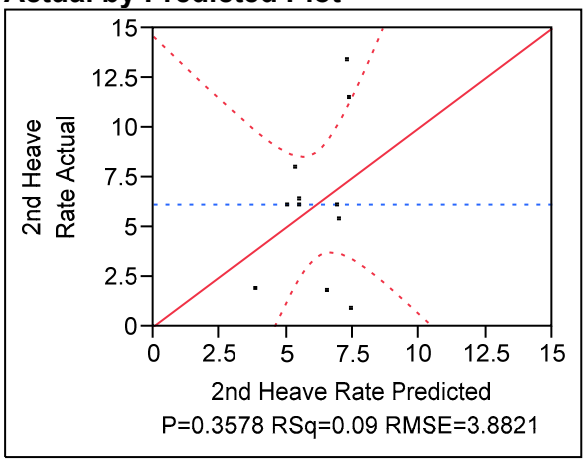


### Summary of Fit

| | |
|---|---|
| RSquare | 0.094497 |
| RSquare Adj | -0.00611 |
| Root Mean Square Error | 3.882051 |
| Mean of Response | 6.145455 |
| Observations (or Sum Wgts) | 11 |

### Analysis of Variance

| Source | DF | Sum of Squares | Mean Square | F Ratio |
|---|---|---|---|---|
| Model | 1 | 14.15442 | 14.1544 | 0.9392 |
| Error | 9 | 135.63285 | 15.0703 | **Prob > F** |
| C. Total | 10 | 149.78727 | | 0.3578 |

### Parameter Estimates

| Term | Estimate | Std Error | t Ratio | Prob>\|t\| |
|---|---|---|---|---|
| Intercept | 7.6769889 | 1.966572 | 3.90 | 0.0036* |
| D30 | -0.522643 | 0.539288 | -0.97 | 0.3578 |

### Residual by Predicted Plot

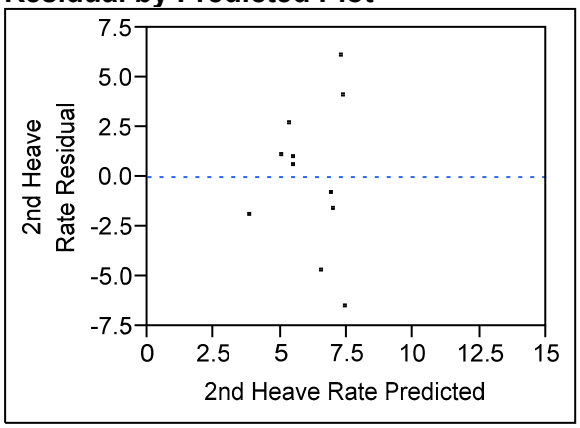

$D_{60}$

**Response 2nd Heave Rate**
**Whole Model**
**Regression Plot**

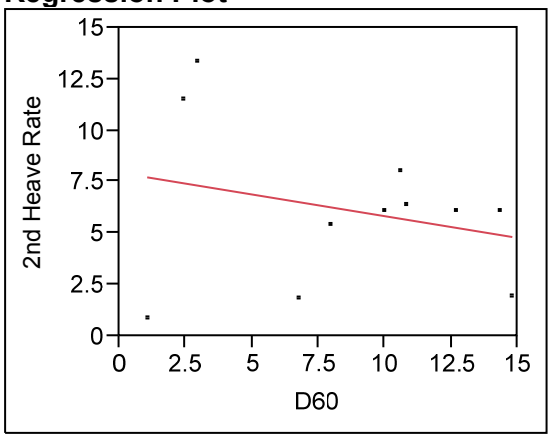


**Actual by Predicted Plot**

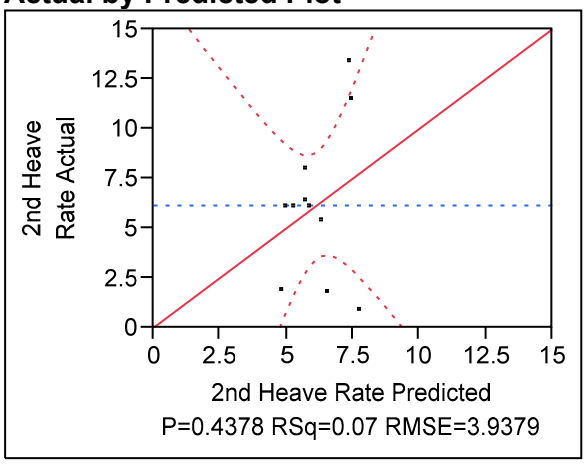


## Summary of Fit

| | |
|---|---|
| RSquare | 0.068236 |
| RSquare Adj | -0.03529 |
| Root Mean Square Error | 3.93794 |
| Mean of Response | 6.145455 |
| Observations (or Sum Wgts) | 11 |

## Analysis of Variance

| Source | DF | Sum of Squares | Mean Square | F Ratio |
|---|---|---|---|---|
| Model | 1 | 10.22095 | 10.2209 | 0.6591 |
| Error | 9 | 139.56633 | 15.5074 | **Prob > F** |
| C. Total | 10 | 149.78727 | | 0.4378 |

## Parameter Estimates

| Term | Estimate | Std Error | t Ratio | Prob>\|t\| |
|---|---|---|---|---|
| Intercept | 7.9533095 | 2.523595 | 3.15 | 0.0117* |
| D60 | -0.210907 | 0.259785 | -0.81 | 0.4378 |

**Residual by Predicted Plot**

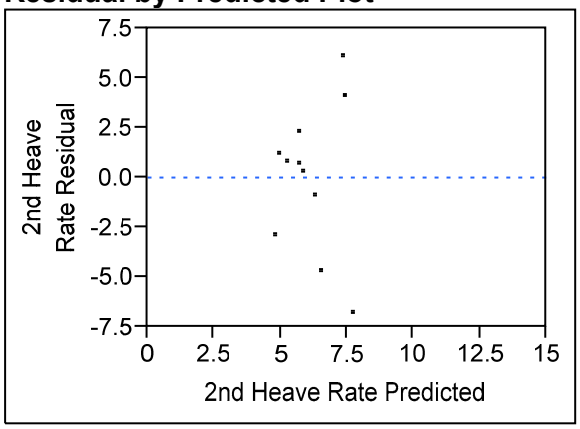


## Gravel Content

**Response 2nd Heave Rate**
**Whole Model**
**Regression Plot**

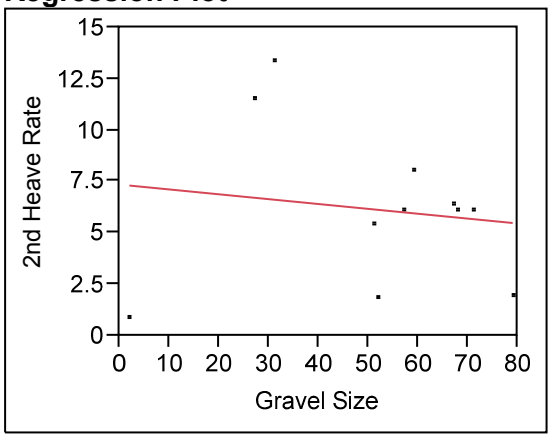


**Actual by Predicted Plot**

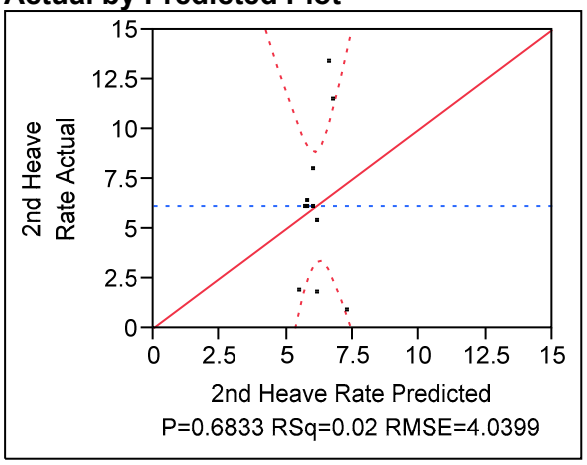

### Summary of Fit

| | |
|---|---|
| RSquare | 0.019349 |
| RSquare Adj | -0.08961 |
| Root Mean Square Error | 4.039926 |
| Mean of Response | 6.145455 |
| Observations (or Sum Wgts) | 11 |

### Analysis of Variance

| Source | DF | Sum of Squares | Mean Square | F Ratio |
|---|---|---|---|---|
| Model | 1 | 2.89824 | 2.8982 | 0.1776 |
| Error | 9 | 146.88903 | 16.3210 | **Prob > F** |
| C. Total | 10 | 149.78727 | | 0.6833 |

### Parameter Estimates

| Term | Estimate | Std Error | t Ratio | Prob>\|t\| |
|---|---|---|---|---|
| Intercept | 7.3552001 | 3.118512 | 2.36 | 0.0427* |
| Gravel Size | -0.023594 | 0.05599 | -0.42 | 0.6833 |

### Residual by Predicted Plot

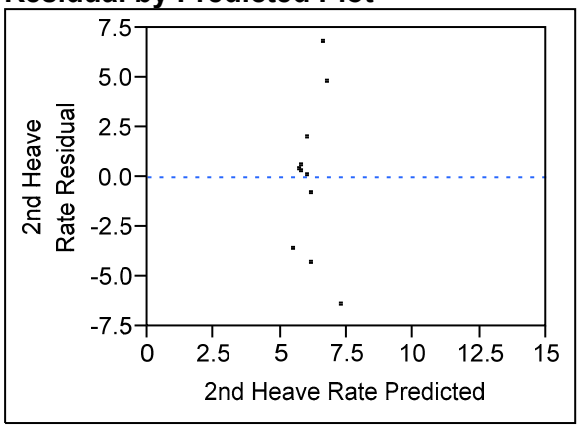


## Sand Content

### Response 2nd Heave Rate
### Whole Model
### Regression Plot

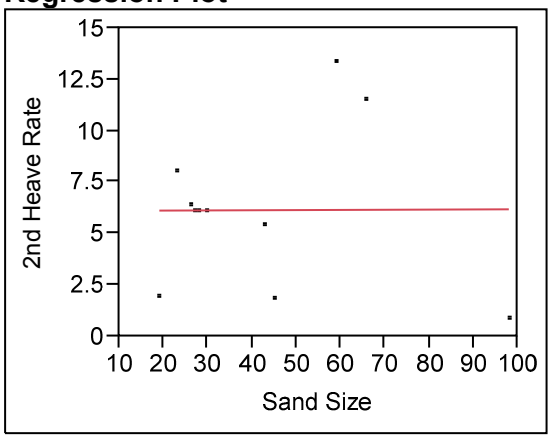

### Actual by Predicted Plot

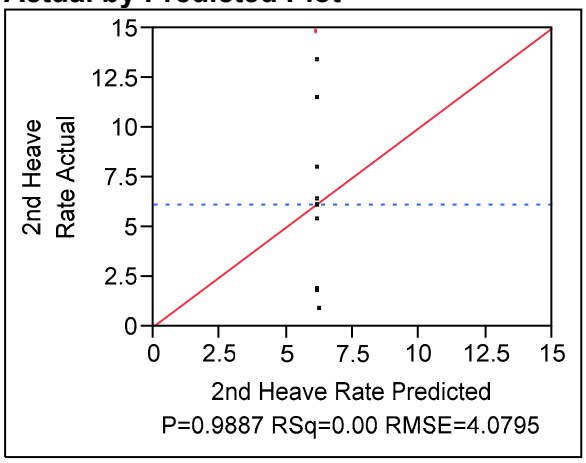


### Summary of Fit

| | |
|---|---|
| RSquare | 2.372e-5 |
| RSquare Adj | -0.11108 |
| Root Mean Square Error | 4.079539 |
| Mean of Response | 6.145455 |
| Observations (or Sum Wgts) | 11 |

### Analysis of Variance

| Source | DF | Sum of Squares | Mean Square | F Ratio |
|---|---|---|---|---|
| Model | 1 | 0.00355 | 0.0036 | 0.0002 |
| Error | 9 | 149.78372 | 16.6426 | **Prob > F** |
| C. Total | 10 | 149.78727 | | 0.9887 |

### Parameter Estimates

| Term | Estimate | Std Error | t Ratio | Prob>\|t\| |
|---|---|---|---|---|
| Intercept | 6.112212 | 2.586207 | 2.36 | 0.0424* |
| Sand Size | 0.0007881 | 0.053933 | 0.01 | 0.9887 |

### Residual by Predicted Plot

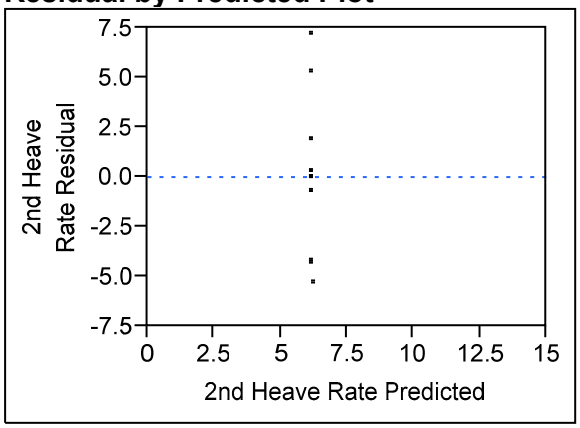

## Silt Content

**Response 2nd Heave Rate**
**Whole Model**
**Regression Plot**

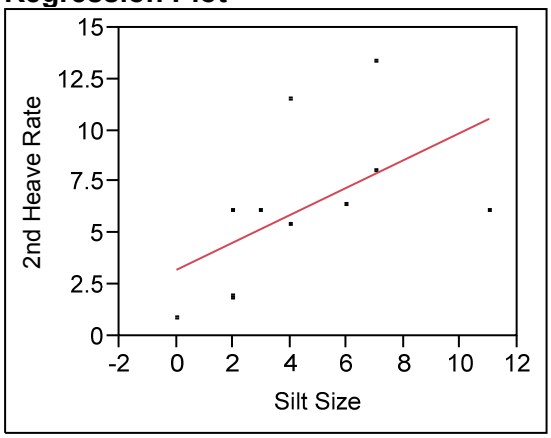


**Actual by Predicted Plot**

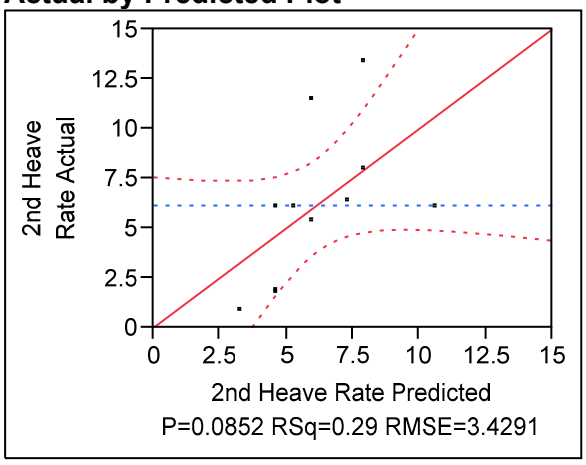


### Summary of Fit

| | |
|---|---|
| RSquare | 0.293481 |
| RSquare Adj | 0.214979 |
| Root Mean Square Error | 3.429084 |
| Mean of Response | 6.145455 |
| Observations (or Sum Wgts) | 11 |

### Analysis of Variance

| Source | DF | Sum of Squares | Mean Square | F Ratio |
|---|---|---|---|---|
| Model | 1 | 43.95975 | 43.9597 | 3.7385 |
| Error | 9 | 105.82753 | 11.7586 | **Prob > F** |
| C. Total | 10 | 149.78727 | | 0.0852 |

### Lack Of Fit

| Source | DF | Sum of Squares | Mean Square | F Ratio |
|---|---|---|---|---|
| Lack Of Fit | 5 | 60.59586 | 12.1192 | 1.0717 |
| Pure Error | 4 | 45.23167 | 11.3079 | **Prob > F** |
| Total Error | 9 | 105.82753 | | 0.4868 |

| Source | DF | Sum of Squares | Mean Square | F Ratio<br>Max RSq<br>0.6980 |
|---|---|---|---|---|

**Parameter Estimates**

| Term | Estimate | Std Error | t Ratio | Prob>\|t\| |
|---|---|---|---|---|
| Intercept | 3.2309963 | 1.827843 | 1.77 | 0.1109 |
| Silt Size | 0.6678967 | 0.34543 | 1.93 | 0.0852 |

**Residual by Predicted Plot**

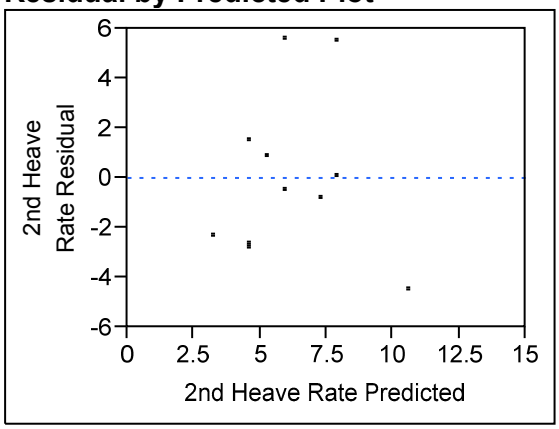


## Clay Content

**Response 2nd Heave Rate**
**Whole Model**
**Regression Plot**

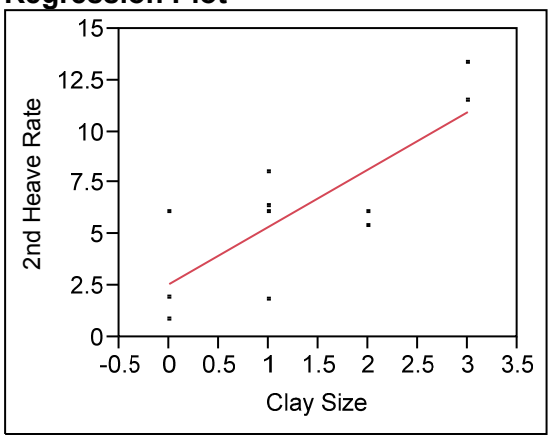

## Actual by Predicted Plot

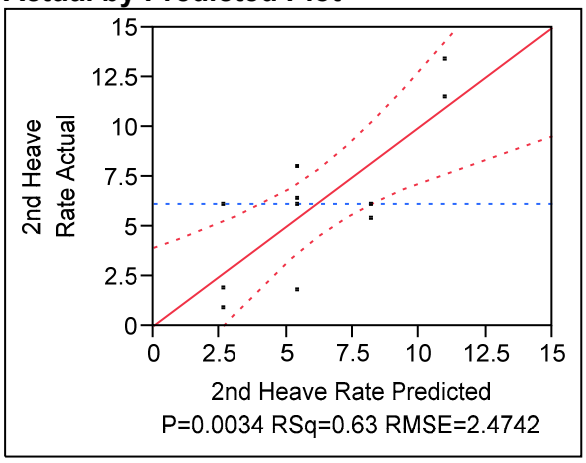


## Summary of Fit

| | |
|---|---|
| RSquare | 0.632181 |
| RSquare Adj | 0.591312 |
| Root Mean Square Error | 2.474192 |
| Mean of Response | 6.145455 |
| Observations (or Sum Wgts) | 11 |

## Analysis of Variance

| Source | DF | Sum of Squares | Mean Square | F Ratio |
|---|---|---|---|---|
| Model | 1 | 94.69265 | 94.6926 | 15.4685 |
| Error | 9 | 55.09463 | 6.1216 | **Prob > F** |
| C. Total | 10 | 149.78727 | | 0.0034* |

## Lack Of Fit

| Source | DF | Sum of Squares | Mean Square | F Ratio |
|---|---|---|---|---|
| Lack Of Fit | 2 | 16.730460 | 8.36523 | 1.5263 |
| Pure Error | 7 | 38.364167 | 5.48060 | **Prob > F** |
| Total Error | 9 | 55.094627 | | 0.2817 |
| | | | | **Max RSq** |
| | | | | 0.7439 |

## Parameter Estimates

| Term | Estimate | Std Error | t Ratio | Prob>\|t\| |
|---|---|---|---|---|
| Intercept | 2.5970149 | 1.170689 | 2.22 | 0.0537 |
| Clay Size | 2.7880597 | 0.708887 | 3.93 | 0.0034* |

**Residual by Predicted Plot**

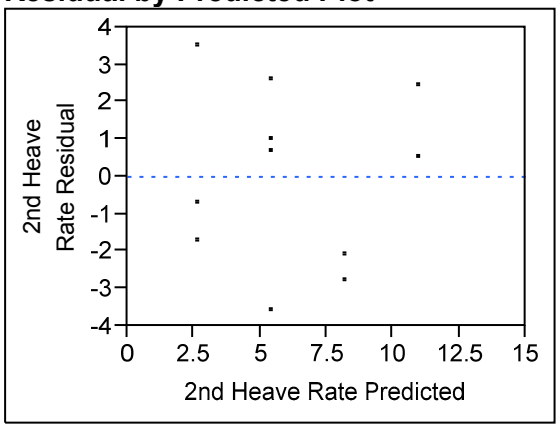


**Passing 0.02mm**

**Response 2nd Heave Rate**
**Whole Model**
**Regression Plot**

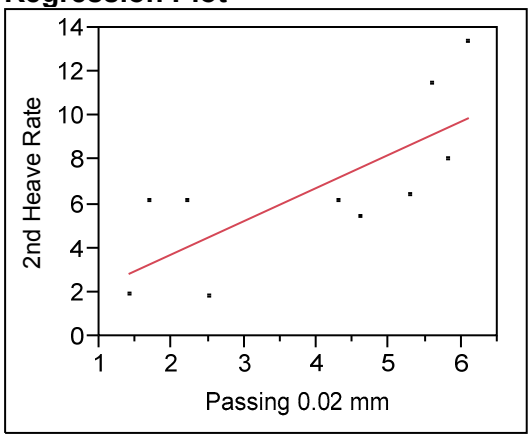


**Actual by Predicted Plot**

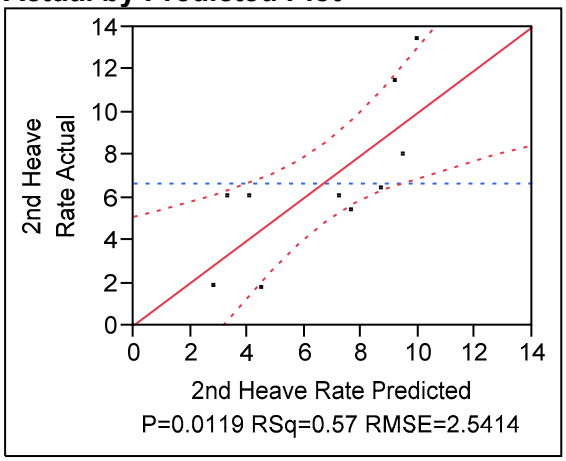

## Summary of Fit

| | |
|---|---|
| RSquare | 0.567685 |
| RSquare Adj | 0.513646 |
| Root Mean Square Error | 2.541423 |
| Mean of Response | 6.67 |
| Observations (or Sum Wgts) | 10 |

## Analysis of Variance

| Source | DF | Sum of Squares | Mean Square | F Ratio |
|---|---|---|---|---|
| Model | 1 | 67.85033 | 67.8503 | 10.5050 |
| Error | 8 | 51.67067 | 6.4588 | **Prob > F** |
| C. Total | 9 | 119.52100 | | 0.0119* |

## Parameter Estimates

| Term | Estimate | Std Error | t Ratio | Prob>\|t\| |
|---|---|---|---|---|
| Intercept | 0.716233 | 2.005043 | 0.36 | 0.7302 |
| Passing 0.02 mm | 1.5072828 | 0.465046 | 3.24 | 0.0119* |

## Residual by Predicted Plot

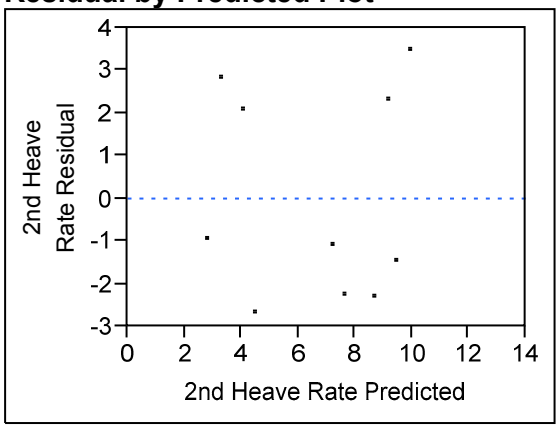

# APPENDIX F. AMES, IA MUNICIPAL POWER PLANT FLY ASH PROPERTIES

**Table 161. Ames, IA Municipal Power Plant fly ash XRF analysis on an oven-dry basis**

| | Content |
|---|---|
| $SiO_2$ | 35.3 |
| $Al_2O_3$ | 17.4 |
| $Fe_2O_3$ | 5.2 |
| $SO_3$ | 2.1 |
| CaO | 25.2 |
| MgO | 5.9 |
| $Na_2O$ | 2.50 |
| $K_2O$ | 0.71 |
| $P_2O_5$ | 1.33 |
| $TiO_2$ | 1.56 |
| SrO | 0.33 |
| BaO | 0.76 |
| Total | 98.24 |

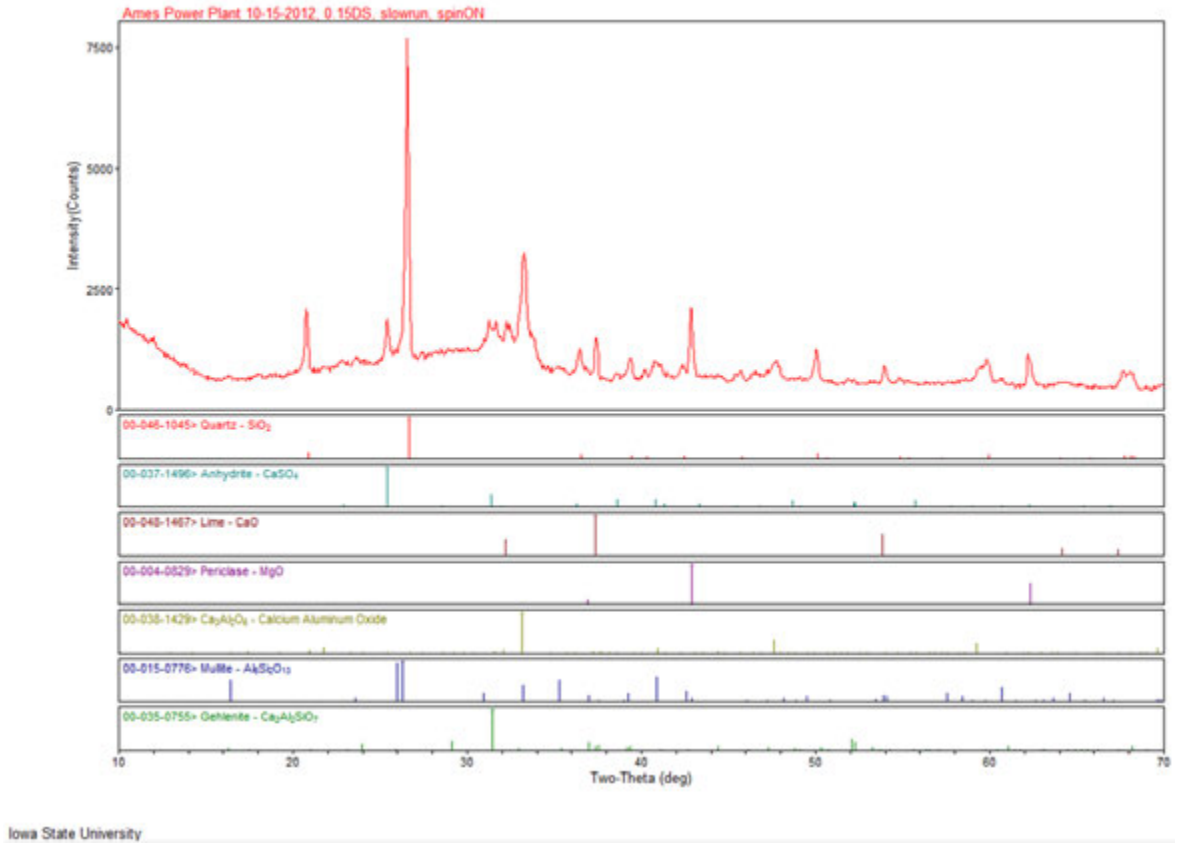


**Figure 277. Ames, IA Municipal Power Plant fly ash XRF analysis on an oven-dry basis**

A set time test was performed on the fly ash from the Ames, IA Municipal Power Plant. The test was performed by mixing 55 g of water with 200 g of fly ash and measuring the strength change of the fly ash with time using a calibrated pocket penetrometer.

**Figure 278. Set time test on Ames, IA Municipal Power Plant fly ash**

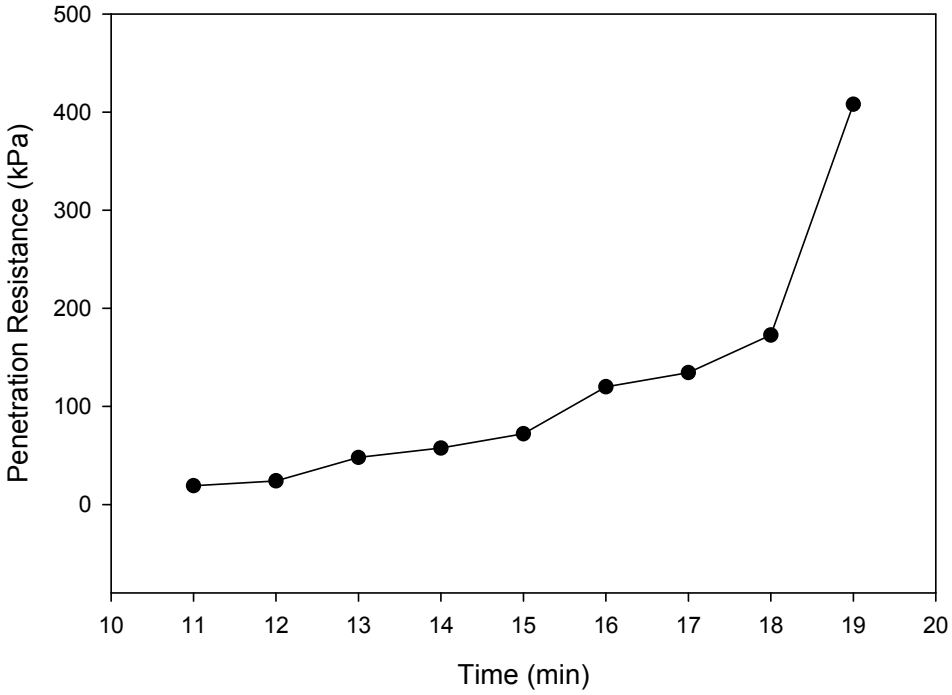


**Figure 279. Set time test results on Ames, IA Municipal Power Plant fly ash**

## ACKNOWLEGEMENTS

It is with immense gratitude that I would like to acknowledge the support and help of my major professor, Dr. David White. His patience, enthusiasm, motivation, and knowledge allowed me to complete the goals of my research. He constantly pushed me to become a better engineer by mentoring me in and out of the classroom. I would like to thank him for the financial support and opportunity that allowed me to pursue a Master of Science degree. I would also like to thank the members of my committee, Dr. Robert Horton, Dr. Peter Taylor, and Dr. Pavana Vennapusa for improving my thesis by providing their advice and suggestions.

I would like to thank the Transportation Pooled Fund Program FHWA TPF-5 (183), California DOT, Iowa DOT, Michigan DOT, Pennsylvania DOT, and Wisconsin DOT for sponsoring this research.

I am grateful for everyone at the Center for Earthworks Engineering Research at Iowa State University that assisted me in completing my research. I would especially like to thank Dr. Pavana Vennapusa for sharing his technical expertise and Dr. Christianna White for all the time she spent helping me improve my writing and communication skills.

Lastly, I am thankful for my loving family and their support that allowed me to complete my studies. My wife, Sadie, constantly motivated and supported me in my efforts to earn a Master of Science degree. I thank God for the wisdom and perseverance He provided to me during my work on this research project.